frontiers | Research Topics

Inherited retinal dystrophies: A light at the end of the tunnel?

Edited by
José M. Millan, Brian Perkins, Altaf A. Kondkar and Glenn Prazere Lobo

Coordinated by
Rakesh Radhakrishnan

Published in
Frontiers in Cell and Developmental Biology
Frontiers in Genetics

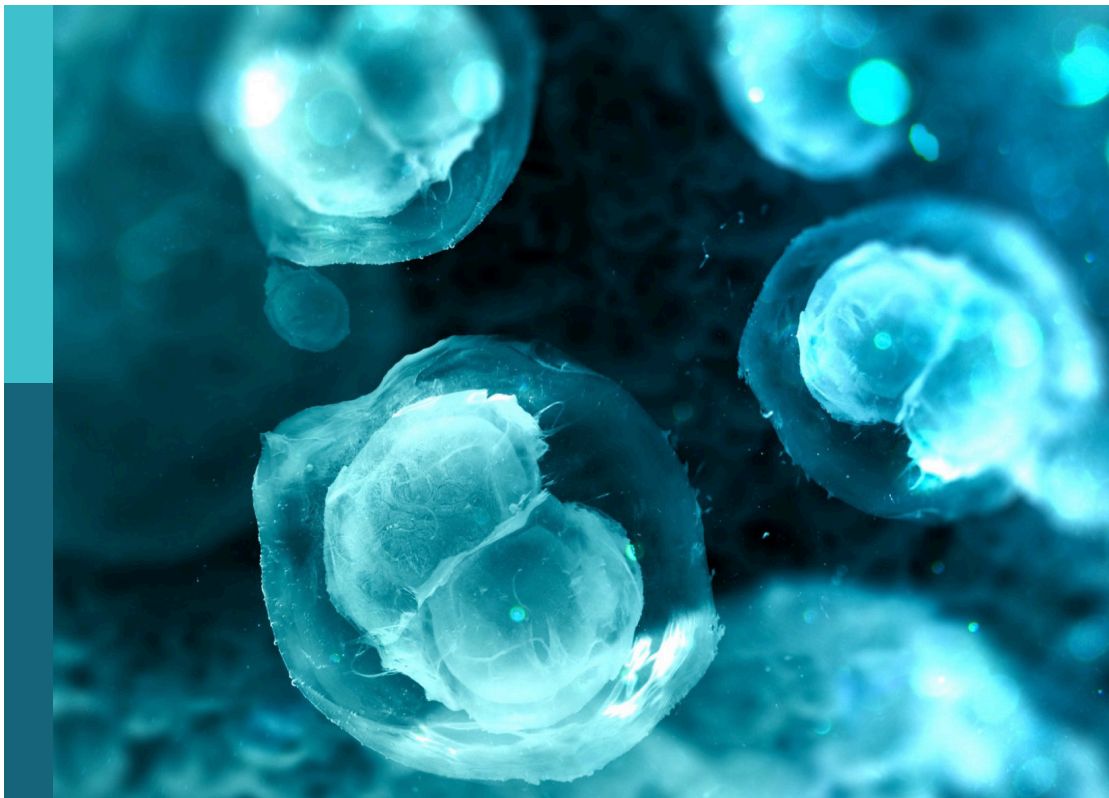

ISSN 1664-8714
ISBN 978-2-8325-3738-1
DOI 10.3389/978-2-8325-3738-1

About Frontiers

Frontiers is more than just an open access publisher of scholarly articles: it is a pioneering approach to the world of academia, radically improving the way scholarly research is managed. The grand vision of Frontiers is a world where all people have an equal opportunity to seek, share and generate knowledge. Frontiers provides immediate and permanent online open access to all its publications, but this alone is not enough to realize our grand goals.

Frontiers journal series

The Frontiers journal series is a multi-tier and interdisciplinary set of open-access, online journals, promising a paradigm shift from the current review, selection and dissemination processes in academic publishing. All Frontiers journals are driven by researchers for researchers; therefore, they constitute a service to the scholarly community. At the same time, the *Frontiers journal series* operates on a revolutionary invention, the tiered publishing system, initially addressing specific communities of scholars, and gradually climbing up to broader public understanding, thus serving the interests of the lay society, too.

Dedication to quality

Each Frontiers article is a landmark of the highest quality, thanks to genuinely collaborative interactions between authors and review editors, who include some of the world's best academicians. Research must be certified by peers before entering a stream of knowledge that may eventually reach the public - and shape society; therefore, Frontiers only applies the most rigorous and unbiased reviews. Frontiers revolutionizes research publishing by freely delivering the most outstanding research, evaluated with no bias from both the academic and social point of view. By applying the most advanced information technologies, Frontiers is catapulting scholarly publishing into a new generation.

What are Frontiers Research Topics?

Frontiers Research Topics are very popular trademarks of the *Frontiers journals series*: they are collections of at least ten articles, all centered on a particular subject. With their unique mix of varied contributions from Original Research to Review Articles, Frontiers Research Topics unify the most influential researchers, the latest key findings and historical advances in a hot research area.

Find out more on how to host your own Frontiers Research Topic or contribute to one as an author by contacting the Frontiers editorial office: frontiersin.org/about/contact

Inherited retinal dystrophies: A light at the end of the tunnel?

Topic editors

José M. Millan — La Fe Health Research Institute, Spain
Brian Perkins — Cole Eye Institute, Cleveland Clinic, United States
Altaf A. Kondkar — King Saud University, Saudi Arabia
Glenn Prazere Lobo — University of Minnesota Twin Cities, United States

Topic coordinator

Rakesh Radhakrishnan – University of Minnesota Twin Cities, United States

Citation

Millan, J. M., Perkins, B., Kondkar, A. A., Lobo, G. P., Radhakrishnan, R., eds. (2023). *Inherited retinal dystrophies: A light at the end of the tunnel?* Lausanne: Frontiers Media SA. doi: 10.3389/978-2-8325-3738-1

Table of contents

frontiers | Frontiers in Cell and Developmental Biology

TYPE Editorial
PUBLISHED 04 October 2023
DOI 10.3389/fcell.2023.1301279

OPEN ACCESS

EDITED AND REVIEWED BY
Ramani Ramchandran,
Medical College of Wisconsin,
United States

*CORRESPONDENCE
Brian D. Perkins,
perkinb2@ccf.org

RECEIVED 24 September 2023
ACCEPTED 27 September 2023
PUBLISHED 04 October 2023

CITATION
Perkins BD, Lobo GP, Kondkar AA and Millan JM (2023), Editorial: Inherited retinal dystrophies: a light at the end of the tunnel?
Front. Cell Dev. Biol. 11:1301279.
doi: 10.3389/fcell.2023.1301279

Editorial: Inherited retinal dystrophies: a light at the end of the tunnel?

Brian D. Perkins[1]*, Glenn P. Lobo[2], Altaf A. Kondkar[3] and Jose M. Millan[4]

[1]Department of Ophthalmic Research, Cole Eye Institute, Cleveland Clinic, Cleveland, OH, United States, [2]Department of Ophthalmology and Visual Neurosciences, University of Minnesota Medical School, Minneapolis, MN, United States, [3]Department of Ophthalmology, College of Medicine, King Saud University, Riyadh, Saudi Arabia, [4]Molecular, Cellular and Genomics Biomedicine, La Fe Health Research Institute, Valencia, Spain

KEYWORDS

retinal dystrophy, inherited retinal degeneration (IRD), gene therapy, retinal regeneration, genetic testing, photoreceptor degeneration

Editorial on the Research Topic
Inherited retinal dystrophies: a light at the end of the tunnel?

Inherited retinal dystrophies (IRDs) are a Research Topic of more than two dozen diseases affecting rod and cone photoreceptors and the retinal pigment epithelium (RPE) of the retina. Patients with IRDs suffer from progressive vision loss that may lead to blindness resulting from retinal degeneration. Building off the revolutionary advances in human genetics knowledge over the past 30 years, hundreds of mutations in more than 280 unique disease genes responsible for IRDs have been identified. The clinical and genetic complexity of IRDs complicates efforts to make rapid and accurate clinical diagnoses and to develop effective therapeutic treatments for IRDs. The 11 selected papers in this special Research Topic entitled "*Inherited Retinal Dystrophies: A light at the end of the tunnel?*" highlight the development of novel stem cell and animal models to study disease progression, advances in genetic screening technologies, and biochemical studies that reveal disease mechanisms that are all central to finding treatments and the eventual cures for patients suffering from IRDs. Included are review articles by Chew and Iannaccone discuss advances in stem cell therapies, optogenetics, and retinal prosthetics as therapeutic options and by Miller et al.that explain how epigenetic changes contribute to photoreceptor death in IRDs.

A major challenge to clinicians is to accurately diagnose patients with IRDs based on clinical presentations and to combine this information with diagnostic results from genetic testing services. While whole-genome sequencing (WGS) and whole-exome sequencing (WES) can identify genetic variants, the cost and necessary infrastructure makes these technologies prohibitive for wide-spread use. Diagnostic genetic testing by WGS or WES in the United States can cost several thousand dollars per patient. To address this problem, Panneman et al. describe a panel of single molecule Molecular Inversion Probes (smMIPs) that cost $30 per sample. This smMIPs panel targets exons and splice sites for all known genes associated with Retinitis Pigmentosa (RP) and Leber congenital amaurosis (LCA). The group discussed the outcomes of using this smMIPs panel to screen almost 1,200 probands and compared the effectiveness of this approach with that of WES.

Determining whether novel genetic variants identified by WGS and WES are causal for pathogenicity also remains a significant obstacle for accurate disease diagnosis. In particular, genetic variants that occur in elements that regulate RNA splicing often require functional assays to validate and confirm the effect of these variants. Rodriquez-Hidalgo et al. describe the identification of two candidate variants in the *ABCA4* gene and subsequent functional assays to determine pathogenicity. Similarly, Fernandez-Suarez et al. used WGS to identify a novel genetic variant in the gene encoding thyroid hormone receptor beta (*THRB*) as a disease-associated variant for a family with a dominantly-inherited form of cone dystrophy. Subsequent genetic analysis revealed this pathogenic variant was also found in individuals with Stargardt disease and macular dystrophy, thus expanding the possible clinical outcomes of genetic variants in *THRB*. These papers highlight the utility of WGS to identify novel variants, but also the need for functional testing to confirm pathogenicity.

Once genetic variants are deemed pathogenic, additional work is necessary to explain disease mechanisms. Jones et al. describe the complementary use of human pluripotent stem cell retinal organoids and preclinical mouse models to investigate the role of *DRAM2* in cone-rod dystrophy. The *DRAM2* gene encodes a transmembrane protein with poorly defined cellular function. Mutations in *DRAM2* lead to a rare form of age-related maculopathy but the details of disease progression remained unclear. The authors discuss how different disease models can be leveraged to study disease progression and the advantages and caveats of making comparisons between human stem cell-derived organoids and mouse models.

Three papers describe efforts to uncover the molecular mechanisms driving photoreceptor dysfunction and vision loss. Sadeh et al. explored the impact of 10 distinct disease-causing missense mutations in the *CACNA1F* gene, which encodes the $Ca_v1.4\alpha_1$ calcium channel. Using a combination of molecular modeling, patch-clamp analysis, and protein stability assays, the authors discovered that mutations in this calcium channel altered protein structure and decreased ion current through the mutant channels. Importantly, they discovered that the mutant proteins were degraded by the proteosome and that inhibition of proteosome machinery could partially restore channel function, suggesting a potential therapeutic option for individuals with congenital stationary night blindness. Radhakrishnan et al. sought to determine the binding domain in the receptor retinol binding protein 4 receptor 2 (RBPR2) protein for the ligand retinol binding protein 4 (RBP4). RBP4 binds to all-*trans*-retinol (ROL) in the bloodstream and transports ROL to cells throughout the body. ROL is the major form of vitamin A within the bloodstream and serves as the precursor to 11-*cis* retinaldehyde, which is the vitamin A derivative essential for light detection. RBPR2 is a receptor for RBP4 and the absence of RBPR2 leads to vision loss, underscoring the importance of RBPR2 in maintaining ROL homeostasis within the eye. To better understand how RBPR2 binds to RBP4, the authors utilized molecular modeling and biochemical binding assays to interrogate specific amino acid changes in RPBR2 and to identify a critical binding domain for RBP4. Finally, Linnert et al. sought to identify interacting partners for ADGRV1 and CIB2, two proteins which when mutated cause Usher Syndrome. Using affinity proteomics and biochemical assays, the authors discovered that these USH proteins shared numerous interacting proteins and, unexpectedly, interacted with proteins of the Bardet Biedl Syndrome (BBS) complex. These data suggest that USH and BBS may share similar pathogenic mechanisms that lead to vision loss.

Given the clinical and genetic heterogeneity of IRDs, the development of regenerative medicine strategies could provide treatments that are not specific to a particular mutation or even a specific gene. To this end, Boyd et al. explore the role of cardiotrophin-like cytokine factor 1 (Clcf1) and cytokine receptor-like factor 1a (Crlf1a) to induce Muller glia to proliferate in the zebrafish retina. The zebrafish has an innate ability to regenerate retinal cells following injury. By leveraging knowledge of how this process is regulated in zebrafish, regenerative strategies for humans with IRDs may be developed. Other gene-agnostic approaches may include mitigating the effect of inflammation. Sarici et al. use retrospective clinical data to demonstrate that managing inflammation in IRDs can potentially mitigate disease progression regardless of the genetic mutation. Such efforts may prolong the window of opportunity for bespoke gene therapy interventions.

In conclusion, this Research Topic provides current insights into the complexities faced by clinicians and researchers in accurately diagnosing and investigating the pathomechanisms of IRDs. This Research Topic should benefit investigators interested in the latest advances in clinical genetics and the approaches used to investigate the functional consequences of genetic variants associated with IRDs.

Author contributions

BDP: Conceptualization, Writing–original draft, Writing–review and editing. GPL: Writing–review and editing. AAK: Writing–review and editing. JMM: Writing–review and editing.

Funding

The author(s) declare financial support was received for the research, authorship, and/or publication of this article. BDP was supported by NIH grants EY034755, EY030574 and EY034493. GPL was supported by NIH grant EY030889.

Conflict of interest

The authors declare that the research was conducted in the absence of any commercial or financial relationships that could be construed as a potential conflict of interest.

The author(s) declared that they were an editorial board member of Frontiers, at the time of submission. This had no impact on the peer review process and the final decision.

Publisher's note

frontiers | Frontiers in Cell and Developmental Biology

TYPE Original Research
PUBLISHED 03 February 2023
DOI 10.3389/fcell.2023.1112270

OPEN ACCESS

EDITED BY
Glenn Prazere Lobo,
University of Minnesota Twin Cities, United States

REVIEWED BY
Michael Farkas,
University at Buffalo, United States
Francisco Javier del Castillo,
Ramón y Cajal University Hospital, Spain

*CORRESPONDENCE
Daan M. Panneman,
Daan.Panneman@radboudumc.nl

SPECIALTY SECTION
This article was submitted to Molecular and Cellular Pathology, a section of the journal Frontiers in Cell and Developmental Biology

RECEIVED 30 November 2022
ACCEPTED 20 January 2023
PUBLISHED 03 February 2023

CITATION
Panneman DM, Hitti-Malin RJ, Holtes LK, de Bruijn SE, Reurink J, Boonen EGM, Khan MI, Ali M, Andréasson S, De Baere E, Banfi S, Bauwens M, Ben-Yosef T, Bocquet B, De Bruyne M, Cerda Bdl, Coppieters F, Farinelli P, Guignard T, Inglehearn CF, Karali M, Kjellström U, Koenekoop R, de Koning B, Leroy BP, McKibbin M, Meunier I, Nikopoulos K, Nishiguchi KM, Poulter JA, Rivolta C, Rodríguez de la Rúa E, Saunders P, Simonelli F, Tatour Y, Testa F, Thiadens AAHJ, Toomes C, Tracewska AM, Tran HV, Ushida H, Vaclavik V, Verhoeven VJM, van de Vorst M, Gilissen C, Hoischen A, Cremers FPM and Roosing S (2023), Cost-effective sequence analysis of 113 genes in 1,192 probands with retinitis pigmentosa and Leber congenital amaurosis.
Front. Cell Dev. Biol. 11:1112270.
doi: 10.3389/fcell.2023.1112270

Cost-effective sequence analysis of 113 genes in 1,192 probands with retinitis pigmentosa and Leber congenital amaurosis

Daan M. Panneman[1,2]*, Rebekkah J. Hitti-Malin[1,2], Lara K. Holtes[1], Suzanne E. de Bruijn[1,2], Janine Reurink[1,2], Erica G. M. Boonen[1], Muhammad Imran Khan[1], Manir Ali[3], Sten Andréasson[4], Elfride De Baere[5,6], Sandro Banfi[7,8], Miriam Bauwens[5,6], Tamar Ben-Yosef[9], Béatrice Bocquet[10,11], Marieke De Bruyne[5,6], Berta de la Cerda[12], Frauke Coppieters[5,6,13], Pietro Farinelli[14], Thomas Guignard[15], Chris F. Inglehearn[3], Marianthi Karali[8,16], Ulrika Kjellström[4], Robert Koenekoop[17,18], Bart de Koning[19], Bart P. Leroy[20,21,22,23], Martin McKibbin[3,24], Isabelle Meunier[10,11], Konstantinos Nikopoulos[25], Koji M. Nishiguchi[26], James A. Poulter[3], Carlo Rivolta[27,28,29], Enrique Rodríguez de la Rúa[30], Patrick Saunders[31], Francesca Simonelli[16], Yasmin Tatour[9], Francesco Testa[16], Alberta A. H. J. Thiadens[32], Carmel Toomes[3], Anna M. Tracewska[1], Hoai Viet Tran[33], Hiroaki Ushida[26], Veronika Vaclavik[33], Virginie J. M. Verhoeven[32,34], Maartje van de Vorst[1], Christian Gilissen[1,35], Alexander Hoischen[1,35,36], Frans P. M. Cremers[1,2] and Susanne Roosing[1,2]

[1]Department of Human Genetics, Radboud University Medical Center, Nijmegen, Netherlands, [2]Donders Institute for Brain, Cognition and Behavior, Radboud University Medical Center, Nijmegen, Netherlands, [3]Division of Molecular Medicine, Leeds Institute of Medical Research, St. James's University Hospital, University of Leeds, Leeds, United Kingdom, [4]Department of Ophthalmology and Clinical Sciences Lund, Lund University, Skane University Hospital, Lund, Sweden, [5]Department of Biomolecular Medicine, Ghent University, Ghent, Belgium, [6]Center for Medical Genetics, Ghent University Hospital, Ghent, Belgium, [7]Telethon Institute of Genetics and Medicine, Pozzuoli, Italy, [8]Department of Precision Medicine, University of Campania "Luigi Vanvitelli", Naples, Italy, [9]Rappaport Faculty of Medicine, Technion-Israel Institute of Technology, Haifa, Israel, [10]National Reference Centre for Inherited Sensory Diseases, University of Montpellier, Montpellier University Hospital, Sensgene Care Network, ERN-EYE Network, Montpellier, France, [11]Institute for Neurosciences of Montpellier (INM), L'Institut National de la Santé et de la Recherche Médicale, University of Montpellier, L'Institut National de la Santé et de la Recherche Médicale, Montpellier, France, [12]Andalusian Center for Molecular Biology and Regenerative Medicine (CABIMER), Seville, Spain, [13]Department of Pharmaceutics, Ghent University, Ghent, Belgium, [14]Department of Computational Biology, Unit of Medical Genetics, University of Lausanne, Lausanne, Switzerland, [15]Chromosomal Genetics Unit, University Hospital of Montpellier, Montpellier, France, [16]Eye Clinic, Multidisciplinary Department of Medical, Surgical and Dental Sciences, University of Campania Luigi Vanvitelli, Naples, Italy, [17]McGill University Health Center (MUHC) Research Institute, Montreal, QC, Canada, [18]Departments of Paediatric Surgery, Human Genetics, and Adult Ophthalmology, McGill University Health Center, Montreal, QC, Canada, [19]Department of Clinical Genetics, Maastricht University Medical Center+ (MUMC+), Maastricht, Netherlands, [20]Department of Ophthalmology, Ghent University Hospital, Ghent, Belgium, [21]Department of Head & Skin, Ghent University, Ghent, Belgium, [22]Division of Ophthalmology & Center for Cellular & Molecular Therapeutics, Children's Hospital of Philadelphia, Philadelphia, PA, United States, [23]Center for Medical Genetics, Ghent University Hospital, Ghent, Belgium, [24]Department of Ophthalmology, St. James's University Hospital, Leeds, United Kingdom, [25]Laboratory of molecular diagnostics, UNILABS SA, Lausanne, Switzerland, [26]Department of Ophthalmology, Nagoya University Graduate School of Medicine, Nagoya, Japan, [27]Institute of Molecular and Clinical Ophthalmology Basel, Basel, Switzerland, [28]Department of Ophthalmology, University of Basel, Basel, Switzerland, [29]Department of Genetics and Genome Biology, University of Leicester, Leicester, United Kingdom, [30]Department of Ophthalmology, Retics Patologia Ocular, OFTARED, Instituto de Salud Carlos III, University Hospital Virgen Macarena, Madrid, Spain, [31]Molecular Loop Biosciences Inc., Woburn, MA, United States, [32]Department of Ophthalmology, Erasmus, Rotterdam, Netherlands, [33]Oculogenetic Unit, University Eye Hospital Jules Gonin, Geneva, Switzerland, [34]Department of Clinical Genetics, Erasmus, Rotterdam, Netherlands, [35]Radboud Institute of Molecular Life Sciences, Radboud University Medical Center, Nijmegen, Netherlands, [36]Department of Internal Medicine and Radboud Center for Infectious Diseases, Radboud University Medical Center, Nijmegen, Netherlands

Introduction: Retinitis pigmentosa (RP) and Leber congenital amaurosis (LCA) are two groups of inherited retinal diseases (IRDs) where the rod photoreceptors degenerate followed by the cone photoreceptors of the retina. A genetic diagnosis for IRDs is challenging since >280 genes are associated with these conditions. While whole exome sequencing (WES) is commonly used by diagnostic facilities, the costs and required infrastructure prevent its global applicability. Previous studies have shown the cost-effectiveness of sequence analysis using single molecule Molecular Inversion Probes (smMIPs) in a cohort of patients diagnosed with Stargardt disease and other maculopathies.

Methods: Here, we introduce a smMIPs panel that targets the exons and splice sites of all currently known genes associated with RP and LCA, the entire *RPE65* gene, known causative deep-intronic variants leading to pseudo-exons, and part of the RP17 region associated with autosomal dominant RP, by using a total of 16,812 smMIPs. The RP-LCA smMIPs panel was used to screen 1,192 probands from an international cohort of predominantly RP and LCA cases.

Results and discussion: After genetic analysis, a diagnostic yield of 56% was obtained which is on par with results from WES analysis. The effectiveness and the reduced costs compared to WES renders the RP-LCA smMIPs panel a competitive approach to provide IRD patients with a genetic diagnosis, especially in countries with restricted access to genetic testing.

KEYWORDS

inherited retinal diseases, targeted gene sequencing, cost-effective, high-throughput, smMIPs

1 Introduction

Inherited retinal diseases (IRDs) are a group of clinically and genetically heterogeneous disorders that are characterized by the dysfunction and subsequent death of the photoreceptor and/or retinal pigment epithelium (RPE) cells, which leads to reduced vision and can ultimately result in complete blindness. Phenotypic classification of IRDs is based on the affected cell type, the affected region within the retina, and the disease progression. For instance, retinitis pigmentosa (RP) is characterized by degeneration of rod photoreceptors and subsequently cone photoreceptors. This results in night blindness followed by peripheral vision loss and, for many persons, ultimately in blindness (Verbakel et al., 2018). In contrast, Leber congenital amaurosis (LCA) results in severe visual impairment or even complete blindness before the first year of life and is caused by degeneration of rod and cone photoreceptors, and often the RPE (den Hollander et al., 2008). The identification of genetic variants underlying IRDs is challenging as over 280 genes are currently known to be involved and pathogenic variants in many of these genes are known to cause multiple phenotypes (http://sph.uth.edu/retnet). Whole exome sequencing (WES) is often used in diagnostic facilities to identify causal variants explaining these phenotypes but the costs and the requirement for suitable infrastructure and bioinformatics support are still prohibiting its global applicability (Black et al., 2021). An efficient and cost-effective targeted sequencing method is therefore desirable. Recently, single molecule Molecular Inversion Probes (smMIPs)-based targeted sequencing has been shown to fulfil this need in the field of IRDs. Using this approach, all genes associated with inherited macular degeneration (iMD) were sequenced, achieving a good overall detection and initial solve rate (Hitti-Malin et al., 2022).

In a similar approach, we have developed a smMIPs panel that targets all genes associated with the rod-dominated forms of the IRD spectrum. All genes known to be mutated in persons with RP and/or LCA, as well as genes associated with other rod-dominant IRDs such as congenital stationary night blindness (CSNB), gyrate atrophy, choroideremia, and Sørsby fundus dystrophy, were included. In contrast to standard WES without customized enrichment, the targeted smMIPs approach allows for enrichment and the sequencing of non-coding, deep-intronic regions of genes in which splice-altering variants have been detected previously. This was exemplified by an earlier smMIPs-based sequencing effort, in which the entire 128-kb *ABCA4* gene, including coding and non-coding regions, was sequenced in 1,054 Stargardt cases (Khan et al., 2020). In this study, a total of 13 novel causative deep-intronic variants (DIVs) were identified. Besides targeting DIVs, the smMIPs approach also allows for the investigation of other genomic regions of interest, such as the RP17 locus in which several different structural variants (SVs) have been identified causing autosomal dominant RP (RP ad) (de Bruijn et al., 2020). Finally, to identify cases eligible for available gene therapies, we have targeted the coding and non-coding regions of the *RPE65* gene.

Here, we present the outcome for 1,192 probands that underwent smMIPs-based sequencing using the RP-LCA smMIPs panel. We sequenced 360 probands in parallel per sequencing run in a highly cost-effective manner and obtained sequencing data that enabled the detection of single nucleotide variants (SNVs), small insertions and deletions (indels), and SVs, including copy number variants (CNVs), and revealed pathogenic variants underlying IRD in these individuals.

2 Material and methods

2.1 Gene selection and generation of the RP-LCA smMIPs panel

All genes implicated in RP and/or LCA, as well as genes associated with other rod-dominant IRDs (e.g., congenital stationary night blindness (CSNB)), were included in the design for smMIPs in

order to completely target all rod-dominant IRDs (Supplementary Table S1). The selection of genes was based on the Retinal Information network online resource (https://sph.uth.edu/retnet/; accessed on 07-08-2020). Additionally, 417 smMIPs covering the RP17 locus, in which several pathogenic duplications and duplication-inversion events were identified, were added to the panel, and allowed detection of known and novel SVs at this locus. *ZNF513* was included in the panel but was later withdrawn as a candidate gene and therefore not included in the final analysis (Supplementary Figure S1) (de Bruijn et al., 2020).

For all genes included in the RP-LCA panel, the 5' and 3' untranslated regions (UTRs), exons, and alternative protein-coding exons were selected as targets. Additionally, all pseudo-exons (PEs) resulting from causal published DIVs, including 20 nucleotides (nt) upstream and downstream these PEs, as well as sequences resulting from exon skipping, intron retention, or with an effect on promoter activity, were included. A complete list of these targets and their genomic coordinates can be found in Supplementary Table S2. For *RPE65*, for which gene augmentation therapy is available (Russell et al., 2017), all intronic regions were also included as targets since they can harbor DIVs that could have an effect on novel or aberrant splicing. Transcript numbers for the protein coding transcript (or the longest transcript) were selected from the Alamut Visual software version 2.13 (Interactive Biosoftware) and subsequently visualized using the UCSC Genome browser (Karolchik et al., 2004). All transcripts were evaluated for the presence of alternative protein coding exons and alternative 5' UTRs using the Ensembl Genome Browser (GRCh37; Ensembl release 101) (Yates et al., 2020). Using the UCSC Genome Browser, hg19 (GRCh37) genomic coordinates were extracted and provided to Molecular Loop Biosciences, USA (Haeussler et al., 2019). A total of 16,812 smMIPs were designed to cover the regions described above with flanking regions of at least 20 nt on both the 5' and 3' ends of the provided regions, resulting in a total of 453,462 nt that are covered by the RP-LCA smMIPs panel.

2.2 smMIPs design

The Molecular Loop Biosciences' smMIPs design includes 225 nt captured regions that are flanked by a 20 nt extension and a 20 nt ligation probe arm at the 5' and 3' end, respectively. All smMIPs are dual-indexed using two 10-nt unique index primer sequences, or "barcodes", that act as a patient barcoding system to generate uniquely tagged libraries. To tag each individual smMIP, two 5 nt Unique Molecular Identifiers are included next to the probe arms and are used to detect duplicate reads and enable the detection of unique reads. A schematic overview of the smMIPs design has been published previously (Hitti-Malin et al., 2022).

2.3 Sample selection and preparation

Prior to shipment to the host institution, collaborators prepared the DNA samples. First, DNA concentrations of the samples were quantified using the Qubit dsDNA HS assay kit (Thermo Fisher, US), according to manufacturer's instructions. Second, DNA was diluted to a concentration of 16.7 ng/μL and 100 ng of DNA was loaded on a 0.8% agarose gel flanked by uncut lambda DNA (25, 50, 100, 200, and 400 ng) and 0.5 μg of a 1-kb ladder. Based on this gel, the DNA concentration was compared to the uncut lambda DNA and, subsequently, labeled as high or low molecular weight (MW) DNA based on the size distribution. The DNA was considered high MW when the DNA fragment was ≥23 kilobases (kb) and low when ≤23 kb and appeared as a smear on the gel. DNA samples of high MW were plated into a 96-well capture plate and subsequently pre-treated by incubating the DNA at 92°C for 5 minutes to briefly shear the DNA prior to library preparation. Next, DNA samples of low MW were added to the capture plate. Additionally, each plate contained six positive controls (five on every fourth plate) and one non-template control (NTC) containing only MilliQ.

2.4 Library preparation

Sequencing libraries were generated as described previously (Hitti-Malin et al., 2022). The High Input DNA Capture Kit, Chemistry 2.3.0H (Molecular Loop Biosciences, Inc.), was used according to Protocol version 2.4.1H. In short, smMIPs were hybridized for 18 h followed by the fill-in reaction to circularize the probe and, subsequently, a combined clean-up and PCR step. Prior to pooling of all samples, the appropriate size (413 bp) of each individual product was evaluated by agarose gel electrophoresis. The pooled library was purified using bead purification and quantified using the Qubit Fluorimeter and the TapeStation system to assess library concentration and fragment sizes, respectively.

2.5 Sequencing

Four sequencing library pools, generated with the High Input DNA capture kit, were combined in an equimolar fashion to form one 100 μL mega-pool of 1.5 nmol (nM). This pool was denatured according to Illumina's NovaSeq 6,000 System Denature and Dilute Libraries Guide, yielding a 300 pM. library. Each library was sequenced by paired-end sequencing on the NovaSeq 6,000 platform (Illumina, California, United States) using SP reagent kits v1.5 (300 cycles).

2.6 Variant calling and annotation

All reads generated by the NovaSeq 6,000 run were converted into raw sequencing data files (FASTQ) using bcl2fastq (v2.20). These files were subsequently processed using the a bioinformatics pipeline developed in-house, as described previously (Khan et al., 2019). In short, the random identifiers were removed from the sequencing reads and added to the read identifier for later use. After exclusion of duplicate reads, the remaining reads were added to patient specific BAM files based on the index barcoding system. In order to determine the overall average smMIPs coverage, forward and reverse read were combined and subsequently divided by two.

2.7 Average coverage per nucleotide

To determine the number of reads covering each nucleotide in sequencing run 01, the base calls of aligned reads to a reference sequence were counted in BAM files corresponding to individual

probands using the 'pileups' function of SAMtools (Li et al., 2009). Data was obtained using the following parameters: minimum mapping quality = 0, minimum base quality = 12, anomalous read pairs were discarded, overlapping base pairs from a single paired read as a depth of 1 were counted. An average coverage per nucleotide was generated for each nucleotide position across all samples sequenced in RP-LCA run 01, followed by an average coverage for all genes/loci targeted in the RP-LCA panel. The average coverage per nucleotide for *RPGR* was calculated excluding exon 15 of the *RPGR-ORF15* transcript, and the coverage of exon 15 of the *RPGR-ORF15* transcript was determined independently. Coverage plots for all reads across each gene/locus were generated. The average coverage per nucleotide was used to assess whether regions were poorly covered (≤10 reads), moderately covered (11-49 reads), or well-covered (≥50 reads).

2.8 Variant prioritization and classification

CNV analysis was performed for all samples using an Excel script described previously (Khan et al., 2020). We presumed a deletion when six (or more) consecutive smMIPs with a normalized coverage across all samples in that run was equal to or smaller than 0.65. Conversely, a duplication was assumed if six (or more) consecutive smMIPs yielded a normalized coverage of ≥1.20.

Subsequently, all SNVs and indels were evaluated. First, previously published pathogenic DIVs were included in the filtering and prioritization steps. Secondly, all homozygous and heterozygous variants with an individual minor allele frequency (MAF) of ≤0.5% in genes associated with autosomal recessive IRDs and all heterozygous variants in genes associated with autosomal dominant IRDs with a MAF of ≤0.1% were assessed. MAFs were obtained from the Genome Aggregation Database (gnomAD v2.1.1; 125,748 exomes and 15,708 genomes), as well as from an in-house WES cohort consisting of data from 24,488 individuals with a large variety of clinical phenotypes. All three MAFs needed to meet the cut-offs described above. Variants that were called in ≥80% of the sequencing reads were considered homozygous and variants that were called in 35%–80% of the sequencing reads were considered heterozygous. Variants that were called in ≥10% of probands included in a sequencing run (i.e., ≥ 38 probands) or were detected with less than 10 reads across that genomic position were excluded from further analysis.

Prioritization of variants was based on variant types, predicted protein effect, and pathogenicity scores. First, all stop gain, stop loss, frameshift, start loss, and canonical splice site variants were considered. Thereafter, in-frame insertions and/or deletions were assessed followed by missense variants that met the pre-defined thresholds of all three *in silico* pathogenicity prediction tools. Namely, PhyloP (threshold: ≥2.7, range: −14.1–6.4), CADD-PHRED (threshold: ≥15, range 1—99), and Grantham (threshold: ≥80, range 0—215) (Grantham, 1974; Pollard et al., 2010; Kircher et al., 2014).

Missense variants that met either one or two thresholds were prioritized thereafter. Subsequently, all variants were investigated using SpliceAI, except for variants affecting the canonical splice acceptor (+1 and +2 position) and donor splice sites (−1 and −2 position) (Jaganathan et al., 2019). Variants with a predicted delta score ≥0.2 (using the default settings with a window of −50 bp to +50 bp) on any of the four parameters (acceptor gain, acceptor loss, donor gain, or donor loss) were prioritized. All non-canonical splice-site (NCSS), near-exon variants and DIVs were investigated using *in silico* tools available *via* Alamut Visual. Splice Site Finder-like (Zhang, 1998), MaxEntScan (Yeo and Burge, 2004), NNSPLICE (Reese et al., 1997), and GeneSplicer (Pertea et al., 2001) were utilized to predict the effect on splicing according to parameters described before (Fadaie et al., 2019). ESEfinder was used to predict the effect on exon splicing enhancers (Cartegni et al., 2003).

Using the ACMG/AMP classification system, all variants were assigned one of five classes: class 1 (benign), class 2 (likely benign), class 3 (variant of uncertain significance, or VUS), class 4 (likely pathogenic) or class 5 (pathogenic) (Richards et al., 2015). These classes were assigned according to the ACMG/AMP guidelines using the Franklin Genoox Platform (https://franklin.genoox.com, accessed before November 2022). For *ABCA4*, the severity scores as published in Cornelis et al. (2022), were used to reach a final classification instead of the ACMG classification. For RP, we considered the proband to be very likely solved by a combination of moderate and/or severe *ABCA4* alleles. Mild *ABCA4* alleles, although sometimes classified as either class 3, 4, or 5, were deemed not to be causative for RP in this study.

Each proband was assigned an outcome indicating whether the proband was genetically "very likely solved", "possibly solved", or "unsolved". Segregation analysis was not performed in this study and, therefore, no definitive "solved" label could be assigned. When at least two variants in a given gene were observed, they were listed in two alleles, although segregation analysis was not performed. Compound heterozygosity therefore was not proven and also was not added as proof for the ACMG classification. All modes of inheritance were taken into consideration when assessing the prioritized variants identified in a proband. When a class 4 or 5 variant was detected in a homozygous state in genes known to be associated with autosomal recessive IRDs, the proband was considered "very likely solved". The genomic region in which the homozygous variant was detected was subsequently assessed for potential heterozygous deletions. In cases with two heterozygous variants in a gene associated with an autosomal recessive retinal disease, a combination of class 4 and/or 5 variants were sufficient to assign a "very likely solved" verdict. This was also the case for probands in which one class 5 and one class 3 variant was identified. Probands with one class 4 and one class 3 variant or two compound heterozygous class 3 variants were deemed "possibly solved". Probands with a heterozygous class 4 or 5 variants observed in a gene associated with autosomal dominant inheritance were assumed to be "very likely solved", whereas a proband with a single heterozygous class 3 variant remained genetically "unsolved".

2.9 Minigene analysis

Minigene analysis was performed as previously described (Sangermano et al., 2018; Verbakel et al., 2019). In short, the regions of interest of the genomic DNA sample was amplified by primers that contain attB1 and attB2 tags at their 5′end to facilitate Gateway cloning. After obtaining the entry clone, the wild-type and mutant construct containing the *RPE65*:c.675C>A variant were separately inserted into the pCI-NEO-RHO Gateway-adapted vector to generate wild-type and mutant minigenes. Both minigenes were independently transfected into HEK293T cells and

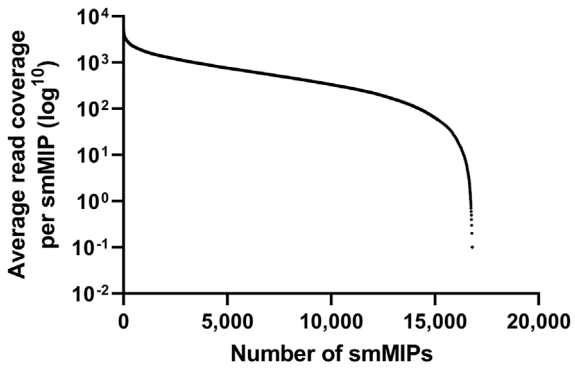

FIGURE 1
Average read coverage per smMIP in the RP-LCA panel.

after 48 h of incubation, mRNA was isolated and amplified by RT-PCR with primers in the flanking *RHO* exon 3 and 5 regions. All primers used for this splice assay are available upon request. Fragment sizes were assessed using gel electrophoresis and identified using Sanger sequencing.

2.10 Ethical considerations

The study adhered to the tenets of the Declaration of Helsinki and was approved by the local ethics committee of the Radboud University Medical Center (Nijmegen, The Netherlands). Written informed consent was obtained from patients prior to DNA analysis and inclusion in this study.

3 Results

Prior to sequencing 360 probands in a single sequencing run, a test run was performed including 32 control samples, harboring a total of 22 CNVs and 19 SNVs, together with 15 genetically unsolved probands. This test run was used to assess the average coverage across all targets and the performance of the RP-LCA smMIPs pool. A total of 496,610,877 reads were obtained after exclusion of duplicate reads, averaging at 10,566,189 reads per proband. An average of 629 reads per smMIP was obtained across the entire pool of 16,812 smMIPs and, since all nucleotides are covered by eight smMIPs on average, each nucleotide was covered by approximately 5,032 smMIPs on average. As this confirmed solid read characteristics, we continued to increase the number of probands sequenced in a single run to 360 cases whilst maintaining adequate read numbers to call variants (approximately 629 reads per nucleotide on average). Since even read coverage was achieved, no rebalancing of the smMIPs pool was required (Figure 1). All previously identified SNVs and CNVs from the positive controls could be detected and prioritized correctly, validating our filtering and prioritization procedure.

In the first complete run (RP-LCA run 01), a total of 360 unsolved cases and 20 controls containing known CNVs, were sequenced. A total number of 596,889,627 reads were obtained after exclusion of duplicate reads. The amount of reads per proband was 1,570,762 on average and an average of 93 reads per smMIP was obtained. Using pileups data, we extracted the amount of reads covering each individual nucleotide and observed an average coverage per nucleotide of 374x. Nucleotides that were covered by ≥ 50 reads were considered well covered, nucleotides covered by 11–49 reads moderately covered, and nucleotides covered by ≤ 10 reads were deemed to be poorly covered. In RP-LCA run 01, 431,878 nt were well covered (95.8%), 14,932 nt (3.3%) were moderately covered, and 3,832 nt (0.9%) were poorly covered. From this, we calculated the coverage per target gene (Figure 2). We observed that the last exon of the *RPGR-ORF15* transcript, together with the *PRCD*, *NYX*, *SAMD11*, and *WDR34* genes, were the five genes/regions with the lowest average nucleotide coverage (72x, 152x, 156x, 157x, and 174x, respectively). The coverage of these genes/regions exceeded our threshold to be considered sufficient for variant calling (i.e. 50x). However, the validity of variants called in the *RPGR-ORF15* transcript was difficult to assess because of the repetitive nature of the region and would therefore need additional long-read sequencing validation.

To further validate our CNV analysis and SNV prioritization and classification workflow, we included another group of 63 probands diagnosed with either RP or LCA and previously screened by a MIPs panel targeting 108 genes associated with IRD (Weisschuh et al., 2018; Sharon et al., 2020). Using our workflow, we obtained a very likely or possibly solved verdict for 40 probands (Supplemental table 3). Of those 40, the variants detected in 28 probands were in concurrence with previous findings (group 1), nine were solved by variants previously not detected (group 2), three probands that were considered to be possibly solved through our workflow, were solved by variants in other genes (group 3). Of those three genes, two genes were not covered by our panel, and one variant in *PRPF8* (c.3394_3396del, p.(Lys1132del)) was detected but excluded based on our workflow since we did not consider class 3 variants in autosomal dominant genes. Eight out of 22 probands that were considered unsolved after our analysis, were known to be genetically solved (group 4). Of those eight, five probands were solved with variants in genes not included in this panel since they are associated with other IRD phenotypes. Furthermore, one duplication was not detected in our CNV analysis, one SNV was detected but only with one read, and therefore excluded, and one proband was considered solved by a class 3 variant in an AD gene.

To enable a focused analysis, we took forward probands that were submitted with an RP (83.7%), LCA (8.7%) or retinal dystrophy (RD, 7.6%) phenotype. After exclusion of 32 samples that failed library preparation, a total of 1,192 probands were analyzed from five sequencing runs. After CNV and SNV analysis, 566 probands were considered very likely solved (47.5%) and 100 probands were considered possibly solved (8.4%), respectively. This resulted in a diagnostic yield of 55.9% when combining these groups (Supplementary Table S4). The 666 very likely and possibly solved probands could be explained by variants in 76 genes (Figure 3). For probands submitted with an RP phenotype (n = 573), the most prevalent mutated genes were *USH2A* (17.3%), *EYS* (9.6%), *RHO* (5.4%), *RP1* (4.7%), and *PDE6A* (4.2%). Probands with an LCA phenotype (n = 57) were mostly genetically explained by pathogenic variants residing in *CRB1* (14.5%), *ABCA4* (12.7%), *RPGRIP1* (9.1%), *CEP290* (5.5%), *GUCY2D* (5.5%), *RDH12* (5.5%) and *TULP1* (5.5%) while those with an RD phenotype (n = 36) could be genetically explained by variants in 10 different genes (each in two cases) *ABCA4, CRB1, EYS, GUCY2D, NRE2E3, PROM1, PRPH2, RLPBP1, TRPM1,* and *USH2A* (all 3.6%).

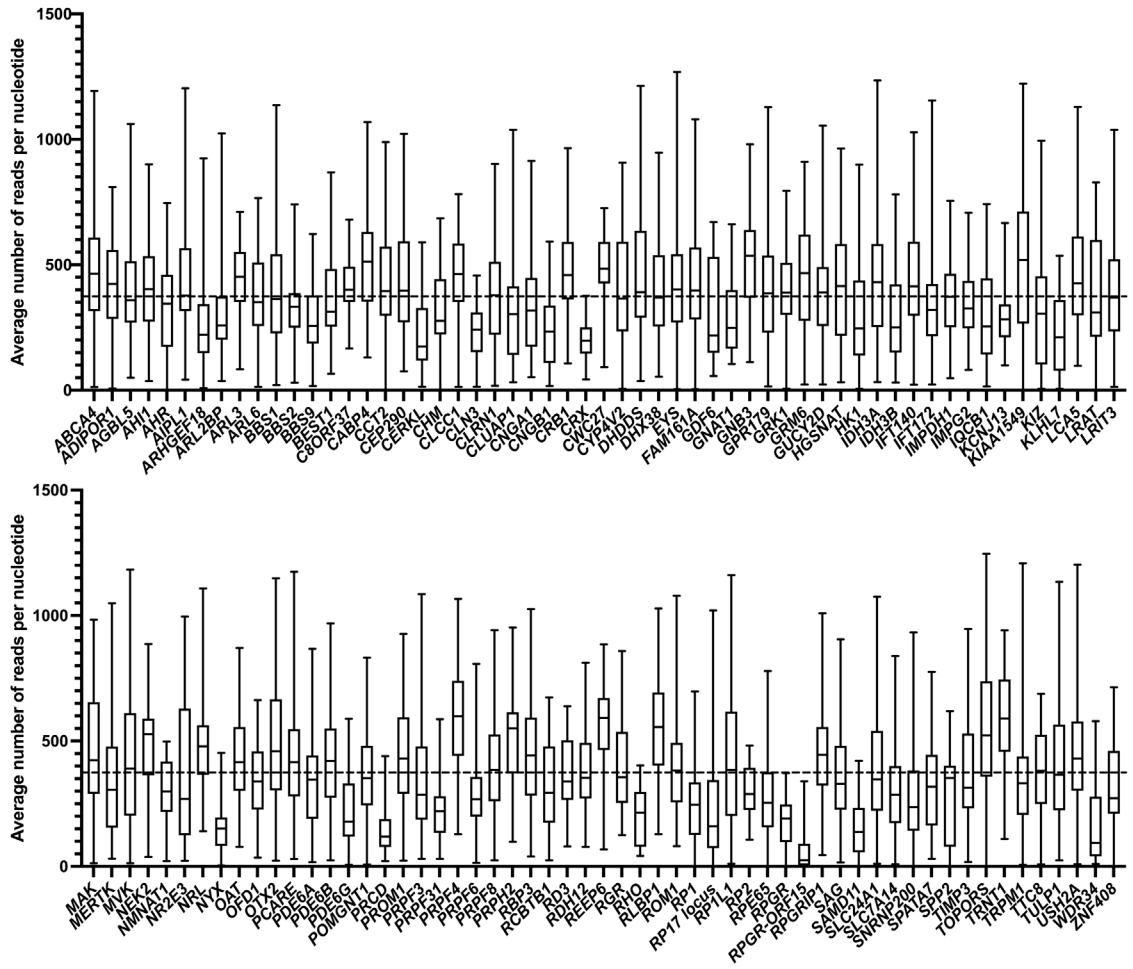

FIGURE 2
Average coverage per nucleotide. The average number of reads per nucleotide for each individual gene are indicated by the black horizontal line within the box, the range is indicated by the whiskers. The horizontal dashed line depicts the average overall coverage (374x).

For CNV, SNV, and indel analysis, all possible phenotypes and modes of inheritance were considered, regardless of the details provided by the collaborator. In total, 39 CNVs and one SV were identified in 18 genes amongst all cases. Twenty-five heterozygous deletions, eight homozygous deletions, three hemizygous deletions, two heterozygous duplications, and one SV in the RP17 locus were detected by CNV analysis (Supplementary Table S5). All probands with heterozygous CNVs could be genetically explained by an additional pathogenic SNV on the presumed second allele. All class 3, 4, and 5 SNVs, CNVs, and indels were taken forward if detected in a homozygous or compound heterozygous state in a gene associated with autosomal recessive inheritance. In this way, 509 probands were possibly (85 probands) or very likely (423 probands) solved by assumed compound heterozygous (300 probands) or homozygous variants (210 probands) (Supplementary Table S6). For variants in genes associated with autosomal dominant inheritance, only class 4 and 5 SNVs and indels were assessed. All variants that were very likely (108 probands) or possibly solving (9 probands) a case were listed in Supplementary Table S7. Moreover, all class 3, 4, and 5 variants identified in X-chromosomal genes were also analyzed. All variants that were considered to possibly (6 probands) or very likely (33 probands) solve the proband are listed in Supplementary Table S8. In this study, 275 variants were detected that were not previously reported in literature. All variants and cases have been uploaded into the respective Leiden Open Variation Databases.

Among the called SNVs, we were able to detect known splice-site altering variants published previously in literature as they were included as targets for the RP-LCA smMIPs panel. We identified five probands with the deep-intronic c.2991+1655A>G variant in *CEP290* (den Hollander et al., 2006), two probands with the c.1374+654C>G in *PRPF31* (Frio et al., 2009), and one proband with the c.7595-2144A>G variant in *USH2A* (Vache et al., 2012). The probands in which the *CEP290* c.2911+1655A>G and *USH2A* c.7595-2144A>G variants were detected, could be genetically explained as they also carried a (likely) pathogenic variant on the assumed second allele. All three DIVs were shown to lead to pseudo-exon inclusion and have been published previously (den Hollander et al., 2006; Frio et al., 2009; Vache et al., 2012).

For proband DNA13-01427, we detected the pathogenic c.886dup (p.(Arg296Lysfs*7)) and the synonymous c.675C>A variant that was classified as VUS in *RPE65*. SpliceAI predictions for c.675C>A yielded a delta score of 0.39 and a donor loss with a delta score of

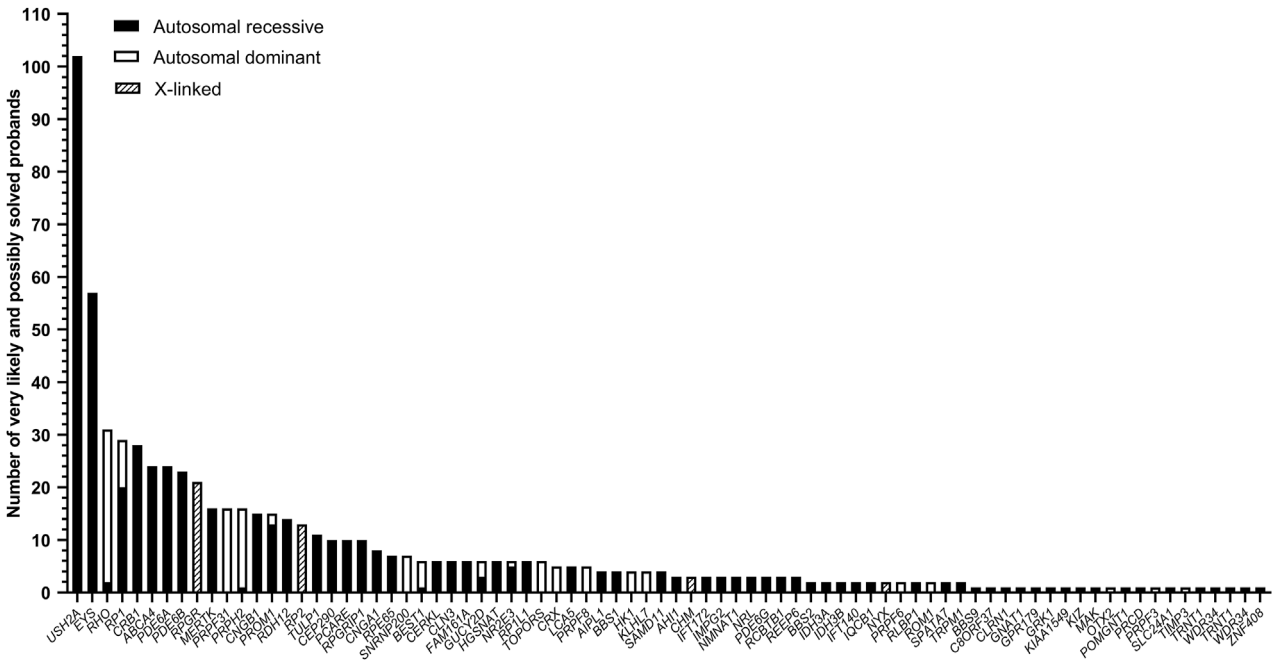

FIGURE 3
Number of solved cases per individual gene. For all genes, the inheritance mode is depicted in either black (autosomal recessive), white (autosomal dominant), or dashed (X-linked inheritance).

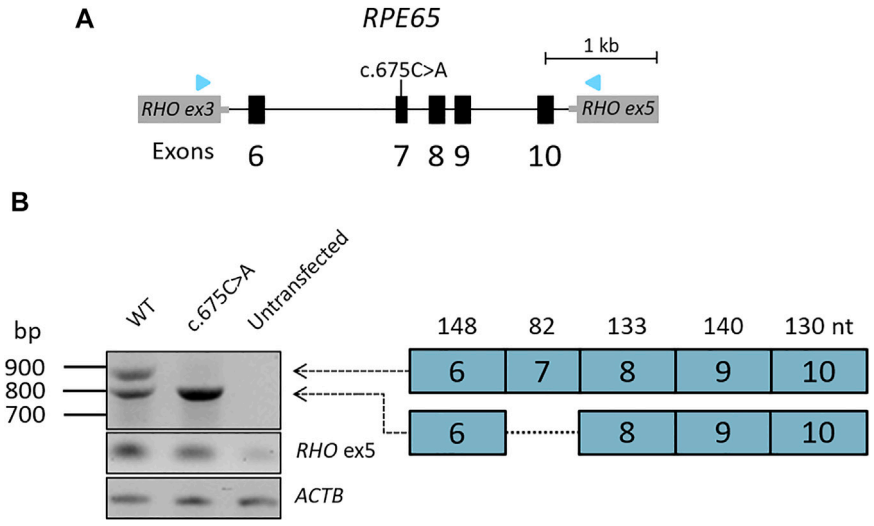

FIGURE 4
Minigene analysis of the splicing effect of *RPE65*:c.675C>A. **(A)** A minigene construct containing either wild-type sequence or the mutant c.675C>A variant in exon 7 was generated spanning exons 6-10 of *RPE65* and was flanked by exons 3 and 5 of the *RHO* gene in the pCI-NEO-RHO vectors **(B)** After gel electrophoresis of the RT-PCR product, we observed two fragments in the wild-type situation. One fragment of 907 nt and one fragment of 825 nt corresponding to the skipping of the 82 nt exon 7. For 675C>A, we exclusively observed the 825 nt fragment, suggesting complete skipping of exon 7.

0.31 suggesting putative skipping of exon 7. Because of the therapeutic relevance of *RPE65*, the variant was assessed in a minigene splice assay with a genomic DNA insert of 3.8 kb containing *RPE65* exons 6 through 10 (Figure 4A). The wild-type construct showed the expected wild-type fragment of 907 nt and also showed a fragment of 825 nt corresponding to the skipping of exon 7 (82 nt)suggesting natural exon 7 skipping (Figure 4B). A similar phenomenon was observed in control photoreceptor precursor cells (PPCs) and pure cultures of control retinal pigment epithelium (RPE) cells (data not shown). RT-PCR analysis of the RNA resulting from the *RPE65* c.675C>A minigene, showed the same fragment of 825 nt corresponding to the skipping of exon 7 which leads to frameshift

variant after 4 amino acids (p.Asp215Valfs*4). The RNA products resulting from the transfection of the mutant *RPE65* c.675C>A showed with no remaining wild-type RNA and therefore the allele was classified as severe (Figure 4B). Adding this functional evidence to the ACMG classification resulted in a re-classification as pathogenic. Segregation for both variants was confirmed in both parents for this proband. In total from 1,192 probands, seven probands were very likely or possibly solved by pathogenic variants in *RPE65*.

In addition to known DIVs, we also targeted the RP17 locus in the RP-LCA panel. SVs in this locus have been shown to cause RP ad (de Bruijn et al., 2020). We identified two probands with duplicated regions of the RP17 locus. In proband 067984, we could confirm that the SV was identical to the UK-SV2 variants published previously (de Bruijn et al., 2020). The second proband (RP ar phenotype) did not harbor a known SV from the de Bruijn *et al.*, study. Using SNP array analysis, it was revealed that this SV it unlikely to cause alteration of the topologically associating domain (TAD) organization of the RP17 locus and is therefore, in combination with the phenotype, considered to be benign (data not shown).

4 Discussion

Using the RP-LCA smMIPs panel, we sequenced all exonic regions of the genes associated with RP and LCA and, additionally, the intronic regions of the *RPE65*, all previously published DIVs in RP/LCA genes, as well as the RP17 locus associated with RP ad in 1,192 probands. After CNV analysis and prioritization of SNVs and indels, we very likely or possibly solved 666 probands (55.9%) with causative variants distributed over 76 genes. When comparing the diagnostic yield of groups of probands originating from different collaborators, a range of 51%–63% was observed. A previous study that used WES to analyze 266 probands with various types of IRDs, had reached a slightly higher diagnostic yield of 63% in a RP subgroup (Haer-Wigman et al., 2017). This difference can possibly be attributed to differences in the genetic screening methods that probands had received prior to inclusion in our RP-LCA smMIPs sequencing. For example, in a group of probands originating from Italy, which had previously undergone APEX microarray analysis, we obtained a diagnostic yield of 51% (26/51 cases) after our analysis, whereas another cohort from France, that received no prior genetic screening showed a diagnostic yield of 63% (116/184 cases).

In the RP subgroup, the top five genes in which variants that solved the proband were detected consisted of *USH2A*, *EYS*, *RHO*, *RP1*, and *PDE6A*. This set of genes is comparable to the genes listed in a recent review by Verbakel *et al.* on RP, which includes a shortlist of frequently mutated genes (*USH2A*, *RPGR*, *EYS*, *RHO*, and *RP1*) (Verbakel et al., 2018). The large proportion (approximately 4x higher than expected) of probands solved by variants in *ABCA4* is likely explained by the extensive efforts on determining the complex pathogenicity of variants in *ABCA4* compared to other genes (Al-Khuzaei et al., 2021; Cornelis et al., 2022; Lee et al., 2022). The underrepresentation of variants detected in genes on the X chromosome might be explained by more extensive targeted testing of X-linked IRD genes such as *RPGR* (prior to smMIPs sequencing) in probands with X-linked diseases. As previously mentioned, variants in *USH2A* solve the largest number of cases in this study. Common variants such as c.2276G>T and c.2299del were observed in 28 and 17 cases, respectively. Furthermore, we could possibly or very likely solve 13 probands with variants in very rarely mutated disease genes such as *IDH3A* (2x), *IDH3B* (2x), *KIAA1549* (1x), *KIZ* (1x), *RCBTB1* (3x), *REEP6* (3x), and *TRNT1* (1x). For instance, *KIAA1549* was determined to be causative in only three probands from three families previously (Abu-Safieh et al., 2013; de Bruijn et al., 2018). Here, we detected a novel homozygous c.4427dup variant (p.(Glu1477Glyfs*3)), which very likely solves proband 067904.

Variant prioritization was completed without taking into consideration the phenotype and possible mode of inheritance provided by the collaborator. This genotype-first approach implies that the variant prioritization may establish an unexpected genetic outcome for a proband, which may not fit the phenotype and/or inheritance pattern provided by the collaborator. For instance, in seven probands diagnosed with LCA we observed pathogenic variants in *ABCA4*. These probands were very likely solved based on our workflow, but variants in *ABCA4* have never been associated with LCA previously. Six out of seven probands carried two protein-truncating variants and one proband carried a homozygous missense variant (p.(Glu1022Lys)), which was deemed to have a moderate/severe effect on ABCA4 function (Cornelis et al., 2022). The phenotype of the proband in which the latter variant was found was re-assessed and Stargardt disease was considered to be more likely. Segregation analysis and in-depth clinical investigation could confirm this new genotype-phenotype correlation. Additionally, genes associated with autosomal dominant inheritance, such as *PRPF31*, can show reduced penetrance and therefore a proband with a proposed autosomal recessive disorder might be explained with a variant in this gene (McGee et al., 1997). In fact, of the 15 probands that were solved through likely pathogenic and pathogenic variants in *PRPF31*, only three were included with a suspected autosomal dominant inheritance pattern. Furthermore, we identified two pathogenic heterozygous variants in *ROM1* and *PRPH2* in proband 075765 (diagnosed with RP ar) that are known to cause digenic RP, a finding that was first observed by Kajiwara et al. (1994). These findings underline the added benefit of using this genotype-first approach and thereby considering all prioritized variants, regardless of associated phenotypes or inheritance patterns. Additionally, in 30 cases variants in two or three genes could explain the phenotype of the probands (Supplementary Table S9). For these cases, the phenotype and inheritance pattern provided by the collaborator, as well as the zygosity and the ACMG classification of the variants were taken into consideration. All variants, including the most likely, causative variant, are listed in Supplementary Table S9 and are labeled as "primary" in the verdict column, all additional findings are labeled as "secondary". In most cases, segregation analysis could already give an indication as to which variants are more likely to solve the proband.

While the smMIPs approach has multiple advantages over other sequencing techniques, such as the ability to sequence large groups of probands in a single sequencing run, the ability to curate and include all desired target regions and the low costs compared to WES or WGS, it does have limitations. For instance, the exact nature of CNVs cannot be identified from the sequencing data, which necessitates additional validation and breakpoint analysis. Moreover, duplications, balanced inversions, and to a lesser extent deletions, are hard to detect since only the genes of interest are sequenced and no comparisons in read counts can be made to neighboring genes on the chromosome. Lastly, as capture and sequencing costs of the RP-LCA smMIPs panel were $30 per sample (excluding design and synthesis of the smMIPs panel),

it makes the smMIPs approach an attractive approach since the costs are lower than commercial WES, WGS, and other forms of IRD gene panel sequencing. However, the extensive infrastructure required for both sequencing capacity and bioinformatic processing of the data hampers an universal applicability.

In conclusion, the low costs and high-throughput capacity of smMIPs sequencing allowed us to effectively sequence all RP and LCA associated genes and loci in 1,192 probands. Alongside previously published variants, a large group of novel variants could also be detected. As new genetic therapies directed against specific IRD genes are becoming available, easy access to genetic/genomic testing and early genetic diagnosis is of the utmost importance to allow the patient to optimally benefit from these treatments.

Data availability statement

The datasets presented in this study can be found in online repositories. The names of the repository/repositories and accession number(s) can be found in the article/Supplementary Material.

Ethics statement

The studies involving human participants were reviewed and approved by local ethics committee of the Radboud University Medical Center (Nijmegen, The Netherlands). Written informed consent to participate in this study was provided by the participants' legal guardian/next of kin.

Author contributions

DP, RH-M, LH, JR, EGMB, and MIK performed data analysis. DP, RH-M, LH, and EGMB, performed library preparations and experiments. FC, SR, RH-M, AMT, and SB selected targets for the smMIPs panel design. CG, TG, BK, PS, and MV provided infrastructure and bioinformatic expert input. SR, FC, and AH contributed significantly to the design of the study, provided infrastructure, and strategic support. DP, FC, and SR wrote the manuscript. SA, MTK, UK, RK, BL, MM, IM, KN, ER, FS, FT, AT, HT, HU, and VV collected clinical cases and performed clinical examinations of patients. DP, FC, SR, EDB, SB, TB-Y, BB, BC, FC, CI, MTK, RK, CR, and VV contributed to data interpretation and curation of the genetic findings. MA, MB, MBB, PF, KN, JP, CT, YT, and CT contributed to proband registration, DNA extraction, purification, quality control, and shipping of samples. All authors read and approved the manuscript.

Funding

This study received funding from Novartis. The funder was not involved in the study design, collection, analysis, interpretation of data, the writing of this article or the decision to submit it for publication. This work was supported by grants from Foundation Fighting Blindness Career Development Award CDGE-0621-0809-RAD (SR), Foundation Fighting Blindness project program award PPA-0123-0841-UCL (SR and SdB), Retinitis Pigmentosa Fighting Blindness, Fight for Sight UK (RP Genome Project GR586), Ghent University Special Research Fund (BOF20/GOA/023) (EDB and BL); EJP RD Solve-RET EJPRD19-234 (EDB, BL, SB, CR, FC, and SR). EDB (1802220N) and BL (1803816N) are FWO Senior Clinical Investigators of the Research Foundation Flanders (FWO). EDB, BL, SB, FC, and SR are members of ERN-EYE (Framework Partnership Agreement No. 739534).

Acknowledgments

The authors would like to thank all patients involved and their families for taking part in this research. We thank Saskia D. van der Velde-Visser, Ellen A.W. Blokland, Marlie Jacobs-Camps, Anita Roelofs, Michiel Oorsprong, Marcel Nelen, Simon van Reijmersdal, and Martine van Zweeden, and the Radboud Genomics Technology Center for technical assistance. Sarah De Jaegere (Center for Medical Genetics Ghent Belgium) is thanked for her technical support. We also thank Greg Porreca and Eric Boyden at Molecular Loop Biosciences Inc. for their contribution and expertise. We want to acknowledge the Biobank Nodo Hospital Virgen Macarena (Biobanco del Sistema Sanitario Público de Andalucía) integrated in the Spanish National biobanks Network (PT20/00069) supported by ISCIII and FEDER funds for their collaboration in this work. The work in the Chromosomal Genetics Unit is supported by the CHROMOSTEM research platform.

Conflict of interest

PS is an employee of Molecular Loop Biosciences Inc.

The remaining authors declare that the research was conducted in the absence of any commercial or financial relationships that could be construed as a potential conflict of interest.

Supplementary material

The Supplementary Material for this article can be found online at: https://www.frontiersin.org/articles/10.3389/fcell.2023.1112270/full#supplementary-material

References

Abu-Safieh, L., Alrashed, M., Anazi, S., Alkuraya, H., Khan, A. O., Al-Owain, M., et al. (2013). Autozygome-guided exome sequencing in retinal dystrophy patients reveals pathogenetic mutations and novel candidate disease genes. *Genome Res.* 23 (2), 236–247. doi:10.1101/gr.144105.112

Al-Khuzaei, S., Broadgate, S., Foster, C. R., Shah, M., Yu, J., Downes, S. M., et al. (2021). An overview of the genetics of ABCA4 retinopathies, an evolving story. *Genes* 12 (8), 1241. doi:10.3390/genes12081241

Black, G. C., Sergouniotis, P., Sodi, A., Leroy, B. P., Van Cauwenbergh, C., Liskova, P., et al. (2021). The need for widely available genomic testing in rare eye diseases: An ERN-EYE position statement. *Orphanet J. Rare Dis.* 16 (1), 142. doi:10.1186/s13023-021-01756-x

Cartegni, L., Wang, J., Zhu, Z., Zhang, M. Q., and Krainer, A. R. (2003). ESEfinder: A web resource to identify exonic splicing enhancers. *Nucleic Acids Res.* 31 (13), 3568–3571. doi:10.1093/nar/gkg616

Cornelis, S. S., Runhart, E. H., Bauwens, M., Corradi, Z., De Baere, E., Roosing, S., et al. (2022). Personalized genetic counseling for Stargardt disease: Offspring risk estimates based on variant severity. *Am. J. Hum. Genet.* 109 (3), 498–507. doi:10.1016/j.ajhg.2022.01.008

de Bruijn, S. E., Fiorentino, A., Ottaviani, D., Fanucchi, S., Melo, U. S., Corral-Serrano, J. C., et al. (2020). Structural variants create new topological-associated domains and ectopic retinal enhancer-gene contact in dominant retinitis pigmentosa. *Am. J. Hum. Genet.* 107 (5), 802–814. doi:10.1016/j.ajhg.2020.09.002

de Bruijn, S. E., Verbakel, S. K., de Vrieze, E., Kremer, H., Cremers, F. P. M., Hoyng, C. B., et al. (2018). Homozygous variants in KIAA1549, encoding a ciliary protein, are associated with autosomal recessive retinitis pigmentosa. *J. Med. Genet.* 55 (10), 705–712. doi:10.1136/jmedgenet-2018-105364

den Hollander, A. I., Koenekoop, R. K., Yzer, S., Lopez, I., Arends, M. L., Voesenek, K. E., et al. (2006). Mutations in the CEP290 (NPHP6) gene are a frequent cause of Leber congenital amaurosis. *Am. J. Hum. Genet.* 79 (3), 556–561. doi:10.1086/507318

den Hollander, A. I., Roepman, R., Koenekoop, R. K., and Cremers, F. P. (2008). Leber congenital amaurosis: Genes, proteins and disease mechanisms. *Prog. Retin Eye Res.* 27 (4), 391–419. doi:10.1016/j.preteyeres.2008.05.003

Fadaie, Z., Khan, M., Del Pozo-Valero, M., Cornelis, S. S., Ayuso, C., Cremers, F. P. M., et al. (2019). Identification of splice defects due to noncanonical splice site or deep-intronic variants in ABCA4. *Hum. Mutat.* 40 (12), 2365–2376. doi:10.1002/humu.23890

Frio, T. R., McGee, T. L., Wade, N. M., Iseli, C., Beckmann, J. S., Berson, E. L., et al. (2009). A single-base substitution within an intronic repetitive element causes dominant retinitis pigmentosa with reduced penetrance. *Hum. Mutat.* 30 (9), 1340–1347. doi:10.1002/humu.21071

Grantham, R. (1974). Amino acid difference formula to help explain protein evolution. *Science* 185 (4154), 862–864. doi:10.1126/science.185.4154.862

Haer-Wigman, L., van Zelst-Stams, W. A., Pfundt, R., van den Born, L. I., Klaver, C. C., Verheij, J. B., et al. (2017). Diagnostic exome sequencing in 266 Dutch patients with visual impairment. *Eur. J. Hum. Genet.* 25 (5), 591–599. doi:10.1038/ejhg.2017.9

Haeussler, M., Zweig, A. S., Tyner, C., Speir, M. L., Rosenbloom, K. R., Raney, B. J., et al. (2019). The UCSC genome browser database: 2019 update. *Nucleic Acids Res.* 47 (D1), D853–D858. doi:10.1093/nar/gky1095

Hitti-Malin, R. J., Dhaenens, C. M., Panneman, D. M., Corradi, Z., Khan, M., Hollander, A. I. D., et al. (2022). Using single molecule Molecular Inversion Probes as a cost-effective, high-throughput sequencing approach to target all genes and loci associated with macular diseases. *Hum. Mutat.* 43, 2234–2250. doi:10.1002/humu.24489

Jaganathan, K., Kyriazopoulou Panagiotopoulou, S., McRae, J. F., Darbandi, S. F., Knowles, D., Li, Y. I., et al. (2019). Predicting splicing from primary sequence with deep learning. *Cell* 176 (3), 535–548. doi:10.1016/j.cell.2018.12.015

Kajiwara, K., Berson, E. L., and Dryja, T. P. (1994). Digenic retinitis pigmentosa due to mutations at the unlinked peripherin/RDS and ROM1 loci. *Science* 264 (5165), 1604–1608. doi:10.1126/science.8202715

Karolchik, D., Hinrichs, A. S., Furey, T. S., Roskin, K. M., Sugnet, C. W., Haussler, D., et al. (2004). The UCSC Table Browser data retrieval tool. *Nucleic Acids Res.* 32, D493–D496. Database issue). doi:10.1093/nar/gkh103

Khan, M., Cornelis, S. S., Khan, M. I., Elmelik, D., Manders, E., Bakker, S., et al. (2019). Cost-effective molecular inversion probe-based ABCA4 sequencing reveals deep-intronic variants in Stargardt disease. *Hum. Mutat.* 40 (10), 1749–1759. doi:10.1002/humu.23787

Khan, M., Cornelis, S. S., Pozo-Valero, M. D., Whelan, L., Runhart, E. H., Mishra, K., et al. (2020). Resolving the dark matter of ABCA4 for 1054 Stargardt disease probands through integrated genomics and transcriptomics. *Genet. Med.* 22 (7), 1235–1246. doi:10.1038/s41436-020-0787-4

Kircher, M., Witten, D. M., Jain, P., O'Roak, B. J., Cooper, G. M., and Shendure, J. (2014). A general framework for estimating the relative pathogenicity of human genetic variants. *Nat. Genet.* 46 (3), 310–315. doi:10.1038/ng.2892

Lee, W., Zernant, J., Su, P.-Y., Nagasaki, T., Tsang, S. H., and Allikmets, R. (2022). A genotype-phenotype correlation matrix for ABCA4 disease based on long-term prognostic outcomes. *JCI insight* 7 (2), e156154. doi:10.1172/jci.insight.156154

Li, H., Handsaker, B., Wysoker, A., Fennell, T., Ruan, J., Homer, N., et al. (2009). The sequence alignment/map format and SAMtools. *Bioinformatics* 25 (16), 2078–2079. Epub 2009 Jun 8. doi:10.1093/bioinformatics/btp352

McGee, T., Devoto, M., Ott, J., Berson, E., and Dryja, T. (1997). Evidence that the penetrance of mutations at the RP11 locus causing dominant retinitis pigmentosa is influenced by a gene linked to the homologous RP11 allele. *Am. J. Hum. Genet.* 61 (5), 1059–1066. doi:10.1086/301614

Pertea, M., Lin, X., and Salzberg, S. L. (2001). GeneSplicer: A new computational method for splice site prediction. *Nucleic Acids Res.* 29 (5), 1185–1190. doi:10.1093/nar/29.5.1185

Pollard, K. S., Hubisz, M. J., Rosenbloom, K. R., and Siepel, A. (2010). Detection of nonneutral substitution rates on mammalian phylogenies. *Genome Res.* 20 (1), 110–121. doi:10.1101/gr.097857.109

Reese, M. G., Eeckman, F. H., Kulp, D., and Haussler, D. (1997). Improved splice site detection in Genie. *J. Comput. Biol.* 4 (3), 311–323. doi:10.1089/cmb.1997.4.311

Richards, S., Aziz, N., Bale, S., Bick, D., Das, S., Gastier-Foster, J., et al. (2015). Standards and guidelines for the interpretation of sequence variants: A joint consensus recommendation of the American college of medical genetics and genomics and the association for molecular Pathology. *Genet. Med.* 17 (5), 405–424. doi:10.1038/gim.2015.30

Russell, S., Bennett, J., Wellman, J. A., Chung, D. C., Yu, Z.-F., Tillman, A., et al. (2017). Efficacy and safety of voretigene neparvovec (AAV2-hRPE65v2) in patients with RPE65-mediated inherited retinal dystrophy: A randomised, controlled, open-label, phase 3 trial. *Lancet* 390 (10097), 849–860. doi:10.1016/S0140-6736(17)31868-8

Sangermano, R., Khan, M., Cornelis, S. S., Richelle, V., Albert, S., Garanto, A., et al. (2018). ABCA4 midigenes reveal the full splice spectrum of all reported noncanonical splice site variants in Stargardt disease. *Genome Res.* 28 (1), 100–110. doi:10.1101/gr.226621.117

Sharon, D., Ben-Yosef, T., Goldenberg-Cohen, N., Pras, E., Gradstein, L., Soudry, S., et al. (2020). A nationwide genetic analysis of inherited retinal diseases in Israel as assessed by the Israeli inherited retinal disease consortium (IIRDC). *Hum. Mutat.* 41 (1), 140–149. doi:10.1002/humu.23903

Vache, C., Besnard, T., le Berre, P., Garcia-Garcia, G., Baux, D., Larrieu, L., et al. (2012). Usher syndrome type 2 caused by activation of an USH2A pseudoexon: Implications for diagnosis and therapy. *Hum. Mutat.* 33 (1), 104–108. doi:10.1002/humu.21634

Verbakel, S. K., Fadaie, Z., Klevering, B. J., van Genderen, M. M., Feenstra, I., Cremers, F. P., et al. (2019). The identification of a RNA splice variant in TULP1 in two siblings with early-onset photoreceptor dystrophy. *Mol. Genet. Genomic Med.* 7 (6), e660. doi:10.1002/mgg3.660

Verbakel, S. K., van Huet, R. A. C., Boon, C. J. F., den Hollander, A. I., Collin, R. W. J., Klaver, C. C. W., et al. (2018). Non-syndromic retinitis pigmentosa. *Prog. Retin Eye Res.* 66, 157–186. doi:10.1016/j.preteyeres.2018.03.005

Weisschuh, N., Feldhaus, B., Khan, M. I., Cremers, F. P., Kohl, S., Wissinger, B., et al. (2018). Molecular and clinical analysis of 27 German patients with Leber congenital amaurosis. *PLoS One* 13 (12), e0205380. doi:10.1371/journal.pone.0205380

Yates, A. D., Achuthan, P., Akanni, W., Allen, J., Allen, J., Alvarez-Jarreta, J., et al. (2020). Ensembl 2020. *Nucleic Acids Res.* 48 (D1), D682–D688. doi:10.1093/nar/gkz966

Yeo, G., and Burge, C. B. (2004). Maximum entropy modeling of short sequence motifs with applications to RNA splicing signals. *J. Comput. Biol.* 11 (2-3), 377–394. doi:10.1089/1066527041410418

Zhang, M. Q. (1998). Statistical features of human exons and their flanking regions. *Hum. Mol. Genet.* 7 (5), 919–932. doi:10.1093/hmg/7.5.919

frontiers | Frontiers in Cell and Developmental Biology

TYPE Original Research
PUBLISHED 10 February 2023
DOI 10.3389/fcell.2023.1142586

OPEN ACCESS

EDITED BY
José M Millan,
La Fe Health Research Institute, Spain

REVIEWED BY
Volker Enzmann,
University Hospital of Bern, Switzerland
Ryan Thummel,
Wayne State University, United States

*CORRESPONDENCE
David R. Hyde,
dhyde@nd.edu

SPECIALTY SECTION
This article was submitted to Molecular and Cellular Pathology, a section of the journal Frontiers in Cell and Developmental Biology

RECEIVED 11 January 2023
ACCEPTED 30 January 2023
PUBLISHED 10 February 2023

CITATION
Boyd P, Campbell LJ and Hyde DR (2023), Clcf1/Crlf1a-mediated signaling is neuroprotective and required for Müller glia proliferation in the light-damaged zebrafish retina.
Front. Cell Dev. Biol. 11:1142586.
doi: 10.3389/fcell.2023.1142586

Clcf1/Crlf1a-mediated signaling is neuroprotective and required for Müller glia proliferation in the light-damaged zebrafish retina

Patrick Boyd, Leah J. Campbell and David R. Hyde*

Department of Biological Sciences, Center for Stem Cells and Regenerative Medicine, and Center for Zebrafish Research, Galvin Life Sciences Building, University of Notre Dame, Notre Dame, IN, United States

Zebrafish possess the innate ability to fully regenerate any neurons lost following a retinal injury. This response is mediated by Müller glia that reprogram and divide asymmetrically to produce neuronal precursor cells that differentiate into the lost neurons. However, little is understood about the early signals that induce this response. Ciliary neurotrophic factor (CNTF) was previously shown to be both neuroprotective and pro-proliferative within the zebrafish retina, however CNTF is not expressed following injury. Here we demonstrate that alternative ligands of the Ciliary neurotrophic factor receptor (CNTFR), such as Cardiotrophin-like cytokine factor 1 (Clcf1) and Cytokine receptor-like factor 1a (Crlf1a), are expressed within Müller glia of the light-damaged retina. We found that CNTFR, Clcf1, and Crlf1a are required for Müller glia proliferation in the light-damaged retina. Furthermore, intravitreal injection of CLCF1/CRLF1 protected against rod photoreceptor cell death in the light-damaged retina and induced proliferation of rod precursor cells in the undamaged retina, but not Müller glia. While rod precursor cell proliferation was previously shown to be Insulin-like growth factor 1 receptor (IGF-1R)-dependent, co-injection of IGF-1 with CLCF1/CRLF1 failed to induce further proliferation of either Müller glia or rod precursor cells. Together, these findings demonstrate that CNTFR ligands have a neuroprotective effect and are required for induction of Müller glia proliferation in the light-damaged zebrafish retina.

KEYWORDS

zebrafish, retina, regeneration, Müller glia, CLCF1, CNTFR, CRLF1

1 Introduction

The zebrafish retina possesses the ability to regenerate all retinal cell types following injury (Lahne et al., 2020). Regeneration involves Müller glia reprogramming and asymmetric division to produce neuronal precursor cells (NPCs). These NPCs continue to proliferate and eventually differentiate into the lost cell types to restore visual function (Fimbel et al., 2007; Sherpa et al., 2008; Wan & Goldman, 2016; Angueyra & Kindt, 2018; Lahne et al., 2020). Several different signalling pathways have been shown to regulate this process, including Delta/Notch (Conner

Abbreviations: DAPI, 4′,6-diamidino-2-phenylindol; DMSO, dimethyl sulfoxide; EdU, 5-ethynyl-2′-deoxyuridine; EGFP, enhanced green fluorescent protein; GCL, ganglion cell layer; INL, inner nuclear layer; NPC, neuronal precursor cell; NVP, NVP-ADW742; ONL, outer nuclear layer; PBS, phosphate buffered saline; PCNA, proliferating cell nuclear antigen; TUNEL, terminal deoxynucleotidyl transferase dUTP nick end labelling.

et al., 2014; Wan & Goldman, 2017; Elsaeidi et al., 2018; Campbell et al., 2021), Hippo/Yap (Hoang et al., 2020; Lourenço et al., 2021), EGF (Wan et al., 2012; Ueki & Reh, 2013), and TNFα pathways (Nelson et al., 2013; Iribarne et al., 2019).

One pathway of particular interest is the ciliary neurotrophic factor receptor (CNTFR) mediated signalling pathway. CNTFR is a tripartite receptor that binds a ligand, which recruits both Il6st (Gp130) and M17 (LIFR), resulting in CNTFR phosphorylation (samuel et al., 1993; Stahl & Yancopoulos, 1994). This allows CNTFR to signal *via* the Stat3, MAPK, and PI3K pathways (Rezende et al., 2009; Leibinger et al., 2013; Askvig & Watt, 2015; Hu et al., 2020), all of which were shown to regulate the Müller glia response to injury (Kassen et al., 2009; Nelson et al., 2012; Wan et al., 2012; Wan et al., 2014). CNTFR was previously found to be expressed within zebrafish Müller glia following injury (Zhao et al., 2014). Several studies also demonstrated that CNTFR and its ligand, ciliary neurotrophic factor (CNTF), have a wide array of effects within the zebrafish retina. Knockdown of *gp130* in the damaged zebrafish retina decreased Müller glia proliferation (Zhao et al., 2014), suggesting that Gp130-mediated signalling is required for retinal regeneration. Further, intravitreal injection of CNTF was sufficient to induce zebrafish Müller glia proliferation in a Stat3-dependent manner and was neuroprotective in a MAPK pathway-dependent manner (Kassen et al., 2009; Zhao et al., 2014). CNTF treatment also resulted in reduced photoreceptor cell death in both rodents (Rhee et al., 2013; Lipinksi et al., 2015) and humans (Sieving et al., 2006; Zhang et al., 2011). Additionally, several different cell types, including Müller glia, rods, and cones, were shown to be CNTF-sensitive (Leibinger et al., 2009; Rhee et al., 2013; Li et al., 2018), with CNTF exposure stimulating significant transcriptional changes (Wang et al., 2020). Interestingly, CNTF also induced regeneration of cones in a rat model of retinal degeneration (Li et al., 2010). Finally, CNTF was also shown to confer neuroprotective effects in other areas of the central nervous system (Beurrier et al., 2010; Jeong et al., 2015).

Despite the effects CNTF exert *in vivo*, *cntf* was not shown to be expressed within the regenerating zebrafish retina, however, the alternative CNTFR ligands Cardiotrophin-like cytokine factor 1 (Clcf1) and Cytokine receptor-like factor 1a (Crlf1a), which form a ligand complex, were expressed within the retina following injury (Zhao et al., 2014). Additionally, knockdown of either *clcf1* or *crlf1a* inhibited regeneration following optic nerve crush in zebrafish (Elsaeidi et al., 2014). Despite the presence of these ligands within the retina, no in-depth studies have examined their role in Müller glia-dependent regeneration of retinal neurons. Understanding the roles of the different CNTFR ligands during zebrafish retinal damage and regeneration may guide the development of cell-based retinal therapeutics in humans.

2 Material and methods

2.1 Zebrafish husbandry

Adult *albino* and transgenic *albino; Tg[gfap:EGFP]*^{nt11} zebrafish were maintained in the Center for Zebrafish Research at the University of Notre Dame Freimann Life Sciences Center as previously described (Recasens et al., 2021). Fish were maintained on a 14h/10h light-dark cycle for standard conditions. Approximately equal numbers of male and female fish were used in the study. All fish used in these experiments were 6–12 months of age and 2–3 cm in length. All animal care protocols were approved by the University of Notre Dame Animal Care and Use Committee and are compliant with the National Institutes of Health guide for the care and use of laboratory animals.

2.2 Light damage paradigm

Adult *albino* and *albino; Tg[gfap:EGFP]*^{nt11} zebrafish were dark-adapted for 14 days and then exposed to constant intense light for up to 36 h as previously described (Garner et al., 2018). Zebrafish were euthanized by anesthetic overdose in 2-phenoxyethanol (2-PE, 1:500, Sigma-Aldrich, St. Louis, MO).

2.3 Drug and protein treatments

2.3.1 CLCF1/CRLF1 & IGF-1

Adult *albino* and *albino; Tg[gfap:EGFP]*^{nt11} zebrafish were anesthetized in 2-phenoxyethanol (2-PE, 1:1000) until unresponsive to tail pinch and intravitreally injected every 12 h with 0.5 µl of either PBS (vehicle), 1 mg/ml recombinant mouse CLCF1/CRLF1 (R&D systems; Minneapolis, MN), 1 mg/ml recombinant human IGF-1 (R&D systems; Minneapolis, MN), or a combination of both, using a 2.5 µl syringe with 33-gauge rounded needle (Hamilton; Reno, NV) and then maintained at 32°C. Eyes were collected 72 h after the initial injection (hpi). For light treatments, dark-adapted *albino* zebrafish received intravitreal injections every 12 h for 48 h, at which point the fish were exposed to constant light and received an additional injection at 12 h of light treatment. These eyes were collected at 24 h of light treatment. For EdU treatment, fish received intraperitoneal injections of 1 mg/ml EdU using a 30-gauge needle while simultaneously receiving intravitreal injections of CLCF1/CRLF1 every 12 h and eyes were collected at 72 h hpi.

2.3.2 NVP-ADW742 (NVP)

albino; Tg[gfap:EGFP]^{nt11} zebrafish were intraperitoneally injected with 50 µl of either 5% DMSO (vehicle) or 500 µM NVP (Selleck Chemical; Houston, TX) every 12 h throughout the course of either constant light treatment or intravitreal injection of CLCF1/CRLF1, using a 30-gauge needle. For light treatment experiments, the initial intraperitoneal injection of NVP corresponded with the commencement of light treatment and the final injection occurred at 24 h of light treatment, with the eyes collected at 36 h of light treatment. During CLCF1/CRLF1 treatment, intraperitoneal injections of NVP were performed simultaneously with intravitreal CLCF1/CRLF1 injections every 12 h and the eyes were collected at 72 hpi.

2.4 Morpholino-mediated knockdowns

Dark-adapted *albino; Tg[gfap:EGFP]*^{nt11} zebrafish were intravitreally injected with 0.5 µl of either standard control, *cntfr*, a mixture of *clcf1/crlf1a*, or a combination of all 3 translation-blocking morpholinos (Gene Tools; Philomath, OR). Eyes were then electroporated as previously described (Thummel et al., 2011) before beginning constant light treatment. The following translation blocking morpholinos were used: standard control: 5′

CCTCTTACCTCAGTTACAATTTATA 3′ (Nasevicius & Ekker, 2000), *clcf1*: 5′ CCTGACCAACTTTCCAGGGACACAT 3′ (Elsaeidi et al., 2014), *cntfr:* 5′ GCGTAATGCTTCCCTCCTTAT CTTC 3′, *crlf1a:* 5′ CAATAAGCAGATCATCTTACGAGGA 3′ (Elsaeidi et al., 2014).

2.5 Immunohistochemistry and EdU labelling

Immunohistochemistry was performed as previously described (Lahne et al., 2015; Lahne et al., 2021). Briefly, eyes were fixed in 9: 1 ethanolic formaldehyde overnight at 4°C. The eyes were rehydrated through an ethanol gradient and incubated overnight at 4°C in 30% sucrose in PBS, followed by incubation overnight in a 2:1 mixture of tissue freezing medium (TFM):30% sucrose at 4°C. Eyes were frozen in TFM and 14 µm cryosections prepared. Sections were rehydrated in PBS for 20 min and blocked (2% normal goat serum, 2% DMSO, 1% Triton-X, 1% Tween-20 in PBS) for 1 h at room temperature. Slides were incubated with primary antibodies diluted in blocking solution overnight at room temperature. Primary antibodies used were rabbit anti-PCNA (1:2000; Abcam; Cambridge, United Kingdom; AB18197) and chicken anti-GFP (1:1000; Abcam; Cambridge, United Kingdom; AB13970). Slides were washed 3 times for 5 min in 0.1% Tween-20 in PBS (PBS-T), incubated for 1 hour with secondary antibodies and 4′,6-diamidino-2-phenylindol (DAPI; Life Technologies; Carlsbad, CA) in blocking solution at room temperature. AlexaFluor-conjugated secondary antibodies (Life Technologies; Carlsbad, CA) used were goat anti-chicken-488 (1:1000; A11039) and goat anti-rabbit-647 (1:1000; A21245). Finally, slides were washed 3 times for 5 min in PBS-T and mounted in Prolong Gold Antifade Reagent (Life Technologies; Carlsbad, CA).

For EdU labelling, slides were washed and rehydrated in PBS for 20 min, washed in 3% bovine serum albumin (BSA) in PBS for 10 min, then permeabilized by washing in 0.5% Triton X-100 (Fisher Scientific; Pittsburgh, PA) in PBS for 20 min. Slides were then labelled using the Click-iT EdU labeling kit (Life Technologies; Carlsbad, CA), per the manufacturer's instructions, and washed in 3% BSA for 5 min before blocking and continuing with immunohistochemistry as described above.

2.6 *In situ* hybridization

RNA *in situ* hybridization was performed using the RNAscope Multiplex Fluorescent v2 Assay (Advanced Cell Diagnostics; Newark, CA) according to the protocol for fixed-frozen tissue sample preparation with some modifications (Campbell et al., 2021). Tissue sections were prepared as described for immunohistochemistry. Frozen sections were washed in PBS for 5 min followed by baking for 1 h at 55°C in an oven. Tissue sections were post-fixed with 4% paraformaldehyde (PFA; Sigma Aldrich; St. Louis, MO) at room temperature for 1 h. Slides were dehydrated for 5 min each in 50%, 70%, and twice in 100% ethanol and then baked for 1 h at 55°C. Sections were treated with hydrogen peroxide solution (Advanced Cell Diagnostics; Newark, CA) for 10 min at room temperature, followed by a distilled water wash and placed in boiling Target Retrieval Buffer (Advanced Cell Diagnostics; Newark, CA) for 15 min. The slides were immediately washed with distilled water, dehydrated with 100% ethanol, and dried. Slides were baked for 1 h at 55°C, during which time a hydrophobic barrier was applied to the slide (ImmEdge Hydrophobic Pen; Vector Laboratories; Burlingame, CA) and dried overnight at room temperature. Sections were treated with the Protease III solution (Advanced Cell Diagnostics; Newark, CA) for 30 min at 40°C and washed with distilled water prior to probe incubation at 40°C for 2 h. The following probes (Advanced Cell Diagnostics; Newark, CA) were used: Dr-il6st-C1 (cat no. 1108591), Dr-clcf1-C2 (cat no. 1102851), Dr-cntfr-C2 (cat no. 1102711), and Dr-crlf1a-C3 (cat no. 1102861). The 3-plex negative control probe mixture was used on a separate slide. Probe amplification with AMP1, AMP2, and AMP3 proceeded according to manufacturer instructions. Development of the HRP signal also proceeded according to manufacturer instructions with the Opal 520, Opal 570, and Opal 690 dyes (1:1000; Akoya Biosciences; Menlo Park, CA). After signal development for each probe, slides were either incubated for 5 min at room temperature with DAPI solution (Advanced Cell Diagnostics), mounted with Prolong Gold Antifade Mountant (Thermo Fisher Scientific; Waltham, MA), and coverslipped or washed in PBS-T for 5 min before proceeding with immunohistochemistry. The primary antibodies used were rabbit anti-GFP (1:1000; Abcam; Cambridge, United Kingdom; AB6556) and mouse anti-PCNA (1:1000; MilliporeSigma; Burlington, MA; P8825), followed by secondary antibodies Alexa Fluor 488-conjugated goat anti-rabbit (1:500; Thermo Fisher Scientific; Waltham, MA; A11034) and Alexa Fluor 647-conjugated goat anti-mouse (1:500; Thermo Fisher Scientific; Waltham, MA; A21245).

2.7 Terminal deoxynucleotidyl transferase dUTP nick end labelling (TUNEL)

Slides were washed and rehydrated in PBS and fixed in 4% PFA for 5 min at room temperature. Slides were washed 3 times for 5 min in PBS and permeabilized for 15 min in PBS-T (5% Tween-20) at room temperature. Slides were washed 3 times for 5 min in PBS and incubated for 30 min with 1:150 proteinase K (Takara Bio; Kusatsu, Shiga, Japan) in PBS at room temperature. Slides were then washed 3 times for 5 min in PBS, before the TUNEL protocol was performed as described previously (Lahne et al., 2021).

2.8 Image acquisition and analysis

A Nikon A1 confocal microscope, equipped with a ×40 plan-fluor oil immersion objective, was used to acquire 6.5 µm z-stacks in 0.8 µm steps, of 1024 × 1024 images of the central-dorsal region of the retina. Counts were performed manually using Fiji software throughout the 6.5 µm z-stack and normalized to a 300 µm length of the retina as previously described (Lahne et al., 2015). Statistical analyses were performed using GraphPad Prism 9 (San Diego, CA). Statistical tests used included either a Student's *t*-test or a one-way ANOVA with a Tukey or Dunnett *post hoc* test. A *p*-value of less than 0.05 was considered significant. The mean ± SEM for each experiment is stated in the text of the appropriate Results section and the sample size (n) is stated in the appropriate figure legend.

2.9 Single cell RNA-seq (scRNA-seq) analysis

We used scRNA-seq data from whole light-damaged retinas that was previously published (Hoang et al., 2020). scRNA-seq analysis was

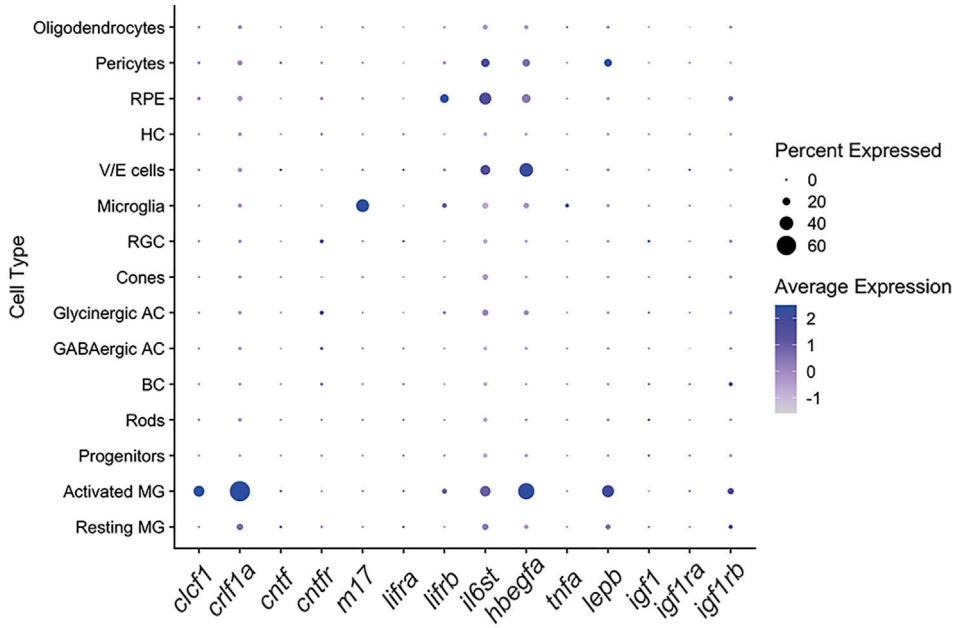

FIGURE 1
The CNTFR ligands Clcf1 and Crlf1a are expressed by Müller glia within the zebrafish retina. Dot plot showing expression of the CNTFR ligands *clcf1, crlf1a* and *cntf,* and CNTFR receptor components *cntfr, lifrb* and *il6st* in all retinal cell types in a single-cell RNA-Seq data set (Hoang et al., 2020). Expression of other pro-proliferative factors is also shown. Cells are from combined whole retina samples of 0 h, 4 h, 10 h, 20 h and 36 h of light treatment.

performed using Seurat (Hao et al., 2021). Established clusters from the previous publication were maintained and differential expression analysis was performed comparing resting and activated Müller glia.

3 Results

3.1 CNTFR ligands Clcf1 and Crlf1a are expressed in the activated Müller glia in light-damaged retinas

To investigate the spatial expression of CNTFR ligands in the light-damaged retina, we analyzed previously published scRNA-seq datasets (Hoang et al., 2020). We did not detect expression of *cntf* in any of the retinal cell types (Figure 1). In contrast, we observed expression of both *clcf1* and *crlf1a* primarily within activated Müller glia (Figure 1), suggesting that Müller glia express and secrete the Clcf1 and Crlf1a ligands in response to retinal damage. These expression patterns were similar to other key pro-proliferative factors within the zebrafish retina, such as *hbegfa* and *lepb* (Wan et al., 2012; Zhao et al., 2014). In contrast, the cytokine LIF (encoded by the *m17* gene) was expressed predominantly in microglia and not in Müller glia (Figure 1). To begin to understand how these ligands interact with cells within the damaged retina, we determined what cell types expressed any of the corresponding receptor components. We observed only low levels of *cntfr* expression in the scRNA-seq datasets, suggesting its expression was not induced during the first 36 h of retinal regeneration. Additionally, of the two LIF receptor genes encoded in zebrafish (Ogai et al., 2014), *lifra* was not significantly expressed in the retina and *lifrb* expression was upregulated in the activated Müller glia relative to the resting Müller glia (Figure 1). Finally, expression of *il6st* (encoding Gp130) was primarily limited to activated Müller glia, vascular endothelial, retinal pigmented epithelium, and pericytes, suggesting these cells are particularly sensitive to Gp130-mediated signalling. Together, these data suggest that Clcf1 and Crlf1a are released from activated Müller glia following injury and potentially interact with a variety of different cell types within the retina.

We further explored the expression of *clcf1* and *crlf1a*, and several associated genes, in both resting and activated Müller glia, as well as across the damage time course within the activated Müller glia population. Both *clcf1* ($p < 1.00 \times 10^{-200}$) and *crlf1a* ($p < 1.00 \times 10^{-200}$) exhibited a significant increase in expression within the activated population of Müller glia (Figures 2A,B, respectively). In addition, *clcf1* and *crlf1a* expression were upregulated by 10 h and 4 h of light damage (Figures 2A,B, respectively). This suggests that Müller glia upregulates the expression of both genes prior to photoreceptor cell death and they both may be required for either neuroprotection or proliferation. Little expression of *cntf* was observed in either resting or activated Müller glia (Figure 2C), indicating that Clcf1 and Crlf1a are the primary CNTFR ligands expressed within the retina. In contrast, *clcf1* expression was significantly increased ($p = 7.40 \times 10^{-183}$) in activated Müller glia in the light-treated mouse retina (Supplementary Figure S1A), while *crlf1* expression was significantly decreased ($p = 0.03$) in activated Müller glia relative to resting Müller glia (Supplementary Figure S1B). Similar to zebrafish, we did not detect expression of *cntf* in either mouse Müller glia population following light treatment (Supplementary Figure S1C).

In the zebrafish retina, expression of the receptor components *cntfr* (Figure 2D) and *lifra* (Figure 1) was relatively low in both Müller glia populations. In contrast, *lifrb* expression (Figure 2E) was significantly higher in activated Müller glia ($p = 6.00 \times 10^{-153}$) and

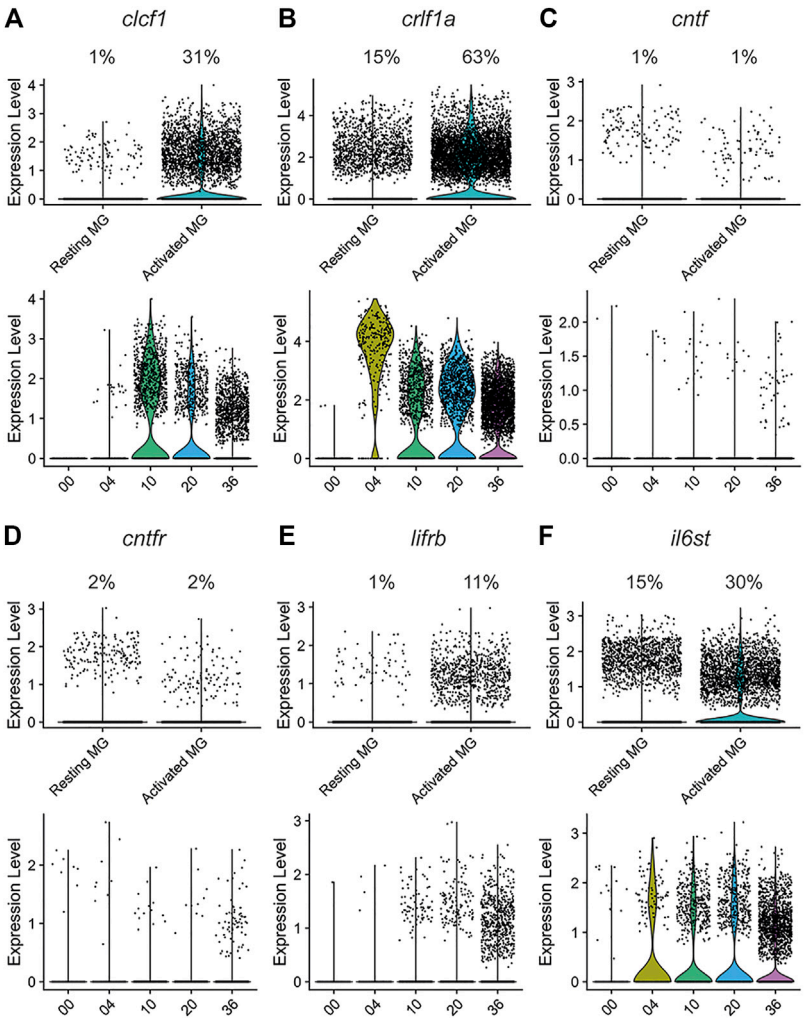

FIGURE 2
The CNTFR ligands *clcf1* and *crlf1a,* but not *cntf,* are differentially expressed by activated Müller glia during regeneration in the light-treated retina. The expression of *clcf1* **(A)**, *crlf1a* **(B)**, *cntf* **(C)**, *cntfr* **(D)**, *lifrb* **(E)**, and *il6st* **(F)** were examined in a single-cell RNA-Seq data set (Hoang et al., 2020). Upper violin plots show number of UMI expressed in individual resting and activated Müller glia. Percentage of Müller glia in each cluster expressing the gene of interest is shown above the plot. Lower violin plots show number of UMI expressed across time in activated Müller glia.

increased from 10 through 36 h of light treatment. Similarly, *il6st* significantly increased in expression in activated Müller glia ($p = 2.80 \times 10^{-71}$) from 4 through at least 36 h of light treatment (Figure 2F). This rapid induction and sustained expression of *il6st* suggests that Gp130-mediated signalling may have both neuroprotective and pro-proliferative effects. The expression differences seen in the receptor genes may be due to Gp130 forming a receptor complex in both a CNTFR- and LIFR-independent manner, and therefore is likely required for additional processes (White & Stevens, 2011). Interestingly, *Cntfr* expression was observed in resting mouse Müller glia, however *Cntfr* was significantly downregulated in activated Müller glia (Supplementary Figure S1D; $p = 7.11 \times 10^{-24}$). No change was observed in *Lifr* expression (Supplementary Figure S1E), but *Il6st* expression was significantly increased within activated Müller glia (Supplementary Figure S1F; $p = 3.80 \times 10^{-11}$).

To confirm that *clcf1* and *crlf1a* were expressed in Müller glia, we performed *in situ* hybridization using the RNAscope system. Dark-adapted *albino; Tg[gfap:EGFP]*^{nt11} fish were placed in intense light treatment for either 0 (undamaged), 10, 20, or 36 h before eyes were collected and retinal sections were labeled for either *clcf1 or crlf1a,* GFP, and PCNA. A broad and low level of *clcf1* expression was detected at 0 h (Figures 3A–A"). However, *clcf1* expression increased and colocalized with GFP-expressing Müller glia (*Tg(gfap:EGFP)*) from 10 through 20 h (Figures 3B–C"). By 36 h of light treatment, the *clcf1* signal appeared weaker and more dispersed throughout the retina (Figures 3D–D"). However, *clcf1* puncta were still observed within proliferating Müller glia (Figures 3D, D"), suggesting that *clcf1* was expressed in Müller glia that would enter the cell cycle. Little expression of *crlf1a* was observed at 0 h (Figures 3E–E"). However, by 10 and 20 h of light treatment, *crlf1a* was observed within Müller glia (Figures 3F–G") and persisted within proliferating Müller glia through 36 h of light treatment (Figures 3H–H"). Furthermore, *clcf1* and *crlf1a* were observed within the same Müller glia at 36 h of light treatment (Supplementary Figures S2A, S2B). Additionally, PCNA-negative Müller glia also did not

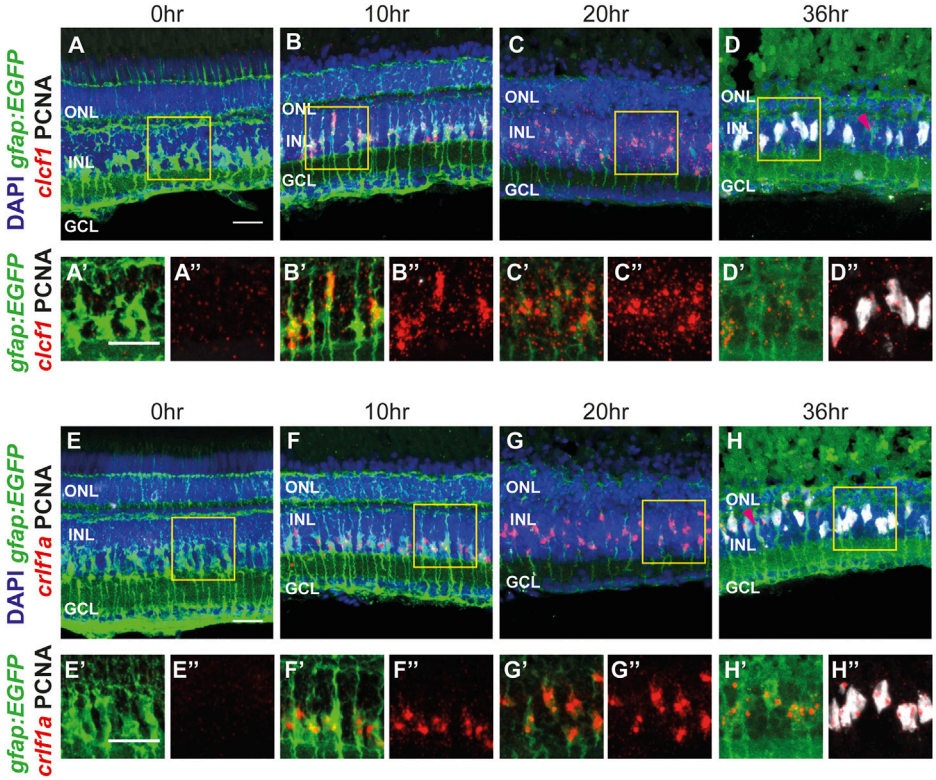

FIGURE 3
The CNTFR ligands *clcf1* and *crlf1a* are detected within Müller glia following injury, consistent with scRNA-seq data. **(A**–H")Maximum projection images of dark-adapted *albino; Tg[gfap:EGFP]*^{nt11} zebrafish that were light-treated for up to 36 h, with *in situ* hybridization performed utilizing either *clcf1* **(A**–D") or *crlf1a* **(E**–H") probes. Sections were also labeled for GFP and PCNA to assess proliferating Müller glia and nuclei were counterstained with DAPI. Yellow boxes in **(A-H)** represent areas chosen for greater magnification (in A'-H' and A"-H"). Magenta arrowheads **(D, H)** show resting Müller glia. ONL, outer nuclear layer, INL, inner nuclear layer, GCL, ganglion cell layer. Scale bar represents 20 μm.

express either *clcf1* or *crlf1a* (Figures 3D,H), which likely represent resting Müller glia. These expression patterns closely resemble the expression time course identified by scRNA-seq and revealed that *clcf1* and *crlf1a* are highly upregulated within Müller glia early in the damage paradigm, before photoreceptor cell death.

We also examined the expression patterns of the *cntfr* and *il6st* receptors. Expression of *cntfr* was observed broadly throughout the retina from 0 to 36 h of light treatment (Supplementary Figures S3A–S3D") with no obvious changes in expression level or pattern, which is consistent with the scRNA-seq data (Figure 1). A similar expression pattern was observed for *il6st* (Supplementary Figures S3E–S3H"). This data suggests that cells within each nuclear layer may respond to the release of Clcf1 and Crlf1a from Müller glia following injury.

3.2 Intravitreal injection of recombinant CLCF1/CRLF1 protects against photoreceptor cell death during light treatment

Previous studies determined that CNTF is neuroprotective within both the zebrafish and mammalian retinas (Kassen et al., 2009; Aslam et al., 2013). We examined whether Clcf1 and Crlf1a, which are alternative ligands for the CNTF receptor, can provide similar neuroprotective benefits. We intravitreally injected *albino* zebrafish with either PBS (vehicle) or 1 mg/ml CLCF1/CRLF1 every 12 h until 48 h after the initial injection, at which point fish were placed in constant intense light. They received a further injection at 12 h of constant light and eyes were collected 12 h later (24 h light treatment). To quantify cell death, we performed the TUNEL assay on retinal sections (Figures 4A–D). We observed a significant decrease in the number of TUNEL-positive ONL cells in Clcf1/Crlf1a-co-injected retinas relative to vehicle control (Figure 4E; PBS: 86.68 ± 6.19, CLCF1/CRLF1: 47.34 ± 7.18, p = 0.0005). This demonstrates that *clcf1/crlf1a* co-expression by zebrafish Müller glia may be neuroprotective in the light-damaged retina.

3.3 CNTFR and the associated ligands Clcf1 and Crlf1a are required for Müller glia proliferation in the light-treated retina

We examined whether CNTFR, Clcf1, or Crlf1a contribute to Müller glia proliferation following light-induced photoreceptor cell death. Dark-adapted *albino; Tg[gfap:EGFP]*^{nt11} fish were electroporated with either standard control morpholino (S.C. MO) (Figures 5A,E), which does not correspond to any known sequence in the zebrafish genome (Nasevicius & Ekker, 2000), *cntfr* morpholino (Figures 5B,F), a combination of the *clcf1* and *crlf1a* MOs (Figures 5C,G), or a mixture of all three (Triple; Figures 5D,H) before being

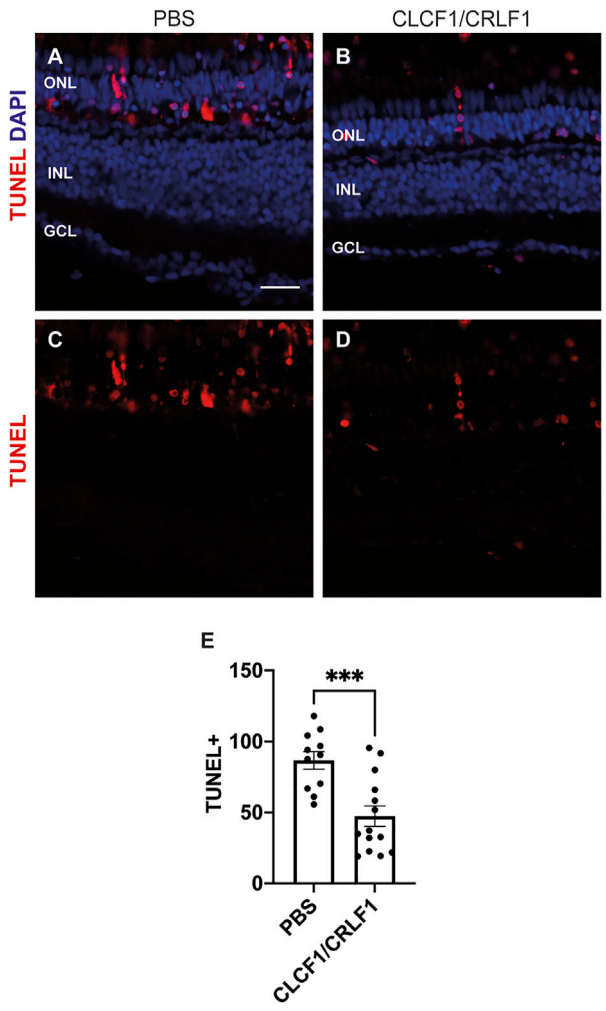

FIGURE 4
Intravitreal injection of CLCF1/CRLF1 protects against photoreceptor cell death during light treatment. **(A–D)** Single z-plane confocal images from dark-adapted *albino* zebrafish that were light-treated for 24 h while being intravitreally injected with either PBS **(A, C)** or CLCF1/CRLF1 **(B, D)**. TUNEL assay was performed to assess cell death, and nuclei were counterstained with DAPI. **(E)** Quantification showing significant decrease in the number of TUNEL-positive nuclei within the ONL of CLCF1/CRLF1-treated retinas. Student's *t*-test, $p = 0.0005$, n ≥ 11. Mean ± SEM, ***$p < 0.001$. ONL, outer nuclear layer, INL, inner nuclear layer, GCL, ganglion cell layer. Scale bar represents 20 µm.

placed in constant light treatment. Retinas were collected at 36 h of constant light and labelled for GFP and PCNA to quantify proliferating Müller glia. As compared to the S.C. MO group (Figure 5I; S.C.: 36.59 ± 2.15 PCNA-positive Müller glia), a significant decrease in the number of proliferating Müller glia was observed in the *cntfr* MO group (Figure 5I; *cntfr*: 17.82 ± 2.83, $p < 0.0001$), the *clcf1/crlf1* MO group (Figure 5I; *clcf1/crlf1a:* 21.62 ± 2.84, $p = 0.0003$), and the Triple MO groups (Figure 5I; Triple: 24.31 ± 3.16, $p = 0.0072$). There was no significant difference between the *cntfr* MO, *clcf1/crlf1* MO, and the Triple MO groups. This suggests that both the receptor and the Clcf1/Crlf1a ligands are required for Müller glia proliferation following light-induced damage. Additionally, this result suggested that while Clcf1/Crlf1a co-expression may be neuroprotective in the light-damaged retina (Figure 4), it is not necessary.

We next examined whether the reduction in Müller glia proliferation was a result of reduced cell death in the morphants by electroporating *albino* zebrafish with either S.C. (Supplementary Figures S4A, S4E), *cntfr* (Supplementary Figures S4B, S4F), *clcf1/crlf1a* (Supplementary Figures S4C, S4G), or all three morpholinos (Triple MO, Supplementary Figures S4D, S4H) and collecting the retinas at 24 h of light treatment. The TUNEL assay was performed to assess cell death (Supplementary Figures S4A–S4H). No significant differences in the number of TUNEL-positive cells were observed between any treatment group relative to S.C. (Supplementary Figure S4I; S.C.: 109.9 ± 8.75 TUNEL-positive cells, *cntfr*: 112.5 ± 4.19 $p = 0.98$, *clcf1/crlf1a*: 114.7 ± 7.46 $p = 0.92$, Triple: 112.4 ± 5.12 $p = 0.99$), suggesting that the reduced number of proliferating Müller glia in either the *cntfr, clcf1/crlf1a* or the Triple morphants was not due to decreased cell death, but rather their requirement for stimulating Müller glia proliferation, with Clf1/Crlf1a likely acting as ligands for CNTFR in the light-treated retina.

3.4 Intravitreal injection of recombinant CLCF1/CRLF1 induces rod precursor cell proliferation

Since Clcf1/Crlf1a signalling is required for Müller glia proliferation, we examined whether co-injection of mouse CLCF1/CRLF1 was sufficient to induce zebrafish Müller glia proliferation. Either PBS (vehicle, Figures 6A–C) or 1 mg/ml of both mouse CLCF1 and CRFL1 (Figures 6D–F) was intravitreally injected into *albino; Tg[gfap:EGFP]*^{nt11} fish along with an interperitoneal injection of the thymidine analogue EdU to label proliferating cells. Injections occurred every 12 h until 72 h after the initial injection, at which time eyes were collected and retinal sections were labelled for GFP, PCNA, and EdU to assess proliferating Müller glia and EdU-labelled cells. We observed no significant difference in the number of PCNA-positive Müller glia (Figure 6G; PBS: 0.26 ± 0.13, CLCF1/CRFL1: 0.98 ± 0.36, $p = 0.08$) or EdU-positive Müller glia (Figure 6I; PBS: 0.17 ± 0.11, CLCF1/CRFL1: 0.52 ± 0.16, $p = 0.09$) between vehicle and CLCF1/CRFL1-treated groups. This suggests that CLCF1/CRFL1-mediated signalling was insufficient to induce Müller glia proliferation. However, we observed a significant increase in the number of PCNA-positive ONL cells (Figure 6H; PBS: 6.56 ± 1.06, CLCF1/CRFL1: 16.0 ± 2.16, $p = 0.0008$) and EdU-positive ONL cells (Figure 6J; PBS: 6.23 ± 0.88, CLCF1/CRFL1: 15.3 ± 2.27, $p = 0.0014$) in the CLCF1/CRFL1-injected retinas relative to vehicle control. These proliferating ONL cells may represent rod precursor cells that produce rod photoreceptors during persistent retinal neurogenesis (Morris et al., 2008; Wilson et al., 2016) and CLCF1/CRFL1 treatment may be sufficient to induce further rod precursor cell proliferation without increased Müller glia proliferation.

3.5 CLCF1/CRFL1-induced rod precursor cell proliferation is IGF-1R dependent

Previous studies showed that rod precursor cell proliferation requires Insulin-like growth factor 1 receptor 1 (IGF-1R) (Zygar et al., 2005; Lahne et al., 2019). To determine if CLCF1/CRFL1-induced rod precursor cell proliferation is IGF-1R-dependent, *albino; Tg[gfap:EGFP]*^{nt11} zebrafish were intravitreally injected with 1 mg/ml CLCF1/CRFL1 and intraperitoneally injected with either DMSO (vehicle; Figures 7A,C) or the IGF-1R inhibitor NVP

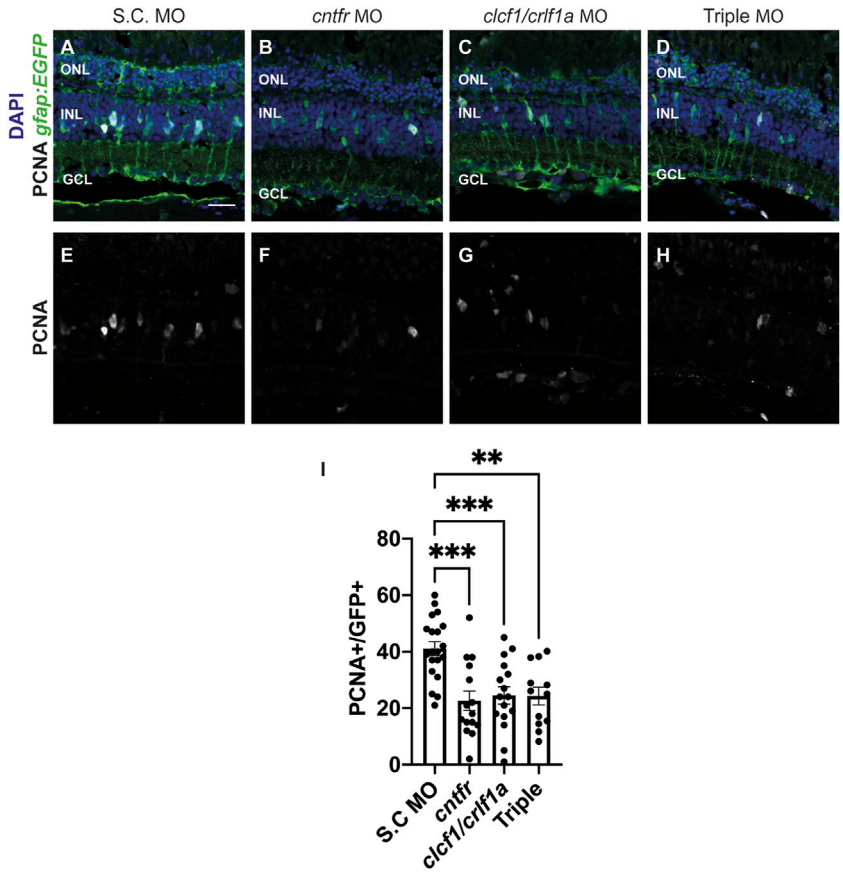

FIGURE 5
Knockdown of CNTFR and Clcf1/Crlf1a reduces Müller glia proliferation. **(A–H)** Single confocal images from dark-adapted *albino; Tg[gfap:EGFP]*^{nt11} zebrafish which were light-treated for 36 h after electroporation of either S.C. **(A)**, *cntfr* **(B),** *clcf1/crlf1a* morpholinos **(C),** or a combination of all three *cntfr/clcf1/crlf1a* (Triple) **(D)**. Sections were labeled for GFP and PCNA to assess proliferating Müller glia and nuclei were counterstained with DAPI **(E, F, G, H)**. **(I)** Quantification showing significant decrease in the number of PCNA-positive Müller glia within the INL in *cntfr* and *clcf1/crlf1a* electroporated retinas. One-way ANOVA with Dunnett *post hoc*, *cntfr* vs. S.C. $p < 0.0001$, *clcf1/crlf1a* vs. S.C. $p = 0.0003$, Triple vs. S.C. $p = 0.0072$. n ≥ 12. Mean ± SEM, $^{**}p < 0.001$, $^{***}p < 0.001$, $^{****}p < 0.0001$. ONL, outer nuclear layer, INL, inner nuclear layer, GCL, ganglion cell layer. Scale bar represents 20 µm.

(Figures 7B,D). Fish received both injections every 12 h. At 72 h after the initial injection, retinas were isolated, sectioned, and labelled for GFP and PCNA to assess Müller glia proliferation. We observed no significant difference in the number of PCNA-positive Müller glia between the DMSO and NVP-treated groups (Figure 7E; DMSO: 0.57 ± 0.38, NVP: 0.49 ± 0.33, $p = 0.87$). However, there was a significant decrease in the number of proliferating rod precursor cells in the NVP-treated group relative to vehicle control (Figure 7F; DMSO: 25.17 ± 2.43, NVP: 11.23 ± 1.36, $p < 0.0001$). This suggests that CLCF1/CRFL1-induced rod precursor cell proliferation was IGF-1R dependent. To confirm that increased rod precursor cell proliferation was not a product of increased Müller glia proliferation, dark-adapted *albino; Tg[gfap:EGFP]*^{nt11} zebrafish were placed in constant intense light treatment, while also receiving intraperitoneal injections of either DMSO (Figures 7G,I) or NVP (Figures 7H,J) beginning at the start of the light treatment and every 12 h thereafter. Eyes were collected after 36 h of constant light treatment and sections were labelled for GFP and PCNA to assess Müller glia proliferation. We did not detect a significant change in the number of PCNA-positive Müller glia between treatment groups (Figure 7K; DMSO: 38.04 ± 2.63, NVP: 40.03 ± 1.88, $p = 0.54$), suggesting that inhibiting IGF-1R does not affect Müller glia proliferation. This is consistent with scRNA-seq data that revealed little expression of either *igf1* or the associated receptor components (*igf1ra* and *igf1rb*) in Müller glia in the light-damaged retina (Figure 1). Together these data suggest that CLCF1/CRFL1 induces rod precursor proliferation in an IGF-1R-dependent manner.

3.6 Intravitreal co-injection of IGF-1 and Clcf1/Crlf1a is not sufficient to induce Müller glia proliferation or additional rod precursor proliferation

Since Clcf1/Crlf1a-dependent rod precursor cell proliferation is IGF-1R-dependent, we examined if co-injection of IGF-1 and Clcf1/Crlf1a was sufficient to induce further proliferation. Previous studies demonstrated that IGF-1 synergizes with FGF2 to induce significant Müller glia proliferation within the zebrafish retina (Wan et al., 2014), therefore we hypothesized that the combination of IGF-1 and Clcf1/Crlf1a would induce a similar response in the absence of retinal damage. Either PBS (vehicle) (Figures 8A,E), IGF-1 (Figures 8B,F), Clcf1/Crlf1a (Figures 8C,G), or a combination of IGF-1 and Clcf1/Crlf1a (Figures 8D,H) were intravitreally injected into *albino;Tg[gfap:*

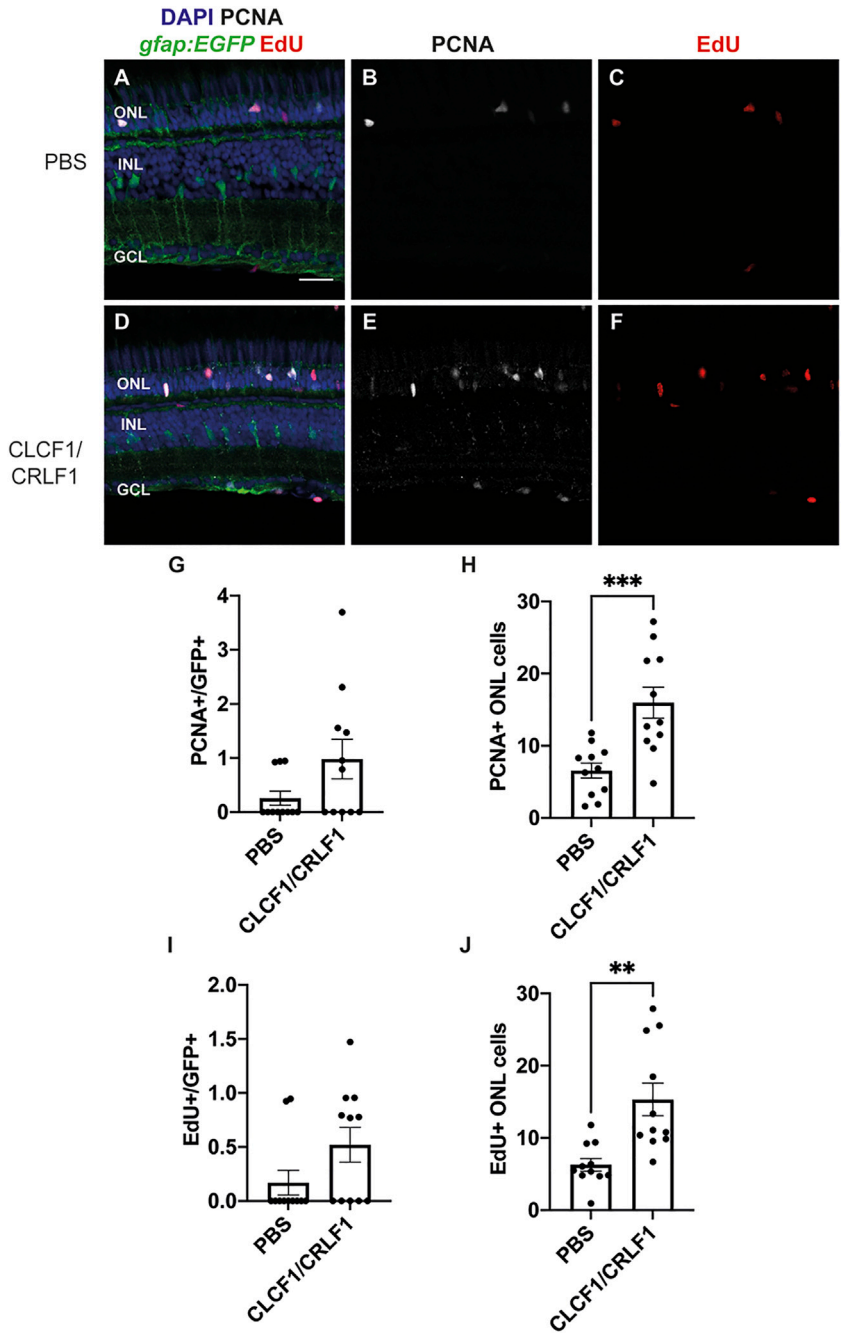

FIGURE 6
Intravitreal injection of recombinant mouse CLCF1/CRLF1 induces rod precursor cell proliferation. **(A–F)** Single confocal images from *albino; Tg[gfap: EGFP]*^{nt11} zebrafish which were intravitreally injected every 12 h with either PBS **(A)** or CLCF1/CRLF1 **(D)** for 72 h. Sections were labeled for GFP, PCNA, and EdU to assess proliferating Müller glia and nuclei were counterstained with DAPI **(B, C, E, F)**. **(G)** Quantification showing no significant change in the number of PCNA-positive Müller glia within the INL of CLCF1/CRLF1-injected retinas. Student's t-test, $p = 0.08$. **(H)** Quantification showing significant increase in the number of PCNA-positive cells within the ONL of CLCF1/CRLF1-injected retinas. Student's *t*-test, $p = 0.0008$. **(I)** Quantification showing no significant difference in the number of EdU-positive Müller glia within the INL of CLCF1/CRLF1-injected retinas. Student's *t*-test, $p = 0.09$. **(J)** Quantification showing significant increase in the number of EdU-positive cells within the ONL of CLCF1/CRLF1-injected retinas. Student's *t*-test, $p = 0.0014$. $n \geq 11$. Mean ± SEM, $^{**}p < 0.01$, $^{***}p < 0.001$. ONL, outer nuclear layer, INL, inner nuclear layer, GCL, ganglion cell layer. Scale bar represents 20 μm.

EGFP]^{nt11} fish every 12 h. At 72 h after the initial injection, eyes were collected, sectioned, and labelled for GFP and PCNA to assess proliferation (Figures 8A–H). We observed no significant difference in the number of PCNA-positive Müller glia between any groups (Figure 8I; PBS: 0.51 ± 0.22, IGF-1: 1.01 ± 0.43, Clcf1/Crlf1a: 0.11 ± 0.11, IGF-1/Clcf1/Crlf1a: 1.36 ± 0.33), suggesting that co-injection of IGF-1 and Clcf1/Crlf1a was not sufficient to induce Müller glia proliferation in the absence of retinal damage. Furthermore, no significant difference was observed in the number of PCNA-positive rod precursor cells between PBS and IGF-1-injected groups (Figure 8J; PBS: 9.24 ± 1.52, IGF-1: 14.76 ± 2.18, $p = 0.34$), indicating that IGF-1 was not sufficient to induce rod precursor cell proliferation.

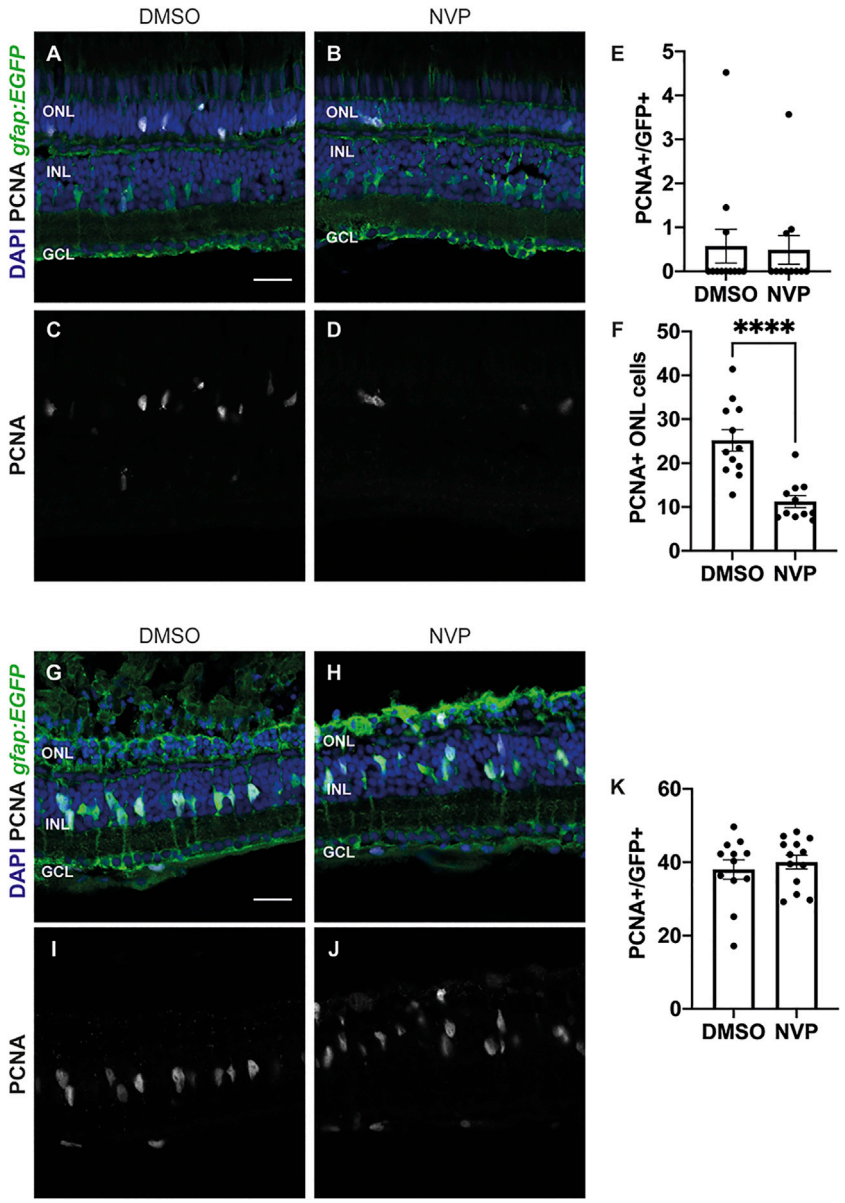

FIGURE 7
CLCF/CRLF1 induces rod precursor cell proliferation in an IGF-1R dependent manner. **(A–D)** Single confocal images from *albino; Tg[gfap:EGFP]*^{nt11} zebrafish which were intravitreally injected every 12 h with CLCF1/CRLF1 and simultaneously receiving injections of either DMSO (vehicle) **(A)** or the IGF-1R inhibitor NVP **(B)** for 72 h. Sections were labeled for GFP and PCNA to assess proliferating Müller glia and nuclei were counterstained with DAPI **(C, D)**. **(E)** Quantification showing no significant change in the number of PCNA-positive Müller glia within the INL of NVP-treated fish. Student's *t*-test, $p = 0.87$, n ≥ 11. **(F)** Quantification showing significant decrease in the number of PCNA-positive cells within the ONL of NVP-treated fish. Student's *t*-test, $p = 0.0001$, n ≥ 11. **(G–J)** Single confocal images from dark-adapted *albino; Tg[gfap:EGFP]*^{nt11} zebrafish which were light-treated for 36 h while receiving injections of either DMSO (vehicle) **(G)** or the IGF-1R inhibitor NVP **(H)**. Sections were labeled for GFP and PCNA to assess proliferating Müller glia and nuclei were counterstained with DAPI **(I, J)**. **(K)** Quantification showing no significant change in the number of PCNA-positive Müller glia between DMSO and NVP-treated fish. Student's t-test, $p = 0.54$, n ≥ 12. Mean ± SEM, ****$p < 0.0001$. ONL, outer nuclear layer, INL, inner nuclear layer, GCL, ganglion cell layer. Scale bar represents 20 µm.

However, there was a significant difference in the number of proliferating rod precursor cells between the PBS and Clcf1/Crlf1a-treated groups (Clcf1/Crlf1a: 24.32 ± 3.23, $p = 0.0007$), and PBS and IGF-1/Clcf1/Crlf1a-treated groups (IGF-1/Clcf1/Crlf1a: 24.44 ± 2.09, $p = 0.0001$). Additionally, a significant increase in the number of proliferating rod precursor cells was observed between Clcf1/Crlf1a and IGF-1-treated groups ($p = 0.036$), and the IGF-1/Clcf1/Crlf1a and IGF-1 groups ($p = 0.013$), but there was no significant difference between the Clcf1/Crlf1a and IGF-1/Clcf1/Crlf1a-treated groups ($p = 0.99$). This suggests that although Clcf1/Crlf1a-induced rod precursor cell proliferation is IGF-1R-dependent, addition of IGF-1 does not induce further proliferation of rod precursor cells.

4 Discussion

This is the first demonstration that the Ciliary neurotrophic factor receptor (CNTFR) ligands Cardiotrophin-like cytokine factor 1

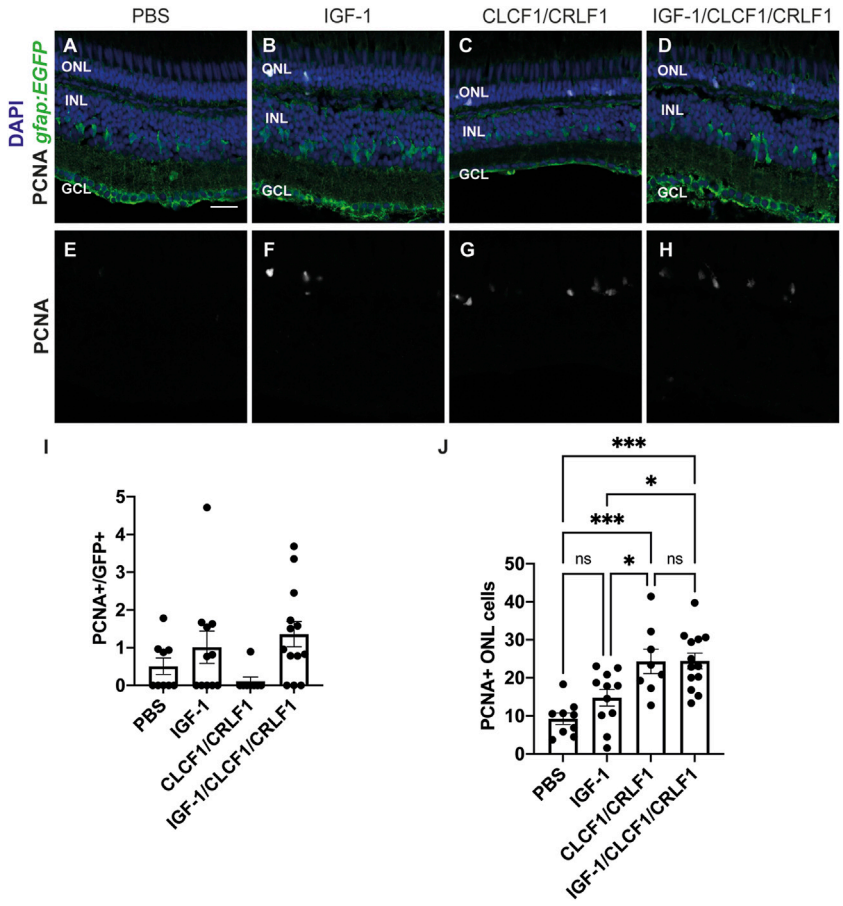

FIGURE 8
Co-injection of CLCF/CRLF and IGF-1 does not induce additional proliferation. **(A–D)** Single confocal images from *albino; Tg[gfap:EGFP]*^{nt11} zebrafish which were intravitreally injected every 12 h with either PBS **(A)**, IGF-1 **(B)**, CLCF1/CRLF1 **(C),** or a combination of IGF-1 and Clcf1/Crlf1a **(D)** for 72 h. Sections were labeled for GFP and PCNA to assess proliferating Müller glia and nuclei were counterstained with DAPI **(E, F, G, H)**. **(I)** Quantification showing no change in the number of PCNA-positive Müller glia within the INL of IGF-1 and IGF-1/CLCF1/CRLF1-injected retinas. **(J)** Quantification showing significant difference in the number of PCNA-positive cells within the ONL of IGF-1 and IGF-1/CLCF1/CRLF1-injected retinas. One-way ANOVA with Tukey *post hoc*, IGF-1/CLCF1/CRLF1 vs. PBS $p = 0.0001$, CLCF1/CRLF1 vs. PBS $p = 0.0007$, IGF-1 vs. CLCF1/CRLF1 $p = 0.0362$, IGF-1/CLCF1/CRLF1 vs. IGF-1 $p = 0.0127$. $n \geq 8$. Mean ± SEM, $*p < 0.05$,$***p < 0.001$. ONL, outer nuclear layer, INL, inner nuclear layer, GCL, ganglion cell layer. Scale bar represents 20 μm.

(Clcf1) and Cytokine receptor-like factor 1a (Crlf1a) are required for retinal regeneration. We investigated expression of these ligands and their corresponding receptor components within the damaged retina and showed that Clcf1 and Crlf1a are neuroprotective, are required for Müller glia proliferation, and can induce rod precursor proliferation in an IGF-1R-dependent manner.

Previously, it was demonstrated that both *clcf1* and *crlf1a* are expressed in Müller glia-derived precursor cells at 96 h post injury (Zhao et al., 2014), however no in-depth analyses have fully investigated the spatio-temporal expression or function of either ligand. Our scRNA-seq data demonstrate that both *clcf1* and *crlf1a* are expressed rapidly following retinal damage with Müller glia expressing these ligands as early as 4 h post injury and maintaining expression until at least 36 h post injury. This expression pattern was further confirmed by *in situ* hybridization, which demonstrates co-expression of *clcf1* and *crfl1a* in proliferating MG, indicating that these ligands are expressed specifically in activated MG. In contrast, we observed little expression of *cntf*, which was previously shown to be neuroprotective in both mammalian (Tao et al., 2002; Sieving et al., 2006; Azadi et al., 2007; Rhee et al., 2013) and zebrafish models of retinal damage (Kassen et al., 2009) and can induce Müller glia proliferation within zebrafish (Kassen et al., 2009; Zhao et al., 2014). This suggests that Clcf1 and Crlf1a are the primary CNTFR ligands expressed within the regenerating retina and may have similar effects on the retina.

Similar to the effects of CNTF (Kassen et al., 2009), intravitreal injection of CLCF1/CRLF1 significantly reduces photoreceptor cell death during light treatment, indicating that Clcf1 and Crlf1a may play a neuroprotective role following damage, which is further supported by the expression of these ligands prior to the occurrence of cell death. Additionally, knockdown of *clcf1* and *crlf1a* significantly reduced Müller glia proliferation following light treatment, however intravitreal injection of CLCF1/CRLF1 was insufficient to induce Müller glia proliferation in the undamaged retina. Therefore, Clcf1 and Crlf1a are necessary, but not sufficient, for the induction of Müller glia proliferation. Clcf1 and Crlf1a have also been shown to be required for optic nerve regeneration (Elsaeidi et al., 2014), suggesting a general role for these ligands in neuronal regeneration.

The contrast in Müller glia proliferation between CNTF and CLCF1/CRLF1-treated retinas may be due to differences in downstream actions of these ligands. Mutations in CRLF1 or CLCF1 have been linked to cold-induced sweating syndrome, however mutations in CNTF do not induce similar effects (Murakami et al., 2019), although both have been demonstrated to induce expression and phosphorylation of Stat3 (Kassen et al., 2009; Nahlé et al., 2019; Rezende et al., 2009; Savin et al., 2015 which has been shown to be essential in Müller glia for retinal regeneration (Nelson et al., 2012).

Despite the inability to increase Müller glia proliferation, intravitreal injection of CLCF1/CRLF1 did induce a significant increase in rod precursor cell proliferation. A similar increase in rod precursor cell proliferation was observed following intravitreal CNTF injection (Kassen et al., 2009). It has previously been demonstrated that proliferation of rod precursor cells is IGF-1R1R-dependent (Lahne et al., 2019). We demonstrated that CLCF1/CRLF1-induced rod precursor cell proliferation is IGF-1R-dependent, although Müller glia proliferation following injury is not. It has previously been shown that IGF-1 can synergize with FGF2 to induced Müller glia proliferation, and that *igfra* is required for Müller glia proliferation following injury (Wan et al., 2014), however co-injection of IGF-1 with CLCF1/CRLF1 failed to induce additional Müller glia or rod precursor cell proliferation. Therefore, the factors that may synergize with Clcf1 and Crlf1a to induce Müller glia proliferation following injury remain unclear.

To better understand how these ligands operate within the zebrafish retina, we also investigated expression of the receptor complex components. NPCs have previously been shown to express *cntfr* at 96 h post injury (Zhao et al., 2014). Within scRNA-seq datasets we observed little expression of *cntfr*, however *in situ* hybridization demonstrated that *cntfr* is expressed throughout the retina at all timepoints studied. Knockdown of *cntfr* also demonstrated that CNTFR is required for Müller glia proliferation. We observed a significant increase in expression of *lifrb* and *il6st* within activated Müller glia, and *in situ* hybridization confirmed that *il6st* is expressed throughout the retina at all timepoints. These findings suggest that Müller glia, and likely most cell types of the retina, are sensitive to CNTFR ligands. This is further supported by transcriptional changes in multiple cell types following CNTF exposure in the mouse retina (Wang et al., 2020).

Together this data suggests a model in which Müller glia respond to injury by producing the CNTFR ligands Clcf1 and Crlf1a, which play a dual role within the regenerating retina showing both neuroprotective and pro-proliferative properties. Based upon expression of receptor components, Clcf1 and Crlf1a can signal to most cell types. It has previously been shown within the mouse retina that the neuroprotective effects of CNTF require GP130 within Müller glia (Rhee et al., 2013), therefore changes induced in Müller glia in response to CNTFR ligands may provide the observed neuroprotective effects, rather than direct CNTFR-mediated signalling within damaged cell types. CNTF has also previously been shown to interact with microglia (Kahn et al., 1995; Baek et al., 2018), which are known to be required during retinal regeneration (Conedera et al., 2019; Mitchell et al., 2019). Therefore, the potential interaction of Clcf1 and Crlf1a with microglia within the damaged retina may be one way in which these two cell types interact.

Data availability statement

The datasets presented in this study can be found in online repositories. All scRNA-seq data and source codes are available at GitHub https://github.com/jiewwwang/Single-cell-retinalregeneration. The scRNA-seq data can be queried interactively at https://proteinpaint.stjude.org/F/2019.retina.scRNA.html.

Ethics statement

The animal study was reviewed and approved by University of Notre Dame Animal Care and Use Committee.

Author contributions

PB and DH conceived and designed the study. PB and LC carried out all the experiments and image analysis. PB and DH wrote the manuscript. PB, LC, and DH edited the manuscript. DH supervised the study. All authors contributed to the article and approved the submitted version.

Funding

This work was funded by the National Institutes of Health/National Eye Institute grant (U01-EY027267), the Hiller Family Endowment for Excellence in Stem Cell Research, and the Center for Zebrafish Research, University of Notre Dame.

Acknowledgments

We thank the staff of the Freimann Life Science Center for providing outstanding zebrafish husbandry and care, NDIIF for support with imaging, and members of the Hyde lab for thoughtful discussions.

Conflict of interest

The authors declare that the research was conducted in the absence of any commercial or financial relationships that could be construed as a potential conflict of interest.

Publisher's note

Supplementary material

The Supplementary Material for this article can be found online at: https://www.frontiersin.org/articles/10.3389/fcell.2023.1142586/full#supplementary-material

References

Angueyra, J. M., and Kindt, K. S. (2018). Leveraging zebrafish to study retinal degenerations. *Front. Cell Dev. Biol.* 6, 110. doi:10.3389/fcell.2018.00110

Askvig, J. M., and Watt, J. A. (2015). The MAPK and PI3K pathways mediate CNTF-induced neuronal survival and process outgrowth in hypothalamic organotypic cultures. *J. Cell Commun. Signal.* 9, 217–231. doi:10.1007/s12079-015-0268-8

Aslam, S. A., Davies, W. I. L., Singh, M. S., Charbel Issa, P., Barnard, A. R., Scott, R. A. H., et al. (2013). Cone photoreceptor neuroprotection conferred by CNTF in a novel *in vivo* model of battlefield retinal laser injury. *Invest. Ophthalmol. Vis. Sci.* 54, 5456–5465. doi:10.1167/iovs.13-11623

Azadi, S., Johnson, L. E., Paquet-Durand, F., Perez, M. R., Zhang, Y., Ekström, P. A. R., et al. (2007). CNTF+BDNF treatment and neuroprotective pathways in the rd1 mouse retina. *Brain Res.* 1129, 116–129. doi:10.1016/j.brainres.2006.10.031

Baek, J. Y., Jeong, J. Y., Kim, K. I., Won, S., Chung, Y. C., Nam, J. H., et al. (2018). Inhibition of microglia-derived oxidative stress by ciliary neurotrophic factor protects dopamine neurons *in vivo* from MPP$^+$ neurotoxicity. *Int. J. Mol. Sci.* 19, 3543. doi:10.3390/ijms19113543

Beurrier, C., Faideau, M., Bennouar, K., Escartin, C., Kerkerian-Le Goff, L., Bonvento, G., et al. (2010). Ciliary neurotrophic factor protects striatal neurons against excitotoxicity by enhancing glial glutamate uptake. *Plos One* 5, e8550. doi:10.1371/journal.pone.0008550

Campbell, L. J., Hobgood, J. S., Jia, M., Boyd, P., Hipp, R. I., and Hyde, D. R. (2021). Notch3 and DeltaB maintain Müller glia quiescence and act as negative regulators of regeneration in the light-damaged zebrafish retina. *Glia* 69, 546–566. doi:10.1002/glia.23912

Conedera, F. M., Pousa, A. M. Q., Mercader, N., Tschopp, M., and Enzmann, V. (2019). Retinal microglia signaling affects Müller cell behavior in the zebrafish following laser injury induction. *Glia* 67, 1150–1166. doi:10.1002/glia.23601

Conner, C., Ackerman, K. M., Lahne, M., Hobgood, J. S., and Hyde, D. R. (2014). Repressing notch signaling and expressing TNFα are sufficient to mimic retinal regeneration by inducing Müller glial proliferation to generate committed progenitor cells. *J. Neurosci. Official J. Soc. Neurosci.* 34, 14403–14419. doi:10.1523/JNEUROSCI.0498-14.2014

Elsaeidi, F., Bemben, M. A., Zhao, X., and Goldman, D. (2014). Jak/Stat signaling stimulates zebrafish optic nerve regeneration and overcomes the inhibitory actions of Socs3 and Sfpq. *J. Neurosci. Official J. Soc. Neurosci.* 34, 2632–2644. doi:10.1523/JNEUROSCI.3898-13.2014

Elsaeidi, F., Macpherson, P., Mills, E. A., Jui, J., Flannery, J. G., and Goldman, D. (2018). Notch suppression collaborates with Ascl1 and Lin28 to unleash a regenerative response in fish retina, but not in mice. *J. Neurosci.* 38, 2246–2261. doi:10.1523/JNEUROSCI.2126-17.2018

Fimbel, S. M., Montgomery, J. E., Burket, C. T., and Hyde, D. R. (2007). Regeneration of inner retinal neurons after intravitreal injection of ouabain in zebrafish. *J. Neurosci.* 27, 1712–1724. doi:10.1523/JNEUROSCI.5317-06.2007

Garner, K. M., Amin, R., Johnson, R. W., Scarlett, E. J., and Burton, M. D. (2018). Microglia priming by interleukin-6 signaling is enhanced in aged mice. *J. Neuroimmunol.* 324, 90–99. doi:10.1016/j.jneuroim.2018.09.002

Hao, Y., Hao, S., Andersen-Nissen, E., Mauck, W. M., Zheng, S., Butler, A., et al. (2021). Integrated analysis of multimodal single-cell data. *Cell* 184, 3573–3587.e29. doi:10.1016/j.cell.2021.04.048

Hoang, T., Wang, J., Boyd, P., Wang, F., Santiago, C., Jiang, L., et al. (2020). Gene regulatory networks controlling vertebrate retinal regeneration. *Science* 370, eabb8598. doi:10.1126/science.abb8598

Hu, Z., Deng, N., Liu, K., Zhou, N., Sun, Y., and Zeng, W. (2020). CNTF-STAT3-IL-6 Axis mediates neuroinflammatory cascade across schwann cell-neuron-microglia. *Cell Rep.* 31, 107657. doi:10.1016/j.celrep.2020.107657

Iribarne, M., Hyde, D. R., and Masai, I. (2019). TNFα induces müller glia to transition from non-proliferative gliosis to a regenerative response in mutant zebrafish presenting chronic photoreceptor degeneration. *Front. Cell Dev. Biol.* 7, 296. doi:10.3389/fcell.2019.00296

Jeong, K. H., Nam, J. H., Jin, B. K., and Kim, S. R. (2015). Activation of CNTF/CNTFRα signaling pathway by hRheb(S16H) transduction of dopaminergic neurons *in vivo*. *Plos One* 10, e0121803. doi:10.1371/journal.pone.0121803

Kahn, M. A., Ellison, J. A., Speight, G. J., and de Vellis, J. (1995). CNTF regulation of astrogliosis and the activation of microglia in the developing rat central nervous system. *Brain Res.* 685, 55–67. doi:10.1016/0006-8993(95)00411-i

Kassen, S. C., Thummel, R., Campochiaro, L. A., Harding, M. J., Bennett, N. A., and Hyde, D. R. (2009). CNTF induces photoreceptor neuroprotection and Müller glial cell proliferation through two different signaling pathways in the adult zebrafish retina. *Exp. Eye Res.* 88, 1051–1064. doi:10.1016/j.exer.2009.01.007

Lahne, M., Brecker, M., Jones, S. E., and Hyde, D. R. (2021). The regenerating adult zebrafish retina recapitulates developmental fate specification programs. *Front. Cell Dev. Biol.* 8, 617923. doi:10.3389/fcell.2020.617923

Lahne, M., Li, J., Marton, R. M., and Hyde, D. R. (2015). Actin-cytoskeleton- and rock-mediated INM are required for photoreceptor regeneration in the adult zebrafish retina. *J. Neurosci.* 35, 15612–15634. doi:10.1523/JNEUROSCI.5005-14.2015

Lahne, M., Nagashima, M., Hyde, D. R., and Hitchcock, P. F. (2020). Reprogramming müller glia to regenerate retinal neurons. *Annu. Rev. Vis. Sci.* 6, 171–193. doi:10.1146/annurev-vision-121219-081808

Lahne, M., Piekos, S. M., O'Neill, J., Ackerman, K. M., and Hyde, D. R. (2019). Photoregulation of rod precursor cell proliferation. *Exp. Eye Res.* 178, 148–159. doi:10.1016/j.exer.2018.09.015

Leibinger, M., Andreadaki, A., Diekmann, H., and Fischer, D. (2013). Neuronal STAT3 activation is essential for CNTF- and inflammatory stimulation-induced CNS axon regeneration. *Cell Death Dis.* 4, e805. doi:10.1038/cddis.2013.310

Leibinger, M., Müller, A., Andreadaki, A., Hauk, T. G., Kirsch, M., and Fischer, D. (2009). Neuroprotective and axon growth-promoting effects following inflammatory stimulation on mature retinal ganglion cells in mice depend on ciliary neurotrophic factor and leukemia inhibitory factor. *J. Neurosci.* 29, 14334–14341. doi:10.1523/JNEUROSCI.2770-09.2009

Li, S., Sato, K., Gordon, W. C., Sendtner, M., Bazan, N. G., and Jin, M. (2018). Ciliary neurotrophic factor (CNTF) protects retinal cone and rod photoreceptors by suppressing excessive formation of the visual pigments. *J. Biol. Chem.* 293, 15256–15268. doi:10.1074/jbc.RA118.004008

Li, Y., Tao, W., Luo, L., Huang, D., Kauper, K., Stabila, P., et al. (2010). CNTF induces regeneration of cone outer segments in a rat model of retinal degeneration. *Plos One* 5, e9495. doi:10.1371/journal.pone.0009495

Lipinski, D. M., Barnard, A. R., Singh, M. S., Martin, C., Lee, E. J., Davies, W. I. L., et al. (2015). CNTF gene therapy confers lifelong neuroprotection in a mouse model of human retinitis pigmentosa. *Mol. Ther.* 23, 1308–1319. doi:10.1038/mt.2015.68

Lourenço, R., Brandão, A. S., Borbinha, J., Gorgulho, R., and Jacinto, A. (2021). Yap regulates müller glia reprogramming in damaged zebrafish retinas. *Front. Cell Dev. Biol.* 9, 667796. doi:10.3389/fcell.2021.667796

Mitchell, D. M., Sun, C., Hunter, S. S., New, D. D., and Stenkamp, D. L. (2019). Regeneration associated transcriptional signature of retinal microglia and macrophages. *Sci. Rep.* 9, 4768. doi:10.1038/s41598-019-41298-8

Morris, A. C., Scholz, T., and Fadool, J. M. (2008). Rod progenitor cells in the mature zebrafish retina. *Adv. Exp. Med. Biol.* 613, 361–368. doi:10.1007/978-0-387-74904-4_42

Murakami, M., Kamimura, D., and Hirano, T. (2019). Pleiotropy and specificity: Insights from the interleukin 6 family of cytokines. *Immunity* 50, 812–831. doi:10.1016/j.immuni.2019.03.027

Nahlé, S., Pasquin, S., Laplante, V., Rousseau, F., Sharma, M., and Gauchat, J. (2019). Cardiotrophin-like cytokine (CLCF1) modulates mesenchymal stem cell osteoblastic differentiation. *J. Biol. Chem.* 294, 11952–11959. doi:10.1074/jbc.AC119.008361

Nasevicius, A., and Ekker, S. C. (2000). Effective targeted gene 'knockdown' in zebrafish. *Nat. Genet.* 26, 216–220. doi:10.1038/79951

Nelson, C. M., Ackerman, K. M., O'Hayer, P., Bailey, T. J., Gorsuch, R. A., and Hyde, D. R. (2013). Tumor necrosis factor-alpha is produced by dying retinal neurons and is required for müller glia proliferation during zebrafish retinal regeneration. *J. Neurosci.* 33, 6524–6539. doi:10.1523/JNEUROSCI.3838-12.2013

Nelson, C. M., Gorsuch, R. A., Bailey, T. J., Ackerman, K. M., Kassen, S. C., and Hyde, D. R. (2012). Stat3 defines three populations of Müller glia and is required for initiating maximal müller glia proliferation in the regenerating zebrafish retina. *J. Comp. Neurol.* 520, 4294–4311. doi:10.1002/cne.23213

Ogai, K., Kuwana, A., Hisano, S., Nagashima, M., Koriyama, Y., Sugitani, K., et al. (2014). Upregulation of leukemia inhibitory factor (LIF) during the early stage of optic nerve regeneration in zebrafish. *Plos One* 9, e106010. doi:10.1371/journal.pone.0106010

Recasens, M., Almolda, B., Pérez-Clausell, J., Campbell, I. L., González, B., and Castellano, B. (2021). Chronic exposure to IL-6 induces a desensitized phenotype of the microglia. *J. Neuroinflammation* 18, 31. doi:10.1186/s12974-020-02063-1

Rezende, L. F., Vieira, A. S., Negro, A., Langone, F., and Boschero, A. C. (2009). Ciliary neurotrophic factor (CNTF) signals through STAT3–SOCS3 pathway and protects rat pancreatic islets from cytokine-induced apoptosis. *Cytokine* 46, 65–71. doi:10.1016/j.cyto.2008.12.014

Rhee, K. D., Nusinowitz, S., Chao, K., Yu, F., Bok, D., and Yang, X. (2013). CNTF-mediated protection of photoreceptors requires initial activation of the cytokine receptor gp130 in Müller glial cells. *Proc. Natl. Acad. Sci. U. S. A.* 110, E4520–E4529. doi:10.1073/pnas.1303604110

Samuel, D., Aldrich Thomas, H., Neil, S., Li, P., Tetsuya, T., Tadamitsu, K., et al. (1993). LIFRβ and gp130 as heterodimerizing signal transducers of the tripartite CNTF receptor. *Science* 260, 1805–1808. doi:10.1126/science.8390097

Savin, V. J., Sharma, M., Zhou, J., Gennochi, D., Fields, T., Sharma, R., et al. (2015). Renal and hematological effects of CLCF-1, a B-Cell-Stimulating cytokine of the IL-6 family. *J. Immunol. Res.* 2015, 714964. doi:10.1155/2015/714964

Sherpa, T., Fimbel, S. M., Mallory, D. E., Maaswinkel, H., Spritzer, S. D., Sand, J. A., et al. (2008). Ganglion cell regeneration following whole-retina destruction in zebrafish. *Dev. Neurobiol.* 68, 166–181. doi:10.1002/dneu.20568

Sieving, P. A., Caruso, R. C., Tao, W., Coleman, H. R., Thompson, D. J. S., Fullmer, K. R., et al. (2006). Ciliary neurotrophic factor (CNTF) for human retinal degeneration: Phase I

trial of CNTF delivered by encapsulated cell intraocular implants. *Proc. Natl. Acad. Sci. U. S. A.* 103, 3896–3901. doi:10.1073/pnas.0600236103

Stahl, N., and Yancopoulos, G. D. (1994). The tripartite CNTF receptor complex: Activation and signaling involves components shared with other cytokines. *J. Neurobiol.* 25, 1454–1466. doi:10.1002/neu.480251111

Tao, W., Wen, R., Goddard, M. B., Sherman, S. D., O'Rourke, P. J., Stabila, P. F., et al. (2002). Encapsulated cell-based delivery of CNTF reduces photoreceptor degeneration in animal models of retinitis pigmentosa. *Invest. Ophthalmol. Vis. Sci.* 43, 3292–3298.

Thummel, R., Bailey, T.,J., and Hyde, D.,R. (2011). *In vivo* electroporation of morpholinos into the adult zebrafish retina. *Jove* 23, e3603. doi:10.3791/3603

Ueki, Y., and Reh, T. A. (2013). EGF stimulates müller glial proliferation via a BMP-dependent mechanism. *Glia* 61, 778–789. doi:10.1002/glia.22472

Wan, J., and Goldman, D. (2017). Opposing actions of Fgf8a on notch signaling distinguish two muller glial cell populations that contribute to retina growth and regeneration. *Cell Rep.* 19, 849–862. doi:10.1016/j.celrep.2017.04.009

Wan, J., and Goldman, D. (2016). Retina regeneration in zebrafish. *Curr. Opin. Genet. Dev.* 40, 41–47. doi:10.1016/j.gde.2016.05.009

Wan, J., Ramachandran, R., and Goldman, D. (2012). HB-EGF is necessary and sufficient for müller glia dedifferentiation and retina regeneration. *Dev. Cell* 22, 334–347. doi:10.1016/j.devcel.2011.11.020

Wan, J., Zhao, X., Vojtek, A., and Goldman, D. (2014). Retinal injury, growth factors, and cytokines converge on β-catenin and pStat3 signaling to stimulate retina regeneration. *Cell Rep.* 9, 285–297. doi:10.1016/j.celrep.2014.08.048

Wang, Y., Rhee, K., Pellegrini, M., and Yang, X. (2020). Impacts of ciliary neurotrophic factor on the retinal transcriptome in a mouse model of photoreceptor degeneration. *Sci. Rep.* 10, 6593. doi:10.1038/s41598-020-63519-1

White, U. A., and Stephens, J. M. (2011). The gp130 receptor cytokine family: Regulators of adipocyte development and function. *Curr. Pharm. Des.* 17, 340–346. doi:10.2174/138161211795164202

Wilson, S. G., Wen, W., Pillai-Kastoori, L., and Morris, A. C. (2016). Tracking the fate of her4 expressing cells in the regenerating retina using her4:Kaede zebrafish. *Exp. Eye Res.* 145, 75–87. doi:10.1016/j.exer.2015.11.002

Zhang, K., Hopkins, J. J., Heier, J. S., Birch, D. G., Halperin, L. S., Albini, T. A., et al. (2011). Ciliary neurotrophic factor delivered by encapsulated cell intraocular implants for treatment of geographic atrophy in age-related macular degeneration. *Proc. Natl. Acad. Sci. U. S. A.* 108, 6241–6245. doi:10.1073/pnas.1018987108

Zhao, X., Wan, J., Powell, C., Ramachandran, R., Myers, M. G., Jr, and Goldman, D. (2014). Leptin and IL-6 family cytokines synergize to stimulate Müller glia reprogramming and retina regeneration. *Cell Rep.* 9, 272–284. doi:10.1016/j.celrep.2014.08.047

Zygar, C. A., Colbert, S., Yang, D., and Fernald, R. D. (2005). IGF-1 produced by cone photoreceptors regulates rod progenitor proliferation in the teleost retina. *Dev. Brain Res.* 154, 91–100. doi:10.1016/j.devbrainres.2004.10.009

frontiers | Frontiers in Cell and Developmental Biology

TYPE Original Research
PUBLISHED 22 February 2023
DOI 10.3389/fcell.2023.1105657

OPEN ACCESS

EDITED BY
David Wei Chang,
University of Texas MD Anderson Cancer Center, United States

REVIEWED BY
Ross F Collery,
Medical College of Wisconsin, United States
Ghulam Mohammad,
Wayne State University, United States

*CORRESPONDENCE
Glenn P. Lobo,
lobo0023@umn.edu

SPECIALTY SECTION
This article was submitted to Molecular and Cellular Pathology, a section of the journal Frontiers in Cell and Developmental Biology

RECEIVED 22 November 2022
ACCEPTED 07 February 2023
PUBLISHED 22 February 2023

CITATION
Radhakrishnan R, Leung M, Solanki AK and Lobo GP (2023), Mapping of the extracellular RBP4 ligand binding domain on the RBPR2 receptor for Vitamin A transport.
Front. Cell Dev. Biol. 11:1105657.
doi: 10.3389/fcell.2023.1105657

Mapping of the extracellular RBP4 ligand binding domain on the RBPR2 receptor for Vitamin A transport

Rakesh Radhakrishnan[1], Matthias Leung[1], Ashish K. Solanki[2] and Glenn P. Lobo[1,2,3]*

[1]Department of Ophthalmology, University of Minnesota, Minneapolis, MN, United States, [2]Department of Medicine, Medical University of South Carolina, Charleston, SC, United States, [3]Department of Ophthalmology, Medical University of South Carolina, Charleston, SC, United States

The distribution of dietary vitamin A/all-*trans* retinol/ROL throughout the body is critical for maintaining retinoid function in peripheral tissues and for retinoid delivery to the eye in the support of visual function. In the circulation, all-*trans*-retinol bound to the RBP4 protein is transported and sequestered into target tissues for long-term storage. Two membrane receptors that facilitate all-*trans* retinol uptake from RBP4 have been proposed. While it is well established that the membrane receptor, STRA6, binds to circulatory RBP4 for ROL transport into the eye, the second vitamin A receptor, RBPR2, which is expressed in non-ocular tissues, is less characterized. Based on the structural homology between these two RBP4 receptors, published literature, and from our recent work in *Rbpr2*$^{-/-}$ deficient mice, we hypothesized that RBPR2 might also have high-binding affinity for RBP4 and this mechanism facilitates ROL transport. Herein, we aimed to elucidate the membrane topology and putative RBP4 binding residues on RBPR2 to understand its physiological function for retinoid homeostasis. Using *in silico* analysis and site-directed mutagenesis, we identified a potential RBP4 binding domain on RBPR2. We employed an *in vitro* cell-based system and confirmed that mutations of these residues on RBPR2 affected its binding to exogenous RBP4 and subsequently vitamin A uptake. Using Surface Plasmon Resonance assays, we analyzed both the binding affinities and kinetic parameters of wild-type RBPR2 and individual mutants affecting the RBPR2-RBP4 binding domain with its physiological ligand RBP4. These studies not only revealed a putative RBP4 binding domain on RBPR2 but also provided new structural, biochemical, and critical information on its proposed role in RBP4 binding for ROL transport and retinoid homeostasis.

KEYWORDS

vitamin A, RBP4, Rbpr2, STRA6, all-trans retinol

Abbreviations: ROL, all-*trans* retinol; 11-*cis* RAL, 11-*cis* retinaldehyde; RBPR2, Retinol binding protein 4 receptor 2; LRAT, Lecithin:ROL acyltransferase; RA, all-*trans* retinoic acid; STRA6, stimulated by retinoic acid protein 6; RBP4, Retinol binding protein 4; Stra6l, Stimulated by retinoic acid protein 6 like.

Introduction

All-*trans* retinol (ROL) is the major form of vitamin A found within circulation. It is essential for normal embryonic development, reproduction, immunity, and is critical for ocular retinoid (von Lintig, 2012; Sun, 2012; Wassef and Quadro, 2011; D'Ambrosio et al., 2011). Within tissues, ROL is the precursor for all-*trans* retinoic acid (RA), an essential ligand for nuclear receptors such as the retinoic acid receptor (RAR), which regulate gene transcription. ROL is also the precursor for 11-*cis* retinaldehyde (RAL), the essential visual chromophore that isomerizes through exposure to light, and by extension allows photoreceptor cells to detect light (von Lintig, 2012; Borel and Desmarchelier, 2017). Humans cannot synthesize vitamin A *de novo*, so all vitamin A and its derivatives in the human body, collectively called retinoids, originate from dietary consumption of vitamin A precursors (von Lintig, 2012; Borel and Desmarchelier, 2017). The bulk of dietary retinoids (80%–85%) are stored within the liver as retinyl esters (RE). Under fasting conditions, the liver is responsible for maintaining retinoic homeostasis through the conversion of its RE storage into ROL, and secreting ROL bound to retinol binding protein 4 (RBP4) into the bloodstream. (Biesalski et al., 1999; Quadro et al., 1999; Kawaguchi et al., 2007; Harrison, 2012; Lobo et al., 2012; Amengual et al., 2014; Kelly and von Lintig, 2015; Borel and Desmarchelier, 2017).

For retinol to perform its biological function it must first be absorbed within cells and this requires membrane receptors specific to the complex formed by RBP4 and retinol (RBP4-ROL) (Harrison, 2012; Lobo et al., 2012). Currently, two membrane receptors that facilitate the uptake of retinol from circulatory RBP4-ROL have been proposed (von Lintig, 2012; Kawaguchi et al., 2007; Kelly and von Lintig, 2015; Amengual et al., 2014). In 2007, the Sun lab discovered the stimulated by retinoic acid 6 (STRA6) cell membrane receptor, which is proposed to transport retinol intracellularly from circulatory RBP4-ROL into target tissues, such as the eye (Kawaguchi et al., 2007). STRA6 is highly expressed in blood-organ barrier structures and organs that require high amounts of retinoid for proper function, such as the retinal pigment epithelium (RPE), reproductive organs, brain, and kidney (Amengual et al., 2014; Kelly and von Lintig, 2015) Correspondingly, Matthew-Wood Syndrome is characterized by visual abnormalities and developmental problems linked to mutations in the human *STRA6* gene (Golzio et al., 2007; Pasutto et al., 2007; Isken et al., 2008). Studies from the von Lintig lab and others have genetically confirmed in zebrafish and mouse models the importance of STRA6 for vitamin A homeostasis of peripheral tissues, where severe ocular defects were reported in animals lacking STRA6 (Isken et al., 2008; Berry et al., 2013; Amengual et al., 2014; Kelly and von Lintig, 2015). To understand the importance of STRA6 in RBP4 binding for ROL transport, the Sun lab used a large-scale mutagenesis approach and identified an essential RBP4 binding domain in STRA6, where they showed that mutations within individual amino acid residues within this RBP4 binding domain affects binding of STRA6 to exogenous RBP4, and this consequently affected ROL transport (Kawaguchi et al., 2008a; Kawaguchi et al., 2008b; Kawaguchi and Sun, 2010; Sun and Kawaguchi, 2011). From these studies, it is apparent that membrane receptors that interact with RBP4-ROL, such as STRA6, must contain one or more binding residues/domains, which are essential for receptor binding to circulatory RBP4 for ROL internalization into target tissues, such as the eye (Golzio et al., 2007; Pasutto et al., 2007; Isken et al., 2008; Kawaguchi et al., 2008a; Kawaguchi et al., 2008b; Kawaguchi and Sun, 2010; Sun and Kawaguchi, 2011; Berry et al., 2013).

Another less studied receptor for RBP4 binding and ROL transport is the retinol binding protein 4 receptor 2 (RBPR2) protein, also annotated as STRA6like (Alapatt et al., 2013; Shi et al., 2017; Lobo et al., 2018; Radhakrishnan et al., 2022a). RBPR2 was first identified by the Graham group in 2013, where they proposed its function in the regulation of retinol homeostasis in the liver and in non-ocular tissues (Alapatt et al., 2013). RBPR2 is expressed both in zebrafish and mouse liver, intestine, and other non-ocular tissues, but not in the eye. As such, RBPR2 could act as the RBP4-ROL receptor in these STRA6 lacking tissues, contributing to the maintenance of proper ocular retinoid concentrations for retinal homeostasis and visual function through the regulation of serum retinoid homeostasis (Shi et al., 2017; Lobo et al., 2018; Martin et al., 2021; Radhakrishnan et al., 2022a). Our recent study in *Rbpr2* knockout (*Rbpr2*$^{-/-}$) mice showed that under vitamin A deficient diets, *Rbpr2*$^{-/-}$ mice failed to maintain retinal function and showed decreased systemic and ocular retinoid concentrations, which manifested as photoreceptor phenotypes (Radhakrishnan et al., 2022a). These *Rbpr2*$^{-/-}$ mice also displayed an imbalance in opsin pigment synthesis and stoichiometry, resulting in decreased visual function, when compared to control mice on similar vitamin A diets (Radhakrishnan et al., 2022a). While the observed ocular phenotypic changes in mice lacking a systemic membrane receptor for RBP4-ROL are apparent, the coordination between retinol consumption in the eye for vision and retinol supply from long-term storage at the systemic level, is one of the less characterized areas in understanding retinoid homeostasis. Even less characterized is the non-ocular RBP4 receptor RBPR2 itself, its mechanisms for RBP4 binding and ROL transport in target tissues, and its role for retinoid homeostasis (Kelly and von Lintig, 2015; Borel and Desmarchelier, 2017; Solanki et al., 2020; Martin et al., 2021; Radhakrishnan et al., 2022a). In this study, we aimed to identify putative RBP4 binding residues on the membrane receptor, RBPR2, to establish the importance of these RBP4 binding residues on RBPR2 for ROL transport.

Materials and methods

Materials

All chemicals, unless stated otherwise were purchased from Sigma-Aldrich (St. Louis, MO, United States).

Homology modeling and molecular docking

Online server SWISS-MODEL (http://swissmodel.expasy.org/) was used to generate homology based models of mouse RBPR2, mouse STRA6, and zebrafish Stra6. The model with maximum coverage and lowest Z score for each was selected for further studies. The template selected (by online server SWISS-MODEL) was the cryoEM structure of STRA6, receptor for retinol (PDB ID

5sy1, Chain B) which showed nearly 44% sequence identity and Q mean close to −5 for STRA6 identity; and nearly 22% sequence identity and Q mean close to −7 for RBPR2. The structure for RBP4 was obtained from PDB database (RSCB PDB ID: 2wqa, Chain E). The models generated were used for docking studies to analyze the protein-protein interactions employing the online data-driven docking program HADDOCK. HADDOCK requires a set of ambiguous interaction restraints (AIRs) at the binding interface that are divided into "active" and "passive" categories where active residues are those directly implicated in binding from experimental data and passive residues are their near neighbors. The docking process included a rigid body energy minimization step. The residues S294, Y295 and L296 for mouse RBPR2 were assigned as active residues for interaction as per the previous published papers to be essential for binding (Alapatt et al., 2013; Chen et al., 2016). The residues between 8 and 12 Å from these three residues were defined as passive. HADDOCK clustered 187 structures in 11 cluster (s), which represents 93.5% of the water-refined models HADDOCK generated for RBP4-Stra6. HADDOCK clustered 138 structures in 12 cluster(s), which represents 69.0% of the water-refined models HADDOCK generated for RBP4-RBPR22. The top cluster with the minimal haddock scores of −95.1 +/− 2.0; and lowest Z-score of −1.5 for RBP4-RBPR2 was selected for analysis (van Zundert et al., 2016; Waterhouse et al., 2018).

Cloning of the mouse *Rbpr2* cDNA

Total RNA (~2 µg) from liver of a 2-month-old wild-type C57/B6 mouse was reverse transcribed using the SuperScript One-Step RT-PCR for LongTemplates system (Invitrogen, Grand Island, NY). The full-length mouse *Rbpr2* cDNA was amplified by using mouse gene specific *Rbpr2* primers with the Expand High Fidelity PCR system (Roche, Indianapolis, IN, USA). The amplified *Rbpr2* cDNA product was cloned in frame into the pCDNA3.1 V5/His TOPO vector (Invitrogen, Carlsbad, CA). Appropriate construction of the wild-type *Rbpr2* plasmid in the pCDNA 3.1 V5/His TOPO vector (pRbpr2-V5) was verified by sequence analysis of both strands (GENEWIZ, USA) and by comparing the sequences to the reference mouse *Rbpr2*/Stra6like cDNA sequences deposited in Ensembl (www.ensembl.org). The WT-Rbpr2 plasmid was used as a template and mutagenic Rbpr2 primer pairs were used to engineer each of the RBP4 binding residue mutants by *in vitro* site-directed mutagenesis (Quick Change II XL: Stratagene/Agilent, Santa Clara, CA), as previously achieved (Shi et al., 2017; Solanki et al., 2020). Appropriate construction of the WT-Rbpr2 and mutant-Rbpr2 plasmids were verified by DNA sequence analysis of both strands using pCDNA3.1 vector primers (GENEWIZ, USA).

Generation of stable cell lines expressing Rbpr2 and Rbpr2/lrat

Mouse NIH3T3 cells obtained from American Type Tissue Culture (ATCC-1658) were maintained in high-glucose DMEM supplemented with 10% FBS and 1% penicillin-streptomycin sulfate and cultured at 37°C with 5% CO_2. NIH3T3 cells were used in this experiment as they are a well-established cell line to study the *in vitro* function of vitamin A membrane receptors for RBP4 binding and ROL transport (Amengual et al., 2014; Shi et al., 2017; Lobo et al., 2018; Solanki et al., 2020). To generate constitutively expressing mouse RBPR2 in NIH3T3 cells, parental NIH3T3 or NIH3T3/LRAT expressing cells were transiently transfected with the pRbpr2-V5 plasmid, as described previously (Solanki et al., 2020). Approximately 40 h post transfection, media was replaced to contain 400 µg/mL Geneticin (G418) selection agent. After 2 weeks of selection with G418, surviving individual cells (n = 12) were selected by placing cloning rings around each surviving cell. Each clonal cell was then carefully detached by adding 10 µL of trypsin into each clonal ring. Detached cells were transferred to 6-well culture plates containing 200 µg/mL G418 selection media. Once individual clones reached ~80% confluence they were expanded into 100 mm dishes containing 200 µg/mL of G418 selection media. To confirm stable integration of the Rbpr2 gene and expression in these cells, we isolated total protein from each clone and subject them to western blot analysis. By using the V5-primary antibody, we detected the V5-tagged RBPR2 protein.

Indirect immunofluorescence and confocal microscopy

Cell lines were grown on coverslips and fixed in a freshly prepared mixture of 4% formaldehyde in 1X PBS (137 mM NaCl, 2.7 mM KCl, 10 mM sodium phosphate dibasic, and 2 mM potassium phosphate monobasic, pH 7.4) for 30 min at room temperature and processed as previously described (Lobo et al., 2010; Lobo et al., 2013; Solanki et al., 2020; Solanki et al., 2021). Parental NIH3T3 cells were transiently transfected with the pRbpr2-V5 plasmid, as described previously (Solanki et al., 2020). Subcellular localization of the recombinant mouse Rbpr2-V5 in NIH3T3 cells was achieved by exposure to the anti-V5 primary antibody (which detects the V5-tagged RBPR2) followed by the anti-rabbit conjugated Alexa 488 secondary antibody staining (Invitrogen, Carlsbad, CA). Cells were examined under a Zeiss LSM 510 UV Meta confocal microscope with an HCX Plan × 40 numerical aperture 1.4 oil immersion objective lens (Zeiss, Jena, Germany). Images were acquired with the Zeiss confocal software, version 2.0. All experiments were carried out in triplicate. Approximately 55–75 cells from 7–9 fields were imaged/counted per experiment (Lobo et al., 2010; Lobo et al., 2013; Rohrer et al., 2021).

Exogenous RBP4 binding and retinol uptake studies

RBP4 cDNA cloned into the pET3a bacterial expression vector was used to express RBP4 in *E.Coli* as previously described (Shi et al., 2017). Apo-RBP4 (100 µg) was loaded with retinol in 0.2 mL of PBS by the addition of 100 µm radiolabeled retinol (American Radiolabeled Chemicals; vitamin A alcohol [3H(N)] Retinol-labeled, adjusted to 1 µCi/nmol specific activity by the addition of cold retinol) and incubating for 1 h at room temperature and then

overnight at 4°C in light-protected tubes, as previously described (Shi et al., 2017). Stable NIH3T3 cells expressing either, RBPR2 or RBPR2 and LRAT were plated in 10 cm dishes. Cells were grown to 70% confluence, washed thrice with 1x PBS and incubated for 1 h in serum-free medium, at which point [^{3}H]ROL-RBP4 was added for 60 min. Cells were washed thrice with 1x PBS and lysed in PBS containing 1% Nonidet P-40. Lysates were homogenized and transferred to scintillation tubes for scintillation counting. Parental NIH3T3 incubated with [^{3}H]ROL-RBP4 served as controls. The RBP4-ROL binding and uptake assay was repeated thrice, using stable cells from a different passage.

Expression and purification of human RBP4

Human RBP4 expression and purification from *Escherichia coli* was accomplished essentially as described previously (Shi et al., 2017). Briefly, human RBP4 (hRBP4) cDNA was cloned into a pET3a expression vector and expressed in BL-21 DE3 cells according to a standard protocol. Bacterial cells were harvested and lysed by osmotic shock. Insoluble material was pelleted by centrifugation, washed, and solubilized in 7M guanidine hydrochloride and 10 mM dithiothreitol. After overnight incubation, insoluble material was removed by ultracentrifugation, and the supernatant was used for the hRBP4 refolding procedure. hRBP4 was refolded by the dropwise addition of solubilized material into a mixture containing 150 µCi of [11,12-^{3}H]ROL ([^{3}H]ROL) (PerkinElmer Life Sciences) and non-radiolabeled ROL (Sigma) at a final concentration of 1 mm. Refolded holo-hRBP4 was dialyzed against 10 mM Tris/HCl buffer, pH 8.0, and loaded onto a DE53 anion exchange chromatography column (Whatman, Piscataway, NJ). Holo-hRBP4 was eluted with linear gradient of NaCl (0–1M) in 10 mM Tris/HCl buffer, pH 8.0. Collected fractions were examined by SDS-PAGE and UV-visible spectroscopy to ensure a proper protein/retinoid ratio. Fractions containing at least 90% holo-hRBP4 were pooled together and concentrated in a Centricon centrifugal filter device (cut-off 10,000 Da) (Millipore, Billerica, MA) to 5 mg/mL. [^{3}H]ROL was quantified in a scintillation counter (Beckman Coulter, Indianapolis, IN). Holo-hRBP4 aliquots were stored at −80°C until used.

Western blotting

Total proteins from cells were extracted using the M-PER protein lysis buffer (ThermoScientific, Beverly, MA, United States) containing protease inhibitors (Roche, Indianapolis, IN, United States). Approximately 25 µg of total protein was electrophoresed on 4%–12% SDS-PAGE gels and transferred to PVDF membranes. Membranes were probed with primary antibodies against EGFR (1:1,000; ThermoFisher/Invitrogen, Waltham, MA), HSP90 (1:2500; Invitrogen, Waltham, MA), V5 (1:2500; Sigma/Millipore, Burlington, MA), Rbp4 (1:1,000; Proteintech/Fisher Scientific, Pittsburg, PA), or β-Actin (1:10,000, Sigma) in antibody buffer (0.2% Triton X-100, 2% BSA, 1X PBS). HRP-conjugated secondary antibodies (BioRad, Hercules, CA, United States) were used at 1:10,000 dilution. Protein expression was detected using a LI-COR Odyssey or ChemiDoc Bio-Rad system, and relative intensities of each band were quantified (densitometry) using ImageJ software version 1.49 and normalized to their respective loading controls. Each western blot analysis was repeated thrice.

Co-immunoprecipitation assays to determine binding of RBP4 to RBPR2

Co-immunoprecipitation (Co-IP) assays were performed with exogenous applied human RBP4 protein in NIH3T3/LRAT cells stably expressing V5-tagged WT-RBPR2 or individual V5-tagged RBPR2-RBP4 mutants. Using a well-established Co-IP protocol that determined extracellular STRA6-RBP4 interactions, we added reduced serum medium (8 mL of OptiMEM) containing 12 µM of purified and crosslinked T7 tagged-RBP4 to the cells and incubate this reaction for 60 min (Kawaguchi et al., 2007). After binding purified T7 tagged-RBP4 protein conjugated with the cross-linker to cells expressing WT or mutant RBPR2, followed by ultraviolet (UV) cross-linking, and membrane solubilization, cells were collected, washed thrice with 1x PBS to remove any un-bound hRBP4. Total protein was isolated and subjected to co-immunoprecipitation analysis using an RBP4 antibody, followed by reciprocal western blotting for RBPR2 (using a V5 antibody).

Mouse RBP4 expression, purification, and quality check by circular dichroism spectroscopy and intrinsic tryptophan fluorescence assay

Recombinant mouse RBP4 with 6XHis Tag was expressed *E.coli* expression system and extracted in Tris buffer with composition of 50 mM Tris-HCl, 1 M L-Arginine, 10% Glycerol, pH 8.0. The lysate was purified by nickel NTA column. The msRBP4 protein quality was monitored by western blot using anti His-tag antibody. The structural quality of the recombinant RBP4 protein was confirmed with Circular dichroism (CD) spectroscopy (Jasco 815 circular dichroism, Spectramax Gemini) (Micsonai et al., 2015). The mean residue ellipticity (θ), was calculated using the following formula.

$$[\theta] = (S \times mRw)/(10cl)$$

where S represents the CD signal in mθ, mRw represents the mean residue mass, c represents the concentration of the protein in mg/mL, and l represents the path length in cm. The percent change in molecules structure were calculated using BeStSel Secondary Structure Analysis to Protein Fold Prediction by CD Spectroscopy (https://bestsel.elte.hu), (see Supplementary Information Supplementary Materials S1–S5). The initial interaction quality of the recombinant RBP4 with msSTRA6, msRBPR2, and control peptides were checked with intrinsic tryptophan fluorescence assay. The peptides were diluted in various micromolar concentrations and the incubated with 3 µg RBP4 in room temperature for 5 min and excited at 290 nm and the emission was scanned from 300 nm to 400 nm wavelength. The data were normalized with the blank and peptide only conditions and

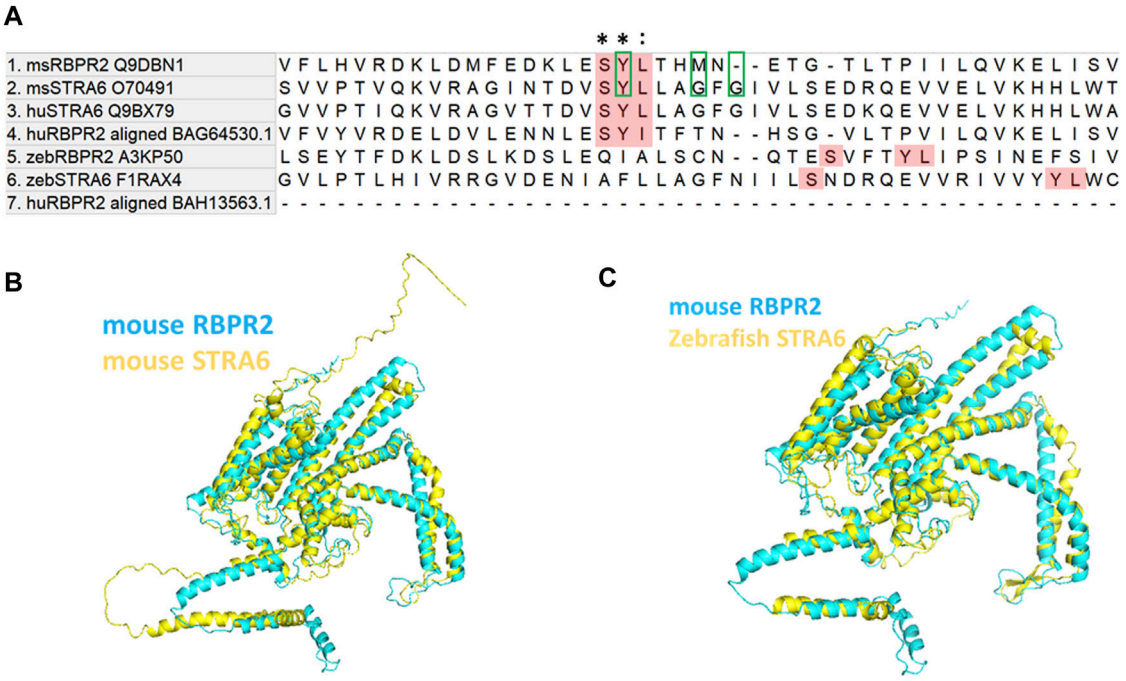

FIGURE 1
Proposed RBP4 binding residues on RBPR2 are conserved across species. **(A)** Proposed RBP4 binding residues on RBPR2 (highlighted Red; amino acid residues S294, Y295 and L296) occurs in exon 11 of mouse RBPR2 (Alapatt et al., 2013). The multiple sequence alignment of mouse and human STRA6, RBPR2 sequences shows conserved residues (Tamura et al., 2021). * indicates conserved residues of the RBP4 binding motif; (colon) indicates strongly similar properties. The previously proposed RBP4 binding residues on mouse STRA6 (Tyrosine Y336, Glycine G340, and Glycine G342) are highlighted with green box. The zebrafish STRA6 and RBPR2 sequence were not highly conserved but surprisingly had an exact topological feature alignment with the mouse sequence to extracellular region of the receptor (https://www.uniprot.org/uniprotkb/Q9DBN1/entry#sequences). **(B,C)** Computer modeling and structure homology between RBPR2 (blue) and STRA6 (yellow) proteins.

plotted in GraphPad prism version 9.3. San Diego, CA, United States. (Supplementary Figure S5).

RBPR2-RBP4 binding assays using surface plasmon resonance (SPR) analysis

Purified RBP4 protein with >90% purity and 0.56 mg/mL concentration was immobilized on Biacore Sensor Chip CM5 (ITDD Biacore S200 Surface Plasmon Resonance instrument at University of Minnesota). The two-flow cell surface activated for using one as blank and other as test. Using Amine Coupling Kit (Cat. No. BR100050; Cytiva, Marlborough, MA, US) 1-ethyl-3-(3-dimethylaminopropyl) carbodiimide hydrochloride (EDC), N-hydroxysuccinimide (NHS), after surface activation, the purified RBP4 with immobilization buffer 10 mM Sodium acetate, pH 5.0, was immobilized with target of 1,200 Response Unit (RU) for achieving Rmax of 30RU in kinetic study. The reaction stopped and washed with Ethanolamine. The system was re-primed with running buffer PBST (phosphate-buffered saline solution with a 0.05% Tween20 detergent solution). The kinetic assay performed on the two flow cells, the blank was used as reference cell and the active cell with RBP4 was used for the binding study. The mouse and zebrafish RBPR2, mouse RBPR2 mutants affecting the "SYL" binding domain, and mouse STRA6 peptides (all containing the predicted RBP4 "SYL" binding residues) were chemically synthesized by Biomatik Corporation, Kitchener, ON, Canada. The peptides were serial diluted in running buffer with range of 0.8–26.6 µM and following parameter was run with contact time: 120 s, flowrate 30 µL/min, Dissociation time 300 s, Regeneration with Glycine-HCl, pH 2.5, contact time 30 s flowrate 30 µL/min and temperature 25°C. The program was run and non-specific binding on the reference cell subtracted bulk refractive index from the active sensorgram and analyzed for the association, dissociation and stabilization of the reads. The plot fitted with 1:1 binding program in Biacore™ Insight Evaluation Software, and the Graph, binding affinity plot, was plotted in GraphPad prism version 9.3.

Results

Mouse RBPR2 contains consensus RBP4 binding residues

Comparison of mouse (*Ms*) RBPR2 protein sequences to human (*Hs*) STRA6 and *Ms* STRA6 revealed several short amino acid segments with >40% amino acid homology, suggesting analogous roles for these residues in the function or structural integrity of these two proteins (Figures 1A–C) (Kawaguchi et al., 2008a; Kawaguchi et al., 2008b; Kawaguchi and Sun, 2010; Sun and Kawaguchi, 2011; Alapatt et al., 2013). Interestingly, a three amino acid consensus was

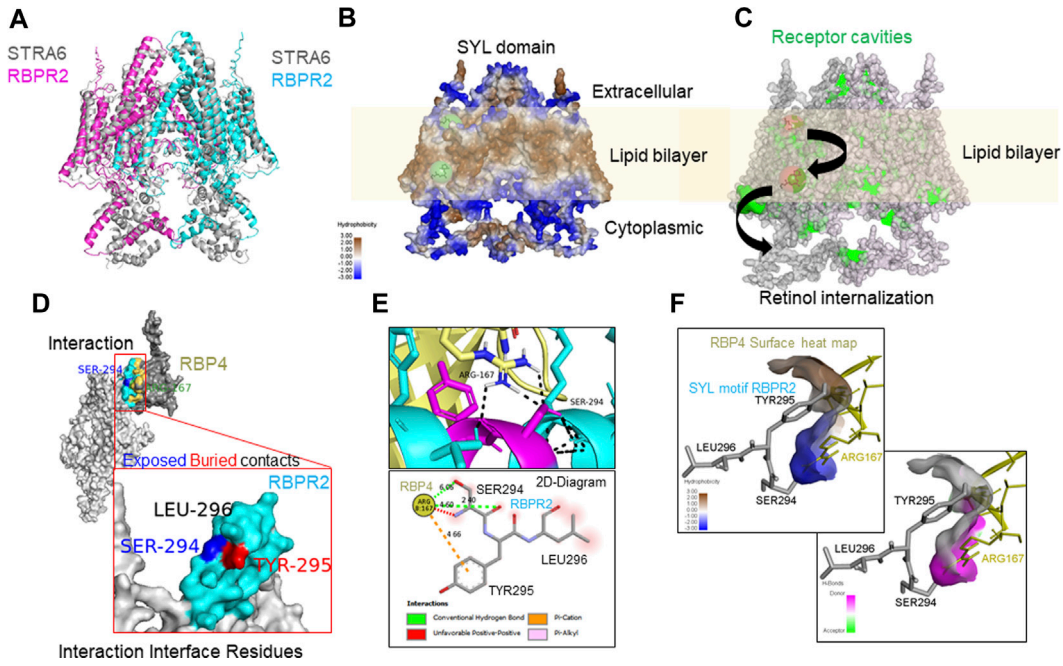

FIGURE 2
Molecular docking analysis of RBPR2-RBP4 protein interaction. **(A)** RBPR2 structural alignment with STRA6 dimer (pdb 5SY1). **(B)** Heat map indicating varying degrees of hydrophobicity within RBPR2, showing the lipid bilayer embedded regions in a RBPR2 dimer complex. The retinol binding prediction on RBPR2 dimer was performed by PyRX showing the possible regions of binding and internalization of retinol from extracellular matrix to cytosol, by utilizing the receptor cavities indicated in green on the right diagram (ref BIOVIA® Discovery Studio Visualizer v21.1). **(C)** The docking of RBPR2 monomer (Light grey) and RBP4 (Dark grey) structure showing the interactions. The interaction interface residues are color-coded, Cyan for RBPR2 residues and Yellow for RBP4. To annotate the positional exposed and buried residues information the SER-294 blue and TYR-295 Red color coded. **(D,E)** The interaction of residues and 2D-Diagram showing the mode of interactions by Hydrogen bonds, Pi-Cation, Pi-Alkyl and solvent accessible surface in Red shade. **(F)** The surface heat map of hydrophobicity and hydrogen bond of RBP4 surface showing the SYL motif of RBPR2 interacting in the pocket, analyzed by BIOVIA® Discovery Studio Visualizer v21.1.

found in the proposed RBP4 binding domain of *Hs*. And *Ms*. STRA6, which was also found to be partially conserved in mouse and zebrafish RBPR2. The proposed RBP4 binding residues in mouse RBPR2 correspond to amino acids Serine294, Tyrosine295, and Leucine296 (SYL) (Figure 1A), which have previously been shown to be required for vitamin A transport to the eye, in zebrafish (Shi et al., 2017; Lobo et al., 2018; Solanki et al., 2020).

Protein-ligand structural analysis confirms the importance of the proposed RBP4 binding residues on RBPR2 for ROL transport

To determine the importance of proposed RBP4 binding residues on mouse RBPR2, we first generated homology-based models of mouse RBPR2 and human STRA6 using the online server SWISS-MODEL (http://swissmodel.expasy.org/), using the cryogenic electron microscopy (cryoEM) structure of zebrafish STRA6 (PDB ID: 5sy1, Chain B) (Chen et al., 2016; van Zundert et al., 2016; Waterhouse et al., 2018), and human RBP4 (PDB ID: 2wqa, Chain E) (Figures 1B, C; Figures 2A, B). The models generated were then utilized in docking studies to analyze the STRA6-RBP4 and RBPR2-RBP4 protein-ligand interactions (docking program HADDOCK2.2) (Chen et al., 2016; van Zundert et al., 2016; Waterhouse et al., 2018). While the *in silico* binding models are assumptions, this analysis showed that the proposed and conserved residues SYL on mouse RBPR2 are part of an extracellular loop that likely plays a critical role in their interaction with RBP4 (Figures 2C–F) and thus stabilizing the complex interface with hydrophobic and hydrophilic contact. The 2D-Diagram shows the complex stabilized by the Conventional Hydrogen bond from Ser294 RBPR2, Pi-Cation and Pi-Alkyl from Tyr295 RBPR2 interacting with the Arg167 on RBP4. Leu296 on RBPR2 was not directly involved in the interaction interface, but could play an essential role in stabilizing the interaction with RBP4.

RBPR2-mutants targeting the proposed RBP4 binding residues show normal trafficking to the plasma membrane

To study the importance of RBP4 binding residues on RBPR2, we used site-directed mutagenesis to individually alter these putative binding residues on mouse RBPR2. Using the wild-type (WT) RBPR2-pCDNA3.1-V5 tagged vector as a template, the polar amino acids (Ser294 and Tyr295) were mutated to hydrophobic amino acids (Ser294Ala and Tyr295Pro), while the hydrophobic amino acid (Leu296) was mutated to a polar amino acid (Leu296Ser)

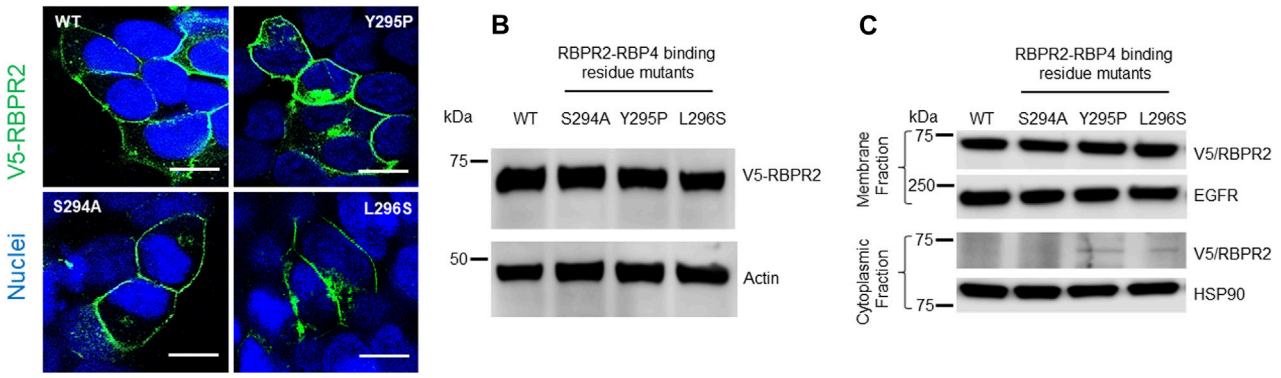

FIGURE 3
Cellular localization and expression of WT-RBPR2 and RBPR2-mutants.**(A)** Transient expression and staining of mouse V5-tagged WT-RBPR2 and variants in NIH3T3 cells using the V5-antibody. Nucleus, DAPI, blue; RBPR2-V5, Green. Scale bar = 50 μm. **(B)** Protein expression and representative western blot images of WT-RBPR2 and RBPR2-mutant proteins, which affect the "SYL" domain; anti-Actin = protein loading control. **(C)** Subcellular fractionation of stable cells expressing WT-RBPR2 or individual RBPR2-RBP4 mutants. Stable NIH3T3/LRAT cells expressing either WT-RBPR2 or individual RBPR2-RBP4 binding residues mutants were fractionated as outlined in the methods. Normalized portions of each extract (~30 μg) were analyzed by Western blotting using antibodies against proteins from cytoplasmic (HSP90) and plasma membrane (EGFR).

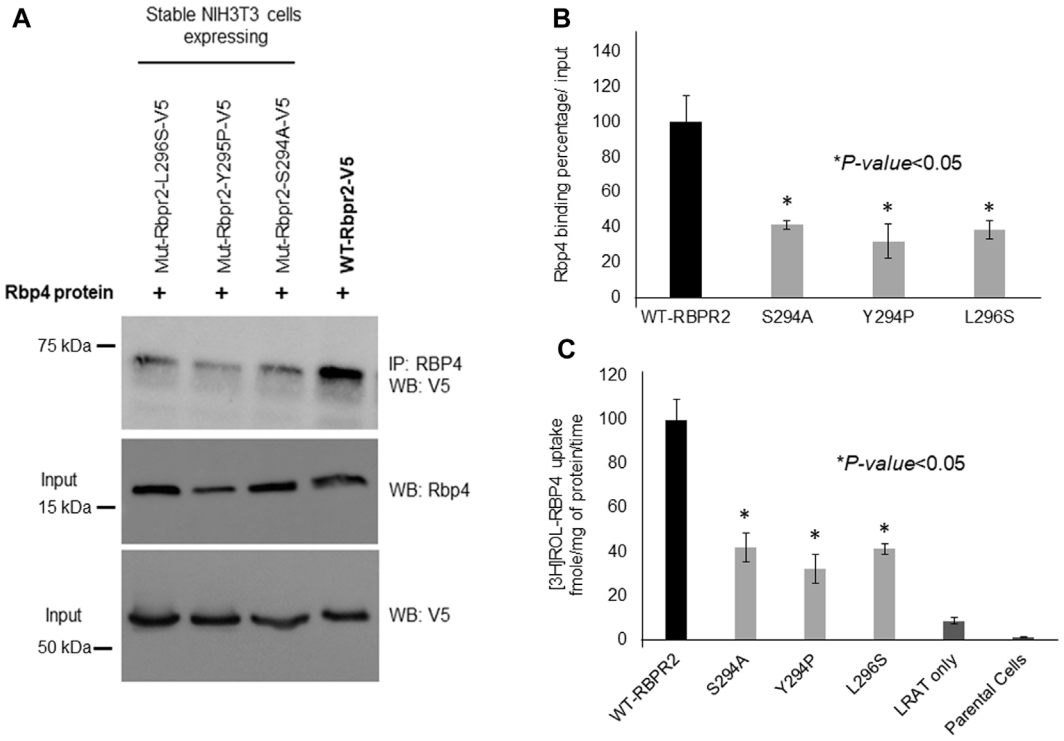

FIGURE 4
Extracellular RBP4 binding capabilities of RBPR2 and Vitamin A uptake assays. **(A,B)** Co-IP experiments showed a strong interaction between wild type (WT) RBPR2 and exogenous applied human RBP4 protein. Conversely, mutants targeting the proposed RBP4 binding sites on RBPR2, showed weaker interaction with RBP4 (62%–73% decreased binding capability compared to WT-RBPR2; $p < 0.05$). **(C)** Compared to NIH3T3/LRAT/WT-RBPR2 expressing cells, all NIH3T3/LRAT/RBPR2-mutant expressing cells showed decreased ability (<81% of WT-RBPR2 activity; *$p < 0.05$) to uptake extracellular applied [^{3}H]ROL bound RBP4.

(Kawaguchi et al., 2008a; Kawaguchi et al., 2008b). WT-RBPR2 and individual RBPR2-mutants were transiently transfected into NIH3T3 cells, and at 72 h post-transfection, WT and mutant RBPR2 expressing cells were subjected to both immunostaining and western blot analysis using the V5-antibody. Confocal microscopy analyses revealed that similar to WT-RBPR2 protein, all three single RBPR2-RBP4 binding residue mutants trafficked properly to the plasma membrane in transiently transfected NIH3T3 cells (green = V5-tagged RBPR2) (Figure 3A). Western blot and densitometry analysis further revealed that like WT-RBPR2, all three single RBPR2-mutants were equally expressed (Figure 3B). To confirm the specific subcellular localization of WT and mutant RBPR2 proteins, we subjected the transfected cells to subcellular fractionation. This analysis confirmed that individual RBPR2-mutants, like WT-RBPR2 protein, localized predominantly within the plasma membrane fractions, with only two RBPR2-mutants showing minimal cytoplasmic retention (<2% of total fractionated protein), indicating that individual RBPR2 mutants, like WT-RBPR2, trafficked properly to the plasma membrane and was expressed in this fraction (Figures 3A, C).

RBPR2 mutants targeting the RBP4 binding sites are defective in extracellular RBP4-ROL uptake

To determine the importance of proposed RBP4 binding residues on RBPR2 for RBP4 binding and ROL transport, we generated stable NIH3T3/LRAT cells expressing WT-RBPR2 or individual RBPR2-mutants (Shi et al., 2017; Lobo et al., 2018). Using both V5 antibody, we first confirmed equal expression of all recombinant proteins in stable cells (Figure 4A). To determine the interaction of RBPR2 with exogenous RBP4, we performed Co-IP experiments. Stable NIH3T3/LRAT cells expressing WT or individual RBPR2 mutants were seeded in 10 cm dishes. Upon reaching ~70% confluence, a reduced serum medium (8 mL of OptiMEM) containing 12 μM of purified RBP4 was added to the cells and incubated for 120 min. Cells were collected, and total protein was isolated and subjected to co-immunoprecipitation analysis using an RBP4 antibody, followed by reciprocal western blotting for RBPR2 (using a V5 antibody). While cells expressing WT-RBPR2 showed strong binding to exogenous RBP4 protein, individual mutant RBPR2-expressing cells showed decreased binding to RBPR2 ($p < 0.005$) (Figures 4A, B). To confirm this observation, individual stable cell lines were incubated with [^{3}H]ROL-RBP4 and analyzed for their ability to uptake extracellular [^{3}H]ROL-RBP4 at the 60-minute time point through Liquid Scintillation Counting (Shi et al., 2017; Lobo et al., 2018). This analysis showed that control cells (NIH3T3 and NIH3T3/LRAT cells) displayed insignificant levels of [^{3}H]ROL-RBP4 uptake (Figure 4C). However, [^{3}H]ROL was evident in cells expressing WT-RBPR2 with co-expressed LRAT (Figure 4C). In contrast, individual RBPR2-mutant expressing cells showed significantly reduced ability (<81% decreased activity compared to WT-RBPR2; $p < 0.005$) to uptake [^{3}H]ROL-RBP4, indicating that the amino acids Ser294, Tyr295, and Leu296 likely encompass the RBP4 binding residues on RBPR2 that would be crucial for ROL transport (Figure 1). Based on proper membrane trafficking of mutant RBPR2 protein (Figure 3A), but with decreased RBP4 binding (Figures 4A, B) and [^{3}H]ROL-RBP4 uptake capabilities (Figure 4C), indicates the importance of these residues on RBPR2 for extracellular RBP4 interaction/binding, which is in turn critical for ROL transport.

Surface plasmon resonance (SPR) analysis reveals binding kinetics of RBPR2 with its proposed ligand RBP4

Surface Plasmon Resonance (SPR) is a common technique used to study protein-ligand interactions. SPR can measure the binding affinities and association/dissociation kinetics of protein to ligand complexes in real-time. The interaction levels measured in Response Units (RU), and real-time plot sensorgram displays the dynamics of the analysis. The purified mouse Retinol Binding Protein, RBP4 (Supplementary Figure S1), was immobilized as the ligand, and various concentrations of the SYL motif containing peptides as analytes were run to measure SPR affinity and kinetics. The analytes examined were mouse RBPR2, zebrafish RBPR2, and mouse STRA6, known to interact with the mouse RBP4 ligand (Supplementary Figures S2–S5). To determine the K_d (ligand concentration in which half of the total receptor sites are occupied), the site-specific binding fitting model described below was used.

$$Y = \frac{Bmax*X}{Kd + X}$$

where B_{max} represents the maximum number of binding sites (Response Unit/RU), X represents the analyte concentration, and Y represents the binding affinity (Response Unit). Interestingly, the binding affinity of mouse RBPR2 to RBP4 approximates to the affinity of mouse STRA6 peptides to RBP4. The K_d of WT-*ms*RBPR2 peptide with *ms*RBP4 was 25.42 ± 6.01 μM, and B_{max} was 183.17 ± 25.66 μM (mean ± S.E). The K_d of *ms*STRA6 peptide with *ms*RBP4 was 26.73 ± 5.67 μM, and B_{max} was 178.45 ± 22.26 (mean ± S.E) (Figures 5, 6). The difference between the binding affinities and dissociation rate (K_{off}) of *ms*RBPR2 and *ms*STRA6 to *ms*RBP4 was not statistically significant ($p < 0.99$) in an unpaired *t*-test, suggesting similar K_d values and binding affinities of these two proteins for its extracellular ligand (Supplementary Figure S6). SPR analysis was then performed on SYL mutant mouse RBPR2 with its physiological ligand RBP4. This analysis showed that RBPR2 mutants (S294A and Y295P), had higher K_d values of 89.33 μM and 34.91 μM respectively, while the RBPR2 mutant (L296S) had a lower K_d value of 21.30 μM, compared to K_d value of 25.42 μM for WT-RBPR2, dissociation rate (K_{off}) for mutant msRBPR2 was significantly lower, suggesting a tighter bond formation between the RBP4 protein and mutant peptides (Figures 7A–C; Supplementary Figure S7).

Discussion

Given our results and those previously shown by the Sun and von Lintig laboratories, we can speculate that evolutionary vitamin A receptor (s) selection and distribution in a tissue-specific manner provides an advantage in the proper transport, storage, and utilization of all-*trans* retinol in the mammalian system, where retinoids are not a product of *de-novo* synthesis and thus require an active transport mechanism/membrane receptor to reach their target

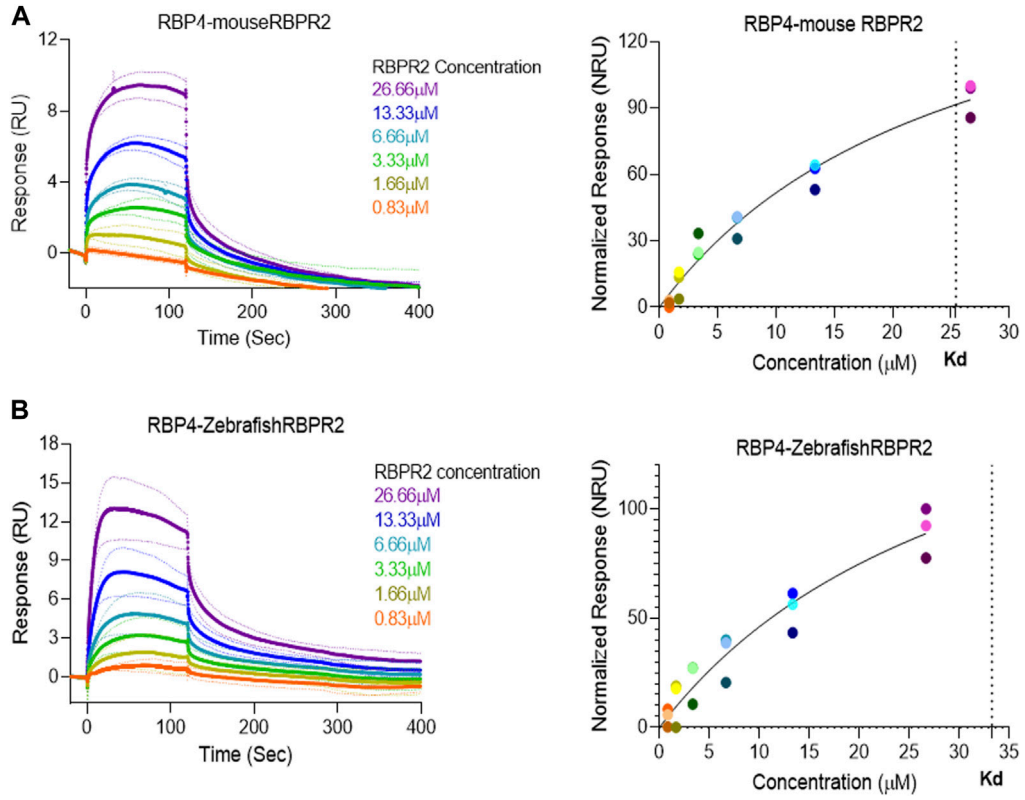

FIGURE 5
Surface Plasmon Resonance binding studies between RBPR2 and its ligand RBP4.Binding studies using SPR between mouse RBPR2 **(A)** and Zebrafish RBPR2 **(B)** and immobilized mouse RBP4 protein is shown, together with the respective kinetic values (K_d) in the right panel. The interaction levels are measured in response units (RU) and real time plot sensorgram display the dynamics of the analysis.

A

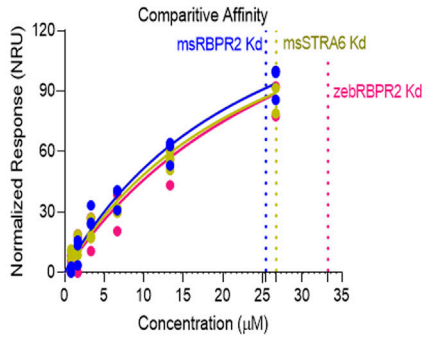

B

RBP4 to mouse RBPR2 Specific binding	
Y = Bmax*X/(Kd + X)	
Best-fit values	
Bmax	183.2
Kd	**25.43μM**
95% CI (profile likelihood)	
Bmax	140.8 to 268.3
Kd	15.84 to 46.08
Goodness of Fit	
Degrees of Freedom	16
R squared	0.9665
Sum of Squares	604.8
Sy.x	6.148

RBP4 to mouse STRA6 Specific binding	
Y = Bmax*X/(Kd + X)	
Best-fit values	
Bmax	178.5
Kd	**26.73μM**
95% CI (profile likelihood)	
Bmax	140.7 to 250.8
Kd	17.35 to 45.71
Goodness of Fit	
Degrees of Freedom	25
R squared	0.9636
Sum of Squares	887.9
Sy.x	5.959

RBP4 to zebrafish RBPR2 Specific binding	
Y = Bmax*X/(Kd + X)	
Best-fit values	
Bmax	199.3
Kd	**33.25μM**
95% CI (profile likelihood)	
Bmax	127.4 to 538.5
Kd	15.36 to 125.2
Goodness of Fit	
Degrees of Freedom	16
R squared	0.9245
Sum of Squares	1210
Sy.x	8.698

FIGURE 6
Kinetics of surface plasmon resonance binding studies between RBPR2 and its ligand RBP4. **(A,B)** Detailed SPR kinetics shown for mouse and zebrafish RBPR2 and for mouse STRA6 with its immobilized ligand mouse RBP4 protein. The affinity K_d values are shown in bold.

organs (Figure 8) (Chelstowska et al., 2016; Borel and Desmarchelier, 2017; Martin et al., 2021). In almost all mammalian systems, all-*trans*-retinol is the most abundant retinoid in the circulation and would serve as the probable form of retinoid delivered to body systems and would additionally serve as the substrate for the previously discussed membrane receptor. Due to its lipophilic nature, all-*trans*-retinol requires a carrier protein to reach target organs (Quadro et al., 1999; Chelstowska et al., 2016; Borel and Desmarchelier, 2017; Martin et al., 2021). With the discovery of the liver-secreted protein retinol binding protein 4 (RBP4) in 1968 as the specific carrier

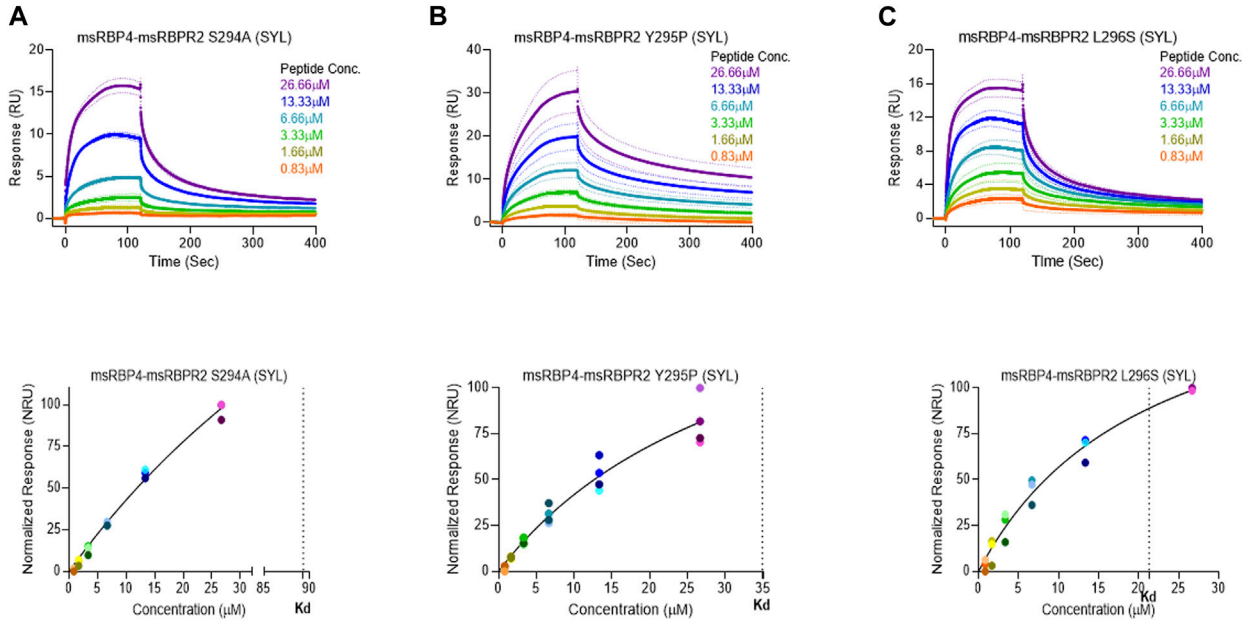

FIGURE 7
Surface plasmon resonance binding studies between mutant RBPR2 and its ligand RBP4. Binding studies using SPR between mouse RBPR2-S294A **(A)**, RBPR2-Y295P **(B)**, RBPR2-L296S **(C)** and immobilized mouse RBP4 protein is shown, together with the respective kinetic values (K_d) in the bottom respective panels. The interaction levels measured in Response Units (RU) and real time plot sensorgram display the dynamics of the analysis.

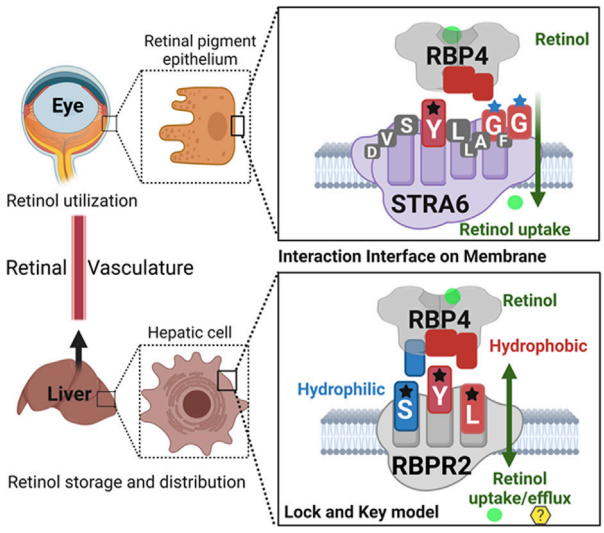

FIGURE 8
Schematic representation of the proposed RBP4 binding motif on RBPR2 for retinol uptake, storage, and distribution.Shown are the proposed RBP4 amino acid binding residues on STRA6 (YGG) and RBPR2 (SYL) that utilize a lock and key model mechanism to bind and stabilize the extracellular RBP4-retinol complex. The interaction interface between the membrane receptor and its' ligand is stabilized by both hydrophilic and hydrophobic interactions for retinol internalization. The proposed binding residues for both RBP4-ROL receptors are color-coded based on the property of the amino acid residues.

for retinol and subsequent investigation in *Rbp4* and *Stra6* deficient mice. The mechanism of transport and uptake of retinol to specific target organs can now be elucidated to a further degree (Quadro et al., 1999; Kawaguchi et al., 2007; Amengual et al., 2014; Shen et al., 2016; Borel and Desmarchelier, 2017).

In this study, we hypothesized that the second vitamin A/retinol binding protein 4 (RBP4) receptor, RBPR2, is necessary for the systemic facilitation of dietary retinoid uptake, storage, and transport to targeted organs, specifically the liver and eye (Alapatt et al., 2013). We based our hypothesis on published literature stating that RBPR2 shares amino acid and structural homology with the well-characterized vitamin A/RBP4 receptor, STRA6 (Alapatt et al., 2013; Chen et al., 2016). In the circulation, vitamin A/all-*trans* retinol is bound to RBP4 (RBP4-ROL/holo-RBP4), and on the binding of RBP4 to STRA6, retinol is transported into the cell without internalization of RBP4 (Blomhoff et al., 1990; Kawaguchi et al., 2008a; Isken et al., 2008; Kawaguchi et al., 2008b; Kawaguchi and Sun, 2010; Sun and Kawaguchi, 2011; Sun, 2012; Zhong et al., 2012; Alapatt et al., 2013; Breen et al., 2015; Chelstowska et al., 2016; Shen et al., 2016; Shi et al., 2017; Borel and Desmarchelier, 2017; Lobo et al., 2018; Solanki et al., 2020; Martin et al., 2021; Radhakrishnan et al., 2022a). To understand the mechanism(s) of RBPR2 binding to RBP4, we first employed an *in silico* protein-ligand interaction approach, multiple *in vitro* biochemical assays, and utilized an *Rbpr2*$^{-/-}$ deficient mouse model to predict RBPR2-RBP4 binding characteristics, to assess its empirical binding characteristics, and to observe the physiological consequences of RBPR2 deletion, respectively.

In the past, the Sun lab expanded upon the mechanism (s) of how the membrane expressed vitamin A receptor STRA6 facilitates retinol transport from its carrier protein, RBP4, into cells, where they used an elegant large-scale mutagenesis approach and identified three essential residues on STRA6 that might be essential for RBP4 binding and subsequent ROL transport into target tissues (Kawaguchi et al., 2008a; Kawaguchi et al., 2008b; Kawaguchi and Sun, 2010; Sun and Kawaguchi, 2011; Chen et al., 2016). These residues (Tyr336, Gly340,

TABLE 1 Amino acid sequences of individual RBPR2 peptides used in SPR analysis. The putative mouse RBP4 "SYL" binding residues on RBPR2 and STRA6 are shown in bold. HPLC and Mass spectrophotometry analysis confirmed purity and sizes of individual proteins.

Peptide name	Peptide sequence	Molecular weight	HPLC-purity (%)	Mass spec
msRbpr2 (42)	HVRDKLDMFEDKLE**SYL**THMNETGTLTPIILQVKELISVTKG	4845.12	92.14	Confirms
msStra6 (40)	SVVPTVQKVRAGINTDV**SYL**LAGFGIVLSEDRQEVVELVK	4329.94	90.84	Confirms
zebRBPR2 (34)	DKLDSLKDSLEQIALSCNQTE**S**VFT**YL**IPSINEF	3862.57	95.94	Confirms

and Gly342) on STRA6 are highly conserved among mammals and, interestingly, are in close proximity to the proposed "SYL" RBP4 binding domain on the less defined vitamin A receptor, RBPR2 (Figures 1A, 8) (Alapatt et al., 2013). The SYL residues (S294, Y295 and L296) on mouse RBPR2 were previously shown by the Graham group to be of importance through both *in vitro* and CRISPR mutant zebrafish model (s), and are critical for RBP4-ROL binding and retinol uptake and transport, in supporting visual function (Seeliger et al., 1999; Kawaguchi et al., 2008a; Kawaguchi et al., 2008b; Kawaguchi and Sun, 2010; Sun and Kawaguchi, 2011; Alapatt et al., 2013; Shi et al., 2017; Lobo et al., 2018; Martin et al., 2021).

Based on the work of the Sun Lab, we propose that a similar SYL binding motif might also be found in RBPR2, given its similar capability in binding RBP4-ROL (Figure 8) (Radhakrishnan et al., 2022b). Through homology and docking studies, an SYL amino acid consensus was found on the proposed RBP4 binding domain of mouse RBPR2. The importance of the RBPR2 SYL domain was then examined through the mutagenesis of individual residues in the proposed "SYL" binding domain of RBPR2 and by overexpression in NIH3T3 cells, where we observed that all three RBPR2-mutants, like the WT-RBPR2, localized predominantly within the plasma membrane. Subsequent subcellular fractions indicated that individual RBPR2 mutants, like WT-RBPR2, trafficked properly to the plasma membrane (Figure 4). However, in RBP4-vitamin A uptake experiments, all three RBPR2-SYL mutants failed to properly uptake exogenous RBP4-ROL, indicating that these three residues likely contribute to a specific RBP4 binding domain on RBPR2 for ROL transport. However, we were unable to test the combined effects of mutant RBPR2-SYL in a single mutant peptide, as the peptide synthesis and HPLC analysis was not optimal. The calculated binding affinity (K_d) of RBP4 for RBPR2 peptides (encompassing the SYL domain) was 25.43 μM for mouse RBPR2 and 33.25 μM for zebrafish RBPR2. The calculated binding affinity (K_d) of RBP4 for mouse STRA6 peptide encompassing the previously reported Tyr^{336}, Gly^{340}, and Gly^{342} residues was 26.73 μM and this was comparable to mouse RBPR2. The binding affinity (K_d) values for RBPR2 binding for its ligand RBP4 were comparable to previously published values for STRA6 for its physiological ligand RBP4 (K_d = 22.4 μM). Interestingly, we observed a reduced binding affinity (K_d) and stronger dissociation rate (K_{off}) for the RBPR2 mutants to its ligand RBP4, compared to the WT. In our docking analysis, we observed Ser294 and Tyr295 on RBPR2 to interact with Arg167 on RBP4, while Leu296 RBPR2 was not directly involved in the interaction. Leu296 might play an essential role in structure stabilization for the interaction; if we compare its observed K_d values to the other RBPR2 mutants and WT-RBPR2, it becomes evident that structural stabilization is equally important. The K_d values for RBPR2 peptides interaction with RBP4, S294A = 89.33 μM, Y295P = 34.91 μM, and L296S = 21.30 μM, indicating that the S294A and Y295P mutant peptides required a higher concentration of RBP4 for binding saturation, while the L296S mutant retained a comparable K_d value when compared to WT-RBPR2 (Figures 2C–E; Figures 5–7). The SYL motif on RBPR2 is crucial in RBP4 complex formation and stabilization, with significantly reduced dissociation rates in mutant RBPR2 peptides and RBP4 interactions. Any changes in these residues result in lower dissociation rates, indicating that the natural behavior of the interaction is affected. This suggests a tighter and possibly non-specific binding for the mutant RBPR2 to RBP4, which demands a more detailed study (Supplementary Figure S7). Based on our studies, it would be fascinating to study the serum kinetics of RBP4-ROL binding and uptake in *Rbpr2*-KO mice (Radhakrishnan et al., 2022a), to determine the contribution of RBPR2 for serum and ocular vitamin A homeostasis (Martin et al., 2021). Therefore, in the future, it would be important to determine the crystal or cryoEM structure of RBPR2 to gain further insight into the physiological role of this RBP4-vitamin A receptor in systemic retinoid homeostasis and for visual function. Table 1.

Data availability statement

The raw data supporting the conclusions of this article will be made available by the authors, without undue reservation.

Ethics statement

The animal study was reviewed and approved by University of Minnesota. Written informed consent was obtained from the owners for the participation of their animals in this study.

Author contributions

GL and RR, designed the research studies. RR, AS and ML, conducted the experiments and acquired data. GL, AS and RR, analyzed and interpreted the data. GL wrote the manuscript. GL, ML and RR, revised and edited the manuscript.

Funding

This work was supported by NIH-NEI grants (EY025034 and EY030889) and an R01-Administrative Supplement (3R01EY030889-03S1) and in part by the University of Minnesota start-up funds to GL University of Minnesota S10 Shared Instrument Grant 1S10OD021539-01 funded by the Office of Research Infrastructure Programs (ORIP)/NIH)).

Acknowledgments

The authors thank Jon Hawkinson, Ph.D. and Deepti Mudaliar, Ph.D. (University of Minnesota) for training, use of the SPR instrumentation, and data analysis. Robyn Rebbeck, Ph.D. and Jonathan Solberg, Ph.D. (University of Minnesota) for training, use of the Jasco J-815 spectropolarimeter instrument, and data analysis.

Conflict of interest

The authors declare that the research was conducted in the absence of any commercial or financial relationships that could be construed as a potential conflict of interest.

Publisher's note

All claims expressed in this article are solely those of the authors and do not necessarily represent those of their affiliated organizations, or those of the publisher, the editors and the reviewers. Any product that may be evaluated in this article, or claim that may be made by its manufacturer, is not guaranteed or endorsed by the publisher.

Supplementary material

The Supplementary Material for this article can be found online at: https://www.frontiersin.org/articles/10.3389/fcell.2023.1105657/full#supplementary-material

References

Alapatt, P., Guo, F., Komanetsky, S. M., Wang, S., Cai, J., Sargsyan, A., et al. (2013). Liver retinol transporter and receptor for serum retinol-binding protein (RBP4). *J. Biol.Chem.* 288, 1250–1265. doi:10.1074/jbc.M112.369132

Amengual, J., Zhang, N., Kemerer, M., Maeda, T., Palczewski, K., and von Lintig, J. (2014). STRA6 is critical for cellular vitamin A uptake and homeostasis. *Hum. Mol. Genet.* 23, 5402–5417. doi:10.1093/hmg/ddu258

Berry, D. C., Jacobs, H., Marwarha, G., Gely-Pernot, A., O'Byrne, S. M., DeSantis, D., et al. (2013). The STRA6 receptor is essential for retinol-binding protein-induced insulin resistance but not for maintaining vitamin A homeostasis in tissues other than the eye. *J. Biol. Chem.* 23, 24528–24539. doi:10.1074/jbc.M113.484014

Biesalski, H. K., Frank, J., Beck, S. C., Heinrich, F., Illek, B., Reifen, R., et al. (1999). Biochemical but not clinical vitamin A deficiency results from mutations in the gene for retinol binding protein. *Am. J. Clin. Nutr.* 69, 931–936. doi:10.1093/ajcn/69.5.931

Blomhoff, R., Green, M. H., Berg, T., and Norum, K. R. (1990). Transport and storage of vitamin A. *Science* 250, 399–404. doi:10.1126/science.2218545

Borel, P., and Desmarchelier, C. (2017). Genetic variations associated with vitamin A status and vitamin A bioavailability. *Nutrients* 9, 246–251. doi:10.3390/nu9030246

Breen, C. J., Martin, D. S., Ma, H., McQuaid, K., O'Kennedy, R., and Findlay, J. B. (2015). Production of functional human vitamin A transporter/RBP receptor (STRA6) for structure determinationPMCID:PMC 25816144. *PLoS One* 10 (3), e0122293. doi:10.1371/journal.pone.0122293

Chelstowska, S., Widjaja-Adhi, M. A. K., Silvaroli, J. A., and Golczak, M. (2016). Molecular basis for vitamin A uptake and storage in vertebrates. *Nutrients* 8, 676–686. doi:10.3390/nu8110676

Chen, Y., Clarke, O. B., Kim, J., Stowe, S., Kim, Y. K., Assur, Z., et al. (2016). Structure of the STRA6 receptor for retinol uptake. *Science* 353 (6302), aad8266. doi:10.1126/science.aad8266

D'Ambrosio, D. N., Clugston, R. D., and Blaner, W. S. (2011). Vitamin A metabolism. An update. *Nutrients* 3, 63–103. doi:10.3390/nu3010063

Golzio, C., Martinovic-Bouriel, J., Thomas, S., Mougou-Zrelli, S., Grattagliano-Bessieres, B., Bonniere, M., et al. (2007). Matthew-Wood syndrome is caused by truncating mutations in the retinol-binding protein receptor gene STRA6. *Am. J. Hum. Genet.* 80 (6), 1179–1187. doi:10.1086/518177

Harrison, E. H. (2012). Mechanisms involved in the intestinal absorption of dietary vitamin A and provitamin A carotenoids. *Biochim. Biophys. Acta.* 1821, 70–77. doi:10.1016/j.bbalip.2011.06.002

Isken, A., Golczak, M., Oberhauser, V., Hunzelmann, S., Driever, W., Imanishi, Y., et al. (2008). RBP4 disrupts vitamin A uptake homeostasis in a STRA6-deficient animal model for Matthew-Wood syndrome. *Cell Metab.* 7 (3), 258–268. doi:10.1016/j.cmet.2008.01.009

Kawaguchi, R., and Sun, H. (2010). Techniques to study specific cell-surface receptor-mediated cellular vitamin A uptake. *Methods Mol. Biol.* 652, 341–361. doi:10.1007/978-1-60327-325-1_20

Kawaguchi, R., Yu, J., Wiita, P., Honda, J., and Sun, H. (2008). An essential ligand-binding domain in the membrane receptor for retinol-binding protein revealed by large-scale mutagenesis and a human polymorphism. *J. Biol. Chem.* 283 (22), 15160–15168. doi:10.1074/jbc.M801060200

Kawaguchi, R., Yu, J., Wiita, P., Ter-Stepanian, M., and Sun, H. (2008). Mapping the membrane topology and extracellular ligand binding domains of the retinol binding protein receptor. *Biochemistry* 47 (19), 5387–5395. doi:10.1021/bi8002082

Kawaguchi, R., Yu, J., Honda, J., Hu, J., Whitelegge, J., Ping, P., et al. (2007). A membrane receptor for retinol binding protein mediates cellular uptake of vitamin A. *Science* 315, 820–825. doi:10.1126/science.1136244

Kelly, M., and von Lintig, J. (2015). STRA6: Role in cellular retinol uptake and efflux. *Hepatobiliary Surg. Nutr.* 4, 229–242. doi:10.3978/j.issn.2304-3881.2015.01.12

Lobo, G. P., Amengual, J., Palczewski, G., Babino, G., and von Lintig, J. (2012). Mammalian carotenoid-oxygenases: Key players for carotenoid function and homeostasis. *Biochim. Biophys. Acta.* 1821, 78–87. doi:10.1016/j.bbalip.2011.04.010

Lobo, G. P., Hessel, S., Eichinger, A., Noy, N., Moise, A. R., Wyss, A., et al. (2010). ISX is a retinoic acid-sensitive gatekeeper that controls intestinal beta,beta-carotene absorption and vitamin A production. *FASEB J.* 24, 1656–1666. doi:10.1096/fj.09-150995

Lobo, G. P., Jaume, A., Diane, B., Ramesh, A. S., and Derek, T. (2013). Genetics and diet regulate vitamin A production via the homeobox transcription factor ISX. *J. Biol. Chem.* 288, 9017–9027. doi:10.1074/jbc.M112.444240

Lobo, G. P., Pauer, G., Lipschutz, J. H., and Hagstrom, S. A. (2018). The retinol-binding protein receptor 2 (Rbpr2) is required for photoreceptor survival and visual function in the zebrafish. *Adv. Exp. Med. Biol.* 1074, 569–576. doi:10.1007/978-3-319-75402-4_69

Martin, A. N., Leung, M., Radhakrishnan, R., and Lobo, G. P. (2021). Vitamin A transporters in visual function: A mini review on membrane receptors for dietary vitamin A uptake, storage, and transport to the eye. *Nutr.* 13 (11), 3987. doi:10.3390/nu13113987

Micsonai, A., Wien, F., Kernya, L., Lee, Y. H., Goto, Y., Réfrégiers, M., et al. (2015). Accurate secondary structure prediction and fold recognition for circular dichroism spectroscopy. *Proc. Natl. Acad. Sci. U. S. A.* 112 (24), E3095–E3103. doi:10.1073/pnas.1500851112

Pasutto, F., Sticht, H., Hammersen, G., Gillessen-Kaesbach, G., Fitzpatrick, D. R., Nürnberg, G., et al. (2007). Mutations in STRA6 cause a broad spectrum of malformations including anophthalmia, congenital heart defects, diaphragmatic hernia, alveolar capillary dysplasia, lung hypoplasia, and mental retardation. *Am. J. Hum. Genet.* 80 (3), 550–560. doi:10.1086/512203

Quadro, L., Blaner, W. S., Salchow, D. J., Vogel, S., Piantedosi, R., Gouras, P., et al. (1999). Impaired retinal function and vitamin A availability in mice lacking retinol-binding protein. *EMBO J.* 18, 4633–4644. doi:10.1093/emboj/18.17.4633

Radhakrishnan, R., Dronamraju, V. R., Leung, M., Gruesen, A., Solanki, A. K., Walterhouse, S., et al. (2022a). The role of motor proteins in photoreceptor protein transport and visual function. *Ophthalmic Genet.* 26, 285–300. doi:10.1080/13816810.2022.2062391

Radhakrishnan, R., Walterhouse, S., Roehrich, H., Fitzgibbon, W., Kondkar, A. A., Biswal, M., et al. (2022b). Mice lacking the systemic vitamin A receptor RBPR2 show decreased ocular retinoids and loss of visual function. *Nutrients* 14 (12), 2371. doi:10.3390/nu14122371

Rohrer, B., Biswal, M. R., Obert, E., Dang, Y., Su, Y., Zuo, X., et al. (2021). Conditional loss of the exocyst component Exoc5 in retinal pigment epithelium (RPE) results in RPE dysfunction, photoreceptor cell degeneration, and decreased visual function. *Int. J. Mol. Sci.* 22 (10), 5083. doi:10.3390/ijms22105083

Seeliger, M. W., Biesalski, H. K., Wissinger, B., Gollnick, H., Gielen, S., Frank, J., et al. (1999). Phenotype in retinol deficiency due to a hereditary defect in retinol binding protein synthesis. *Invest. Ophthalmol. Vis. Sci.* 40, 3–11.

Shen, J., Shi, D., Suzuki, T., Xia, Z., Zhang, H., Araki, K., et al. (2016). Severe ocular phenotypes in Rbp4-deficient mice in the C57BL/6 genetic background. *Lab. Invest.* 96 (6), 680–691. doi:10.1038/labinvest.2016.39

Shi, Y., Obert, E., Rahman, B., Rohrer, B., and Lobo, G. P. (2017). The retinol binding protein receptor 2 (Rbpr2) is required for photoreceptor outer segment morphogenesis and visual function in zebrafish. *Sci. Rep.* 7, 16207–16217. doi:10.1038/s41598-017-16498-9

Solanki, A. K., Biswal, M. R., Walterhouse, S., Martin, R., Kondkar, A. A., Knölker, H. J., et al. (2021). Loss of motor protein MYO1C causes rhodopsin mislocalization and results in impaired visual function. *Cells* 10 (6), 1322. doi:10.3390/cells10061322

Solanki, A. K., Kondkar, A. A., Fogerty, J., Su, Y., Kim, S. H., Lipschutz, J. H., et al. (2020). A functional binding domain in the Rbpr2 receptor is required for vitamin A transport, ocular retinoid homeostasis, and photoreceptor cell survival in zebrafish. *Cells* 9 (5), 1099. doi:10.3390/cells9051099

Sun, H., and Kawaguchi, R. (2011). The membrane receptor for plasma retinol-binding protein, a new type of cell-surface receptor. *Int. Rev. Cell Mol. Biol.* 288, 1–41. doi:10.1016/B978-0-12-386041-5.00001-7

Sun, H. (2012). Membrane receptors and transporters involved in the function and transport of vitamin A and its derivatives. *Biochim. Biophys. Acta* 1821, 99–112. doi:10.1016/j.bbalip.2011.06.010

Tamura, K., Stecher, G., and Kumar, S. (2021). MEGA11: Molecular evolutionary genetics analysis version 11. *Mol. Biol. Evol.* 38 (7), 3022–3027. doi:10.1093/molbev/msab120

van Zundert, G. C. P., Rodrigues, J. P. G. L. M., Trellet, M., Schmitz, C., Kastritis, P. L., Karaca, E., et al. (2016). The HADDOCK2.2 web server: User-friendly integrative modeling of biomolecular complexes. *J. Mol. Biol.* 428, 720–725. doi:10.1016/j.jmb.2015.09.014

von Lintig, J. (2012). Metabolism of carotenoids and retinoids related to vision. *J. Biol. Chem.* 287, 1627–1634. doi:10.1074/jbc.R111.303990

Wassef, L., and Quadro, L. (2011). Uptake of dietary retinoids at the maternal-fetal barrier: *In vivo* evidence for the role of lipoprotein lipase and alternative pathways. *J. Biol. Chem.* 286, 32198–32207. doi:10.1074/jbc.M111.253070

Waterhouse, A., Bertoni, M., Bienert, S., Studer, G., Tauriello, G., Gummienny, R., et al. (2018). SWISS-MODEL: Homology modelling of protein structures and complexes. *Nucleic Acids Res.* 46, W296–W303. doi:10.1093/nar/gky427

Zhong, M., Kawaguchi, R., Kassai, M., and Sun, H. (2012). Retina, retinol, retinal and the natural history of vitamin A as a light sensor. *Nutrients* 19, 2069–2096. doi:10.3390/nu4122069

frontiers | Frontiers in Cell and Developmental Biology

TYPE Original Research
PUBLISHED 13 April 2023
DOI 10.3389/fcell.2023.1177711

OPEN ACCESS

EDITED BY
Brian Perkins,
Cleveland Clinic, United States

REVIEWED BY
Rafael Ufret-Vincenty,
UT Southwestern Medical Center, United States
Ninel Gregori,
University of Miami Health System, United States

*CORRESPONDENCE
Alessandro Iannaccone,
aiannacc@yahoo.com

RECEIVED 01 March 2023
ACCEPTED 03 April 2023
PUBLISHED 13 April 2023

CITATION
Sarici K, Vyas A and Iannaccone A (2023), The double-edged sword of inflammation in inherited retinal degenerations: Clinical and preclinical evidence for mechanistically and prognostically impactful but treatable complications.
Front. Cell Dev. Biol. 11:1177711.
doi: 10.3389/fcell.2023.1177711

The double-edged sword of inflammation in inherited retinal degenerations: Clinical and preclinical evidence for mechanistically and prognostically impactful but treatable complications

Kubra Sarici, Aanal Vyas and Alessandro Iannaccone*

Duke Center for Retinal Degenerations and Ophthalmic Genetic Diseases, Duke Eye Center, Department of Ophthalmology, Duke University School of Medicine, Durham, NC, United States

We present retrospective data from our clinical research efforts of the past several years alongside a review of past and current clinical and preclinical data independently by several investigators supporting our clinical evidence for the importance of inflammation in inherited retinal degenerations (IRDs). We show how inflammation is a complicating factor in IRDs but, if recognized and managed, also a great opportunity to mitigate disease severity immediately, improve patient prognosis and quality of life, extend the treatment windows for gene-specific and agnostic therapeutic approaches, mitigate the impact of inflammatory complications on the accurate estimate of vision changes in IRD natural history studies, improve the chances of safer outcomes following cataract surgery, and potentially reduce the likelihood of inflammatory adverse events and augment the efficacy of viral vector-based treatment approaches to IRDs. Manuscript contribution to the field. Inflammation has been suspected to be at play in IRDs since the beginning of the 1900s and became a research focus through the early 1990s but was then largely abandoned in favor of genetic-focused research. Thanks to regained cognizance, better research tools, and a more holistic approach to IRDs, the recent reappraisal of the role of inflammation in IRDs has brought back to the surface its importance. A potential confounder in natural history studies and a limiting factor in clinical trials if not accounted for, inflammation can be managed and often offers an opportunity for immediately improved prognosis and outcomes for IRD patients. We present our retrospective clinical evidence for connections with a measurable secondary autoimmune component that can develop in IRDs and contribute to vision loss but is at least in part treatable. We also present ample lines of evidence from the literature corroborating our clinical observations at the preclinical level.

KEYWORDS

inherited retinal degeneration (IRD), inflammation, immune activation, treatment, prognosis

Introduction

Inherited retinal degenerations (IRDs) comprise a genetically and clinically heterogeneous group of conditions due to mutations in over 300 distinct genes characterized by the common leitmotif causing the progressive degeneration of photoreceptors and vision loss (Daiger, 2020). The mechanisms of degeneration in IRDs have been under investigation for decades and remain under further characterization. The presence of clinically visible inflammatory changes in IRD patients has been noted since the early days of the field, leading to the development of the term "*retinitis* pigmentosa" to characterize RP, the most common of the IRDs. The most apparent clinical change related to ongoing inflammation at the tissue level is the presence of cystoid macular edema (CME), a well-known and common complication of IRDs. In addition to CME, virtually every IRD specialist has seen IRD patients also present with retinal exudates, perivascular sheathings, vascular staining, and/or leakage of the far peripheral vessels or at the vascular arcades on intravenous fluorescein angiography (IVFA). It has been our experience that far less appreciated appear to be signs of late leakage on IVFA at or around the optic nerve head and swelling of the retinal nerve fiber layer (RNFL) on optical coherence tomography (OCT)—but it has been our experience that they are also present. The less frequent appreciation of these features is in part since inflammatory disc changes in IRDs tend to be best appreciated in the very late IVFA frames (>6 min), and that glaucoma specialists or neuro-ophthalmologists routinely ask for RNFL OCTs, but not by IRD—or more in general, retinal—specialists.

The presence of these inflammatory findings in IRDs led researchers in the field to investigate, in the late 1980s, the immune system reactivity against retinal antigens in patients with RP (Chant et al., 1985; Detrick et al., 1985; Heckenlively et al., 1985; Chan et al., 1986; Detrick et al., 1986; Percopo et al., 1990). In early studies, in addition to immune cellular activation, high levels of anti-retinal auto-antibodies (AR-AAbs) were also found in various cohorts of RP patients (Brinkman et al., 1980; Heckenlively et al., 1985; Broekhuyse et al., 1988). Furthermore, CME was shown independently by several investigators to be associated with elevated AR-AAb levels (Heckenlively et al., 1996; Heckenlively et al., 1999; Wolfensberger et al., 2000). In RP, it also shown that CME can be treated with carbonic anhydrase inhibitors (CAIs) administered either orally, topically, or both (Marmor, 1990; Grover et al., 1997; Wolfensberger, 1999; Grover et al., 2006; Apushkin et al., 2007), the "fluid-draining" ability of which is due to the expression of membrane-bound carbonic anhydrase II (CA-II) in the RPE (Wolfensberger et al., 1994). It suggested that responsiveness to CAIs may be linked to the presence of anti-CA-II AAbs, which are common in RP patients with CME (Wolfensberger et al., 2000). However, there can be rebound effects from prolonged treatment or following discontinuation (Apushkin et al., 2007), since CAIs do not address any underlying inflammatory component, as noted in uveitis patients with CME (Schilling et al., 2005). Therefore, in the uveitis subspecialty world, in which the inflammatory etiology of CME is well established and accepted, CME is far more commonly treated with topical steroids, non-steroidal anti-inflammatory drugs (NSAIDs), in conjunction with oral steroids, various types of steroid-sparing immuno-modulating treatment (IMT) regimens such as mycophenolate mofetil (MMF), methotrexate (MTX), azathioprine (AZT), and more recently a variety of biologic agents such as adalimumab, with or without subtenon, intravitreal and—more recently also—suprachoroidal steroid injections or injectable/implantable steroid slow-releasing devices (Steinmetz et al., 1991; Tanner et al., 1998; Tranos et al., 2004; Androudi et al., 2005; Jain et al., 2005; Perry and Donnenfeld, 2006; Hariprasad and Callanan, 2008; Hogewind et al., 2008; Jones and Francis, 2009; Slabaugh et al., 2012; Wu et al., 2012; Bourgault et al., 2013; Koop et al., 2013; Rossetto et al., 2015; Sen et al., 2015; Grixti et al., 2016; Asproudis et al., 2017; Feiler et al., 2017; Frere et al., 2017; Juthani et al., 2017; Khurana et al., 2017; Pichi et al., 2017; Doycheva et al., 2018; Petrushkin et al., 2018; Schallhorn et al., 2018; Hasanreisoglu et al., 2019; Ansari et al., 2021; Saade et al., 2021; Wong et al., 2021; Chronopoulos et al., 2022; Studsgaard et al., 2022; Miguel-Escuder et al., 2023). These remedies have been used successfully to manage CME in RP patients who are refractory or incompletely responsive to CAIs (Forte et al., 1994; Heckenlively et al., 1999; Saraiva et al., 2003; Kim, 2006; Scorolli et al., 2007; Park et al., 2013; Ahn et al., 2014; Patil and Lotery, 2014; Lemos Reis et al., 2015; Schaal et al., 2016; Sudhalkar et al., 2017; Bakthavatchalam et al., 2018; Mansour et al., 2018; Karasu, 2020; Park et al., 2020; Veritti et al., 2020; Chen et al., 2022), and this has also been our experience thus far.

The early investigations into the role of the immune system in RP pathogenesis and progression led us to investigate the therapeutic potential of an IMT agent available in the 1990s, thymopentin (Rispoli et al., 1990; Rispoli et al., 1991; Vingolo et al., 1993a; Vingolo et al., 1993b; Iannaccone et al., 1994a). Administered i.v., thymopentin reduces immune system activation. In brief, in an open-label, prospective, pilot trial comparing automated visual field (VF) sensitivity and retinal function by virtue of the mixed full-field flash electroretinogram (ffERG) b-wave amplitudes to a historical natural history control group (Berson et al., 1985), serial intravenous thymopentin administration improved both parameters at 18 and 36 mos (Rispoli et al., 1990; Rispoli et al., 1991; Vingolo et al., 1993a; Vingolo et al., 1993b; Iannaccone et al., 1994a) vs. both declining progressively in the historical control group (Berson et al., 1985). These results supported the hypothesis that immune system activation is a contributing factor to IRD pathobiology and progression. Unfortunately, this drug is no longer available on the market, yet numerous IMT regimens are possible nowadays.

Over 3 years have gone by since the time when the role of the immune system in IRDs was being first investigated, and this hypothesis was set aside as the focus of IRD researchers rapidly shifted towards the discovery of new genes and the characterization of genotype-phenotype correlations. More recently, though, there has been a progressive reappraisal of the role of inflammation and activation of the immune system in IRDs (Iannaccone et al., 1994b; Iannaccone et al., 1995; Epstein et al., 2014; Epstein et al., 2015; Hollingsworth et al., 2015; Iannaccone et al., 2015; Hollingsworth et al., 2017; Iannaccone et al., 2017; Adamus, 2018; Hollingsworth et al., 2018; McMurtrey and Tso, 2018; Iannaccone and Radic, 2019; Birch et al., 2020; Duncan et al., 2020; Hollingsworth and Gross, 2020; Liu et al., 2020; Yang et al., 2020; Adamus, 2021; Alekseev et al., 2021; Iannaccone et al., 2021; Alekseev et al., 2022; Funatsu et al., 2022; Gupta et al., 2022). Several lines of evidence will be

reviewed further in the discussion section to provide additional support to immune-mediated inflammation representing a potential treatment target for IRDs (Adamus et al., 2004; Xiong et al., 2013; McMurtrey and Tso, 2018; Hollingsworth and Gross, 2020; Funatsu et al., 2022), including work from our group (Epstein et al., 2014; Hollingsworth et al., 2015; Gattegna et al., 2019; Iannaccone and Radic, 2019). Independently, also two IMTs commonly used to manage inflammatory eye disease, including autoimmune retinopathy and/or optic neuropathy (AIR/AINR), MMF and MTX, have been shown to have potential treatment effects on animal models of RP (Liu et al., 2020; Yang et al., 2020), whereby further investigations on these drugs are in progress and intravitreal MTX is already being tested in a human clinical trial of RP (NCT05392179, Aldeyra Therapeutics). While these specific drugs have exhibited mechanistic effects on specific aspects of the retinal degenerative process that make them attractive as treatments for RP, MMF also clearly showed a normalization of the intraretinal microglial activation patterns (Yang et al., 2020). Therefore, the effects of MMF and MTX on RP-induced inflammation cannot be ignored and may be in part responsible for some of the observed benefits.

Some investigators have questioned the potential pathogenicity of AR-AAbs, and the need for standardized testing methods has been emphasized (Fox et al., 2016). In prior studies, we have found that control subjects, too, can exhibit autoreactivities. (Iannaccone et al., 2012; Iannaccone et al., 2015; Iannaccone et al., 2017). Thus, the presence of AR- or ON-AAbs is not automatically diagnostic of AIR/AINR. Autoreactivities need to be interpreted in the context of the entire clinical picture before considering initating treatment. A consensus on the diagnostic approaches to AIR/AINR has been reached and more refined testing standards have been instituted (Fox et al., 2016; Adamus, 2020). Notwithstanding these caveats, the pathogenicity of AR-AAbs implicated in AIR/AINR and its paraneoplastic form, cancer-associated retinopathy (CAR), has been extensively characterized and confirmed (Adamus et al., 1997; Adamus et al., 1998a; Adamus et al., 1998b; Kyger et al., 2013; Xiong et al., 2013; Adamus, 2018). We further showed previously that as many as 60%–70% of AIR and CAR patients exhibit also an anti-optic nerve AAb (AON-AAb) associated optic neuropathy phenotype (i.e., AINR or CARON) independent of being paraneoplastic or not (Adamus et al., 2011). Treating these conditions with steroids and various IMT regimens has been shown to lead to disease mitigation, halting, or even partial reversal (Adamus et al., 2012; Davoudi et al., 2017; Heckenlively and Lundy, 2018a; Finn et al., 2020; Grewal et al., 2021).

Despite all these lines of evidence, detection of the very same AR- or AON-AAbs is not presently considered equally relevant in IRDs, and is most often dismissed as a mere after-the-fact secondary marker of prior degeneration. However, our clinical experience with many IRD patients has been quite different. IRD patients exhibiting inflammatory complications virtually invariably present also with AR- and/or AON-AAb patterns that correlate quite well with clinical and functional findings, especially at the retinal immunohistochemistry (rIHC) testing level, and respond favorably to the treatment of these complications. This is in line with a pathogenic view of these AAbs also in IRDs (Adamus, 2021). Thus, we sought out to conduct a systematic retrospective review of our patients who presented with signs and symptoms of a possible IRD and also exhibited inflammatory signs and, thus, underwent AAb and rIHC testing between 2016 and 2022. We will present data on the incidence of AR- and/or AON-AAbs in IRDs, and show that some genotypes appear to be more commonly associated with these secondary autoimmune reactions. We will illustrate in-depth analyses of these associations in certain genetic subgroups that are a) quite common and b) of enhanced interest because of ongoing natural history studies (RUSH2A, NCT03146078, and Pro-EYS, NCT04127006), and we will illustrate some representative examples of IRD patients with very clear improvements in visual function following treatment of these immune-mediated complications. Far from claiming that IRDs are outright autoimmune disorders, our data will show that the proposed pathogenicity and prognostic relevance of these AAbs is well supported, falls in line with preexisting evidence going back to the 1980s, advocates for increased efforts to tackle these treatable aspects in IRDs, and paves the way for additional avenues to ensure that there is indeed a light at the end of the tunnel for IRD patients.

Methods

We conducted a retrospective analysis, approved by the Duke Institutional Review Board, of subjects seen at the Duke Center for Retinal Degenerations and Ophthalmic Genetic Diseases who had been referred for a possible diagnosis of IRD but also exhibited inflammatory signs and symptoms, thus, underwent AAb and rIHC testing between 2016 and the summer of 2022 according to published methods (Adamus et al., 2004; Adamus, 2020). The study adhered to the ethical principles of the Helsinki Declaration. Given the retrospective nature of the study, written informed consent was not required.

Patients meeting clinical or imaging criteria that we defined as suggestive or outright indicative of inflammatory complications during their examination (Table 1) underwent a complete eye examination inclusive of best corrected visual acuity (BCVA) to ETDRS charts, VF and ffERGs according to ISCEV (McCulloch et al., 2015) standards (Espion3 system, Diagnosys LLC, Lowell, MA, United States). VFs were most often of the semiautoamated kinetic (SKP) type (Octopus 900 Pro; Haag-Streit AG; Koeniz, Switzerland). When appropriate to better characterize the patterns of VF loss, supplemental VFs with photopic or scotopic (Dark-Adapted Cromatic Perimetry, Medmont Int PTY LTD.; Nunawading, Australia) full-field testing static approaches were also obtained. ERG testing included also, when appropriate, supplemental recordings to assess the specific integrity of the ON- and OFF pathways and the photopic negative response (PhNR), an ffERG photopic response originating from the RGCs (Viswanathan et al., 1999; Frishman et al., 2018). Imaging studies included on every subject macular linear and volume spectral domain optical coherence tomography (SD-OCT, Spectralis, Heidelberg Engineering, Heidelberg, Germany) fundus autofluorescence (FAF), and color fundus photography. FAF and photos were obtained in the vast majority of cases with Optos Wide-Field imaging devices (California model or prior versions). Based on medical indication and necessity when optic nerve involvement was apparent or suspected, a more selected subset of patients underwent also peripapillary (PP) ON SD-OCTs to estimate the

TABLE 1 Visual function and clinical/imaging criteria used to identify subjects with IRD-like presentations associated with inflammatory complications.

Clinical/imaging criteria associated with suspected inflammatory complications	*Visual function criteria associated with suspected inflammatory complications*
• Absence of waxy pallor on DFE	• Late-onset visual function loss or sudden acceleration in the vision loss process
• Presence of outright overt disc hyperemia and/or swelling on DFE	• BCVA less than potential predicted by foveal EZ preservation not explained by media opacities or other factors (e.g., amblyopia)
• Thickened RNFL on OCT imaging (macular and/or PP scans)	• Worse VF loss than predicted by the level of ffERG reduction
• Late leakage and/or staining on FA of the disc, arcades, macula, peripheral vascular, focal or disseminated	• Asymmetry in VF loss not explained by other factors
• Presence of significant CME (especially if unresponsive/only partially responsive to CAIs)	• Enlarged blind spots or centro-cecal scotomas on VF testing not associated with PP atrophy or other PP chorioretinal lesions
• Disseminated and/or flame-shaped retinal exudates on DFE (as frequently seen in primary and paraneoplastic AIR and AIR/ARRON patients)	• Delayed pattern VEPs despite normal or reasonable (20/25–20/30) BCVA
• Disseminated chorioretinal peripheral nummular "punched-out" atrophic lesions on DFE	• Electronegative ffERGs with evidence of post-receptoral dysfunction and/or (when measurable) disproportionate RGC-driven response (PhNR) reduction

DFE, dilated fundus examination; RNFL, retinal nerve fiber layer; OCT, optical coherence tomography; PP, peripapillary; FA, fluorescein angiography; CAIs, carbonic anhydrase inhibitors; AIR, autoimmune retinopathy; ARRON, autoimmune-related retinopathy and optic neuropathy; BCVA, best corrected visual acuity; EZ, ellipsoid zone; VF, visual field; VEPs, visual evoked potentials; ffERGs full-field electroretinogram; RGC, retinal ganglion cells.

thickness of the PP RNFL, assessment of optic nerve functional status via pattern-reversal visual evoked potentials (PVEPs) and IVFAs, typically extended in duration (at least 6–8 min from the injection of the fluorescent dye). In these patients, retinal SD-OCT segmentation analysis of the RGC layer was also usually conducted to ascertain the selective integrity of the RGCs and correlate it as appropriate to PVEP, PhNR, rIHC and ON-AAb test results.

All subjects meeting the above clinical and functional criteria also underwent CLIA-certified diagnostic testing for AAb/rIHC at the Ocular Immunology Laboratory at the Casey Eye Institute, Oregon Health and Sciences University, Portland, OR, meeting updated and refined testing standards as of 2018 (Fox et al., 2016; Adamus, 2020). Tests obtained prior to these new standards by Western blot (WB)-based methods showed specific reactivities only when possible (Adamus et al., 2004). AON-AAb testing was and remains exclusively WB-based, as it is directed against a lysate of a retrobulbar portion of the optic nerve (Adamus et al., 2011). We also strived to obtain in all subjects rIHC, which is performed on normal human donor eye thin retinal sections that are then stained with the patients' sera and then counterstained with a secondary fluorescent anti-IgG antibody to detect and quantitate reactivities (Adamus et al., 2004). We found rIHC to be especially important to identify the subcellular localization of autoreactivities at the tissue level and help us establish better correlates with clinical and functional findings. While depending on the type and location of the autoreactive epitopes, a patient may be positive for AAb testing but not for rIHC and *vice versa*. In the vast majority of cases, AAb-positive patients were also positive for rIHC testing which allowed us to establish such cellular level correlates with precision. For example, a patient presenting with inflammatory optic nerve findings (disc swelling on SD-OCT and leakage on IVFA) may well present without AON-AAbs but exhibit AR-AAbs and RNFL and/or RGC staining on rIHC, whereas one with mild if any disc changes but exhibiting PVEP delays suggestive of an inflammatory optic nerve component may present exclusively with AON-AAbs and no AR-AAbs and no RNFL and/or RGC staining on rIHC. Also, patients presenting with more complex pictures such as electronegative ffERG due to selective or prevailing b-wave compromise would most often exhibit retinal bipolar cell (BC)/inner nuclear layer (INL) and/or outer plexiform layer (OPL) staining and/or AR-AAbs directed against known BC/INL- and/or OPL-expressed antigens—or even against arrestin, a protein of the visual cycle that, when compromised genetically like in Oguchi disease (Fuchs et al., 1995; Nakazawa et al., 1997), is associated with electronegative ffERG responses. A similar effect on the ffERG response has also been observed when the partner visual cycle protein, rhodopsin kinase, is compromised in Oguchi disease (Yamamoto et al., 1997; Cideciyan et al., 1998; Khani et al., 1998; Yoshii et al., 1998).

All patients who presented not only with inflammatory findings but also a positive family history of an IRD, a clinical picture strongly suggestive of an IRD, or a longtime history of visual symptoms (e.g., night blindness since birth or early childhood) suggestive of a likely IRD, and/or a diagnosis of an RP or macular dystrophy—e.g., Stargardt disease—in childhood also underwent CLIA-certified molecular genetic testing to confirm the presumed or suspected diagnosis of an IRD. Whenever possible, samples from other affected members (ideally both parents when available and, when applicable, also confirmed affected or unaffected siblings) or from the presumed healthy carrier parents in suspected recessive disease were also obtained and tested as part of the diagnostic process to establish the phase of any detected gene mutations and confirm the pathogenicity of detected mutations. All patients underwent as a minimum IRD-focused broad CLIA-certified next-generation sequencing (NGS) testing. The most commonly used labs for diagnostic molecular genetic testing included GeneDx (Gaithersburg, MD) and the Molecular Vision Lab (Hillsboro, OR). Initially negative or inconclusive results generally led also to escalation to deletion/duplication analyses and/or whole exome sequencing (WES) testing when the suspicion of an IRD was especially high. Further details about our approach to molecular

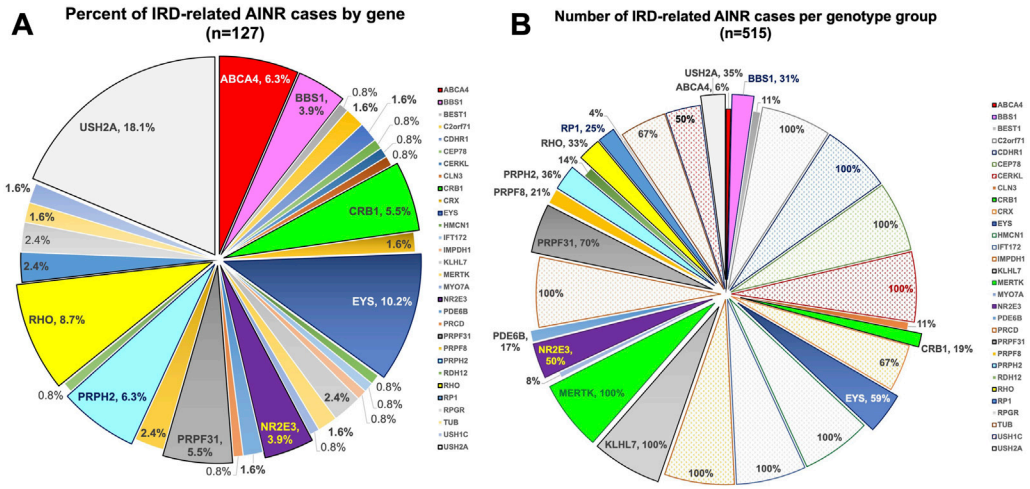

FIGURE 1
Pie charts illustrating the breakdown by gene of the IRD cases with associated AAb-related inflammatory complications. **(A)** Percentage of cases by gene within the 127 positive IRD cases; **(B)** Percentage of cases within each gene subgroup within our IRD database (n = 515 for the genes in which AAbs were observed in 2022). The percentages are cumulative for all AAbs observed, whether only AR-AAbs, only AON-AAbs, or both.

genetic testing and diagnostic management of our IRD patients have been recently published (Gupta et al., 2022).

Based on all these criteria, the records of 418 subjects who exhibited positive AAb and/or rIHC test results were reviewed retrospectively. All clinical and imaging findings and test results such as VF and electrophysiological were reviewed. Their correlation with positive AR-AAbs and AON-AAbs and rIHC findings was characterized to infer more precisely the potential pathogenicity of the observed autoreactivities applying criteria as briefly outlined above. When applicable, genetic test results were also reviewed and the presence of any pathogenic, disease-causing genetic changes was confirmed. In addition, we will present more in-depth (but earlier) analyses of our findings in genetic subgroups of patients harboring *EYS* and *USH2A* mutations—these are subsets of genetically well defined patients in which we initially empirically noted an unusually high frequency of inflammatory findings and that have been presented but not published before (Gattegna et al., 2019; Alekseev et al., 2021; Alekseev et al., 2022). These initial observations and our prior presented and published data prompted the more systematic review of our findings that is also presented herein.

Results

Autoreactivity patterns in IRD patients by genotype

Of the 418 records reviewed with positive autoreactivities, there were 127 cases (30.3%) with AR-AAbs, AON-AAbs, or both (and/or positive rIHC) who had a molecularly confirmed IRD. All other AAb-positive cases (n = 261) had either primary AIR or (more commonly) AINR/ARRON or a paraneoplastic form thereof (CAR/CARON). The latter diagnoses were established based on age and modality of presentation [most often late- and acute/subacute onset, most often asymmetric in nature—i.e., affecting one eye significantly more than the other, which is seldom observed in IRDs except for X-linked RP female carriers (Jacobson et al., 1989)—whether or not in association to a known/confirmed diagnosis of cancer and/or another underlying autoimmune disorder in the affected patient or a family member (Heckenlively and Ferreyra, 2008; Ferreyra et al., 2009; Heckenlively and Lundy, 2018b)] and, in select more ambiguous cases, also based on of inconclusive or outright negative molecular genetic test results. Despite being suspected of having secondary autoimmune complications due to the presence of visible or suspected inflammatory complications based on our selection criteria to warrant AAb and rIHC testing, 9 additional IRD subjects tested negative for any type of AAb and exhibited no staining upon rIHC.

The breakdown of the various genetic etiologies of the 127 IRD cases with positive AR-AAbs, AON-AAbs, or both (and/or positive rIHC) is illustrated in Figure 1A, which illustrates the frequency of the genotypes at play within this data set. To further gain into the prevalence of these positive autoreactivities among all subjects found to have disease-causing in the genes identified by this initial retrospective data analysis, we further reviewed the records of all subjects who, by the end of the data review window period, exhibited mutations in these same genes (n = 515). This breakdown is illustrated in Figure 1B and helps us appreciate how, for some rarer genes (such as *MERTK* or *KLHL7*), the within-gene frequency of AAb-associated inflammatory findings was actually very high—in some cases, in as much as 100% of the patients diagnosed with these rarer forms of IRDs. In brief, from this dual-level review of our data, we observed that inflammatory manifestations were especially common among patients with mutations in the *EYS, USH2A, MERTK, CRB1, BBS1, NR2E3, ABCA4, RHO, RP1, KLHL7,* and the *PRPF* family of genes among the latter ones, the *PRPF31* gene more commonly than the *PRPF8* one).

In most of these IRD cases, there was a dual retinal (most often, CME) and optic nerve inflammatory component. Not uncommonly,

the latter was a main determinant of the visual acuity and/or field loss above and beyond the CME. A concominant optic neuropathy becomes recognizable not only from measurable RNFL swelling, but also from mismatches between VF areas and extent of ffERG loss. For example, a disproportionate VF loss vis-à-vis far better ffERG responses—with or without asymmetric findings between the two eyes, neither one of which are expected based on published evidence of VF-ERG correlations in IRDs (Iannaccone et al., 1995; Sandberg et al., 1996; Iannaccone et al., 2003)—was a recurrent and particularly telling finding. Other lines of evidence in favor an inflammatory optic nerve component included delayed pattern visual evoked potentials (PVEPs) and/or overt angiographic epi-pr peri-papillary inflammatory findings. In some cases, as it will be illustrated below and as it has been previously reported (Iannaccone and Radic, 2019), the picture could also be associated with a disseminated chorioretinitis-type pattern. Unlike classical uveitis patients, there were typically no anterior chamber cells in IRD patients with secondary AINR, as the process is mostly far posterior. No patient exhibited clear signs of vitritis either, withour instances of vitreal haze. However, it is very important to note that the vast majority of IRD patients affected by a diffuse retinopathy have anterior vitreous cells and, also very commonly, posterior vitreous detachments. These vitreal cells have already been shown to be largely inflammatory in nature (Albert et al., 1986; Newsome and Michels, 1988). A substantial breakdown in the blood-retinal barrier in IRD patients accompanies this process—this is not just clinically intuitive, but it has also been well characterized in the past (Gieser et al., 1980; Fishman and Cunha-Vaz, 1981; Miyake et al., 1984; Travassos et al., 1985; Fishman et al., 1986).

A deeper level analysis of the clinical and functional correlations with AAb reactivity patterns is presented below for the *EYS* and the *USH2A* gene, which are common causes of autosomal recessive RP (ARRP), in the latter case whether with or without hearing loss (Birch et al., 2020; Duncan et al., 2020) and that are also the ongoing object of natural history characterization (NCT03146078, NCT04127006).

Subgroup analysis of results in ARRP associated with EYS gene mutations

In 2021(76), we retrospectively identified 20 subjects positive for biallelic disease-causing *EYS* mutations (M = 8/F = 12, age 23–80), all of whom had undergone a complete eye examination, inclusive of VFs) and ffERGs, macular (n = 20) and optic nerve (n = 13) SD-OCTs and, in 12 of them, also IVFA and CLIA-certified AAb/rIHC testing. Of the total 24 tested eyes with IVFA, 8 showed optic nerve head leakage, 3 showed leakage at the vascular arcades, and 11 showed combined nerve and vascular leakage. The RNFL was thickened, most often sectorally, in 24 of 26 eyes assessed, and correlated well with IVFA leakage, helping explain disproportionate visual acuity losses compared to foveal findings, or disproportionate VF loss compared to retinal imaging or functional findings. CME was seen by SD-OCT in only 3 of the 20 *EYS* patients, all of them presenting with the latter alone or other associated inflammatory signs. AAbs were identified in all 12 tested subjects. AR-AAbs were found in 11 of the 12 tested

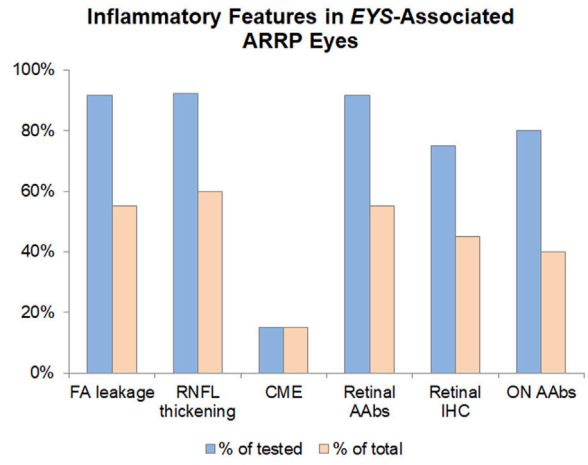

FIGURE 2
Inflammatory features in *EYS*-Associated ARRP Eyes. The inflammatory component of *EYS*-ARRP was evaluated by leakage on FA (performed in 24 eyes), RNFL thickening on OCT (performed in 26 eyes), and cystoid macular edema on OCT (performed in 40 eyes). Additionally, CLIA-certified testing was performed to detect circulating AAbs against retinal (performed in 12 patients) and retrobulbar optic nerve antigens (performed in 10 patients), as well as retinal immunohistochemistry (performed in 12 patients). Blue bars show positivity as a percentage of tested eyes/patients, whereas orange bars show positivity in the total cohort of 20 *EYS*-ARRP patients.

patients [most common: against enolase (8/12) and TULP1 (4/12)]. AON-AAbs were found in 8 out of 9 tested patients. AAbs against both tissues were seen in 6 patients, and rIHC showed positive staining in 9 of 12 cases, labeling predominantly photoreceptors (8/12) and less frequently RGCs and the RNFL. The specifics of the observed autoreactivities and related correlations are illustrated in Figure 2, Figure 3, Figure 4.

Altogether, 70% (14/20) of patients exhibited subclinical signs of inflammation and, in 12 of them, they were associated with an autoimmune component that correlated closely with imaging and functional findings. These patients received intravitreal and/or sub-Tenon steroid injections, with both subjective and measurable increases in vision (visual acuity, VFs, or both), associated with improved SD-OCT and IVFA characteristics in most.

Subgroup analysis of results in USH2A-associated retinal degeneration

In 2022 (Alekseev et al., 2022), we retrospectively identified 75 subjects (M = 38/F = 37, age 4–84) with confirmed disease-causing *USH2A* gene mutations, all of whom had a complete eye exam, including visual acuity (VA), visual fields (VFs), ffERG, macular (n = 75) and, in many, optic nerve (n = 40) SD-OCT, IVFAs in about 45% of the subjects (n = 31), and CLIA-certified testing in 50% (n = 35) for circulating AR-AAbsand/or AON-AAbs by antigen-speficic immunoblot, WB, and rIHC.

Of the 62 tested eyes tested with IVFA, 38 eyes had leakage of optic nerve head, vascular arcades, macula, or a combination thereof. The RNFL was thickened on SD-OCT, most often

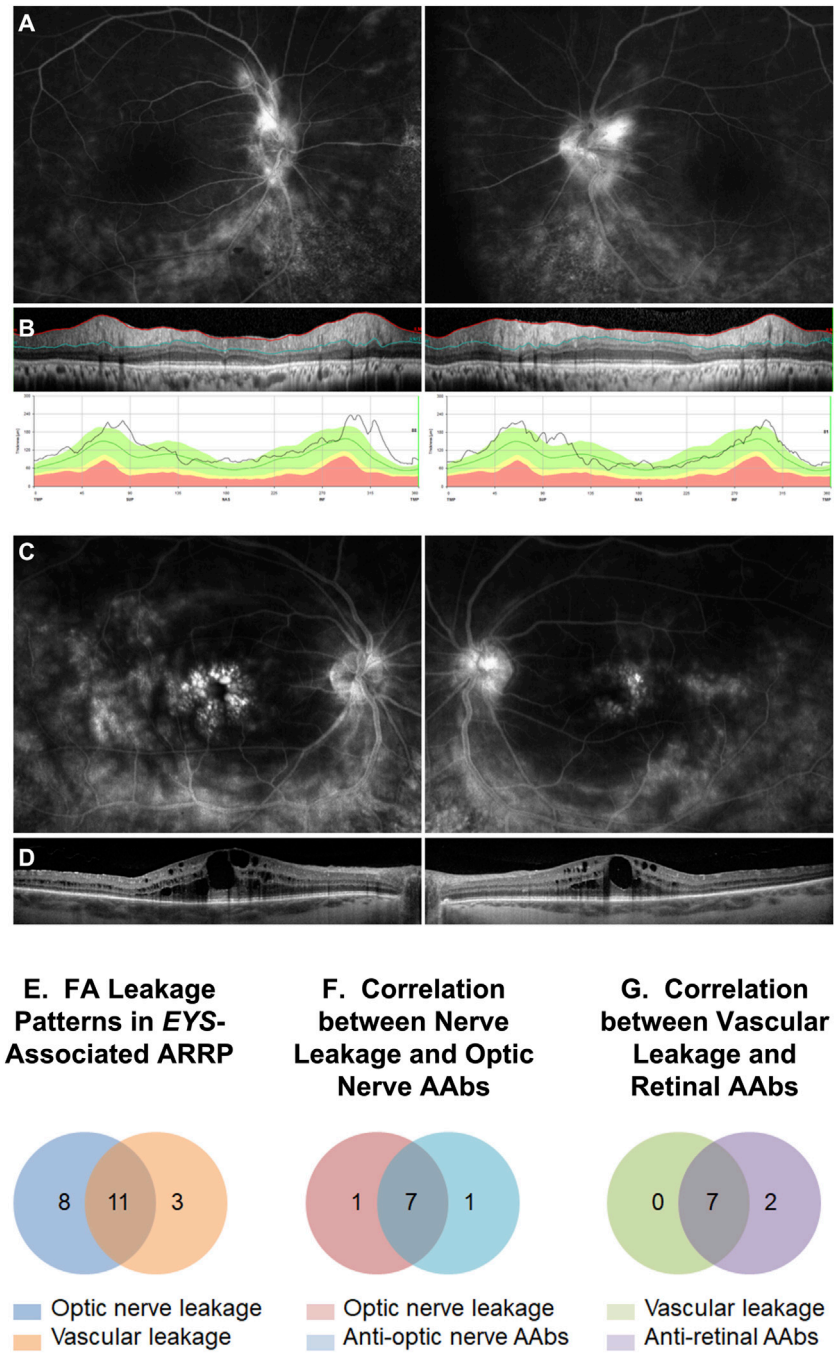

FIGURE 3
Intravenous fluorescein angiography (IVFA) features in *EYS*-ARRP eyes. Example of optic nerve leakage **(A)** in a patient with sectoral thickening of the retinal nerve fiber layer on disc SD-OCT **(B)**. Example of foveal leakage **(C)** in a patient with CME on macular SD-OCT **(D)**. **(E)** Analysis of IVFA leakage patterns: of 24 analyzed eyes, 19 eyes showed optic nerve leakage, 14 eyes showed perivascular leakage, and 2 eyes showed no leakage. Combined optic nerve and perivascular leakage was seen in 11 eyes. **(F)** Optic nerve leakage on IVFA correlated strongly with presence of circulating AON-AAbs on Western blot. Of the 8 patients who tested positive for the AON-AAbs, 7 showed nerve leakage on FA in at least one eye. Conversely, of the 8 patients with FA nerve leakage, 7 tested positive for AON-AAbs. **(G)** Vascular leakage on IVFA correlated strongly with presence of circulating AR-AAbs. Of the 9 patients who tested positive for AR-AAbs, 7 showed vascular leakage on IVFA in at least one eye. Conversely, all 7 patients with IVFA vascular leakage tested positive for AR-AAbs.

sectorally, in 49 of 80 eyes, and correlated well with IVFA leakage, helping explain disproportionate VA losses compared to foveal SD-OCT findings. CME was seen by SD-OCT in 47 of 150 eyes (31%). AR-AAbswere found in 32 of the 35 tested patients [most often against carbonic anhydrase II (16/35) and enolase (15/35)]. AON-AAbs were found in 28 of 34 tested patients, and rIHC showed positive staining in 28 of 34 cases, labeling predominantly photoreceptors (26/34) and less frequently RGC (11/34) and

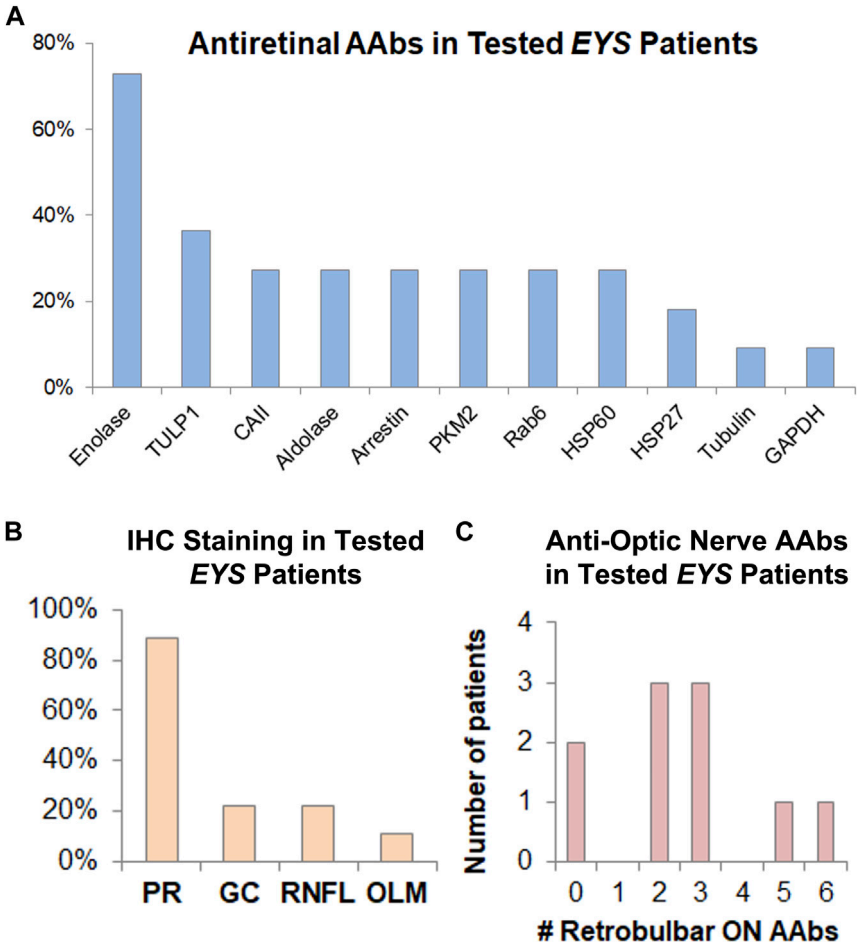

FIGURE 4
AAbs against retinal and optic nerve antigens are frequently present in *EYS*-ARRP patients. **(A)** Among those patients who tested positive for AR-AAbs, the most prevalent retinal antigen was enolase (involved in 75% of positive patients), followed by TULP1 and others, as shown above. **(B)** Among those patients who had positive tissue staining to rIHC on human retinal tissue sections stained with patient serum, the photoreceptor (PR) layer was the most commonly involved, with less frequent staining of RGCs, RNFL, and outer limiting membrane (OLM). **(C)** Human retrobulbar optic nerve lysates were used for WB-based AON-AAAb testing. The 10 patients who underwent testing, showed positivity, on average, for 2.6 optic nerve antigens, ranging from 0 (no reactivity against retrobulbar antigens) to as many as 6 antigens per patient. Of note, presence of AON-AAbs correlated strongly with optic nerve leakage on IVFA (Figure 3F), and presence of AR-AAbscorrelated strongly with vascular leakage on IVFA (Figure 3G).

RNFL (8/34). Altogether, 66.7% (50/75) of patients exhibited subclinical signs of inflammation, which correlated directly with the presence of circulating AAbs in 25 of them. The specifics of the observed autoreactivities and related correlations are illustrated in Figure 5, Figure 6, Figure 7.

Also, these patients, after modest to no response to initial trials of topical and/or oral CAIs for CME and in all cases when significant optic nerve inflammatory involvement was present (which would not be expected to respond to CAIs), received intravitreal and/or sub-Tenon steroid injections in doses and frequencies dictated by the severity of the observed inflammatory findings, with or without subsequent addition of IMT regimens based on response to the intra/periocular steroids. Most patients experienced both subjective and measurable increase in vision (by VA criteria, VF criteria, or both), associated with improved SD-OCT and IVFA characteristics in virtually all treatment-responsive cases.

Examples of treatment-responsive IRD patients following management of inflammatory complications

How much vision can IRD patients recover from ongoing inflammatory complications? The short answer is—it depends on the severity of the complications at the time of evaluation, the timing of the identification of the complication with respect to any more sudden-onset, abrupt vision changes, and the stage of the underlying disease itself. We have previously briefly reported two cases of IRDs who experienced marked visual loss recovery after management of inflammatory complications associated with detectable AR- and AON-AAbs (Iannaccone and Radic, 2019). One with *RHO*-linked autosomal dominant (AD) RP will be re-reviewed and illustrated in further detail here, alongside a representative case of *EYS*-associated ARRP and even one with *ABCA4*-associated cone-rod dystrophy (CORD). These 3 cases have been specifically chosen to emphasize

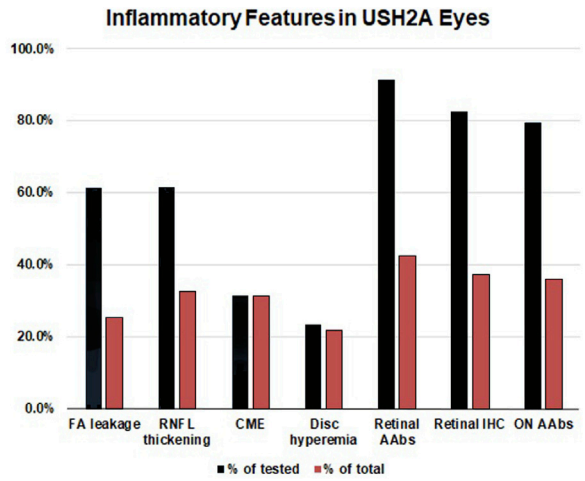

FIGURE 5
Inflammatory features in USH2A-associated retinal degeneration. The inflammatory component of USH2A-linked ARRP was evaluated by leakage on fluorescein angiography (FA) (n = 62 eyes), retinal nerve fiber layer (RNFL) thickening on optical coherence tomography (OCT) (n = 80 eyes), cystoid macular edema (CME) on OCT (performed in 150 eyes), and assessment of disc hyperemia on fundoscopy (n = 142 eyes). CLIA-certified testing was performed to detect circulating autoantibodies (AAbs) against retinal (n = 35) and retrobulbar optic nerve antigens (n = 30), as well as retinal immunohistochemistry (IHC, n = 34). Blue bars: positivity as a percentage of tested eyes/patients, Red bars: positivity in the total USH2A cohort (n = 75).

the very important role of optic nerve inflammatory complications, in IRDs, well beyond CME (if at all present) and how treatment of these cases can allow patients in glaring cases like these ones to achieve their "true retinal potential".

P23H RHO-linked ADRP: Full visual field potential restoration treating inflammatory optic nerve complications

This 51-yo White female [briefly reported in (80)] presented with a family history of RP consistent with dominant inheritance. BCVA was 20/20–2 in the right eye and 20/30 in the left. However, the patient complained of blurred vision. Fundus examination showed altitudinal RP limited to the inferior retina (Figure 8A, arrows), a presentation that would predict an altitudinal VF defect. The ffERG (not shown) was reduced but still robust and also rod responses remained partially measurable, attesting to an overall mild to moderate disease stage consistent with the clinical presentation. Of note, the patient's fundus did not exhibit the typical waxy disc pallor of RP (Figure 8A, asterisks). VF loss was instead disproportionately severe compared to the fundus exam and the ffERG findings, showing a concentric constriction (Figure 8C, left).

Via molecular genetic testing, she was confirmed to harbor an *RHO* P23H mutation. Because of the VF/ffERG and fundus exam mismatch, disc inflammation was also suspected. PVEPs were obtained (not shown), exhibiting marked delays at all tested spatial frequencies (120–140 ms P100 peak times, which is in the optic neuritis range) without amplitude response loss. An IVFA (Figure 8B) showed marked papillary and peri-papillary staining and leakage increasing substantially in the late IVF frames, and peripapillary SD-OCT showed mild but measurable nasal RNFL swelling in both eyes (Figure 8C, right). This suggested a secondary autoimmune component affecting both the optic nerve and retina, causing far more vision loss than caused by the RP alone. The patient serum was positive for anti-ON AAbs against 30-kDa, 35–40-kDa complex, and 46-kDa proteins and for anti-retinal Aabs against 30-kDa (CA-İİ), 33-kDa, 46-kDa (alpha-enolase), 56-, 60-, and 62-kDa proteins, with mild photoreceptor staining and marked RGC and RNFL staining on rIHC. It was therefore decided at this stage to initiate serial subtenon triamcinolone acetonide injections. After 3 years of continued treatment, the disc inflammation and swelling progressively diminished and resolved (Figure 8D, right), and the VF was restituted to her "true retinal potential", limited to the expected altitudinal VF defect (Figure 8D, left).

EYS-linked ARRP: CME resolution and substantial reduction in visual field loss

This 28yo White female presented with a history of night blindness, VF loss and photopsia that suggested ARRP. Baseline BCVA was 20/50 in the right eye and 20/30 in the left. Her fundus exam (Figure 9A) showed bone spicule-like changes both nasally and, less so, temporally, with only mild nasal/superonasal disc hyperemia bilaterally. These changes were also associated with speckled loss of AF signal in these same areas and a wide ring of hyperautofluorescence was visible at and well outside the vascular arcades, encircling an area of well preserved central retinal integrity (Figure 9B). Genetic testing identified two *EYS* mutations in trans, a c.2259 + 1G>T splice site mutation and c.4103dupT, p. Ser1369IlefsTer18 frameshift mutation. A baseline IVFA (Figure 9C) showed florid CME, which was also apparent on SD-OCT (Figure 9D) and, in addition to this expected finding, it also revealed marked late optic nerve inflammatory involvement and hyperfluorescence at the arcades in both eyes. Baseline SKPs (Figure 9D, far left) showed bilateral temporal and nasal VF loss with other patchy absolute scotomas superiorly and inferiorly in the right eye. There was no response of CME to an initial oral and topical CAI regimen. A secondary autoimmune inflammatory component was suspected, prompting testing for Aabs and rIHC, which identified AON-Aabs against 44, 46, 52, 62, and 136 kDa proteins and for AR-Aabs against 34 k (CRALBP), 46 k (enolase), 52 k (tubulin), 58 k, 58 k (PKM2), and 76 kDa proteins. After adding to the treatment regimen serial bilateral intravitreal triamcinolone acetonide injections, followed by a transition to subtenon injections of the same due to intervening intraocular pressure elevations and oral IMT with long-term MMF, escalated progressively from 500 mg BID to 1,500 mg BID, SKPs at 2 years showed sustained nasal and temporal widening and disappearance of the absolute scotomas seen at baseline with overall improved size and sensitivity, and macular SD-OCTs also showed a significant reduction in CME in the right eye and resolution in the efte ye (Figure 9E). A follow-up IVFA also exhibited markedly reduced leakage at the disc and the arcades (not shown), whereby the improved VF could be attributed to resolved inflammation at the optic nerve and arcade level. These improvements were also associated with a marked reduction in photopsia. After over 5 years of follow up, despite long-term IMT, there have been periodic relapses of the CME, the disc inflammation and portions of the VF loss in conjunction with reductions in the

10.3389/fcell.2023.1177711

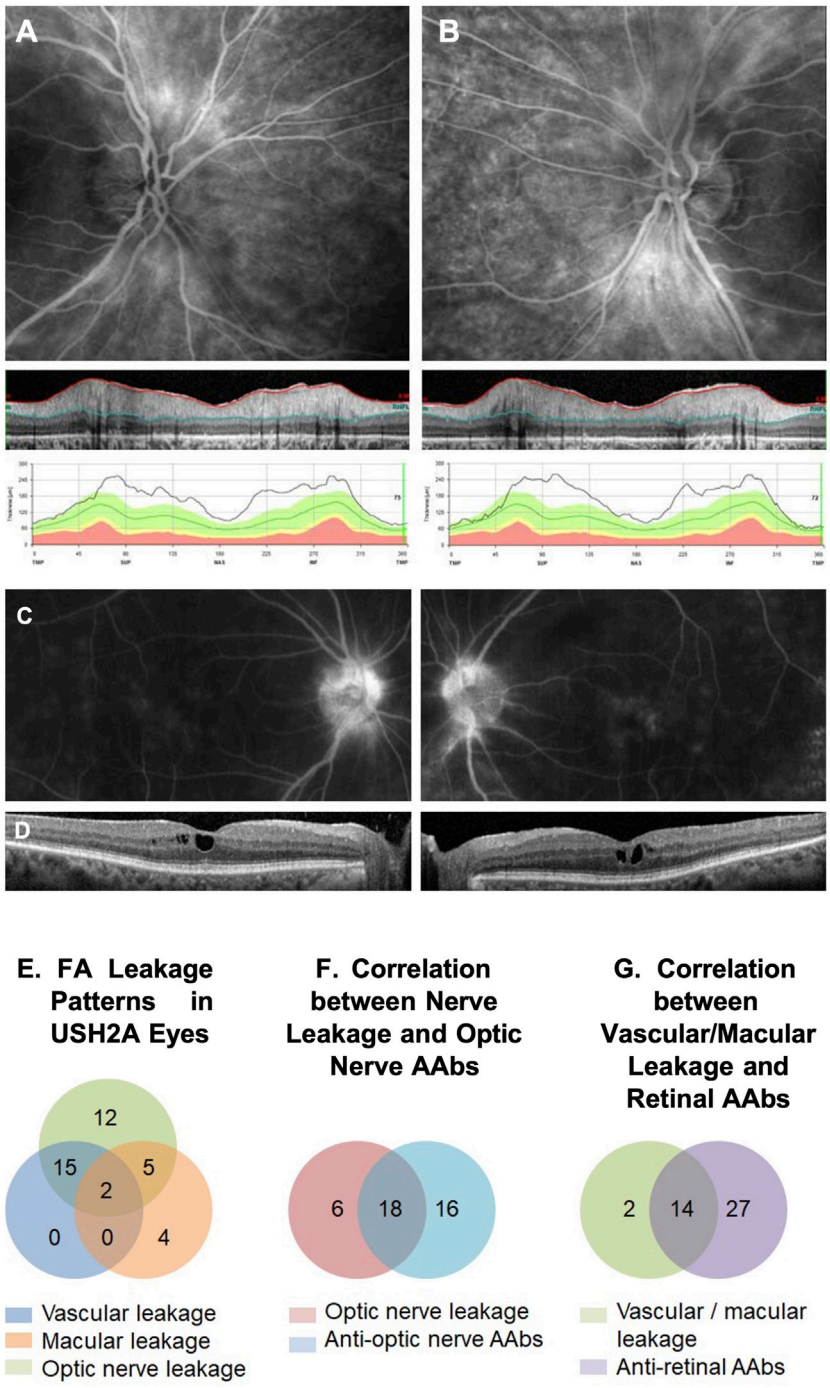

FIGURE 6
IVFA features and AAb findings in USH2A. An example of a late-phase fluorescein angiography (FA) image of an USH2A-associated retinal degeneration patient shows optic nerve head leakage in both eyes correlated with retinal nerve fiber layer (RNFL) thickening in SD-OCT images **(A, B)**. Similarly, an example of macular leakage on late-phase FA correlated cystoid macular edema (CME) on SD-OCT **(C, D)**. FA leakage pattern in USHA2 eyes showed all ON head, macular, and vascular leakage patterns with overlapping **(E)**. Optic nerve leakage on FA correlated strongly with the presence of circulating anti-optic nerve autoantibodies (ON-AAbs) **(F)**, and Vascular/macular leakage on IVFA correlated strongly with the presence of circulating anti-retinal AAbs (AR-AAbs) **(G)**.

steroid regimen, implemented in an effort to balance this regimen with the IOP status (both oral and topical CAIs have been reintegrated into the regimen to assist with longterm CME and IOP co-management, and a topical NSAID has been added as well), but they all remained susceptible of re-improvement after repeat steroid injections. The current IOP conditions would permit us also to consider transitioning this patient to suprachoroidal triamcinolone acetonide injections at the next CME relapse

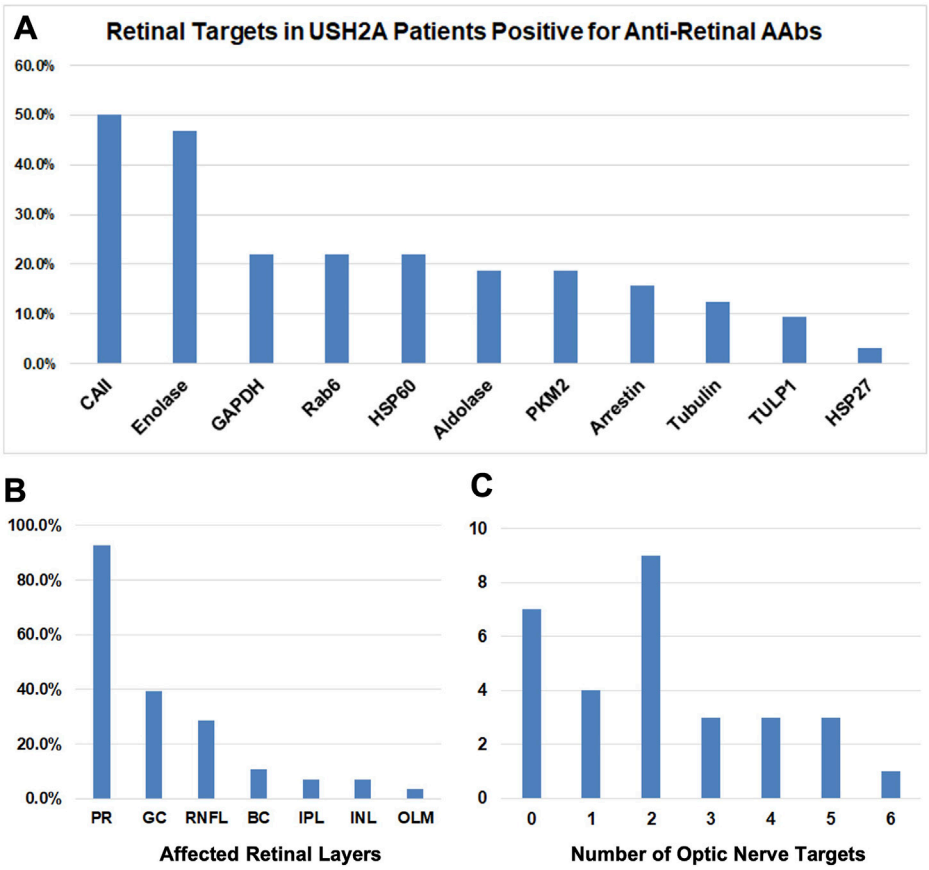

FIGURE 7
Breakdown of AAbs in USH2A. **(A)** Bar graphs showing results of the retinal targets in USHA 2 patients positive for anti-retinal autoantibodies (AR-AAbs). The presence of autoantibodies against Carbonic anhydrase II and Enolase retinal antigens was demonstrated. **(B)** Bar graphs showing retinal immunohistochemistry (rIHC) results with positive staining predominantly in photoreceptors and less frequently retinal ganglion cells and retinal neural fiber layer. **(C)** Bar graphs showing the number of optic nerve targets.

episode. Because of the precarious IOP status, long-term steroid implants, which would appear to be an ideal solution for this patient, have been deferred for now, but also remain under consideration.

ABCA4-linked CORD: From light perception to partial acuity and substantial visual field restitution

A 29-year-old White male with a history of "Stargardt" since childhood presented with a best corrected visual acuity (BCVA) 20/200 with severe loss of ffERG and a widespread phenotype characterized by disseminated atrophic spots, compatible with an advanced stage CORD (Figures 10A, B). The patient was molecularly confirmed to have *ABCA4*-related CORD (2 disease-causing mutations in trans, one of which is a deep intronic c.5461–10T>C mutation, which are usually associated with a more severe and progressive phenotype). Typical features of *ABCA4*-related disease such as peripapillary FAF sparing and hyperautofluorescent flecks peripheral to the atrophic spots were noticeable. At this stage, the patient was not subjectively noticing any VF loss and VF was normal to confrontation.

This initial presentation was followed by a sudden, precipitous bilateral BCVA to 20/400 and severe subjective VF loss, which was confirmed by SKP testing (Figure 10C). A Full-Field Stimulus Test (FST) (Birch et al., 2020) obtained at this stage showed severe sensitivity depression to white light stimuli (Figure 10D). At this point, a subacute secondary autoimmune retinal complication was suspected and AAb and rIHC testing was ordered, revealing 4 AR-AAbs (vs. carbonic anhydrase II, aldolase, arrestin, pyruvate kinase M2) and positive rIHC for staining of photoreceptor and RGCs. By the time test results were received and the patient could be seen in follow up, though, BCVA had already declined to light perception (LP) in the right eye and count finger (CF) in the left eye, without cataract or apparent changes in exam or imaging from baseline. A brain MRI had also been obtained to exclude any central origin to the vision loss, and that too was normal. An initial subtenon triamcinolone acetonide injection did not improve the findings, thus MMF 500 mg twice daily and bilateral intravitreal triamcinolone acetonide injections (IVTAs) were started. After the first IVTA injection, BCVA recovered rapidly to the 20/300–20/400 range at distance and 20/70 near, whereby the patient was already able to work successfully at the computer. After serial IVTA injections and continued MMF 500 mg twice daily (18-mo treatment course), BCVA recovered to baseline levels (20/200), VF improved dramatically, and FST testing improved equally dramatically by 3.5–4.5 log units (Figures 10D–F).

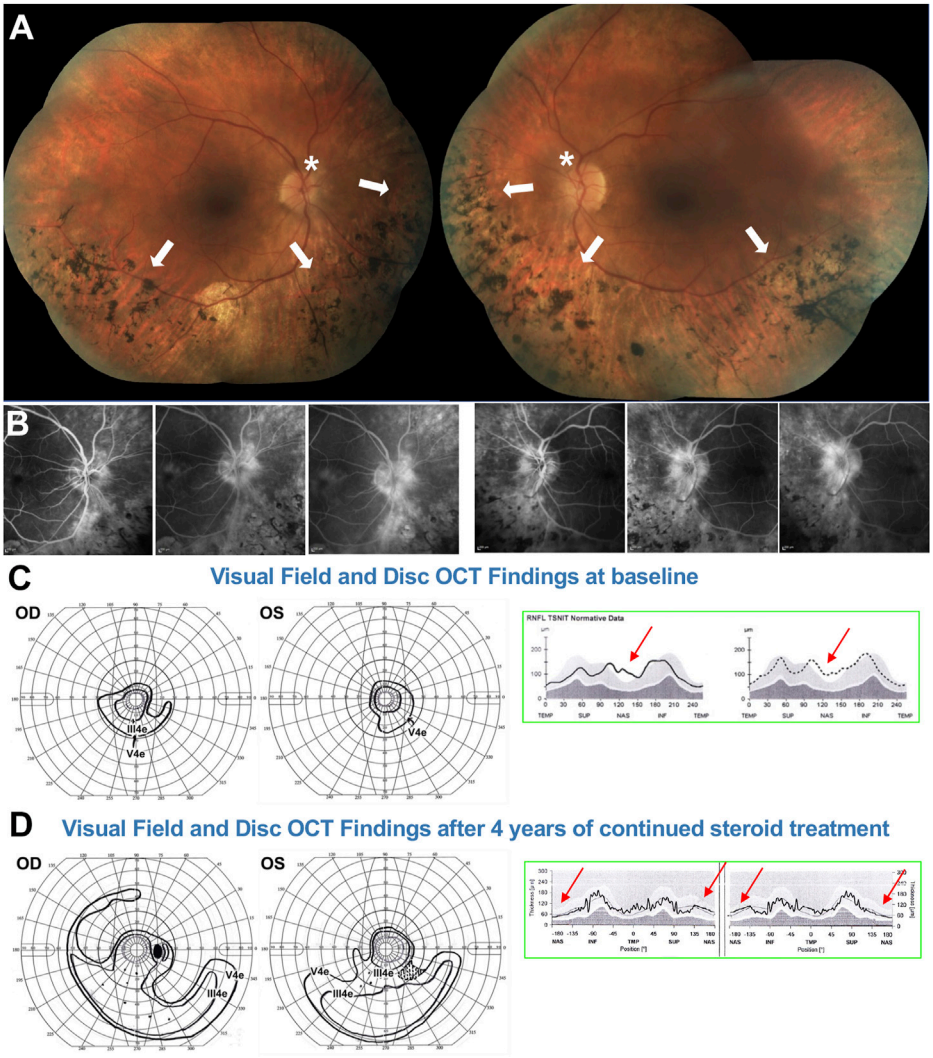

FIGURE 8
51-yo female with ADRP confirmed to be due to a *RHO* P23H mutation. **(A)** Fundus photos showing altitudinal (inferior) bone spicules (arrows) without disc waxy pallor (asterisk). **(B)** Fluorescein angiography at baseline shows marked papillary and peri-papillary staining and leakage increasing in the later frames. **(C)** left: Baseline kinetic visual fields showing concentric constriction of the visual field, inconsistent with the fundus presentation. **(C)** right: Disc OCT scans show (arrows) nasal RNFL swelling in both eyes. **(D)** left: After treatment, the visual field was markedly improved, with a pattern now consistent with to "true retinal potential" of the patient, and the disc OCT shows resolution of the RNFL swelling in both eyes **(D)** right. Please refer to main text for further details.

Discussion

We have illustrated the anti-retinal and anti-optic nerve autoreactivity patterns observed in 127 patients reviewed retrospectively with a confirmed molecular genetic diagnosis of an IRD. This patient sample represented 30.3% of the patients with a suspected IRD at referral who tested positive for AAbs. The remainder of the AAb-positive patients were found to haave primary AIR/AINR or its paraneoplastic counterparts (CAR/CARON). Contrary to a common belief that virtually any IRD patient tested will exhibit autoreactivities, we had 9 subjects who, despite being suspected of having secondary autoimmune complications due to the presence of visible or strongly suspected inflammatory complications, tested negative for any type of AAb and exhibited no staining upon rIHC. Thus, despite the sample being upfront more likely to exhibit autoreactivies by virtue of the criteria used to make it medically appropriate to order AAb and rIHC testing, not even everyone in this enriched sample always showed autoreactivity. Our findings show that secondary autoimmune complications in IRDs are indeed common and appear to be more associated with certain genotypes than others. In our retrospective case series, the *EYS, USH2A, MERTK, CRB1, BBS1, NR2E3, ABCA4, RHO, RP1, KLHL7,* and the *PRPF* family of genes were among the others more commonly associated with AAb-associated inflammatory manifestations—and among the latter ones, the *PRPF31* gene was more commonly so than the *PRPF8* one. It is not presently known if more immunogenic phenomena associated with certain genotypes may be behind the clustering of AAb autoreactivities within the aforementioned genes. Based on the evidence associated with MERTK gene mutations (reviewed in further detail below), this would be expected to be the case in conjunction with this one gene and may also be the case for the

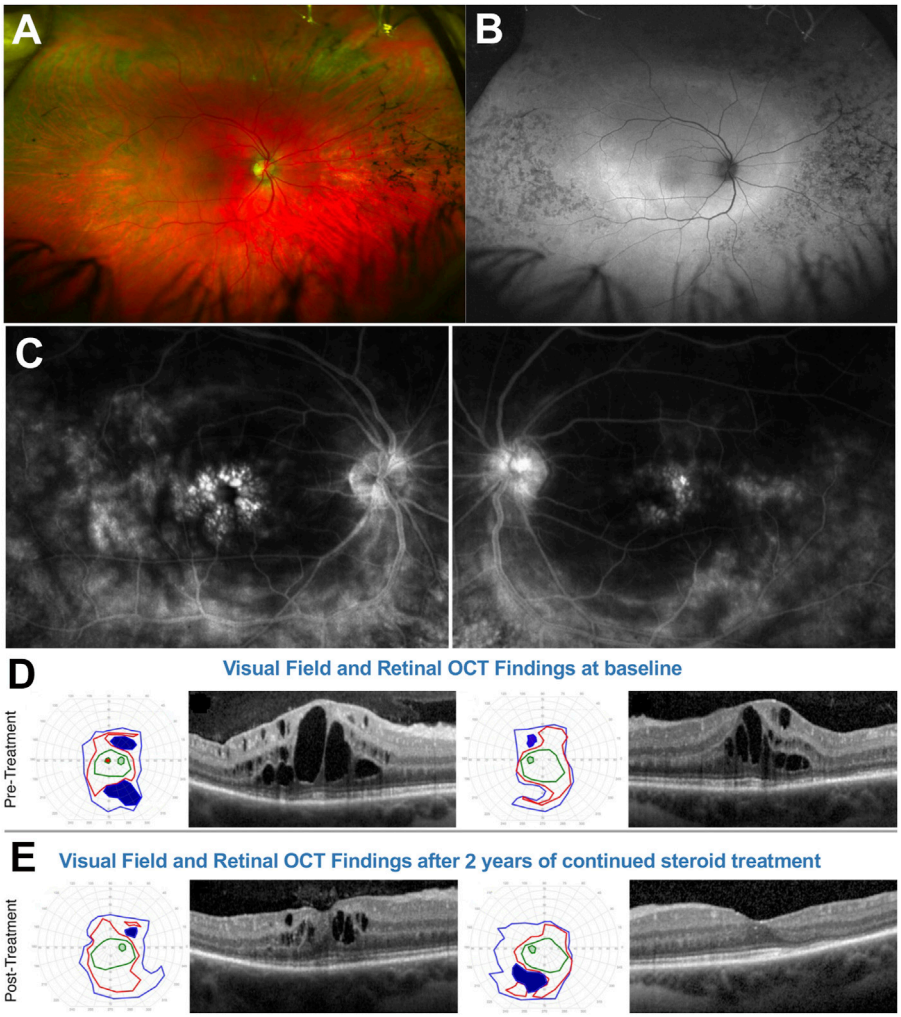

FIGURE 9
28-yo female with ARRP confirmed to be due to *EYS* mutations. **(A)** Fundus photos. **(B)** Fundus autofluorescence. **(C)** Fluorescein angiography at baseline shows shows marked cystoid macular edema (CME), late optic nerve inflammatory involvement, and hyperfluorescence at the arcades/posterior pole on both eyes. At baseline **(D)** Semiautomated kinetic perimetries (SKPs) show baseline marked bilateral temporal and nasal visual field (VF) loss with other absolute scotomas and macular SD-OCTs also show florid CME. **(E)** After treatment, SKPs show nasal and temporal visual field widening and disappearance of the absolute scotomas seen at baseline. Macular SD-OCTs significantly reduce CME in OD and resolution in OS. Please refer to main text for further details.

others. This aspect deserves further investigation at the preclinical level. For *BBS1*, the association we found is also quite interesting in light of very recent evidence pointing to this gene, and potentially more in general the BBSome, in being involved in immune synapse assembly by promoting the centrosome polarization to the antigen-presenting cells and in the regulation of selective functions of T cells that predispone BBS patients to other autoimmune and inflammatory diseases (Kanie and Jackson, 2021; Tsyklauri et al., 2021; Stump et al., 2023).

Evidence for stereotyped pathogenic autoreactivities in MERTK-associated retinal disease

The work of Adamus et al. (Xiong et al., 2013) on the RCS rats, whose retinal dystrophy is due to a mutation in the Mertk gene, has clearly shown how AR-AAbs [directed against arrestin and interphotoreceptor binding protein (IRBP)] develop early in the course of the RCS rat disease. Adamus et al. (Xiong et al., 2013) also showed intense staining of outer photoreceptor segments, TUNEL-positive apoptotic cells that coincide with AAb production, and intense intraretinal microglial and T-lymphocyte reactivity. The microglial reactivity patterns were different than the physiological ones both by tissue level localization and intensity/patterns of activation (Xiong et al., 2013). In line with our observation that these AAb-associated inflammatory reactions often have an optic nerve and retinal vasculitic component, also RCS rats exhibit marked disc and retinal vascular leakage on IVFA (Adamus et al., 2004). Even more importantly, systemic treatment of RCS rats every other day as of P21 (thus once disease had already started to occur) with an epitope-specific biologic agent blocking the anti-IRBP AAbs retain significantly more outer nuclear layer (ONL)

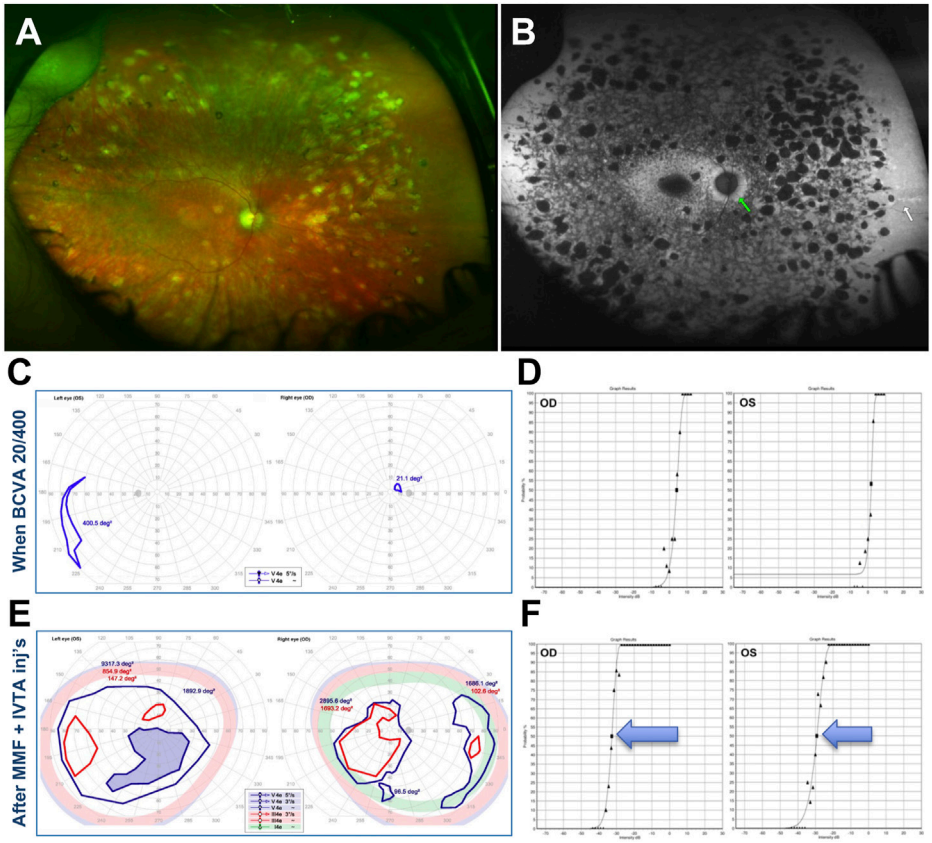

FIGURE 10
29-year-old White male with confirmed recessive cone-rod dystrophy due to *ABCA4* mutations. **(A)** Fundus photos. **(B)** Fundus autofluorescence. **(C)** Semiautomated kinetic perimetries (SKPs) obtained after the first bout of severe subacute vision loss. **(D)** Full-field Stimulus Threshold (FST) test at this same time point. **(E)** Markedly improved SKPs after treatment. **(F)** Markedly improved FSTs after treatment. Please refer to main text for further details.

thickness than untreated ones or the ones treated with vehicule alone, and neither vascular nor disc leakage and subclinical signs of inflammation are appreciable any longer after active treatment (Adamus et al., 2004).

Following this evidence, we investigated *Mertk*-deficient mice and we observed the same type of anti-arrestin and anti-IRBP in the sera of these mice (Epstein et al., 2015; Iannaccone and Radic, 2019) and that, upon rIHC, *Mertk*-deficient mouse sera stain intensely also the optic nerve head region (Iannaccone and Radic, 2019), which could explain well the disc leakage seen in RCS rats. We further showed that patients harboring the null *MERTK* mutation, p. R775X (Ksantini et al., 2012), exhibit these very same reactivities, indicating that this specific pattern of AAb response is conserved across species when the *MERTK* gene is involved (Epstein et al., 2015; Iannaccone and Radic, 2019). We then showed also that, in conjunction with this AAb response, in *Mertk*-deficient mice there is abundant intraretinal accumulation of large clumps of strongly citrullinated peptides (Hollingsworth et al., 2015; Iannaccone and Radic, 2019), a biochemical reaction that is well known from the rheumatoid arthritis world to be strongly immunogenic and proinflammatory (Iannaccone and Radic, 2019). In addition, we showed that, when *Mertk*-deficient mice are crossed with mice lacking PAD4, which we have demonstrated to be the main retinal peptidylarginine deiminase that mediates intraretinal citrullination under physiological conditions (Hollingsworth et al., 2017; Hollingsworth et al., 2018), the severity of the retinal degenerative phenotype in *Mertk*-deficient mice is approximately half at corresponding time points compared to the same mice with intact PAD4, free to accumulate large amount of immunogenic and proinflammatory citrullinated peptide aggregates (Iannaccone and Radic, 2019). Thus, reducing what we interpret to be a key trigger to the anti-retinal activation of the immune system and production of AAbs in *MERTK*-related disease in mice appears to have at least as meaningful a treatment impact as anti-IRBP AAb blockage has been shown to be in RCS rats.

The presence of a robust inflammatory component in *Mertk*-associated retinal disease has been recently confirmed independently in full by Mercau et al. (Mercau et al., 2023). Thus, one can readily envision how treatment strategies of this type, especially if early enough in the course of the disease, could prove very impactful on patients as well, and not only for patients with *MERTK*-associated disease.

Evidence for IMT agents as treatments for IRDs

As mentioned in the introduction section, there is now evidence that some IMTs may exert outright beneficial effects on IRDs *via*

interactions with the mechanisms intrinsic to the retinal degenerative process itself. One of them is MMF, the very same IMT agent used to help treat inflammatory complications in 2 of our 3 representative cases described above. MMF is a prodrug of mycophenolic acid (MPA), worldwide approved for medical use, which potently suppresses *de novo* guanine nucleotide production by reversibly inhibiting inosine monophosphate dehydrogenase (IMPDH). Yang et al. have discovered that intraperitoneally administered MMF suppresses retinal cyclic guanosine monophosphate (cGMP)-dependent photoreceptor toxicity in both the *rd1* and *rd10* ARRP mouse models, both caused by *PDE6B* mutations (Yang et al., 2020). After treatment, the authors observed marked improvement in retinal microanatomical and functional preservation (cone ffERGs). Since cGMP dysregulation may be a common mechanism of photoreceptor cell death in up to 30% of forms of RP, pursuing additional studies to investigate further the IRD cGMP-dependent mechanism-specific effects of MMF is ongoing. Of further interest, though, MMF is known to be neuroprotective after excitatory injury, to inhibit microglia activation, to inhibit leukocytes, and even act as an antioxidant [reviewed in (90)]. Accordingly, in the *rd1* and *rd10* mouse models treated with MMF, Yang et al. also observed much improved (more physiological state) microglial morphological and migration patterns, and far less photoreceptor layer infiltration by microglial cells. While microglial activation may be important to remove debris resulting from inflammatory events, they also trigger a cascade of inflammatory events, as it has been shown in the *Mertk* murine models discussed above that are connected both directly and indirectly to their migration to non-physiological retinal locations. Thus, notwithstanding the noted cGMP-related effects that make MMF and derivatives thereof attractive as an outright treatment candidate for various forms of RP, a benefit to the inflammatory side of IRDs through its impact on local intraretinal inflammation pathways provides an important validation for its observed clinical benefits in IRD patients with inflammatory, autoimmune-associated complications.

MTX is a drug already routinely used to treat cancer, rheumatoid, psoriatic and other forms of inflammatory arthritis, posterior non-infectious inflammatory eye disease and, intravitreally, ocular lymphoma. The anti-inflammatory actions of MTX encompass multiple mechanisms, including an antimetabolite effect *via* the inhibition of purine and pyrimidine synthesis, transmethylation reactions, translocation of nuclear factor-κB to the nucleus, signaling *via* the Janus kinase–signal transducer and activator of transcription (JAK–STAT) pathway and nitric oxide production, as well as the promotion of adenosine release and expression of certain long non-coding RNAs (Cronstein and Aune, 2020). Like MMF, MTX has been shown to have important, mechanistically specific efficacy in another model of RP, the P23H *RHO* knock-in mouse model (Liu et al., 2020), the same mutation affecting one of the patients we illustrated. Via an *in vitro* screen of hundreds of compounds, Liu et al. discovered that MTX increases the clearance of misfolded P23H *via* the lysosomal pathway and increases also autophagy flux. Intravitreal injections (IVIs) of MTX were then tested *in vitro* in the P23H *RHO* knock-in mouse model for potential therapeutic efficacy at stages when rods were still sufficiently intact to respond to treatment. A regimen of four weekly 25 pmol IVIs started at post-natal day 15 increased misfolded P23H clearance *via* the lysosomal pathway and autophagy also *in vivo*, and led to significantly better functional (ffERG), increased outer segment rhodopsin levels and better ONL preservation compared to untreated mice. A single IVI was insufficient to attain these results, and the 25 pmol dosing outperformed 100 pmol, indicating that there is an optimal therapeutic range for MTX IVIs. Since MTX is a widely available drug and worldwide approved for systemic medical use, and is also available as for IVI regimens in humans, Aldeyra Therapeutics has initiated a human clinical trial (NCT05392179) of IVIs of MTX in ADRP patients with P23H *RHO* mutations and other such mutations in which rhodopsin misfolding and aggregation has already been shown to occur (Iannaccone et al., 2006; Mitchell et al., 2019). Liu et al. did not investigate the behavior of microglial cells in the P23H *RHO* knock-in mice treated with MTX IVIs, thus is it uncertain if, in addition to the noted effects on the clearance of misfolded P23H *via* the lysosomal pathway and the improved autophagy flux, MTX IVIs also improved any inflammatory manifestations that may be at play in this murine model—along the same lines of the case we illustrated. If it did, it too, like MMF, could offer a dual benefit to RP patients and this approach may prove beneficial to other IRD patients who also exhibit inflammatory, autoimmune-mediated complications regardless of any specific effects on the misfolding of accumulating proteins at the intracellular level. More research is needed to this effect and appears worth pursuing—and the outcome of the Aldeyra trial will be of definite interest.

Limitations and take-home messages from our clinical investigation into the pathogenic potential of AAb-associated inflammation in IRDs

One important limitation of our investigation is its retrospective nature. A prospective investigation would certainly be beneficial. In addition, not all of our IRD patients were tested for AAbs/rIHC, as this can only be done in the setting of a research study and not one where the decision to test for AAbs/rIHC is driven by the presence or suspected presence of inflammation—and, thus, by a criterion of medical necessity. Therefore, the actual prevalence of positive AAbs and IHC tests in IRD patients is not presently known. Furthermore, the mechanism underlying AAb-related vision loss in positive patients with IRDs remains to be elucidated. On the other hand, the pathogenic potential of the same type of AAbs is known from the AIR (Fox et al., 2016; Adamus, 2018) and CAR literature (Adamus et al., 1997; Adamus et al., 1998a; Adamus et al., 1998b; Adamus et al., 2011; Kyger et al., 2013; Xiong et al., 2013). While the exact epitopes involved in the processes may admittedly vary between IRDs, AIR and CAR, one can make the parsimonious assumption that, in the presence of treatable inflammation with tangible benefits associated with these AAbs in IRDs, the pathogenic potential of the AAbs observed in AIR/CAR patients is likely at play also in IRD subjects. Further investigations will be needed to elucidate these nuances.

An important take home message from our experience is that IRD patients with secondary autoimmune complications can,

indeed, truly benefit from treatment. As the examples presented herein illustrate well, when the component is impacting primarily the optic nerves, treatment is aimed at letting patients achieve their "full retinal potential" and can be especially impactful. When the secondary autoimmune component affects also the retina beyond mere CME, such as retinal vasculitis or disseminated chorioretinitis-like features, like in the CORD case we presented, treatment can be fundamentally prognosis-altering. Based on these observations, autoimmunity in IRDs cannot be considered just an epiphenomenon, but appears to be an event of pathogenic and prognostic relevance, and of substantial therapeutic importance, a conclusion that is in line with the framework already proposed by Adamus (Adamus, 2021).

We did not perform a case-by-case assessment of the individual therapeutic benefits in our large case series yet, and this will be the object of future retrospective evaluations. However, we have observed how the few patients who would typically exhibit the most modest benefits from steroidal treatment were typically those with more severe, long-lasting vision loss, more severe retinal and optic nerve damage by SD-OCT criteria [loss of central ellipsoid zone (EZ) and external (or outer) limiting membrane (ELM/OLM) or RNFL loss, especially if affecting the papillo-macular bundle (PMB)] and more modest IVFA findings. Most of these patients reported, in their prior history, slow progression of their vision loss over the years until they experienced a sudden acceleration and relatively rapid vision loss that could not be otherwise explained by previous treating physicians. This suggests in these poorly responsive cases that the autoreactivities, at these "burnt-out" stages, truly reflected biomarkers of likely *past* inflammatory autoimmune-mediated manifestations vis-à-vis low levels of ongoing, active inflammation—or, when the IVFA findings were still significant, simply too much preexisting retinal and/or optic nerve damage to respond any further to treatment, emphasizing the likely importance of early detection and treatment of these inflammatory complications.

A common account reported by IRD patients exhibiting autorectivities was also the exacerbation of vision loss within months of undergoing cataract surgery, performed elsewhere, whereby some patients had subsequently refused to have the fellow eye operated on out of fear of experiencing the same outcome. It has been recently reported that CME, the most frequent post-operative inflammatory complication of cataract surgery (also known as the Irvine-Gass syndrome) is much more common in RP patients than in the general population (Hong et al., 2020; Antonio-Aguirre et al., 2022; Nguyen et al., 2023). There is no accounting in the literature for the optic nerve inflammatory complications in IRDs. However, over the past 6+ years, it has been our experience that the risk for post-cataract inflammatory complications can be minimized in IRD patients. Due to our heightened level of awareness of these issues, we instituted early on a systematic protocol whereby no IRD patient undergoes cataract surgery at our facility until examined by the IRD specialist and confirmed to have minimal to no underlying inflammatory findings. When present, AAb testing has been obtained and, if positive, surgeries have been strategically delayed until inflammation has been subdued. To date, contrary to what has been reported in the literature (Hong et al., 2020; Antonio-Aguirre et al., 2022; Nguyen et al., 2023), among hundreds of IRD patients who have undergone cataract surgery at our facility since 2016, we have observed less than a handful of cases of minimal and rapidly resolved post-operative CME, having had each of these "inflammation-prone" IRD cases pretreated shortly before cataract surgery with—usually posterior subtenon—steroids, typically within a week of surgery. None of these patients, even after years of follow up, has to date suffered any sudden or major disease progression or vision loss after surgery not even in the patients who had experienced as much no-light-perception outcomes in the fellow eye operated on previously elsewhere before the autoimmune-mediated inflammatory substrate had been recognized and managed. We aim to conduct a detailed retrospective review of cataract surgery-specific outcomes in our IRD patient population pretreated with our protocol in a separate setting, since this is not the focus of this manuscript. However, we wanted to emphasize herein the substantial practical relevance of this observation to outcomes and prognosis for IRD patients who so often need to undergo cataract surgery and, otherwise, tend to benefit greatly from cataract removal (Hong et al., 2020; Antonio-Aguirre et al., 2022; Nguyen et al., 2023). We have found this to be yet another very important and immediately relevant ramification of our findings that has impactful implications when it comes to ensuring that we do everything possible to avoid accidentally contributing closing the door on the light that *is* at the end of the tunnel for IRDs. We sincerely hope that, having shared this experience, the same caution and prudence in preevaluating (and pretreating, if need be) IRD patients that we use ahead of cataract surgery will be used by everyone henceforth.

Conclusion

In summary, AAb-associated inflammation in IRDs is not a mere epiphenomenon and, at least in many cases, it is truly impactful yet treatable, in line with the mechanistic framework already proposed by Adamus (Adamus, 2021). Thus, while this double-edged sword can prove to be a significant worsening factor for the prognosis of affected patients, recognizing the presence of inflammation in IRDs and treating it can be truly beneficial. The benefits are multiple: a) inflammation can be a potentially strong confounder in natural history studies, if not accounted for; since inflammation appears to be part of the natural history of IRDs, assessing patients for these issues should be incorporated in natural history studies, and should not lead to excluding patients who have such complications; b) inflammation can impact adversely safety and efficacy outcomes in gene therapy trial efforts and other gene-agnostic treatments (e.g., optogenetics, stem cell-related applications); c) successful treatment of inflammatory complications in IRDs can significantly expand the viable therapeutic window for many IRD patients, thereby making them more likely to ultimately remain eligible for gene-specific and agnostic treatment approaches—some of which could, in a not too distant future, include also approaches to better management of intraretinal inflammation including use of existing IMTs or as, but by no means not limited to, PAD4 blockage/inhibition as we showed potentially possible in *Mertk*-deficient mice (Iannaccone and Radic, 2019). Ultimately, one may envision a future in which one may also be able to recognize, perhaps with the aid of artificial intelligence and machine learning-based approaches, patterns of better response to treatment associated with certain

pharmacological regimens and, perhaps, certain AAb profiles, allowing us also to refine the management of inflammation in IRDs, identify optimal treatment protocols, and achieve a better level of truly personalized medicine-type approaches also for IRDs.

Data availability statement

The datasets presented in this article are not readily available because There are no datasets that can be made available for this investigation because the data cannot be made publicly available for both medicolegal and ethical reasons related to HIPAA regulations protecting access to personal health information, or PHI. Requests to access the datasets should be directed to aiannacc@yahoo.com.

Ethics statement

The studies involving human participants were reviewed and approved by Duke IRB. Written informed consent from the participants'; legal guardian/next of kin was not required to participate in this study in accordance with the national legislation and the institutional requirements. Written informed consent was obtained from the minor(s)'; legal guardian/next of kin for the publication of any potentially identifiable images or data included in this article.

Author contributions

Substantial contributions to the conception or design of the work were made by KS and AI. Substantial contributions to the acquisition, analysis, or interpretation of the data presented in this manuscript. Were made by all authors. All authors also contributed to the drafting of the manuscript and revising it critically for important intellectual content and agree to be accountable for all aspects of the work in ensuring that questions related to the accuracy or integrity of any part of the work are appropriately investigated and resolved.

Funding

Supported by an unrestricted departmental research grant to the Duke Eye Center by Research to Prevent Blindness, Inc., New York, NY, and by private donations to AI made under the Duke Retinal Degenerations Research Fund, the Duke Retina Genetics Fund, and the Maria Laura Ciccarelli Memorial Duke Fund.

Acknowledgments

We thank Dr. Oleg Alekseev for his invaluable initial work on the *EYS* and *USH2A* case series and his many helpful comments to our retrospective investigation over the past 2 years.

Conflict of interest

The authors declare that the research was conducted in the absence of any commercial or financial relationships that could be construed as a potential conflict of interest.

Publisher's note

All claims expressed in this article are solely those of the authors and do not necessarily represent those of their affiliated organizations, or those of the publisher, the editors and the reviewers. Any product that may be evaluated in this article, or claim that may be made by its manufacturer, is not guaranteed or endorsed by the publisher.

Supplementary material

The Supplementary Material for this article can be found online at: https://www.frontiersin.org/articles/10.3389/fcell.2023.1177711/full#supplementary-material

References

Adamus, G., Amundson, D., Seigel, G., and Machnicki, M. (1998). Anti-enolase-alpha autoantibodies in cancer-associated retinopathy: Epitope mapping and cytotoxicity on retinal cells. *J. Autoimmun.* 11 (6), 671–677. doi:10.1006/jaut.1998.0239

Adamus, G. (2018). Are anti-retinal autoantibodies a cause or a consequence of retinal degeneration in autoimmune retinopathies? *Front. Immunol.* 9, 765. doi:10.3389/fimmu.2018.00765

Adamus, G., Brown, L., Schiffman, J., and Iannaccone, A. (2011). Diversity in autoimmunity against retinal, neuronal, and axonal antigens in acquired neuro-retinopathy. *J. Ophthalmic Inflamm. Infect.* 1 (3), 111–121. doi:10.1007/s12348-011-0028-8

Adamus, G. (2020). Current techniques to accurately measure anti-retinal autoantibodies. *Expert Rev. Ophthalmol.* 15 (2), 111–118. doi:10.1080/17469899.2020.1739522

Adamus, G. (2021). Importance of autoimmune responses in progression of retinal degeneration initiated by gene mutations. *Front. Med. (Lausanne)* 8, 672444. doi:10.3389/fmed.2021.672444

Adamus, G., Machnicki, M., Elerding, H., Sugden, B., Blocker, Y. S., and Fox, D. A. (1998). Antibodies to recoverin induce apoptosis of photoreceptor and bipolar cells*in vivo*. *J. Autoimmun.* 11 (5), 523–533. doi:10.1006/jaut.1998.0221

Adamus, G., Machnicki, M., and Seigel, G. M. (1997). Apoptotic retinal cell death induced by antirecoverin autoantibodies of cancer-associated retinopathy. *Investigative Ophthalmol. Vis. Sci.* 38 (2), 283–291.

Adamus, G., Ren, G., and Weleber, R. G. (2004). Autoantibodies against retinal proteins in paraneoplastic and autoimmune retinopathy. *BMC Ophthalmol.* 4, 5. doi:10.1186/1471-2415-4-5

Adamus, G., Wang, S., Kyger, M., Worley, A., Lu, B., and Burrows, G. G. (2012). Systemic immunotherapy delays photoreceptor cell loss and prevents vascular pathology in Royal College of Surgeons rats. *Mol. Vis.* 18, 2323–2337.

Ahn, S. J., Kim, K. E., Woo, S. J., and Park, K. H. (2014). The effect of an intravitreal dexamethasone implant for cystoid macular edema in retinitis pigmentosa: A case report and literature review. *Ophthalmic Surg. Lasers Imaging Retina* 45 (2), 160–164. doi:10.3928/23258160-20140131-03

Albert, D. M., Pruett, R. C., and Craft, J. L. (1986). Transmission electron microscopic observations of vitreous abnormalities in retinitis pigmentosa. *Am. J. Ophthalmol.* 101 (6), 665–672. doi:10.1016/0002-9394(86)90766-x

Alekseev, O., Adamus, G., and Iannaccone, A. (2021). Inflammatory findings in autosomal recessive retinitis pigmentosa (ARRP) associated with EYS gene mutations. *Invest. Ophthalmol. Vis. Sci.* 62 (7), 3234.

Alekseev, O., Krauss, E., Kedrov, M., Adamus, G., and Iannaccone, A. (2022). Retinal and optic nerve inflammatory findings are a common feature in patients with USH2A-associated retinal degeneration. *Invest. Ophthalmol. Vis. Sci.* 63 (7), 4498.

Androudi, S., Letko, E., Meniconi, M., Papadaki, T., Ahmed, M., and Foster, C. S. (2005). Safety and efficacy of intravitreal triamcinolone acetonide for uveitic macular edema. *Ocul. Immunol. Inflamm.* 13 (2-3), 205–212. doi:10.1080/09273940590933511

Ansari, A. S., Amir, Z., and Williams, G. S. (2021). Bilateral 0.19 mg fluocinolone acetonide intravitreal implant in the successful treatment of juvenile idiopathic arthritis-associated uveitis and secondary macular oedema: A case report and review of intravitreal therapies. *Ophthalmol. Ther.* 10 (1), 193–200. doi:10.1007/s40123-020-00328-9

Antonio-Aguirre, B., Swenor, B., Canner, J. K., and Singh, M. S. (2022). Risk of cystoid macular edema after cataract surgery in retinitis pigmentosa: An analysis of United States claims from 2010 to 2018. *Ophthalmol. Retina* 6 (10), 906–913. doi:10.1016/j.oret.2022.04.018

Apushkin, M. A., Fishman, G. A., Grover, S., and Janowicz, M. J. (2007). Rebound of cystoid macular edema with continued use of acetazolamide in patients with retinitis pigmentosa. *Retina* 27 (8), 1112–1118. doi:10.1097/IAE.0b013e31805f6b79

Asproudis, I., Katsanos, A., Kozeis, N., Tantou, A., and Konstas, A. G. (2017). Update on the treatment of uveitis in patients with juvenile idiopathic arthritis: A review. *Adv. Ther.* 34 (12), 2558–2565. doi:10.1007/s12325-017-0635-3

Bakthavatchalam, M., Lai, F. H. P., Rong, S. S., Ng, D. S., and Brelen, M. E. (2018). Treatment of cystoid macular edema secondary to retinitis pigmentosa: A systematic review. *Surv. Ophthalmol.* 63 (3), 329–339. doi:10.1016/j.survophthal.2017.09.009

Berson, E. L., Sandberg, M. A., Rosner, B., Birch, D. G., and Hanson, A. H. (1985). Natural course of retinitis pigmentosa over a three-year interval. *Am. J. Ophthalmol.* 99, 240–251. doi:10.1016/0002-9394(85)90351-4

Birch, D. G., Cheng, P., Duncan, J. L., Ayala, A. R., Maguire, M. G., Audo, I., et al. (2020). The RUSH2A study: Best-corrected visual acuity, full-field electroretinography amplitudes, and full-field Stimulus thresholds at baseline. *Transl. Vis. Sci. Technol.* 9 (11), 9. doi:10.1167/tvst.9.11.9

Bourgault, S., Aroichane, M., Wittenberg, L. A., Lavallee, A., and Ma, P. E. (2013). Treatment of refractory uveitic macular edema with dexamethasone intravitreal implants in a pediatric patient with bilateral granulomatous idiopathic panuveitis: A case report. *J. Ophthalmic Inflamm. Infect.* 3 (1), 61. doi:10.1186/1869-5760-3-61

Brinkman, C., Pinckers, A., and Broekhuyse, R. (1980). Immune reactivity to different retinal antigens in patients suffering from retinitis pigmentosa. *Investigative Ophthalmol. Vis. Sci.* 19 (7), 743–750.

Broekhuyse, R., Van Herck, M., Pinckers, A., Winkens, H., Van Vugt, A., Ryckaert, S., et al. (1988). Immune responsiveness to retinal S-antigen and opsin in serpiginous choroiditis and other retinal diseases. *Doc. Ophthalmol.* 69 (1), 83–93. doi:10.1007/BF00154420

Chan, C. C., Hooks, J. J., Nussenblatt, R. B., and Detrick, B. (1986). Expression of Ia antigen on retinal pigment epithelium in experimental autoimmune uveoretinitis. *Curr. Eye Res.* 5 (4), 325–330. doi:10.3109/02713688609020059

Chant, S. M., Heckenlively, J., and Meyers-Elliott, R. H. (1985). Autoimmunity in hereditary retinal degeneration. I. Basic studies. *Br. J. Ophthalmol.* 69 (1), 19–24. doi:10.1136/bjo.69.1.19

Chen, C., Liu, X., and Peng, X. (2022). Management of cystoid macular edema in retinitis pigmentosa: A systematic review and meta-analysis. *Front. Med. (Lausanne).* 9, 895208. doi:10.3389/fmed.2022.895208

Chronopoulos, A., Chronopoulos, P., Hattenbach, L. O., Ashurov, A., Schutz, J. S., Pfeiffer, N., et al. (2022). Intravitreal fluocinolone acetonide implant for chronic postoperative cystoid macular edema - two years results. *Eur. J. Ophthalmol.* 33, 1054–1060. doi:10.1177/11206721221124688

Cideciyan, A. V., Zhao, X., Nielson, L., Khani, S. C., Jacobson, S. G., and Palczewski, K. (1998). Null mutation in the rhodopsin kinase gene slows recovery kinetics of rod and cone phototransduction in man. *Proc. Natl. Acad. Sci. U. S. A.* 95, 328–333. doi:10.1073/pnas.95.1.328

Cronstein, B. N., and Aune, T. M. (2020). Methotrexate and its mechanisms of action in inflammatory arthritis. *Nat. Rev. Rheumatol.* 16 (3), 145–154. doi:10.1038/s41584-020-0373-9

Daiger, S. (2020). *Summaries of genes and loci causing retinal diseases (RetNet)*. Houston, TX, USA: The University of Texas Health Science Center.

Davoudi, S., Ebrahimiadib, N., Yasa, C., Sevgi, D. D., Roohipoor, R., Papavasilieou, E., et al. (2017). Outcomes in autoimmune retinopathy patients treated with rituximab. *Am. J. Ophthalmol.* 180, 124–132. doi:10.1016/j.ajo.2017.04.019

Detrick, B., Newsome, D. A., Percopo, C. M., and Hooks, J. J. (1985). Class II antigen expression and gamma interferon modulation of monocytes and retinal pigment epithelial cells from patients with retinitis pigmentosa. *Clin. Immunol. Immunopathol.* 36 (2), 201–211. doi:10.1016/0090-1229(85)90121-7

Detrick, B., Rodrigues, M., Chan, C. C., Tso, M. O., and Hooks, J. J. (1986). Expression of HLA-DR antigen on retinal pigment epithelial cells in retinitis pigmentosa. *Am. J. Ophthalmol.* 101 (5), 584–590. doi:10.1016/0002-9394(86)90949-9

Doycheva, D., Deuter, C., and Grajewski, R. (2018). Topical corticosteroids and non-steroidal anti-inflammatory drugs in the therapy of non-infectious uveitis. *Klin. Monatsblatter fur Augenheilkd.* 235 (5), 586–591. doi:10.1055/a-0590-4546

Duncan, J. L., Liang, W., Maguire, M. G., Audo, I., Ayala, A. R., Birch, D. G., et al. (2020). Baseline visual field findings in the RUSH2A study: Associated factors and correlation with other measures of disease severity. *Am. J. Ophthalmol.* 219, 87–100. doi:10.1016/j.ajo.2020.05.024

Epstein, R. S., New, D. D., Hollingsworth, T. J., Meunier, I., Lenchik, N. I., Lu, Q., et al. (2015). Defective mer-tyrosine kinase (mer-TK) function is associated with anti-arrestin and anti-interphotoreceptor retinoid-binding protein (IRBP) autoantibodies (AAbs) in Mer, Axl, Tyro3 -/- (TAM) mice and in autosomal recessive retinitis pigmentosa (arRP) patients with a null MERTK mutation. *Invest. Ophthalmol. Vis. Sci.* 56. E-Abstract 169.

Epstein, R. S., Sollenberger, E., Adamus, G., and Iannaccone, A. (2014). *Clinical, functional, and imaging characteristics of cancer-associated retinopathy and optic neuropathy*. Chicago, IL: American Academy of Ophthalmology meeting. Oct. 18-22,.

Feiler, D. L., Srivastava, S. K., Pichi, F., Bena, J., and Lowder, C. Y. (2017). Resolution of noninfectious uveitic cystoid macular edema with topical difluprednate. *Retina* 37 (5), 844–850. doi:10.1097/IAE.0000000000001243

Ferreyra, H. A., Jayasundera, T., Khan, N. W., He, S., Lu, Y., and Heckenlively, J. R. (2009). Management of autoimmune retinopathies with immunosuppression. *Arch. Ophthalmol.* 127 (4), 390–397. doi:10.1001/archophthalmol.2009.24

Finn, A. P., Keenan, R. T., and Jaffe, G. J. (2020). Reconstitution of the ellipsoid zone with tocilizumab in autoimmune retinopathy. *Retin. Cases Brief Rep.* 14 (4), 297–300. doi:10.1097/ICB.0000000000000766

Fishman, G. A., and Cunha-Vaz, J. E. (1981). Carriers of X-linked recessive retinitis pigmentosa: Investigation by vitreous fluorophotometry. *Int. Ophthalmol.* 4 (1-2), 37–44. doi:10.1007/BF00139579

Fishman, G. A., Rhee, A. J., and Blair, N. P. (1986). Blood-retinal barrier function in patients with cone or cone-rod dystrophy. *Arch. Ophthalmol.* 104 (4), 545–548. doi:10.1001/archopht.1986.01050160101022

Forte, R., Pannarale, L., Iannaccone, A., Vingolo, E. M., Santi, G., and Pannarale, M. R. (1994). Cystoid macular edema in retinitis pigmentosa: Clinical and functional evaluation of patients treated with deflazacort. [ARVO abstracts]. *Invest. Ophthalmol. VisSci* 35 (4), 1958.

Fox, A. R., Gordon, L. K., Heckenlively, J. R., Davis, J. L., Goldstein, D. A., Lowder, C. Y., et al. (2016). Consensus on the diagnosis and management of nonparaneoplastic autoimmune retinopathy using a modified delphi approach. *Am. J. Ophthalmol.* 168, 183–190. doi:10.1016/j.ajo.2016.05.013

Frere, A., Caspers, L., Makhoul, D., Judice, L., Postelmans, L., Janssens, X., et al. (2017). Single dexamethasone intravitreal implant in the treatment of noninfectious uveitis. *J. ocular Pharmacol. Ther. official J. Assoc. Ocular Pharmacol. Ther.* 33 (4), 290–297. doi:10.1089/jop.2016.0139

Frishman, L., Sustar, M., Kremers, J., McAnany, J. J., Sarossy, M., Tzekov, R., et al. (2018). ISCEV extended protocol for the photopic negative response (PhNR) of the full-field electroretinogram. *Doc. Ophthalmol.* 136 (3), 207–211. doi:10.1007/s10633-018-9638-x

Fuchs, S., Nakazawa, M., Maw, M., Tamai, M., Oguchi, Y., and Gal, A. (1995). A homozygous 1-base pair deletion in the arrestin gene is a frequent cause of Oguchi disease in Japanese. *Nat. Genet.* 10 (3), 360–362. doi:10.1038/ng0795-360

Funatsu, J., Murakami, Y., Shimokawa, S., Nakatake, S., Fujiwara, K., Okita, A., et al. (2022). Circulating inflammatory monocytes oppose microglia and contribute to cone cell death in retinitis pigmentosa. *PNAS Nexus* 1 (1), pgac003. doi:10.1093/pnasnexus/pgac003

Gattegna, R., Bleicher, I., and Iannaccone, A. (2019). Emerging phenotypic characteristics and identification of novel mutations in autosomal recessive retinitis pigmentosa (ARRP) associated with the EYS gene. *Invest. Ophthalmol. Vis. Sci.* 60 (7), 4508.

Gieser, D. K., Fishman, G. A., and Cunha-Vaz, J. (1980). X-linked recessive retinitis pigmentosa and vitreous fluorophotometry. A study of female heterozygotes. *Arch. Ophthalmol.* 98 (2), 307–310. doi:10.1001/archopht.1980.01020030303013

Grewal, D. S., Jaffe, G. J., and Keenan, R. T. (2021). Sarilumab for recalcitrant cystoid macular edema in non-paraneoplastic autoimmune retinopathy. *Retin. Cases Brief Rep.* 15 (5), 504–508. doi:10.1097/ICB.0000000000000872

Grixti, A., Hagan, R., Nayak, H., and Chandna, A. (2016). Multifocal choroiditis with panuveitis in an 8-year-old boy with long-standing idiopathic acute anterior uveitis. *Eur. J. Ophthalmol.* 26 (5), e114–e117. doi:10.5301/ejo.5000772

Grover, S., Apushkin, M. A., and Fishman, G. A. (2006). Topical dorzolamide for the treatment of cystoid macular edema in patients with retinitis pigmentosa. *Am. J. Ophthalmol.* 141 (5), 850–858. doi:10.1016/j.ajo.2005.12.030

Grover, S., Fishman, G. A., Fiscella, R. G., and Adelman, A. E. (1997). Efficacy of dorzolamide hydrochloride in the management of chronic cystoid macular edema in patients with retinitis pigmentosa. *Retina* 17 (3), 222–231. doi:10.1097/00006982-199705000-00009

Gupta, P., Kheir, W., Peng, B., Chiang, J. P-W., and Iannaccone, A. (2022). Careful clinical-functional phenotyping combined with systematic, broad NGS Panel-based genotyping identify numerous novel disease-causing mutations and deletions in inherited retinal disease patients. *Mol. Vis.* 28, 202–217.

Hariprasad, S. M., and Callanan, D. (2008). Topical nepafenac 0.1% for treatment of chronic uveitic cystoid macular edema. *Retin Cases Brief. Rep.* 2 (4), 304–308. doi:10.1097/ICB.0b013e31809ed9db

Hasanreisoglu, M., Ozdemir, H. B., Ozkan, K., Yuksel, M., Aktas, Z., Atalay, H. T., et al. (2019). Intravitreal dexamethasone implant in the treatment of non-infectious uveitis. *Turk J. Ophthalmol.* 49 (5), 250–257. doi:10.4274/tjo.galenos.2019.81594

Heckenlively, J. R., Aptsiauri, N., Nusinowitz, S., Peng, C., and Hargrave, P. A. (1996). Investigations of antiretinal antibodies in pigmentary retinopathy and other retinal degenerations. *Trans. Am. Ophthalmol. Soc.* 94, 179–200. discussion 200-6.

Heckenlively, J. R., and Ferreyra, H. A. (2008). Autoimmune retinopathy: A review and summary. *Semin. Immunopathol.* 30 (2), 127–134. doi:10.1007/s00281-008-0114-7

Heckenlively, J. R., Jordan, B. L., and Aptsiauri, N. (1999). Association of antiretinal antibodies and cystoid macular edema in patients with retinitis pigmentosa. *Am. J. Ophthalmol.* 127 (5), 565–573. doi:10.1016/s0002-9394(98)00446-2

Heckenlively, J. R., and Lundy, S. K. (2018). "Autoimmune retinopathy: An immunologic cellular-driven disorder," in *Retinal degenerative diseases* (Springer), 193–201.

Heckenlively, J. R., and Lundy, S. K. (2018). Autoimmune retinopathy: An immunologic cellular-driven disorder. *Adv. Exp. Med. Biol.* 1074, 193–201. doi:10.1007/978-3-319-75402-4_24

Heckenlively, J. R., Solish, A. M., Chant, S. M., and Meyers-Elliott, R. H. (1985). Autoimmunity in hereditary retinal degenerations. II. Clinical studies: Antiretinal antibodies and fluorescein angiogram findings. *Br. J. Ophthalmol.* 69 (10), 758–764. doi:10.1136/bjo.69.10.758

Hogewind, B. F., Zijlstra, C., Klevering, B. J., and Hoyng, C. B. (2008). Intravitreal triamcinolone for the treatment of refractory macular edema in idiopathic intermediate or posterior uveitis. *Eur. J. Ophthalmol.* 18 (3), 429–434. doi:10.1177/112067210801800318

Hollingsworth, T. J., and Gross, A. K. (2020). Innate and autoimmunity in the pathogenesis of inherited retinal dystrophy. *Cells* 9 (3), 630. doi:10.3390/cells9030630

Hollingsworth, T. J., New, D. D., Giorgianni, F., Lenchik, N. I., Beranova-Giorgianni, S., Gerling, I. C., et al. (2015). Peptidylarginine deiminase (PAD4) expression and citrullination levels in normal and mouse retinas and in murine models of late (Sod1-/-) and early-onset (Tyro3-/-, Axl-/-, Mertk-/- or TAM mice) retinal degeneration. *Invest. Ophthalmol. Vis. Sci.* 56. E-Abstract 4636.

Hollingsworth, T. J., Radic, M. Z., Beranova-Giorgianni, S., Giorgianni, F., Wang, Y., and Iannaccone, A. (2018). Murine retinal citrullination declines with age and is mainly dependent on peptidyl arginine deiminase 4 (PAD4). *Invest. Ophthalmol. Vis. Sci.* 59 (10), 3808–3815. doi:10.1167/iovs.18-24118

Hollingsworth, T. J., Radic, M. Z., Giorgianni, F., Beranova-Giorgianni, S., Koirala, D., Wang, Y., et al. (2017). Peptidylarginine deiminase 4 (PAD4) is the primary mediator of retinal citrullination in mice. *Invest. Ophthalmol. Vis. Sci.* 58. [E-Abstract no. assignement in progress].

Hong, Y., Li, H., Sun, Y., and Ji, Y. (2020). A review of complicated cataract in retinitis pigmentosa: Pathogenesis and cataract surgery. *J. Ophthalmol.* 2020, 6699103. doi:10.1155/2020/6699103

Iannaccone, A., Alekseev, O., and Adamus, G. (2021). *Recognizing, characterizing, and managing inflammation in inherited retinal degenerations: Treatable, visually impactful complications beyond cystoid macular edema RD2021 Meeting*. Nashville.

Iannaccone, A., Giorgianni, F., New, D. D., Hollingsworth, T. J., Umfress, A. C., Alhatem, A. H., et al. (2015). Circulating autoantibodies in age-related macular degeneration recognize human macular tissue antigens implicated in autophagy, immunomodulation, and protection from oxidative stress and apoptosis. *PLoS ONE* 10 (12), e0145323. doi:10.1371/journal.pone.0145323

Iannaccone, A., Hollingsworth, T. J., Koirala, D., New, D. D., Lenchik, N. I., Beranova-Giorgianni, S., et al. (2017). Retinal pigment epithelium and microglia express the CD5 antigen-like protein, a novel autoantigen in age-related macular degeneration. *Exp. Eye Res.* 155, 64–74. doi:10.1016/j.exer.2016.12.006

Iannaccone, A., Man, D., Waseem, N., Jennings, B. J., Ganapathiraju, M., Gallaher, K., et al. (2006). Retinitis pigmentosa associated with rhodopsin mutations: Correlation between phenotypic variability and molecular effects. *Vis. Res.* 46 (27), 4556–4567. doi:10.1016/j.visres.2006.08.018

Iannaccone, A., Neeli, I., Krishnamurthy, P., Lenchik, N. I., Wan, H., Gerling, I. C., et al. (2012). Autoimmune biomarkers in age-related macular degeneration: A possible role player in disease development and progression. *Adv. Exp. Med. Biol.* 723, 11–16. doi:10.1007/978-1-4614-0631-0_2

Iannaccone, A., and Radic, M. Z. (2019). Increased protein citrullination as a trigger for resident immune system activation, intraretinal inflammation, and promotion of anti-retinal autoimmunity: Intersecting paths in retinal degenerations of potential therapeutic relevance. *Adv. Exp. Med. Biol.* 2019 (1185), 175–179. doi:10.1007/978-3-030-27378-1_29

Iannaccone, A., Rispoli, E., Vingolo, E. M., Onori, P., Steindl, K., Rispoli, D., et al. (1995). Correlation between Goldmann perimetry and maximal electroretinogram response in retinitis pigmentosa. *Doc. Ophthalmol.* 90, 129–142. doi:10.1007/BF01203333

Iannaccone, A. (2003). "Usher syndrome: Correlation between visual field size and maximal ERG response b-wave amplitude," in *Retinal degenerations: Mechanisms and experimental therapy. Adv exp med biol. 533*. Editors M. M. LaVail, J. G. Hollyfield, and R. E. Anderson (New York: Plenum Publishers), 123–131.

A. Iannaccone, E. M. Vingolo, P. Tanzilli, P. Del Beato, and M. R. Pannarale (Editors) (1994). *Long-term results of a pilot study on thymopentin in the treatment of retinitis pigmentosa: Pathophysiological considerations [Italian] IV national congress of the Italian association for ocular pharmacology (AISFO)* (Catania, Italy: Mediconsult). Isola di Capri.

Iannaccone, A., Vingolo, E. M., Tanzilli, P., Del Beato, P., and Pannarale, M. R. (1994). "Long-term results of a pilot study on thymopentin in the treatment of retintitis pigmentosa: Pathophysiological considerations [Italian]," in *The IV national congress of the Italian association for ocular pharmacology (AISFO)* (Catania: MediConsult), 461–473.

Jacobson, S. G., Yagasaki, K., Feuer, W. J., and Roman, A. J. (1989). Interocular asymmetry of visual function in heterozygotes of X-linked retinitis pigmentosa. *Exp. Eye Res.* 48, 679–691. doi:10.1016/0014-4835(89)90009-2

Jain, R., Ferrante, P., Reddy, G. T., and Lightman, S. (2005). Clinical features and visual outcome of intermediate uveitis in children. *Clin. Exp. Ophthalmol.* 33 (1), 22–25. doi:10.1111/j.1442-9071.2005.00938.x

Jones, J., and Francis, P. (2009). Ophthalmic utility of topical bromfenac, a twice-daily nonsteroidal anti-inflammatory agent. *Expert Opin. Pharmacother.* 10 (14), 2379–2385. doi:10.1517/14656560903188425

Juthani, V. V., Clearfield, E., and Chuck, R. S. (2017). Non-steroidal anti-inflammatory drugs versus corticosteroids for controlling inflammation after uncomplicated cataract surgery. *Cochrane Database Syst. Rev.* 7 (7), CD010516. doi:10.1002/14651858.CD010516.pub2

Kanie, T., and Jackson, P. K. (2021). Connecting autoimmune disease to Bardet-Biedl syndrome and primary cilia. *EMBO Rep.* 22 (2), e52180. doi:10.15252/embr.202052180

Karasu, B. (2020). Short-term outcomes of subtenon triamcinolone acetonide injections in patients with retinitis pigmentosa-associated cystoid macular edema unresponsive to carbonic anhydrase inhibitors. *Int. Ophthalmol.* 40 (3), 677–687. doi:10.1007/s10792-019-01228-z

Khani, S. C., Nielsen, L., and Vogt, T. M. (1998). Biochemical evidence for pathogenicity of rhodopsin kinase mutations correlated with the oguchi form of congenital stationary night blindness. *Proc. Natl. Acad. Sci. U. S. A.* 95, 2824–2827. doi:10.1073/pnas.95.6.2824

Khurana, R. N., Bansal, A. S., Chang, L. K., Palmer, J. D., Wu, C., and Wieland, M. R. (2017). Prospective evaluation of a sustained-release dexamethasone intravitreal implant for cystoid macular edema in quiescent uveitis. *Retina* 37 (9), 1692–1699. doi:10.1097/IAE.0000000000001406

Kim, J. E. (2006). Intravitreal triamcinolone acetonide for treatment of cystoid macular edema associated with retinitis pigmentosa. *Retina* 26 (9), 1094–1096. doi:10.1097/01.iae.0000254897.86389.a5

Koop, A., Ossewaarde, A., and Rothova, A. (2013). Peripheral multifocal chorioretinitis: Complications, prognosis and relation with sarcoidosis. *Acta Ophthalmol.* 91 (6), 492–497. doi:10.1111/j.1755-3768.2012.02483.x

Ksantini, M., Lafont, E., Bocquet, B., Meunier, I., and Hamel, C. P. (2012). Homozygous mutation in MERTK causes severe autosomal recessive retinitis pigmentosa. *Eur. J. Ophthalmol.* 22 (4), 647–653. doi:10.5301/ejo.5000096

Kyger, M., Worley, A., and Adamus, G. (2013). Autoimmune responses against photoreceptor antigens during retinal degeneration and their role in macrophage recruitment into retinas of RCS rats. *J. Neuroimmunol.* 254 (1-2), 91–100. doi:10.1016/j.jneuroim.2012.10.007

Lemos Reis, R. F., Moreira-Goncalves, N., Estrela Silva, S. E., Brandao, E. M., and Falcao-Reis, F. M. (2015). Comparison of topical dorzolamide and ketorolac treatment for cystoid macular edema in retinitis pigmentosa and Usher's syndrome. *Ophthalmologica* 233 (1), 43–50. doi:10.1159/000368052

Liu, X., Feng, B., Vats, A., Tang, H., Seibel, W., Swaroop, M., et al. (2020). Pharmacological clearance of misfolded rhodopsin for the treatment of RHO-associated retinitis pigmentosa. *FASEB J.* 34 (8), 10146–10167. doi:10.1096/fj.202000282R

Mansour, A. M., Sheheitli, H., Kucukerdonmez, C., Sisk, R. A., Moura, R., Moschos, M. M., et al. (2018). Intravitreal dexamethasone implant in retinitis pigmentosa-related cystoid macular edema. *Retina* 38 (2), 416–423. doi:10.1097/IAE.0000000000001542

Marmor, M. F. (1990). Hypothesis concerning carbonic anhydrase treatment of cystoid macular edema: Example with epiretinal membrane. *Arch. Ophthalmol.* 108 (11), 1524–1525. doi:10.1001/archopht.1990.01070130026013

McCulloch, D. L., Marmor, M. F., Brigell, M. G., Hamilton, R., Holder, G. E., Tzekov, R., et al. (2015). ISCEV Standard for full-field clinical electroretinography (2015 update). *Doc. Ophthalmol.* 130 (1), 1–12. doi:10.1007/s10633-014-9473-7

McMurtrey, J. J., and Tso, M. O. M. (2018). A review of the immunologic findings observed in retinitis pigmentosa. *Surv. Ophthalmol.* 63 (6), 769–781. doi:10.1016/j.survophthal.2018.03.002

Mercau, M. E., Akalu, Y. T., Mazzoni, F., Gyimesi, G., Alberto, E. J., Kong, Y., et al. (2023). Inflammation of the retinal pigment epithelium drives early-onset photoreceptor degeneration in Mertk-associated retinitis pigmentosa. *Sci. Adv.* 9 (3), eade9459. doi:10.1126/sciadv.ade9459

Miguel-Escuder, L., Olate-Perez, A., Sala-Puigdoners, A., Moll-Udina, A., Figueras-Roca, M., Navarro-Angulo, M. J., et al. (2023). Intravitreal fluocinolone acetonide implant for the treatment of persistent post-surgical cystoid macular edema in vitrectomized eyes. *Eur. J. Ophthalmol.* 33 (1), NP23–NP27. doi:10.1177/11206721211046718

Mitchell, J., Balem, F., Tirupula, K., Man, D., Dhiman, H. K., Yanamala, N., et al. (2019). Comparison of the molecular properties of retinitis pigmentosa P23H and N15S amino acid replacements in rhodopsin. *PLoS ONE* 14 (5), e0214639. doi:10.1371/journal.pone.0214639

Miyake, Y., Goto, S., Ota, I., and Ichikawa, H. (1984). Vitreous fluorophotometry in patients with cone-rod dystrophy. *Br. J. Ophthalmol.* 68 (7), 489–493. doi:10.1136/bjo.68.7.489

Nakazawa, M., Wada, Y., Fuchs, S., Gal, A., and Tamai, M. (1997). Oguchi disease: Phenotypic characteristics of patients with the frequent 1147DELA mutation in the arrestin gene. *Retina* 17, 17–22. doi:10.1097/00006982-199701000-00004

Newsome, D. A., and Michels, R. G. (1988). Detection of lymphocytes in the vitreous gel of patients with retinitis pigmentosa. *Am. J. Ophthalmol.* 105 (6), 596–602. doi:10.1016/0002-9394(88)90050-5

Nguyen, X. T., Thiadens, A., Fiocco, M., Tan, W., McKibbin, M., Klaver, C. C. W., et al. (2023). Outcome of cataract surgery in patients with retinitis pigmentosa. *Am. J. Ophthalmol.* 246, 1–9. doi:10.1016/j.ajo.2022.10.001

Park, S., Lim, L. T., and Gavin, M. P. (2013). Topical steroidal and nonsteroidal antiinflammatory drugs for the treatment of cystoid macular edema in retinitis pigmentosa. *Retin Cases Brief. Rep.* 7 (2), 134–136. doi:10.1097/ICB.0b013e31825a300f

Park, U. C., Park, J. H., Ma, D. J., Cho, I. H., Oh, B. L., and Yu, H. G. (2020). A randomized paired-eye trial of intravitreal dexamethasone implant for cystoid macular edema in retinitis pigmentosa. *Retina* 40 (7), 1359–1366. doi:10.1097/IAE.0000000000002589

Patil, L., and Lotery, A. J. (2014). Coat's-like exudation in rhodopsin retinitis pigmentosa: Successful treatment with an intravitreal dexamethasone implant. *Eye (Lond).* 28 (4), 449–451. doi:10.1038/eye.2013.314

Percopo, C. M., Hooks, J. J., Shinohara, T., Caspi, R., and Detrick, B. (1990). Cytokine-mediated activation of a neuronal retinal resident cell provokes antigen presentation. *J. Immunol.* 145 (12), 4101–4107. doi:10.4049/jimmunol.145.12.4101

Perry, H. D., and Donnenfeld, E. D. (2006). An update on the use of ophthalmic ketorolac tromethamine 0.4%. *Expert Opin. Pharmacother.* 7 (1), 99–107. doi:10.1517/14656566.7.1.99

Petrushkin, H., Rogers, D., and Pavesio, C. (2018). The use of topical non-steroidal anti-inflammatory drugs for uveitic cystoid macular edema. *Ocul. Immunol. Inflamm.* 26 (5), 795–797. doi:10.1080/09273948.2016.1269931

Pichi, F., Nucci, P., Baynes, K., Lowder, C. Y., and Srivastava, S. K. (2017). Sustained-release dexamethasone intravitreal implant in juvenile idiopathic arthritis-related uveitis. *Int. Ophthalmol.* 37 (1), 221–228. doi:10.1007/s10792-016-0265-9

Rispoli, E., Vingolo, E. M., and Iannaccone, A. (1991). Thymopentin in Retinitis Pigmentosa. Evaluation of its possible therapeutical effects after 18 months of treatment, preliminary results. *New Trends Ophthalmol.* 6, 235–241.

Rispoli, E., Vingolo, E. M., and Iannaccone, A. (1990). "Thymopentin (Timunox) in retinitis pigmentosa: Evaluation of its therapeutical effects after 18 months of treatment. Preliminary results," in *XXVI international congress of ophthalmology (ICO)* (Singapore. March 18-24.

Rossetto, J. D., Nascimento, H., Fernandes, D. D., Belfort, R., Jr., and Muccioli, C. (2015). Treatment of cystoid macular edema secondary to chronic non-infectious intermediate uveitis with an intraocular dexamethasone implant. *Arq. Bras. Oftalmol.* 78 (3), 190–193. doi:10.5935/0004-2749.20150049

Saade, J. S., Istambouli, R., AbdulAal, M., Antonios, R., and Hamam, R. N. (2021). Bromfenac 0.09% for the treatment of macular edema secondary to noninfectious uveitis. *Middle East Afr. J. Ophthalmol.* 28 (2), 98–103. doi:10.4103/meajo.meajo_134_21

Sandberg, M. A., Weigel-DiFranco, C., Rosner, B., and Berson, E. L. (1996). The relationship between visual field size and electroretinogram amplitude in retinitis pigmentosa. *Invest. Ophthalmol. Vis. Sci.* 37, 1693–1698.

Saraiva, V. S., Sallum, J. M., and Farah, M. E. (2003). Treatment of cystoid macular edema related to retinitis pigmentosa with intravitreal triamcinolone acetonide. *Ophthalmic Surg. Lasers Imaging* 34 (5), 398–400. doi:10.3928/1542-8877-20030901-11

Schaal, Y., Hondur, A. M., and Tezel, T. H. (2016). Subtenon triamcinolone for cystoid macular edema due to retinitis pigmentosa unresponsive to oral acetazolamide. *Can. J. Ophthalmol.* 51 (4), e113–e115. doi:10.1016/j.jcjo.2015.12.021

Schallhorn, J. M., Niemeyer, K. M., Browne, E. N., Chhetri, P., and Acharya, N. R. (2018). Difluprednate for the treatment of uveitic cystoid macular edema. *Am. J. Ophthalmol.* 191, 14–22. doi:10.1016/j.ajo.2018.03.027

Schilling, H., Heiligenhaus, A., Laube, T., Bornfeld, N., and Jurklies, B. (2005). Long-term effect of acetazolamide treatment of patients with uveitic chronic cystoid macular edema is limited by persisting inflammation. *Retina* 25 (2), 182–188. doi:10.1097/00006982-200502000-00011

Scorolli, L., Morara, M., Meduri, A., Reggiani, L. B., Ferreri, G., Scalinci, S. Z., et al. (2007). Treatment of cystoid macular edema in retinitis pigmentosa with intravitreal triamcinolone. *Arch. Ophthalmol.* 125 (6), 759–764. doi:10.1001/archopht.125.6.759

Sen, E. S., Dick, A. D., and Ramanan, A. V. (2015). Uveitis associated with juvenile idiopathic arthritis. *Nat. Rev. Rheumatol.* 11 (6), 338–348. doi:10.1038/nrrheum.2015.20

Slabaugh, M. A., Herlihy, E., Ongchin, S., and van Gelder, R. N. (2012). Efficacy and potential complications of difluprednate use for pediatric uveitis. *Am. J. Ophthalmol.* 153 (5), 932–938. doi:10.1016/j.ajo.2011.10.008

Steinmetz, R. L., Fitzke, F. W., and Bird, A. C. (1991). Treatment of cystoid macular edema with acetazolamide in a patient with serpiginous choroidopathy. *Retina* 11 (4), 412–415. doi:10.1097/00006982-199110000-00008

Studsgaard, A., Clemmensen, K. O., and Nielsen, M. S. (2022). Intravitreal fluocinolone acetonide 0.19 mg (Iluvien®) for the treatment of uveitic macular edema: 2-year follow-up of 20 patients. *Graefes Arch. Clin. Exp. Ophthalmol.* 260 (5), 1633–1639. doi:10.1007/s00417-021-05504-6

Stump, M., Guo, D. F., and Rahmouni, K. (2023). T cell-specific deficiency in BBSome component BBS1 interferes with selective immune responses. *Am. J. Physiol. Regul. Integr. Comp. Physiol.* 324 (2), R161–R170. doi:10.1152/ajpregu.00243.2022

Sudhalkar, A., Kodjikian, L., and Borse, N. (2017). Intravitreal dexamethasone implant for recalcitrant cystoid macular edema secondary to retinitis pigmentosa: A pilot study. *Graefes Arch. Clin. Exp. Ophthalmol.* 255 (7), 1369–1374. doi:10.1007/s00417-017-3660-7

Tanner, V., Kanski, J. J., and Frith, P. A. (1998). Posterior sub-Tenon's triamcinolone injections in the treatment of uveitis. *Eye (Lond).* 12 (4), 679–685. doi:10.1038/eye.1998.168

Tranos, P. G., Wickremasinghe, S. S., Stangos, N. T., Topouzis, F., Tsinopoulos, I., and Pavesio, C. E. (2004). Macular edema. *Surv. Ophthalmol.* 49 (5), 470–490. doi:10.1016/j.survophthal.2004.06.002

Travassos, A., Fishman, G., and Cunha-Vaz, J. G. (1985). Vitreous fluorophotometry studies in retinitis pigmentosa. *Graefes Arch. Clin. Exp. Ophthalmol.* 222 (4-5), 237–240. doi:10.1007/BF02133687

Tsyklauri, O., Niederlova, V., Forsythe, E., Prasai, A., Drobek, A., Kasparek, P., et al. (2021). Bardet-Biedl Syndrome ciliopathy is linked to altered hematopoiesis and dysregulated self-tolerance. *EMBO Rep.* 22 (2), e50785. doi:10.15252/embr.202050785

Veritti, D., Sarao, V., De Nadai, K., Chizzolini, M., Parmeggiani, F., Perissin, L., et al. (2020). Dexamethasone implant produces better outcomes than oral acetazolamide in patients with cystoid macular edema secondary to retinitis pigmentosa. *J. ocular Pharmacol. Ther. official J. Assoc. Ocular Pharmacol. Ther.* 36 (3), 190–197. doi:10.1089/jop.2018.0153

E. M. Vingolo, A. Iannaccone, R. Forte, P. Tanzilli, and F. Sciò (Editors) (1993). "Thymopentin in the treatment of retinitis pigmentosa: Results after a three-year follow-up," *Retinitis pigmentosa present knowledge and outlook* (Naples, Italy: Edizioni Liviana Medicina).

Vingolo, E. M., Iannaccone, A., Rispoli, E., Pannarale, L., Amodeo, S., and Pannarale, M. R. (1993). "Three-year experience in the treatment of retinitis pigmentosa with thymopentin," in *4th meeting of the schepens international society* (Hong Kong. March 30-April 2.

Viswanathan, S., Frishman, L. J., Robson, J. G., Harwerth, R. S., and Smith, E. L., III (1999). The photopic negative response of the macaque electroretinogram: Reduction by experimental glaucoma. *Invest. Ophthalmol. Vis. Sci.* 40, 1124–1136.

Wolfensberger, T. J., Aptsiauri, N., Godley, B., Downes, S., and Bird, A. C. (2000). Antiretinale Antikörper assoziiert mit zystoidem Makulaödem1. *Klin. Monatsblatter fur Augenheilkd.* 216 (5), 283–285. doi:10.1055/s-2000-10561

Wolfensberger, T. J., Mahieu, I., Jarvis-Evans, J., Boulton, M., Carter, N. D., Nogradi, A., et al. (1994). Membrane-bound carbonic anhydrase in human retinal pigment epithelium. *Invest. Ophthalmol. Vis. Sci.* 35 (9), 3401–3407.

Wolfensberger, T. J. (1999). The role of carbonic anhydrase inhibitors in the management of macular edema. *Doc. Ophthalmol.* 97 (3-4), 387–397. doi:10.1023/a:1002143802926

Wong, C. W., Metselaar, J. M., Storm, G., and Wong, T. T. (2021). A review of the clinical applications of drug delivery systems for the treatment of ocular anterior segment inflammation. *Br. J. Ophthalmol.* 105 (12), 1617–1622. doi:10.1136/bjophthalmol-2020-315911

Wu, L., Arevalo, J. F., Hernandez-Bogantes, E., and Roca, J. A. (2012). Intravitreal infliximab for refractory pseudophakic cystoid macular edema: Results of the pan-American collaborative retina study group. *Int. Ophthalmol.* 32 (3), 235–243. doi:10.1007/s10792-012-9559-8

Xiong, W-H., Duvoisin, R. M., Adamus, G., Jeffrey, B. G., Gellman, C., and Morgans, C. W. (2013). Serum TRPM1 autoantibodies from melanoma associated retinopathy patients enter retinal on-bipolar cells and attenuate the electroretinogram in mice. *PLoS One* 8 (8), e69506. doi:10.1371/journal.pone.0069506

Yamamoto, S., Sippel, K. C., Berson, E. L., and Dryja, T. P. (1997). Defects in the rhodopsin kinase gene in the Oguchi form of stationary night blindness. *Nat. Genet.* 15 (2), 175–178. doi:10.1038/ng0297-175

Yang, P., Lockard, R., Titus, H., Hiblar, J., Weller, K., Wafai, D., et al. (2020). Suppression of cGMP-dependent photoreceptor cytotoxicity with mycophenolate is neuroprotective in murine models of retinitis pigmentosa. *Invest. Ophthalmol. Vis. Sci.* 61 (10), 25. doi:10.1167/iovs.61.10.25

Yoshii, M., Murakami, A., Akeo, K., Nakamura, A., Shimoyama, M., Ikeda, Y., et al. (1998). Visual function and gene analysisin a family with oguchi's disease. *Ophthalmic Res.* 30, 394–401. doi:10.1159/000055501

frontiers | Frontiers in Cell and Developmental Biology

TYPE Review
PUBLISHED 13 April 2023
DOI 10.3389/fcell.2023.1177838

OPEN ACCESS

EDITED BY
Glenn Prazere Lobo,
University of Minnesota Twin Cities,
United States

REVIEWED BY
Valeria Marigo,
University of Modena and Reggio Emilia,
Italy
Janosch P. Heller,
Dublin City University, Ireland

*CORRESPONDENCE
Alessandro Iannaccone,
aiannacc@yahoo.com

SPECIALTY SECTION
This article was submitted to Molecular and Cellular Pathology, a section of the journal Frontiers in Cell and Developmental Biology

RECEIVED 02 March 2023
ACCEPTED 31 March 2023
PUBLISHED 13 April 2023

CITATION
Chew LA and Iannaccone A (2023), Gene-agnostic approaches to treating inherited retinal degenerations. *Front. Cell Dev. Biol.* 11:1177838. doi: 10.3389/fcell.2023.1177838

Gene-agnostic approaches to treating inherited retinal degenerations

Lindsey A. Chew[1,2] and Alessandro Iannaccone[1]*

[1]Duke Center for Retinal Degenerations and Ophthalmic Genetic Diseases, Department of Ophthalmology, Duke Eye Center, Duke University School of Medicine, Durham, NC, United States, [2]Department of Cell Biology, Duke University School of Medicine, Durham, NC, United States

Most patients with inherited retinal degenerations (IRDs) have been waiting for treatments that are "just around the corner" for decades, with only a handful of seminal breakthroughs happening in recent years. Highlighting the difficulties in the quest for curative therapeutics, Luxturna required 16 years of development before finally obtaining United States Food and Drug Administration (FDA) approval and its international equivalents. IRDs are both genetically and phenotypically heterogeneous. While this diversity offers many opportunities for gene-by-gene precision medicine-based approaches, it also poses a significant challenge. For this reason, alternative (or parallel) strategies to identify more comprehensive, across-the-board therapeutics for the genetically and phenotypically diverse IRD patient population are very appealing. Even when gene-specific approaches may be available and become approved for use, many patients may have reached a disease stage whereby these approaches may no longer be viable. Thus, alternate visual preservation or restoration therapeutic approaches are needed at these stages. In this review, we underscore several gene-agnostic approaches that are being developed as therapeutics for IRDs. From retinal supplementation to stem cell transplantation, optogenetic therapy and retinal prosthetics, these strategies would bypass at least in part the need for treating every individual gene or mutation or provide an invaluable complement to them. By considering the diverse patient population and treatment strategies suited for different stages and patterns of retinal degeneration, gene agnostic approaches are very well poised to impact favorably outcomes and prognosis for IRD patients.

KEYWORDS

inherited retinal degenerations, retinal dystrophies, gene therapy, gene-agnostic, optogenetics, photoreceptor transplantation, retinal prosthetics, stem cells

1 Introduction

For years, seminal breakthroughs to restore vision have been "just around the corner," yet most patients with inherited retinal degenerations (IRDs) find themselves continuing to wait. More than 2 decades have passed since the first large animal, Lancelot the Briard dog, was successfully administered gene therapy for Leber's congenital amaurosis type 2 (LCA2), and his vision was restored (Veske et al., 1999; Lorenz et al., 2000; Bainbridge et al., 2008; Hauswirth et al., 2008; Maguire et al., 2008; Russell et al., 2017). However, this treatment (voretigene neparvovec/Luxturna by Spark Therapeutics in the United States (United States) and Novartis outside the United States) required 16 years before completing extensive trials; Luxturna finally obtained approval from the United States Food and Drug Administration

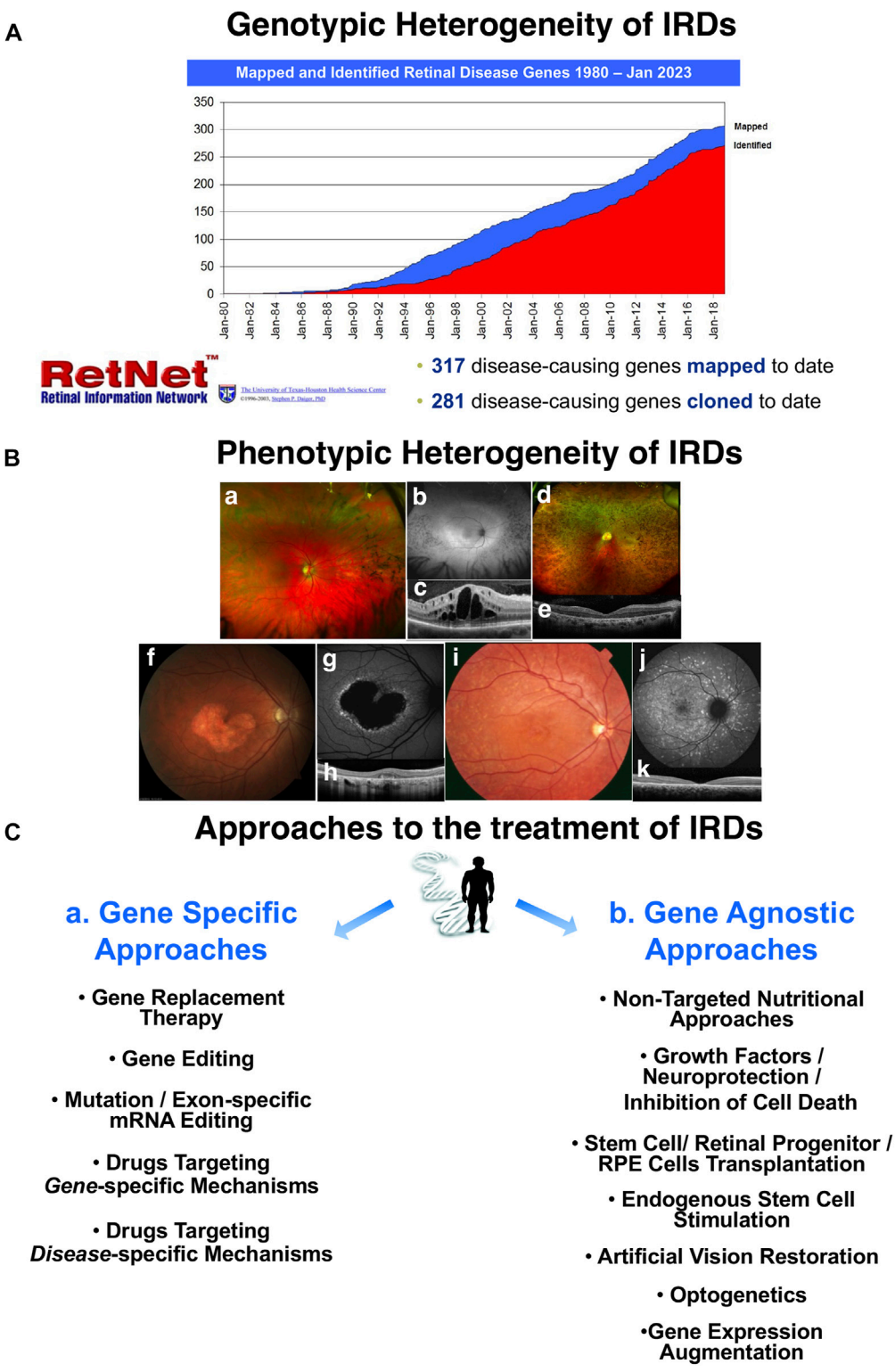

FIGURE 1
The landscape of treatment strategies for inherited retinal degenerations (IRD). Rapid acceleration of research since the 1980s has led to the discovery of 317 disease-causing genes with 281 of these genes now cloned, highlighting genotypic heterogeneity previously described by the RetNet project (hosted by the University of Texas-Houston Health Science Center) **(A)**. The immense phenotypic heterogeneity of IRDs is further illustrated by fundus images **(B, a–k)**. Patients with retinitis pigmentosa (RP) can present with good central retinal preservation **(a–b)** with mild to moderate vision loss and good preservation of the central photoreceptors exemplified by a partially detectable ellipsoid zone (EZ) and retained outer nuclear layer (ONL). However, RP can also induce significant inflammatory complications like cystoid macular edema (CME) **(c)**. In other instances of RP, the macular area may be partially compromised **(d)**, with minimal central EZ preservation **(e)**. In macular, cone, and cone-rod dystrophies, central disruptions are most common, but some present with significant foveal atrophic changes and partial foveal EZ preservation **(f–h)**; others present with global changes marked by central retinal thinning and complete EZ loss **(J–K)**. Gene-specific therapy **(C, a)** is unlikely to benefit patients with severe degeneration **(d–k)**, but gene-agnostic strategies **(C, b)** may still offer these patients a path to recovering vision.

(FDA) and its international equivalents in 2017 (Maguire et al., 2008; Ledford, 2017; Russell et al., 2017). IRDs, are enormously heterogeneous from a genetic standpoint, with over 280 genes cloned to date and over 300 mapped (Figure 1, top). This represents both a great opportunity to deliver gene-by-gene precision medicine-based approaches as it could never be envisioned before, and a major challenge. If genetic heterogeneity was not sufficient, phenotypic heterogeneity adds significantly to the challenge as well (Figure 1B, a-k). Patients with retinitis pigmentosa (RP), the most common form of IRD, can present with good central retinal preservation (Figure 1B, a-b) with mild to moderate vision loss and good preservation of the central photoreceptors exemplified by a partially detectable ellipsoid zone (EZ) and retained outer nuclear layer (ONL) but exhibit important inflammatory complications such as cystoid macular edema (CME, Figures 1B,C), or they can be affected much earlier and more severely in life, whereby the macular area is also partially compromised (Figures 1B,D) and there is minimal central EZ preservation (Figures 1B,E). In macular dystrophies and cone and cone-rod dystrophies, therapeutic help is needed mostly centrally, but a patient could present either with significant atrophic changes around the fovea but partial foveal EZ preservation (Figures 1B,F-H) or could have a more widespread phenotype and, crucially, marked central retinal thinning with complete EZ loss (Figures 1B,J-K). For these patients with exceedingly rare exceptions, gene therapy would be expected to provide no meaningful benefit.

Given the recent advances in our understanding of the mechanisms underlying IRD pathobiology, can we approach IRDs more broadly? Can we use gene-agnostic strategies (Figure 1B) to identify therapeutics that could target a wide range of causative genotypes, therefore bypassing the development of therapies for every individual gene known to impair vision? Where gene-specific therapies already exist, can gene-agnostic strategies still provide complementary support to protect the retina and ultimately preserve vision? While others have tackled similar topics (John et al., 2022), we uniquely explore these questions in the context of IRD progression, examine the intersection of treatment strategies with disease severity, and assess broadly applicable approaches for restoring retinal health—especially those already in or at the cusp of clinical trials.

Several groups have explored this possibility through a wide variety of approaches and ongoing efforts. For example, supplementation with Rod-derived Cone Viability Factor (RdCVF) holds promise for preventing secondary cone demise in primary rod dystrophies (Yang et al., 2009; Aït-Ali et al., 2015; Clérin et al., 2020). Advances in understanding the retina's neuroimmune interactions and oxidative stress tolerance provide alternative avenues for maintaining retinal health (Wang et al., 2020; Wu et al., 2021), especially in the context of microglial maintenance and antioxidant cocktails (Yu et al., 2004; Shen et al., 2005; Komeima et al., 2006; Komeima et al., 2007; Punzo et al., 2012; O'Koren et al., 2019). Given that the vast number of disease-causing mutations are in genes selectively or primarily expressed by photoreceptors (Rosenfeld et al., 1992; McLaughlin et al., 1993), photoreceptor transplantation has garnered enthusiasm as a therapeutic solution (Comyn et al., 2010; Garita-Hernandez et al., 2021; Chiang and Chern, 2022), especially in combination with induced pluripotent stem cells (iPSCs) (Zhong et al., 2014; Takagi et al., 2019; Watari et al., 2023), embryonic stem cells (ESCs) (Da Cruz et al., 2018), mesenchymal stem cells (Bartsch et al., 2008; Gasparini et al., 2019; Mahato et al., 2020; Sharma and Jaganathan, 2021; Zerti et al., 2021) (MSCs), chemically-induced photoreceptor-like cells (CiPCs) (Mahato et al., 2020) or neural stem cells (Liu et al., 2003; Coles et al., 2004; Frøen et al., 2013). Transplanting retinal pigmented epithelial (RPE) cells also warrants consideration, given the critical role of the RPE in providing the photoreceptors with the necessary support for maintaining the visual cycle and recycling metabolites.

There have been notable achievements in the application of optogenetics *via* adeno-associated viral vectors (AAV) to restore vision to patients, while bypassing photoreceptors entirely (Batabyal et al., 2021a; Gauvain et al., 2021; Sahel et al., 2021). Optogenetic strategies take advantage of opsins, light-sensitive proteins often derived from bacteria, to repurpose them for scientific and medical applications. Depending on the particular opsin, this strategy can require partnership with an active stimulative device (such as goggles) (Gauvain et al., 2021; Sahel et al., 2021). For some patients, this additional equipment may be cumbersome. For this reason, exploration of opsins activated by ambient light is desirable and has been proposed in combination with gene therapy targeting ON bipolar cells (Batabyal et al., 2021b). Fusing optogenetics with photoreceptor transplantation has also generated interest, with some progress made by expressing microbial opsins in neonatal murine photoreceptors, which are then transplanted into a mouse model of retinal degeneration (Garita-Hernandez et al., 2019; 2021). The host immune response following both transplantation and AAV delivery remains a concern. However, an adjacent method employing laser assistance for nano-enhanced optical delivery appears capable of similarly facilitating gene delivery to targeted cell populations without instigating an undesirable immune response (Batabyal et al., 2019; Batabyal et al., 2021b). This reduces the likelihood of adverse events while maximizing the therapeutic potential.

These strategies sharply contrast with artificial vision mediated by retinal and cortical prosthetics (Zhou et al., 2013; Farvardin et al., 2018; Niketeghad and Pouratian, 2019; Pio-Lopez et al., 2021). Requirements for successful application of these prosthetics include surgical implantation and multiple pieces of equipment, such as a specialized camera attached to glasses and a video processing unit. As we approach 10 years since the first implantation of the Argus II retinal prosthetic device, clinical outcomes and patient tolerability of this system vis-à-vis limited benefits have represented a barrier to its continuation alongside cost considerations and the complexities of subsequent training and rehabilitation protocols (Vaidya et al., 2014; Berger et al., 2016; Ghodasra et al., 2016; Ostad-Ahmadi et al., 2021). Thus, simpler systems are required, and continued development of retinal and cortical prosthetics remains ongoing and very important.

As IRD patients continue to experience progressive vision loss, we must adopt a sense of urgency and aspire to a research landscape where the next-generation of therapeutics is five instead of 16 years away. While important, tackling IRDs on an individual, mutation-by-mutation or gene-by-gene basis is unlikely to be the most expedient path forward. With the approval of Luxturna, the field is well-poised to tackle these challenges. By centering our commentary on gene-agnostic approaches to treating IRDs, we focus on more broadly applicable treatment strategies that will

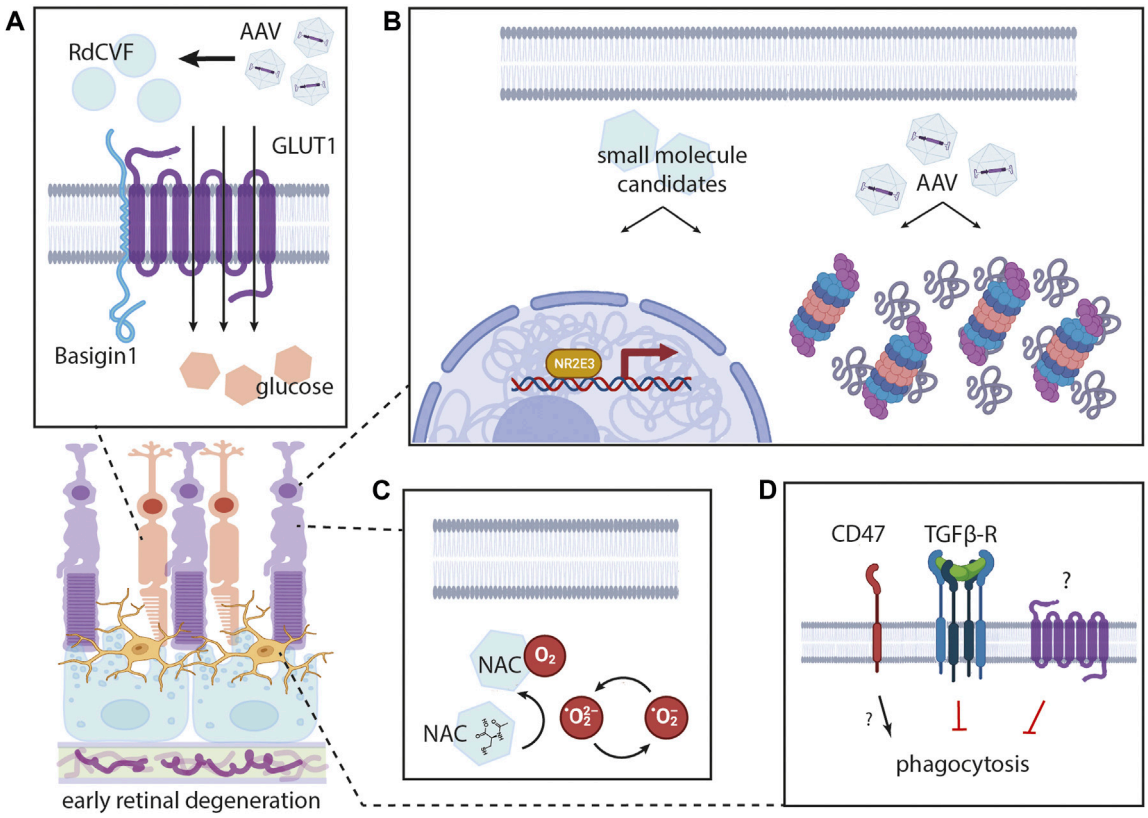

FIGURE 2
Mechanisms for enhancing photoreceptor survival in early retinal degeneration. Introducing Rod-derived Cone Viability Factor (RdCVF) **(A)** through use of AAVs represents one potential strategy for promoting cone photoreceptor survival. The working model for this mechanism includes activation of the Basigin-1/GLUT1 complex to increase transport of glucose and potentially other similar metabolites. Proteasomal enhancement (**(B)**, *right*) to clear excess misfolded proteins represents another possible approach. This strategy could be harnessed through the discovery of small molecules or through gene augmentation for proteasomal machinery. These approaches could also be used for augmenting certain nuclear hormone receptors (like NR2E3) (**(B)**, *left*). Oral supplementation with antioxidants like N-Acetylcysteine (NAC) **(C)** may also support photoreceptor health, with NAC as a known scavenger of reactive oxygen species. Alternative strategies include limiting activation of microglia **(D)**, by inhibiting excessive phagocytosis (*i.e.*, inhibiting the TGFβ receptor), while harnessing their role in maintenance of the retina.

expedite and increase treatment access for diverse IRD patients across the globe.

2 A photoreceptor survival guide

Patients in early and intermediate stages of IRD progression may still retain intact photoreceptors. For these individuals, minimally invasive treatments (Figure 2) that can rescue vision or reduce the risk of further vision loss are especially desirable and feasible. We discuss several promising developments that may support patients' existing rod and cone photoreceptors to limit further cell death (Aït-Ali et al., 2015; Lobanova et al., 2018; Vighi et al., 2018) and deterioration of visual function. While supporting retinal health may be insufficient to improve patients' visual acuity, maintaining photoreceptor survival prevents critical and significant declines in visual function. To this end, each of the following approaches aim to reduce the likelihood of photoreceptor cell death. Although we do not provide an exhaustive list, these strategies have reached the clinical trial stage, or will imminently achieve that status, and therefore warrant consideration additional consideration.

2.1 Rod-derived cone viability factor (RdCVF)

IRDs involving primary rod photoreceptor death and secondary cone demise have a unique presentation. At times, even patients experiencing late stages of disease with advanced cone loss may continue to retain substantial visual acuity (Cideciyan et al., 1998; Iannaccone et al., 2006). For this reason, supporting the health and function of cone photoreceptors is an extraordinary opportunity for vision preservation in the many such patients worldwide (Wright, 1997).

In vitro observations of significantly higher cone photoreceptor survival in the presence of rod photoreceptors, as compared to cultures deprived of rods, have given basis for the idea of a "diffusible trophic factor . . . released from . . . rod cells" (Mohand-Said et al., 1998). Rod photoreceptors are approximately 20 times more numerous than cones in many mammalian species (Rodieck, 1998). However, the hypotheses of rod death simply resulting in structural collapse of cones, or causing cone death by toxic byproduct release are contravened by a lack of widespread cone demise immediately following rod death (Hicks and Sahel, 1999). Furthermore, the insoluble glycocalyx surrounding each cone

provides significant structural integrity and a link to the nearby RPE cells (Hicks and Sahel, 1999). Eventually the existence of Rod-derived Cone Viability Factor (RdCVF) was discovered (Léveillard et al., 2004).

RdCVF shares 33% similarity with thioredoxin but does not have detectable oxidoreductase activity (Léveillard et al., 2004). Evidence suggests that RdCVF binds to a complex formed by the photoreceptor-specific transmembrane protein Basigin-1 and glucose transporter GLUT1 (Figure 2A) (Aït-Ali et al., 2015). This binding appears to promote cone survival by stimulating intracellular glucose uptake and increasing aerobic glycolysis (Aït-Ali et al., 2015). A redox-sensitive interaction between RdCVF and Basigin-1 might even serve as a prerequisite for full activation of GLUT1 transport activity in photoreceptors (Cepko and Punzo, 2015). Complementary findings indicate that lactose supports photoreceptor health *in vitro* and point to a supportive role of glucose, lactose, and other similar metabolites (Jablonski et al., 2001; Wang et al., 2003). Demonstrating functional RdCVF-mediated cone rescue in a rhodopsin P23H rat model of retinitis pigmentosa served as another critical milestone (Yang et al., 2009; Léveillard et al., 2014). Understanding RdCVF's mechanism of action has underscored its salient role in retinal physiology in health and disease, ultimately reinforcing the potential for RdCVF's use in therapies for IRDs (Sahel et al., 2001; Chalmel et al., 2007). At this time, SparingVision is leading multiple preclinical studies to translate these findings into clinical solutions, with advancement to clinical trials in the near future.

2.2 Cellular stress management

2.2.1 Oxidative stress, N-Acetylcysteine (NAC), and antioxidant supplementation

There is growing clinical interest across many disciplines in the management of oxidative stress to restore cellular homeostasis (Ferrante et al., 1997; Gilgun-Sherki et al., 2001; Ildefonso et al., 2016; Pinilla et al., 2022). Several clinical trials for retinal supplements (*i.e.,* vitamin A, lutein, zeaxanthin, docosahexaenoic acid) have explored their capacity to slow the progression of retinitis pigmentosa (RP) (Iannaccone et al., 2021a). These initial trials paved the way to continued clinical interest across many disciplines in the management of oxidative stress to restore cellular homeostasis in IRDs (Ildefonso et al., 2016; Pinilla et al., 2022). Identification of the Nrf2 pathway and its role in regulation of oxidative stress responses has generated significant attention (Lee et al., 2003; St-Pierre et al., 2006). Consequently, efforts to enhance Nrf2 signaling have been attempted as a mechanism for inhibiting the cellular oxidative stress response. In *rd1* and *rd10* mouse models, AAV-mediated overexpression of Nrf2 in the RPE demonstrated measurable benefits, preserving RPE morphology and increasing survival, improving photoreceptor health, and boosting visual function as measured by optomotor responses (Wu et al., 2021). Given the high baseline metabolic activity of rod photoreceptors, their death in IRDs may lead to an unfettered hyperoxic microenvironment in the outer nuclear layer, thereby inducing oxidative stress in the surviving photoreceptors (Punzo et al., 2012; Wu et al., 2021). To counteract this imbalance, increasing photoreceptor mitochondrial expression of antioxidant proteins, like glutathione peroxidase and superoxide dismutase 2, resulted in delays in retinal degeneration (Lu et al., 2009; Usui et al., 2009).

A well-established antioxidant agent and reactive oxygen species (ROS) scavenger, N-acetylcysteine (NAC) has been studied for over a decade (Lee et al., 2011; Schimel et al., 2011; Raghu et al., 2021), and there is special interest in its therapeutic use as an oral antioxidant supplement) (Iannaccone et al., 2021b). In both the *rd1* and *rd10* mouse models of retinitis pigmentosa, oral NAC reduced cone cell death and preserved cone function by mitigating oxidative damage (Lee et al., 2011). Evidence also suggests that NAC acts mechanistically by scavenging existing ROS and reversing lipid peroxidation to limit further ROS production (Figure 2C) (Schimel et al., 2011). In a human RPE culture model, the degenerative state is known to correlate with reduced glutathione and glutathione peroxidase levels. NAC treatment increased the expression of both of these enzymes, suggesting its capacity to mitigate the overall redox state of cells and reduce oxidative stress (Schimel et al., 2011; Nuhu et al., 2020). In a mouse model of phototoxic retinal degeneration, oral NAC treatment protected the outer nuclear layer and preserved photoreceptor function on electroretinography (Schimel et al., 2011). Preclinical success has advanced this strategy into clinical trials, where oral NAC has already been reported to improve cone function in retinitis pigmentosa patients in a phase I trial (Campochiaro et al., 2020). While this study primarily focused on validating NAC's safety profile, patients' best correct visual acuity significantly improved during a 24-week oral NAC treatment period across all cohorts (Campochiaro et al., 2020). In this regimen, patients received 600, 1,200, or 1800 mg of NAC twice daily for 3 months, followed by a 3 times/day regimen for another 3 months (Campochiaro et al., 2020; Kong et al., 2021). Additional retrospective analysis of this study revealed that the higher NAC dosing regimens reduced the risk of macular sensitivity loss (Kong et al., 2021). In the context of RP, there is an ongoing multicenter, randomized, placebo-controlled trial to determine whether oral NAC treatment can improve cone function (NAC-Attack; NCT05537220).

In parallel efforts toward oxidative stress reduction, other investigations have focused on the potential of multiple other exogenous antioxidants, alpha-tocopherol, ascorbic acid, Mn(III) tetrakis (4-benzoic acid) porphyrin, and alpha-lipoic acid (Komeima et al., 2006). Findings suggested that these compounds could also limit oxidative stress to improve cone photoreceptor survival in models of both slowly- and quickly-progressing retinal degeneration (the Q433ter *RHO* and *rd10* mouse models, respectively) (Komeima et al., 2007; Lu et al., 2009; Usui et al., 2009). While global reduction of reactive oxygen species would likely bear significant side effects, given their important signaling functions (Finkel, 2003), tissue specific regulation of oxidative stress could be adapted for use in IRD treatments (Qi et al., 2007; Koilkonda et al., 2010).

2.2.2 Microglial maintenance

Long-standing dogma dictated that microglia in the retina are always detrimental (Itagaki et al., 1989; Yamasaki et al., 2014; Krasemann et al., 2017), with microglial overactivation causing an excessive oxidative stress response and metabolic dysregulation (Block et al., 2007; Smith et al., 2012; Peng et al., 2014; Zhao et al., 2015; Subhramanyam et al., 2019). In the context

of the *rd1* and *rd10* mouse models of retinal degeneration, treatment with the anti-inflammatory cytokine transforming growth factor beta (TGF-β) rescued degenerating cones and protected against loss of visual function (Wang et al., 2020). These results suggested broad benefits of TGF-β on cone survival through a mechanism dependent on microglial activation (Wang et al., 2020). However, recent evidence suggests that microglia also occupy a purposeful physiological niche in the healthy retina (Keren-Shaul et al., 2017; O'Koren et al., 2019). In mice, depleting native microglia from the inner plexiform layer of the retina led to a selective reduction in scotopic and photopic b-wave responses without gross changes in synapse number (O'Koren et al., 2019). Evidence also demonstrated that eliminating retinal microglia failed to augment cone survival by a separate CD47-dependent mechanism, which had been previously hypothesized to be mediated by microglia (Wang et al., 2021). This collection of work highlights the complexity of microglia (Figure 2D) and their various roles in the retinal landscape. Further research to selectively promote their role in maintenance while avoiding excess activation may prove fruitful in the development of treatments.

2.2.3 Proteasomal enhancement

Proteasome overload is another common factor in cellular stress, and evidence points to this being a significant contributor to photoreceptor degeneration in IRDs (Tzekov et al., 2011; Lobanova et al., 2013; 2018). This natural sequela follows the accumulation of misfolded and mistrafficked proteins driven by various disease-causing mutations (Kosmaoglou et al., 2008). In the context of retinitis pigmentosa, the frequently diagnosed rhodopsin P23H mutation causes rhodopsin misfolding and accumulation in the endoplasmic reticulum (Illing et al., 2002; Saliba et al., 2002). Ultimately, these stressors induce the unfolded protein response and photoreceptor death (Lin et al., 2007; Gorbatyuk et al., 2010).

In a Gγ1 knockout mouse model of photoreceptor degeneration (Lobanova et al., 2008; Kolesnikov et al., 2011), the degenerative phenotype features the misfolding of proteins like $G\beta_1$, which appears to require Gγ1's chaperone-like activity for correct folding. Cellular stress in this model is derived from accumulation of $G\beta_1$ and other misfolded proteins. Promising evidence from this work demonstrated that preventing this accumulation, by reducing $G\beta_1$ expression, led to a complete reversal in the degenerative phenotype of the $G\gamma1^{-/-}$ mouse (Lobanova et al., 2013). Furthermore, the severity of photoreceptor retinal degeneration correlated with the misfolded protein levels (Lobanova et al., 2013). Subsequent studies have indicated that increasing photoreceptor proteasomal activity can significantly delay retinal degeneration, with the most substantial benefits conferred by overexpression of the 11S proteasome cap subunit PA28α to enhance ubiquitin-independent protein degradation (Lobanova et al., 2018). In a rhodopsin P23H heterozygous mouse model of retinitis pigmentosa, this strategy quadrupled the number of surviving photoreceptors in the inferior retina of 6 month-old mice (Lobanova et al., 2018). Repeating this approach in a mouse model of Bardet-Biedl Syndrome (Zaghloul and Katsanis, 2009; Liu et al., 2014), a multisystemic disorder affecting photoreceptors alongside other ciliated cells, similarly demonstrated a delay in retinal degeneration (Wang, 2022).

Alternatively, phosphorylation of specific downstream targets in the mammalian target of rapamycin complex 1 (mTORC1) pathway also appears to be a viable strategy for increasing proteasomal activity (Wang et al., 2003). By contrast, reducing the proteolytic capacity of photoreceptors through genetic manipulation in otherwise normal retinas induced retinitis pigmentosa-like pathology (Ando et al., 2014). Altogether, this combination of findings heavily emphasizes the critical role of proteostasis in retinal physiology, with significant degenerative consequences stemming from proteasomal overload. The presence of proteasomal machinery in all photoreceptors also augments their attractiveness as therapeutic targets for IRDs, and evidence strongly supports the pursuit of proteasomal enhancement (Figure 2B) as a gene-agnostic treatment strategy.

2.3 Nuclear hormone receptor enhancement

Nuclear hormone receptor enhancement (Figure 2B) is another potential strategy for preserving visual function in IRDs. Mutations in the human nuclear hormone receptor gene *NR2E3* (Haider et al., 2000) with two rather different conditions, a recessive one due to insufficient *NR2E3,* resulting in a disorder of photoreceptor cell fate known as the Enhanced S-Cone Syndrome (ESCS) in which rods are replaced by S-cones that remain preserved for extended periods of time (Roman et al., 2019; Iannaccone et al., 2021a), and in a dominant disorder in which abnormal gain of function mutations cause instead a form of RP without enhanced function or selective preservation of the S-cones (S. Li et al., 2021a). In the *rd7* mouse model, which lacks *Nr2e3* and we have shown that faithfully replicated human ESCS (Roman et al., 2019; Batabyal and Kim, 2021), augmenting expression of the nuclear hormone receptor NR1D1 led to histological and molecular restoration of the *rd7* retina (Cruz et al., 2014). However, due to the pleiotropic effects of this gene on photoreceptor health, *NR2E3* has been studied beyond these two conditions and shown to act also as a genetic modifier that can rescue also other forms of RP (Gire et al., 2007). In pursuit of this strategy for restoring vision, Ocugen has initiated an ongoing clinical trial (NCT05203939) in an effort to test the safety and initial efficacy of *NR2E3*-based gene therapy. This trial aims not only to treat ESCS patients and dominant forms of RP linked to *NR2E3* mutations, but is also trying to harness *NR2E3*'s potential to promote homeostasis in the degenerating retina with other forms of RP (S. Li et al., 2021b). If successful, this therapy could become available for not only patients with ESCS, but also for other forms of RP not linked to *NR2E3* mutations.

3 Stem Cell Transplantation and Regeneration

As illustrated in Figure 1, patients with end-stage IRDs, who have lost virtually all of their photoreceptors, are outside of the treatment window wherein protective therapies could make a substantive impact. Such patients require restorative approaches that aim to replace rather than protect photoreceptors, or otherwise circumvent their loss. This includes patients with macular

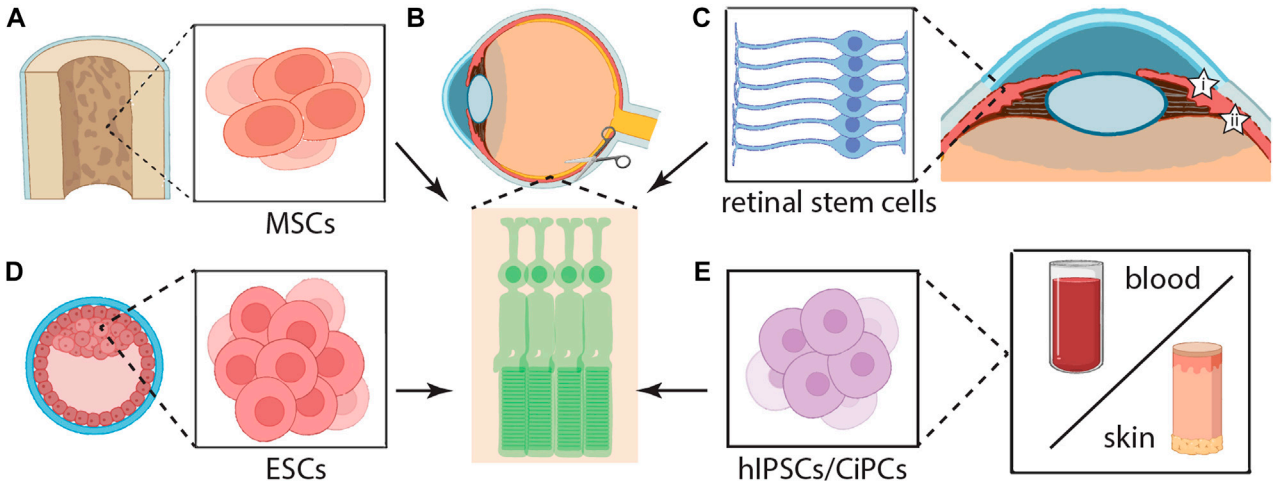

FIGURE 3
Stem Cell Transplantation and Regeneration. Many stem cells sources are being explored, and research efforts are focusing on streamlining regeneration methods to convert these stem cells **(B)** into healthy photoreceptors that can survive subretinal transplantation (*scissors*) while retaining light-responsive properties. Here, we highlight the origin and conversion of the following cells into photoreceptors, mesenchymal stem cells (MSCs) **(A)**, retinal stem cells **(C)** from the ciliary margin (*shown by i & ii*), embryonic stem cells (ESCs) **(D)**, human induced pluripotent stem cells (hiPSCs) **(E)**, and chemically-induced photoreceptor-like cells (CiPCs) **(E)** derived from fibroblasts.

dystrophies such as Stargardt disease or related conditions in whom, despite good peripheral retinal functional preservation, central visual loss may be associated with irreparable photoreceptor loss and restorative approaches are needed as well. To this end, numerous stem cell research (Figure 3) efforts have focused on photoreceptor differentiation and transplantation. Harnessing stem cell transplantation technologies has the potential to play a key role in the treatment of patients with advanced IRDs.

3.1 Photoreceptors and RPE derived from embryonic stem cells (ESCs) or induced pluripotent stem cells (iPSCs)

Early efforts to direct embryonic stem cells into retinal precursors with the competence for photoreceptor differentiation (Ikeda et al., 2005) provided the basis for subsequent development of transplantable retinal sheets (Zhong et al., 2014; Han et al., 2022). Further optimization of these protocols shortened the minimum time to maturation, with expression of putative photoreceptor markers like OPN1SW (the blue cone pigment) and rhodopsin (Mellough et al., 2012). The development of murine ESC- or iPSC-derived 3D retinal sheets (Figures 3D,E) for transplantation into the *rd1* mouse and other models of retinal degeneration advanced these approaches further (Assawachananont et al., 2014; Jayakody et al., 2015; Ribeiro et al., 2021). Evidence from these studies indicated successful establishment of synaptic connections between host-graft bipolar cells and photoreceptors (Assawachananont et al., 2014; Jayakody et al., 2015; Ribeiro et al., 2021), and provide crucial validation for photoreceptor replacement therapy and its potential to rescue cone-mediated vision. Others have identified the capacity of human iPSCs to autonomously proliferate and spontaneously organize themselves into three-dimensional retinal cups containing properly arranged retinal cell types (Zhong et al., 2014). More recently, efforts have identified three-dimensional retinal organoids as a promising graft source for transplantation therapy (Watari et al., 2023). Evidence also points to preclinical stage success storing associated tissue-sheets for 3, 4 days using a novel preservation method, with functional light responses following retinal transplantation in a rodent model (Watari et al., 2023).

In theory, iPSC-derived RPE bears similar potential for clinical application, particularly when differentiation methods generate and maintain the apical-basolateral polarity characteristic of native RPE structure and function (Miyagishima et al., 2016). Donor-to-donor variability impacts iPSC-derived RPE quality and elevates the requirement for validation of individual graft features prior to consideration for clinical application. Select clinical trials have achieved incremental success for this field, and subretinally transplanted ESC- and iPSC-derived RPE improved visual acuity in some patients (Mandai et al., 2017; Da Cruz et al., 2018; Takagi et al., 2019; Li et al., 2021a), including a cohort with Stargardt macular dystrophy. Intravitreal injection of retinal progenitor cells have also been investigated by jCyte, with a Phase 3 trial that is in the planning phase is required to make determinations beyond safety and efficacy (NCT03073733; NCT04604899; NCT02320812). Multiple clinical trials focusing on stem cell-derived RPE for treating IRDs remain ongoing (ReNeuron Limited, NCT02464436; Southwest Hospital, China, NCT02941991, NCT02749734; Centre d'Etude des Cellules Souches, France, NCT03963154). Further evidence from emerging trials will be required to demonstrate that this strategy can be successful in practice and yield significant improvements for patients' vision.

3.2 Mesenchymal stem cell (MSC) transplantation

Multiple characteristics of mesenchymal stem cells (MSCs) make them suitable for clinical use, including their anti-inflammatory properties derived from extracellular vesicle release (Kou et al., 2022) or their enhancement of autophagy pathways (Liu et al., 2020). The latter was highlighted by a study of rat bone marrow-derived MSC rescue (Figure 3A) of outer nuclear layer thickness in an *in vitro* photoreceptor model (Liu et al., 2020). In a sodium iodate model of retinal degeneration, intravitreal injection of human dental pulp-derived MSCs improved retinal function on electroretinography (Alsaeedi et al., 2019). A proteomic study in a N-methyl-N-nitrosourea injury model of retinal degeneration demonstrated that MSC transplantation conferred a protective effect on photoreceptors, which was attributed to attenuated activation of Pdcd4-mediated programmed cell death pathways (Deng et al., 2021). These rudimentary models provide important insight into the potential of MSC transplantation and establish the basis for subsequent advancement to translational models and clinical trials.

In a non-randomized clinical trial for RP patients, intravitreal injection of autologous bone marrow-derived MSCs improved the best-corrected visual acuity of all participants for several months after the procedure (Tuekprakhon et al., 2021). Unfortunately, the improvements were not sustainable, as their visual acuity reverted to baseline within 12 months of treatment (Tuekprakhon et al., 2021). However, subsequent clinical trials in retinitis pigmentosa patients have reported much success following bone marrow-derived MSC transplantation (Adak et al., 2021). A phase III clinical trial involving suprachoroidal injection of umbilical cord-derived MSC also improved patients' visual acuity through the 6-month follow-up, without changes in average visual field sensitivity or visual evoked potentials (Kahraman and Oner, 2020; Zhao et al., 2020). Sub-tenon injection of Wharton's jelly-derived MSCs led to improvements in patients' visual acuity as well, although this study remains ongoing (Özmert and Arslan, 2020). These advances point to the promise of MSC technologies for vision restoration, although long-term efficacy studies will be required to validate the potential of these treatments.

3.3 Chemically-induced photoreceptor-like cells (CiPCs)

Recent seminal work has identified a set of five small molecules capable of chemically inducing transformation of fibroblast into photoreceptor-like cells (CiPCs) (Figure 3E) without first reverting them into pluripotent states or employing transcription factors (Mahato et al., 2020). In the *rd1* mouse model, which is characterized by rapid onset retinal degeneration akin to RP, CiPC transplantation into the subretinal space partially restored the pupillary reflex and visual function, as measured by the light-aversion behavioral paradigm (Mahato et al., 2020). In some tests, this effect was detected under scotopic illumination conditions assessing rod-mediated vision (Mahato et al., 2020). Evidence suggests that CiPC development relies on translocation of AXIN2 to the mitochondria to promote reactive oxygen species production and subsequent activation of NFkB and Ascl1 upregulation (Shin et al., 2016; Mahato et al., 2020). While larger preclinical and clinical studies of CiPC will be required to fully assess the potential of this strategy, more efficient conversion of fibroblasts into photoreceptor-like cells may play a key role in lowering costs and increasing patient access to regenerative medicine.

3.4 Neural stem cells of the retina

Reports of true retinal stem cells in the adult human eye raise the possibility of an endogenous source for cellular regeneration (Coles et al., 2004; Frøen et al., 2013). Adult neural stem cells do not require reprogramming, and a retinal stem cell population would fall into this category (Liu et al., 2003). A study of human ocular cell types showed that the human eye contains a small population of approximately 10,000 multipotent, retinal stem cells (Figure 3C) with the potential for proliferation and self-renewal (Coles et al., 2004). Capitalizing on this population in the ciliary margin (Figure 3C, i and ii), the biotechnology company Endogena Therapeutics has focused on a regenerative medicine approach to stimulate proliferation and migration of these retinal stem cells as a therapeutic alternative. While this technology remains proprietary, ongoing clinical trials are evaluating the efficacy of several cocktails of intravitreally delivered small molecules (NCT05392751). Activating endogenous retinal stem cell populations for development into photoreceptors would be exciting; however, any genetic defects would persist in this reactivated stem cell population. These cells might mature into photoreceptors and function normally for some time, but the genetic basis for degeneration would remain. Eventually, degeneration would likely occur at the same rate experienced by the patient prior to any intervention. For early onset IRDs, such as LCA2, this strategy may not be viable; however, slower progressing IRDs, like RP, may be well-suited for treatment by this approach. Further studies will be required to assess the feasibility of repeating treatment to activate retinal stem cells multiple times over a patient's lifetime. Extended-release formulations could also play a role in long-term activation of patients' retinal stem cells.

4 Optogenetic strategies for restoring vision

Optogenetic therapy provides an unparalleled opportunity for restoring vision to patients who have experienced significant photoreceptor cell death. Through AAV-mediated expression of opsins (*i.e.*, channelrhodopsin, ChrimsonR and Opto-mGluR6) in bipolar cells and retinal ganglion cells, direct stimulation of these secondary and tertiary cell types of the neural retina can bypass photoreceptors while maximizing the activation of typical visual circuits of the brain.

4.1 Targeting retinal ganglion cells

A series of non-human primate studies established the proof of concept for optogenetic gene therapy targeting retinal ganglion cells

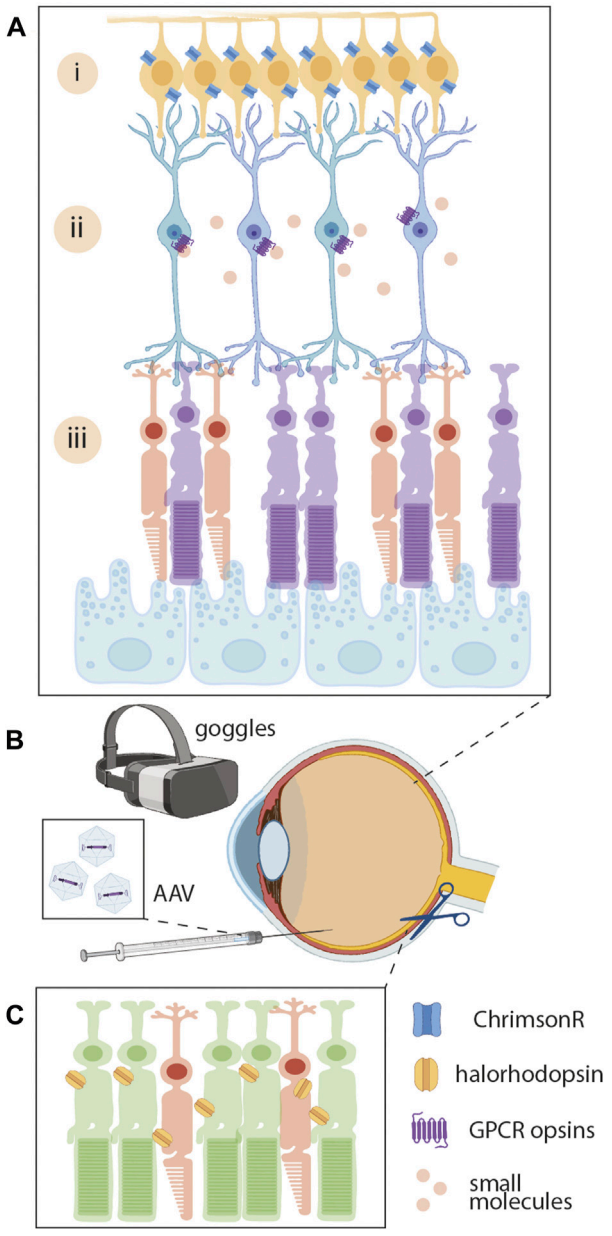

FIGURE 4
Optogenetic strategies for restoring vision. In the degenerating retina **(A)**, dying photoreceptors (iii) fail to detect light or provide the retinal interneurons with signals about visual input. Solutions include targeting retinal ganglion cells (i) with channelrhodopsins (such as ChrimsonR, *blue*). Another option is to target bipolar cells (ii) with GPCR opsins (*purple*) or to combine this approach with small molecules (*red circles*) that further increase light sensitivity. **(B)** Administration of therapy requires intravitreal delivery of AAVs mediating opsin expression in the bipolar cells and retinal ganglion cells. Use of optogenetic goggles convert digital images from a camera into light stimulation of the treated retina to support patients' restoration of vision **(C)** Another possible solution is to replace dying photoreceptors with a graft of human iPSC-photoreceptors that have been transduced with optogenetic proteins like halorhodopsin.

(Figures 4A, i) and demonstrated the capacity for AAV-mediated opsin expression without a deleterious immune response (Picaud et al., 2019; Gauvain et al., 2021). Importantly, this work overcame differences in murine and primate immunology, and collaborative efforts identified an AAV-variant (AAV2.7m8) that could effectively transduce retinal ganglion cells following intravitreal injection (Dalkara et al., 2013; Sahel et al., 2021). Translating this strategy into clinic has been enormously successful and restored significant visual perception in a patient with RP, whose visual acuity had been limited to light perception for over a decade (Sahel et al., 2021). By pairing intravitreal injections with active stimulation goggles designed exclusively for converting camera inputs into opsin stimulation, this therapy maximizes the functionality of the newly expressed opsins in patients' retinal ganglion cells (Gauvain et al., 2021; Sahel et al., 2021; Kralik et al., 2022). Physiotherapy also forms a key component of the therapeutic process, and patients must train themselves to interpret the new format of visual information transmitted by optogenetic goggles (GenSight Biologics; NCT03326336). For patients with severe photoreceptor loss, optogenetic therapy represents hope of regaining some level of vision.

Further advances in optogenetic therapy may be capable of improving the best visual acuity that treatment can offer. For example, rather than achieving vision at the level of object localization within arm's length (Sahel et al., 2021), future therapies may be able to allow for counting fingers at several feet. These seemingly modest improvements would lead to significant practical possibilities for patients.

4.2 Amplifying optogenetic signals in bipolar cells

Following severe photoreceptor degeneration, many retinal interneurons remain physiologically and metabolically stable. Imbuing bipolar cells (Figure 4A, ii) with light sensitivity could maximize the utility of native retinal circuits and restore visual function. Inducing the expression of light-sensitive G-protein coupled receptors, such as vertebrate rhodopsin, in bipolar cells represents another attractive alternative for restoring vision (Gaub et al., 2018). Expanding on this concept, Vedere Bio II is also developing a library of intravitreally injectable small molecules to augment the sensitivity of rhodopsin and increase its signal amplification. Together, AAV-mediated delivery of rhodopsin to bipolar cells followed by intravitreally injectable small molecules that can act as a "molecular switch" has the potential to restore patient's visual function using ambient light.

Protein engineering to improve the kinetics of opsins used in optogenetic therapy may also facilitate improved outcomes. AAV-mediated delivery of Opto-mGluR6, a chimera of melanopsin with the intracellular domains exchanged for those of mGluR6, represents an early foray into this space (Kralik et al., 2022). This design aimed to optimize activation of the $G\alpha_o$ signaling pathway, the G-protein pathway traditionally activated by mGluR6 at the photoreceptor-ON bipolar cell synapse (Nawy, 1999). Harnessing the natural signal amplification capacity of metabotropic receptors makes GPCR opsins approximately 1000-fold more light sensitive compared to traditional channelrhodopsins (Kralik et al., 2022). Targeting bipolar cells also maximizes the capacity of light signals to naturally propagate to diverse retinal ganglion cell populations and their inherently varied receptive fields (Hulliger et al., 2020). The

immense potential of this strategy is highlighted by the encouraging results demonstrating improved visual function and contrast sensitivity in optogenetically stimulated *rd1* mice (Kralik et al., 2022).

4.3 Optogenetic photoreceptor transplantation

Combining optogenetic therapy with photoreceptor transplantation may represent a viable strategy for restoring function of the entire retinal circuit, even in patients who have experienced significant photoreceptor loss (Garita-Hernandez et al., 2021; Sakai et al., 2022). Optogenetic transduction of human iPSC-photoreceptors with halorhodopsin eNpHR2.0 has shown success in preclinical studies, following transplantation into *rd1* mice, optogenetic stimulation of eNpHR2.0-expressing photoreceptors led to robust activity in downstream retinal ganglion cells (Garita-Hernandez et al., 2019). Furthermore, immunofluorescence studies from treated *rd1* mice revealed the development of synaptic connections between transplanted photoreceptors and host bipolar cells (Garita-Hernandez et al., 2019). These advances may pave the way toward new treatments for patients with late-stage IRDs.

4.4 Evolution of gene therapy

Despite the ocular immune privilege, immune consequences of AAV-mediated therapies remain a consideration in the translational vision research community (Taylor, 2016). Attempts to enhance the transduction of retinal cells by increasing viral loads will likely result in higher toxicity (Khabou et al., 2018), as seen in certain studies involving non-human primates (Vandenberghe et al., 2011; Ramachandran et al., 2017; Hinderer et al., 2018). Selection of the ideal promoter based on its activity and cell-type-specific tropism is a key factor in reducing gene therapy-associated toxicity and optimizing its therapeutic effect. For this reason, promoters with activity restricted to specific cell types (such as human rhodopsin (Allocca et al., 2007; Busskamp et al., 2010) [rods], cone arrestin [cones] (Zhu et al., 2002), and bestrophin-1 (Snodderly et al., 1992; Zhu et al., 2002; Xiong et al., 2019) [RPE] promoters) are typically preferred to globally active potent promoters (such as cytomegalovirus immediate-early (Boshart et al., 1985) [CMV] and chicken beta actin (Hitoshi et al., 1991) [CAG] promoters). Cell-specific promoters eliminate the physiologic stress of indiscriminate expression across cell types that leads to treatment toxicity. These findings highlight the need for more detailed examination of tropism and immune responses associated with viral constructs intended for therapeutic use.

To this end, Vedere Bio (whose assets have now been acquired by Novartis) and Vedere Bio II have initiated recent advances harnessing *in vivo*-directed evolution of new AAV capsids significantly expand the therapeutic potential and applications of AAV gene therapy for IRDs (Dalkara et al., 2013). AAV variants capable of delivering gene cargo to the outer retina following intravitreal injection are especially sought after, with dense tissue of the inner limiting membrane posing a major barrier to successful gene therapy for naturally-occurring AAV serotypes (Snodderly et al., 1992; Fischer et al., 2009). By contrast, *in vivo*-directed evolution of new AAV serotypes appears to have partially overcome these obstacles, and in mouse models of X-linked retinoschisis and LCA2, novel AAV2.7m8 mediated highly efficient gene delivery across retinal layers (Dalkara et al., 2013). Furthermore, AAV2.7m8 facilitated successful transduction of primate photoreceptors following intravitreal injection (Dalkara et al., 2013). Spearheading a segment of these efforts, GenSight Biologics is already invested in ongoing clinical trials (NCT03326336) to integrate this technology with optogenetic approaches.

Continued improvement of AAVs toward increasingly efficient transduction of the outer retina and RPE will be fundamental to the future of gene therapy for IRDs. In combination with selective promoters to achieve minimal toxicity, these novel AAV serotypes will also increase treatment accessibility by enabling patients to receive injections in-office as opposed to in the operating room. Multiple surgical steps that carry significant risks will also be avoided, such as vitrectomy and retinotomy associated with subretinal injections.

4.5 Gene therapy without AAV, without goggles, and without immune rejection

For some patients, cytotoxicity may eliminate AAV-mediated gene therapy as an option. A novel method for nano-enhanced optical delivery may alleviate these concerns and serve as a laser-assisted gene therapy alternative (Batabyal et al., 2021a). Known as optoporation, this strategy depends on a pulsed femtosecond near-infrared laser microbeam to facilitate high-efficiency, transient perforations in the cell membrane; this leads to spatially localized transfection of cells with the desired genetic material (Matsuda and Cepko, 2004; Lagali et al., 2008; Doroudchi et al., 2011; Mohanty, 2012). In several optogenetic studies utilizing this method, the neural retina of *rd10* mice remained healthy following optoporation of multicharacteristics opsin (MCO1), a broad-band activatable white-opsin that can be reliably stimulated by ambient light (Batabyal et al., 2015; 2019). In previous work, MCO1-treated mice also showed improvements in visually guided behaviors like the Morris water maze (Wright et al., 2017). This was true even under illumination levels ten times lower than the thresholds typically required for channelrhodopsin stimulation in traditionally optogenetically modified mice (Wright et al., 2017; Batabyal et al., 2021a; Batabyal et al., 2021b). Furthermore, chronic ambient light exposure for 8 h per day did not induce photobleaching in the treated mice (Batabyal et al., 2021b). Nanoscope Therapeutics has launched subsequent clinical trials based on this technology (NCT05417126; NCT04945772). These promising studies may lead to novel therapies that do not require active stimulation goggles, while nano-enhanced optical delivery may obviate the need for AAV and reduce immune response concerns. Immunogenic risks associated with introducing synthetic opsins will remain, but eliminating the introduction of AAV particles will remove the major exacerbating factor.

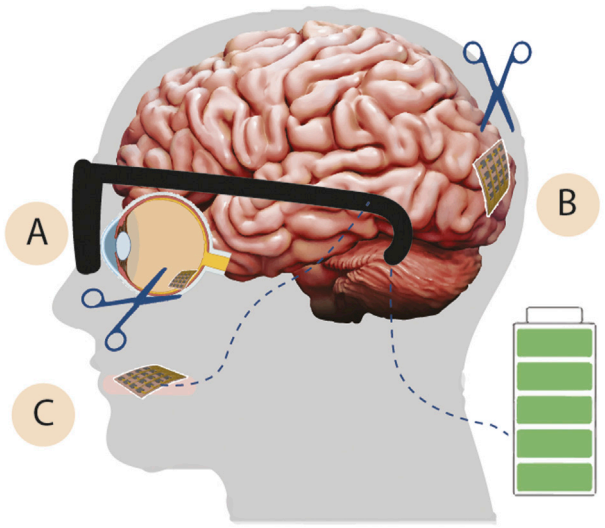

FIGURE 5
Artificial visual prosthetic designs. Goggles with an integrated camera and transmitter (*black*) connected to a battery and visual processing unit (*green, right side*) are required for existing artificial visual prosthetics. The goggles transmit stimulation signals to **(A)** retinal prosthetic devices, surgical implantation (*scissors*) of an electrode array with a receiving coil facilitates stimulation of retinal ganglion cells **(B)** cortical prosthetic devices, surgical implantation of an electrode array in the primary visual cortex (V1) with a receiving coil facilitates stimulation of these cortical neurons **(C)** non-implanted visual prosthetics, placed on the user's tongue contains integrated receiver for delivering electrical stimulation to the tongue (*pink*).

5 Artificial vision and prosthetics

Developments in artificial vision over the last few decades illustrate significant advances in retinal and cortical prosthetic devices. Creative approaches harness reprogramming of other sensory systems for prosthetics as well. The impressive success of several implantable and wearable prosthetic designs (summarized in Figure 5) warrants particular attention and will be especially valuable for the diverse IRD patient population. In the case of retinal and cortical prosthetics, patients with IRDs often experience a complex conglomeration of symptoms, which makes them candidates for only some of the surgical implantation techniques. The parallel pursuit of multiple prosthetic options will better serve the visually impaired community overall.

5.1 Retinal prosthetics

Significant progress in artificial vision research led to approval of Second Sight's Argus II retinal prosthetic system by the European Union and FDA in 2011 and 2013, respectively (Fernandes et al., 2012; Ghodasra et al., 2016). Argus II, and other similar retinal prosthetics (Figure 5A) required surgical implantation of a receiving coil to the lateral rectus muscle and placement of an electrode array over the macula (Farvardin et al., 2018). As of 2018, four patients had been treated by this strategy and re-gained the ability to perceive hand motions and to perform vague pattern recognition (Farvardin et al., 2018). In addition to the implanted components, these patients used complementary goggles equipped with a sensor-containing camera, a video processing unit, and a transmitting coil (Farvardin et al., 2018). While Argus II featured an array with only 60 electrodes, a next-generation implant in development could incorporate 240 central and peripheral electrodes to improve the resolution of vision (Duncan et al., 2017). Ultimately, electrodes with sizes comparable to that of a retinal ganglion cell would provide optimal vision for the patient (Duncan et al., 2017). However, low resolution of visual restoration has not been the only problem confronting Argus II users. Patients have reported poor battery life for the Argus II system and other features that limit its user friendliness. These are a few reasons why Argus II is no longer available. To address these problems and further enhance this technology, Second Sight (now a division of Vivani Medical) has a new device, Orion II, which is currently in development. These upgrades will be critical to make a retinal prosthetic implant worthwhile for patients, especially given the additional inconveniences posed by surgical implantation, vision rehabilitation, equipment burden, and the associated high costs (Ostad-Ahmadi et al., 2021).

Other prosthetics currently in development include Alpha AMS (Edwards et al., 2018), the Intelligent Retinal Implant System (IRIS V2; NCT02670980), Suprachoroidal Retinal Prosthesis (SRP; NCT01603576), and the PRIMA high-resolution photovoltaic retinal prosthetic system (PRIMA; NCT03333954). The Alpha AMS implant successfully improved visual performance in multiple participants for up to 24 months (Edwards et al., 2018). As with other visual prosthetics, surgical implantation remains challenging, but ongoing improvements in real-time optical coherence tomography microscope guidance and in surgical methods continue to bolster this intervention as a promising option for patients.

The SRP appears to have an acceptable safety profile, yet limitations still exist in the quality of visual contrast discrimination and object localization achieved by this device (Ayton et al., 2014; Slater et al., 2015). Results appear especially mixed in terms of the patients' ability to use the SRP to identify meaningful characters and localize objects (Shivdasani et al., 2017).

The PRIMA system targets patients with dry age-related macular degeneration (AMD) (Hageman et al., 2005; Toomey, 2015; Landowski et al., 2019), not IRDs; however, advances in this system are likely to become applicable to IRD patients as well. PRIMA has been shown in clinical trials to restore vision in the central scotoma of several patients (Palanker et al., 2020). Importantly, visual acuity correlated with the expectations derived from the pixel pitch (20/420) of the PRIMA device, and higher resolution of pixels in future versions of the implant will likely further improve the maximum achievable visual acuity (Palanker et al., 2020; 2022).

5.2 Cortical prosthetics

Cortical visual prosthetics have also been in development for many decades (Dobelle and Mladejovsky, 1974; Dobelle et al., 1976). Recent progress in electrode design, wireless power, and data transmission has generated devices that can support much

higher resolution of vision and greater implant stability (Kim et al., 2006; Rush and Troyk, 2012; PR, 2017; Niketeghad and Pouratian, 2019; Pio-Lopez et al., 2021). Importantly, cortical prosthetics implanted in the primary visual cortex (Figure 5B) can also bring vision to patients who are not candidates for retinal implants. This includes patients without functional retinal tissue due to severe IRD progression, as well as those with dysfunctional image forming corticothalamic pathways (*i.e.,* optic nerve-lateral geniculate nucleus-visual cortex) due to developmental and neurological disorders or ocular malformations (*i.e.,* microphthalmia).

5.3 Non-implanted visual prosthetics

Patients without any functional vision could also benefit from tactile based visual sensory substitution (Figure 5C) using devices like BrainPort Vision Pro, which remains in clinical trials (Nau et al., 2013; Lee et al., 2014; Stronks et al., 2016; Grant et al., 2018). BrainPort Vision Pro converts image information from a video camera into electrical stimulation patterns emitted from an oral device placed on the user's tongue (Nau et al., 2013; Lee et al., 2014; Stronks et al., 2016; Grant et al., 2018). Users learn to interpret the electrical stimulation patterns as visual stimuli including shapes, sizes, relative location, and object motion over the course of multiple training sessions, typically totaling 10 hours of one-on-one training over 3 days (Nau et al., 2013; Lee et al., 2014; Stronks et al., 2016; Grant et al., 2018). This strategy does not require any surgical implantation, and the intraoral device can be easily removed for cleaning (Lee et al., 2014; Grant et al., 2018). BrainPort Vision Pro likely harnesses synaptic plasticity in the brain to modulate the visual cortex in a manner conceptually similar to tactile interpretation of Braille lettering (Bola et al., 2017; Silson et al., 2022). BrainPort Vision Pro is currently available in China, with an ongoing clinical trial in the United States (NCT04725760) and expansion efforts in the European Union following Conformité Européene (CE) Mark approval. This technology augments visual prosthetic devices and is currently intended for use alongside traditional assistive technologies like the white cane or a guide dog.

6 Discussion

There are many viable, gene-agnostic strategies for treating IRDs. While most of them are best suited for treating patients at a particular stage of disease progression, in combination, they could constitute a powerful arsenal for maintaining or restoring vision across the disease-stage spectrum.

For patients who remain early in their IRD diagnosis, oral supplementation with NAC or other antioxidant cocktails remains a very useful therapeutic option. Mounting evidence in ongoing clinical trials suggests good efficacy for this strategy. Given that NAC and many other supplements can be self-administered by patients daily and at home, adherence to these regimens will likely be high. Delivery of RdCVF or proteasomal enhancers to patients with early disease represents a more definitive opportunity to prevent or at least delay otherwise inevitable visual impairment. Compliance with these treatments is likely to be high for stand-alone delivery by intravitreal injection, while extended-release formulations or AAV-based approaches may limit the burden of frequent repeat treatments.

For IRD patients with intermediate stage of disease progression, combinatorial treatment is even more likely to provide the necessary synergy to restore or protect visual function. In some instances, subretinal surgical implantation of ESCs, iPSCs, or CiPCs may be necessary to augment native photoreceptors. However, surgical and immune rejection risks can be significant, making some patients poor candidates for these procedures. By contrast, intravitreal delivery of a small molecule cocktail is much more accessible for most patients, and activation of a patient's own retinal stem cells eliminates immune rejection concerns. For patients with early onset disease that obliterates function of their own retinal stem cells, optogenetic strategies targeting bipolar cells or retinal ganglion cells remain gene-agnostic without relying on a patient's degenerating photoreceptors. Advances in AAV design may also allow the field to transition from subretinal to intravitreal treatment delivery. Optoporation or electro-transfection *via* a proprietary injection system (ETIS) developed by Eyevensys represent competing delivery strategies for both gene therapies and pharmacological/neuroprotective approaches to IRDs. Furthermore, improvements in the design of synthetic opsins may eventually support IRD patients' ability to regain vision without relying on goggles, which are traditionally required by optogenetic therapies.

For advanced-stage IRD patients with significant outer retina loss, vision restoration will focus on bipolar cells, retinal ganglion cells and the image-forming pathways in the brain. Optogenetic technologies would be ideal for patients whose bipolar cells and retinal ganglion cells remain responsive. By contrast, implantable retinal and cortical visual prosthetics are best suited to create artificial vision in patients whose inner retinal function is compromised as well. Creative approaches using tactile devices, like BrainPort Vision Pro, can also expand the population of patients for whom vision restoration is possible.

From retinal supplementation and stem cell transplantation to optogenetic therapy and retinal prosthetics, a variety of creative strategies hold promise in the quest to protect or restore vision for a broad population of people living with IRDs. Focusing on gene-agnostic approaches to treating IRDs will expedite the development of meaningful therapeutic solutions for patients. Distinct approaches will be suited to IRD patients at various stages of disease progression. Other aspects of health and financial access may also contribute to the "best treatment" for a given patient. Gene specific approaches represent the ultimate example of precision medicine and remain highly desirable and critically important to pursue. However, by investigating common targetable disease pathways and putting sufficient parallel emphasis on the development of gene-agnostic IRD therapeutics as well, we can hope to achieve the long-promised "just around the corner" treatments in time to make a difference for the vast majority of IRD patients.

Author contributions

Both LAC and AI contributed to the overall concept for this review, writing the manuscript, assembling/editing the figures, manuscript revisions and approved the submitted version.

Funding

This work was supported by an Unrestricted Research Award from Research to Prevent Blindness, Inc., New York, NY to the Duke Eye Center; AI's work was supported by private donations to the Duke Retinal Degenerations Research Fund, the Duke Retinal Genetics Fund, and the Maria Laura Ciccarelli Duke Memorial Fund. LAC is supported by NIH 5T32GM007171-48 (to the Duke University School of Medicine Medical Scientist Training Program).

Acknowledgments

We would like to thank Marios L. Tringides and Oleg Alekseev, MD, PhD for feedback on the manuscript and figure layout. Some artwork inspired by Biorender; all figures were hand-drawn.

Conflict of interest

LAC has no conflicts of interest. AI is a consultant for the following, GLG Group; Teladoc Health (formerly Advance Medical, Inc.); Rhythm Pharmaceuticals; Applied Genetic Technologies Corporation; Acucela; Allergan/AbbVie; Guidepoint Clinical; 4D Molecular Therapeutics; MeiraGTX; Jannsen Pharmaceuticals; M. Arkin Ltd.; Allievex Corp; Biogen; Aldeyra Therapeutics; Clarivate Analytics; EluminexBio; IQVIA; Adverum Biotechnologies; Tegus; Twenty-Twenty; and Baker Brother Investments. AI participates on the scientific advisory boards for the following, Foundation for Fighting Blindness; the Choroideremia Research Foundation; Alia Therapeutics.

Publisher's note

References

Adak, S., Magdalene, D., Deshmukh, S., Das, D., and Jaganathan, B. G. (2021). A review on mesenchymal stem cells for treatment of retinal diseases. *Stem Cell Rev. Rep.* 17 (4), 1154–1173. doi:10.1007/S12015-020-10090-X

Aït-Ali, N., Fridlich, R., Millet-Puel, G., Clérin, E., Delalande, F., Jaillard, C., et al. (2015). Rod-derived cone viability factor promotes cone survival by stimulating aerobic glycolysis. *Cell* 161 (4), 817–832. doi:10.1016/J.CELL.2015.03.023

Allocca, M., Mussolino, C., Garcia-Hoyos, M., Sanges, D., Iodice, C., Petrillo, M., et al. (2007). Novel adeno-associated virus serotypes efficiently transduce murine photoreceptors. *J. virology* 81 (20), 11372–11380. doi:10.1128/JVI.01327-07

Alsaeedi, H. A., Koh, A. E. H., Lam, C., Rashid, M. B. A., Harun, M. H. N., Saleh, M. F. B. M., et al. (2019). Dental pulp stem cells therapy overcome photoreceptor cell death and protects the retina in a rat model of sodium iodate-induced retinal degeneration. *J. Photochem. Photobiol. B, Biol.* 198, 111561. doi:10.1016/J.JPHOTOBIOL.2019.111561

Ando, R., Noda, K., Tomaru, U., Kamoshita, M., Ozawa, Y., Notomi, S., et al. (2014). Decreased proteasomal activity causes photoreceptor degeneration in mice. *Investigative Ophthalmol. Vis. Sci.* 55 (7), 4682–4690. doi:10.1167/IOVS.13-13272

Assawachananont, J., Mandai, M., Okamoto, S., Yamada, C., Eiraku, M., Yonemura, S., et al. (2014). Transplantation of embryonic and induced pluripotent stem cell-derived 3D retinal sheets into retinal degenerative mice. *Stem Cell Rep.* 2 (5), 662–674. doi:10.1016/J.STEMCR.2014.03.011

Ayton, L. N., Blamey, P. J., Guymer, R. H., Luu, C. D., Nayagam, D. A. X., Sinclair, N. C., et al. (2014). First-in-Human trial of a novel suprachoroidal retinal prosthesis. *PLoS ONE* 9 (12), 115239. doi:10.1371/JOURNAL.PONE.0115239

Bainbridge, J. W. B., Smith, A. J., Barker, S. S., Robbie, S., Henderson, R., Balaggan, K., et al. (2008). Effect of gene therapy on visual function in Leber's congenital amaurosis. *N. Engl. J. Med.* 358 (21), 2231–2239. doi:10.1056/NEJMOA0802268

Bartsch, U., Oriyakhel, W., Kenna, P. F., Linke, S., Richard, G., Petrowitz, B., et al. (2008). Retinal cells integrate into the outer nuclear layer and differentiate into mature photoreceptors after subretinal transplantation into adult mice. *Exp. eye Res.* 86 (4), 691–700. doi:10.1016/J.EXER.2008.01.018

Batabyal, S., Cervenka, G., Ha, J. H., Kim, Y. T., and Mohanty, S. (2015). Broad-band activatable white-opsin. *PloS one* 10 (9), e0136958. doi:10.1371/JOURNAL.PONE.0136958

Batabyal, S., Gajjeraman, S., Bhattacharya, S., Wright, W., and Mohanty, S. (2019). Nano-enhanced optical gene delivery to retinal degenerated mice. *Curr. Gene Ther.* 19 (5), 318–329. doi:10.2174/1566523219666191017114044

Batabyal, S., Gajjeraman, S., Pradhan, S., Bhattacharya, S., Wright, W., and Mohanty, S. (2021b). Sensitization of ON-bipolar cells with ambient light activatable multi-characteristic opsin rescues vision in mice. *Gene Ther.* 28 (3–4), 162–176. doi:10.1038/S41434-020-00200-2

Batabyal, S., and Kim, S. (2021). Layer-specific nanophotonic delivery of therapeutic opsin-encoding genes into retina. *Exp. eye Res.* 205, 108444. doi:10.1016/J.EXER.2021.108444

Batabyal, S., Kim, S., Wright, W., and Mohanty, S. (2021a). Laser-assisted targeted gene delivery to degenerated retina improves retinal function. *J. Biophot.* 14 (1), e202000234. doi:10.1002/JBIO.202000234

Berger, A., Devenyi, R., and Héon, E. (2016). Retinal prosthesis system for advanced retinitis pigmentosa, A health technology assessment. *Ont. Health Technol. Assess. Ser.* 16 (14), 1–63.

Block, M. L., Zecca, L., and Hong, J. S. (2007). Microglia-mediated neurotoxicity, uncovering the molecular mechanisms. *Nat. Rev. Neurosci.* 8 (1), 57–69. doi:10.1038/NRN2038

Bola, Ł., Siuda-Krzywicka, K., Paplińska, M., Sumera, E., Zimmermann, M., Jednoróg, K., et al. (2017). Structural reorganization of the early visual cortex following Braille training in sighted adults. *Sci. Rep.* 7 (1), 17448. doi:10.1038/S41598-017-17738-8

Boshart, M., Weber, F., Jahn, G., Dorsch-Häsler, K., Fleckenstein, B., and Schaffner, W. (1985). A very strong enhancer is located upstream of an immediate early gene of human cytomegalovirus. *Cell* 41 (2), 521–530. doi:10.1016/S0092-8674(85)80025-8

Busskamp, V., Duebel, J., Balya, D., Fradot, M., Viney, T. J., Siegert, S., et al. (2010). Genetic reactivation of cone photoreceptors restores visual responses in retinitis pigmentosa. *Science* 329 (5990), 413–417. doi:10.1126/SCIENCE.1190897

Campochiaro, P. A., Iftikhar, M., Hafiz, G., Akhlaq, A., Tsai, G., Wehling, D., et al. (2020). Oral N-acetylcysteine improves cone function in retinitis pigmentosa patients in phase I trial. *J. Clin. investigation* 130 (3), 1527–1541. doi:10.1172/JCI132990

Cepko, C., and Punzo, C. (2015). Cell metabolism, Sugar for sight. *Nature* 522 (7557), 428–429. doi:10.1038/522428a

Chalmel, F., Léveillard, T., Jaillard, C., Lardenois, A., Berdugo, N., Morel, E., et al. (2007). Rod-derived Cone Viability Factor-2 is a novel bifunctional-thioredoxin-like protein with therapeutic potential. *BMC Mol. Biol.* 8, 74. doi:10.1186/1471-2199-8-74

Chiang, M. C., and Chern, E. (2022). Current development, obstacle and futural direction of induced pluripotent stem cell and mesenchymal stem cell treatment in degenerative retinal disease. *Int. J. Mol. Sci.* 23 (5), 2529. doi:10.3390/IJMS23052529

Cideciyan, A. V., Hood, D. C., Huang, Y., Banin, E., Li, Z. Y., Stone, E. M., et al. (1998). Disease sequence from mutant rhodopsin allele to rod and cone photoreceptor

degeneration in man. *Proc. Natl. Acad. Sci. U. S. A.* 95 (12), 7103–7108. doi:10.1073/PNAS.95.12.7103

Clérin, E., Marussig, M., Sahel, J. A., and Léveillard, T. (2020). Metabolic and redox signaling of the nucleoredoxin-like-1 gene for the treatment of genetic retinal diseases. *Int. J. Mol. Sci.* 21 (5), 1625. doi:10.3390/IJMS21051625

Coles, B. L. K., Angénieux, B., Inoue, T., Del Rio-Tsonis, K., Spence, J. R., McInnes, R. R., et al. (2004). Facile isolation and the characterization of human retinal stem cells. *Proc. Natl. Acad. Sci. U. S. A.* 101 (44), 15772–15777. doi:10.1073/PNAS.0401596101

Comyn, O., Lee, E., and MacLaren, R. E. (2010). Induced pluripotent stem cell therapies for retinal disease. *Curr. Opin. neurology* 23 (1), 4–9. doi:10.1097/WCO.0B013E3283352F96

Cruz, N. M., Yuan, Y., Leehy, B. D., Baid, R., Kompella, U., DeAngelis, M. M., et al. (2014). Modifier genes as therapeutics, the nuclear hormone receptor Rev Erb alpha (Nr1d1) rescues Nr2e3 associated retinal disease. *PloS one* 9 (1), e87942. doi:10.1371/JOURNAL.PONE.0087942

Da Cruz, L., Fynes, K., Georgiadis, O., Kerby, J., Luo, Y. H., Ahmado, A., et al. (2018). Phase 1 clinical study of an embryonic stem cell-derived retinal pigment epithelium patch in age-related macular degeneration. *Nat. Biotechnol.* 36 (4), 328–337. doi:10.1038/NBT.4114

Dalkara, D., Byrne, L. C., Klimczak, R. R., Visel, M., Yin, L., Merigan, W. H., et al. (2013). *In vivo*-directed evolution of a new adeno-associated virus for therapeutic outer retinal gene delivery from the vitreous. *Sci. Transl. Med.* 5 (189), 189ra76. doi:10.1126/SCITRANSLMED.3005708

Deng, C. L., Hu, C. B., Ling, S. T., Zhao, N., Bao, L. H., Zhou, F., et al. (2021). Photoreceptor protection by mesenchymal stem cell transplantation identifies exosomal MiR-21 as a therapeutic for retinal degeneration. *Cell death Differ.* 28 (3), 1041–1061. doi:10.1038/S41418-020-00636-4

Dobelle, W. H., Mladejovsky, M. G., Evans, J. R., Roberts, T. S., and Girvin, J. P. (1976). Braille" reading by a blind volunteer by visual cortex stimulation. *Nature* 259 (5539), 111–112. doi:10.1038/259111A0

Dobelle, W. H., and Mladejovsky, M. G. (1974). Phosphenes produced by electrical stimulation of human occipital cortex, and their application to the development of a prosthesis for the blind. *J. physiology* 243 (2), 553–576. doi:10.1113/JPHYSIOL.1974.SP010766

Doroudchi, M. M., Greenberg, K. P., Liu, J., Silka, K. A., Boyden, E. S., Lockridge, J. A., et al. (2011). Virally delivered channelrhodopsin-2 safely and effectively restores visual function in multiple mouse models of blindness. *Mol. Ther. , J. Am. Soc. Gene Ther.* 19 (7), 1220–1229. doi:10.1038/MT.2011.69

Duncan, J. L., Richards, T. P., Arditi, A., da Cruz, L., Dagnelie, G., Dorn, J. D., et al. (2017). Improvements in vision-related quality of life in blind patients implanted with the Argus II Epiretinal Prosthesis. *Clin. Exp. optometry* 100 (2), 144–150. doi:10.1111/CXO.12444

Edwards, T. L., Cottriall, C. L., Xue, K., Simunovic, M. P., Ramsden, J. D., Zrenner, E., et al. (2018). Assessment of the electronic retinal implant alpha AMS in restoring vision to blind patients with end-stage retinitis pigmentosa. *Ophthalmology* 125 (3), 432–443. doi:10.1016/J.OPHTHA.2017.09.019

Farvardin, M., Afarid, M., Attarzadeh, A., Johari, M. K., Mehryar, M., Nowroozzadeh, M. H., et al. (2018). The Argus-II retinal prosthesis implantation; from the global to local successful experience. *Front. Neurosci.* 12, 584. doi:10.3389/fnins.2018.00584

Fernandes, R. A. B., Diniz, B., Ribeiro, R., and Humayun, M. (2012). Artificial vision through neuronal stimulation. *Neurosci. Lett.* 519 (2), 122–128. doi:10.1016/J.NEULET.2012.01.063

Ferrante, R. J., Browne, S. E., Shinobu, L. A., Bowling, A. C., Baik, M. J., MacGarvey, U., et al. (1997). Evidence of increased oxidative damage in both sporadic and familial amyotrophic lateral sclerosis. *J. Neurochem.* 69 (5), 2064–2074. doi:10.1046/J.1471-4159.1997.69052064.X

Finkel, T. (2003). Oxidant signals and oxidative stress. *Curr. Opin. Cell Biol.* 15 (2), 247–254. doi:10.1016/S0955-0674(03)00002-4

Fischer, M. D., Huber, G., Beck, S. C., Tanimoto, N., Muehlfriedel, R., Fahl, E., et al. (2009). Noninvasive, *in vivo* assessment of mouse retinal structure using optical coherence tomography. *PloS one* 4 (10), e7507. doi:10.1371/JOURNAL.PONE.0007507

Frøen, R., Erik, O. J., Bjørn, N., Andrea, F., Goran, P., and Morten, C. M. (2013). Does the adult human ciliary body epithelium contain "true" retinal stem cells? *BioMed Res. Int.* 2013, 531579. doi:10.1155/2013/531579

Garita-Hernandez, M., Chaffiol, A., Guibbal, L., Routet, F., Khabou, H., Riancho, L., et al. (2021). Control of microbial opsin expression in stem cell derived cones for improved outcomes in cell therapy. *Front. Cell. Neurosci.* 15, 70. doi:10.3389/fncel.2021.648210

Garita-Hernandez, M., Lampič, M., Chaffiol, A., Guibbal, L., Routet, F., Santos-Ferreira, T., et al. (2019). Restoration of visual function by transplantation of optogenetically engineered photoreceptors. *Nat. Commun.* 10 (1), 4524–4613. doi:10.1038/s41467-019-12330-2

Gasparini, S. J., Llonch, S., Borsch, O., and Ader, M. (2019). Transplantation of photoreceptors into the degenerative retina, Current state and future perspectives. *Prog. Retin. eye Res.* 69, 1–37. doi:10.1016/J.PRETEYERES.2018.11.001

Gaub, B. M., Berry, M. H., Visel, M., Holt, A., Isacoff, E. Y., and Flannery, J. G. (2018). Optogenetic retinal gene therapy with the light gated GPCR vertebrate rhodopsin. *Methods Mol. Biol.* 1715, 177–189. doi:10.1007/978-1-4939-7522-8_12

Gauvain, G., Akolkar, H., Chaffiol, A., Arcizet, F., Khoei, M. A., Desrosiers, M., et al. (2021). Optogenetic therapy, high spatiotemporal resolution and pattern discrimination compatible with vision restoration in non-human primates. *Commun. Biol.* 4 (1), 125. doi:10.1038/s42003-020-01594-w

Ghodasra, D. H., Chen, A., Arevalo, J. F., Birch, D. G., Branham, K., Coley, B., et al. (2016). Worldwide Argus II implantation, Recommendations to optimize patient outcomes. *BMC Ophthalmol.* 16 (1), 52–58. doi:10.1186/s12886-016-0225-1

Gilgun-Sherki, Y., Melamed, E., and Offen, D. (2001). Oxidative stress induced-neurodegenerative diseases, the need for antioxidants that penetrate the blood brain barrier. *Neuropharmacology* 40 (8), 959–975. doi:10.1016/S0028-3908(01)00019-3

Gire, A., Sullivan, L. S., Bowne, S. J., Birch, D. G., Hughbanks-Wheaton, D., Heckenlively, J. R., et al. (2007). The Gly56Arg mutation in NR2E3 accounts for 1-2% of autosomal dominant retinitis pigmentosa. *Mol. Vis.* 13, 1970–1975.

Gorbatyuk, M. S., Knox, T., LaVail, M. M., Gorbatyuk, O. S., Noorwez, S. M., Hauswirth, W. W., et al. (2010). Restoration of visual function in P23H rhodopsin transgenic rats by gene delivery of BiP/Grp78. *Proc. Natl. Acad. Sci. U. S. A.* 107 (13), 5961–5966. doi:10.1073/PNAS.0911991107

Grant, P., Maeng, M., Arango, T., Hogle, R., Szlyk, J., and Seiple, W. (2018). Performance of real-world functional tasks using an updated oral electronic vision device in persons blinded by trauma. *Optometry Vis. Sci. , official Publ. Am. Acad. Optometry* 95 (9), 766–773. doi:10.1097/OPX.0000000000001273

Hageman, G. S., Anderson, D. H., Johnson, L. V., Hancox, L. S., Taiber, A. J., Hardisty, L. I., et al. (2005). A common haplotype in the complement regulatory gene factor H (HF1/CFH) predisposes individuals to age-related macular degeneration. *Proc. Natl. Acad. Sci. U. S. A.* 102 (20), 7227–7232. doi:10.1073/PNAS.0501536102

Haider, N. B., Jacobson, S. G., Cideciyan, A. V., Swiderski, R., Streb, L. M., Searby, C., et al. (2000). Mutation of a nuclear receptor gene, NR2E3, causes enhanced S cone syndrome, a disorder of retinal cell fate. *Nat. Genet.* 24 (2), 127–131. doi:10.1038/72777

Han, I. C., Bohrer, L. R., Gibson-Corley, K. N., Wiley, L. A., Shrestha, A., Harman, B. E., et al. (2022). Biocompatibility of human induced pluripotent stem cell-derived retinal progenitor cell grafts in immunocompromised rats. *Cell Transplant.* 31, 9636897221104451. doi:10.1177/09636897221104451

Hauswirth, W. W., Aleman, T. S., Kaushal, S., Cideciyan, A. V., Schwartz, S. B., Wang, L., et al. (2008). Treatment of leber congenital amaurosis due to RPE65 mutations by ocular subretinal injection of adeno-associated virus gene vector, short-term results of a phase I trial. *Hum. gene Ther.* 19 (10), 979–990. doi:10.1089/HUM.2008.107

Hicks, D., and Sahel, J. A. (1999). The implications of rod-dependent cone survival for basic and clinical research. *Investigative Ophthalmol. Vis. Sci.* 40, 3071–3074.

Hinderer, C., Katz, N., Buza, E. L., Dyer, C., Goode, T., Bell, P., et al. (2018). Severe toxicity in nonhuman primates and piglets following high-dose intravenous administration of an adeno-associated virus vector expressing human SMN. *Hum. gene Ther.* 29 (3), 285–298. doi:10.1089/HUM.2018.015

Hitoshi, N., Ken-ichi, Y., and Jun-ichi, M. (1991). Efficient selection for high-expression transfectants with a novel eukaryotic vector. *Gene* 108 (2), 193–199. doi:10.1016/0378-1119(91)90434-D

Hulliger, E. C., Hostettler, S. M., and Kleinlogel, S. (2020). Empowering retinal gene therapy with a specific promoter for human rod and cone ON-bipolar cells. *Mol. Ther. Methods & Clin. Dev.* 17, 505–519. doi:10.1016/J.OMTM.2020.03.003

Iannaccone, A., Alekseev, O., and Krauss, E. (2021b). *Retinitis pigmentosa, rare diseases*. National Organization of Rare Diseases.

Iannaccone, A., Brabbit, E., Lopez-Miro, C., Love, Z., Griffiths, V., Kedrov, M., et al. (2021a). Interspecies correlations between human and mouse nr2e3-associated recessive disease. *J. Clin. Med.* 10 (3), 475–527. doi:10.3390/JCM10030475

Iannaccone, A., Man, D., Waseem, N., Jennings, B. J., Ganapathiraju, M., Gallaher, K., et al. (2006). Retinitis pigmentosa associated with rhodopsin mutations, Correlation between phenotypic variability and molecular effects. *Vis. Res.* 46 (27), 4556–4567. doi:10.1016/J.VISRES.2006.08.018

Ikeda, H., Osakada, F., Watanabe, K., Mizuseki, K., Haraguchi, T., Miyoshi, H., et al. (2005). Generation of Rx+/Pax6+ neural retinal precursors from embryonic stem cells. *Proc. Natl. Acad. Sci. U. S. A.* 102 (32), 11331–11336. doi:10.1073/PNAS.0500010102

Ildefonso, C. J., Jaime, H., Brown, E. E., Iwata, R. L., Ahmed, C. M., Massengill, M. T., et al. (2016). Targeting the Nrf2 signaling pathway in the retina with a gene-delivered secretable and cell-penetrating peptide. *Investigative Ophthalmol. Vis. Sci.* 57 (2), 372–386. doi:10.1167/IOVS.15-17703

Illing, M. E., Rajan, R. S., Bence, N. F., and Kopito, R. R. (2002). A rhodopsin mutant linked to autosomal dominant retinitis pigmentosa is prone to aggregate and interacts with the ubiquitin proteasome system. *J. Biol. Chem.* 277 (37), 34150–34160. doi:10.1074/JBC.M204955200

Itagaki, S., McGeer, P. L., Akiyama, H., Zhu, S., and Selkoe, D. (1989). Relationship of microglia and astrocytes to amyloid deposits of Alzheimer disease. *J. Neuroimmunol.* 24 (3), 173–182. doi:10.1016/0165-5728(89)90115-X

Jablonski, M. M., Tombran-Tink, J., Mrazek, D. A., and Iannaccone, A. (2001). Pigment epithelium-derived factor supports normal Müller cell development and glutamine synthetase expression after removal of the retinal pigment epithelium. *GLIA* 35 (1), 14–25. doi:10.1002/glia.1066

Jayakody, S. A., Gonzalez-Cordero, A., Ali, R. R., and Pearson, R. A. (2015). Cellular strategies for retinal repair by photoreceptor replacement. *Prog. Retin. eye Res.* 46, 31–66. doi:10.1016/J.PRETEYERES.2015.01.003

John, M. C., Quinn, J., Hu, M. L., Cehajic-Kapetanovic, J., and Xue, K. (2022). Gene-agnostic therapeutic approaches for inherited retinal degenerations. *Front. Mol. Neurosci.* 15, 1068185. doi:10.3389/FNMOL.2022.1068185

Kahraman, N. S., and Oner, A. (2020). Umbilical cord derived mesenchymal stem cell implantation in retinitis pigmentosa, a 6-month follow-up results of a phase 3 trial. *Int. J. Ophthalmol.* 13 (9), 1423–1429. doi:10.18240/IJO.2020.09.14

Keren-Shaul, H., Spinrad, A., Weiner, A., Matcovitch-Natan, O., Dvir-Szternfeld, R., Ulland, T. K., et al. (2017). A unique microglia type associated with restricting development of alzheimer's disease. *Cell* 169 (7), 1276–1290. doi:10.1016/J.CELL.2017.05.018

Khabou, H., Cordeau, C., Pacot, L., Fisson, S., and Dalkara, D. (2018). Dosage thresholds and influence of transgene cassette in adeno-associated virus-related toxicity. *Hum. gene Ther.* 29 (11), 1235–1241. doi:10.1089/HUM.2018.144

Kim, T., Troyk, P. R., and Bak, M. (2006). "Active floating micro electrode arrays (AFMA)," in Conference proceedings, Annual International Conference of the IEEE Engineering in Medicine and Biology Society, United Kingdom, 10 April 2006, 2807–2810. doi:10.1109/IEMBS.2006.259981

Koilkonda, R. D., Chou, T. H., Porciatti, V., Hauswirth, W. W., and Guy, J. (2010). Induction of rapid and highly efficient expression of the human ND4 complex I subunit in the mouse visual system by self-complementary adeno-associated virus. *Archives Ophthalmol. Chic. Ill* 128 (7), 876–883. doi:10.1001/ARCHOPHTHALMOL.2010.135

Kolesnikov, A. V., Rikimaru, L., Hennig, A. K., Lukasiewicz, P. D., Fliesler, S. J., Govardovskii, V. I., et al. (2011). G-protein betagamma-complex is crucial for efficient signal amplification in vision. *J. Neurosci. , official J. Soc. Neurosci.* 31 (22), 8067–8077. doi:10.1523/JNEUROSCI.0174-11.2011

Komeima, K., Rogers, B. S., and Campochiaro, P. A. (2007). Antioxidants slow photoreceptor cell death in mouse models of retinitis pigmentosa. *J. Cell. physiology* 213 (3), 809–815. doi:10.1002/JCP.21152

Komeima, K., Rogers, B. S., Lu, L., and Campochiaro, P. A. (2006). Antioxidants reduce cone cell death in a model of retinitis pigmentosa. *Proc. Natl. Acad. Sci. U. S. A.* 103 (30), 11300–11305. doi:10.1073/PNAS.0604056103

Kong, X., Gulnar, H., Dagmar, W., Anam, A., and Peter, A. C. (2021). Locus-level changes in macular sensitivity in patients with retinitis pigmentosa treated with oral N-acetylcysteine. *Am. J. Ophthalmol.* 221, 105–114. doi:10.1016/j.ajo.2020.08.002

Kosmaoglou, M., Schwarz, N., Bett, J. S., and Cheetham, M. E. (2008). Molecular chaperones and photoreceptor function. *Prog. Retin. eye Res.* 27 (4), 434–449. doi:10.1016/J.PRETEYERES.2008.03.001

Kou, M., Huang, L., Yang, J., Chiang, Z., Chen, S., Liu, J., et al. (2022). Mesenchymal stem cell-derived extracellular vesicles for immunomodulation and regeneration, a next generation therapeutic tool? *Cell Death Dis.* 13 (7), 580–616. doi:10.1038/s41419-022-05034-x

Kralik, J., van Wyk, M., Stocker, N., and Kleinlogel, S. (2022). Bipolar cell targeted optogenetic gene therapy restores parallel retinal signaling and high-level vision in the degenerated retina. *Commun. Biol.* 5, 1116–1215. doi:10.1038/s42003-022-04016-1

Krasemann, S., Madore, C., Cialic, R., Baufeld, C., Calcagno, N., El Fatimy, R., et al. (2017). The TREM2-APOE pathway drives the transcriptional phenotype of dysfunctional microglia in neurodegenerative diseases. *Immunity* 47 (3), 566–581. doi:10.1016/J.IMMUNI.2017.08.008

Lagali, P. S., Balya, D., Awatramani, G. B., Münch, T. A., Kim, D. S., Busskamp, V., et al. (2008). Light-activated channels targeted to ON bipolar cells restore visual function in retinal degeneration. *Nat. Neurosci.* 11 (6), 667–675. doi:10.1038/NN.2117

Landowski, M., Kelly, U., Klingeborn, M., Groelle, M., Ding, J. D., Grigsby, D., et al. (2019). Human complement factor H Y402H polymorphism causes an age-related macular degeneration phenotype and lipoprotein dysregulation in mice. *Proc. Natl. Acad. Sci. U. S. A.* 116 (9), 3703–3711. doi:10.1073/PNAS.1814014116

Ledford, H. (2017). FDA advisers back gene therapy for rare form of blindness. *Nature* 550 (7676), 314. doi:10.1038/NATURE.2017.22819

Lee, J. M., Calkins, M. J., Chan, K., Kan, Y. W., and Johnson, J. A. (2003). Identification of the NF-E2-related factor-2-dependent genes conferring protection against oxidative stress in primary cortical astrocytes using oligonucleotide microarray analysis. *J. Biol. Chem.* 278 (14), 12029–12038. doi:10.1074/JBC.M211558200

Lee, S. Y., Usui, S., Zafar, A. B., Oveson, B. C., Jo, Y. J., Lu, L., et al. (2011). N-Acetylcysteine promotes long-term survival of cones in a model of retinitis pigmentosa. *J. Cell. physiology* 226 (7), 1843–1849. doi:10.1002/JCP.22508

Lee, V. K., Nau, A. C., Laymon, C., Chan, K. C., Rosario, B. L., and Fisher, C. (2014). Successful tactile based visual sensory substitution use functions independently of visual pathway integrity. *Front. Hum. Neurosci.* 8, 291. doi:10.3389/FNHUM.2014.00291

Léveillard, T., Fridlich, R., Clérin, E., Aït-Ali, N., Millet-Puel, G., Jaillard, C., et al. (2014). Therapeutic strategy for handling inherited retinal degenerations in a gene-independent manner using rod-derived cone viability factors. *Comptes rendus Biol.* 337 (3), 207–213. doi:10.1016/J.CRVI.2013.12.002

Léveillard, T., Mohand-Saïd, S., Lorentz, O., Hicks, D., Fintz, A. C., Clérin, E., et al. (2004). Identification and characterization of rod-derived cone viability factor. *Nat. Genet.* 36 (7), 755–759. doi:10.1038/NG1386

Li, S., Datta, S., Brabbit, E., Love, Z., Woytowicz, V., Flattery, K., et al. (2021a). Nr2e3 is a genetic modifier that rescues retinal degeneration and promotes homeostasis in multiple models of retinitis pigmentosa. *Gene Ther.* 28 (5), 223–241. doi:10.1038/S41434-020-0134-Z

Li, S., Liu, Y., Wang, L., Wang, F., Zhao, T. T., Li, Q. Y., et al. (2021b). A phase I clinical trial of human embryonic stem cell-derived retinal pigment epithelial cells for early-stage Stargardt macular degeneration, 5-years' follow-up. *Cell Prolif.* 54 (9), e13100. doi:10.1111/CPR.13100

Lin, J. H., Li, H., Yasumura, D., Cohen, H. R., Zhang, C., Panning, B., et al. (2007). IRE1 signaling affects cell fate during the unfolded protein response. *Science* 318 (5852), 944–949. doi:10.1126/SCIENCE.1146361

Liu, C. Y., Westerlund, U., Svensson, M., Moe, M. C., Varghese, M., Berg-Johnsen, J., et al. (2003). Artificial niches for human adult neural stem cells, possibility for autologous transplantation therapy. *J. hematotherapy stem Cell Res.* 12 (6), 689–699. doi:10.1089/15258160360732713

Liu, X., Xie, J., Yang, L., Li, Y., He, Y., Liu, Z., et al. (2020). Bone marrow mesenchymal stem cells enhance autophagy and help protect cells under hypoxic and retinal detachment conditions. *J. Cell. Mol. Med.* 24 (6), 3346–3358. doi:10.1111/JCMM.15008

Liu, Y. P., Tsai, I. C., Morleo, M., Oh, E. C., Leitch, C. C., Massa, F., et al. (2014). Ciliopathy proteins regulate paracrine signaling by modulating proteasomal degradation of mediators. *J. Clin. investigation* 124 (5), 2059–2070. doi:10.1172/JCI71898

Lobanova, E. S., Finkelstein, S., Herrmann, R., Chen, Y. M., Kessler, C., Michaud, N. A., et al. (2008). Transducin gamma-subunit sets expression levels of alpha- and beta-subunits and is crucial for rod viability. *J. Neurosci. , official J. Soc. Neurosci.* 28 (13), 3510–3520. doi:10.1523/JNEUROSCI.0338-08.2008

Lobanova, E. S., Finkelstein, S., Li, J., Travis, A. M., Hao, Y., Klingeborn, M., et al. (2018). Increased proteasomal activity supports photoreceptor survival in inherited retinal degeneration. *Nat. Commun.* 9 (1), 1738. doi:10.1038/S41467-018-04117-8

Lobanova, E. S., Stella, F., Nikolai, P. S., and Vadim, Y. A. (2013). Proteasome overload is a common stress factor in multiple forms of inherited retinal degeneration. *Proc. Natl. Acad. Sci. U. S. A.* 110 (24), 9986–9991. doi:10.1073/PNAS.1305521110

Lorenz, B., Gyürüs, P., Preising, M., Bremser, D., Gu, S., Andrassi, M., et al. (2000). Early-onset severe rod–cone dystrophy in young children with RPE65 mutations. *Investigative Ophthalmol. Vis. Sci.* 41, 2735–2742.

Lu, L., Oveson, B. C., Jo, Y. J., Lauer, T. W., Usui, S., Komeima, K., et al. (2009). Increased expression of glutathione peroxidase 4 strongly protects retina from oxidative damage. *Antioxidants redox Signal.* 11 (4), 715–724. doi:10.1089/ARS.2008.2171

Maguire, A. M., Simonelli, F., Pierce, E. A., Pugh, E. N., Jr, Mingozzi, F., Bennicelli, J., et al. (2008). Safety and efficacy of gene transfer for Leber's congenital amaurosis. *N. Engl. J. Med.* 358 (21), 2240–2248. doi:10.1056/NEJMOA0802315

Mahato, B., Kaya, K. D., Fan, Y., Sumien, N., Shetty, R. A., Zhang, W., et al. (2020). Pharmacologic fibroblast reprogramming into photoreceptors restores vision. *Nature* 581 (7806), 83–88. doi:10.1038/S41586-020-2201-4

Mandai, M., Watanabe, A., Kurimoto, Y., Hirami, Y., Morinaga, C., Daimon, T., et al. (2017). Autologous induced stem-cell-derived retinal cells for macular degeneration. *N. Engl. J. Med.* 376 (11), 1038–1046. doi:10.1056/NEJMOA1608368

Matsuda, T., and Cepko, C. L. (2004). Electroporation and RNA interference in the rodent retina *in vivo* and *in vitro*. *Proc. Natl. Acad. Sci. U. S. A.* 101 (1), 16–22. doi:10.1073/PNAS.2235688100

McLaughlin, M. E., Sandberg, M. A., Berson, E. L., and Dryja, T. P. (1993). Recessive mutations in the gene encoding the beta-subunit of rod phosphodiesterase in patients with retinitis pigmentosa. *Nat. Genet.* 4 (2), 130–134. doi:10.1038/NG0693-130

Mellough, C. B., Sernagor, E., Moreno-Gimeno, I., Steel, D. H. W., and Lako, M. (2012). Efficient stage-specific differentiation of human pluripotent stem cells toward retinal photoreceptor cells. *Stem cells* 30 (4), 673–686. doi:10.1002/STEM.1037

Miyagishima, K. J., Wan, Q., Corneo, B., Sharma, R., Lotfi, M. R., Boles, N. C., et al. (2016). In pursuit of authenticity, induced pluripotent stem cell-derived retinal pigment epithelium for clinical applications. *Stem Cells Transl. Med.* 5 (11), 1562–1574. doi:10.5966/sctm.2016-0037

Mohand-Said, S., Deudon-Combe, A., Hicks, D., Simonutti, M., Forster, V., Fintz, A. C., et al. (1998). Normal retina releases a diffusible factor stimulating cone survival in the retinal degeneration mouse. *Proc. Natl. Acad. Sci. U. S. A.* 95 (14), 8357–8362. doi:10.1073/PNAS.95.14.8357

Mohanty, S. (2012). Non-viral delivery and optimized optogenetic stimulation of retinal ganglion cells led to behavioral restoration of vision. *Nat. Preced.* 2012, 1. doi:10.1038/npre.2012.6869.1

Nau, A., Bach, M., and Fisher, C. (2013). Clinical tests of ultra-low vision used to evaluate rudimentary visual perceptions enabled by the BrainPort vision device. *Transl. Vis. Sci. Technol.* 2 (3), 1. doi:10.1167/TVST.2.3.1

Nawy, S. (1999). The metabotropic receptor mGluR6 may signal through G(o), but not phosphodiesterase, in retinal bipolar cells. *J. Neurosci. , official J. Soc. Neurosci.* 19 (8), 2938–2944. doi:10.1523/JNEUROSCI.19-08-02938.1999

Niketeghad, S., and Pouratian, N. (2019). Brain machine interfaces for vision restoration, the current state of cortical visual prosthetics. *Neurother. , J. Am. Soc. Exp. Neurother.* 16 (1), 134–143. doi:10.1007/S13311-018-0660-1

Nuhu, F., Gordon, A., Sturmey, R., Seymour, A. M., and Bhandari, S. (2020). Measurement of glutathione as a tool for oxidative stress studies by high performance liquid chromatography. *Molecules* 25 (18), 4196. doi:10.3390/MOLECULES25184196

O'Koren, E. G., Yu, C., Klingeborn, M., Wong, A. Y. W., Prigge, C. L., Mathew, R., et al. (2019). Microglial function is distinct in different anatomical locations during retinal homeostasis and degeneration. *Immunity* 50 (3), 723–737. doi:10.1016/J.IMMUNI.2019.02.007

Ostad-Ahmadi, Z., Daemi, A., Modabberi, M. R., and Mostafaie, A. (2021). Safety, effectiveness, and cost-effectiveness of Argus II in patients with retinitis pigmentosa, a systematic review. *Int. J. Ophthalmol.* 14 (2), 310–316. doi:10.18240/IJO.2021.02.20

Özmert, E., and Arslan, U. (2020). Management of retinitis pigmentosa by Wharton's jelly derived mesenchymal stem cells, preliminary clinical results. *Stem Cell Res. Ther.* 11 (1), 25. doi:10.1186/S13287-020-1549-6

Palanker, D., Le Mer, Y., Mohand-Said, S., Muqit, M., and Sahel, J. A. (2020). Photovoltaic restoration of central vision in atrophic age-related macular degeneration. *Ophthalmology* 127 (8), 1097–1104. doi:10.1016/j.ophtha.2020.02.024

Palanker, D., Le Mer, Y., Mohand-Said, S., and Sahel, J. A. (2022). Simultaneous perception of prosthetic and natural vision in AMD patients. *Nat. Commun.* 13 (1), 513. doi:10.1038/s41467-022-28125-x

Peng, B., Xiao, J., Wang, K., So, K. F., Tipoe, G. L., and Lin, B. (2014). Suppression of microglial activation is neuroprotective in a mouse model of human retinitis pigmentosa. *J. Neurosci. , official J. Soc. Neurosci.* 34 (24), 8139–8150. doi:10.1523/JNEUROSCI.5200-13.2014

Picaud, S., Dalkara, D., Marazova, K., Goureau, O., Roska, B., and Sahel, J. A. (2019). The primate model for understanding and restoring vision. *Proc. Natl. Acad. Sci. U. S. A.* 116 (52), 26280–26287. doi:10.1073/PNAS.1902292116

Pinilla, I., Maneu, V., Campello, L., Fernández-Sánchez, L., Martínez-Gil, N., Kutsyr, O., et al. (2022). Inherited retinal dystrophies, role of oxidative stress and inflammation in their physiopathology and therapeutic implications. *Antioxidants* 11 (6), 1086. doi:10.3390/antiox11061086

Pio-Lopez, L., Poulkouras, R., and Depannemaecker, D. (2021). Visual cortical prosthesis, an electrical perspective. *J. Med. Eng. Technol.* 45 (5), 394–407. doi:10.1080/03091902.2021.1907468

Pr, T. (2017). "The intracortical visual prosthesis project," in *Artificial vision* (Germany: Springer), 203–214.

Punzo, C., Xiong, W., and Cepko, C. L. (2012). Loss of daylight vision in retinal degeneration, are oxidative stress and metabolic dysregulation to blame? *J. Biol. Chem.* 287 (3), 1642–1648. doi:10.1074/JBC.R111.304428

Qi, X., Sun, L., Lewin, A. S., Hauswirth, W. W., and Guy, J. (2007). Long-term suppression of neurodegeneration in chronic experimental optic neuritis, antioxidant gene therapy. *Investigative Ophthalmol. Vis. Sci.* 48 (12), 5360–5370. doi:10.1167/IOVS.07-0254

Raghu, G., Berk, M., Campochiaro, P. A., Jaeschke, H., Marenzi, G., Richeldi, L., et al. (2021). The multifaceted therapeutic role of N-acetylcysteine (NAC) in disorders characterized by oxidative stress. *Curr. Neuropharmacol.* 19 (8), 1202–1224. doi:10.2174/1570159X19666201230144109

Ramachandran, P. S., Lee, V., Wei, Z., Song, J. Y., Casal, G., Cronin, T., et al. (2017). Evaluation of dose and safety of AAV7m8 and AAV8BP2 in the non-human primate retina. *Hum. Gene Ther.* 28 (2), 154–167. doi:10.1089/HUM.2016.111

Ribeiro, J., Procyk, C. A., West, E. L., O'Hara-Wright, M., Martins, M. F., Khorasani, M. M., et al. (2021). Restoration of visual function in advanced disease after transplantation of purified human pluripotent stem cell-derived cone photoreceptors. *Cell Rep.* 35 (3), 109022. doi:10.1016/J.CELREP.2021.109022

Rodieck, R. W. (1998). *The first steps in seeing*. 1st edn. Oxford: Sinauer Associates.

Roman, A. J., Powers, C. A., Semenov, E. P., Sheplock, R., Aksianiuk, V., Russell, R. C., et al. (2019). Short-wavelength sensitive cone (S-cone) testing as an outcome measure for NR2E3 clinical treatment trials. *Int. J. Mol. Sci.* 20 (10), 2497. doi:10.3390/IJMS20102497

Rosenfeld, P. J., Cowley, G. S., McGee, T. L., Sandberg, M. A., Berson, E. L., and Dryja, T. P. (1992). A null mutation in the rhodopsin gene causes rod photoreceptor dysfunction and autosomal recessive retinitis pigmentosa. *Nat. Genet.* 1 (3), 209–213. doi:10.1038/NG0692-209

Rush, A. D., and Troyk, P. R. (2012). A power and data link for a wireless-implanted neural recording system. *IEEE Trans. bio-medical Eng.* 59 (11), 3255–3262. doi:10.1109/TBME.2012.2214385

Russell, S., Bennett, J., Wellman, J. A., Chung, D. C., Yu, Z. F., Tillman, A., et al. (2017). Efficacy and safety of voretigene neparvovec (AAV2-hRPE65v2) in patients with RPE65-mediated inherited retinal dystrophy, a randomised, controlled, open-label, phase 3 trial. *Lancet* 390, 849–860. doi:10.1016/S0140-6736(17)31868-8

Sahel, J.-A. A., Boulanger-Scemama, E., Pagot, C., Arleo, A., Galluppi, F., Martel, J. N., et al. (2021). Partial recovery of visual function in a blind patient after optogenetic therapy. *Nat. Med.* 27, 1223–1229. doi:10.1038/s41591-021-01351-4

Sahel, J. A., Mohand-Said, S., Léveillard, T., Hicks, D., Picaud, S., and Dreyfus, H. (2001). Rod-cone interdependence, implications for therapy of photoreceptor cell diseases. *Prog. Brain Res.* 131, 649–661. doi:10.1016/S0079-6123(01)31051-8

Sakai, D., Tomita, H., and Maeda, A. (2022). Optogenetic therapy for visual restoration. *Int. J. Mol. Sci.* 23 (23), 15041. doi:10.3390/IJMS232315041

Saliba, R. S., Munro, P. M. G., Luthert, P. J., and Cheetham, M. E. (2002). The cellular fate of mutant rhodopsin, quality control, degradation and aggresome formation. *J. Cell Sci.* 115, 2907–2918. doi:10.1242/JCS.115.14.2907

Schimel, A. M., Abraham, L., Cox, D., Sene, A., Kraus, C., Dace, D. S., et al. (2011). N-acetylcysteine amide (NACA) prevents retinal degeneration by up-regulating reduced glutathione production and reversing lipid peroxidation. *Am. J. Pathology* 178 (5), 2032–2043. doi:10.1016/J.AJPATH.2011.01.036

Sharma, A., and Jaganathan, B. G. (2021). Stem cell therapy for retinal degeneration, the evidence to date. *Biol. , targets & Ther.* 15, 299–306. doi:10.2147/BTT.S290331

Shen, J., Yang, X., Dong, A., Petters, R. M., Peng, Y. W., Wong, F., et al. (2005). Oxidative damage is a potential cause of cone cell death in retinitis pigmentosa. *J. Cell. physiology* 203 (3), 457–464. doi:10.1002/JCP.20346

Shin, J. H., Kim, H. W., Rhyu, I. J., and Kee, S. H. (2016). Axin is expressed in mitochondria and suppresses mitochondrial ATP synthesis in HeLa cells. *Exp. Cell Res.* 340 (1), 12–21. doi:10.1016/J.YEXCR.2015.12.003

Shivdasani, M. N., Sinclair, N. C., Gillespie, L. N., Petoe, M. A., Titchener, S. A., Fallon, J. B., et al. (2017). Identification of characters and localization of images using direct multiple-electrode stimulation with a suprachoroidal retinal prosthesis. *Investigative Ophthalmol. Vis. Sci.* 58 (10), 3962–3974. doi:10.1167/IOVS.16-21311

Silson, E. H., Gouws, A. D., Legge, G. E., and Morland, A. B. (2022). In a case of longstanding low vision regions of visual cortex that respond to tactile stimulation of the finger with Braille characters are not causally involved in the discrimination of those same Braille characters. *Cortex; a J. devoted study Nerv. Syst. Behav.* 155, 277–286. doi:10.1016/J.CORTEX.2022.07.012

Slater, K. D., Sinclair, N. C., Nelson, T. S., Blamey, P. J., McDermott, H. J., and Bionic Vision Australia Consortium (2015). neuroBi, A highly configurable neurostimulator for a retinal prosthesis and other applications. *IEEE J. Transl. Eng. health Med.* 3, 3800111. doi:10.1109/JTEHM.2015.2455507

Smith, J. A., Das, A., Ray, S. K., and Banik, N. L. (2012). Role of pro-inflammatory cytokines released from microglia in neurodegenerative diseases. *Brain Res. Bull.* 87 (1), 10–20. doi:10.1016/J.BRAINRESBULL.2011.10.004

Snodderly, D. M., Weinhaus, R. S., and Choi, J. C. (1992). Neural-vascular relationships in central retina of macaque monkeys (*Macaca fascicularis*). *J. Neurosci. , official J. Soc. Neurosci.* 12 (4), 1169–1193. doi:10.1523/JNEUROSCI.12-04-01169.1992

St-Pierre, J., Drori, S., Uldry, M., Silvaggi, J. M., Rhee, J., Jäger, S., et al. (2006). Suppression of reactive oxygen species and neurodegeneration by the PGC-1 transcriptional coactivators. *Cell* 127 (2), 397–408. doi:10.1016/J.CELL.2006.09.024

Stronks, H. C., Mitchell, E. B., Nau, A. C., and Barnes, N. (2016). Visual task performance in the blind with the BrainPort V100 vision aid. *Expert Rev. Med. devices* 13 (10), 919–931. doi:10.1080/17434440.2016.1237287

Subhramanyam, C. S., Wang, C., Hu, Q., and Dheen, S. T. (2019). Microglia-mediated neuroinflammation in neurodegenerative diseases. *Seminars Cell & Dev. Biol.* 94, 112–120. doi:10.1016/J.SEMCDB.2019.05.004

Takagi, S., Mandai, M., Gocho, K., Hirami, Y., Yamamoto, M., Fujihara, M., et al. (2019). Evaluation of transplanted autologous induced pluripotent stem cell-derived retinal pigment epithelium in exudative age-related macular degeneration. *Ophthalmol. Retina* 3 (10), 850–859. doi:10.1016/J.ORET.2019.04.021

Taylor, A. W. (2016). Ocular immune privilege and transplantation. *Front. Immunol.* 7, 37. doi:10.3389/FIMMU.2016.00037

Toomey, C. B. (2015) 'Regulation of age-related macular degeneration-like pathology by complement factor H', doi:10.1073/pnas.1424391112

Tuekprakhon, A., Sangkitporn, S., Trinavarat, A., Pawestri, A. R., Vamvanij, V., Ruangchainikom, M., et al. (2021). Intravitreal autologous mesenchymal stem cell transplantation, a non-randomized phase I clinical trial in patients with retinitis pigmentosa. *Stem Cell Res. Ther.* 12 (1), 52. doi:10.1186/S13287-020-02122-7

Tzekov, R., Stein, L., and Kausha, S. (2011). Protein misfolding and retinal degeneration. *Cold Spring Harb. Perspect. Biol.* 3 (11), a007492. doi:10.1101/CSHPERSPECT.A007492

Usui, S., Komeima, K., Lee, S. Y., Jo, Y. J., Ueno, S., Rogers, B. S., et al. (2009). Increased expression of catalase and superoxide dismutase 2 reduces cone cell death in

retinitis pigmentosa. *Mol. Ther. , J. Am. Soc. Gene Ther.* 17 (5), 778–786. doi:10.1038/MT.2009.47

Vaidya, A., Borgonovi, E., Taylor, R. S., Sahel, J. A., Rizzo, S., Stanga, P. E., et al. (2014). The cost-effectiveness of the Argus II retinal prosthesis in Retinitis Pigmentosa patients. *BMC Ophthalmol.* 14 (1), 49. doi:10.1186/1471-2415-14-49

Vandenberghe, L. H., Bell, P., Maguire, A. M., Cearley, C. N., Xiao, R., Calcedo, R., et al. (2011). Dosage thresholds for AAV2 and AAV8 photoreceptor gene therapy in monkey. *Sci. Transl. Med.* 3, 88ra54. doi:10.1126/SCITRANSLMED.3002103

Veske, A., Nilsson, S. E., Narfström, K., and Gal, A. (1999). Retinal dystrophy of Swedish briard/briard-beagle dogs is due to a 4-bp deletion in RPE65. *Genomics* 57 (1), 57–61. doi:10.1006/GENO.1999.5754

Vighi, E., Trifunović, D., Veiga-Crespo, P., Rentsch, A., Hoffmann, D., Sahaboglu, A., et al. (2018). Combination of cGMP analogue and drug delivery system provides functional protection in hereditary retinal degeneration. *Proc. Natl. Acad. Sci. U. S. A.* 115 (13), E2997–E3006. doi:10.1073/PNAS.1718792115

Wang, S. K., Xue, Y., and Cepko, C. L. (2021). Augmentation of CD47/SIRPα signaling protects cones in genetic models of retinal degeneration. *JCI insight* 6 (16), e150796. doi:10.1172/JCI.INSIGHT.150796

Wang, S. K., Xue, Y., and Cepko, C. L. (2020). Microglia modulation by TGF-β1 protects cones in mouse models of retinal degeneration. *J. Clin. investigation* 130 (8), 4360–4369. doi:10.1172/JCI136160

Wang, X., Iannaccone, A., and Jablonski, M. M. (2003). Permissive glycan support of photoreceptor outer segment assembly occurs via a non-metabolic mechanism. *Mol. Vis.* 9, 701–709.

Wang, Y. (2022). Tsc2 knockout counteracts ubiquitin-proteasome system insufficiency and delays photoreceptor loss in retinitis pigmentosa. *Proc. Natl. Acad. Sci. U. S. A.* 119 (11). doi:10.1073/PNAS.2118479119

Watari, K., Yamasaki, S., Tu, H. Y., Shikamura, M., Kamei, T., Adachi, H., et al. (2023). Self-organization, quality control, and preclinical studies of human iPSC-derived retinal sheets for tissue-transplantation therapy. *Commun. Biol.* 6 (1), 164. doi:10.1038/S42003-023-04543-5

Wright, A. F. (1997). A searchlight through the fog. *Nat. Genet.* 17 (2), 132–134. doi:10.1038/NG1097-132

Wright, W. W., Gajjeraman, S., Batabyal, S., Pradhan, S., Bhattacharya, S., Mahapatra, V., et al. (2017). Restoring vision in mice with retinal degeneration usingmulticharacteristic opsin. *Neurophotonics* 4 (4), 041505. doi:10.1117/1.NPH.4.4.041505

Wu, D. M., Ji, X., Ivanchenko, M. V., Chung, M., Piper, M., Rana, P., et al. (2021). Nrf2 overexpression rescues the RPE in mouse models of retinitis pigmentosa. *JCI insight* 6 (2), e145029. doi:10.1172/JCI.INSIGHT.145029

Xiong, W., Wu, D. M., Xue, Y., Wang, S. K., Chung, M. J., Ji, X., et al. (2019). AAV cis-regulatory sequences are correlated with ocular toxicity. *Proc. Natl. Acad. Sci. U. S. A.* 116 (12), 5785–5794. doi:10.1073/PNAS.1821000116

Yamasaki, R., Lu, H., Butovsky, O., Ohno, N., Rietsch, A. M., Cialic, R., et al. (2014). Differential roles of microglia and monocytes in the inflamed central nervous system. *J. Exp. Med.* 211 (8), 1533–1549. doi:10.1084/JEM.20132477

Yang, Y., Mohand-Said, S., Danan, A., Simonutti, M., Fontaine, V., Clerin, E., et al. (2009). Functional cone rescue by RdCVF protein in a dominant model of retinitis pigmentosa. *Mol. Ther. , J. Am. Soc. Gene Ther.* 17 (5), 787–795. doi:10.1038/MT.2009.28

Yu, D. Y., Cringle, S., Valter, K., Walsh, N., Lee, D., and Stone, J. (2004). Photoreceptor death, trophic factor expression, retinal oxygen status, and photoreceptor function in the P23H rat. *Investigative Ophthalmol. Vis. Sci.* 45 (6), 2013–2019. doi:10.1167/IOVS.03-0845

Zaghloul, N. A., and Katsanis, N. (2009). Mechanistic insights into Bardet-Biedl syndrome, a model ciliopathy. *J. Clin. investigation* 119 (3), 428–437. doi:10.1172/JCI37041

Zerti, D., Hilgen, G., Dorgau, B., Collin, J., Ader, M., Armstrong, L., et al. (2021). Transplanted pluripotent stem cell-derived photoreceptor precursors elicit conventional and unusual light responses in mice with advanced retinal degeneration. *Stem cells* 39 (7), 882–896. doi:10.1002/STEM.3365

Zhao, L., Zabel, M. K., Wang, X., Ma, W., Shah, P., Fariss, R. N., et al. (2015). Microglial phagocytosis of living photoreceptors contributes to inherited retinal degeneration. *EMBO Mol. Med.* 7 (9), 1179–1197. doi:10.15252/EMMM.201505298

Zhao, T., Liang, Q., Meng, X., Duan, P., Wang, F., Li, S., et al. (2020). Intravenous infusion of umbilical cord mesenchymal stem cells maintains and partially improves visual function in patients with advanced retinitis pigmentosa. *Stem cells Dev.* 29 (16), 1029–1037. doi:10.1089/SCD.2020.0037

Zhong, X., Gutierrez, C., Xue, T., Hampton, C., Vergara, M. N., Cao, L. H., et al. (2014). Generation of three-dimensional retinal tissue with functional photoreceptors from human iPSCs. *Nat. Commun.* 5, 4047. doi:10.1038/NCOMMS5047

Zhou, D. D., Dorn, J. D., and Greenberg, R. J. (2013). "The Argus® II retinal prosthesis system, an overview," in Electronic Proceedings of the 2013 IEEE International Conference on Multimedia and Expo Workshops, 15-19 July 2013. *ICMEW 2013* [Preprint]. doi:10.1109/ICMEW.2013.6618428

Zhu, X., Ma, B., Babu, S., Murage, J., Knox, B. E., and Craft, C. M. (2002). Mouse cone arrestin gene characterization, Promoter targets expression to cone photoreceptors. *FEBS Lett.* 524 (1–3), 116–122. doi:10.1016/S0014-5793(02)03014-4

frontiers | Frontiers in Cell and Developmental Biology

TYPE Original Research
PUBLISHED 03 May 2023
DOI 10.3389/fcell.2023.1161548

OPEN ACCESS

EDITED BY
José M. Millan,
La Fe Health Research Institute, Spain

REVIEWED BY
Ivan Salazar,
University of Coimbra, Portugal
Gladys Y.-P. Ko,
Texas A&M University, United States

*CORRESPONDENCE
Graeme C. Black,
graeme.black@manchester.ac.uk

RECEIVED 08 February 2023
ACCEPTED 17 April 2023
PUBLISHED 03 May 2023

CITATION
Sadeh TT, Baines RA, Black GC and Manson F (2023), $Ca_v1.4$ congenital stationary night blindness is associated with an increased rate of proteasomal degradation.
Front. Cell Dev. Biol. 11:1161548.
doi: 10.3389/fcell.2023.1161548

$Ca_v1.4$ congenital stationary night blindness is associated with an increased rate of proteasomal degradation

Tal T. Sadeh[1], Richard A. Baines[2], Graeme C. Black[1,3]* and Forbes Manson[1]

[1]Division of Evolution, Infection and Genomics, Faculty of Biology, Medicine and Health, University of Manchester, Manchester, United Kingdom, [2]Division of Neuroscience, Faculty of Biology, Medicine and Health, University of Manchester, Manchester, United Kingdom, [3]Manchester Centre for Genomic Medicine, Manchester Academic Health Sciences Centre, Manchester University NHS Foundation Trust, St Mary's Hospital, Manchester, United Kingdom

Pathogenic, generally loss-of-function, variants in *CACNA1F*, encoding the $Ca_v1.4\alpha_1$ calcium channel, underlie congenital stationary night blindness type 2 (CSNB2), a rare inherited retinal disorder associated with visual disability. To establish the underlying pathomechanism, we investigated 10 clinically derived *CACNA1F* missense variants located across pore-forming domains, connecting loops, and the carboxy-tail domain of the $Ca_v1.4\alpha$ subunit. Homology modeling showed that all variants cause steric clashes; informatics analysis correctly predicted pathogenicity for 7/10 variants. *In vitro* analyses demonstrated that all variants cause a decrease in current, global expression, and protein stability and act through a loss-of-function mechanism and suggested that the mutant $Ca_v1.4\alpha$ proteins were degraded by the proteasome. We showed that the reduced current for these variants could be significantly increased through treatment with clinical proteasome inhibitors. In addition to facilitating clinical interpretation, these studies suggest that proteasomal inhibition represents an avenue of potential therapeutic intervention for CSNB2.

KEYWORDS

$Ca_v1.4$, CACNA1, voltage-gated calcium channel, variant pathogenicity, proteasome inhibitor, bortezomib

Introduction

Voltage-gated calcium channels (VGCCs) are integral membrane proteins that regulate calcium influx from the extracellular space. They activate through membrane depolarization that gates the channel open, permitting calcium influx along an electrochemical gradient (Catterall et al., 2005). There are 10 VGCCs, grouped by the α subunit's voltage sensitivity, with L-type channels ($Ca_v1.1$–1.4) being high-voltage channels (Striessnig et al., 2004). Pathogenic variation of all four Ca_v1 channels is associated with human diseases across a wide range of pathologies, including cardiovascular (Antzelevitch et al., 2007), neurological (Tumienė et al., 2018), psychiatric (Torrico et al., 2019), and retinal diseases (Strom et al., 1998), reflecting the expression patterns of the encoding genes to a considerable degree.

Congenital stationary night blindness type 2 (CSNB2), also known as incomplete CSNB, is a static X-linked inherited retinal disorder that results in nystagmus and

reduced visual acuity in affected individuals. Combined molecular and phenotypic testing is essential for the diagnosis of CSNB2 that is caused by pathogenic variants in the *CACNA1F* gene, encoding the $Ca_v1.4\alpha_1$ calcium channel. $Ca_v1.4\alpha_1$ sustains continuous calcium-dependent glutamate release between retinal photoreceptors and bipolar cells. More than 200 CSNB2 *CACNA1F* variants have been reported, including both missense (n = 96) and small insertion–deletion (indel; n = 67) variants (Boycott et al., 2000; Striessnig et al., 2004; Zeitz et al., 2015; Men et al., 2017).

The mechanisms through which missense mutations act to disrupt each Ca_v1 channel vary and include both gain of function (GoF) and loss of function (LoF) (Sadeh et al., 2021). Across the spectrum of these disorders, however, it remains unclear whether the phenotypes arise from decreased protein expression, protein instability, or changes to channel kinetics (Hoda et al., 2005; Burtscher et al., 2014). While many studies have sought to establish whether pathogenic variants can be grouped by structural features, residue properties, or topology (Brunklaus et al., 2014; Heyne et al., 2020; Indelicato and Boesch, 2021; Sadeh et al., 2021), it remains the case that a majority of missense mutations, which are identified in a clinical context, lack sufficient evidence to confirm pathogenicity. This frequently results in inappropriate designation (Hosseini et al., 2018) and/or in variants being reported as variants of uncertain significance (VUS), precluding the provision of a molecular diagnosis to patients and families (Hoda et al., 2005). These limitations hinder the development of therapies and highlight that a refined pipeline is required to identify and classify clinically relevant pathogenic variants.

In this study, we selected 10 novel *CACNA1F* VUS from patients who lack a molecular diagnosis and have a putative diagnosis of CSNB2. We confirmed a number of informatics predictions and advanced the understanding of the underlying pathogenic mechanism. We established that all the pathogenic missense variants under study act by LoF, as evidenced by a combination of reduced channel current, protein stability, and channel expression. We further showed that the reduced current for these variants can be significantly increased through treatment with clinical proteasome inhibitors, thus identifying a target pathway for possible therapeutic intervention.

Materials and methods

Experimental design

In this study, we predicted the effects of *CACNA1F* variants *in silico* and empirically tested the predictions to improve the interpretation of clinical variants that alter current amplitudes. We investigated 10 *CACNA1F* missense variants using the gold standard whole-cell patch-clamp analysis to quantify current amplitude as a measure of channel function and Western blotting for protein expression. We selected previously used inhibitors to identify the pathways that degrade mutant proteins and tested their potency in rescuing protein expression and current amplitude. A minimum of three biological replicates were used in this study.

Samples

We selected 10 novel *CACNA1F* VUS from patients that lack a molecular diagnosis and have a putative CSNB2 diagnosis. Such patients were previously tested at the Manchester Genomic Diagnostic Laboratory (MGDL).

Informatics analysis

Physicochemical analysis

The physicochemical properties of each mutation were manually analyzed using NCBI's Amino Acid Explorer tools (https://www.ncbi.nlm.nih.gov/Class/Structure/aa/aa_explorer.cgi). The "Structure and Chemistry" and "Common Substitutions" tools were used to compare specific physicochemical constraints of the amino acid pair, such as a change in amino acid size, charge, and hydrophobicity. The latter tool relies on the BLOSUM62 matrix to sort the frequency of the substitution.

Population database search (gnomAD)

The minor allele frequencies (MAFs) of *CACNA1F* VUS analyzed in this study were searched in the general population on gnomAD (Karczewski et al., 2019). The MAF is the number of times a variant allele occurs in a population for any data set.

CACNA1F homology model

To analyze the distribution of mutations across channel domains, a computational model was generated. As the crystallography structure of human *CACNA1F* has not been resolved, a homology model was generated. The CACNA1F protein sequence (accession number: O60840.2) was uploaded to the SWISS-MODEL protein structure homology modeling server (Waterhouse et al., 2018). This identified the homologous rabbit *CACNA1S* ($Ca_v1.1$) structure generated by cryo-electron microscopy (PDB ID: 5GJV) that has 85% protein sequence homology to human (Wu et al., 2016). PyMOL was used for model visualization (The PyMOL Molecular Graphics System, Version 2.0 Schrödinger, LLC). This is consistent with the approach and structure used by CACNA1F-vp.

CACNA1F-vp pathogenicity prediction analysis and comparison with other tools were performed as described in Sallah et al. (2020).

Cloning

Mutations were generated by directional sub-cloning into the wild-type *CACNA1F* plasmid and verified by DNA sequencing (Source Bioscience, https://www.sourcebioscience.com). Fragments containing the single-base substitutions were designed and ordered from GeneArt (Thermo Fisher Scientific, United Kingdom). Mutant fragments were cloned into a pUC18 vector with unique restriction enzymes to allow their excision with complementary ends to the wild-type recipient vector. Restriction sites were digested in the mutant and the wild-type vectors and separated by electrophoresis. The corresponding fragments were excised and gel-purified (Bioline

TABLE 1 Clinical details and properties of the 10 novel *CACNA1F* variants of unknown significance (VUS) identified at the Manchester Genomics Diagnostic Laboratory in patients with congenital stationary night blindness (CSNB). The degree of residue conservation is calculated using Clustal Omega (Sievers et al., 2011) on three paralogues and 20 orthologues. CACNA1F-vp (Sallah et al., 2020) prediction of pathogenicity.

VUS (cDNA, protein)	Clinical detail	Structural location	Conservation	CACNA1F-vp	Reference
c.355G>T, p. (Asp119Tyr)	Consistent with CSNB2	R1S1 EL	High	Pathogenic	
	Attenuated light adapted and attenuated B waves on light-adapted ERG				
	No family history				
c.868C>T, p. (Arg290Cys)	VA (LogMAR) 0.92/0.76	R1S5 EL	High	Benign	10.1016/j.ophtha.2017.02.005
	Refractive correction (diopter) −7/-8				
	Horizontal nystagmus				
	Two siblings				
	Consistent with CSNB2				
	Affected cousin				
	Attenuated light-adapted and attenuated B waves on light-adapted ERG				
	Affected cousin				
	Electronegative ERG				
c.2020G>A, p. (Gly674Ser)	Consistent with CSNB2	R2S5	High	Pathogenic	
c.2390 A>T, p. (Glu797Val)	Unknown	R2S6 CL	Low	Benign	DOI:10.1167/iovs.16-19445
c.3289G>A, p. (Asp1097Asn)	VA (LogMAR) 0.82/0.64	R3S5 EL	High	Pathogenic	10.1016/j.ophtha.2017.02.005
	Refractive correction (diopter) −17/-16D				
	Cone dysfunction with abnormal B wave on dark-adapted bright flash ERG				
	No family history				
c.4301 A>G, p. (Asn1434Ser)	Consistent with CSNB2	R4S6	High	Pathogenic	10.1016/j.ophtha.2017.02.005
	VA (LogMAR) 0.70/0.77				
	Horizontal nystagmus				
	Male cousins				
	ERG consistent with CSNB2				
c.4472C>T, p. (Pro1491Leu)	Suggestive CSNB2	CTD	High	Pathogenic	DOI:10.1016/j.ajhg.2016.12.003, DOI:10.1038/s41586-020-2434-2
	VA (LogMAR) 0.26/0.34				
	Refractive correction (diopter) +6				
	Poor cone responses with attenuated B waves in dark ERG				
c.4480G>A, p. (Gly1494Arg)	Unknown	CTD	High	Pathogenic	DOI:10.1016/j.preteyeres.2014.09.001
c.4518G>T, p. (Lys1506Asn)	Consistent with CSNB2	CTD	High	Pathogenic	
c.4594C>T, p. (Arg1532Trp)	Four affected in the family; X-linked (but no co-segregation)	CTD	High	Pathogenic	DOI:10.1167/iovs.16-19445
	Nystagmus				
	Normal fundus appearance				
	ERG suggests combined cone and rod problem				

Structural location: CL, cytoplasmic loop; CTD, carboxyl-tail domain; EL, extracellular loop; R, repeat; S, segment. Clinical details: ERG, electroretinogram; CSNB2, incomplete congenital stationary night blindness type 2; VA, visual acuity.

ISOLATE II PCR and Gel Kit, United Kingdom), and the recipient and mutant fragments were ligated (Promega T4 ligation kit, United States of America) and transformed by electroporation (XL1 electroporation-competent cells, Agilent Technologies, United States). This enabled the insertion of the mutant fragments into the recipient vector.

The plasmids used in this study are listed in Supplementary Table S1.

Cell culture

Human embryonic kidney 293T (HEK293T) cells were grown in Dulbecco's modified Eagle's medium (DMEM) (Sigma-Aldrich, United Kingdom) supplemented with 10% (v/v) heat-inactivated fetal bovine serum (FBS) (Life Technologies, United States) and 1% (v/v) 2 mM L-glutamine (Sigma-Aldrich, United Kingdom). Cells were incubated at 37°C in 5% CO_2. Versene solution (Life Technologies, United States) was used for non-enzymatic cell dissociation.

Transient transfection

HEK293T cells were transfected with either wild-type *CACNA1F* or mutant constructs using FuGENE HD Transfection Reagent (Promega Ltd., United States) in Opti-MEM media (Life Technologies, United States) in a 1 $\alpha_{1.4}$: 0.6 β_3: 0.8 $\alpha_2\delta$ ratio. A pEGFP plasmid was used for detection (1 α: 0.2 pEGFP). Transfected cells were incubated at 37°C in 5% CO_2, and for electrophysiological analysis, the temperature was reduced to 30°C after 6–8 h at 37°C to ensure stable calcium ion currents (Koschak et al., 2003). The transfection medium was replaced with culture medium 24 h post-transfection and incubated for a further 24 h.

A β_3 subunit was used instead of the retina-specific β_2 for better expression, and higher currents are recorded with no changes in gating properties (Koschak et al., 2003; Hoda et al., 2005).

Inhibitor treatment

Each drug was added directly to the cell culture media for the stated time prior to harvesting for patch-clamp or Western blot analysis.

A measure of 20 μg/mL cycloheximide (CHX) was added to the cell culture media at different time points prior to harvesting for Western blot analysis.

The inhibitors used in this study are listed in Supplementary Table S2.

Whole-cell patch-clamp analysis

Transfected HEK293T cells expressing $Ca_v1.4$ were dissociated and seeded on poly-L-lysine (0.05%)-coated coverslips 24 h prior to analysis and maintained at 30°C in 5% CO_2. For electrophysiology recording, the coverslips were placed in extracellular buffer supplemented with calcium ions as the permeating ion (15 mM $CaCl_2$, 150 mM choline-Cl, 10 mM HEPES, and 1 mM $MgCl_2$, adjusted to pH 7.3 with 1 M CsOH). Borosilicate glass capillaries GC100F-10 (Harvard Apparatus, United Kingdom) were pulled with a Model P-97 pipette puller (Sutter Instrument Co., United States of America) to a resistance of 2–4 MΩ (unpolished). The pipettes were filled with intracellular buffer (5 mM EGTA, 140 mM *N*-methyl-*D*-glucamine, 2 mM $MgCl_2$, 10 mM HEPES, and 2 mM Mg-ATP, adjusted to pH 7.3 with 1 M methanesulfonic acid). The osmolarity of all buffers was adjusted to 290–310 using D-mannitol (Osmomat 3000: Gonotec, Germany). Only cells co-expressing GFP were patched. Cells were held at −80 mV, and currents were evoked by 5 ms depolarization from −80 to 80 mV using an online leak subtraction protocol (P/4). Three separate traces were recorded and averaged per cell. No significant difference in cell capacitance (average capacitance being 12 pF) was observed, negating the need to represent the data as current density.

Conventional whole-cell recordings were performed using a MultiClamp 700A amplifier, Digidata 1440A digitizer, and pCLAMP v10 (Molecular Devices, CA, United States of America). Recordings were digitized at 20 KHz and filtered at 10 KHz. Leak-subtracted currents were analyzed on Clampfit software v11.0.3.

SDS-PAGE and Western blotting

Membrane protein lysates were harvested from 60-mm dishes following the instructions in the Mem-PER Plus Membrane Protein Extraction Kit (Thermo Fisher, United Kingdom), supplemented with proteasome inhibitor cocktail (Sigma-Aldrich, United Kingdom). Protein lysates were prepared with 2x Laemmli sample buffer (1: 1) (Sigma-Aldrich, United Kingdom) supplemented with β-mercaptoethanol (Sigma-Aldrich, United Kingdom). These were loaded on a 4%–20% Mini-PROTEAN TGX Stain-Free Gel (Bio-Rad, United Kingdom). Gels were transferred onto a nitrocellulose membrane (LI-COR Biosciences, United Kingdom) by wet transfer at 350 mA for 90 min at 4°C. The membrane was blocked in 5% milk in TBS-T at room temperature for 1 h before adding the primary antibody in 2% milk TBS-T for 1 h at room temperature. The membrane was washed three times in TBS-T and incubated with the secondary antibody in 2% milk TBS-T for 1 h at room temperature. After three washes in TBS-T, the membrane was imaged using the LI-COR Odyssey CLx system, and LI-COR Image Studio v5.0 was used to analyze the image. The antibodies used in this study are listed in Supplementary Tables S3, S4.

Data analysis

Quantitative data for Western blots were combined from at least three independent experiments and expressed as mean ± standard error of the mean (S.E.M). A minimum of three biological replicates were used for statistical analysis. Patch-clamp data were acquired from at least three independent experiments and expressed as mean ± standard error of the mean (S.E.M), with each individual cell recording repeated three times and averaged. Statistical

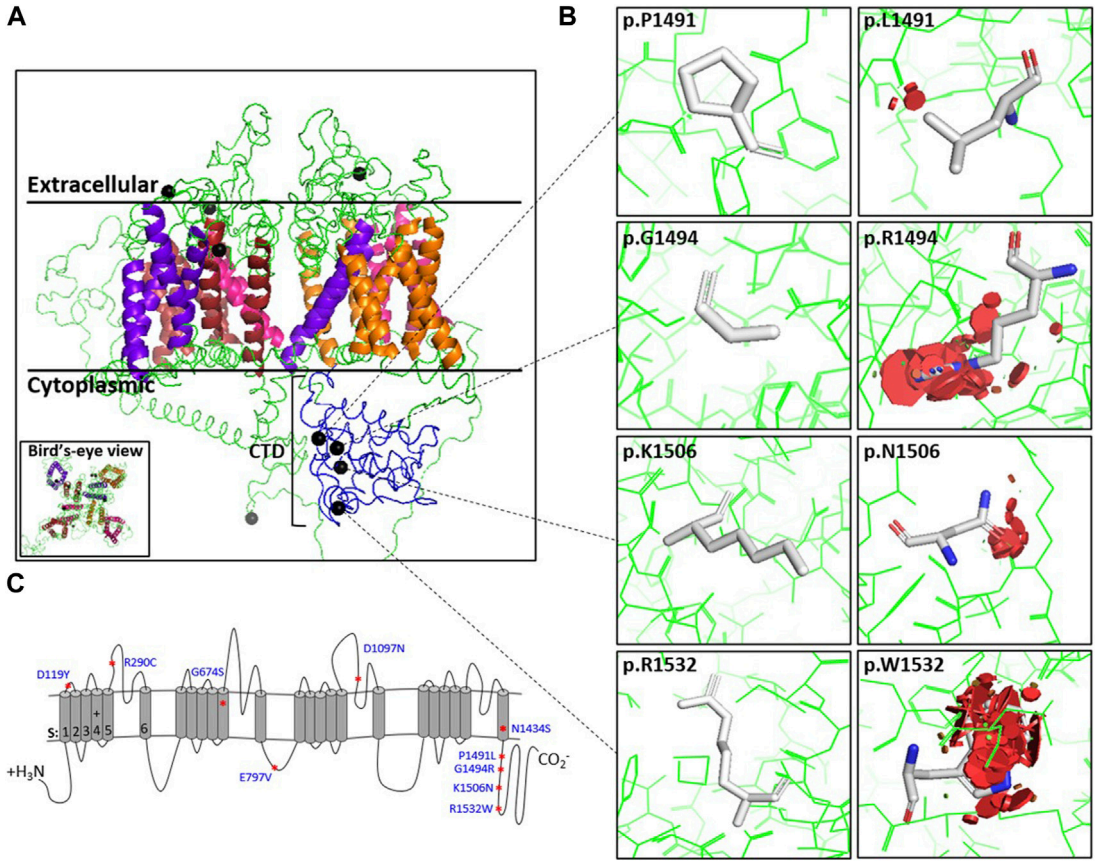

FIGURE 1
Position and steric clashes of $Ca_v1.4$ missense variants. The locations of the $Ca_v1.4$ variants from this study are shown on a homology model of $Ca_v1.4$. **(A)** Cross-section of the $Ca_v1.4$ homology model (extracellular, transmembrane, and cytoplasmic regions indicated). Helices are colored for each repeat. Blue indicates the carboxyl-tail. The black spheres indicate the position of the $Ca_v1.4$ variant. **(B)** Modeling of the $Ca_v1.4$ variants of uncertain significance (VUS) (shown as PyMOL images) predicted that they are likely to cause protein hindrance by inducing steric clashes. The red discs demonstrate the predicted degree of steric clashes between the mutated residue and surrounding residues. **(C)** Picture representation of $Ca_v1.4$'s linear structure. Additional variant PyMOL images are provided in Supplementary Figure S1.

significance was determined by Student's t-test or one-way ANOVA with the Bonferroni correction, with a statistically significant difference defined at $p < 0.05$. The Student's t-test was used when the limitation of replicates prevented the use of the Kruskal–Wallis test. All data were analyzed and plotted on GraphPad Prism v8.0 (GraphPad, La Jolla, United States).

Results

Selection of *CACNA1F* variants for functional analysis

We selected 10 *CACNA1F* VUS from local patients via a putative CSNB2 diagnosis (Table 1). As it was shown previously that the connecting loops are the most frequently substituted regions in the Ca_v1 family (Sadeh et al., 2021), we selected two variants in these loops: p.D119Y (identified in a male patient with an electronegative electroretinogram (ERG)) and p.E797V (identified in two unrelated families (Hove et al., 2016)). We further chose four variants in the pore-forming domains: p.R290C, p.G674S, p.D1097N, and p.N1434S. These pore variants are functionally constrained and likely to dysregulate Ca^{2+} influx (Sadeh et al., 2021). All four $Ca_v1.4$ pore variants are novel and were present in male patients that had ERGs consistent with diagnosis of CSNB2; p. R290C was present in four family members and p.N1434S was present in two cousins, all affected with CSNB2 (Table 1).

The carboxyl-tail domain (CTD) of $Ca_v1.4$ is structurally unresolved, thus preventing accurate predictions of the functional consequence of variation in this region. To address this, we characterized four *CACNA1F* VUS in the CTD (p.P1491L, p.G1494R, p.K1506N, and p.R1532W) that were predicted as pathogenic by CACNA1F-vp (Sallah et al., 2020) (Table 1). We and other researchers have reported p.P1491L in patients with ERGs typical of CSNB2 (Carss et al., 2017; Turro et al., 2020) and identified the previously reported p.R1532W variant in multiple affected family members (Hove et al., 2016).

We modeled all 10 mutations on an *in silico* homology model of $Ca_v1.4$. The model was used to predict the physiochemical consequences of each missense variant on steric clashes due to charge, polarity, or bond disturbances (Figure 1; Supplementary Figure S1). Although all *in silico* modeling techniques have their

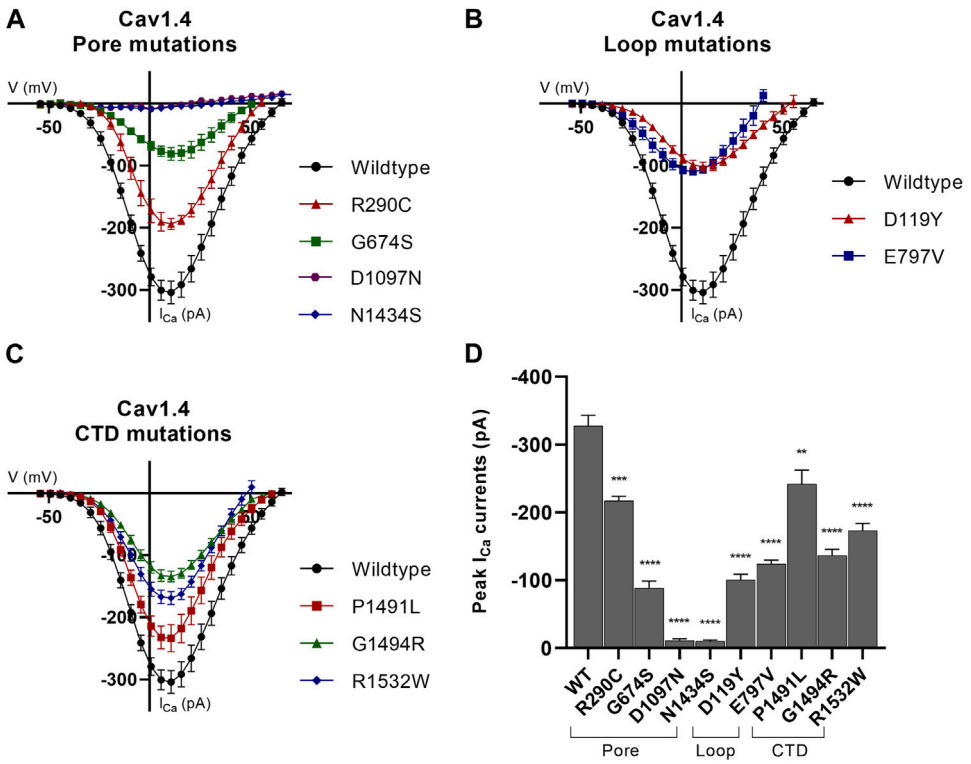

FIGURE 2
Whole-cell ion currents of $Ca_v1.4$ variants. I/V plots for **(A)** wild-type $Ca_v1.4$, pore-forming domains, and associated loop mutations, **(B)** wild-type $Ca_v1.4$ and loop (excluding the pore-forming S5–S6 loop) mutations, and **(C)** wild-type $Ca_v1.4$ and carboxyl-tail domain (CTD) mutations. The CTD variant, p.K1506N, is omitted from this figure as no statistical significance from the wild type was identified (data are presented in Supplementary Table S5). The wild-type $Ca_v1.4$ I_{Ca} activates at ~−45 mV and reverses at ~45 mV. All nine variants significantly reduce the peak I_{Ca} compared to the wild type. Representative raw traces are presented in Supplementary Figure S2. Currents were evoked by 5 ms depolarization from −80 to 80 mV with P/4 leak subtraction. The wild-type $Ca_v1.4$ traces are an accumulation from multiple experiments (n = 30). A minimum of n = 10 traces per variant with three separate recordings were taken per cell and averaged. Error bars represent mean ± S.E.M. **(D)** Peak I_{Ca} currents for wild-type and mutant $Ca_v1.4$ channels. Peak current differences between wild type and mutant were analyzed by one-way ANOVA with the Bonferroni correction. *$p < 0.05$, **$p < 0.01$, and ***$p < 0.001$ indicate the degrees of significance (p-values are provided in Supplementary Table S5). Error bars represent mean ± S.E.M. Pore mutations, S5–S6 pore-forming membrane segments and connecting loop mutations; loop mutations, mutations in loops excluding pore-forming S5–S6 loop; CTD mutations, mutations in the carboxyl-tail domain; WT, wild type.

limitations, our modeling and informatics analyses predict that all 10 variants would likely result in steric clashes that are likely to cause instability to the variant channel (Table 1).

CACNA1F missense mutations reduce channel stability, expression, and function

We next sought to confirm the pathogenic predictions of the 10 variants on channel function by whole-cell patch-clamp analysis, quantifying channel current as a measure of channel function. The global expression and protein stability of the 10 novel variants were determined by Western blotting and cycloheximide (CHX) chase assay, respectively.

We identified a significant reduction in expressed Ca^{2+} current (I_{Ca}) for all but one variant. There was a 62% mean (range 26%–96%) reduction in peak I_{Ca} compared to the human wild-type $Ca_v1.4$ channel (Figure 2; Supplementary Table S5). There was also a significant reduction in global protein expression for nine of the 10 novel variants, with a mean reduction of 34% (range 12%–51%) compared to the wild-type (Supplementary Figure S3; Supplementary Table S5).

Protein turnover was significantly increased for nine variant proteins relative to the wild-type. On average, just over half (52%) of the variant protein remained after 8 h CHX chase compared to the wild-type variant protein (range 17%–77%) (Figure 3A, Supplementary Figure S4, Supplementary Table S5). The rate of protein turnover for the $Ca_v1.4$ pore variant p.E797V and two $Ca_v1.4$ CTD variants (p.G1494R and p.R1532W) increased compared to that of the wild-type protein (Figure 3B; Supplementary Figure S4). There was an average 3 h half-life for these three mutant proteins, whereas 75% of the wild-type protein remained till the end of the chase (Figure 3B).

The increased turnover in mutant proteins is consistent with the homology model's prediction of protein instability due to steric clashes (Figure 1; Supplementary Figure S1). This protein instability was observed in all the $Ca_v1.4$ mutations studied.

For three variants, the functional data did not support the informatics predictions. The $Ca_v1.4$ variants p.R290C and p.E797V, neither of which is found in gnomAD, were

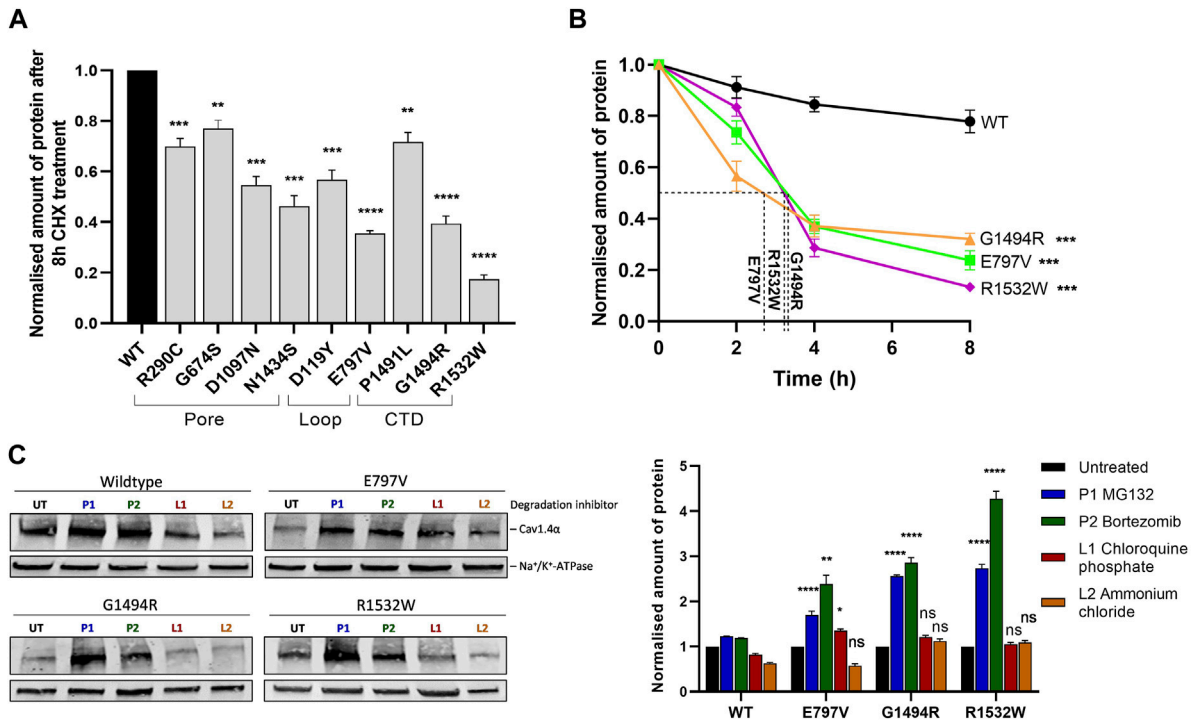

FIGURE 3
$Ca_v1.4$ variants reduce protein stability and are degraded by the proteasome. **(A)** Quantified Western blotting data from cells expressing $Ca_v1.4$ variants treated with 20 μg/mL cycloheximide (CHX) for 8 h. Error bars represent mean ± S.E.M of three independent experiments. Wild-type expression is set at 1. *$p < 0.05$, **$p < 0.01$, and ***$p < 0.001$ indicate the degrees of significance for the remaining protein between each variant and the wild-type protein analyzed by a one-way, unpaired Student's t-test (p-values are provided in Supplementary Table S5). A representative Western blot is shown in Supplementary Figure S4A. **(B)** Quantified Western blot data of the three least stable mutations (p.E797V, p.G1494R, and p.R1532W) after different CHX treatment times (0, 2, 4, and 8 h) with the protein half-life shown. Error bars represent mean ± S.E.M of three independent experiments. The amount of protein is shown relative to untreated (0 h) expression, which is set at 1. A one-way, unpaired Student's t-test analysis compares the amount of mutant protein remaining after 8 h relative to the wild type. Representative Western blots are shown in Supplementary Figure S4B. **(C)** Representative Western blot **(left)** and quantified expression **(right)** of wild-type $Ca_v1.4$ and the three least stable proteins treated with proteasome or lysosome inhibitors for 6 h. Error bars represent mean ± S.E.M of three independent experiments. The amount of $Ca_v1.4$ protein (220 kDa) was normalized to the loading control (Na^+/K^+-ATPase, 110 kDa) and is relative to the untreated controls that are set at 1. *$p < 0.05$, **$p < 0.01$, and ***$p < 0.001$ indicate the degrees of significance between treated and untreated cells using a one-way, unpaired Student's t-test. WT, wild type; UT, untreated; P1 (bortezomib, 10 nM) and P2 (MG132, 20 μM), proteasome inhibitors; L1 (chloroquine phosphate, 50 μM) and L2 (ammonium chloride, 50 mM), lysosome inhibitors.

hypomorphic on functional analysis but were classified as benign variants by CACNA1F-vp. Additionally, the $Ca_v1.4$ CTD variant p.K1506N, which was predicted to be pathogenic by CACNA1F-vp, had currents, expression, and stability comparable to the wild-type channel (Supplementary Table S4).

Mutant Cav1.4α proteins are degraded by the proteasome

We used the three least stable novel variants (p.E797V, p.G1494R, and p.R1532W) to identify the route of degradation for $Ca_v1.4α$ variants. Non-native proteins can be degraded *via* proteasomes or lysosomes through the ubiquitin-proteasome pathway or autophagy, respectively (Levine and Klionsky, 2004; Collins and Goldberg, 2017). We inhibited each pathway using either the proteasome inhibitors (PIs) (bortezomib (BTZ) and MG132) or the lysosome inhibitors (LIs) (chloroquine phosphate and ammonium chloride) for 6 h. BTZ and MG132 are highly selective PIs that inhibit the proteolytic activity of the 26S proteasome complex (Han et al., 2009; Fricker, 2020), whereas chloroquine phosphate and ammonium chloride are weak bases that inhibit autophagy by changing the lysosomal pH or by inhibiting phagosome–lysosome fusion, respectively (Hart and Young, 1991; Redmann et al., 2017). We found that the ubiquitin-proteasome degradation pathway is the major route of degradation for the $Ca_v1.4α$ variants investigated. After treatment with PIs, the amount of mutant $Ca_v1.4α$ proteins detected increased by 2– 4-fold relative to untreated cells (Figure 3C). This increase was highly significant. In contrast, ammonium chloride made no significant difference to the detectable mutant $Ca_v1.4α$ proteins, and chloroquine phosphate only marginally increased the expression of one mutant protein (p.E797V) (Figure 3C).

Proteasome inhibitors restore expression and function of $Ca_v1.4$ mutant channels

Having determined that the proteasome is the most likely route for degradation of mutant Cav1.4α proteins, we postulated that

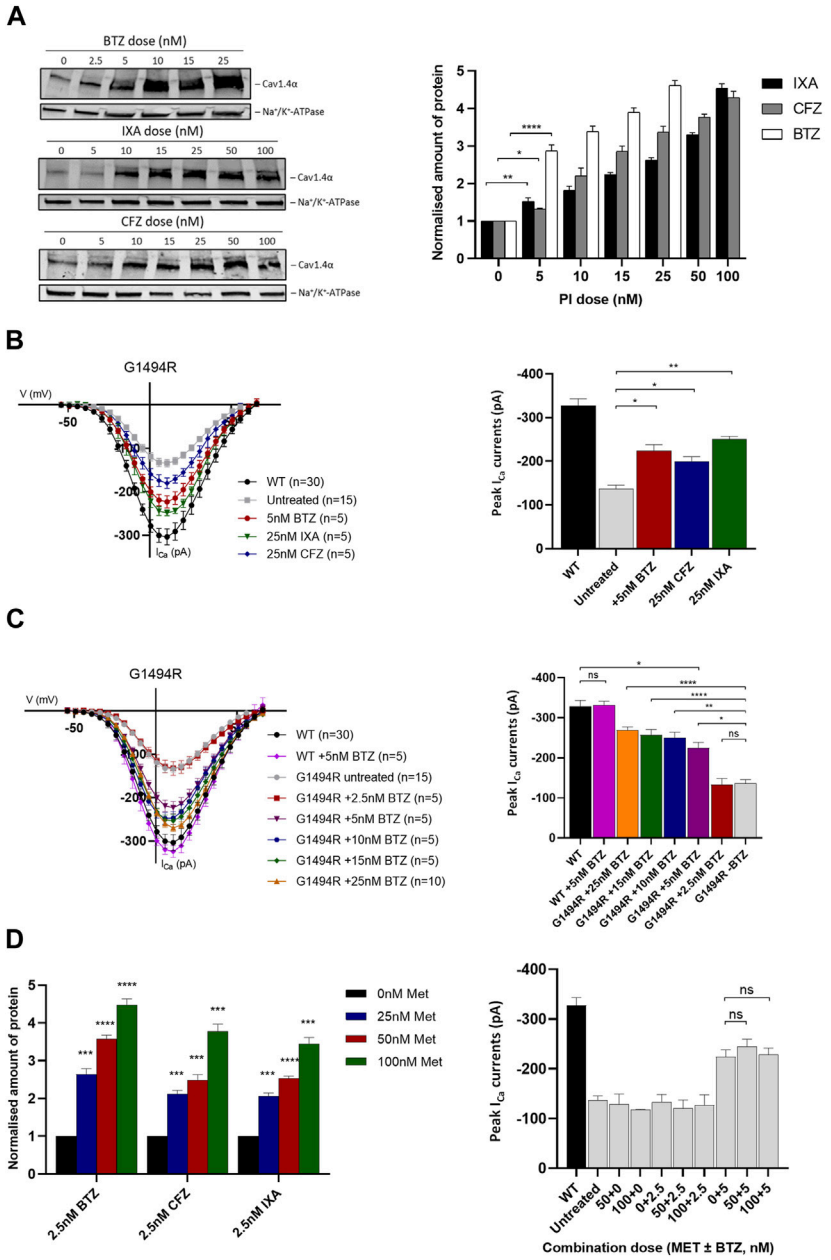

FIGURE 4
$Ca_v1.4$ protein expression and channel function following treatment with proteasome inhibitors and metformin. **(A)** Dose–response relationship of $Ca_v1.4$ p.G1494R and proteasome inhibitors (PIs) after 6 h treatment. Representative Western blot **(left)** and quantified plot **(right)** of p.G1494R treated with increasing doses of each PI. Error bars represent mean ± S.E.M of three independent experiments, and statistical significance is measured by a one-way, unpaired Student's t-test. The $Ca_v1.4$ protein (220 kDa) was normalized to the loading control (Na^+/K^+-ATPase, 110 kDa) and is relative to the untreated control set at 1. **(B)** I/V plots of $Ca_v1.4$ p.G1494R treated with different PIs for 6 h **(left)** and the peak I_{Ca} **(right)**. Error bars represent mean ± S.E.M., and statistical significance is analyzed by a one-way, unpaired Student's t-test. **(C)** I/V plots of I_{Ca} for $Ca_v1.4$ p.G1494R treated with increasing concentrations of bortezomib (BTZ) for 6 h **(left)** and the peak I_{Ca} **(right)**. Error bars represent mean ± S.E.M., and statistical significance is analyzed by a one-way, unpaired Student's t-test. **(D)** Quantified Western blot data of $Ca_v1.4$ p.G1494R treated with each PI combined with different concentrations of metformin for 6 h **(left)**. Error bars represent mean ± S.E.M of three independent experiments. A one-way, unpaired Student's t-test analysis was used to compare the relative amount of protein per drug combination relative to metformin alone. A representative Western blot is shown in Supplementary Figure S5A. Peak I_{Ca} **(right)** of $Ca_v1.4$ p.G1494R treated with different combinations of metformin and BTZ. I/V plots are shown in Supplementary Figure S5B. For I/V plots, the currents were evoked by 5 ms depolarization from −80 to 80 mV with P/4 leak subtraction. The wild-type $Ca_v1.4$ traces are an accumulation from multiple experiments (n = 30). Each cell trace was recorded three times, and an average was taken. Error bars represent mean ± S.E.M. The peak I_{Ca} are normalized to the wild type. *p < 0.05, **p < 0.01, and ***p < 0.001 indicate the degrees of significance between groups analyzed by a one-way, unpaired Student's t-test. Met, metformin; BTZ, bortezomib; CFZ, carfilzomib; IXA, ixazomib; WT, wild type.

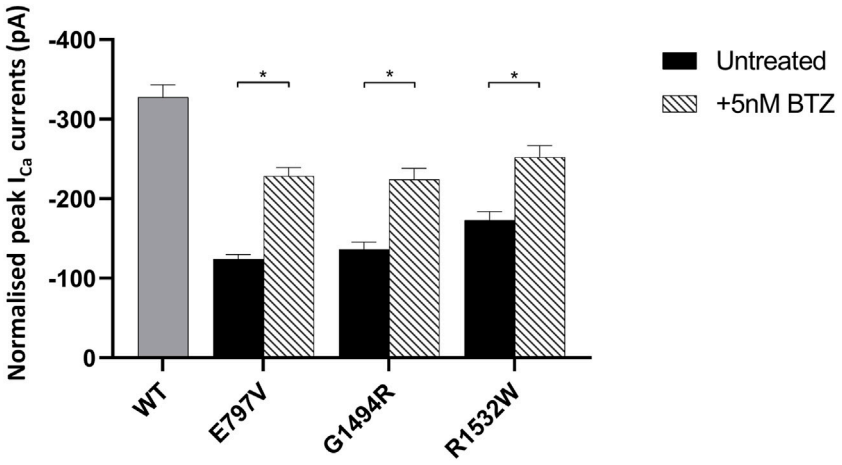

FIGURE 5
Effect of bortezomib on the function of mutant $Ca_v1.4$ channels. Bar chart plot of the peak I_{Ca} for wild-type and mutant $Ca_v1.4$ treated with 5 nM bortezomib (BTZ) for 6 h compared to untreated controls. BTZ had no effect on wild type (data not shown). Error bars represent mean ± S.E.M. *$p < 0.05$, **$p < 0.01$, and ***$p < 0.001$ indicate the degrees of significance between treated and untreated channels analyzed by a one-way, unpaired Student's t-test. WT, wild type; BTZ, bortezomib.

inhibiting this pathway may be therapeutically beneficial by increasing the levels of mutant channel expression/function. We tested three clinically approved PIs: BTZ, carfilzomib (CFZ), and ixazomib (IXA). We first tested their effects on $Ca_v1.4\alpha$ p.G1494R since this mutant channel had significantly reduced expression and was particularly unstable. All three PIs had comparable toxic effects *in vitro*, and we selected a treatment time of 6 h as >50% of the cells were still viable after this time (data not shown). All three inhibitors significantly increased the amount of detectable protein after 6 h treatments, with the highest doses of PIs resulting in a 5-fold increase in protein expression relative to untreated samples (Figure 4A). Bortezomib was the most potent PI, with ×5 as much as CFZ (25 nM compared to 5 nM) and ×10 as much as IXA (50 nM compared to 5 nM) being required to achieve a similar increase in protein expression.

Using whole-cell peak I_{Ca} as a measure of channel function, we were able to significantly increase the cellular function of $Ca_v1.4$ p.G1494R in cells treated with each PI compared to untreated ones (Figure 4B). BTZ was the most potent, while higher concentrations of CFZ and IXA were required to achieve comparable increases (Figure 4B). As 2.5 nM BTZ had no significant effect on the peak I_{Ca} or protein expression compared to untreated cells (Figure 4C), we titrated the concentration of BTZ and determined 5 nM as the threshold to achieve a significant increase in function and expression whilst maintaining minimal toxicity to cells expressing $Ca_v1.4$ p.G1494R (Figure 4C). Higher concentrations of BTZ further increased mutant channel I_{Ca}, achieving >80% wild type with 25 nM BTZ.

Given the toxicity of the PIs tested, we tried to reduce the PI concentration required to achieve a significant increase in expressed I_{Ca} by combining each with metformin (Met). Metformin is not only approved for the treatment of type 2 diabetes but also acts to suppress the expression of GRP78-dependent autophagy and enhance the pharmacological effects of BTZ (Jagannathan et al., 2015). We combined a low concentration of each PI that had no effect on expressed I_{Ca} (2.5 nM) with increasing concentrations of Met and measured the channel expression and function of the p.G1494R mutant after 6 h. Metformin had no effect on either protein expression or peak I_{Ca} on its own at any of the concentrations tested (Figure 4D; Supplementary Figure S5A). However, in combination with any of the three PIs, it significantly increased mutant p.G1494R $Ca_v1.4\alpha$ expression, and this combination was Met dose-dependent (Figure 4D, Supplementary Figure S5A). Despite the increase in channel expression, no Met–PI combination had any effect on mutant p.G1494R $Ca_v1.4$ peak I_{Ca} (Figure 4D; Supplementary Figure S5B).

Having discounted the combined use of Met with a PI, we next investigated the ability of 5 nM BTZ to increase expressed peak I_{Ca} for the two least stable $Ca_v1.4$ mutant proteins (p.E797V and p.R1532W) (Figure 5; Supplementary Figure S6). BTZ significantly increased the peak current of both mutants, with a mean increase in peak I_{Ca} greater than 70% relative to each wild type after a 6-h treatment (Figure 5).

Discussion

The Ca_v1 protein family is evolutionarily conserved (Catterall et al., 2005; Zamponi et al., 2015). The encoded genes are mutated in a range of rare disorders inherited as autosomal dominant, recessive, and X-linked traits affecting a wide range of organ systems reflecting their expression patterns. Pathogenic variants in *CACNA1F*, which is highly expressed in the retina, cause X-linked CSNB2, a rare disorder causing visual disability in males. In this context, the interpretation of missense variant pathogenicity across the entire Ca_v1 family remains challenging (Brunklaus et al., 2014; Heyne et al., 2020; Indelicato and Boesch, 2021; Sadeh et al., 2021) and can delay diagnosis and treatment. To this end, we and other researchers have developed informatics tools, including CACNA1F-vp and funNCIon (Heyne et al., 2020; Sallah et al., 2020), and in this

experimental follow-up study, have undertaken functional studies to examine the efficacy of these tools.

We examined 10 missense variants that are located throughout the $Ca_v1.4\alpha$ protein, including those within connecting loops, pores, and C-terminal tail. Nine of the 10 variants showed a dramatic reduction in whole-cell Ca^{2+} current (I_{Ca}) compared to cells expressing the wild-type channel, associated with low levels of expression and an increased rate of protein turnover. The increased turnover of mutant proteins is consistent with the predicted impact of steric clashes from homology modeling and suggests a common pathological mechanism. Of the parameters examined, there was a correlation between the expression level of the mutant protein compared to the wild-type channel. The four pore mutants were the most highly expressed, all being above 70% of the wild-type channel. Associations between I_{Ca} and protein stability were less clear-cut. The three mutants with the largest decrease in I_{Ca} were all in the pore (p.G674S, p.D1097N, and p.N1434S). Two of the three most stable mutant channels (protein remaining after CHX treatment) were in the pore (p.R290C and p.G674S) along with p.P1491L in the CTD. The p.K1506N CTD mutant channel showed little difference from the wild-type channel, and it is likely that this splice site variant is non-pathogenic.

A wide range of mutations underlies *CACNA1F*-related CSNB2, including both classical LoF variants (nonsense, splice site, and indel) and missense alterations. Our data highlight that pathogenic missense changes in $Ca_v1.4\alpha$ act through an LoF mechanism and, using three novel variants, that this is consequent upon protein instability and ubiquitin-proteasome degradation. Proteasome inhibition with four different inhibitors resulted in increased protein expression and ion conductance (Figure 3C; Figures 4A–C). This suggests that mutant Cav1.4α is degraded by endoplasmic reticulum-associated protein degradation and prevents trafficking of the mutant protein to the plasma membrane. This has been described for a number of inherited conditions, including the degenerative retinal condition retinitis pigmentosa (RP) (Abriel et al., 2000; Benhorin et al., 2000; Macías-Vidal et al., 2014; Zhang et al., 2019). A drug capable of targeting mutations across a family of proteins and a range of disorders is an attractive property for a therapeutic, as exemplified by the use of flecainide to target voltage-gated sodium channels in the heart (SCN5A) and skeletal muscle (SCN4A) (Ward et al., 1995; Rosenfeld et al., 1997; Galbiati et al., 2000; Zheng et al., 2012). Inhibiting the turnover of mutant proteins has been investigated as a possible therapeutic treatment for dominant negative mutations in caveolin-3 associated with limb-girdle muscular dystrophy (Galbiati et al., 2000). For cystic fibrosis, two general PIs restored deltaF508 CFTR expression in the plasma membrane, although these were immature forms and so of limited therapeutic value (Ward et al., 1995). We found three clinically approved PIs, and all significantly increased the channel density of $Ca_v1.4\alpha$ mutations, with BTZ being the most potent. This is consistent with other studies using BTZ to increase the gross cellular function of proteins mutated in a range of conditions, including RP, Niemann–Pick disease type C, mitochondrial leukoencephalopathy, and Lynch syndrome (Macías-Vidal et al., 2014; Zhang et al., 2019). There are trials for more than 600 conditions investigating BTZ as a therapy (ClinicalTrials.gov), although its long-term use has been associated with side effects, such as peripheral neurotoxicity and mitotoxicity (Cavaletti et al., 2007; Nowis et al., 2010; Zheng et al., 2012; Kaplan et al., 2017). The BTZ concentrations that are shown to be effective against $Ca_v1.4\alpha$ mutations are within the range approved for clinical use, suggesting that BTZ proteasomal inhibition also has therapeutic potential for the treatment of CSNB2.

Metformin is a first-line treatment for type 2 diabetes and has been researched for its many other effects, including the management of polycystic ovary syndrome. In model systems, it can alleviate polycystic kidney disease (Pastor-Soler et al., 2022), and for cancer treatment, it can modulate the unfolded protein response resulting from bortezomib treatment (Jagannathan et al., 2015; Granato et al., 2017). In an RP mouse model, metformin was able to stabilize mutant rhodopsin and enhance its trafficking to the rod outer segment. The latter effect appears to be predominant as this resulted in increased photoreceptor death (Athanasiou et al., 2017). Given these reported modes of action, we tested whether metformin, either alone or in combination with PIs, could increase the function of mutant $Ca_v1.4\alpha$. Although metformin significantly increased the expression of mutant $Ca_v1.4\alpha$ higher than that achieved with a PI alone, it had no effect on current density and was possibly inhibitory to the positive effect of bortezomib. This is in contrast to a previous report that metformin downregulated the expression of $Ca_v1.2$, although a study observed that metformin suppressed channel current (Wang et al., 2020). The current density of the Nav1.7 channel is reduced by metformin acting through the E3 ubiquitin ligase NEDD4-2 (Deftu et al., 2022).

The functional consequences of putative pathogenic missense variants in the $Ca_v1.4\alpha$ CTD have not been previously investigated. The CTD is unresolved in the crystal structure of rabbit $Ca_v1.1\alpha$ from which the $Ca_v1.4\alpha$ structure is derived. This reduces the confidence in the $Ca_v1.4\alpha$ homology model, and consequently, the prediction of variant pathogenicity, and most likely underlies the incorrect functional consequence predictions for three of the 10 $Ca_v1.4$ variants (p.R290C, p.E797V, and p.K1506N) (Sallah et al., 2020). We show that mutations in this domain have identical consequences to those in connecting, or pore-forming, loops, namely, a significant reduction in whole-cell I_{Ca}, which we correlate to a reduced channel expression resulting from protein instability. CACNA1F-vp correctly predicted the pathological functional consequence of three of the four CTD variants tested (p.P1491L, p.G1494R, and p.R1532W), all of which significantly reduced I_{Ca} of the expressed channel variant. Interestingly, the fourth CTD variant (p.K1506N) that was functionally comparable to wild type lies at the intron–exon boundary with exon 38 and is predicted to alter splicing. Two previously reported pathogenic variants also lie at the same exon–intron boundary: c.4519-1G>A and c.4518 + 2T>A (Rosenfeld et al., 1997; Galbiati et al., 2000).

Like previous electrophysiological studies on $Ca_v1.4$, we used heterologous expression in HEK293 cells due to their low expression of native channels and reproducible phenotype observed in mouse models and induced pluripotent stem cells (Burtscher et al., 2014; Hu et al., 2018; Koschak et al., 2021). Future studies should scrutinize the mutant channel physiology in more detail by

quantifying changes in gating and deactivation kinetics. Ideally, these experiments should be performed using a more physiological cell line to confirm the pathogenic mechanism of altered protein expression. Quantification of $Ca_v1.4\alpha$ channel expression on the cell surface would have been beneficial in showing how it changed following proteasomal inhibition. This proved impossible and is consistent with what other laboratories have experienced. Therefore, we relied on the gold-standard whole-cell patch-clamp electrophysiology in combination with semi-quantitative Western blotting as a measure of how ion conductance correlates with channel expression and function.

Being able to provide a molecular diagnosis is important to patients, their families, and their doctors as it confirms the cause of the condition and allows appropriate treatment, support, and counseling. In this study, we empirically test novel *CACNA1F* variants and show that bioinformatics prediction of pathogenicity was 70% accurate. This and future studies are important for refining and improving future prediction algorithms. We show that all *CACNA1F* variants with a functional consequence act via a LoF mechanism, irrespective of the variant's location in the subunit. The mutant subunits were degraded by the proteasome, and inhibition of this pathway by clinically approved drugs increased the cellular function of the mutant channels. This finding suggests that the use of proteasomal inhibitors may be useful therapeutic drugs for the treatment of CSNB2.

Data availability statement

The original contributions presented in the study are included in the article/Supplementary material; further inquiries can be directed to the corresponding author.

Author contributions

TS performed and analyzed all the data presented. FM and GB contributed to data interpretations, and RB contributed to the analysis of the electrophysiology work. All authors contributed to and approved the manuscript.

Funding

The authors thank the Manchester Academic Health Science Centre and the Manchester National Institute for Health Research Biomedical Research Centre for their support. This work was also supported by Fight for Sight (5079/5080) (TS).

Acknowledgments

The authors thank Dr Shalaw Sallah for his contribution to CACNA1F-vp. The authors also thank Prof Alexandra Koschak (University of Innsbruck) for providing the β3 plasmid as a gift and her support with the electrophysiology experiments. The authors extend their thanks to Prof Amy Lee (University of Texas) for providing the wild-type $Ca_v1.4\alpha$, β2a, and α2δ as a gift. This study would not have been possible without their combined contributions.

Conflict of interest

The authors declare that the research was conducted in the absence of any commercial or financial relationships that could be construed as a potential conflict of interest.

Publisher's note

Supplementary material

The Supplementary Material for this article can be found online at: https://www.frontiersin.org/articles/10.3389/fcell.2023.1161548/full#supplementary-material

References

Abriel, H., Wehrens, X. H., Benhorin, J., Kerem, B., and Kass, R. S. (2000). Molecular pharmacology of the sodium channel mutation D1790G linked to the long-QT syndrome. *Circulation* 102 (8), 921–925. doi:10.1161/01.cir.102.8.921

Antzelevitch, C., Pollevick, G. D., Cordeiro, J. M., Casis, O., Sanguinetti, M. C., Aizawa, Y., et al. (2007). Loss-of-function mutations in the cardiac calcium channel underlie a new clinical entity characterized by ST-segment elevation, short QT intervals, and sudden cardiac death. *Circulation* 115 (4), 442–449. doi:10.1161/CIRCULATIONAHA.106.668392

Athanasiou, D., Aguila, M., Opefi, C. A., South, K., Bellingham, J., Bevilacqua, D., et al. (2017). Rescue of mutant rhodopsin traffic by metformin-induced AMPK activation accelerates photoreceptor degeneration. *Hum. Mol. Genet.* 26 (2), 305–319. doi:10.1093/hmg/ddw387

Benhorin, J., Taub, R., Goldmit, M., Kerem, B., Kass, R. S., Windman, I., et al. (2000). Effects of flecainide in patients with new SCN5A mutation: Mutation-specific therapy for long-QT syndrome? *Circulation* 101 (14), 1698–1706. doi:10.1161/01.cir.101.14.1698

Boycott, K. M., Pearce, W. G., and Bech-Hansen, N. T. (2000). Clinical variability among patients with incomplete X-linked congenital stationary night blindness and a founder mutation in CACNA1F. *Can. J. Ophthalmol.* 35 (4), 204–213. doi:10.1016/s0008-4182(00)80031-9

Brunklaus, A., Ellis, R., Reavey, E., Semsarian, C., and Zuberi, S. M. (2014). Genotype phenotype associations across the voltage-gated sodium channel family. *J. Med. Genet.* 51 (10), 650–658. doi:10.1136/jmedgenet-2014-102608

Burtscher, V., Schicker, K., Novikova, E., Pöhn, B., Stockner, T., Kugler, C., et al. (2014). Spectrum of Cav1.4 dysfunction in congenital stationary night blindness type 2. *Biochim. Biophys. Acta BBA - Biomembr.* 1838 (8), 2053–2065. doi:10.1016/j.bbamem.2014.04.023

Carss, K. J., Arno, G., Erwood, M., Stephens, J., Sanchis-Juan, A., Hull, S., et al. (2017). Comprehensive rare variant analysis via whole-genome sequencing to determine the molecular Pathology of inherited retinal disease. *Am. J. Hum. Genet.* 100 (1), 75–90. doi:10.1016/j.ajhg.2016.12.003

Catterall, W. A., Perez-Reyes, E., Snutch, T. P., and Striessnig, J. (2005). International Union of Pharmacology. XLVIII. Nomenclature and structure-function relationships of voltage-gated calcium channels. *Pharmacol. Rev.* 57 (4), 411–425. doi:10.1124/pr.57.4.5

Cavaletti, G., Gilardini, A., Canta, A., Rigamonti, L., Rodriguez-Menendez, V., Ceresa, C., et al. (2007). Bortezomib-induced peripheral neurotoxicity: A neurophysiological

and pathological study in the rat. *Exp. Neurol.* 204 (1), 317–325. doi:10.1016/j.expneurol.2006.11.010

Collins, G. A., and Goldberg, A. L. (2017). The logic of the 26S proteasome. *Cell* 169 (5), 792–806. doi:10.1016/j.cell.2017.04.023

Deftu, A. F., Chung, P. C. S., Laedermann, C. J., Gillet, L., Pertin, M., Kirschmann, G., et al. (2022). The antidiabetic drug metformin regulates voltage-gated sodium channel NaV1.7 via the ubiquitin-ligase NEDD4-2. *eNeuro* 9, 0409–0421. doi:10.1523/ENEURO.0409-21.2022

Fricker, L. D. (2020). Proteasome inhibitor drugs. *Annu. Rev. Pharmacol. Toxicol.* 60 (1), 457–476. doi:10.1146/annurev-pharmtox-010919-023603

Galbiati, F., Volonte, D., Minetti, C., Bregman, D. B., and Lisanti, M. P. (2000). Limb-girdle muscular dystrophy (LGMD-1C) mutants of caveolin-3 undergo ubiquitination and proteasomal degradation. Treatment with proteasomal inhibitors blocks the dominant negative effect of LGMD-1C mutanta and rescues wild-type caveolin-3. *J. Biol. Chem.* 275 (48), 37702–37711. doi:10.1074/jbc.M006657200

Granato, M., Gilardini Montani, M. S., Romeo, M. A., Santarelli, R., Gonnella, R., D'Orazi, G., et al. (2017). Metformin triggers apoptosis in PEL cells and alters bortezomib-induced Unfolded Protein Response increasing its cytotoxicity and inhibiting KSHV lytic cycle activation. *Cell Signal* 40, 239–247. doi:10.1016/j.cellsig.2017.09.020

Han, Y. H., Moon, H. J., You, B. R., and Park, W. H. (2009). The effect of MG132, a proteasome inhibitor on HeLa cells in relation to cell growth, reactive oxygen species and GSH. *Oncol. Rep.* 22 (1), 215–221.

Hart, P. D., and Young, M. R. (1991). Ammonium chloride, an inhibitor of phagosome-lysosome fusion in macrophages, concurrently induces phagosome-endosome fusion, and opens a novel pathway: Studies of a pathogenic mycobacterium and a nonpathogenic yeast. *J. Exp. Med.* 174 (4), 881–889. doi:10.1084/jem.174.4.881

Heyne, H. O., Baez-Nieto, D., Iqbal, S., Palmer, D. S., Brunklaus, A., May, P., et al. (2020). Predicting functional effects of missense variants in voltage-gated sodium and calcium channels. *Sci. Transl. Med.* 12 (556), eaay6848. doi:10.1126/scitranslmed.aay6848

Hoda, J. C., Zaghetto, F., Koschak, A., and Striessnig, J. (2005). Congenital stationary night blindness type 2 mutations S229P, G369D, L1068P, and W1440X alter channel gating or functional expression of Ca(v)1.4 L-type Ca2+ channels. *J. Neurosci. Off. J. Soc. Neurosci.* 25 (1), 252–259. doi:10.1523/JNEUROSCI.3054-04.2005

Hosseini, S. M., Kim, R., Udupa, S., Costain, G., Jobling, R., Liston, E., et al. (2018). Reappraisal of reported genes for sudden arrhythmic death: Evidence-based evaluation of gene validity for brugada syndrome. *Circulation* 138 (12), 1195–1205. doi:10.1161/CIRCULATIONAHA.118.035070

Hove, M. N., Kilic-Biyik, K. Z., Trotter, A., Grønskov, K., Sander, B., Larsen, M., et al. (2016). Clinical characteristics, mutation spectrum, and prevalence of åland eye disease/incomplete congenital stationary night blindness in Denmark. *Invest. Ophthalmol. Vis. Sci.* 57 (15), 6861–6869. doi:10.1167/iovs.16-19445

Hu, J., Han, J., Li, H., Zhang, X., Liu, L. L., Chen, F., et al. (2018). Human embryonic kidney 293 cells: A vehicle for biopharmaceutical manufacturing, structural Biology, and electrophysiology. *Cells Tissues Organs* 205 (1), 1–8. doi:10.1159/000485501

Indelicato, E., and Boesch, S. (2021). From genotype to phenotype: Expanding the clinical spectrum of CACNA1A variants in the era of next generation sequencing. *Front. Neurol.* 12, 639994. doi:10.3389/fneur.2021.639994

Jagannathan, S., Abdel-Malek, M. A. Y., Malek, E., Vad, N., Latif, T., Anderson, K. C., et al. (2015). Pharmacologic screens reveal metformin that suppresses GRP78-dependent autophagy to enhance the anti-myeloma effect of bortezomib. *Leukemia* 29 (11), 2184–2191. doi:10.1038/leu.2015.157

Kaplan, G. S., Torcun, C. C., Grune, T., Ozer, N. K., and Karademir, B. (2017). Proteasome inhibitors in cancer therapy: Treatment regimen and peripheral neuropathy as a side effect. *Free Radic. Biol. Med.* 103, 1–13. doi:10.1016/j.freeradbiomed.2016.12.007

Karczewski, K. J., Francioli, L. C., Tiao, G., Cummings, B. B., Alföldi, J., Wang, Q., et al. (2019). Variation across 141,456 human exomes and genomes reveals the spectrum of loss-of-function intolerance across human protein-coding genes. *bioRxiv* 30, 531210.

Koschak, A., Fernandez-Quintero, M. L., Heigl, T., Ruzza, M., Seitter, H., and Zanetti, L. (2021). Cav1.4 dysfunction and congenital stationary night blindness type 2. *Pflugers Arch.* 473 (9), 1437–1454. doi:10.1007/s00424-021-02570-x

Koschak, A., Reimer, D., Walter, D., Hoda, J. C., Heinzle, T., Grabner, M., et al. (2003). Cav1.4alpha1 subunits can form slowly inactivating dihydropyridine-sensitive L-type Ca2+ channels lacking Ca2+-dependent inactivation. *J. Neurosci. Off. J. Soc. Neurosci.* 23 (14), 6041–6049. doi:10.1523/JNEUROSCI.23-14-06041.2003

Levine, B., and Klionsky, D. J. (2004). Development by self-digestion: Molecular mechanisms and biological functions of autophagy. *Dev. Cell* 6 (4), 463–477. doi:10.1016/s1534-5807(04)00099-1

Macías-Vidal, J., Girós, M., Guerrero, M., Gascón, P., Serratosa, J., Bachs, O., et al. (2014). The proteasome inhibitor bortezomib reduced cholesterol accumulation in fibroblasts from Niemann-Pick type C patients carrying missense mutations. *FEBS J.* 281 (19), 4450–4466. doi:10.1111/febs.12954

Men, C. J., Bujakowska, K. M., Comander, J., Place, E., Bedoukian, E. C., Zhu, X., et al. (2017). The importance of genetic testing as demonstrated by two cases of CACNA1F-associated retinal generation misdiagnosed as LCA. *Mol. Vis.* 23, 695–706.

Nowis, D., Maczewski, M., Mackiewicz, U., Kujawa, M., Ratajska, A., Wieckowski, M. R., et al. (2010). Cardiotoxicity of the anticancer therapeutic agent bortezomib. *Am. J. Pathol.* 176 (6), 2658–2668. doi:10.2353/ajpath.2010.090690

Pastor-Soler, N. M., Li, H., Pham, J., Rivera, D., Ho, P. Y., Mancino, V., et al. (2022). Metformin improves relevant disease parameters in an autosomal dominant polycystic kidney disease mouse model. *Am. J. Physiol-Ren Physiol.* 322 (1), F27–F41. doi:10.1152/ajprenal.00298.2021

Redmann, M., Benavides, G. A., Berryhill, T. F., Wani, W. Y., Ouyang, X., Johnson, M. S., et al. (2017). Inhibition of autophagy with bafilomycin and chloroquine decreases mitochondrial quality and bioenergetic function in primary neurons. *Redox Biol.* 11, 73–81. doi:10.1016/j.redox.2016.11.004

Rosenfeld, J., Sloan-Brown, K., and George, A. L. (1997). A novel muscle sodium channel mutation causes painful congenital myotonia. *Ann. Neurol.* 42 (5), 811–814. doi:10.1002/ana.410420520

Sadeh, T. T., Black, G. C., and Manson, F. (2021). A review of genetic and physiological disease mechanisms associated with Cav1 channels: Implications for incomplete congenital stationary night blindness treatment. *Front. Genet.* 12, 7876387. doi:10.3389/fgene.2021.637780

Sallah, S. R., Sergouniotis, P. I., Barton, S., Ramsden, S., Taylor, R. L., Safadi, A., et al. (2020). Using an integrative machine learning approach utilising homology modelling to clinically interpret genetic variants: CACNA1F as an exemplar. *Eur. J. Hum. Genet. EJHG* 28, 1274–1282. doi:10.1038/s41431-020-0623-y

Sievers, F., Wilm, A., Dineen, D., Gibson, T. J., Karplus, K., Li, W., et al. (2011). Fast, scalable generation of high-quality protein multiple sequence alignments using Clustal Omega. *Mol. Syst. Biol.* 7, 539. doi:10.1038/msb.2011.75

Striessnig, J., Hoda, J. C., Koschak, A., Zaghetto, F., Müllner, C., Sinnegger-Brauns, M. J., et al. (2004). L-type Ca2+ channels in Ca2+ channelopathies. *Biochem. Biophys. Res. Commun.* 322 (4), 1341–1346. doi:10.1016/j.bbrc.2004.08.039

Strom, T. M., Nyakatura, G., Apfelstedt-Sylla, E., Hellebrand, H., Lorenz, B., Weber, B. H. F., et al. (1998). An L-type calcium-channel gene mutated in incomplete X-linked congenital stationary night blindness. *Nat. Genet.* 19 (3), 260–263. doi:10.1038/940

Torrico, B., Shaw, A. D., Mosca, R., Vivó-Luque, N., Hervás, A., Fernàndez-Castillo, N., et al. (2019). Truncating variant burden in high-functioning autism and pleiotropic effects of LRP1 across psychiatric phenotypes. *J. Psychiatry Neurosci. Jpn.* 44 (5), 350–359. doi:10.1503/jpn.180184

Tumienė, B., Maver, A., Writzl, K., Hodžić, A., Čuturilo, G., Kuzmanić-Šamija, R., et al. (2018). Diagnostic exome sequencing of syndromic epilepsy patients in clinical practice. *Clin. Genet.* 93 (5), 1057–1062. doi:10.1111/cge.13203

Turro, E., Astle, W. J., Megy, K., Gräf, S., Greene, D., Shamardina, O., et al. (2020). Whole-genome sequencing of patients with rare diseases in a national health system. *Nature* 583 (7814), 96–102. doi:10.1038/s41586-020-2434-2

Wang, H., Wang, C., Lu, Y., Yan, Y., Leng, D., Tian, S., et al. (2020). Metformin shortens prolonged qt interval in diabetic mice by inhibiting L-type calcium current: A possible therapeutic approach. *Front. Pharmacol.* 11, 614. doi:10.3389/fphar.2020.00614

Ward, C. L., Omura, S., and Kopito, R. R. (1995). Degradation of CFTR by the ubiquitin-proteasome pathway. *Cell* 83 (1), 121–127. doi:10.1016/0092-8674(95)90240-6

Waterhouse, A., Bertoni, M., Bienert, S., Studer, G., Tauriello, G., Gumienny, R., et al. (2018). SWISS-MODEL: Homology modelling of protein structures and complexes. *Nucleic Acids Res.* 46 (1), W296–W303. doi:10.1093/nar/gky427

Wu, J., Yan, Z., Li, Z., Qian, X., Lu, S., Dong, M., et al. (2016). Structure of the voltage-gated calcium channel Ca v 1.1 at 3.6 Å resolution. *Nature* 537 (7619), 191–196. doi:10.1038/nature19321

Zamponi, G. W., Striessnig, J., Koschak, A., and Dolphin, A. C. (2015). The physiology, Pathology, and pharmacology of voltage-gated calcium channels and their future therapeutic potential. *Pharmacol. Rev.* 67 (4), 821–870. doi:10.1124/pr.114.009654

Zeitz, C., Robson, A. G., and Audo, I. (2015). Congenital stationary night blindness: An analysis and update of genotype–phenotype correlations and pathogenic mechanisms. *Prog. Retin Eye Res.* 45, 58–110. doi:10.1016/j.preteyeres.2014.09.001

Zhang, J., Gao, F., Du, C., Wang, J., Pi, X., Guo, W., et al. (2019). A novel RP2 missense mutation Q158P identified in an X-linked retinitis pigmentosa family impaired RP2 protein stability. *Gene* 707, 86–92. doi:10.1016/j.gene.2019.05.006

Zheng, H., Xiao, W. H., and Bennett, G. J. (2012). Mitotoxicity and bortezomib-induced chronic painful peripheral neuropathy. *Exp. Neurol.* 238 (2), 225–234. doi:10.1016/j.expneurol.2012.08.023

frontiers | Frontiers in Cell and Developmental Biology

TYPE Original Research
PUBLISHED 22 June 2023
DOI 10.3389/fcell.2023.1199069

OPEN ACCESS

EDITED BY
José M. Millan,
La Fe Health Research Institute, Spain

REVIEWED BY
Francesc R. Garcia-Gonzalo,
Autonomous University of Madrid, Spain
Maxim Sokolov,
West Virginia University, United States

*CORRESPONDENCE
Uwe Wolfrum,
wolfrum@uni-mainz.de

†These authors have contributed equally to this work and share first authorship

RECEIVED 02 April 2023
ACCEPTED 06 June 2023
PUBLISHED 22 June 2023

CITATION
Linnert J, Knapp B, Güler BE, Boldt K, Ueffing M and Wolfrum U (2023), Usher syndrome proteins ADGRV1 (USH2C) and CIB2 (USH1J) interact and share a common interactome containing TRiC/CCT-BBS chaperonins.
Front. Cell Dev. Biol. 11:1199069.
doi: 10.3389/fcell.2023.1199069

Usher syndrome proteins ADGRV1 (USH2C) and CIB2 (USH1J) interact and share a common interactome containing TRiC/CCT-BBS chaperonins

Joshua Linnert[1†], Barbara Knapp[1†], Baran E. Güler[1], Karsten Boldt[2], Marius Ueffing[2] and Uwe Wolfrum[1*]

[1]Institute of Molecular Physiology, Molecular Cell Biology, Johannes Gutenberg University Mainz, Mainz, Germany, [2]Institute for Ophthalmic Research, Eberhard Karls University of Tuebingen, Tubingen, Germany

The human Usher syndrome (USH) is the most common form of a sensory hereditary ciliopathy characterized by progressive vision and hearing loss. Mutations in the genes *ADGRV1* and *CIB2* have been associated with two distinct sub-types of USH, namely, USH2C and USH1J. The proteins encoded by the two genes belong to very distinct protein families: the adhesion G protein-coupled receptor ADGRV1 also known as the very large G protein-coupled receptor 1 (VLGR1) and the Ca^{2+}- and integrin-binding protein 2 (CIB2), respectively. In the absence of tangible knowledge of the molecular function of ADGRV1 and CIB2, pathomechanisms underlying USH2C and USH1J are still unknown. Here, we aimed to enlighten the cellular functions of CIB2 and ADGRV1 by the identification of interacting proteins, a knowledge that is commonly indicative of cellular functions. Applying affinity proteomics by tandem affinity purification in combination with mass spectrometry, we identified novel potential binding partners of the CIB2 protein and compared these with the data set we previously obtained for ADGRV1. Surprisingly, the interactomes of both USH proteins showed a high degree of overlap indicating their integration in common networks, cellular pathways and functional modules which we confirmed by GO term analysis. Validation of protein interactions revealed that ADGRV1 and CIB2 mutually interact. In addition, we showed that the USH proteins also interact with the TRiC/CCT chaperonin complex and the Bardet Biedl syndrome (BBS) chaperonin-like proteins. Immunohistochemistry on retinal sections demonstrated the co-localization of the interacting partners at the photoreceptor cilia, supporting the role of USH proteins ADGRV1 and CIB2 in primary cilia function. The interconnection of protein networks involved in the pathogenesis of both syndromic retinal dystrophies BBS and USH suggest shared pathomechanisms for both syndromes on the molecular level.

KEYWORDS

usher syndrome, bardet biedl syndrome (BBS), protein networks, retinal ciliopathies, VLGR1, TRiC/CCT chaperonins, primary cilia, photoreceptor cells

Introduction

The human Usher syndrome (USH) is a clinically and genetically heterogeneous autosomal recessive disorder characterized by deafness and vestibular dysfunction combined with vision loss due to *Retinitis pigmentosa* (Reiners et al., 2006; Delmaghani and El-Amraoui, 2022). Three types of USH (USH1, USH2 and USH3) are distinguished, based on the age of onset, disease progression and the severity of the symptoms. To date, only one gene for USH3, *CLRN1*, three genes for USH2, *USH2A*, *ADGRV1* (USH2C), *WHRN* (USH2D), and six USH1 genes, *MYO7A* (USH1B), *USH1C, CDH23* (USH1D), *PCDH15* (USH1F), *USH1G,* and *CIB2* (USH1J) have been assigned to USH (Fuster-García et al., 2021). Recently, the association of mutations in CIB2 with USH and the assignment to USH1J (Riazuddin et al., 2012) has been debated (Dal Cortivo and Dell'orco, 2022; Delmaghani and El-Amraoui, 2022). Clinical analysis on patients with confirmed mutations in *CIB2*, a NGS meta-analysis of USH patients, and work on *cib2* mouse models have recently raised doubts that *CIB2* is a USH-causing gene, but rather a gene for non-syndromic deafness (DFNB48) (Michel et al., 2017; Booth et al., 2018; Jouret et al., 2019). However, a recent study found a distinct visual phenotype alongside deafness in a *cib2*-deficient mouse model, confirming the association of *CIB2* defects with syndromic inherited retinal dystrophies (IRD) such as USH (Sethna et al., 2021).

The various USH genes encode very heterogeneous families and groups of proteins, such as scaffold proteins, transmembrane proteins, or motor proteins, but they share the common feature of being involved in common protein networks called the USH interactome (Reiners et al., 2006; Mathur and Yang, 2015). However, the cellular function of these USH proteins in photoreceptors and hair cells has not been fully elucidated, an understanding that would be necessary to mitigate the phenotypic burden of mutations in any of the USH genes by means of sound treatment. Here, we focus on *ADGRV1* (USH2C) and *CIB2* (USH1J) that codify the very large G protein-coupled receptor 1 (VLGR1) ADGRV1 and the Ca^{2+}- and integrin-binding protein 2 (CIB2), respectively.

CIB2 shares sequence identity with calmodulin and calcineurin B and contains three EF-hand domains, whereby only the last two domains can bind Ca^{2+} (Figure 1) (Dal Cortivo and Dell'orco, 2022). CIB2 is expressed in diverse tissues and cell types, such as the skeletal muscle, platelet cells, diverse nervous tissue as well as the sensory cells in the retina and the inner ear (Riazuddin et al., 2012; Jacoszek et al., 2017). CIB2 is involved in the regulation of Ca^{2+}-homeostasis and interacts with integrins (Häger et al., 2008), important for hair cell differentiation and stereocilia development (Evans and Müller, 2000). In the eye, CIB2 is found in the neuronal retina and the retinal pigment epithelium where it participates in mTORC1 signaling and autophagy (Sethna et al., 2021).

The ADGRV1 protein, also known as VLGR1, GPR98, MASS1, or FEB4 is a seven-transmembrane receptor that belongs to the adhesion GPCR (ADGR) family (McMillan and White, 2010; Hamann et al., 2015). The characteristic very long extracellular domain of ADGRV1 comprises 35 Ca^{2+}-binding Calx-beta domains (Calxβ), a laminin G/pentraxin domain (LamG/PTX), six epitempin/epilepsy-associated repeats (EPTP/EAR) and a G protein-coupled receptor proteolytic site (GPS), which is embedded in the GPCR autoproteolysis-inducing (GAIN) domain and divides the molecule in a N-terminal fragment (NTF) and a C-terminal fragment (CTF) (Figure 1A). The very C-terminal intracellular domain of ADGRV1 displays a terminal class I PDZ-binding motif (PBM).

Like CIB2, ADGRV1 is expressed in various tissues, most abundantly in the retina, the inner ear and the brain (Reiners et al., 2006; McMillan and White, 2010). ADGRV1 is essential for the formation of ankle-links during the development of hair cells (McGee et al., 2006; Michalski et al., 2007; Yagi et al., 2007). Defects in *Adgrv1* result in disorganized hair bundles, which manifest in hearing impairment. In photoreceptor cells, ADGRV1 builds fibrous links between the apical inner segment and the connecting cilium, which resemble the ankle links in hair cells and are lost in *Adgrv1* mutant mice (Maerker et al., 2008).

In the past years, it became evident that USH proteins are part of larger protein networks that are present in cilia, antenna-like structures that emerge from the cell surface (Van Wijk et al., 2009; Wright et al., 2012; May-Simera et al., 2017; Sorusch et al., 2017). Diseases affecting ciliary function - so-called ciliopathies - include besides USH, for example, also the Bardet Biedl syndrome (BBS) and numerous non-syndromic IRDs such as Leber congenital amaurosis (LCA) (Bettencourt-Dias et al., 2011; Braun and Hildebrandt, 2017; Bujakowska et al., 2017). The molecular mechanisms underlying the pathogenesis of these diseases are largely unknown and their analysis is challenging.

In recent studies, we have identified novel functional modules associated with ADGRV1 applying affinity proteomics (Knapp et al., 2019; 2022; Kusuluri et al., 2021; Krzysko et al., 2022). Here, we compared the interactomes of ADGRV1 and CIB2 identified by tandem affinity purification (TAP) and found that there was a large overlap in terms of the interacting proteins included. Interestingly, the data sets for both proteins include all eight subunits of the TRiC/CCT chaperonin complex, which is essential for the correct folding of client protein substrates such as actin and tubulin and thereby for the organization of the entire cytoskeleton (Dekker et al., 2008; Brackley and Grantham, 2009). CCT proteins are specifically enriched at the base of primary cilia, suggesting a role in cilia maintenance and/or cell cycle regulation (Seixas et al., 2010; Seo et al., 2010; Kypri et al., 2014). Recently, mutations in the *CCT2* gene have been related to LCA, a severe visual impairment beginning in infancy (Minegishi et al., 2016). Three gene products that are associated with Bardet-Biedl sydrome (BBS) - MKKS/BBS6, BBS10 and BBS12 - have high sequence identity with CCTs (Alvarez-Satta et al., 2017). Together, the BBS-type chaperones and the TRiC/CCT chaperonin complex cooperate in the assembly of the BBSome (Seo et al., 2010; Zhang et al., 2012). The BBSome is a heterooctomeric protein complex consisting of seven BBS proteins: BBS1, BBS2, BBS4, BBS5, BBS7, BBS8, BBS9, and BBIP10 protein (Jin and Nachury, 2009). It plays a key role in primary cilia homeostasis and is essential for the transport of cargo vesicles to primary cilia and the intraflagellar transport (IFT) of membrane cargo within the ciliary shaft (Jin et al., 2010).

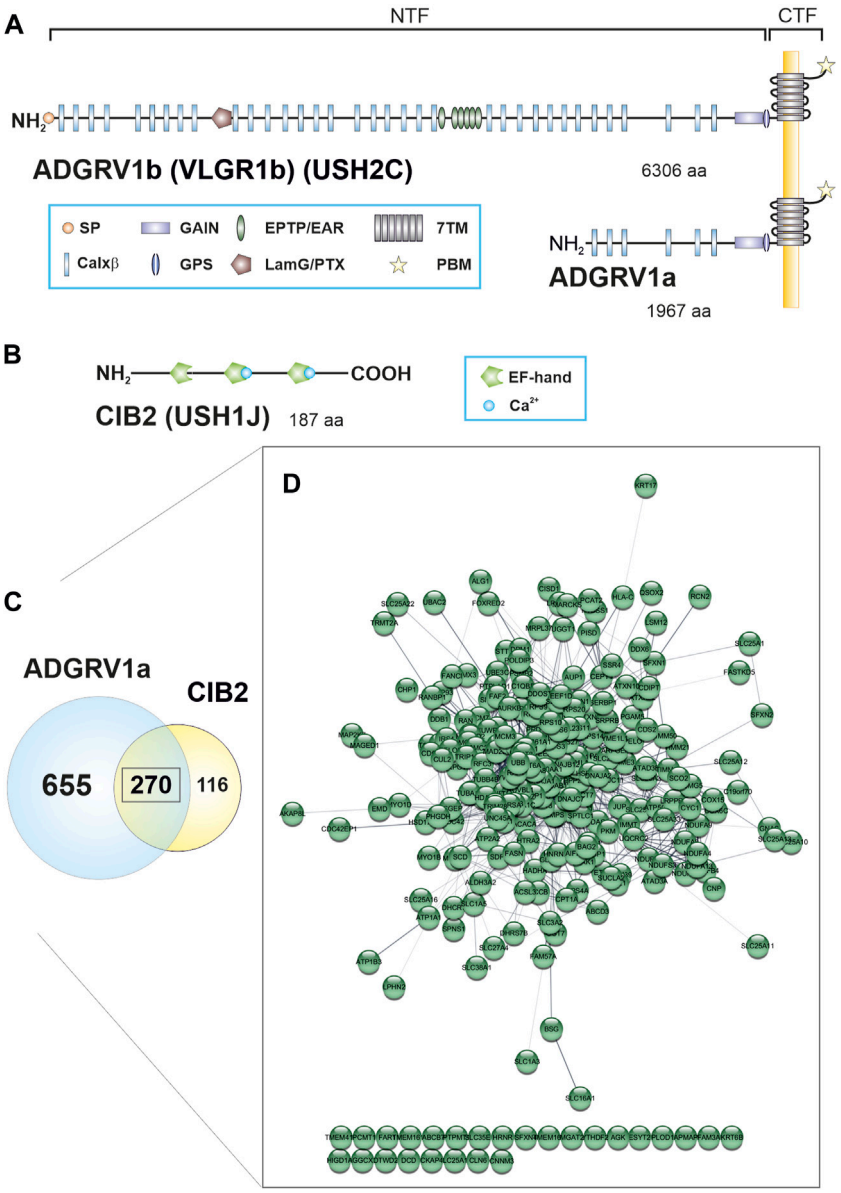

FIGURE 1
ADGRV1 and CIB2 share a common protein network. **(A)** The human full-length ADGRV1 isoform b contains 6,306 amino acids (aa), the ADGRV1a isoform 1,967 aa. Both isoforms can undergo autocleavage at the G protein-coupled receptor proteolytic cleavage site (GPS), resulting in an N-terminal fragment (NTF) and a C-terminal fragment (CTF). The NTF of ADGRV1b contains a signal peptide (SP), 35 calcium-binding Calxβ domains, a laminin G/pentraxin domain (LamG/PTX), epitempin/epilepsy-associated repeats (EPTP/EAR) and the N-terminal part of the G protein-coupled receptor (GPCR) autoproteolysis-inducing (GAIN) domain. The CTF contains the seven transmembrane (7TM) domain and the C-terminal PDZ binding motif (PBM). **(B)** The CIB2 isoform 1 is composed of 187 aa and contains three EF-hand motifs. Only the last two motifs can bind calcium. **(C)** 925 binding partners were identified for ADGRV1a and 386 interactors were found for CIB2 by TAP analysis. 270 prey proteins were contained in both data sets. **(D)** Visualization of the common ADGRV1 and CIB2 network with the STRING application in Cytoscape (confidence view). Most prey (244 out of 270) show a high degree of connectivity, based on STRING interaction data.

Here, we show that ADGRV1 and CIB2 are not only associated with the TRiC/CCT chaperonin complex but also bind to the three BBS chaperones. Moreover, we demonstrate that both USH proteins mutually interact and partially co-localize with the TRiC/CCT subunit CCT3 in the ciliary region of photoreceptor cells. We further demonstrate that the chaperonin complex is essential for the ciliary import of ADGRV1. Our data indicate a functional relation between protein networks involved in the pathomechanisms underlying USH, BBS and LCA.

Materials and methods

Constructs and plasmids

For tandem affinity purification (TAP), CIB2 isoform 1 (O75838-1, aa 1-187) was Strep II-FLAG (SF)-tagged at the N terminus. Plasmids used for pulldowns and immunoprecipitation coded for Strep-II-FLAG (SF)-tagged ADGRV1a (Uni-Prot ID

Q8WXG9-1, aa 4340-6306), (HA-tagged ADGRV1_CTF (Uni-Prot ID Q8WXG9-1, aa 5891-6306), HA-tagged ADGRV1_ICD (Q8WXG9-1, aa 6155-6306), FLAG-myc-tagged CCT3 (P49368-1) and mRFP-tagged BBS6 (Q9NPJ1-1, aa 2-570), BBS10 (Q8TAM1-1, aa 2-723) and BBS12 (Uni-Prot ID Q6ZW61-1, aa 2-710).

Cell culture

hTERT-RPE1 cells and HEK293T cells were cultured in Dulbecco's modified Eagle's medium (DMEM) containing 10% heat-inactivated fetal calf serum (FCS). Cells were transfected with GeneJuice® (Merck Millipore) according to the manufacturer's instructions.

Tandem affinity purification (TAP)

Three TAPs were performed for CIB2 as described (Gloeckner et al., 2007; Knapp et al., 2019). In brief, SF-CIB2 was overexpressed in HEK293T cells for 48 h. Mock-treated cells were used as a control. The cells were lysed, and the lysate was cleared by centrifugation. The supernatant was then subjected to a two-step purification on Strep-Tactin®Superflow® beads (IBA) and anti-FLAG M2 agarose beads (Sigma-Aldrich). Competitive elution was achieved by Desbiothin (IBA) in the first step and FLAG® peptide (Sigma-Aldrich) in the second step. The eluate was precipitated by methanol-chloroform and then subjected to mass spectrometric analysis.

Mass spectrometry

Mass spectrometry was performed as previously described (Boldt et al., 2016). SF-TAP-purified protein complexes were solubilized before subjecting to trypsin cleavage. Resulting peptides were desalted and purified using stage tips before separation on a Dionex RSLC system. Eluted peptides were ionized by Nano spray ionization and detected by an LTQ Orbitrap Velos mass spectrometer (Thermo Fisher Scientific). Raw spectra were searched against the human SwissProt database using Mascot and the results were verified by Scaffold (Version 4.02.01, Proteome Software Inc.) to validate MS/MS-based peptide and protein identifications. The mass spectrometry proteomics data have been deposited to the ProteomeXchange Consortium via the PRIDE (Perez-Riverol et al., 2022) partner repository with the dataset identifier PXD042629.

Data processing

Mass spectrometry data of SF-tagged CIB2 were compared to data for mock-transfected cells. Proteins that occurred in the mock dataset were not considered for subsequent analysis of CIB2 data. The identified prey in CIB2-TAPs were compared with the data for ADGRV1a from Knapp et al. (2022). Gene names (according to HGNC) of ADGRV1 and CIB2 prey were used as input for the Cytoscape (http://www.cytoscape.org/) plugins STRING (http://apps.cytoscape.org/apps/stringapp) and ClueGO (Bindea et al., 2009). The parameter *confidence (score) cutout* was set to 0. 40 and the parameter *maximum number of interactors* was set to 0 for STRING analysis. ClueGO v2.3.3 was used for Gene Ontology (GO) term enrichment analysis. Network specificity was set to default (medium). Only GO terms that are based on experimental data (setting: All_Experimental (EXP, IDA, IPI, IMP, IGI, IEP)) were included for the enrichment analysis and only pathways with a pV ≤ 0,05 were considered.

RFP-Trap® analysis

RFP-fused proteins were immobilized on RFP-Trap® agarose beads (ChromoTek) and used for co-precipitation assays according to the manufacturer's protocol. Briefly, cell lysates from co-transfected HEK293T cells (RFP-tagged proteins or RFP alone together with HA- or SF-tagged proteins, respectively) were suspended in lysis buffer (10 mM Tris-Cl, pH 7.5, 150 mM NaCl, 0.5 mM EDTA, 0.5% NP-40), spun and the supernatant was diluted to 1 mL in dilution buffer (10 mM Tris–Cl, pH 7.5, 150 mM NaCl, 0.5 mM EDTA). Fifty microliters were separated as input (total cell lysate) and samples were added to equilibrated beads for 2 h at 4°C under constant shaking. After washing, precipitated protein complexes were eluted with SDS-sample buffer and subjected to SDS–PAGE and western blotting.

Immunoprecipitation

For co-IP FLAG-myc-CCT3, and HA-ADGRV1_CTF (HA-ADGRV1_ICD, HA-CIB2, HA-centrin) were expressed in HEK293T cells and lysed in TAP lysis buffer. Co-IP was performed using anti-FLAG M2 beads from Sigma according to the manufacturer's protocol. Briefly, cell lysates were incubated with anti-FLAG M2 beads for 1 h at 4°C. Reciprocal Co-IPs were performed with anti-HA agarose beads from Biotool. After three washing steps with TAP washing buffer, samples were eluted with SDS-sample buffer and subjected to SDS-page and Western blot, using antibodies against the FLAG- and HA-tag.

GST pull-down assay

Glutathione S-transferase (GST), GST-tagged BBS6 and 7xHis-tagged ADGRV1-ICD expressed in *E. coli* BL21 AI following the manufacturer's instructions. Equal amounts of GST or GST fusion protein were mixed with lysates of His-tagged ADGRV1-ICD and a protease inhibitor mix (Sigma-Aldrich). Samples were incubated overnight at 4°C followed by incubation with 50 µL glutathione sepharose beads 4B (Amersham Biosciences) for 45 min with gentle agitation. Beads were centrifugated and washed 4 times with 50 mM Tris-HCl, 150 mM NaCl, 5 mM MgCl2, 1 mM EDTA, 10% glycerol, 0.01% polyoxyethylene-10-lauryl ether, pH 7.5. Subsequently, bound proteins were eluted with SDS sample buffer and subjected to SDS-PAGE and Western blotting.

Antibodies

The following antibodies were used: mouse anti-CCT3 (Proteintech 60264-1-Ig), mouse anti-CCT2 (Proteintech 68214-1-Ig), mouse anti-CIB2 (Abnova H00010518-A01), rabbit anti-ADGRV1 (Maerker et al., 2008), mouse anti-FLAG M2 (Sigma F3165), rabbit anti-HA antibody (Roche 11867423001), anti-RFP (Chromotek 5F8), goat-anti-GST (Sigma-Aldrich, SAB 2501414), anti-His antibody (Sigma-Aldrich, SAB1306082), goat anti-centrin 2 antibody (Giessl et al., 2004), anti-paxillin (rabbit polyclonal, Abcam, cat no ab32115; mouse monoclonal, BD Transduction Laboratories, cat no 610052) anti-pericentrin 2 (PCNT2) (Santa Cruz, C-16), mouse anti-Arl13b (Abcam, ab136648). Secondary antibodies conjugated to Alexa 488, Alexa 568, or Alexa 647 were purchased from Molecular Probes (Life Technologies) or from Rockland Inc.

Animals and tissue dissection

All experiments described herein are conforming to the statement by the Association for Research in Vision and Ophthalmology as to care and use of animals in research. C57BL/6J mice and eGFP-Centrin2 mice (Higginbotham et al., 2004) were maintained under a 12 h light-dark cycle, with food and water *ad libitum*. After sacrificing the animals in CO2 and decapitation, appropriate tissues were dissected. The use of mice in research was approved by District administration Mainz-Bingen, 41a/177-5865-§11 ZVTE, 30.04.2014.

Immunohistochemistry

The eyes of mice were cryofixed in melting isopentane and cryosectioned as previously described (Wolfrum 1991). Cryosections were placed on poly-L-lysine-precoated coverslips, incubated with 0.01% Tween 20 in PBS, washed several times, covered with blocking solution, and incubated for a minimum of 30 min followed by overnight incubation at 4°C with primary antibodies. Washed cryosections were incubated with secondary antibodies in a blocking solution containing DAPI (1 mg/mL) (Sigma) for 1.5 h at room temperature. After washing, sections were mounted in Mowiol (Roth).

Immunocytochemistry

hTERT-RPE1 cells were processed for immunohistochemistry as previously described (Krzysko et al., 2022).

Microscopy

Specimen were analyzed on a Leica DM6000B microscope and 3D deconvoluted with Leica imaging software (three iteration steps). Images were processed with Leica imaging software and Adobe Photoshop CS. Fiji/ImageJ software (NIH, Bethesda) was used for image processing and quantifications.

Results

Identification of interacting proteins of CIB2 by tandem affinity purification

To identify novel potential proteins interacting with CIB2 we applied affinity proteomics using tandem affinity purification (TAP) (Boldt et al., 2016). We fused the tandem Strep II-FLAG (SF)-tag to the N-terminus of the CIB2 isoform 1 (Figure 1). The SF-tagged CIB2 was expressed in HEK293T cells, and then subjected to TAP as described previously (Gloeckner et al., 2007; Knapp et al., 2019). Recovered protein complexes were separated by liquid chromatography and the peptide content was determined with tandem mass spectrometry (LC-MS/MS). To identify interacting proteins the raw spectra were searched against SwissProt databases and the results were verified by Scaffold. By applying these strategies we identified 386 potential novel interactors for CIB2 (Supplementary Table S1).

Comparison of the interactome of CIB2 and ADGRV1 revealed a high degree of overlap

We compared the CIB2 TAP data with the data set which we previously described for ADGRV1a (Knapp et al., 2022). This comparison revealed a high degree of overlap (Figure 1C; Supplementary Table S1), which we did not observe for ADGRV1 and TAP results from other USH proteins (e.g., for SANS (USH1G) and harmonin (USH1C), not shown). We found 270 identical prey proteins in the data sets of CIB2 and ADGRV1 (Figure 1C). Analysis by the Cytoscape plugin STRING revealed that of the 270 shared binding partners of ADGRV1 and CIB2, 244 are highly interconnected (https://string-db.org/, confidence view) and form a common protein network (Figure 1D).

ADGRV1 and CIB2 physically interact

The high overlap of the ADGRV1 and CIB2 TAP interactome prompted us to test whether both proteins physically interact. To address this question, we performed RFP-Trap® pulldown experiments (Figure 2A). For this we co-expressed the 3xHA-tagged C-terminal fragment of ADGRV1 (3xHA-ADGRV1_CTF) with either RFP-tagged CIB2 (mRFP-CIB2) or RFP alone in HEK293T cells. Cell lysates were then incubated with RFP-Trap® beads to immobilize RFP-CIB2 and RFP, respectively. Subsequent Western blot analysis of the recovered proteins revealed that 3xHA-ADGRV1_CTF was pulled down by RFP-CIB2, but not by RFP alone. We next performed reciprocal immunoprecipitations with anti-HA agarose beads to immobilize 3xHA-ADGRV1_CTF and the appropriate controls (Supplementary Figure S1). In this case, Western blot analysis of the recovered proteins revealed that RFP-CIB2, but not RFP alone, co-immunoprecipitated with 3xHA-ADGRV1_CTF, but not with the HA beads alone. Taken together, these findings demonstrated the interaction between ADGRV1 and CIB2.

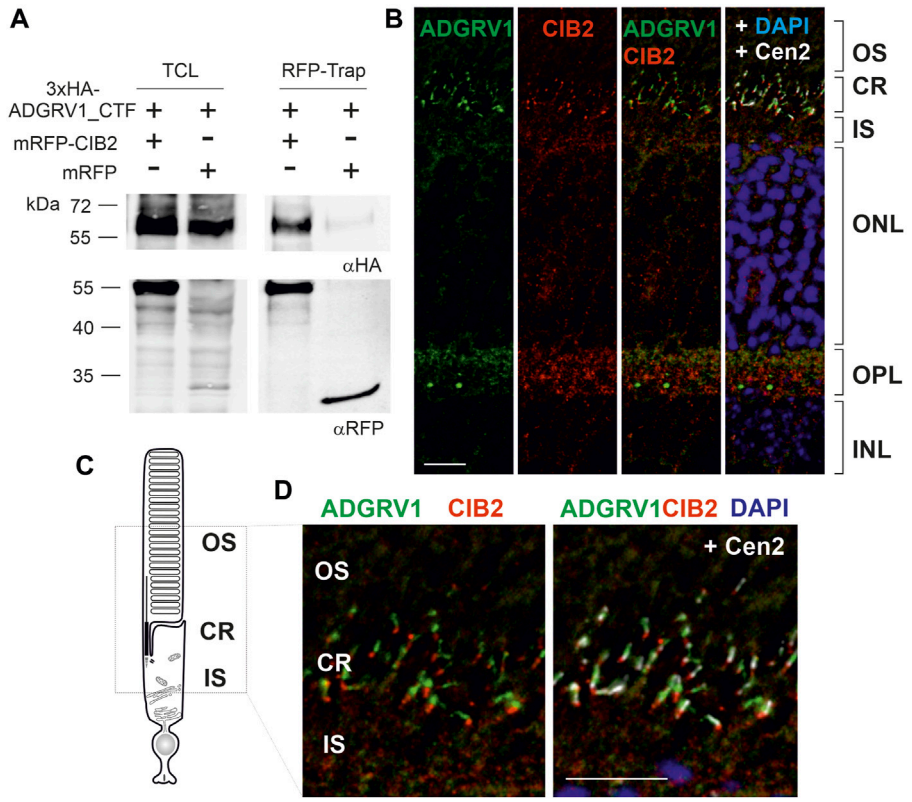

FIGURE 2
ADGRV1 and CIB2 interact and localize to the ciliary region of photoreceptor cells. **(A)** ADGRV1_CTF is pulled down by RFP-CIB2, but not RFP, in an RFP-Trap®. **(B)** Indirect immunolabeling of CIB2, ADGRV1, and the ciliary marker centrin 2 in a cryosection of a murine retina counterstained with the nuclear DNA marker DAPI. Merged images demonstrate ADGRV1 and CIB2 are mainly localized in the ciliary region (CR) and the outer plexiform layer (OPL) where the synapses of photoreceptor cells are present. **(C)** Cartoon of a rod photoreceptor cell: the photoreceptor inner segment (IS) is connected with the outer segment (OS) by the connecting cilium of the CR. **(D)** CIB2 and ADGRV1 localize in close proximity at the proximal end of the basal body, as revealed by the marker protein centrin 2, which localizes to the connecting cilium, the basal body and the adjacent centriole. TCL, total cell lysate; OS, outer segment; IS, inner segment; ONL, outer nuclear layer; OPL, outer plexiform layer; INL, inner nuclear layer; Scale bars: 2b and d = 10 μm.

ADGRV1 and CIB2 localize in the ciliary region of photoreceptor cells

Next, we used indirect immunofluorescence to examine whether ADGRV1 and CIB2 are co-distributed in the mouse retina. Immunostaining of both proteins in longitudinal cryosections through the murine retinas showed that ADGRV1 and CIB2 were most prominently localized in the synaptic and ciliary region of photoreceptor cells (Figure 2B). Triple-labeling with antibodies against centrin 2, a marker for the connecting cilium, the basal body and the adjacent daughter centriole of photoreceptor cells (Trojan et al., 2008), further highlighted the ciliary association of CIB2 and ADGRV1 in photoreceptor cells (Figures 2C, D). Immunostaining of pericentrin and Arl13b, common markers for the cilia base and shaft/axoneme of primary cilia, respectively (Mühlhans et al., 2011), as well as CIB2 and ADGRV1 confirmed the localization of CIB2 and ADGRV1 at the cilia base of primary cilia in hTERT-RPE1 cells (Supplementary Figure S2). Co-staining of CIB2 and paxillin, a focal adhesion component, in hTERT-RPE1 cells did not show CIB2 staining in focal adhesions (Supplementary Figure S2A), where ADGRV1 is also localized (Supplementary Figure S2B) (Kusuluri et al., 2021; Güler et al., 2023).

TAP analysis reveals novel protein complexes associated with ADGRV1 and CIB2

The physical interaction and co-localization of ADGRV1 with CIB2, and the high degree of overlap of their interactomes, indicate their functional relation. To investigate the context of these connections, we further analyzed the shared ADGRV1 and CIB2 network. For this purpose, we used the Cytoscape plugin ClueGO (accessed 10 September 2017) and STRING data (https://string-db.org/) (accessed 20 March 2022) (Bindea et al., 2009), which allows protein enrichment analysis based on Gene Ontology (GO) terms that indicate cellular pathways and processes.

We searched within the three categories *Biological Process*, *Cellular Component,* and *Molecular Function*. GO terms based on experimental data and a significance pV ≤ 0.05 were considered (Figure 3; Supplementary Tables S2–S4). In the *Biological Process* category, seven groups showed enriched GO terms with the leading terms *positive regulation of DNA biosynthetic process*, *protein localization to nuclear body*, *establishment of protein localization to organelle*, *acidic amino acid transport*, *substantia nigra*

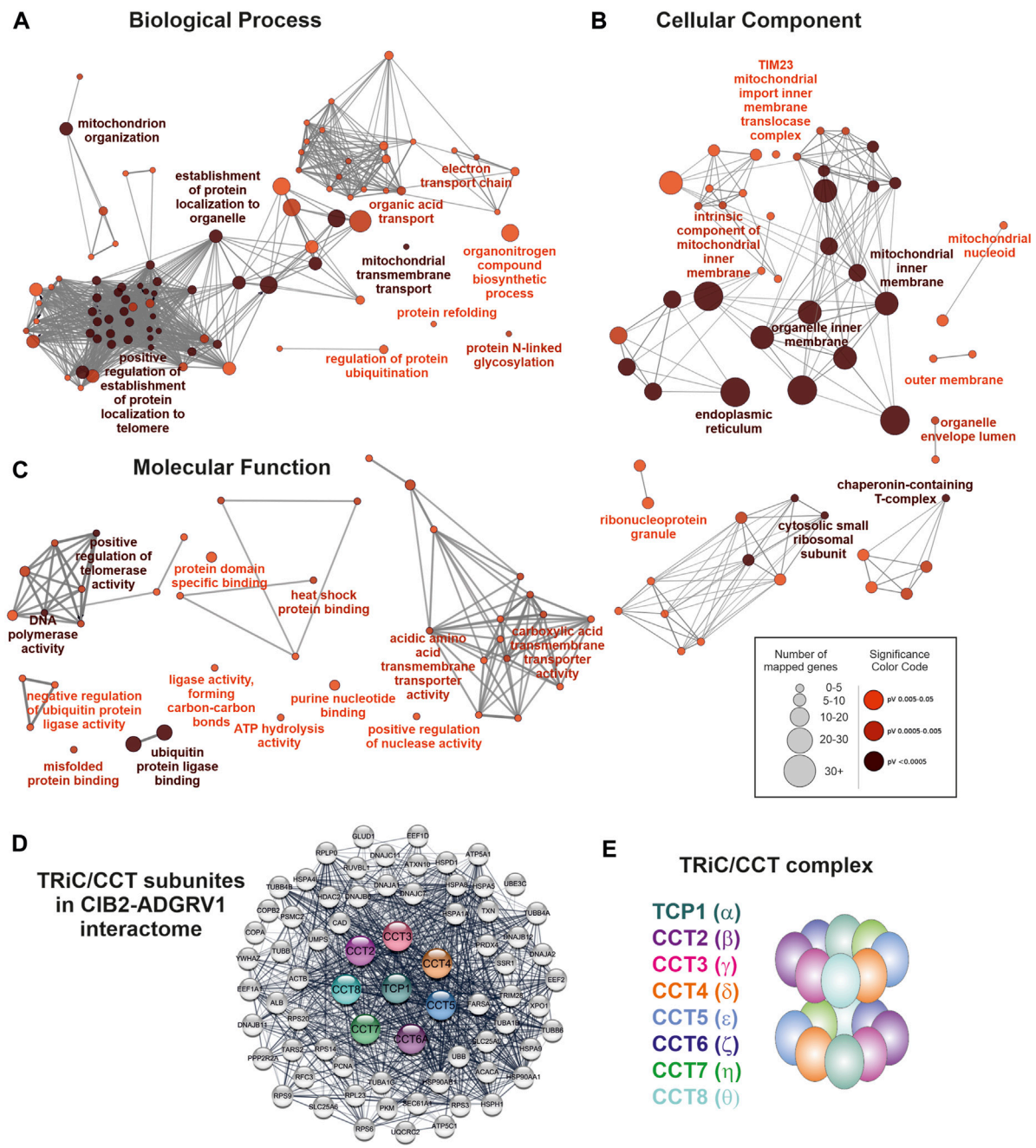

FIGURE 3
Components of the TRiC/CCT-complex are associated with enriched GO terms and build a subnetwork within the ADGRV1-CIB2 interactome. **(A)** GO term enrichment analysis in the category Biological Process. Depicted are the most significant terms for seven different groups. **(B)** GO term enrichment analysis in the category Cellular Component. Depicted are the most significant terms, for eight different groups. **(C)** GO term enrichment analysis in the category Molecular Function. Depicted are the most significant terms, for eleven different groups. **(D)** Protein network of the TRiC/CCT complex and direct network partners within the ADGRV1-CIB2 interactome. **(E)** The TRiC/CCT complex consists of eight CCT subunits that form a double ring, building up a cylindrical structure with a central cavity.

development, *protein refolding* and *mitochondrial membrane organization* (Figure 3A). In the *Cellular Component* category, we identified eight GO term groups with the leading terms *extracellular matrix*, *chaperone complex*, *chaperonin-containing T-complex*, *mitochondrion*, *mitochondrial nucleoid*, *mitochondrial inner membrane presequence translocase complex*, *organelle envelope lumen* and *endoplasmic reticulum* (Figure 3B). In the *Molecular Function* category, we found eleven GO term groups with the leading terms *protein binding involved in protein folding*, *L-glutamate transmembrane transporter activity*, *cation-transporting ATPase activity*, *RNA binding*, *ubiquitin protein ligase binding*, *NADH dehydrogenase activity*, *heat shock protein binding*, *MHC class II protein complex binding*, *cadherin binding* and *protein domain specific binding* (Figure 3C).

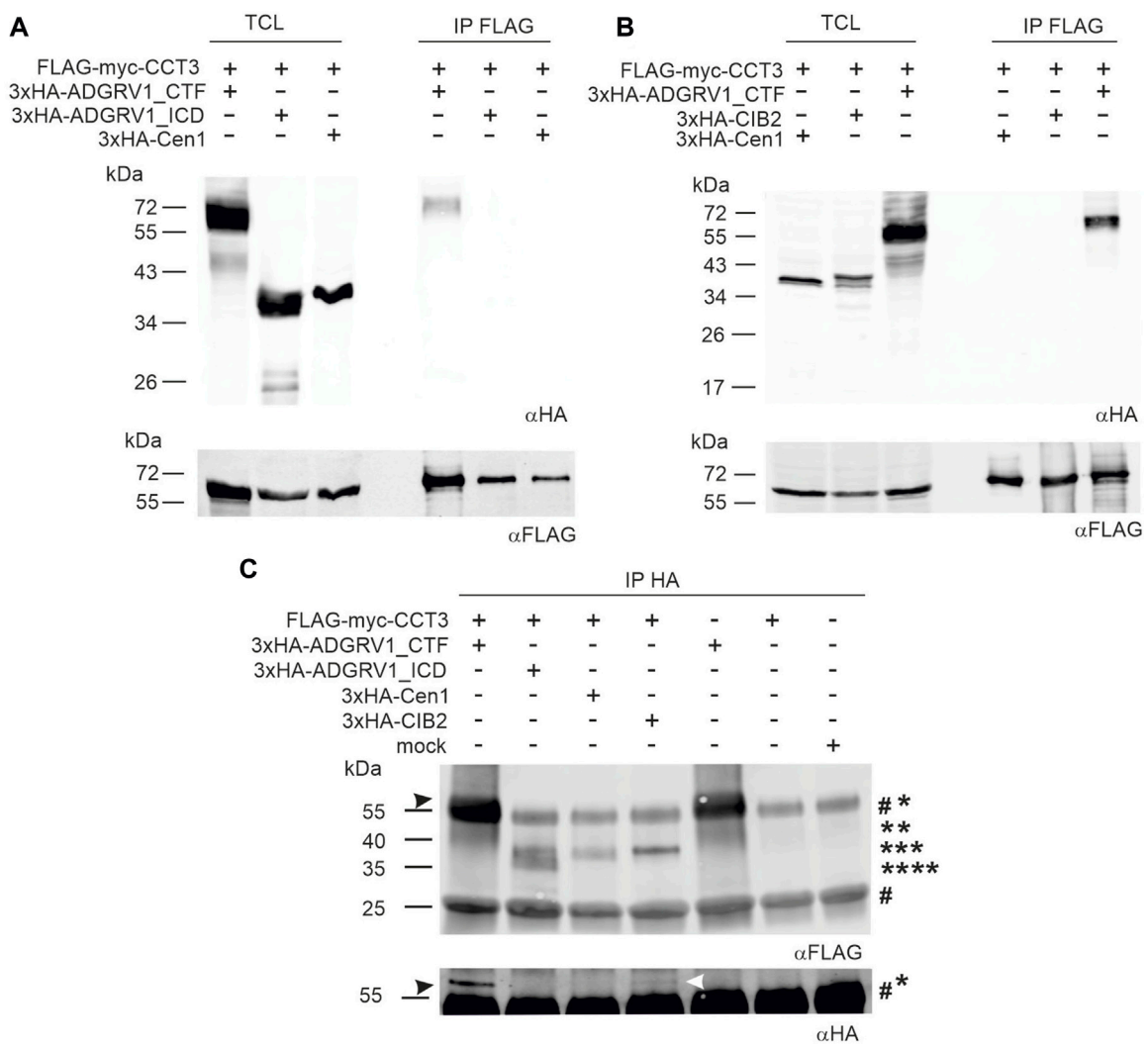

FIGURE 4
Co-immunoprecipitations of ADGRV1 and CIB2 with CCT3. **(A, B)** anti-FLAG-CCT3-immunoprecipitations: **(A)** Western blot analyses of anti-FLAG-Co-immunoprecipitations from HEK293 cells co-expressing the 3xHA-tagged C-terminal fragment of ADGRV1 (ADGRV1_CTF), the C-terminal intracellular domain (ADGRV1_ICD), or centrin 1 (Cen1), respectively, and the FLAG-myc-tagged CCT3. ADGRV1_CTF but not ADGRV1_ICD nor the negative control Cen1 were recovered, indicating the specific interaction of ADGRV1_CTF with CCT3. **(B)** Western blot analyses of anti-FLAG-Co-immunoprecipitations from HEK293 cells co-expressing 3xHA-tagged ADGRV1_CTF, CIB2, or Cen1, respectively, and the FLAG-myc-tagged CCT3. ADGRV1_CTF but not ADGRV1_ICD nor the negative control Cen1 were recovered, indicating specific interaction of CCT3 with ADGRV1_CTF, but not with CIB2. TCL, total cell lysate; IP, immunoprecipitation. **(C)** Reciprocal anti-HA-ADGRV1/CCT3-immunoprecipitations: Western blot analyses of anti-HA-co-immunoprecipitations from HEK293 cells co-expressing the 3xHA-tagged ADGRV1_CTF, ADGRV1_ICD, CIB2, or Cen1, respectively, and the FLAG-myc-tagged CCT3 or from cells expressing only FLAG-myc-tagged CCT3 as well as mock transfected cells. CCT3 (black arrowhead) was recovered in 3xHA-tagged ADGRV1_CTF but not ADGRV1_ICD nor the negative control Cen1 or "single-expressed" FLAG-myc-tagged CCT3 confirming the specific interaction of ADGRV1_CTF with CCT3 observed in **(A, B)**. In addition, a fade FLAG-myc-tagged CCT3 band was observed in the HA-Co-precipitation with 3xHA-tagged CIB2 (white arrowhead), indicating that CIB2 also interacts with CCT3 in this setting. Molecular weight of the used constructs are indicated: * 3xHA-VLGR1_CTF, ** 3xHA-tagged CIB2, *** 3xHA-Cen1, **** 3xHA-ADGRV1_ICD. The two # indicate the precipitated heavy and light IgG chains of anti-HA, respectively, used for the co-immunoprecipitations (Note: the 3xHA-tagged ADGRV1_CTF band runs very close to the IgG heavy chain.). Loading controls to c are shown in Supplementary Figure S3D.

The TAP prey, that was related to most of the GO terms in our enrichment analysis, were the eight components of the chaperonin-containing T (CCT)-complex, also known as the TCP1 ring complex (TRiC) (Ghozlan et al., 2022). In addition, STRING analysis demonstrated that the eight CCT subunits are directly connected to numerous additional prey in the ADGRV1-CIB2 interactome (Figure 3D). The CCT complex subunits form a double ring with inter- and intra-ring contact sites, which build up a cylindrical structure with a central cavity, where polypeptides are inserted and folded (Figure 3E).

ADGRV1 interacts with the CCT3 subunit of the TriC/CCT chaperonin complex

Since there is increasing evidence for the participation of CCTs in retinal function (Sinha et al., 2014; Minegishi et al., 2016), we further dissected the interaction of ADGRV1 and CIB2 with the complex subunit CCT3. For this, we co-expressed FLAG-myc-tagged CCT3 and 3xHA-ADGRV1_CTF in HEK293T cells and incubated the cell lysate with anti-FLAG® M2 beads. After anti-FLAG pull-downs we subjected the recovered proteins to Western blots and

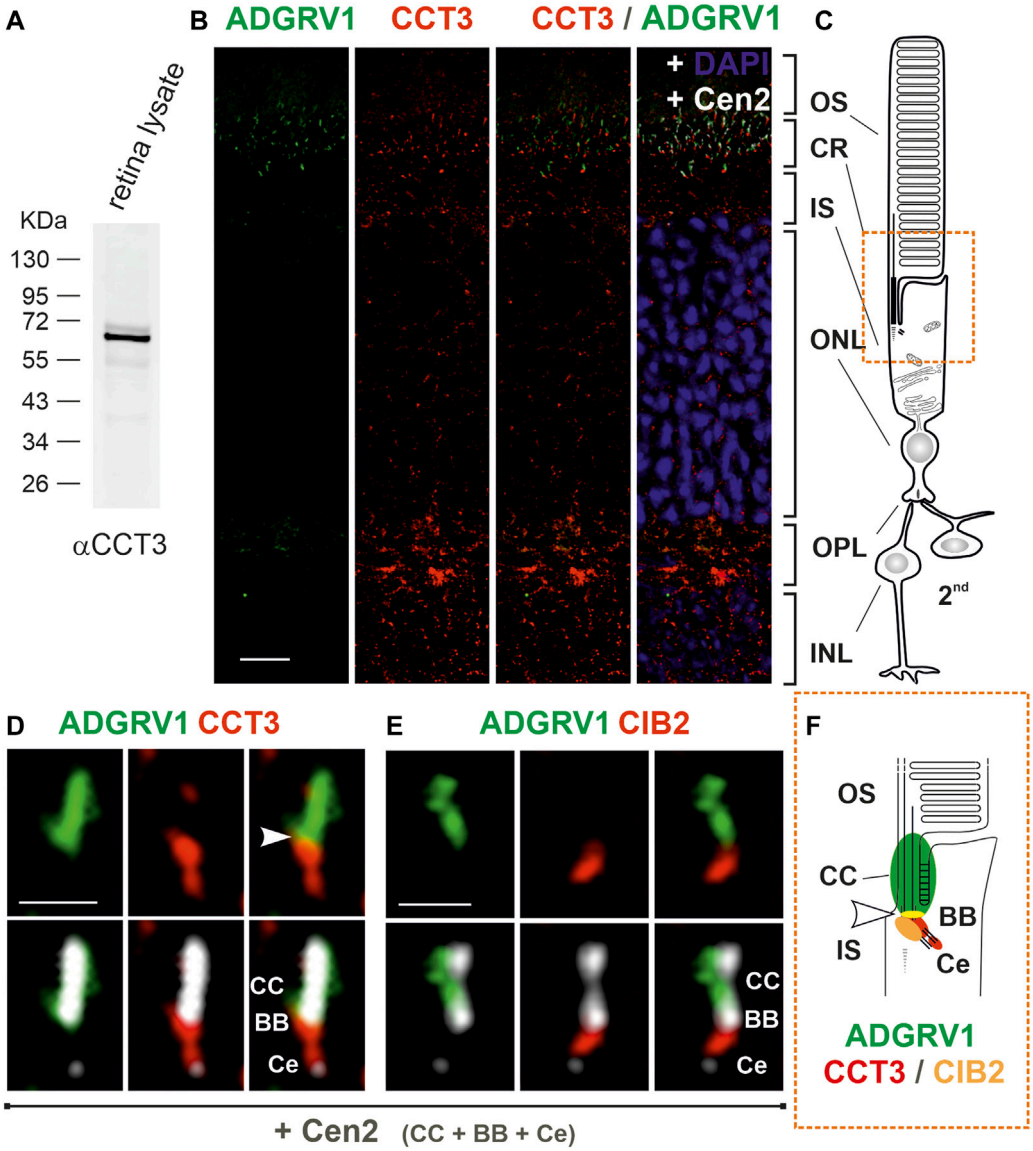

FIGURE 5
Subcellular localization of CCT3, ADGRV1 and CIB2 in murine retinal photoreceptor cells. **(A)** Anti-CCT3 Western blot of murine retina lysate reveals a band at ~ 60 kDa, the predicted molecular weight. **(B)** Immunofluorescence triple-labeling of ADGRV1, CCT3 and centrin 2 (Cen2), a marker for the connecting cilium, basal body and centriole, counterstained with DAPI as a nuclear DNA marker on cryosections through a murine retina. **(C)** Schema of a rod photoreceptor cell, linked to 2nd neurons. The comparison of **(B, C)** demonstrates the localization of CCT3 in the outer plexiform layer (OPL, synapse), the outer nuclear layer (ONL, somata), the inner segment (IS) and the ciliary region (CR, orange box) and CCT3—ADGRV1 co-localization in the ciliary. **(D)** Higher magnification of the ciliary region of a CCT3—ADGRV1—Cen2 triple-stained photoreceptor cell reveals the localization of ADGRV1 at the connecting cilium (CC) and CCT3 in the basal body (BB) and the proximal daughter centriole (Ce) with a little overlap (arrowhead). **(E)** Higher magnification of the ciliary region of a CIB2—ADGRV1—Cen2 triple-stained photoreceptor cell from Figure 2D shows the localization of ADGRV1 at the connecting cilium (CC) and CIB 2 in the basal body (BB) with less overlap (arrowhead). **(F)** Schematic representation of the spatial arrangement of ADGRV1, CIB2 and CCT3 in the primary cilium of photoreceptor cells (ciliary region). CIB2 and CCT3 co-localize the basal body proximal to the ADGRV1 present at the connecting cilium (CC). Arrowhead point to the co-localization of ADGRV1 with CCT3 and CIB2. CCT3 is additionally localized in Ce. INL, inner nuclear layer. Scale bars: b = 10 μm; d, e = 1 μm.

observed binding of CCT3 to ADGRV1_CTF, but not to the intracellular domain of ADGRV1 (ADGRV1_ICD) alone or to the negative control centrin 1, an EF-hand motif-containing Ca^{2+}-binding protein (Trojan et al., 2008) (Figure 4A). In contrast, ADGRV1_CTF was not recovered control precipitations with anti-FLAG beads only (Supplementary Figures S3A–C) and CIB2 was not co-precipitated with CCT3 in this experimental setting (Figure 4B).

Next, we performed reciprocal co-immunoprecipitations and incubated the cell lysate with anti-HA beads (Figure 4C). Western blots of anti-HA-pull-downs also showed the binding of CCT3 to ADGRV1_CTF (Figure 4C, right blot, 1st lane) and no binding to the intracellular domain of ADGRV1 (ADGRV1_ICD) or to centrin 1 (Figure 4C), confirming the findings in anti-FLAG-pull-downs (Figures 4A, B). In addition, however, a small substantial portion of

CCT3 was precipitated by CIB2 in the anti-HA-immunoprecipitation settings (Figure 4C, fade band indicated by *white arrow*). In contrast, in mock-transfected and single transfected cells expressing FLAG-myc-CCT3, respectively no bands were detectable. Taken together, these findings indicated that CCT3 interacts with the cytoplasmic face of the 7-transmembrane part of ADGRV1, most probably with one of the three intracellular loops and that CIB2 also loosely binds to CCT3.

CCT3 localizes to the ciliary region of photoreceptor cells

It has been previously shown that components of the CCT complex are localized at the base of primary cilia (Seixas et al., 2010; Seo et al., 2010; Kypri et al., 2014). Given that the connecting cilium and photosensitive outer segment of photoreceptor cells represent a modified primary cilium (Roepman and Wolfrum, 2007; May-Simera et al., 2017), we aimed to examine the expression and spatial distribution of CCT3 in the murine retina (Figure 5). In Western blots with antibodies against CCT3 we detected in protein lysate of the murine retina a prominent band at a proximal molecular weight of ~ 60 kDa, which is in accordance with the predicted size of CCT3 (Figure 5A). Immunohistochemistry in longitudinal cryosections through murine retina cryosections revealed puncta-like staining of CCT3 (Figure 5B). Triple immunostaining of CCT3, ADGRV1, and the ciliary marker protein centrin 2 in retinal sections demonstrated the localization of CCT3 in the outer plexiform layer, the outer nuclear layer, the inner segments of photoreceptors, and indicated co-localization with ADGRV1 in the ciliary region of photoreceptor cells (Figures 5B, C). Higher magnification of the ciliary region of the triple-stained photoreceptor cells confirmed the localization of ADGRV1 at the connecting cilium and the localization of CCT3 in the basal body and proximal daughter centriole with a slight co-localization of both proteins at the junction of the basal body with the connecting cilium (arrowhead) (Figure 5D). A comparison of this staining pattern with the triple staining for ADGRV1, CIB2, and centrin (Figure 5E) indicated the co-localization of CIB2 with CCT3 in the basal body but only a slight co-localization of both proteins with ADGRV1 (Figure 5F). To determine whether the expression profile of CCT3 in the retina can be extended to other molecules of the TRiC/CCT-chaperonin complex, we also examined the expression of CCT2 in the mouse retina (Supplementary Figure S4). Anti-CCT2 Western of retinal lysates revealed bands of the expected size of CCT2 molecules, but also bands of high molecular weight, possibly representing dimers and oligomers (Supplementary Figure S4A), which were previously suspected (Collier et al. (2021). Immunohistochemistry also revealed punctate labeling of CCT2 in the retinal layers (Supplementary Figure S4B), especially in the inner segments and ciliary region of the photoreceptors (Supplementary Figure S4C).

ADGRV1 and CIB2 interact with the three chaperonin-like BBS proteins

In primary cilia, the interaction of the cytoplasmic TRiC/CCT chaperonin complex with the three chaperonin-like BBS proteins BBS6, BBS10, and BBS12 mediates the assembly of the BBSome (Figure 6A) (Seo et al., 2010). This interaction of CCTs with the chaperonin-like BBS proteins raised the possibility that these may also interact with ADGRV1 and CIB2. To investigate this, we performed RFP-Traps® with ADGRV1a and BBS6, BBS10 and BBS12 (Figures 5B–D). We expressed SF-ADGRV1a or SF-CIB2 together with RFP-tagged BBS6, BBS10, BBS12, or centrin-1, respectively, in HEK293T cells and incubated cell lysates with RFP-Trap® beads for RFP-Trap®-precipitations. Western blot analyses of the recovered proteins revealed the co-precipitation of ADGRV1a and CIB2 with all three BBS chaperone-like proteins (Figures 6B–D). In contrast, neither ADGRV1 nor CIB2 was co-precipitated in the control RFP-Trap®-precipitations with the RFP-tagged centrin 1 (Figures 6B–D). An exemplary GST pull-down with bacterially expressed GST-BBS6 and His-tagged ADGRV1_ICD confirmed the direct interaction between BBS molecules and ADGRV1 (Supplementary Figure S5).

Taken together, the present interaction assays revealed that ADGRV1 and CIB2 interact with the three chaperonin-like BBS proteins.

Discussion

The knowledge of the function of molecules associated with IRDs is an important prerequisite to define targets for cure and treatment. There is broad agreement in the field that the interacting partners of a protein and the associated protein networks provide clues to cellular modules and thus to the function of a protein (Gavin et al., 2006; Boldt et al., 2016). In our search for interaction partners, we have previously identified numerous putative interacting proteins of the USH2C protein ADGRV1 by applying our affinity capture proteomics strategy (Knapp et al., 2022). The identified molecules pointed to cellular modules in which ADGRV1 acts in concert with those molecules. Recent more detailed studies on some of these modules related to ADGRV1 demonstrated the association of ADGRV1 with focal adhesions where it is involved in mechanosensation during cell motility (Kusuluri et al., 2021; Güler et al., 2023). In addition, we showed the localization of ADGRV1 in mitochondria-associated ER membranes (MAMs), important for the maintenance of Ca^{2+}-homeostasis (Krzysko et al., 2022), 2022) and that ADGRV1 controls autophagy processes and cellular proteostasis (Linnert et al., 2023). Moreover, others and we have previously shown that the USH2C protein ADGRV1 is part of the USH interactome interacting with both other USH2 proteins, usherin (USH2A) and whirlin (USH2D), and the two USH1 proteins myosin VIIa (USH1B) and harmonin (USH1C) (Reiners et al., 2005; van Wijk et al., 2006; Michalski et al., 2007; Wang et al., 2023). The putative USH1J protein CIB2 also interacts with the USH proteins whirlin and myosin VIIa (Riazuddin et al., 2012), and the interaction between ADGRV1 and CIB2 that we describe here confirms that CIB2 is part of the USH interactome.

However, the present comparison of the interactomes CIB2 and ADGRV1 revealed that they not only share the USH proteins whirlin and myosin VIIa as binding proteins, but also numerous additional other interaction partners. Of the 386 putative proteins identified as interaction partners of CIB2, 270 (2/3) proteins are also reported to be binding partners of ADGRV1 (Knapp et al., 2019;

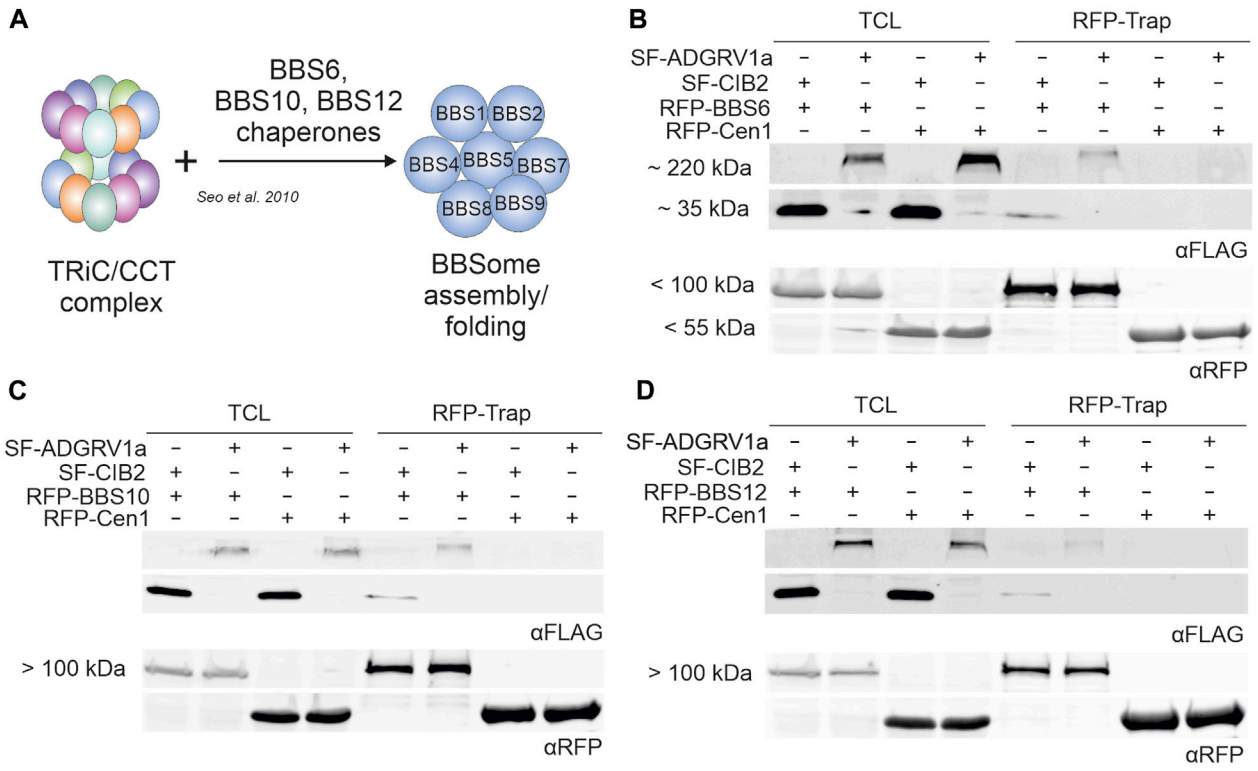

FIGURE 6
RFP-Trap®-precipitations of ADGRV1 and CIB2 with RFP-tagged chaperonin-like BBS proteins BBS6, BBS10 and BBS12. **(A)** Schematic representation of the assembly of the BBSome mediated by the TRiC/CCT chaperonin ring complex and the chaperonin-like BBS proteins BBS6, BBS10, and BBS12. **(B–D)** Anti-FLAG and anti-RFP Western blots of RFP-Trap®-precipitations from cell lysates co-expressing SF-ADGRV1 or SF-CIB2 together with RFP-tagged BBS6 **(B)**, BBS10 **(C)**, BBS12 **(D)** or RFP-centrin 1 (Cen1), respectively. Both ADGRV1 and CIB2 were recovered by all three RFP-tagged chaperonin-like BBS proteins BBS6, BBS10, and BBS12, but not by the control GFP-Cen1, indicating a specific interaction of ADGRV1 and CIB2 with chaperonin-like BBS proteins. TCL, total cell lysate.

Knapp et al., 2022) (Figure 1C). Furthermore, present STRING analyses show that most of the common interaction partners of CIB2 and ADGRV1, namely, 244 proteins, are also interconnected in protein networks (Figure 1D) and are part of functional modules, which we confirmed by GO term analyses. We conclude that the functions of CIB2 and ADGRV1 are linked and that both participate in shared processes and joint pathways in the cell.

We have previously described ADGRV1 as a component of focal adhesions interacting with several of their key components such as integrins (Kusuluri et al., 2021; Güler et al., 2023). α/β-integrin heterodimers play essential roles in outside-in and/or inside-out signaling at focal adhesions (Shen et al., 2012; Sun et al., 2016). Although the binding of integrins to CIB2 is well documented and eponymous for CIB2 (Dal Cortivo and Dell'orco, 2022), we could not detect CIB2 at focal adhesions of murine astrocytes (Supplementary Figure S2). The absence of CIB2 from focal adhesions of astrocytes may be due to the fact that CIB2 binds to the cytoplasmic tails of specific α-/β-integrin heterodimers, namely, αIIbβ3 and α7Bβ1 which have been previously found in platelets and megakaryocytes, and in skeletal muscles, but not related to focal adhesions so far (Denofrio et al., 2008; Häger et al., 2008). In any case, according to our data, CIB2 is not expressed in focal adhesions and, consequently, cannot be a functional partner for ADGRV1 there.

Nevertheless, both CIB2 and ADGRV1 are localized at the base of primary cilia, the sensory "ciliary" outer segment of retinal photoreceptor cells and confirmed in the primary cilia model cell line of hTERT-RPE1 cells (Figures 2D, 5E, F; Supplementary Figure S2B). At the ciliary base of photoreceptor cells ADGRV1 has been previously identified as a component of the periciliary membrane complex (PCM) (Maerker et al., 2008; Cosgrove and Zallocchi, 2014; Mathur and Yang, 2015). In the PCM complex, the cytoplasmic domains of ADGRV1 and USH2A are anchored by the scaffold protein whirlin in the cytoplasm of the apical extension of the photoreceptor inner segment where myosin VIIa and USH1G protein SANS are also localized (Liu et al., 1997; van Wijk et al., 2006; Maerker et al., 2008). It is thought that the PCM complex is important for targeting cargos with outer segment destination to the ciliary base and the subsequent handover of these cargos to the ciliary or intraflagellar transport (IFT) systems associated with kinesin 2 or myosin VIIA in the photoreceptor cilium (Maerker et al., 2008; Sedmak and Wolfrum, 2010; May-Simera et al., 2017; Sorusch et al., 2019). The subcellular localization of CIB2 at the ciliary base together with the interaction of CIB2 to several USH proteins of the PMC suggests that CIB2 is also part of the PMC complex in photoreceptor cells.

Besides the PMC the heterooctameric BBSome is localized in the periciliary region of the cilia base. There the BBSome acts as a cargo adapter for membrane proteins such as GPCRs and links cargo to the intraflagellar transport machinery (Jin and Nachury, 2009; Lechtreck et al., 2022). The BBSome is formed via intrinsic protein-protein interactions of BBS proteins of the complex with the BBS-type chaperones BBS6, BBS10 and BBS12 in cooperation with the double ring-shaped TRiC/CCT chaperonin complex (Figures 3E, 6A) (Seo et al., 2010; Zhang et al., 2012). Here, we have demonstrated the interaction of CIB2 and ADGRV1 with both the TRiC/CCT chaperonin complex and the three BBS-type chaperones. Our data also indicate that this interaction occurs at the ciliary base which is in accordance with previous reports on the presence of CCT subunits in ciliary protein networks, which was revealed by TAP (Boldt et al., 2016) and other affinity proteomic screens with centrosomal and ciliary proteins (Sang et al., 2011; Gupta et al., 2015). This interaction of CIB2 and ADGRV1 with the TRiC/CCT-BBS chaperonins indicates molecular links of CIB2 and ADGRV1 to the assembly machinery of the BBSome at the base of primary cilia. Furthermore, these data suggest that CIB2 and ADGRV1 take part in chaperonin functions or alternatively both proteins may represent substrates for the chaperonin complex. Interestingly, there is growing evidence that USH protein complexes are preassembled in the ER (Blanco-Sánchez et al., 2014) before being transported to their final ciliary destination. It is conceivable that they are transported in a pre-folded inactive state and only achieve full functionality by TRiC/CCT-BBS-chaperonin-mediated folding when they reach the ciliary base. However, in the lack of mechanistic insights, the question of whether CIB2 and ADGRV1 are clients of the TRiC/CCT/BBS chaperone complex like the BBSome or contribute to the activity of the chaperone complex will be the subject of further investigations. This may also shed light on the possible interplay between the machineries of the BBSome and the PCM in ciliary transport.

Mutations in *CIB2* and *ADGRV1* were described as causative for human USH, for the subtypes USH1J and USH2C, respectively (Weston et al., 2004; Riazuddin et al., 2012). The association between mutations in *CIB2* with the retinal and vestibular phenotypes in USH1 has recently been debated (Dal Cortivo and Dell'orco, 2022; Delmaghani and El-Amraoui, 2022). However, the close relation by physical interaction, the ciliary co-localization, and the shared protein interactions in a common large interactome found in the present study support a functional interplay of CIB2 and ADGRV1 in retinal photoreceptor cells. Whether this qualifies CIB2 as a USH1 gene must be determined by future studies.

Are the molecular and functional connections between USH proteins, the components of the TRiC/CCT chaperone complex, and various BBS molecules relevant to ocular diseases? Our results here are consistent with the essential chaperone function of CCTs during the biogenesis of photoreceptor cilia in mice (Sinha et al., 2014), which is supported by the identification of mutations in *CCT2* causing retinal degenerations in LCA patients (Minegishi et al., 2016). Moreover, due to the presence of defects in photoreceptor cilia in cell and animal models for USH, evidence has been accumulating in recent years that USH is considered a retinal ciliopathy (Bujakowska et al., 2017; May-Simera et al., 2017; Grotz et al., 2022) which is consistent with the ciliary association of CIB2 and ADGRV1 described here. In addition, the interaction of both USH proteins with BBS molecules as well as their subcellular localization in photoreceptors may hint at a yet enigmatic function of both proteins at the periciliary membrane complex, which controls transport selectivity of proteins from the inner to the outer segment of photoreceptors via ciliary transport. We have recently observed another molecular link between USH and BBS based on the molecular interaction of the USH1G protein SANS with CEP290 (Sorusch et al., 2014). Like in most BBS genes mutations in *CEP290,* also known as *BBS14*, can lead to other, mostly more severe ciliopathies, such as nephronophthisis (NPHP), Meckel-Gruber syndrome (MKS), and Joubert syndrome (JBTS) but also to non-syndromic retinal dystrophies, namely, LCA (Forsythe and Beales, 2013; McConnachie et al., 2021; Delvallée and Dollfus, 2023). The common visual ciliary phenotype in USH, BBS, and LCA based on the diverse disease molecules participating in common pathways are most probably based on defects in ciliary modules such as post-translational modification by chaperonin complexes.

Conclusion

The association of CIB2 and ADGRV1 with a larger ciliary network shared by USH, BBS, and certain forms of LCA, strongly suggests a role of both proteins in ciliary cargo selection and transport. This is further supported by the fact that mutations in these proteins affect both rod and cone photoreceptors. The overlapping protein networks of both syndromic retinal dystrophies BBS and USH suggest shared pathomechanisms for both syndromes on the molecular level, which bears the chance to identify common therapeutic targets for the correction of the causative defects in a mutation-independent fashion in patients affected by these ciliopathies.

Data availability statement

Full Western blots presented in the study are included in the article/Supplementary Material. The mass spectrometry proteomics data have been deposited to the ProteomeXchange Consortium via the PRIDE partner repository with the dataset identifier PXD042629.

Ethics statement

The animal study was reviewed and approved by The use of mice in research was approved by District administration Mainz-Bingen, 41a/177-5865-§11 ZVTE, 30.04.2014.

Author contributions

All authors contributed to the article and approved the submitted version. JL contributed to the TAP data analyses, immunocytochemistry experiments, and protein-protein interaction assays. BK conducted most of the experiments, analyzed tandem affinity purification (TAP) data sets, and prepared most figures of the publication. BEG performed immunocytochemical analyses in cells. KB and MU carried out mass

spectrometry analysis and analyzed data. BK and UW conceptualized the studies. BK and JL drafted the manuscript and UW revised and wrote the manuscript.

Funding

This work was supported by the Deutsche Forschungsgemeinschaft (DFG): FOR 2149 Elucidation of Adhesion-GPCR signaling, project number 246212759 (UW) and in the framework of the DFG SPP2127—Gene and Cell based therapies to counteract neuroretinal degeneration, project number 399487434 (UW), The Foundation Fighting Blindness (FFB) PPA-0717-0719-RAD (UW and MU), and inneruniversitäre Forschungsförderung ("Stufe I") of the Johannes Gutenberg University Mainz (UW).

Acknowledgments

We thank Ulrike Maas, Yvonne Kerner, and Gabi Stern-Schneider for excellent technical assistance, and Kerstin Nagel-Wolfrum for critical discussion of the present data.

Conflict of interest

The authors declare that the research was conducted in the absence of any commercial or financial relationships that could be construed as a potential conflict of interest.

Publisher's note

Supplementary material

The Supplementary Material for this article can be found online at: https://www.frontiersin.org/articles/10.3389/fcell.2023.1199069/full#supplementary-material

References

Alvarez-Satta, M., Castro-Sánchez, S., and Valverde, D. (2017). Bardet-biedl syndrome as a chaperonopathy: Dissecting the major role of chaperonin-like BBS proteins (BBS6-BBS10-BBS12). *Front. Mol. Biosci.* 4, 55–57. doi:10.3389/fmolb.2017.00055

Bettencourt-Dias, M., Hildebrandt, F., Pellman, D., Woods, G., and Godinho, S. A. (2011). Centrosomes and cilia in human disease. *Trends Genet.* 27, 307–315. doi:10.1016/j.tig.2011.05.004

Bindea, G., Mlecnik, B., Hackl, H., Charoentong, P., Tosolini, M., Kirilovsky, A., et al. (2009). ClueGO: A Cytoscape plug-in to decipher functionally grouped gene ontology and pathway annotation networks. *Bioinformatics* 25, 1091–1093. doi:10.1093/bioinformatics/btp101

Blanco-Sánchez, B., Clément, A., Fierro, J., Washbourne, P., and Westerfield, M. (2014). Complexes of Usher proteins preassemble at the endoplasmic reticulum and are required for trafficking and ER homeostasis. *DMM Dis. Model. Mech.* 7, 547–559. doi:10.1242/dmm.014068

Boldt, K., Van Reeuwijk, J., Lu, Q., Koutroumpas, K., Nguyen, T. M. T., Texier, Y., et al. (2016). An organelle-specific protein landscape identifies novel diseases and molecular mechanisms. *Nat. Commun.* 7, 11491. doi:10.1038/ncomms11491

Booth, K. T., Kahrizi, K., Babanejad, M., Daghagh, H., Bademci, G., Arzhangi, S., et al. (2018). Variants in CIB2 cause DFNB48 and not USH1J. *Clin. Genet.* 93, 812–821. doi:10.1111/cge.13170

Brackley, K. I., and Grantham, J. (2009). Activities of the chaperonin containing TCP-1 (CCT): Implications for cell cycle progression and cytoskeletal organisation. *Cell. Stress Chaperones* 14, 23–31. doi:10.1007/s12192-008-0057-x

Braun, D. A., and Hildebrandt, F. (2017). Ciliopathies. *Cold Spring Harb. Perspect. Biol.* 9, a028191. doi:10.1101/cshperspect.a028191

Bujakowska, K. M., Liu, Q., and Pierce, E. A. (2017). Photoreceptor cilia and retinal ciliopathies. *Cold Spring Harb. Perspect. Biol.* 9, a028274. doi:10.1101/cshperspect.a028274

Collier, M. P., Moreira, K. B., Li, K. H., Chen, Y. C., Itzhak, D., Samant, R., et al. (2021). Native mass spectrometry analyses of chaperonin complex TRiC/CCT reveal subunit N-terminal processing and re-association patterns. *Sci. Rep.* 11, 13084. doi:10.1038/s41598-021-91086-6

Cosgrove, D., and Zallocchi, M. (2014). Usher protein functions in hair cells and photoreceptors. *Int. J. Biochem. Cell. Biol.* 46, 80–89. doi:10.1016/j.biocel.2013.11.001

Dal Cortivo, G., and Dell'orco, D. (2022). Calcium-and integrin-binding protein 2 (CIB2) in Physiology and disease: Bright and dark sides. *Int. J. Mol. Sci.* 23, 3552. doi:10.3390/ijms23073552

Dekker, C., Stirling, P. C., McCormack, E. A., Filmore, H., Paul, A., Brost, R. L., et al. (2008). The interaction network of the chaperonin CCT. *EMBO J.* 27, 1827–1839. doi:10.1038/emboj.2008.108

Delmaghani, S., and El-Amraoui, A. (2022). The genetic and phenotypic landscapes of usher syndrome: From disease mechanisms to a new classification. *Hum. Genet.* 141, 709–735. doi:10.1007/s00439-022-02448-7

Delvallée, C., and Dollfus, H. (2023). Retinal degeneration animal models in bardet– biedl syndrome and related ciliopathies. *Cold Spring Harb. Perspect. Med.* 13, a041303. doi:10.1101/CSHPERSPECT.A041303

Denofrio, J. C., Yuan, W., Temple, B. R., Gentry, H. R., and Parise, L. V. (2008). Characterization of calcium- and integrin-binding protein 1 (CIB1) knockout platelets: Potential compensation by CIB family members. *Thromb. Haemost.* 100, 847–856. doi:10.1160/TH08-06-0351

Evans, A. L., and Müller, U. (2000). Stereocilia defects in the sensory hair cells of the inner ear in mice deficient in integrin alpha8beta1. *Nat. Genet.* 24, 424–428. doi:10.1038/74286

Forsythe, E., and Beales, P. L. (2013). Bardet-Biedl syndrome. *Eur. J. Hum. Genet.* 21, 8–13. doi:10.1038/ejhg.2012.115

Fuster-García, C., García-Bohórquez, B., Rodríguez-Muñoz, A., Aller, E., Jaijo, T., Millán, J. M., et al. (2021). Usher syndrome: Genetics of a human ciliopathy. *Int. J. Mol. Sci.* 22, 6723–6725. doi:10.3390/ijms22136723

Gavin, A. C., Aloy, P., Grandi, P., Krause, R., Boesche, M., Marzioch, M., et al. (2006). Proteome survey reveals modularity of the yeast cell machinery. *Nature* 440, 631–636. doi:10.1038/nature04532

Ghozlan, H., Cox, A., Nierenberg, D., King, S., and Khaled, A. R. (2022). The TRiCky business of protein folding in Health and disease. *Front. Cell. Dev. Biol.* 10, 906530. doi:10.3389/fcell.2022.906530

Gloeckner, C. J., Boldt, K., Schumacher, A., Roepman, R., and Ueffing, M. (2007). A novel tandem affinity purification strategy for the efficient isolation and characterisation of native protein complexes. *Proteomics* 7, 4228–4234. doi:10.1002/pmic.200700038

Grotz, S., Schäfer, J., Wunderlich, K. A., Ellederova, Z., Auch, H., Bähr, A., et al. (2022). Early disruption of photoreceptor cell architecture and loss of vision in a humanized pig model of usher syndromes. *EMBO Mol. Med.* 14, e14817–e14824. doi:10.15252/emmm.202114817

Güler, B. E., Linnert, J., and Wolfrum, U. (2023). Monitoring paxillin in astrocytes reveals the significance of the adhesion G protein coupled receptor VLGR1/ADGRV1 for focal adhesion assembly. *Basic Clin. Pharmacol. Toxicol.* Online ahead of print. doi:10.1111/bcpt.13860

Gupta, G. D., Coyaud, É., Gonçalves, J., Mojarad, B. A., Liu, Y., Wu, Q., et al. (2015). A dynamic protein interaction landscape of the human centrosome-cilium interface. *Cell.* 163, 1484–1499. doi:10.1016/j.cell.2015.10.065

Häger, M., Bigotti, M. G., Meszaros, R., Carmignac, V., Holmberg, J., Allamand, V., et al. (2008). Cib2 binds integrin alpha7Bbeta1D and is reduced in laminin alpha2 chain-deficient muscular dystrophy. *J. Biol. Chem.* 283, 24760–24769. doi:10.1074/jbc.M801166200

Hamann, J., Aust, G., Araç, D., Engel, F. B., Formstone, C., Fredriksson, R., et al. (2015). International union of basic and clinical pharmacology. XCIV. adhesion G protein-coupled receptors. *Pharmacol. Rev.* 67, 338–367. doi:10.1124/pr.114.009647

Higginbotham, H., Bielas, S., Tanaka, T., and Gleeson, J. G. (2004). Transgenic mouse line with green-fluorescent protein-labeled Centrin 2 allows visualization of the centrosome in living cells. *Transgenic. Res.* 13, 155–164. doi:10.1023/b:trag.0000026071.41735.8e

Jacoszek, A., Pollak, A., Płoski, R., and Ołdak, M. (2017). Advances in genetic hearing loss: CIB2 gene. *Eur. Arch. Oto-Rhino-Laryngology* 274, 1791–1795. doi:10.1007/s00405-016-4330-9

Jin, H., and Nachury, M. V. (2009). The BBSome. *Curr. Biol.* 19, 472–473. doi:10.1016/j.cub.2009.04.015

Jin, H., White, S. R., Shida, T., Schulz, S., Aguiar, M., Gygi, S. P., et al. (2010). The conserved bardet-biedl syndrome proteins assemble a coat that traffics membrane proteins to Cilia. *Cell.* 141, 1208–1219. doi:10.1016/j.cell.2010.05.015

Jouret, G., Poirsier, C., Spodenkiewicz, M., Jaquin, C., Gouy, E., Arndt, C., et al. (2019). Genetics of usher syndrome: New insights from a meta-analysis. *Otol. Neurotol.* 40, 121–129. doi:10.1097/MAO.0000000000002054

Knapp, B., Roedig, J., Boldt, K., Krzysko, J., Horn, N., Ueffing, M., et al. (2019). Affinity proteomics identifies novel functional modules related to adhesion GPCRs. *Ann. N. Y. Acad. Sci.* 1456, 144–167. doi:10.1111/nyas.14220

Knapp, B., Roedig, J., Roedig, H., Krzysko, J., Horn, N., Güler, B. E., et al. (2022). Affinity proteomics identifies interaction partners and defines novel insights into the function of the adhesion GPCR VLGR1/ADGRV1. *Molecules* 27, 3108. doi:10.3390/molecules27103108

Krzysko, J., Maciag, F., Mertens, A., Güler, B. E., Linnert, J., Boldt, K., et al. (2022). The adhesion GPCR VLGR1/ADGRV1 regulates the Ca2+ homeostasis at mitochondria-associated ER membranes. *Cells* 11, 2790. doi:10.3390/cells11182790

Kusuluri, D. K., Güler, B. E., Knapp, B., Horn, N., Boldt, K., Ueffing, M., et al. (2021). Adhesion G protein-coupled receptor VLGR1/ADGRV1 regulates cell spreading and migration by mechanosensing at focal adhesions. *iScience* 24, 102283. doi:10.1016/j.isci.2021.102283

Kypri, E., Christodoulou, A., Maimaris, G., Lethan, M., Markaki, M., Lysandrou, C., et al. (2014). The nucleotide-binding proteins Nubp1 and Nubp2 are negative regulators of ciliogenesis. *Cell. Mol. Life Sci.* 71, 517–538. doi:10.1007/s00018-013-1401-6

Lechtreck, K. F., Liu, Y., Dai, J., Alkhofash, R. A., Butler, J., Alford, L., et al. (2022). Chlamydomonas ARMC2/PF27 is an obligate cargo adapter for intraflagellar transport of radial spokes. *Elife* 11, 1–24. doi:10.7554/eLife.74993

Linnert, J., Güler, B., Krzysko, J., and Wolfrum, U. (2023). The adhesion G-protein coupled receptor VLGR1/ADGRV1 controls autophagy. *Basic Clin. Pharmacol. Toxicol.* Online ahead of print. doi:10.1111/bcpt.13869

Liu, X., Vansant, G., Udovichenko, I. P., Wolfrum, U., and Williams, D. S. (1997). Myosin VIIa, the product of the Usher 1B syndrome gene, is concentrated in the connecting cilia of photoreceptor cells. *Cell. Motil. Cytoskelet.* 37, 240–252. doi:10.1002/(SICI)1097-0169(1997)37:3<240::AID-CM6>3.0.CO;2-A

Maerker, T., van Wijk, E., Overlack, N., Kersten, F. F. J., Mcgee, J., Goldmann, T., et al. (2008). A novel Usher protein network at the periciliary reloading point between molecular transport machineries in vertebrate photoreceptor cells. *Hum. Mol. Genet.* 17, 71–86. doi:10.1093/hmg/ddm285

Mathur, P., and Yang, J. (2015). Usher syndrome: Hearing loss, retinal degeneration and associated abnormalities. *Biochim. Biophys. Acta - Mol. Basis Dis.* 1852, 406–420. doi:10.1016/j.bbadis.2014.11.020

May-Simera, H., Nagel-Wolfrum, K., and Wolfrum, U. (2017). Cilia - the sensory antennae in the eye. *Prog. Retin. Eye Res.* 60, 144–180. doi:10.1016/j.preteyeres.2017.05.001

McConnachie, D. J., Stow, J. L., and Mallett, A. J. (2021). Ciliopathies and the kidney: A review. *Am. J. Kidney Dis.* 77, 410–419. doi:10.1053/j.ajkd.2020.08.012

McGee, J. A., Goodyear, R. J., McMillan, D. R., Stauffer, E. A., Holt, J. R., Locke, K. G., et al. (2006). The very large G-protein-coupled receptor VLGR1: A component of the ankle link complex required for the normal development of auditory hair bundles. *J. Neurosci.* 26, 6543–6553. doi:10.1523/JNEUROSCI.0693-06.2006

McMillan, D. R., and White, P. C. (2010). Studies on the very large G protein-coupled receptor: From initial discovery to determining its role in sensorineural deafness in higher animals. *Adv. Exp. Med. Biol.* 706, 76–86. doi:10.1007/978-1-4419-7913-1_6

Michalski, N., Michel, V., Bahloul, A., Lefèvre, G., Barral, J., Yagi, H., et al. (2007). Molecular characterization of the ankle-link complex in cochlear hair cells and its role in the hair bundle functioning. *J. Neurosci.* 27, 6478–6488. doi:10.1523/JNEUROSCI.0342-07.2007

Michel, V., Booth, K. T., Patni, P., Cortese, M., Azaiez, H., Bahloul, A., et al. (2017). CIB2, defective in isolated deafness, is key for auditory hair cell mechanotransduction and survival. *EMBO Mol. Med.* 9, 1711–1731. doi:10.15252/emmm.201708087

Minegishi, Y., Sheng, X., Yoshitake, K., Sergeev, Y., Iejima, D., Shibagaki, Y., et al. (2016). CCT2 mutations evoke leber congenital amaurosis due to chaperone complex instability. *Sci. Rep.* 6, 33742. doi:10.1038/srep33742

Mühlhans, J., Brandstätter, J. H., and Gießl, A. (2011). The centrosomal protein pericentrin identified at the basal body complex of the connecting cilium in mouse photoreceptors. *PLoS One* 6, e26496. doi:10.1371/journal.pone.0026496

Perez-Riverol, Y., Bai, J., Bandla, C., Hewapathirana, S., García-Seisdedos, D., Kamatchinathan, S., et al. (2022). The PRIDE database resources in 2022: A hub for mass spectrometry-based proteomics evidences. *Nucleic Acids Res.* 50 (D1), D543–D552. doi:10.1093/nar/gkab1038

Reiners, J., van Wijk, E., Märker, T., Zimmermann, U., Jürgens, K., te Brinke, H., et al. (2005). Scaffold protein harmonin (USH1C) provides molecular links between Usher syndrome type 1 and type 2. *Hum. Mol. Genet.* 14, 3933–3943. doi:10.1093/hmg/ddi417

Reiners, J., Nagel-Wolfrum, K., Jürgens, K., Märker, T., and Wolfrum, U. (2006). Molecular basis of human Usher syndrome: Deciphering the meshes of the Usher protein network provides insights into the pathomechanisms of the Usher disease. *Exp. Eye Res.* 83, 97–119. doi:10.1016/j.exer.2005.11.010

Riazuddin, S., Belyantseva, I. A., Giese, A. P. J., Lee, K., Indzhykulian, A. A., Nandamuri, S. P., et al. (2012). Alterations of the CIB2 calcium-and integrin-binding protein cause Usher syndrome type 1J and nonsyndromic deafness DFNB48. *Nat. Genet.* 44, 1265–1271. doi:10.1038/ng.2426

Roepman, R., and Wolfrum, U. (2007). Protein networks and complexes in photoreceptor cilia. *Subcell. Biochem.* 43, 209–235. doi:10.1007/978-1-4020-5943-8_10

Sang, L., Miller, J. J., Corbit, K. C., Giles, R. H., Brauer, M. J., Otto, E. A., et al. (2011). Mapping the NPHP-JBTS-MKS protein network reveals ciliopathy disease genes and pathways. *Cell.* 145, 513–528. doi:10.1016/j.cell.2011.04.019

Sedmak, T., and Wolfrum, U. (2010). Intraflagellar transport molecules in ciliary and nonciliary cells of the retina. *J. Cell. Biol.* 189, 171–186. doi:10.1083/jcb.200911095

Seixas, C., Cruto, T., Tavares, A., Gaertig, J., and Soares, H. (2010). CCTalpha and CCTdelta chaperonin subunits are essential and required for cilia assembly and maintenance in Tetrahymena. *PLoS One* 5, e10704. doi:10.1371/journal.pone.0010704

Seo, S., Baye, L. M., Schulz, N. P., Beck, J. S., Zhang, Q., Slusarski, D. C., et al. (2010). BBS6, BBS10, and BBS12 form a complex with CCT/TRiC family chaperonins and mediate BBSome assembly. *Proc. Natl. Acad. Sci. U. S. A.* 107, 1488–1493. doi:10.1073/pnas.0910268107

Sethna, S., Scott, P. A., Giese, A. P. J., Duncan, T., Jian, X., Riazuddin, S., et al. (2021). CIB2 regulates mTORC1 signaling and is essential for autophagy and visual function. *Nat. Commun.* 12, 3906–3919. doi:10.1038/s41467-021-24056-1

Shen, B., Delaney, M. K., and Du, X. (2012). Inside-out, outside-in, and inside-outside-in: G protein signaling in integrin-mediated cell adhesion, spreading, and retraction. *Curr. Opin. Cell. Biol.* 24, 600–606. doi:10.1016/j.ceb.2012.08.011

Sinha, S., Belcastro, M., Datta, P., Seo, S., and Sokolov, M. (2014). Essential role of the chaperonin CCT in rod outer segment biogenesis. *Investig. Ophthalmol. Vis. Sci.* 55, 3775–3785. doi:10.1167/iovs.14-13889

Sorusch, N., Wunderlich, K., Bauss, K., Nagel-Wolfrum, K., and Wolfrum, U. (2014). Usher syndrome protein network functions in the retina and their relation to other retinal ciliopathies. *Adv. Exp. Med. Biol.* 801, 527. doi:10.1007/978-1-4614-3209-8_67

Sorusch, N., Baub, K., Plutniok, J., Samanta, A., Knapp, B., Nagel-Wolfrum, K., et al. (2017). Characterization of the ternary Usher syndrome SANS/ush2a/whirlin protein complex. *Hum. Mol. Genet.* 26, 1157–1172. doi:10.1093/hmg/ddx027

Sorusch, N., Yildirim, A., Knapp, B., Janson, J., Fleck, W., Scharf, C., et al. (2019). SANS (USH1G) molecularly links the human usher syndrome protein network to the intraflagellar transport module by direct binding to IFT-B proteins. *Front. Cell. Dev. Biol.* 7, 216–313. doi:10.3389/fcell.2019.00216

Sun, Z., Guo, S. S., and Fässler, R. (2016). Integrin-mediated mechanotransduction. *J. Cell. Biol.* 215, 445–456. doi:10.1083/jcb.201609037

Trojan, P., Krauss, N., Choe, H. W., Gießl, A., Pulvermüller, A., and Wolfrum, U. (2008). Centrins in retinal photoreceptor cells: Regulators in the connecting cilium. *Prog. Retin. Eye Res.* 27, 237–259. doi:10.1016/j.preteyeres.2008.01.003

van Wijk, E., van der Zwaag, B., Peters, T., Zimmermann, U., te Brinke, H., Kersten, F. F. J., et al. (2006). The DFNB31 gene product whirlin connects to the Usher protein network in the cochlea and retina by direct association with USH2A and VLGR1. *Hum. Mol. Genet.* 15, 751–765. doi:10.1093/hmg/ddi490

Van Wijk, E., Kersten, F. F. J., Kartono, A., Mans, D. A., Brandwijk, K., Letteboer, S. J. F., et al. (2009). Usher syndrome and Leber congenital amaurosis are molecularly linked via a novel isoform of the centrosomal ninein-like protein. *Hum. Mol. Genet.* 18, 51–64. doi:10.1093/hmg/ddn312

Wang, H., Du, H., Ren, R., Du, T., Lin, L., Feng, Z., et al. (2023). Temporal and spatial assembly of inner ear hair cell ankle link condensate through phase separation. *Nat. Commun.* 14, 1657. doi:10.1038/s41467-023-37267-5

Weston, M. D., Luijendijk, M. W. J., Humphrey, K. D., Möller, C., and Kimberling, W. J. (2004). Mutations in the VLGR1 gene implicate G-protein signaling in the pathogenesis of usher syndrome type II. *Am. J. Hum. Genet.* 74, 357–366. doi:10.1086/381685

Wright, R. N., Hong, D. H., and Perkins, B. (2012). Rpgr ORF15 connects to the usher protein network through direct interactions with multiple whirlin isoforms. *Investig. Ophthalmol. Vis. Sci.* 53, 1519–1529. doi:10.1167/iovs.11-8845

Yagi, H., Tokano, H., Maeda, M., Takabayashi, T., Nagano, T., Kiyama, H., et al. (2007). Vlgr1 is required for proper stereocilia maturation of cochlear hair cells. *Genes. Cells* 12, 235–250. doi:10.1111/j.1365-2443.2007.01046.x

Zhang, Q., Yu, D., Seo, S., Stone, E. M., and Sheffield, V. C. (2012). Intrinsic protein-protein interaction-mediated and chaperonin-assisted sequential assembly of stable Bardet-Biedl syndrome protein complex, the BBSome. *J. Biol. Chem.* 287, 20625–20635. doi:10.1074/jbc.M112.341487

frontiers | Frontiers in Cell and Developmental Biology

TYPE Original Research
PUBLISHED 21 July 2023
DOI 10.3389/fcell.2023.1197744

OPEN ACCESS

EDITED BY
José M. Millan,
La Fe Health Research Institute, Spain

REVIEWED BY
Shushu Huang,
Yale University, United States
Douglas Forrest,
National Institutes of Health (NIH),
United States

*CORRESPONDENCE
Salud Borrego,
salud.borrego.sspa@juntadeandalucia.es
Guillermo Antiñolo,
gantinolo@us.es

†These authors have contributed equally to this work and share first authorship

RECEIVED 31 March 2023
ACCEPTED 27 June 2023
PUBLISHED 21 July 2023

CITATION
Fernández-Suárez E, González-del Pozo M, García-Núñez A, Méndez-Vidal C, Martín-Sánchez M, Mejías-Carrasco JM, Ramos-Jiménez M, Morillo-Sánchez MJ, Rodríguez-de la Rúa E, Borrego S and Antiñolo G (2023), Expanding the phenotype of *THRB*: a range of macular dystrophies as the major clinical manifestations in patients with a dominant splicing variant. *Front. Cell Dev. Biol.* 11:1197744. doi: 10.3389/fcell.2023.1197744

Expanding the phenotype of *THRB*: a range of macular dystrophies as the major clinical manifestations in patients with a dominant splicing variant

Elena Fernández-Suárez[1,2†], María González-del Pozo[1,2†], Alejandro García-Núñez[1], Cristina Méndez-Vidal[1,2], Marta Martín-Sánchez[1,2], José Manuel Mejías-Carrasco[1], Manuel Ramos-Jiménez[3], María José Morillo-Sánchez[4], Enrique Rodríguez-de la Rúa[4,5], Salud Borrego[1,2]* and Guillermo Antiñolo[1,2]*

[1]Department of Maternofetal Medicine, Genetics and Reproduction, Institute of Biomedicine of Seville (IBiS), University Hospital Virgen del Rocío/Spanish National Research Council (CSIC)/University of Seville, Seville, Spain, [2]Center for Biomedical Network Research on Rare Diseases (CIBERER), Seville, Spain, [3]Department of Clinical Neurophysiology, University Hospital Virgen Macarena, Seville, Spain, [4]Department of Ophthalmology, University Hospital Virgen Macarena, Seville, Spain, [5]RETICS Patología Ocular, OFTARED, Instituto de Salud Carlos III, Madrid, Spain

Inherited retinal dystrophies (IRDs) are a clinically and genetically heterogeneous group of disorders that often severely impair vision. Some patients manifest poor central vision as the first symptom due to cone-dysfunction, which is consistent with cone dystrophy (COD), Stargardt disease (STGD), or macular dystrophy (MD) among others. Here, we aimed to identify the genetic cause of autosomal dominant COD in one family. WGS was performed in 3 affected and 1 unaffected individual using the TruSeq Nano DNA library kit and the NovaSeq 6,000 platform (Illumina). Data analysis identified a novel spliceogenic variant (c.283 + 1G>A) in the thyroid hormone receptor beta gene (*THRB*) as the candidate disease-associated variant. Further genetic analysis revealed the presence of the same heterozygous variant segregating in two additional unrelated dominant pedigrees including 9 affected individuals with a diagnosis of COD (1), STGD (4), MD (3) and unclear phenotype (1). *THRB* has been previously reported as a causal gene for autosomal dominant and recessive thyroid hormone resistance syndrome beta (RTHβ); however, none of the IRD patients exhibited RTHβ. Genotype-phenotype correlations showed that RTHβ can be caused by both truncating and missense variants, which are mainly located at the 3′ (C-terminal/ligand-binding) region, which is common to both *THRB* isoforms (TRβ1 and TRβ2). In contrast, the c.283 + 1G>A variant is predicted to disrupt a splice site in the 5′-region of the gene that encodes the N-terminal domain of the TRβ1 isoform protein, leaving the TRβ2 isoform intact, which would explain the phenotypic variability observed between RTHβ and IRD patients. Interestingly, although monochromacy or cone response alterations have already been described in a few RTHβ patients, herein we report the first genetic association between a pathogenic variant in *THRB* and non-syndromic IRDs. We thereby expand the phenotype of *THRB* pathogenic variants including COD, STGD, or MD as the main

clinical manifestation, which also reflects the extraordinary complexity of retinal functions mediated by the different *THRB* isoforms.

KEYWORDS

cone dystrophy, Stargardt disease, macular dystrophy, autosomal dominant, *THRB*, thyroid hormone resistance, splicing variant

1 Introduction

Inherited retinal dystrophies (IRDs) constitute a complex group of rare disorders with extreme clinical and genetic heterogeneity, which cause visual loss due to improper development, dysfunction, or premature death of the retinal photoreceptors or the retinal pigment epithelial cells (Schneider et al., 2022). More than 50 major subtypes of IRDs have been described so far, which can be clinically classified based on the photoreceptor type that is primarily involved in disease pathogenesis. In patients starting with rods degeneration like retinitis pigmentosa (RP), the initial clinical symptoms are night blindness and tunnel vision since these cells are primarily located along the peripheral edges of the retina and are responsible for vision at low light levels (scotopic vision) (Himawan et al., 2019). In contrast, cones are mostly concentrated in the macula, the central portion of the retina and, are active at higher light levels (photopic vision). These cells are critical for visual acuity and color discrimination (Himawan et al., 2019). This means that the affected individuals with a primary cone dysfunction manifest poor central vision as the first symptom such as in cone dystrophy (COD), Stargardt disease (STGD), or macular dystrophy (MD) among others.

IRDs can be inherited as autosomal recessive (AR), autosomal dominant (AD), or X-linked (XL) disorders. Although in most cases, the disease is limited to the eye (non-syndromic), over 80 forms of syndromic IRD have been described (Tatour and Ben-Yosef, 2020). To date, more than 290 genes have been associated with some type of IRDs, (https://web.sph.uth.edu/RetNet/, accessed March 2023), of which about 50 genes are involved in cone-dominated diseases (Cremers et al., 2018). However, the overlapping causative genes and phenotypes tremendously complicate the genetic analysis of IRDs, and a relatively large percentage of affected individuals (~40%) remain genetically unsolved after routine analyses (Martín-Sánchez et al., 2020). In this sense, the application of a global approach like whole genome sequencing (WGS) promises to increase the diagnostic yield of IRDs through the identification of challenging variants like structural variants, deep-intronic variants, or variants in novel causative genes (Gonzalez-Del Pozo et al., 2022).

In the human retina, three different cones subtypes are distinguished, based on the expression of opsin proteins with different spectral sensitivities (Zhang et al., 2019). The red-opsin or L-cones are stimulated by long-wavelength light; the green-opsin or M-cones respond to medium-wavelength light; and, the blue-opsin or S-cones, are stimulated by short-wavelength light (Schmidt et al., 2019). In humans, S-cones are first specified, followed by M/L-cones. This specification is regulated by the thyroid hormones triiodothyronine (T3) and thyroxine (T4) signaling (Eldred et al., 2018), through the activation of the thyroid hormone receptor nuclear receptor (*THRB*) gene expression (Emerson et al., 2013). *THRB* gene produces two transcripts using alternative splicing: TRβ1, which is widely distributed, and TRβ2, which is limited to the cochlea, retina, and pituitary gland (Zaig et al., 2018). Both isoforms contain the typical domain structure of a nuclear receptor with an N-terminal domain (A/B) with hormone-independent transactivation activity; a central DNA-binding domain (DBD) consisting of two C4-type zinc fingers that recognized DNA motif in the regulatory regions of genes; a hinge region with a nuclear location signal; the C-terminal ligand-binding domain (LBD) with regions essential for hormone-dependent transactivation, and the AF2 domain (Tian et al., 2006) (Figure 1). These two transcripts only differ in the N-terminal domain (Zaig et al., 2018). Numerous studies in model organisms have established a role for TRβ2 during cone subtype specification (Ng et al., 2001; Roberts et al., 2005; Ng et al., 2009; Suzuki et al., 2013; Aramaki et al., 2022). In mice, the deletion of the specific isoform TRβ2 prompts the expression of only S-cones and the complete loss of M-cones, revealing an essential role for TRβ2 in M-cone identity (Ng et al., 2001). In addition, a wide range of studies in others model organisms, such as zebrafish or rats, also showed retinal abnormalities (McNerney and Johnston, 2021). Moreover, Eldred et al. demonstrated that in the absence of *THRB*, all cones developed into the S subtype using human retinal organoids. In addition to its role in cone opsin specification, THRB also regulates cone survival. Excess of T3 signaling through TRβ2 induces cone apoptosis (Ng et al., 2017). Taken together, these findings suggest an important role for *THRB* in cone-related disorders.

In fact, visual impairment and cones dysfunction have been noted in rare cases of thyroid hormone resistance syndrome beta (RTHβ) (Lindstedt et al., 1982; Frank-Raue et al., 2004; Weiss et al., 2012; Campi et al., 2017), a syndrome caused by variants in the *THRB* gene. RTHβ is a rare disease mainly inherited as an autosomal dominant pattern, although a few cases of autosomal recessive inheritance have been also reported (Refetoff et al., 1967; Takeda et al., 1991). RTHβ is characterized by inappropriate findings in the serum levels of free thyroid hormones (T3 and T4) with high circulating thyroid-stimulating hormone (TSH). Most RTHβ patients are considered clinically euthyroid and present a wide phenotypic variability, even among patients harboring the same variant in *THRB* (Campi et al., 2021). More than 190 truncating and missense variants have been associated with RTHβ (data from HGMD-pro, March 2023), most of which are located in the LBD (T3-binding) domain or in the contiguous hinge region (Figure 1). Interestingly, common SNPs in the intron control region (ICR) have been associated with the clinical variability in RTHβ (Alberobello et al., 2011).

Here, we identified a canonical spliceogenic variant affecting the A/B domain of the TRβ1 isoform of THRB in three unrelated Spanish families with a diagnosis of cone-dominated disorders (COD, STGD, and MD). To our knowledge, this is the first report of the identification of *THRB* variants in IRD patients,

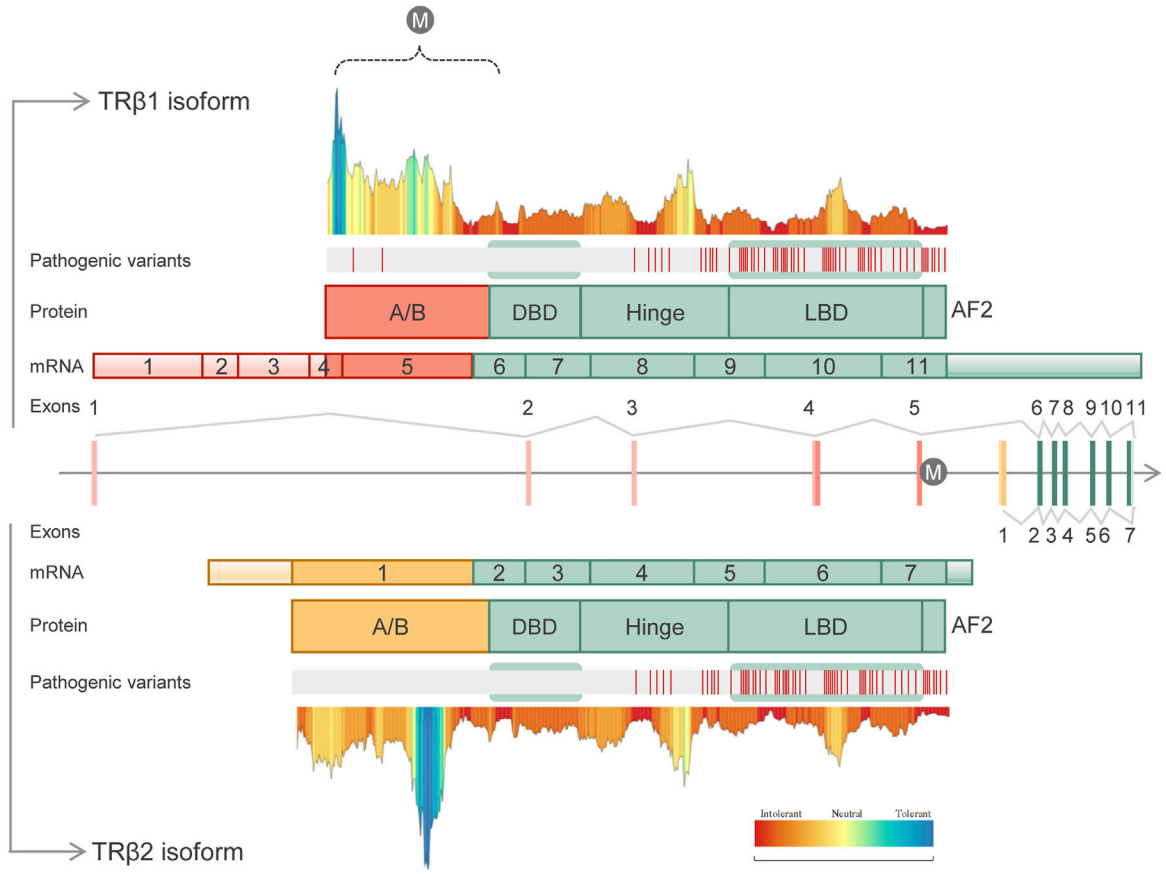

FIGURE 1
Schematic representation of the human *THRB* gene structure, transcripts, protein domains, distribution of known pathogenic variants and tolerance landscape. The identified variant (c.283 + 1G>A) is represented with the "M" letter. Two different isoforms are shown: TRβ1 (UniProtKB, P10828-1) containing 11 exons and 461 amino acids (above panel), and TRβ2 (UniProtKB, P10828-2) containing 7 exons and 476 amino acids (below panel). Both isoforms differ in the A/B domains which are encoded by specific exons. Common domains included DNA-binding domain (DBD), hinge domain, ligand-binding domain (LBD) and the AF2 domain. The distribution of the known pathogenic variants along the THRB domains was done using curated HGMD-pro data (Stenson et al., 2020). Of note, to date disease-causing variants ("DM" class) have been identified only in RTHβ individuals, being mainly located within the common LBD and hinge domains. MetaDome server (Wiel et al., 2019) (https://stuart.radboudumc.nl/metadome) was used to create the tolerance landscape of both THRB isoforms. The variant identified here in IRD patients, c.283 + 1G>A, is predicted to disrupt the A/B domain of the TRβ1 isoform (dashed bracket). In this region, only two pathogenic variants have been identified in RTHβ patients.

with macular degeneration as the major clinical feature, which suggests novel retinal functions of this complex gene.

2 Materials and methods

2.1 Subjects and clinical evaluation

Three unrelated Spanish families consisting of 9 unaffected and 11 affected individuals with a presumed autosomal dominant IRD, were recruited for genetic diagnosis (Figure 2). Genomic DNA was isolated from peripheral blood using standard procedures. An informed consent form was signed by all participants or their legal guardians for clinical and genetic studies. The research was conducted in accordance with the tenets of the Declaration of Helsinki (Edinburgh, 2000), and approved by the Institutional Review Boards of the University Hospital Virgen del Rocio and the University Hospital Virgen Macarena (Seville, Spain).

All affected individuals were derived from the Ophthalmic Departments at the University Hospital Virgen Macarena and University Hospital Virgen del Rocio, and underwent a comprehensive ophthalmic examination including best corrected visual acuity (BCVA), fundus photographs, fundus fluorescein angiography (FA), optical coherence tomography (OCT), visual field, visual evoked potentials (VEP), and electroretinography (ERG).

In addition, clinical data relevant to the disease of each patient were obtained from the electronic health record (EHR), including routine blood tests showing thyroid hormones studies (free thyroxine, FT4, and thyroid-stimulating hormone, TSH).

2.2 Targeted NGS and mutational screening

As part of our diagnostic routine, individual III:1 from family A, individuals IV:1, III:3 and III:7 from family B and III:1 from family

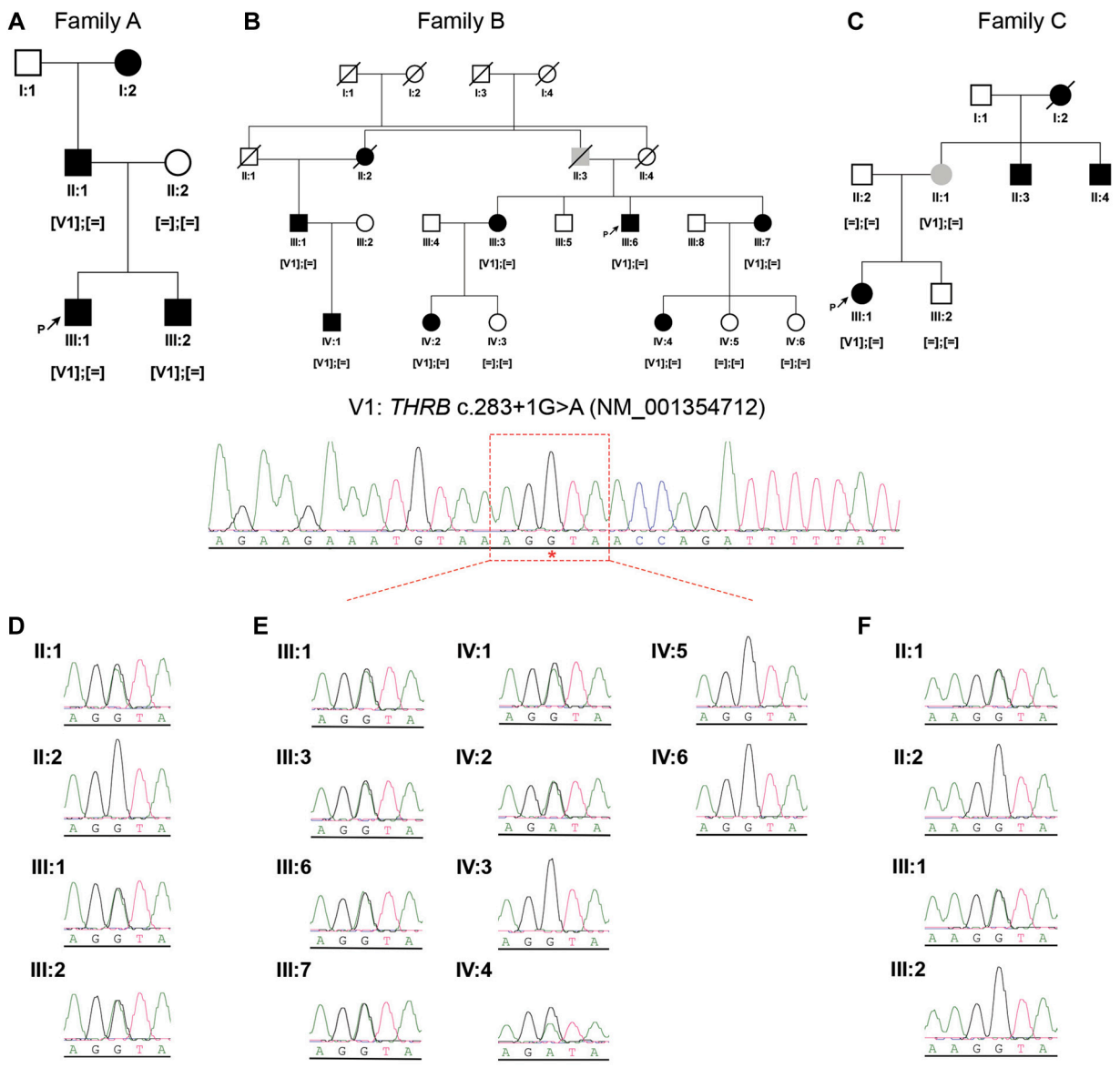

FIGURE 2
Pedigree structures and segregation analysis of the recurrent *THRB* variant (NM_001354712: c.283 + 1G>A; r.spl; NP_001341641.1: p.?) in the three IRD families **(A–C)**. Black symbols represent affected individuals, white symbols represent unaffected individuals and grey symbols represent individuals with uncertain clinical diagnosis. '[=]; [=]': wild-type genotype; '[V1]; [=]': heterozygous genotype. **(D–F)**, Sanger sequencing electropherograms and segregation results in the available members of family A **(D)**, family B **(E)** and family C **(F)**.

C, underwent targeted panel sequencing of 1,166 genes associated with different rare diseases, as previously described (Puppo Moreno et al., 2022). After a negative result using a virtual IRD panel comprising 146 associated genes (https://web.sph.uth.edu/RetNet/), the families were included in the unsolved IRD cohort.

The unsolved IRD cohort was composed of a total of 215 individuals whose genomic information was used to extract local-frequency data and to evaluate the recurrence of novel candidate variants. In fact, as the *THRB* gene was already included in the targeted diagnostic panel for RTHβ patients, we searched for the presence of likely pathogenic variants in all coding exons and its splice junctions of this gene in the unsolved IRD cohort. Prioritization of *THRB* variants was done using the prediction tools and optimized cutoffs previously described elsewhere (Gonzalez-Del Pozo et al., 2022).

2.3 Whole genome sequencing and genetic analysis

Individuals II:1, II:2, III:1 and III:2 from family A (Figure 2) underwent WGS by Macrogen (Seoul, Korea). DNA libraries were constructed using the TruSeq Nano DNA Library Prep Kit (Illumina, CA, United States) according to the manufacturer's

instructions. The quality of the libraries was confirmed using a 2100 Bioanalyzer (Agilent Technologies, CA, United States). WGS was performed using 2 × 150 base paired-end reads on an Illumina NovaSeq 6,000 platform. After sequencing, trimmed reads were mapped to the hg19 human reference genome using BWA-MEM (v. 0.7.17). BAM files were sorted, and duplicates were removed using Picard (v. 2.18.2). GATK (v. 4.0.5.1) was used for base quality recalibration and variant calling of single-nucleotide variants (SNVs). The variant annotation was done using SnpEff (v. 5.0e). The variant calling of structural variants (SVs) was done with Manta (v. 1.5.0) and copy number variations (CNVs) were identified by Control-FREEC (v.11.5) and PennCNV (v. 1.0.5), and both annotated using AnnotSV 2.2 online software (Geoffroy et al., 2021). The final output was a vcf file per sample and type of variants.

The WGS data prioritization was conducted using our validated pipeline as previously described (Gonzalez-Del Pozo et al., 2022). Briefly, the WGS data of the four sequenced individuals were combined using VCF combine (Vcflib). The resulting multi-sample vcf file was annotated with data from gnomaAD browser, CADD v1.6 scores, SpliceAI scores and ClinVar significance (January 2023). Variants with a minor allele frequency (MAF) less than 1% in public databases (gnomAD) were first prioritized and subsequently filtered using the customized filters. Non-splicing variants were prioritized with the prediction tools: CADD (≥22.25), MAPP (≤0.098 or absent), Grantham (≥28 or absent), and SIFT (≤0.175 or absent). The prioritization of splicing variants was done using an update of the worklflow (data unpublished) with SpliceAI (Jaganathan et al., 2019) and MaxEntScan tools (Yeo and Burge, 2004). The application of the "pedigree filtering" helped us to prioritize variants according to their zygosity and phenotype (González-Del Pozo et al., 2020). Finally, a manual curation was carried out according to the American College of Medical Genetics/Association for Molecular Pathology (ACMG/AMP) guidelines (Richards et al., 2015) using the Franklin Genoox Platform (https://franklin.genoox.com/), the clinical significance in databases such as ClinVar, LOVD, or HGMD-pro, and the number of homozygous and heterozygous (absent, 0, 1) in gnomAD, among others criteria. The nomenclature of variants was adjusted to the Human Genome Variation Society (http://varnomen.hgvs.org/) guidelines.

Candidate variants were confirmed and segregated in the available family members by PCR and direct Sanger sequencing according to the manufacturer's protocols (3730 DNA Analyzer, Applied Biosystems, Foster City, CA, United States).

2.4 Protein structural analysis of TRβ1 and its predicted splicing impacts

To evaluate the effect of alternative splice process derivate from c.283 + 1G>A variant, a three-dimensional modeling for TRβ1, TRβ1-skipping exon 5, and TRβ1-skipping exons 5 and 6 were conducted. The modeling of TRβ1-skipping exon 5 was performed using IntFOLD (McGuffin et al., 2023) (Integrated Protein Structure and Function Prediction Server, University of Reading, https://www.reading.ac.uk/bioinf/). The three-dimensional modeling for the THRβ-skipping exons 5 y 6 were conducted using PEP-FOLD4 (Lamiable et al., 2016; Rey et al., 2023) (https://bioserv.rpbs.univ-paris-diderot.fr/services/PEP-FOLD4/) due to the small size of the resulting peptide.

2.5 Statistical analysis

In order to investigate if the prevalence of the variant is significantly increased in affected individuals as compared to controls, a statistical analysis was performed using RStudio 2022.02.3 and R version 4.1.3. The chi-square test, considering a significant value of $p < 0.05$, was performed to compare these categorical variables.

3 Results

3.1 Clinical features in family A

Family A was of Spanish origin. Affected individuals received a clinical diagnosis of COD and had a suspected autosomal dominant pedigree due to the existence of multiple affected individuals of both genders in three consecutive generations (Figure 2). The first symptom in all affected individuals was a decrease in visual acuity, but individuals III:1 and III:2 had a childhood-onset (6–7 years respectively) whereas in individual II:1 the symptoms began during adulthood, showing a milder phenotype. Ophthalmic examination revealed orange-yellowish lesions in the macula, foveal cavitation and the disruption of the photoreceptor and retinal pigment epithelium layers (Figure 3). ERG of these individuals were consistent with central vision defects showing pathological pattern ERG with abnormal responses in both eyes and prolonged P-100 latency in the VEP. Additional clinical findings of the sequenced patients are reported in Table 1.

3.2 WGS data quality

The reliability of WGS data was given by the quality parameters of the generated data. Genome sequencing in the four studied individuals of family A produced an average total yield of 88.76 Gb ± 1.34 (mean ± SD) and an average coverage of 30.63x±0.58 (mean ± SD). Only 0.92% of the bases showed a coverage less than 10x. The percentage of mapped reads and duplicated reads was 99.73% and 6.52%, respectively. The total base Q ≥ 30 was 90.27%. The Q score of 30 to a base is equivalent to the probability of an incorrect base call 1 in 1,000 times. This means that the base call accuracy is 99.9%, thus, all the reads will have zero errors and ambiguities in 90.27% of the bases. All these parameters indicated that WGS rendered high-quality data.

3.3 Identification and assessment of candidate variants in family A

Application of WGS in family A resulted in an average of 5,052,864 SNVs/indels, 691 CNVs, and 8,972 SVs per sample, which were annotated and filtered to identify causative variants.

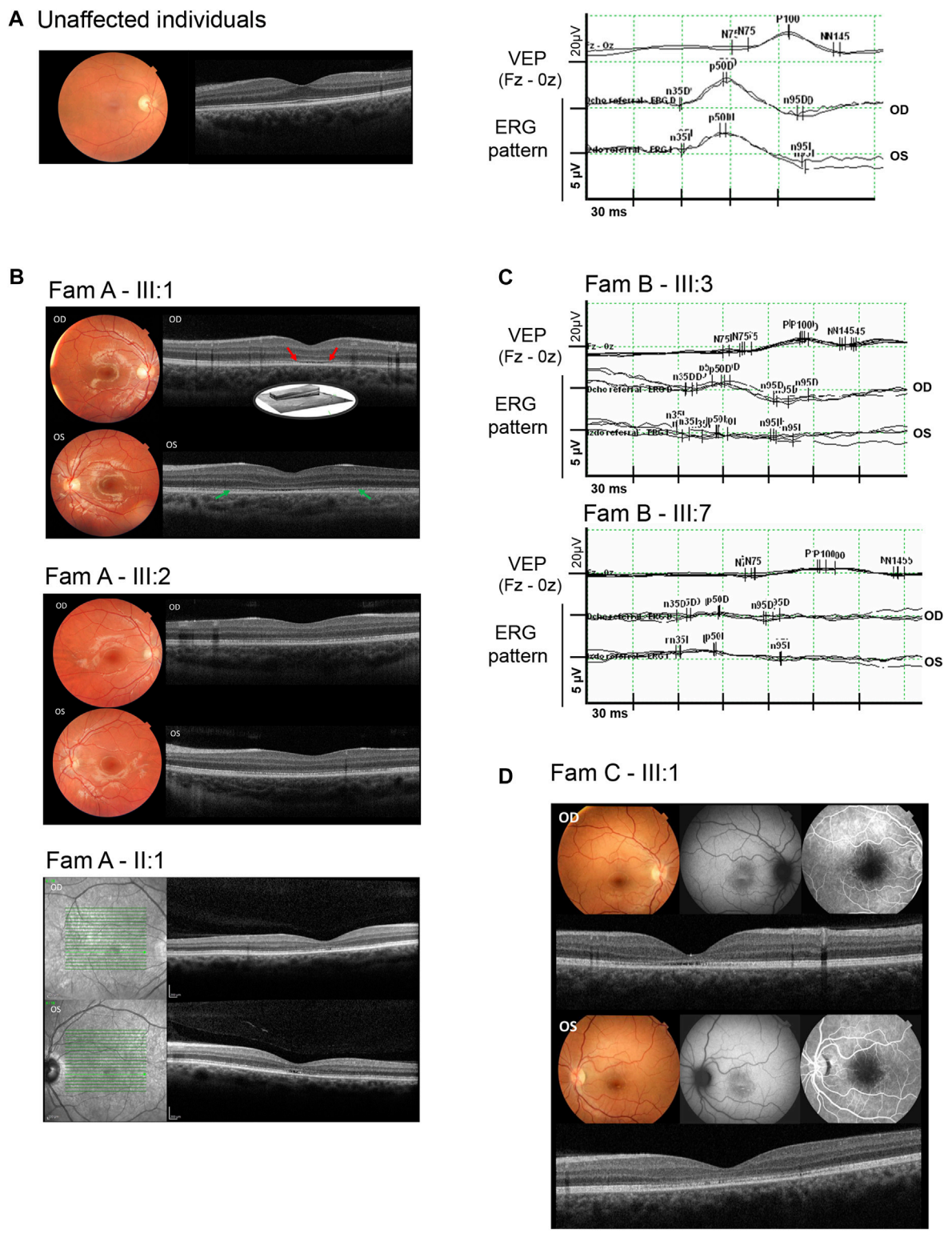

FIGURE 3
Ophthalmic characterization of some of the IRD individuals who harbored the *THRB* variant. **(A)**, Clinical characterization of an unaffected control individual including normal color fundus photographs, optical coherence tomography, visual evoked potentials (VEP), and ERG pattern responses in both eyes. **(B)**, Clinical characterization of affected individuals from family A, including color fundus photographs (individuals III:1, and III:2) showing orange-yellowish lesions in the fovea; fundus autofluorescence imaging (individual II:1), and optical coherence tomography (individuals III:1, III:2 and II:1) showing foveal cavitation (red arrows) and the disruption of the photoreceptor and retinal pigment epithelium layers (green arrows). **(C)**, Visual evoked potentials (VEP) showing prolonged P100 latency and ERG pattern with abnormal responses in both eyes (OD: right eye and OS: left eye) from individuals III:3 and III:7 of family B, **(D)**, Clinical characterization of the affected individual from family C (individual III:1) showing macular atrophy, loss of the ellipsoid zone, foveal cavitation, hyper- and hypoautofluorescent changes in fovea and disruption of the photoreceptor cells layer.

TABLE 1 Clinical characteristics of the individuals harboring the c.283 + 1G>A variant in *THRB*.

Family and pedigree subject	Onset age/age at time of evaluation (years)	First symptom	Ophthalmic examination	ERG	Clinical diagnosis	Additional manifestations
Fam-A II:1	Adulthood	Decreased of visual acuity	Loss of central vision and mild fundus alterations	NA	COD	Milder phenotype
Fam-A III:1	7/9	Decreased of visual acuity	Loss of central vision, photopic response alteration, foveal cavitation, orange-yellowish lesion in fovea	VEP for central vision bilaterally affected (prolonged P100 latency)	COD	NA
				Pathological pERG bilaterally		
			Disruption of the photoreceptor outer segment junction	Affected cone responses		
				Impairment of photopic retinal responses		
Fam-A III:2	6/8	Decreased of visual acuity	Loss of central vision, photopic response alteration, foveal cavitation, orange-yellowish lesion in fovea	NA	COD	NA
Fam-B III:1	Childhood/39	Decreased of visual acuity	NA	NA	STGD	NA
Fam-B III:3	50/54	Decreased of visual acuity			STGD	Multinodular goiter; Hypodense nodules with peripheral rim calcification; Papillary Thyroid Carcinoma
			Loss of central vision and decreased retinal thickness at the macular level	VEP for the function of central vision altered bilaterally (prolonged P100 latency)		Total thyroidectomy
			Disruption of the photoreceptor outer segment junction, mild subfoveal retinal detachment, atrophic lesions, cataracts	pERG: altered bilaterally		Hypothyroidism; Depression; Increased body weight
				No alterations in the function of the RPE, rods or cones		Type II diabetes mellitus
						Hypertension; Hypertriglyceridemia
						Osteoarthritis
Fam-B III:6	Childhood/29	Decreased of visual acuity	Decreased visual acuity, loss of central vision, photophobia, and macular atrophy	NA	MD	Goiter; Headache
Fam-B III:7	Childhood/42	Decreased of visual acuity	Loss of central vision, retinal flecks, chorioretinal atrophy with hypertrophy of the RPE, atrophic macules with hyper- and hypoautofluorescent changes.	VEP for the function of central vision altered bilaterally in a moderate-severe degree (prolonged P100 latency)	STGD	Type II diabetes mellitus; Increased body weight
				pERG: severely altered bilaterally		
				No alterations in the function of the RPE, rods or cones		
Fam-B IV:1	11/11	Decreased of visual acuity	Blurred vision, myopia, and early macular lesions	NA	MD	Migraine
Fam-B IV:2	31/35	Decreased of visual acuity	Loss of central vision, hyperfluorescence at the fovea, RPE atrophy, bright yellow/orange distributed spots consistent with lipofuscin deposits, salt-and-pepper RPE mottling and pigment clumping, macular atrophy, and thinning of the fovea	NA	STGD	Hearing impairment (left ear); Depression; Anxiety

(Continued on following page)

TABLE 1 (*Continued*) Clinical characteristics of the individuals harboring the c.283 + 1G>A variant in *THRB*.

Family and pedigree subject	Onset age/age at time of evaluation (years)	First symptom	Ophthalmic examination	ERG	Clinical diagnosis	Additional manifestations
Fam-B IV:4	20/27	Decreased of visual acuity	Macular scotoma, diffuse posterior pole pigmentation, dull macula, and lack of foveal reflex	NA	MD	Atopic dermatitis; Anxiety
Fam-C II:1	2 nd decade of life/55	Decreased of visual acuity	NA (refused to undergo an ophthalmological evaluation but manifested visual impairment)	NA	Unclear clinical diagnosis	Hyperthyroidism for 14 years, and then subclinic hypothyroidism; Psoriasiform dermatitis; Hyperlipidemia
Fam-C III:1	24/25	Decreased of visual acuity	Loss of central vision, photophobia	Abnormal pERG.	COD	Increased body weight; Depression; Atopic dermatitis
			Macular atrophy and loss of the ellipsoid zone, foveal cavitation, hyper- and hypoautofluorescent changes in fovea			
			RPE atrophy			

Abbreviations: COD, cone dystrophy; ERG, electroretinogram; Fam, family; MD, macular dystrophy; NA, not available; pERG, pattern ERG; RPE, retinal pigment epithelium; STGD, stargardt disease; VEP, visual evoked potentials.

The multi-sample vcf from family A encompassed more than six million of SNVs. After the application of the customized pipeline, we identified 75,199 rare SNVs (MAF≤0.01) and 54 SNVs with MAF>0.01 that were recovered by ClinVar filtering (Supplementary Table S1). The subsequent filters with prediction tools prioritized 1,686 variants, of which 309 variants passed "CADDv1.6 + MAPP + Grantham + SIFT" filtering and 1,377 variants were recovered by "SpliceAI + MaxEnt" filtering (Figure 4). An autosomal dominant inheritance pattern was assumed for the analysis of the family as a first approach, prioritizing those common variants in the three affected individuals and absent in the unaffected mother. After the application of this pedigree filtering 142 variants were considered for further analysis. No coding nor spliceogenic deep-intronic variants in known IRD genes were identified consistent with the disease. Additionally, after the prioritization of CNVs and SVs, only 28 variants passed the applied filters (Figure 4; Supplementary Table S1). All the filtered variants present in affected individuals were manually curated considering the ACMG/AMP classification and the number of heterozygous or homozygous in gnomAD. This curation allowed the identification of four variants (Table 2). A comprehensive bibliography search of the candidate variants allowed us to propose a novel heterozygous *THRB* variant (NM_001354712.2: c.283 + 1G>A; r.spl; NP_001341641.1: p.?) as the most likely cause of the disease due to its role in cone development in different animal models (Supplementary Table S2). Family segregation results are depicted in Figure 2.

According to the ACMG/AMP guidelines, although the variant affects the canonical splicing +1 position, the PVS1 rule cannot be applied because this requires the existence of a prior association between loss-of-function variants and the IRD phenotype, being here reported for first time. However, the application of the PM2 rule (absent from controls), and the PP3 rule (multiple lines of computational evidence support a deleterious effect on the gene or gene product), resulted in a "VUS" classification. Moreover, all splicing prediction tools used in our pipeline predicted a disruption of the canonical donor splicing site with a high score (SpliceAI = 0.98 and MaxEnt variation = 57.74%), and the CADD tool also displayed an elevated score (CADD_phred v1.6 = 34). Based on previous studies (Anna and Monika, 2018) exon skipping is the most frequent consequence of canonical splice site mutations, therefore the identified variant is expected to produce the skipping of exon 5 or exons 5 and 6 of *THRB*, or even a mix of aberrantly spliced transcripts. Using *in silico* predictions, we hypothesized the skipping of exon 5, which would produce a protein with an abnormal N-terminal domain conserving intact the rest of protein. Instead, the skipping of the two exons (exons 5 and 6) would create a premature stop codon producing an incomplete protein. Three-dimensional modeling of these predicted consequences showed conformational differences in the protein folding (Supplementary Figure S1).

Moreover, in order to explain the clinical heterogeneity between the three affected individuals, additional genetic variants in this and other genes were considered. Remarkably, the individual FamA-II: 1 harbored *in trans* with the c.283 + 1G>A variant, two common SNPs, rs2596622 and rs2596623, in the ICR of *THRB,* previously associated with clinical heterogeneity in RTHβ patients (Alberobello et al., 2011).

3.4 Mutational screening of *THRB*

Expanded genetic analysis of the *THRB* gene in the 215 unsolved patients from our IRD cohort allowed the identification of the same variant (c.283 + 1G>A) in two additional unrelated families clinically diagnosed with different autosomal dominant cone diseases (Figure 4). Sanger sequencing revealed segregation of the *THRB* variant with the disease in 8 affected, 6 unaffected and 1 individual with unclear phenotype (Figure 2). No alternative candidate variants (SNVs

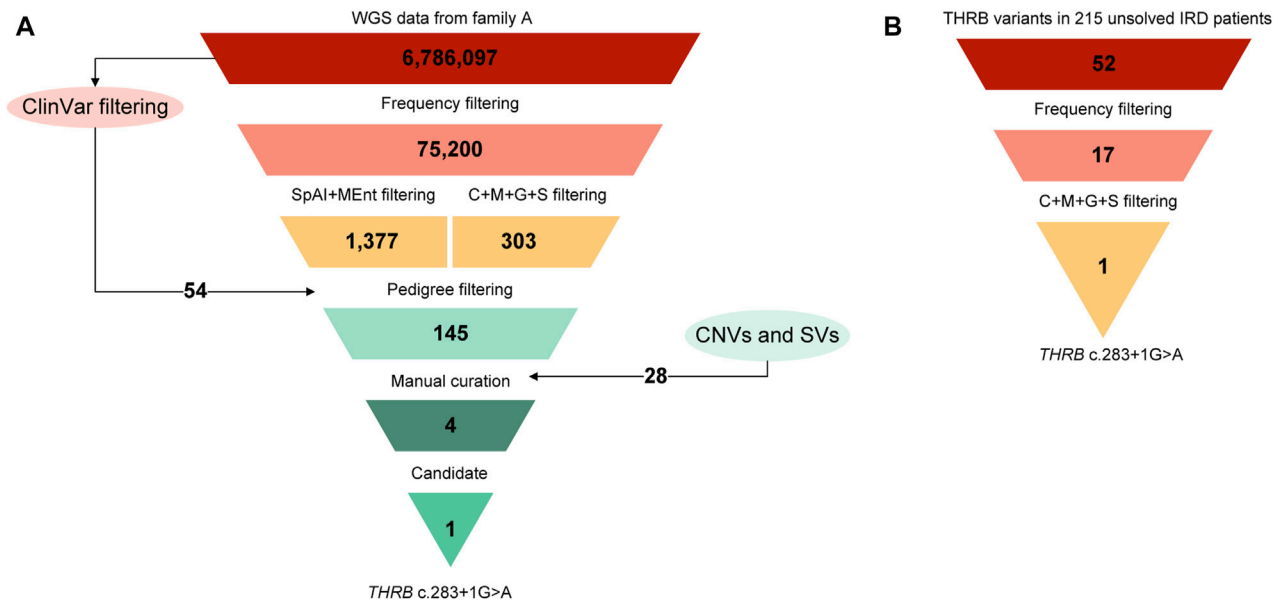

FIGURE 4
Variant filtering scheme used for the prioritization of the NGS data. **(A)** The starting point was the combined vcf file from the four sequenced individuals of family A (FamA-II:1, II:2, III:1, and III:2) that was filtered using the settings and the cutoffs described elsewhere (Gonzalez-Del Pozo et al., 2022). Briefly, variants with a MAF>0.01 in gnomAD database were filtered out except those variants classified as pathogenic (P), likely pathogenic (LP), or as conflicting interpretations of pathogenicity with P or LP entries (CIP: P/LP) in ClinVar database. Then, a combination of predictions tools including 'CADD + MAPP + Grantham + SIFT' (C + M + G + S) for non-splicing variants and 'SpliceAI + MaxEntScan' (SpAI + MEnt) for splicing variants were applied. The pedigree filtering consisted in prioritizing those variants present in the three affected individuals and absent in the unaffected individual. At this point, copy number variations (CNVs) and structural variants (SVs) were also considered. In addition, according to an autosomal dominant inheritance, variants with 2 or more heterozygous individuals in public control databases were filtered out as a first approach. Lastly, the manual curation, including ACMG/AMP classification and a comprehensive bibliography search, led to the identification of one candidate variant in this family. **(B)** Prioritization of the variant in THRB gene in the unsolved IRD cohort applying the workflow described above. The final analysis allows the identification of the THRB **(C)** 283 + 1G>A variant in families B and C.

TABLE 2 Variants prioritized in the family A during the application of the manual curation.

Gene	gDNA (hg19)	cDNA | protein	ACMG/AMP class	MAF (gnomAD)	OMIM phenotype	Phenotype MIM number	Inh	Role in cone function
THRB	chr3: g.24231564C>T	NM_001354712.2: c.283 + 1G>A | NP_001341641.1: p.?	LP	NA	RTHβ	#188570	AD	Yes
					RTHβ	#274300	AR	
					RTHβ, selective pituitary	#145650	AD	
GRM6	chr5: g.178416383G>A	NM_000843.4: c.1036C>T | NP_000834.2: p.Arg346*	P	NA	CSNB 1B	#257270	AR	No
STK38	chr6: g.36507933G>A	NM_001305102.1: c.47C>T | NP_001292031.1: p.Thr16Ile	VUS	0.000115	NA	NA	NA	No
TDRD9	chr14: g.104441854T>G	NM_153046.3: c.975T>G | NP_694591.2: p.Tyr325*	LP	NA	SPGF30	#618110	AR	No

Abbreviations: AD, autosomal dominant; AR, autosomal recessive; CSNB 1B, congenital stationary night blindness 1B; Inh, inheritance; LP, likely pathogenic; MAF, minor allele frequency; NA, not available; P, pathogenic; RTHβ, resistance to thyroid hormone β; SPGF30, spermatogenic failure-30; VUS, variant of unknown significance.

nor CNVs) explaining the retinal condition were identified in any case.

Remarkably, the c.283 + 1G>A variant has been identified in 11 alleles in our IRD cohort whereas it was totally absent in public control databases including gnomAD, Bravo and CSVS (Pena-Chilet et al., 2021). Therefore, the frequency of the variant in IRD patients was significantly higher than in control individuals (p-value = $2.2{\cdot}10^{-16}$, Chi-squared test). The application of two additional pathogenic ACMG/AMP rules, PP1 (cosegregation with the disease in multiple affected family

members) and PS4 (the prevalence of the variant in affected individuals was significantly increased compared to the prevalence in controls) led us to re-classify this variant as "likely pathogenic" (Class IV).

3.5 Genotype-phenotype correlation and thyroid hormones studies

Combining the phenotypic characteristics of the 12 affected individuals, we delineated the updated ophthalmologic spectrum of phenotypes associated with the splicing variant c.283 + 1G>A in *THRB*. Autosomal dominant retinal dystrophies such as COD (n = 4), STGD (n = 4) or MD (n = 3) represented the major clinical diagnoses that motivated the genetic testing (Table 1). One individual (FamC-II:1) who carried the variant (Figure 2), refused to be reevaluated. Affected individuals manifested a reduction in visual acuity as first symptom being the age of onset variable between 6 and 31 years old. Fundus evaluation showed photoreceptor layer thinning at macular area, and foveal cavitation consistent with central visual impairment in most of the patients (Figure 3). Regarding the neuro-ophthalmological studies, VEP revealed pathological changes consisting of prolonged P100 latency and abnormal ERG pattern responses (Figure 3). No color vision alterations were reported among the individuals of our cohort.

Routine blood tests, including thyroid-stimulating hormone (TSH), and free thyroxine (FT4) levels, were conducted in 8 out of 12 patients. Patients showed normal FT4 values (mean: 1.14 ± 0.18 ng/dL; normal range, 0.89–1.80 ng/dL), and normal TSH values (mean: 2.88 ± 2.31 μUI/mL (0.40–4.00 μUI/mL), except two who showed high TSH values (4.24 and 7.72 μUI/mL respectively). Regrettably, free triiodothyronine (FT3) was only measured in one patient, and it was normal (Supplementary Table S3). Of note, none of the affected individuals received a clinical diagnosis of RTHβ because most remain in a euthyroid state with no specific endocrine test recommendations. However, related features such as multinodular goiter (n = 2), increased body weight (n = 3), hyperlipidemia (n = 2), hypothyroidism (n = 1), type II diabetes mellitus (n = 2) or hearing impairment (n = 1) were observed. Additional clinical manifestations included skin diseases (n = 3), anxiety and depression (n = 3). More details about the clinical characterization are summarized in Table 1 and in Supplementary Table S3.

4 Discussion

We present one Spanish family with dominant IRD harboring a novel sequence variant in the *THRB* gene (c.283 + 1G>A). An expanded genetic analysis of the *THRB* gene in our unsolved IRD cohort, resulted in the identification of the same variant in two additional unrelated families. The unusually high frequency of the variant in our population, suggests a possible founder effect. This genetic information enabled us to propose a new genotype-phenotype correlation between cone-dominated diseases and the presence of variants in this gene.

Numerous studies have shown a role for *THRB* in cone development and survival using a wide range of model organisms (Supplementary Table S2). However, monoallelic or biallelic *THRB* variants have only been associated with generalized or selective pituitary RTHβ in humans (Refetoff et al., 1967; Gershengorn and Weintraub, 1975; Weiss et al., 1993; Adams et al., 1994; Ferrara et al., 2012; Ortiga-Carvalho et al., 2014), with just a few patients showing visual impairment (Frank-Raue et al., 2004; Weiss et al., 2012). Here, we have expanded the phenotype of *THRB* with the identification of a putatively spliceogenic variant associated with retinal degeneration, as the main clinical outcome in three unsolved IRD families. Although thyroid involvement was barely observed, multinodular goiter, and hyper- or hypothyroidism were observed in three patients. This suggests that RTHβ and IRD might not be fully independent clinical entities, but different manifestations of the same syndromic disease in which the expressivity of the different clinical features may vary from patient to patient. Additionally, some patients manifested a metabolic disorder, including increased body weight, type II diabetes mellitus, and hyperlipidemia Also, mental health conditions (anxiety and depression) and, skin diseases (atopic dermatitis and psoriasiform dermatitis) were also reported. Altogether these data suggest that *THRB* is associated with a highly variable clinical expression, even within the same family, suggesting the role of phenotype modifiers in THRB-associated conditions or variable *THRB* expression. In this sense, variations in *THRB* enhancer sequences that influence the expression of TRβ2 in both retina and pituitary have been proposed to explain tissue-specific phenotypes (Jones et al., 2007; Alberobello et al., 2011; Liu et al., 2023). Individual II:1 from family A harbored two SNPs within a putative regulatory intronic region that, although still controversial (Zaig et al., 2018), have been hypothesized to modify the expression of THRβ isoforms (Alberobello et al., 2011). Remarkably, individual II:1 presented a milder phenotype than his sons (III:1 and III:2), which could associate with the presence of these SNPs; however, further studies are needed to corroborate this hypothesis.

Despite the phenotypic variability observed in IRD patients harboring the c.283 + 1G>A variant, all individuals were characterized by primary cone dysfunction. This is shown as a reduction in the thickness of the photoreceptor layer, and the foveal cavitation that is characteristically present in most of the patients of our cohort. The visual outcome for these 11 patients was, on average, worse in comparison to RTHβ patients harboring dominant-negative variants in *THRB* (Campi et al., 2017), as none of those patients (n = 27) met the clinical criteria to be diagnosed of MD, STGD or COD, and only color vision changes and a 10% reduction of the cone-response to a single flash of light during the photopic ERG were observed. It was intriguing that previously described dominant variants in *THRB* caused variable but closely related ocular symptoms compared with the recessive variants which consisted mainly of differences in the cone-subtype specification (Weiss et al., 2012). Our patients did not manifest color vision alterations, and regarding the neuro-ophthalmological studies, VEP changes in the form of prolonged P100 latency, and the abnormal pattern electroretinogram responses were consistent with severe central visual defects showing a clinical diagnosis varied from

COD (n = 4), STGD (n = 4), and MD (n = 3). One carrier refused to conduct an ophthalmological revaluation but manifested visual impairment since the second decade of life according to her EHR.

Genotype-phenotype correlations showed that RTHβ can be caused by both truncating and missense variants, which are mainly located at the common domains in the TRβ1 and TRβ2 isoforms, the LBD domain and the contiguous hinge region (Weiss et al., 1993). In contrast, the variant identified here, c.283 + 1G>A, is predicted to disrupt the N-terminal A/B domain of the TRβ1 isoform. This region shows promoter- and cell-specific activity (Aranda and Pascual, 2001) and is target for numerous post-translational modifications including phosphorylation, SUMOylation, and acetylation (Weikum et al., 2018). We hypothesized that the c.283 + 1G>A variant could impact retinal-specific functions mainly involved in cone viability without a major affectation of cone subtype specification that is mediated by TRβ2. In fact, a recent study experimentally demonstrates that TRβ1-knockout mice displayed only minor changes in opsin photopigment expression (Ng et al., 2023), resembling what we observed in our patients. Authors suggest that TRβ1, the predominant TRβ isoform at mature ages, may have a role in the survival of both cone photoreceptors and retinal pigment epithelium cells (Ng et al., 2023), as described in other retinal degeneration models (Ma et al., 2014; Ma et al., 2017; Ma et al., 2022), and now in the IRD patients of our cohort. Of note, only two putatively pathogenic variants have been identified in the TRβ1 N-terminal domain in patients with congenital hypothyroidism and thyroid dysgenesis (Zhou et al., 2018). However, the young age of these patients, the lack of an ophthalmologic evaluation, and the VUS status of these variants hampered the proper establishment of genotype-phenotype correlations. Here, we report the first likely pathogenic splicing variant in *THRB*, which also affects only the TRβ1 isoform, reflecting both the extraordinary intolerance to variation of this gene and the high complexity of retinal functions mediated by the different *THRB* isoforms. Hence, it will be of interest to screen this and other *THRB* variants in IRD patients from different populations in order to evaluate the burden of *THRB* variants in additional IRD cohorts worldwide.

Also, dominant negative effects produced by *THRB* variants in RTHβ patients have been described and are possibly explained by the formation of heterodimers between normal and functionally inactive mutant receptor, which would diminish the activity of the resultant thyroid receptor (TR). This would reduce the amount of normal and potentially functional TR-T3 complexes and, therefore, higher concentrations of the hormone would be required to produce sufficient amount of hormone-saturated TR homodimers (Takeda et al., 1991). In fact, in this scenario, higher demands of thyroid hormones could trigger the activation of compensatory mechanisms like the increase of T3 levels, leading to cone apoptosis if this occurs in certain tissues like the retina (Ma et al., 2014; Ng et al., 2017). This is in line with previous findings that associated high T3 levels with an increased risk of age-related macular degeneration in human populations (Chaker et al., 2015; Gopinath et al., 2016). This is supported by the ocular phenotype described in our patients, who presented the photoreceptor layer thinning and the foveal cavitation without color vision alterations.

On the other hand, our work has also highlighted the importance of reanalysis of NGS data before proceeding with the generation of new genetic data using sequencing protocols such as WES or WGS in unsolved patients. In fact, the *THRB* gene was already included in the targeted diagnostic approach for these patients, but it was not routinely analyzed in IRD patients due to the lack of association. We conclude that sequencing of a smaller set of genomic regions during the diagnostic routine, may show some discovery potential for the identification of genes not yet associated to a particular disease, but routinely sequenced during the diagnostic process, resulting in the establishment of novel genotype-phenotype correlations.

To sum up, given the reported eye findings in a group of nearly 30 RTHβ patients (Weiss et al., 2012; Campi et al., 2017) and the demonstration that ablation of *THRB* in animal models induces retinal changes mainly consisting of cone differentiation defects, ophthalmological monitoring should be recommended together with an endocrine evaluation in patients with suspected THRB-associated syndrome. Similarly, likely pathogenic variants in the *THRB* gene, especially in the TRβ1 specific exons, should also be considered as disease-causing in patients with clinically diagnosed macular dystrophies, cone-dystrophy, or Stargardt disease with or without extra-ocular manifestations. We thereby expanded the phenotype of *THRB* pathogenic variants including a spectrum of IRD as the main clinical manifestation.

Data availability statement

The datasets for this article are not publicly available due to concerns regarding participant/patient anonymity. Requests to access the datasets should be directed to the corresponding authors. The prioritized variant was submitted to ClinVar database under the accession ID: SCV003845203.

Ethics statement

The studies involving human participants were reviewed and approved by Institutional Review Boards of the University Hospital Virgen del Rocio and the University Hospital Virgen Macarena (Seville, Spain). Written informed consent to participate in this study was provided by the participants' legal guardian/next of kin.

Author contributions

GA and SB conceived and designed the study. ER-R and MJM-S performed the ophthalmic evaluations. EF-S, MG-P, AG-N, and JMM-C conducted the experiments. EF-S, MG-P, MM-S, and AG-N analyzed and interpreted the generated data. MR-J conducted the electrophysiological study. MG-P and EF-S wrote the manuscript with the collaboration of all co-authors. GA, SB, MM-S, and CM-V revised the paper critically for important intellectual content. All authors contributed to the article and approved the submitted version.

Funding

This work was supported by the Instituto de Salud Carlos III (ISCIII), Spanish Ministry of Science and Innovation, Spain and co-funded by ERDF ("A way to make Europe") [PI21-00244]; The strategic plan for the Precision Medicine Infrastructure associated with Science and Technology - IMPaCT [IMP-0009], Regional Ministry of Health and Families of the Autonomous Government of Andalusia [PEER-0501-2019] and the Foundation Isabel Gemio/Foundation Cajasol [FGEMIO-2019-01]. EF-S is supported by fellowship FI19/00091 from ISCIII (ESF, "Investing in your future"). MM-S [RH-0049-2021] are supported by a fellowship funded by the Regional Ministry of Health and Families of the Autonomous Government of Andalusia.

Acknowledgments

The authors thank the families who participated in this study, and the Andalusian Association of Retinitis Pigmentosa.

Conflict of interest

The authors declare that the research was conducted in the absence of any commercial or financial relationships that could be construed as a potential conflict of interest.

Publisher's note

All claims expressed in this article are solely those of the authors and do not necessarily represent those of their affiliated organizations, or those of the publisher, the editors and the reviewers. Any product that may be evaluated in this article, or claim that may be made by its manufacturer, is not guaranteed or endorsed by the publisher.

Supplementary material

The Supplementary Material for this article can be found online at: https://www.frontiersin.org/articles/10.3389/fcell.2023.1197744/full#supplementary-material

References

Adams, M., Matthews, C., Collingwood, T. N., Tone, Y., Beck-Peccoz, P., and Chatterjee, K. K. (1994). Genetic analysis of 29 kindreds with generalized and pituitary resistance to thyroid hormone. Identification of thirteen novel mutations in the thyroid hormone receptor beta gene. *J. Clin. Invest.* 94 (2), 506–515. doi:10.1172/JCI117362

Alberobello, A. T., Congedo, V., Liu, H., Cochran, C., Skarulis, M. C., Forrest, D., et al. (2011). An intronic SNP in the thyroid hormone receptor β gene is associated with pituitary cell-specific over-expression of a mutant thyroid hormone receptor β2 (R338W) in the index case of pituitary-selective resistance to thyroid hormone. *J. Transl. Med.* 9, 144. doi:10.1186/1479-5876-9-144

Anna, A., and Monika, G. (2018). Splicing mutations in human genetic disorders: Examples, detection, and confirmation. *J. Appl. Genet.* 59 (3), 253–268. doi:10.1007/s13353-018-0444-7

Aramaki, M., Wu, X., Liu, H., Liu, Y., Cho, Y. W., Song, M., et al. (2022). Transcriptional control of cone photoreceptor diversity by a thyroid hormone receptor. *Proc. Natl. Acad. Sci. U. S. A.* 119 (49), e2209884119. doi:10.1073/pnas.2209884119

Aranda, A., and Pascual, A. (2001). Nuclear hormone receptors and gene expression. *Physiol. Rev.* 81 (3), 1269–1304. doi:10.1152/physrev.2001.81.3.1269

Campi, I., Agostini, M., Marelli, F., de Filippis, T., Romartinez-Alonso, B., Rajanayagam, O., et al. (2021). Clinical consequences of variable results in the measurement of free thyroid hormones: Unusual presentation of a family with a novel variant in the THRB gene causing resistance to thyroid hormone syndrome. *Eur. Thyroid. J.* 10 (6), 533–541. doi:10.1159/000519748

Campi, I., Cammarata, G., Bianchi Marzoli, S., Beck-Peccoz, P., Santarsiero, D., Dazzi, D., et al. (2017). Retinal photoreceptor functions are compromised in patients with resistance to thyroid hormone syndrome (RTHβ). *J. Clin. Endocrinol. Metab.* 102 (7), 2620–2627. doi:10.1210/jc.2016-3671

Chaker, L., Buitendijk, G. H., Dehghan, A., Medici, M., Hofman, A., Vingerling, J. R., et al. (2015). Thyroid function and age-related macular degeneration: A prospective population-based cohort study--the rotterdam study. *BMC Med.* 13, 94. doi:10.1186/s12916-015-0329-0

Cremers, F. P. M., Boon, C. J. F., Bujakowska, K., and Zeitz, C. (2018). Special issue introduction: Inherited retinal disease: Novel candidate genes, genotype-phenotype correlations, and inheritance models. *Genes (Basel)* 9 (4), 215. doi:10.3390/genes9040215

Eldred, K. C., Hadyniak, S. E., Hussey, K. A., Brenerman, B., Zhang, P. W., Chamling, X., et al. (2018). Thyroid hormone signaling specifies cone subtypes in human retinal organoids. *Science* 362 (6411), eaau6348. doi:10.1126/science.aau6348

Emerson, M. M., Surzenko, N., Goetz, J. J., Trimarchi, J., and Cepko, C. L. (2013). Otx2 and Onecut1 promote the fates of cone photoreceptors and horizontal cells and repress rod photoreceptors. *Dev. Cell* 26 (1), 59–72. doi:10.1016/j.devcel.2013.06.005

Ferrara, A. M., Onigata, K., Ercan, O., Woodhead, H., Weiss, R. E., and Refetoff, S. (2012). Homozygous thyroid hormone receptor beta-gene mutations in resistance to thyroid hormone: Three new cases and review of the literature. *J. Clin. Endocrinol. Metab.* 97 (4), 1328–1336. doi:10.1210/jc.2011-2642

Frank-Raue, K., Lorenz, A., Haag, C., Hoppner, W., Boll, H. U., Knorr, D., et al. (2004). Severe form of thyroid hormone resistance in a patient with homozygous/hemizygous mutation of T3 receptor gene. *Eur. J. Endocrinol.* 150 (6), 819–823. doi:10.1530/eje.0.1500819

Geoffroy, V., Guignard, T., Kress, A., Gaillard, J. B., Solli-Nowlan, T., Schalk, A., et al. (2021). AnnotSV and knotAnnotSV: A web server for human structural variations annotations, ranking and analysis. *Nucleic Acids Res.* 49 (W1), W21–W28. doi:10.1093/nar/gkab402

Gershengorn, M. C., and Weintraub, B. D. (1975). Thyrotropin-induced hyperthyroidism caused by selective pituitary resistance to thyroid hormone. A new syndrome of "inappropriate secretion of TSH. *J. Clin. Invest.* 56 (3), 633–642. doi:10.1172/JCI108133

Gonzalez-Del Pozo, M., Fernandez-Suarez, E., Bravo-Gil, N., Mendez-Vidal, C., Martin-Sanchez, M., Rodriguez-de la Rua, E., et al. (2022). A comprehensive WGS-based pipeline for the identification of new candidate genes in inherited retinal dystrophies. *NPJ Genom Med.* 7 (1), 17. doi:10.1038/s41525-022-00286-0

González-Del Pozo, M., Fernández-Suárez, E., Martín-Sánchez, M., Bravo-Gil, N., Méndez-Vidal, C., Rodríguez-de la Rúa, E., et al. (2020). Unmasking retinitis pigmentosa complex cases by a whole genome sequencing algorithm based on open-access tools: Hidden recessive inheritance and potential oligogenic variants. *J. Transl. Med.* 18 (1), 73. doi:10.1186/s12967-020-02258-3

Gopinath, B., Liew, G., Kifley, A., and Mitchell, P. (2016). Thyroid dysfunction and ten-year incidence of age-related macular degeneration. *Invest. Ophthalmol. Vis. Sci.* 57 (13), 5273–5277. doi:10.1167/iovs.16-19735

Himawan, E., Ekstrom, P., Buzgo, M., Gaillard, P., Stefansson, E., Marigo, V., et al. (2019). Drug delivery to retinal photoreceptors. *Drug Discov. Today* 24 (8), 1637–1643. doi:10.1016/j.drudis.2019.03.004

Jaganathan, K., Kyriazopoulou Panagiotopoulou, S., McRae, J. F., Darbandi, S. F., Knowles, D., Li, Y. I., et al. (2019). Predicting splicing from primary sequence with deep learning. *Cell* 176 (3), 535–548.e24. doi:10.1016/j.cell.2018.12.015

Jones, I., Ng, L., Liu, H., and Forrest, D. (2007). An intron control region differentially regulates expression of thyroid hormone receptor beta2 in the cochlea, pituitary, and cone photoreceptors. *Mol. Endocrinol.* 21 (5), 1108–1119. doi:10.1210/me.2007-0037

Lamiable, A., Thevenet, P., Rey, J., Vavrusa, M., Derreumaux, P., and Tuffery, P. (2016). PEP-FOLD3: Faster de novo structure prediction for linear peptides in solution and in complex. *Nucleic Acids Res.* 44 (W1), W449–W454. doi:10.1093/nar/gkw329

Lindstedt, G., Lundberg, P. A., Sjogren, B., Ernest, I., and Sundquist, O. (1982). Thyroid hormone resistance in a 35-year old man with recurrent goitre. *Scand. J. Clin. Lab. Invest.* 42 (7), 585–593. doi:10.3109/00365518209168134

Liu, H., Lu, A., Kelley, K. A., and Forrest, D. (2023). Noncoding mutations in a thyroid hormone receptor gene that impair cone photoreceptor function. *Endocrinology* 164 (3), bqad006. doi:10.1210/endocr/bqad006

Ma, H., Thapa, A., Morris, L., Redmond, T. M., Baehr, W., and Ding, X. Q. (2014). Suppressing thyroid hormone signaling preserves cone photoreceptors in mouse models of retinal degeneration. *Proc. Natl. Acad. Sci. U. S. A.* 111 (9), 3602–3607. doi:10.1073/pnas.1317041111

Ma, H., Yang, F., Butler, M. R., Belcher, J., Redmond, T. M., Placzek, A. T., et al. (2017). Inhibition of thyroid hormone receptor locally in the retina is a therapeutic strategy for retinal degeneration. *FASEB J.* 31 (8), 3425–3438. doi:10.1096/fj.201601166RR

Ma, H., Yang, F., and Ding, X. Q. (2022). Deficiency of thyroid hormone receptor protects retinal pigment epithelium and photoreceptors from cell death in a mouse model of age-related macular degeneration. *Cell Death Dis.* 13 (3), 255. doi:10.1038/s41419-022-04691-2

Martín-Sánchez, M., Bravo-Gil, N., González-Del Pozo, M., Méndez-Vidal, C., Fernández-Suárez, E., Rodríguez-de la Rúa, E., et al. (2020). A multi-strategy sequencing workflow in inherited retinal dystrophies: Routine diagnosis, addressing unsolved cases and candidate genes identification. *Int. J. Mol. Sci.* 21 (24), 9355. doi:10.3390/ijms21249355

McGuffin, L. J., Edmunds, N. S., Genc, A. G., Alharbi, S. M. A., Salehe, B. R., and Adiyaman, R. (2023). Prediction of protein structures, functions and interactions using the IntFOLD7, MultiFOLD and ModFOLDdock servers. *Nucleic Acids Res.*, gkad297. doi:10.1093/nar/gkad297

McNerney, C., and Johnston, R. J., Jr. (2021). Thyroid hormone signaling specifies cone photoreceptor subtypes during eye development: Insights from model organisms and human stem cell-derived retinal organoids. *Vitam. Horm.* 116, 51–90. doi:10.1016/bs.vh.2021.03.001

Ng, L., Hurley, J. B., Dierks, B., Srinivas, M., Salto, C., Vennstrom, B., et al. (2001). A thyroid hormone receptor that is required for the development of green cone photoreceptors. *Nat. Genet.* 27 (1), 94–98. doi:10.1038/83829

Ng, L., Liu, H., Liu, Y., and Forrest, D. (2023). Biphasic expression of thyroid hormone receptor TRβ1 in mammalian retina and anterior ocular tissues. *Front. Endocrinol. (Lausanne)* 14, 1174600. doi:10.3389/fendo.2023.1174600

Ng, L., Liu, H., St Germain, D. L., Hernandez, A., and Forrest, D. (2017). Deletion of the thyroid hormone-activating type 2 deiodinase rescues cone photoreceptor degeneration but not deafness in mice lacking type 3 deiodinase. *Endocrinology* 158 (6), 1999–2010. doi:10.1210/en.2017-00055

Ng, L., Ma, M., Curran, T., and Forrest, D. (2009). Developmental expression of thyroid hormone receptor beta2 protein in cone photoreceptors in the mouse. *Neuroreport* 20 (6), 627–631. doi:10.1097/WNR.0b013e32832a2c63

Ortiga-Carvalho, T. M., Sidhaye, A. R., and Wondisford, F. E. (2014). Thyroid hormone receptors and resistance to thyroid hormone disorders. *Nat. Rev. Endocrinol.* 10 (10), 582–591. doi:10.1038/nrendo.2014.143

Pena-Chilet, M., Roldan, G., Perez-Florido, J., Ortuno, F. M., Carmona, R., Aquino, V., et al. (2021). CSVS, a crowdsourcing database of the Spanish population genetic variability. *Nucleic Acids Res.* 49 (D1), D1130–D1137. doi:10.1093/nar/gkaa794

Puppo Moreno, A. M., Bravo-Gil, N., Mendez-Vidal, C., Adsuar Gomez, A., Gomez Ruiz, F. T., Jimenez De Juan, C., et al. (2022). Genetic profile in patients with complicated acute aortic syndrome: The GEN-AOR study. *Rev. Esp. Cardiol. Engl. Ed.* 76, 434–443. doi:10.1016/j.rec.2022.10.005

Refetoff, S., DeWind, L. T., and DeGroot, L. J. (1967). Familial syndrome combining deaf-mutism, stuppled epiphyses, goiter and abnormally high PBI: Possible target organ refractoriness to thyroid hormone. *J. Clin. Endocrinol. Metab.* 27 (2), 279–294. doi:10.1210/jcem-27-2-279

Rey, J., Murail, S., de Vries, S., Derreumaux, P., and Tuffery, P. (2023). PEP-FOLD4: A pH-dependent force field for peptide structure prediction in aqueous solution. *Nucleic Acids Res.*, gkad376. doi:10.1093/nar/gkad376

Richards, S., Aziz, N., Bale, S., Bick, D., Das, S., Gastier-Foster, J., et al. (2015). Standards and guidelines for the interpretation of sequence variants: A joint consensus recommendation of the American College of medical genetics and genomics and the association for molecular Pathology. *Genet. Med.* 17 (5), 405–424. doi:10.1038/gim.2015.30

Roberts, M. R., Hendrickson, A., McGuire, C. R., and Reh, T. A. (2005). Retinoid X receptor (gamma) is necessary to establish the S-opsin gradient in cone photoreceptors of the developing mouse retina. *Invest. Ophthalmol. Vis. Sci.* 46 (8), 2897–2904. doi:10.1167/iovs.05-0093

Schmidt, B. P., Boehm, A. E., Tuten, W. S., and Roorda, A. (2019). Spatial summation of individual cones in human color vision. *PLoS One* 14 (7), e0211397. doi:10.1371/journal.pone.0211397

Schneider, N., Sundaresan, Y., Gopalakrishnan, P., Beryozkin, A., Hanany, M., Levanon, E. Y., et al. (2022). Inherited retinal diseases: Linking genes, disease-causing variants, and relevant therapeutic modalities. *Prog. Retin Eye Res.* 89, 101029. doi:10.1016/j.preteyeres.2021.101029

Stenson, P. D., Mort, M., Ball, E. V., Chapman, M., Evans, K., Azevedo, L., et al. (2020). The human gene mutation database (HGMD®): Optimizing its use in a clinical diagnostic or research setting. *Hum. Genet.* 139 (10), 1197–1207. doi:10.1007/s00439-020-02199-3

Suzuki, S. C., Bleckert, A., Williams, P. R., Takechi, M., Kawamura, S., and Wong, R. O. (2013). Cone photoreceptor types in zebrafish are generated by symmetric terminal divisions of dedicated precursors. *Proc. Natl. Acad. Sci. U. S. A.* 110 (37), 15109–15114. doi:10.1073/pnas.1303551110

Takeda, K., Balzano, S., Sakurai, A., DeGroot, L. J., and Refetoff, S. (1991). Screening of nineteen unrelated families with generalized resistance to thyroid hormone for known point mutations in the thyroid hormone receptor beta gene and the detection of a new mutation. *J. Clin. Invest.* 87 (2), 496–502. doi:10.1172/JCI115023

Tatour, Y., and Ben-Yosef, T. (2020). Syndromic inherited retinal diseases: Genetic, clinical and diagnostic aspects. *Diagn. (Basel)* 10 (10), 779. doi:10.3390/diagnostics10100779

Tian, H., Mahajan, M. A., Wong, C. T., Habeos, I., and Samuels, H. H. (2006). The N-Terminal A/B domain of the thyroid hormone receptor-beta2 isoform influences ligand-dependent recruitment of coactivators to the ligand-binding domain. *Mol. Endocrinol.* 20 (9), 2036–2051. doi:10.1210/me.2005-0437

Weikum, E. R., Liu, X., and Ortlund, E. A. (2018). The nuclear receptor superfamily: A structural perspective. *Protein Sci.* 27 (11), 1876–1892. doi:10.1002/pro.3496

Weiss, A. H., Kelly, J. P., Bisset, D., and Deeb, S. S. (2012). Reduced L- and M- and increased S-cone functions in an infant with thyroid hormone resistance due to mutations in the THRβ2 gene. *Ophthalmic Genet.* 33 (4), 187–195. doi:10.3109/13816810.2012.681096

Weiss, R. E., Weinberg, M., and Refetoff, S. (1993). Identical mutations in unrelated families with generalized resistance to thyroid hormone occur in cytosine-guanine-rich areas of the thyroid hormone receptor beta gene. Analysis of 15 families. *J. Clin. Invest.* 91 (6), 2408–2415. doi:10.1172/JCI116474

Wiel, L., Baakman, C., Gilissen, D., Veltman, J. A., Vriend, G., and Gilissen, C. (2019). MetaDome: Pathogenicity analysis of genetic variants through aggregation of homologous human protein domains. *Hum. Mutat.* 40 (8), 1030–1038. doi:10.1002/humu.23798

Yeo, G., and Burge, C. B. (2004). Maximum entropy modeling of short sequence motifs with applications to RNA splicing signals. *J. Comput. Biol.* 11 (2-3), 377–394. doi:10.1089/1066527041410418

Zaig, E., Cohen-Ouaknine, O., Tsur, A., Nagar, S., Bril, G., Tolkin, L., et al. (2018). Clinical and molecular characteristics of eight Israeli families with thyroid hormone receptor beta mutations. *Isr. Med. Assoc. J.* 20 (11), 679–686.

Zhang, F., Kurokawa, K., Lassoued, A., Crowell, J. A., and Miller, D. T. (2019). Cone photoreceptor classification in the living human eye from photostimulation-induced phase dynamics. *Proc. Natl. Acad. Sci. U. S. A.* 116 (16), 7951–7956. doi:10.1073/pnas.1816360116

Zhou, Z., Yang, C., Lv, F., Liu, W., Yan, S., Zang, H., et al. (2018). Novel THRB mutation analysis in congenital hypothyroidism with thyroid dysgenesis. *J. Cell Biochem.* 119 (11), 9474–9482. doi:10.1002/jcb.27264

Glossary

ACMG/AMP	American College Of Medical Genetics/Association For Molecular Pathology
AD	Autosomal Dominant
AR	Autosomal Recessive
BCVA	Best Corrected Visual Acuity
BWA	Burrows-Wheeler Alignment Tool
C + M + G + S	Cadd + Mapp + Grantham + Sift
CIP:P/LP	Conflicting Interpretations Of Pathogenicity With P Or LP Entries
CNVs	Copy Number Variations
COD	Cone Dystrophy
CSNB1B	Congenital Stationary Night Blindness 1B
CSVS	Collaborative Spanish Variant Server
DBD	DNA-Biding Domain
EHR	Electronic Health Record
ERG	Electroretinography
FA	Fundus Fluorescein Angiography
fam	Family
FT3	Free Triiodothyronine
FT4	Free Thyroxine
GATK	Genome Analysis Toolkit
gDNA	Genomic DNA
ICR	Intron Control Region
Inh	Inheritance
IRD	Inherited Retinal Dystrophies
LBD	Ligand-Binding Domain
LP	Likely Pathogenic
MAF	Minor Allele Frequency
MD	Macular Dystrophy
NA	Not Available
NGS	Next-generation sequencing
OCT	Optical Coherence Tomography
P	Pathogenic
pERG	Pattern Electroretinography
PM2	Pathogenic Moderate Criteria 2
PP1	Pathogenic Supporting Criteria 1
PP3	Pathogenic Supporting Criteria 3
PS4	Pathogenic Strong Criteria
PVS1	Pathogenic Very Strong Criteria 1
RP	Retinitis Pigmentosa
RPE	Retinal Pigment Epithelium
RTHβ	Thyroid Hormone Resistance Syndrome Beta

SNP	Single Nucleotide Polymorphism
SNVs	Single-Nucleotide Variants
SpAI + MEnt	SpliceAI + MaxEntScan
SPGF30	Spermatogenic Failure-30
STGD	Stargardt Disease
SVs	Structural Variants
T3	Triiodothyronine
T4	Thyroxine
THRB	Thyroid Hormone Receptor Beta Gene
TR	Thyroid Receptor
TRβ1	Thyroid Hormone Receptor Beta Isoform 1 Protein
TRβ2	Thyroid Hormone Receptor Beta Isoform 2 Protein
TSH	Thyroid-Stimulating Hormone
VCF	Variant Call Format
VEP	Visual Evoked Potentials
VUS	Variant Of Uncertain Significance
WGS	Whole Genome Sequencing
XL	X-Linked

frontiers | Frontiers in Cell and Developmental Biology

TYPE Review
PUBLISHED 04 August 2023
DOI 10.3389/fcell.2023.1224078

OPEN ACCESS

EDITED BY
Glenn Prazere Lobo,
University of Minnesota Twin Cities,
United States

REVIEWED BY
Daniela Intartaglia,
Università degli Studi di Napoli Federico II,
Italy
Rakesh Radhakrishnan,
University of Minnesota Twin Cities,
United States

*CORRESPONDENCE
Livia S. Carvalho,
livia.dossantoscarvalho@uwa.edu.au

RECEIVED 17 May 2023
ACCEPTED 20 July 2023
PUBLISHED 04 August 2023

CITATION
Miller AL, James RE, Harvey AR, Trifunović D and Carvalho LS (2023), The role of epigenetic changes in the pathology and treatment of inherited retinal diseases.
Front. Cell Dev. Biol. 11:1224078.
doi: 10.3389/fcell.2023.1224078

The role of epigenetic changes in the pathology and treatment of inherited retinal diseases

Annie L. Miller[1,2], Rebekah E. James[1,2], Alan R. Harvey[2,3,4], Dragana Trifunović[5] and Livia S. Carvalho[1,2,6]*

[1]Centre for Ophthalmology and Visual Science, The University of Western Australia, Crawley, WA, Australia, [2]Retinal Genomics and Therapy Laboratory, Lions Eye Institute, Nedlands, WA, Australia, [3]School of Human Sciences, The University of Western Australia, Crawley, WA, Australia, [4]Perron Institute for Neurological and Translational Science, Nedlands, WA, Australia, [5]Institute for Ophthalmic Research, Tubingen University, Tübingen, Germany, [6]Department of Optometry and Vision Sciences, Faculty of Medicine, Dentistry and Health Sciences, The University of Melbourne, Melbourne, VIC, Australia

Elucidation of the cellular changes that occur in degenerating photoreceptors of people with inherited retinal diseases (IRDs) has been a focus for many research teams, leading to numerous theories on how these changes affect the cell death process. What is clearly emerging from these studies is that there are common denominators across multiple models of IRD, regardless of the underlying genetic mutation. These common markers could open avenues for broad neuroprotective therapeutics to prevent photoreceptor loss and preserve functional vision. In recent years, the role of epigenetic modifications contributing to the pathology of IRDs has been a particular point of interest, due to many studies noting changes in these epigenetic modifications, which coincide with photoreceptor cell death. This review will discuss the two broad categories of epigenetic changes, DNA methylation and histone modifications, that have received particular attention in IRD models. We will review the altered epigenetic regulatory events that are believed to contribute to cell death in IRDs and discuss the therapeutic potential of targeting these alterations.

KEYWORDS

inherited retinal disease, epigenetic changes, DNA methylation, histone methylation, histone acetylation, poly(ADP-ribosyl)ation

1 Introduction

Inherited retinal diseases (IRDs) are a genetically and phenotypically diverse group of blinding diseases that can result in photoreceptor death, dysfunction, or developmental delay (Berger et al., 2010). Collectively, these diseases affect 1:2000 people worldwide and pose a significant socioeconomic problem due to healthcare costs, reduced workplace participation and an increased requirement for carer assistance (Berger et al., 2010; Galvin et al., 2020).

Abbreviations: 5caC, 5-carboxylcytosine; 5fC, 5-formylcytosine; 5hmC, 5-hydroxymethylcytosine; 5mC, 5-methylcytosine; BER, base excision repair; DNMT, DNA methyltransferase; HAT, histone acetyltransferase; HDAC, histone deacetylase; IRD, inherited retinal disease; ONL, outer nuclear layer; PAR, poly (ADP-ribose); PARG, poly (ADP-ribose) glycohydrolase; PARP, poly (ADP-ribose) polymerase; rd, retinal degeneration [mouse model]; RP, retinitis pigmentosa; TDG, thymine DNA glycosylase; TET, ten-eleven translocase; TSA, trichostatin A; TUNEL, t erminal deoxynucleotidyl transferase dUTP nick end labelling; VPA, valproic acid.

However, treatments available for IRD are limited; only people with a mutation in one particular gene, *RPE65*, can receive the FDA-approved gene therapy drug Luxturna, leaving a critical gap in patient care (Maguire et al., 2021). Mutations in over 270 genes have been associated with IRD to date, and more are being discovered (Center DSTUoTHS, 2020). Due to this genetic heterogeneity, many researchers have investigated common targets that are independent of the underlying genetic mutations, with the aim of developing neuroprotective therapies that can treat a broader population of IRD patients. Such studies often focus on understanding the precise cell death mechanisms that lead to photoreceptor death. There is extensive debate in the field, with conflicting reports on whether apoptotic or non-apoptotic cell death mechanisms, or somewhere "in-between", are the predominant cause of photoreceptor loss (Brunet et al., 2022). A seminal study by Arango-Gonzalez et al. (2014) identified a common non-apoptotic cell death pathway that was dysregulated in ten mouse models of IRD, with many of the components of this pathway linked to epigenetic regulation (Arango-Gonzalez et al., 2014). In recent years there has been increased research in this area, strengthening links between epigenomic modifications and cell death in IRD. This review will outline the current understanding of the association of two types of epigenetic modification, DNA methylation and histone modifications, with IRD pathology.

2 DNA methylation

DNA methylation is a heritable genetic mark essential in multiple developmental processes such as genomic imprinting, X-chromosome inactivation and suppression of repetitive element transcription (Jin et al., 2011). DNA methylation functions by recruiting proteins involved in gene repression while also having a role in blocking DNA transcription factors (Moore et al., 2013). In eukaryotes, DNA methylation most often involves the addition of a methyl group to the C5 position of cytosine, forming 5-methylcytosine (5mC) (Moore et al., 2013). Other forms of DNA methylation exist, namely N6-methyladenine and N4-methylcytosine; however, their role in eukaryotes is far less clear, and thus they will not be a focus of this review (Xiao et al., 2018; Rodriguez et al., 2022). The level of methylation and demethylation of DNA is modulated by DNA methyltransferases (DNMTs) and ten-eleven translocase (TET) enzymes (Figure 1) (Moore et al., 2013; Rasmussen and Helin, 2016). DNMTs catalyse DNA methylation by transferring a methyl group to the fifth carbon of a cytosine to form 5mC (Moore et al., 2013). TET enzymes regulate the oxidation of 5mC to 5-hydroxymethylcytosine (5hmC), which can be further oxidised to form 5-formylcytosine (5fC) and 5-carboxylcytosine (5caC), leading to DNA demethylation (Moore et al., 2013). After oxidation to 5fC or 5caC, restoration of the molecule to a cytosine is modulated by thymine DNA glycosylase (TDG), which is an essential component of the base excision repair (BER) pathway (Moore et al., 2013).

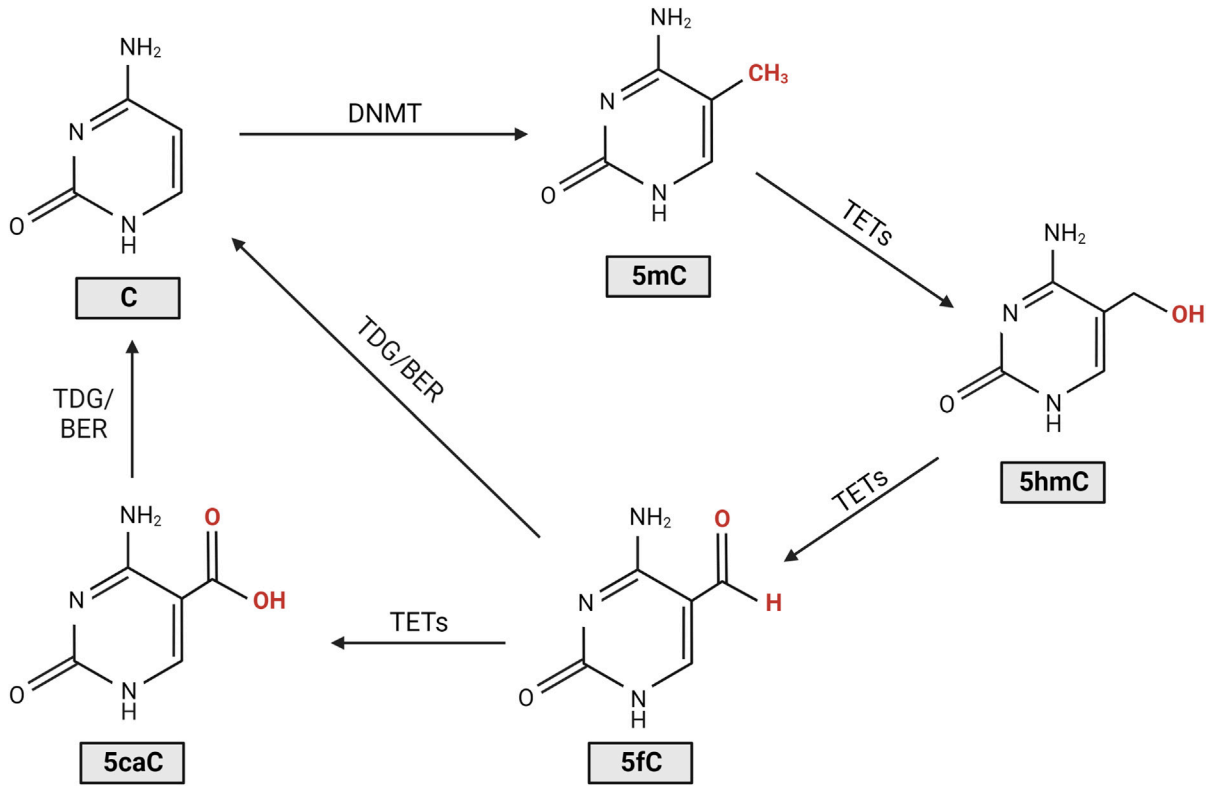

FIGURE 1
Cytosine DNA methylation and demethylation. DNA methyltransferases (DNMTs) introduce a methyl group to the cytosine (C), forming 5-methylcytosine (5mC). Ten-eleven translocase (TET) enzymes then regulate the oxidation of 5mC to 5-hydroxymethylcytosine (5hmC), 5-formylcytosine (5fC), and 5-carboxylcytosine (5caC). Following oxidation to 5fC or 5caC, restoration of the molecule to cytosine is modulated by thymine DNA glycosylase (TDG), an essential component of the base excision repair (BER) pathway (Moore et al., 2013; Rasmussen and Helin, 2016).

Changes to the proportion of oxidised cytosines and DNMTs are involved in multiple pathologies such as cancer and are thought to potentially contribute to photoreceptor degeneration in models of IRD (Wahlin et al., 2013; Farinelli et al., 2014; Locke et al., 2019). 5mC and 5hmC are the best understood of the cytosine derivatives and are thought to be the most biologically relevant thus far. This review will focus on studies that involve their dysregulation in IRDs.

Wahlin et al. (2013) first reported aberrant DNA methylation levels in the *rd1* mouse model of retinitis pigmentosa (RP), a widely used model that displays rapid rod photoreceptor loss that peaks between postnatal days 12–14 (P12-14; for a summary of all preclinical models discussed in this review, refer to Supplementary Table S1) (Keeler, 1924; LaVail and Sidman, 1974; Portera-Cailliau et al., 1994; Wahlin et al., 2013). At timepoints corresponding to this peak of rod cell death, both rod and cone photoreceptors in the *rd1* retina were found to possess increased immunoreactivity for 5mC and 5hmC compared to wildtype controls (Wahlin et al., 2013). This increase in 5hmC positive cells was seen as early as P9, and numbers were even greater at P10, prior to significant thinning of the outer nuclear layer (ONL) which occurs around 2 weeks postnatal (Wahlin et al., 2013). The authors noted that cells stained positively for either 5hmC or 5mC were also positive for the cell death terminal deoxynucleotidyl transferase dUTP nick end labelling (TUNEL) stain (Wahlin et al., 2013). The same group also investigated this phenomenon in homozygous rhodopsin-GFP knock-in mice carrying the P23H *Rho* mutation, which displayed 5mC positive cells in the early stages of degeneration. Similarly, in P23H adult retinal explants that were grown for 4 and 7 days, as the ONL degenerated there was an accumulation of 5mC positive cells, primarily in rods (Wahlin et al., 2013). These results were validated by a similar study that looked at 5mC expression in four models of RP, the *rd1* and *rd2* mouse models, which have mutations in the *Pde6b* and *Prph2* genes, respectively, and the P23H and S334ter rat models, which harbor mutations in the *Rho* gene (Farinelli et al., 2014). It was shown that at the peak of cell death in each model there was an increase in 5mC expression in photoreceptors that was colocalised with TUNEL positivity (Farinelli et al., 2014). The *rd1* mouse retina was further investigated at the ultrastructural level, revealing a severely altered chromatin structure which coincided with increased expression of the DNA methylating isozyme, DNMT3a. In microarray analysis, the *rd1* mouse showed hypermethylation of genes involved in cell death and survival, cell morphology, and nervous system development, correlating with a transcriptional silencing action. Interestingly, *rd1* retinal explants treated with the DNMT inhibitor decitabine showed a reduction in photoreceptor cell death after 4 days of treatment and a reduction in 5mC positive cells (Farinelli et al., 2014). These results suggest a potential role of DNA methylation in the pathological process of IRD and shows that DNA methylation may be a potential target for neuroprotection. However, research into this field is still in comparatively early stages, as only two studies currently have assessed the changes in DNA methylation in the context of IRD (Figure 2). As such, there is a need to understand the role of DNA

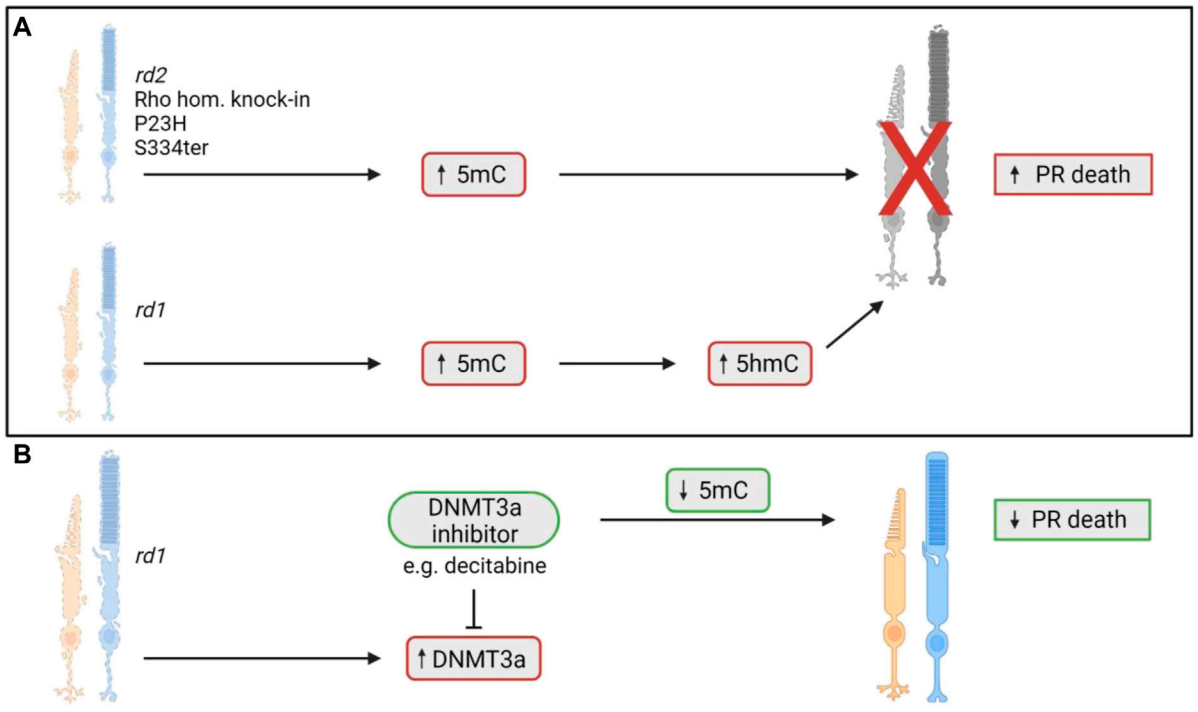

FIGURE 2
DNA methylation changes involved in photoreceptor death in models of IRD. **(A)** Previous studies have shown an upregulation of the demethylated cytosine molecule, 5-methylcytosine (5mC), in five models of IRD (Wahlin et al., 2013; Farinelli et al., 2014). The 5mC upregulation coincides with the photoreceptor degeneration found in each model (Wahlin et al., 2013; Farinelli et al., 2014). In the *rd1* mouse model only, increased levels of the 5-hydroxymethylcytosine (5hmC) molecule was noted as well (Wahlin et al., 2013). 5hmC is an oxidised form of 5mC, with increased levels coinciding with photoreceptor death (Wahlin et al., 2013). **(B)** In the *rd1* mouse, there was increased expression of DNMT3a, an enzyme responsible for the demethylation of cytosine to form 5mC. When *rd1* retinal explants were treated with the DNMT3a inhibitor, decitabine, they noted a decrease in 5mC positive cells and a reduction in photoreceptor cell death (Farinelli et al., 2014). PR = photoreceptor.

methylation in the degenerative process, as well as the links between aberrant DNA methylation and photoreceptor loss in other models of IRD, and how to best translate any beneficial outcomes in preclinical research to the clinic.

3 Histone modifications

3.1 Histone acetylation and deacetylation

3.1.1 The basics of histone acetylation and deacetylation

Histone modifications permit significant changes in the regulation of DNA and play a major role in almost all fundamental biological processes. Modifications are complex, with many chemical groups that can be added to histones such as methyl, acetyl, and ADP-ribose units (Bannister and Kouzarides, 2011). Gene expression changes vary depending on the type and location of these modifications (Bannister and Kouzarides, 2011). Post-translational acetylation and deacetylation of histone proteins allow the bidirectional regulation of gene expression and chromatin architecture by opening (acetylation) or closing (deacetylation) the chromatin structure (Park and Kim, 2020). The dynamic process and balance of acetylation and deacetylation are modulated by histone acetyltransferases (HATs) and histone deacetylases (HDAC), respectively (Figure 3) (Bannister and Kouzarides, 2011). Over the years, many studies have reported an association between altered HDAC activity and the pathology of IRDs. HDACs counteract the acetylation process modulated by HATs by removing acetyl groups from histone proteins, deacetylating histones back to their basal state, thereby suppressing gene expression (Bannister and Kouzarides, 2011). HDACs can be separated into four broad categories: Class I (HDACs 1, 2, 3, 8), Class II (HDACs 4, 5, 6, 7, 9, 10), Class III (NAD-dependent sirtuins) and Class IV (HDAC11) (Bannister and Kouzarides, 2011; Balaiya et al., 2017). Each HDAC class and its isoforms have unique biological functions, tissue specificity, enzymatic activity and more (Balaiya et al., 2017; Park and Kim, 2020). Classical HDACs (Class I, II and IV) are distinct from sirtuins (Class III HDACs), so will be discussed separately.

In the field of IRDs, research has mainly focused on establishing the role of histone deacetylation in the context of photoreceptor degeneration. A substantial decrease in acetylation (hypoacetylation) was identified in the *rd1* retina, thought to be due to an increase in HDAC class I, II, and IV activity (Sancho-Pelluz et al., 2010). Interestingly, approximately 94% of hypoacetylated cells were positive for TUNEL staining, while increased HDAC activity was detected 2 days before TUNEL positivity, suggesting that HDAC activity may precede the final stages of cell death (Sancho-Pelluz et al., 2010). This was further confirmed when *rd1* explants were treated with the pan-HDAC inhibitor, trichostatin A (TSA), which caused a significant reduction in TUNEL-positive cells. However, when treated with the class I HDAC inhibitor, Scriptaid, no neuroprotective effects on photoreceptor survival were reported (Sancho-Pelluz et al., 2010). A later study went on to identify a potential causative role of HDAC in photoreceptor degeneration, highlighting that HDAC overactivity was a common feature in ten animal models of IRD: *rd1*, *rd10*, *rd2*, *Cngb1*$^{-/-}$, *Rho*$^{-/-}$, S334ter, P23H, *Pde6c*^{cpfl1}, *Cnga3*$^{-/-}$, and *Rpe65*$^{-/-}$ (Arango-Gonzalez et al., 2014).

3.1.2 Pan-HDAC inhibitors for the treatment of IRD

Due to the identification of HDAC overactivity in multiple models of IRD, many studies have searched for neuroprotective effects of pharmacological inhibition of HDACs. In the *Pde6c*^{cpfl1} achromatopsia mouse model, treatment with TSA at P14, the time of onset of cone photoreceptor death in this model, resulted in cone rescue up to 10 days post-treatment (Trifunović et al., 2016). This study also showed improved localisation of cone-specific proteins, including opsins and cone transducin (GNAT2), and improved cone developmental migration patterns (Trifunović et al., 2016). When TSA was administered later in the disease stage at P18 the drug still displayed neuroprotective abilities, with a 10% increase in cone numbers and improved cone migration persisting as long as 12 days following a single intravitreal injection (Samardzija et al., 2019). TSA has also shown neuroprotective ability in *rd10* retinal explants, with

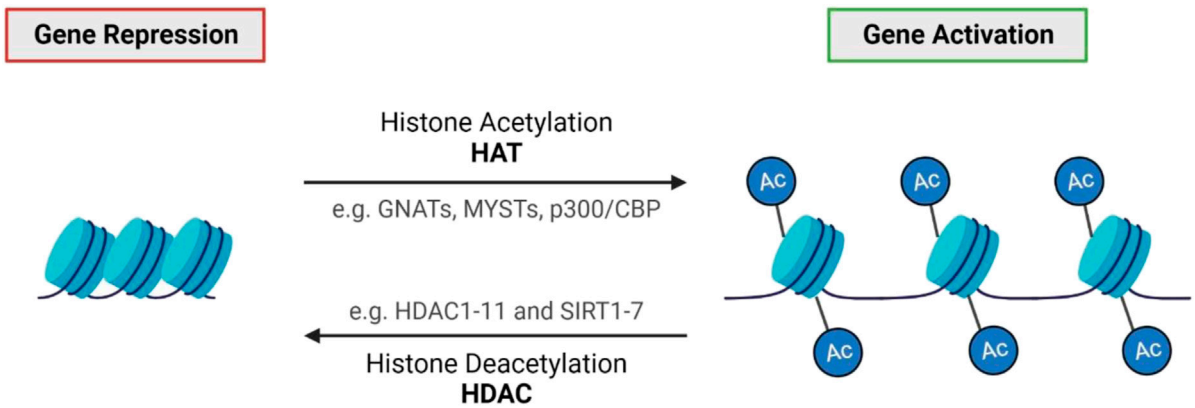

FIGURE 3
Histone acetylation and deacetylation. Histone acetylation generally results in gene activation through chromatin de-condensation, whereas deacetylation results in gene repression (Park and Kim, 2020). The balance of acetylation and deacetylation is modulated by two opposing classes of enzymes: histone acetyltransferases (HATs) and histone deacetylases (HDACs) (Bannister and Kouzarides, 2011; Park and Kim, 2020).

a five-fold increase in surviving photoreceptors (Trifunović et al., 2018). Administration of TSA in the *rd1* and *rd10* models at later stages of the disease, P19 and P42, respectively, was sufficient to preserve and support cone survival long-term while also allowing cones to remain light sensitive with preservation of visual function (Samardzija et al., 2020). Another pan-HDAC inhibitor, SAHA, was tested in 661W cells that were stressed with a non-specific phosphodiesterase inhibitor, resulting in improved cell survival, mitochondrial respiration and reduced mitochondrial fission in the 661W cells (Perron et al., 2021). When *rd1* explants were treated with SAHA, the number of photoreceptors approximately doubled compared to controls (Perron et al., 2021; Dong et al., 2023).

Despite evidence that pharmacological HDAC inhibition is neuroprotective in several models of IRD, the molecular basis for this neuroprotection is poorly understood, mainly because HDAC inhibition drives concurrent transcriptional changes in numerous genes. For example, Samardzija et al. (2021) performed RNA sequencing analysis on *rd1* cones treated with TSA, showing that TSA may have a multi-level protection mechanism via regulation of different pro-survival pathways including MAPK, PI3K-Akt and autophagy (Samardzija et al., 2020). These studies and others have highlighted the complexity of HDAC and the impact of its inhibition. As such, more broad transcriptional studies are required to help understand the mechanisms behind the neuroprotection that arises from HDAC inhibition.

3.1.3 Valproic acid and its controversial clinical translation

Only one HDAC inhibitor has been tested in clinical trials for use in RP, valproic acid (VPA); however, it sparked much debate due to highly variable patient responses and concerns raised about the study design. VPA was already FDA-approved for use in epilepsy, bipolar and migraine disorders. As previous work in animal models of RP showed VPA could inhibit apoptosis, activate microglia and stimulate photoreceptor regeneration from glial cells, drug repurposing was suggested for its therapeutic use in RP (Clemson, 2010). Additionally, VPA was found to be a potent molecular chaperone with the ability to increase the yield of properly folded mutant rhodopsin in the *Rho*$^{P23H/+}$ heterozygous knock-in mouse (Clemson, 2010; Kaushal et al., 2010). The initial human study reported that VPA had improved visual acuity in 9 of the 13 eyes from patients with RP; however, this study was criticised for a number of reasons, including a lack of controls and the failure to properly account for side effects from VPA use (Clemson et al., 2011; Sandberg et al., 2011). VPA was tested in a further three patients, but the trial was ended prematurely as the patients experienced a reduction in visual acuity and significant side effects including intolerable photophobia in one patient and torsional nystagmus in another, both of which were resolved upon cessation of VPA (Sisk, 2012). A subsequent non-randomised trial with ten patients showed an improved mean visual acuity after 3 months of daily VPA oral dosing, with average visual acuity progressing from 20/72 to 20/65 (Shanmugam et al., 2012). Similarly, a fourth study reported that 14 out of 15 RP patients treated with VPA had improved visual acuity (Kumar et al., 2014). Iraha et al. (2016) reported that after 6 months of VPA use, 16 out of 29 patients considered it "easier to see" when undergoing the Humphrey field analyser central 10–2 program. Patients showed improved best corrected visual acuity and visual field testing after treatment, but this improvement was lost once VPA administration was ceased (Iraha et al., 2016). Conversely, Bhalla et al. reported that in 31 patients with a range of different IRDs, there was, on average, a reduction in their visual field after VPA treatment, with most patients experiencing either no change or a slight decrease in visual acuity (Bhalla et al., 2013). Finally, a trial using VPA for 6–12 months on RP patients of unknown genotype, found no improvement in best corrected visual acuity measurements or visual field analyses, while noting potential decreases in some ERG measurement parameters (Totan et al., 2017).

Sisk (2012) suggested that genotype differences may be responsible for the variable patient outcomes (Sisk, 2012), a proposal validated by several studies conducted in animal models. A study conducted in four *Xenopus laevis* models, which expressed different RP-linked alleles of human rhodopsin, showed that administration of VPA in a *Xenopus* line with the P23H rhodopsin mutation was neuroprotective and led to an improvement in visual function (Vent-Schmidt et al., 2017). The other three *Xenopus* lines carrying the Q344ter, T17M, or T4K rhodopsin mutations did not demonstrate these same improvements (Vent-Schmidt et al., 2017). Similarly, a study carried out in two mouse models of autosomal recessive RP, the *rd1* and *rd10* mouse models, showed that daily injections for 12 days of VPA in *rd1* mice resulted in a significant increase in photoreceptor rows, with several extra rows of rod nuclei compared to PBS injected controls (Mitton et al., 2014). On the other hand, when VPA was administered in the *rd10* mouse model there was a failure of photoreceptor rescue and reduced visual function (Mitton et al., 2014). In 2018, the results of a randomised phase 2 multicentre placebo-controlled clinical trial of 90 patients with genetically characterised autosomal dominant RP revealed a small but significantly worse outcome for VPA-treated patients (Birch et al., 2018). Most adverse events reported were mild, but ultimately, the use of VPA in autosomal dominant RP was not supported (Birch et al., 2018). Future clinical translation and research of VPA or other HDAC inhibitors should consider the genotypes and clinical diagnosis of the patient and how that could affect their response to treatment with HDAC inhibitors. Importantly, when considering treatment regimes, different pan-HDAC inhibitors may have slightly different HDAC targets or have stronger affinities to certain isoforms, thus not all HDAC inhibitors will necessarily have the same effect in patients.

3.1.4 Isoform-specific HDAC inhibitors for the treatment of IRD

Isoform-specific HDAC inhibition has also been investigated, allowing for a deeper understanding of HDAC subtypes that may be associated with cell death and potentially reducing off-target toxicity sometimes associated with pan-HDAC inhibitors (Bieliauskas and Pflum, 2008; Vishwakarma et al., 2013). A study that used romidepsin, an HDAC1 and HDAC2 inhibitor, in the *rd10* mouse, found that it caused significant neuroprotection and preservation of the rods, the ONL thickness increasing by approximately three-fold (Popova et al., 2021). Of concern, romidepsin also caused a reduction in weight gain throughout

the treatment when compared to age-matched controls (Popova et al., 2021). In one study, no increase in cell survival was observed when the HDAC6 specific inhibitor, Tubastatin A, was applied to 661W cells that had been stressed with a non-specific phosphodiesterase inhibitor (Perron et al., 2021). Contrastingly, when 661W cells were stressed with hydrogen peroxide, treatment with Tubastatin A promoted cell survival, perhaps due to upregulation of heatshock proteins 25 and 70, heat shock transcription factor 1 and peroxiredoxin 1 (Leyk et al., 2017). Tubastatin A was then tested in the *dye*^{ucd6} zebrafish model of IRD, resulting in improved retinal morphology, as assessed by qualitative improvement of the photoreceptors, a slight improvement in outer segment length, and rescue of visual function (Leyk et al., 2017). The authors suggested that HDAC6 inhibition and the associated regulation of peroxiredoxin may play a role in protecting the photoreceptors in this model (Leyk et al., 2017). In the *atp6v0e1*$^{-/-}$ zebrafish model, HDAC6 inhibition with Tubastatin A led to improved visual function and cell morphology, the treated zebrafish showing an eight-fold improvement in vision and a 44.7% improvement in photoreceptor outer segment area (Sundaramurthi et al., 2020). Proteome sequencing after treatment revealed modulation of ubiquitin-proteasome, phototransduction, metabolism, and phagosome pathways. In addition, when using *rd10* retinal explants, there was an increased number of cone arrestin-positive cells after treatment with Tubastatin A (Sundaramurthi et al., 2020). Another study used electroporation to overexpress HDAC4 to investigate its role in the degenerative process in newborn *rd1* mice (Chen and Cepko, 2009). Retinae transfected to overexpress HDAC4 (but not HDAC5 or HDAC6) contained more rods at P50, at a time when these photoreceptors would usually have degenerated (Chen and Cepko, 2009). Furthermore, compared to the full-length HDAC4 protein, expression of a short N-terminal domain of HDAC4 resulted in a more extensive preservation of *rd1* rods, greater cone survival and partial restoration of cone visual function (Guo et al., 2015). The authors speculated HDAC4s photoreceptor protection ability might be due to a restoration of altered gene expression of cell cycle progression genes *Ccnb1* and *Ccnd1*, the transcription factors c-fos, c-jun, and p53, endoplasmic reticulum stress genes such as *Atf4*, *Chop* and *Casp12* and apoptotic/cell death genes such as *Bid* and *Parp1* (Guo et al., 2015).

In summary, HDAC overactivity seems to be a consistent feature in many preclinical models of IRD, with HDAC inhibition being neuroprotective. More recently, isoform-specific studies have highlighted that not all HDAC overactivity is necessarily deleterious, with evidence that HDAC4 can be neuroprotective. Further studies should validate if such results are consistent across different models of IRD, as well as looking at HDAC isoforms that have not been investigated yet. A summary of all studies that investigate HDAC changes and consequent HDAC modulation is shown in Figure 4.

3.1.5 Sirtuins–function in IRDs

The Class III HDACs, sirtuins, are a unique and highly conserved family of nicotinamide adenine dinucleotide (NAD)-dependent protein deacetylases. They deacetylate both histone and non-histone proteins and are involved in cellular functions such as stress response, apoptosis, DNA repair, cell differentiation and much more (Balaiya et al., 2017). Seven sirtuins have been identified in mammals (SIRT1-7) (Balaiya et al., 2017). The role of sirtuins was investigated in the *rd1* mouse, to ascertain if the overactive HDAC activity was derived from classical HDACs, sirtuins or both (Sancho-Pelluz et al., 2010). In the *rd1* retina, while there was a small increase in overall sirtuin activity compared to wildtype controls, classic HDACs showed a much more substantial increase (Sancho-Pelluz et al., 2010). To further elucidate if sirtuins contributed to *rd1* retinal pathology, the sirtuin inhibitor nicotinamide was administered to *rd1* explants, but no improvement in photoreceptor survival was observed (Sancho-Pelluz et al., 2010). To elucidate which specific sirtuin isoforms might be important in photoreceptor degeneration, Sirt1 immunoreactivity was assessed in retinae from *rd10* mice aged from P14 until 5 months of age (Jaliffa et al., 2009). There was strong Sirt1 staining at P15 in scattered cells throughout the ONL of the central retina (Jaliffa et al., 2009). Over time, Sirt1 immunoreactivity decreased as the *rd10* retina degenerated, following an apparent central-to-periphery gradient (Jaliffa et al., 2009). This staining was seen mostly, if not exclusively, in the nucleus of the photoreceptors, and approximately 85% of the Sirt1-positive cells were also TUNEL-positive (Jaliffa et al., 2009). Additionally, of the Sirt1-positive cells, 82% were also positive for the apoptotic marker caspase-12, and 71% for mitochondrial apoptosis inducing factor, Aif (Jaliffa et al., 2009). In a different IRD model, the *Nmnat1*$^{V9M/V9M}$ mutant mouse, sirtuin expression changes were assessed indirectly by examining the sites they deacetylate, such as H3K9, H3K18, and H4K16 (Greenwald et al., 2021). H3K9ac is deacetylated by Sirt1 and potentially Sirt6, H3K18ac by Sirt7, and H4K16ac, by Sirt1, Sirt2, and possibly Sirt6 (Greenwald et al., 2021). All three sites showed no significant changes compared to wildtype, suggesting that these particular sirtuins were not dysregulated as a part of *Nmnat1*$^{V9M/V9M}$ disease progression (Greenwald et al., 2021). Overall, only one study by Jaliffa et al. (2009) has identified sirtuin expression changes might be relevant in the degeneration seen in models of IRD (Jaliffa et al., 2009). Clearly, more work needs to be done to understand the potential role of sirtuins in different IRDs, especially since sirtuin changes have been noted in several different neurodegenerative disorders such as Alzheimer's and Parkinson's disease (Chandramowlishwaran et al., 2020). Increasing online access to single-cell sequencing data will permit more detailed and potentially revealing information about sirtuin expression in disease photoreceptors.

3.2 Histone methylation

Histone methylation and demethylation are the processes whereby methyl groups are added or removed from histone proteins (Greer and Shi, 2012). The methylation process is dynamic and supported by various enzymes, which can add or remove methyl groups on different histone types, as well as specific residues on those histones (Figure 5).

Significantly, abnormal changes to these methylation marks have been associated with a multitude of diseases, including

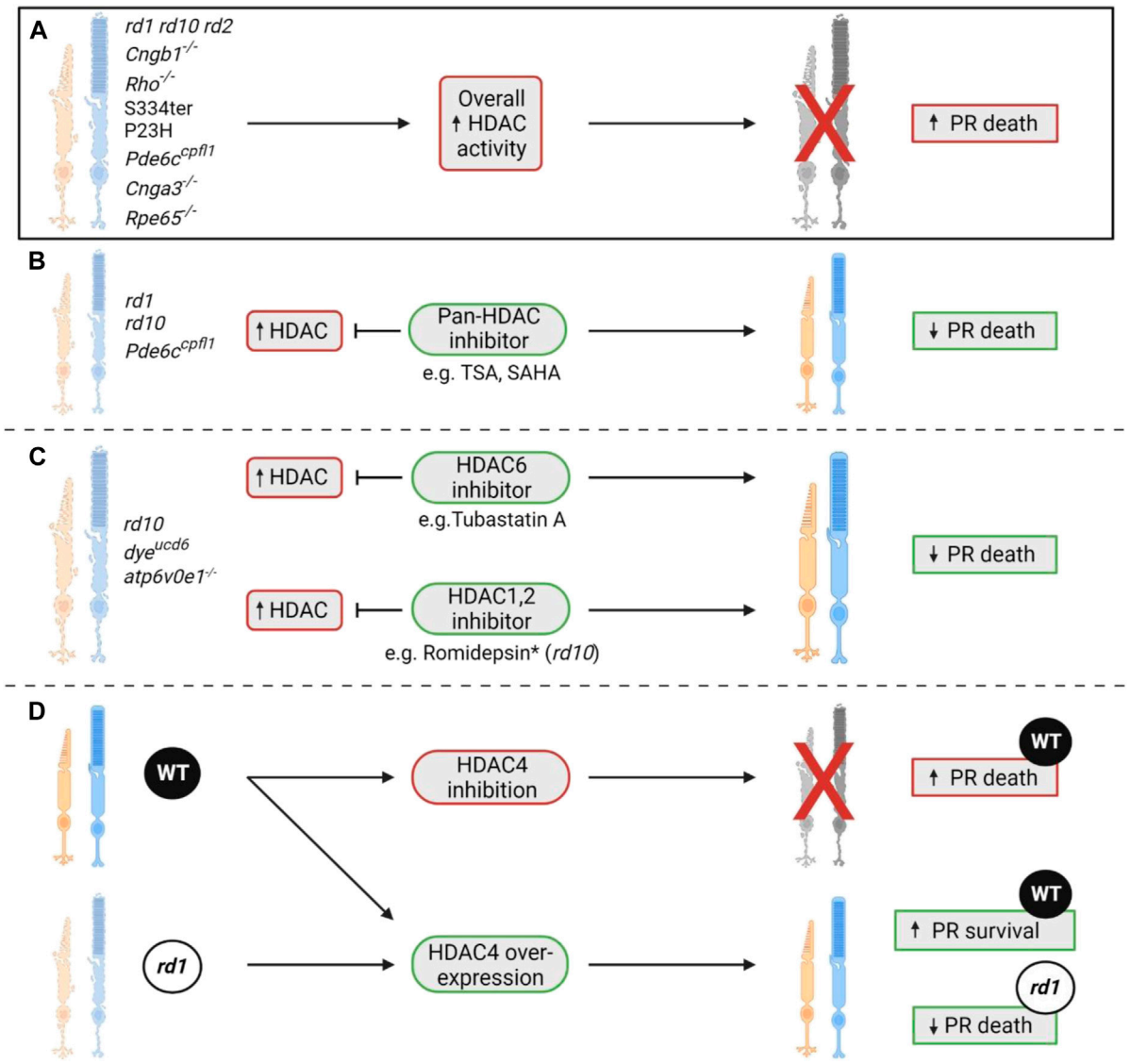

FIGURE 4
The role of HDACs in photoreceptor degeneration. **(A)** A seminal study showcased that histone deacetylase (HDAC) overactivity was a consistent phenomenon observed in ten different rodent models of IRD, namely the *rd1*, *rd10*, *rd2*, *Cngb1*$^{-/-}$, *Rho*$^{-/-}$, S334ter, P23H, *Pde6c*^{cpfl1}, *Cnga3*$^{-/-}$, *and Rpe65*$^{-/-}$ (Sancho-Pelluz et al., 2010; Arango-Gonzalez et al., 2014). This increase in overall HDAC activity coincided with the peak of cell death in each of these models (Sancho-Pelluz et al., 2010; Arango-Gonzalez et al., 2014). **(B)** Previous studies have shown that inhibition of HDAC with a pan-HDAC inhibitor such as trichostatin A (TSA) or SAHA can result in significant retention of photoreceptor numbers. These neuroprotective effects were displayed in two RP models (*rd1* and *rd10*) and one achromatopsia model (*Pde6c*^{cpfl1}) (Trifunović et al., 2016; Trifunović et al., 2018; Samardzija et al., 2019; Samardzija et al., 2020; Perron et al., 2021; Dong et al., 2023). **(C)** Isoform-specific HDAC inhibition has also proven beneficial in various models of IRD, with treatment with the HDAC1/2 inhibitor romidepsin allowing for preservation of rod numbers in the *rd10* model of RP (Popova et al., 2021). *Despite romidepsin having neuroprotective effects in the retina, it caused a reduction in weight gain throughout treatment compared to age-matched wildtype controls, displaying a potential systemic toxicity (Popova et al., 2021). HDAC6 inhibition has also been shown to be neuroprotective in the *dye*^{ucd6}, *atp6v0e1*$^{-/-}$ zebrafish models of inherited blindness and the *rd10* mouse model of RP (Leyk et al., 2017; Sundaramurthi et al., 2020). Each model had HDAC6 inhibited via administration of the HDAC6 inhibitor Tubastatin A. In the two zebrafish models, improvements in retinal morphology and visual function were observed (Leyk et al., 2017; Sundaramurthi et al., 2020). In the *rd10* model, an improvement in the number of cone arrestin positive cells was observed (Sundaramurthi et al., 2020). **(D)** HDAC4 inhibition in wildtype (WT) mice has been shown to cause photoreceptor death, implying that overexpression of HDAC4 is in fact neuroprotective (Chen and Cepko, 2009; Guo et al., 2015). This was validated when HDAC4 overexpression in WT and *rd1* mice showed increased photoreceptor survival in both lines (Chen and Cepko, 2009; Guo et al., 2015). PR = photoreceptor.

cancer and neurodegenerative disease (Song et al., 2016; Basavarajappa and Subbanna, 2021). Some forms of IRDs have also been associated with changes in methylation, but this field is still in its comparative infancy. In 2020, Zheng and colleagues made the first discovery of the involvement of histone methylation in IRDs, reporting increased expression of H3K27me3 in retinae from *rd1* mice (Zheng et al., 2018). The global histone methylation inhibitor DZNep was administered

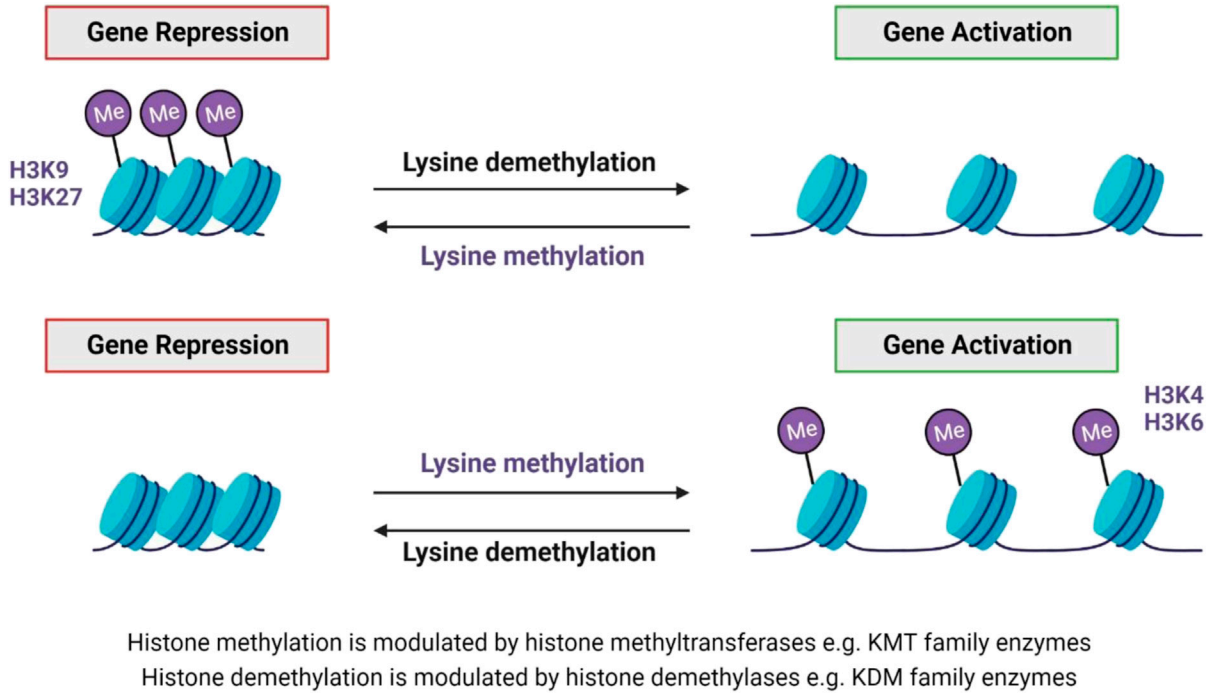

FIGURE 5
Lysine methylation and demethylation. Histone methytransferases modulate histone methylation, while demethylation is modulated by histone demethylases (Greer and Shi, 2012; Song et al., 2016). Both lysine methylation and demethylation can result in either gene repression or activation - dependent on the lysine residue that is methylated, e.g. H3K9 and H3K27 methylation results in gene repression, whereas H3K4 and H3K6 methylation result in gene activation (Basavarajappa and Subbanna, 2021).

subretinally at P0, resulting in the preservation of both the a- and b-wave in scotopic and photopic electroretinogram (ERG) recordings at P14 (Zheng et al., 2018). With the same treatment regime, ONL thickness was significantly retained by 70% compared to untreated controls (Zheng et al., 2018). Significant improvement in ONL thickness was also seen at P21 after treatment at P0; however, improvement in the ERGs was no longer present (Zheng et al., 2018). Another study in the *rd10* model of RP reported that inhibition of the histone methylation eraser, lysine demethylase 1, LSD1, which specifically demethylates H3K4me1/2 and H3K9me1/2, resulted in reduced rod degeneration, preservation of vision, and influenced the expression of multiple genes including maintenance of rod-specific transcripts and downregulation of genes involved in inflammation, gliosis and cell death (Popova et al., 2021). The authors suggested that the neuroprotective activity of LSD1 inhibitors firstly targeted histone modifications, increasing accessibility of chromatin and upregulation of neuroprotective genes, then potentially inhibited transcription of inflammatory genes (Popova et al., 2021). Finally, in a recent study, we found that the ubiquitous H3K27me3 expression seen in wildtype cones was lost in the *Pde6c*^{cpfl1} mouse model of achromatopsia (Miller et al., 2022). Administration of GSK-J4, a histone demethylase inhibitor that targets H3K27me3, resulted in increased immunostaining of H3K27me3 in *Pde6c*^{cpfl1} cones, and increased cone survival in retinal explants. When GSK-J4 was administered to mice via a single intravitreal injection, there were significant transcriptional changes to pathways involved in mitochondrial dysfunction, endoplasmic reticulum stress and key epigenetic pathways (Miller et al., 2022). The role of histone methylation modifications and their contribution to IRD pathology has only recently been investigated, with current studies showing crucial differences in H3K27me3 status in cone and rod photoreceptors, where ubiquitous expression in rods is deleterious to survival, while it is beneficial in cones. A summary of all studies that have assessed changes in histone methylation in preclinical IRD models can be found in Figure 6. Future studies should investigate the differences between histone methylation patterns in rods versus cones and attempt to understand which changes to histone methylation sites are most relevant.

3.3 Poly(ADP-ribosyl)ation and associated processes

3.3.1 The role of PARP

Poly(ADP-ribosyl)ation is a post-translational modification involving the addition of ADP-ribose units on the glutamic or aspartic acid residues of histone and non-histone target proteins, catalysed by poly (ADP-ribose) polymerase (PARP; Figure 7) (Tong et al., 2001; Kraus and Lis, 2003; Quénet et al., 2009). Modifications can involve mono ADP-ribose additions

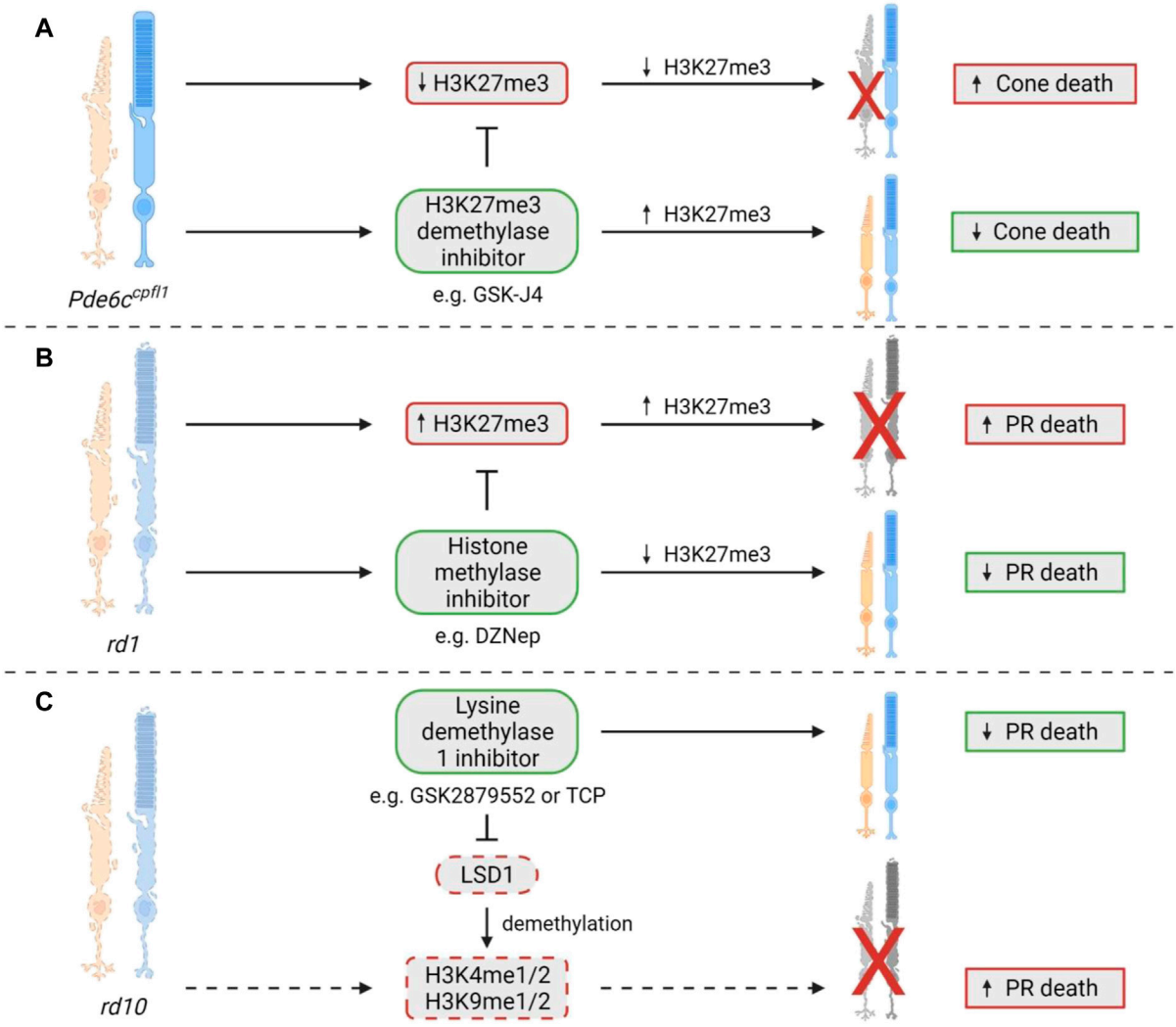

FIGURE 6
Histone methylation changes in IRDs. **(A)** In the *Pde6c*^{cpfl1} mouse model of achromatopsia, decreased expression of the usually ubiquitous H3K27me3 was noted in cone photoreceptors specifically. A significant cone photoreceptor survival was observed when H3K27me3 demethylation was inhibited via GSK-J4 administration in *Pde6c*^{cpfl1} retinal explants (Miller et al., 2022). **(B)** Interestingly, the *rd1* mouse model, which shows degeneration of both rod and cone photoreceptors, showed an increase in H3K27me3 expression that coincides with photoreceptor cell death. After treatment with the histone methylase inhibitor DZNep, there was a significant improvement in photoreceptor survival (Zheng et al., 2018). **(C)** A study in the *rd10* model of RP showed that treatment with a lysine demethylase 1 (LSD1) inhibitor, such as GSK2879552 or TCP, could cause a reduction in photoreceptor cell death. LSD1 is known to demethylate H3K4me1/2 and H3K9me1/2, which may contribute to cell death in this model, although the study did not directly assess this, so it remains to be confirmed (Popova et al., 2021). PR = photoreceptor.

or can involve chains of ADP-ribose polymers being added, called poly (ADP-ribose) (PAR) accumulation (Langelier et al., 2018). PAR accumulation generally causes transcriptional activation via chromatin de-condensation and the alteration of promoter and enhancer activity (Kraus and Lis, 2003; Quénet et al., 2009). This reaction is reversible due to the endo- and exo-glycosidic activity of poly (ADP-ribose) glycohydrolase (PARG) (Quénet et al., 2009). PARP is involved in various cellular roles, including cell proliferation, cell death, DNA repair, genomic stability, and epigenetic regulation (Tong et al., 2001; Quénet et al., 2009). The role of poly(ADP-ribosyl)ation, and the relevant molecules in this process have garnered attention for their potential role in neurodegeneration, including in IRDs.

3.3.2 PARPs in IRDs

Paquet-Durand et al. (2007) first suggested that excessive activation of PARP may have a role in the photoreceptor death seen in *rd1* mice (Paquet-Durand et al., 2007). As photoreceptors degenerated in *rd1* retinae, there was a concomitant increase in PAR positive staining which was identified via immunohistochemistry, and increased PARP activity (Paquet-Durand et al., 2007). Interestingly, in P11 *rd1* sections, 88% of PAR- or PARP-positive cells were also positive for the TUNEL cell death marker. Additionally, PAR- or PARP-positive cells were shown to co-localise with avidin and AIF, an oxidative damage marker and mitochondrial apoptosis-inducing factor, respectively (Paquet-Durand et al., 2007). The role of PARP activation in cell death was also established in two rat models of autosomal

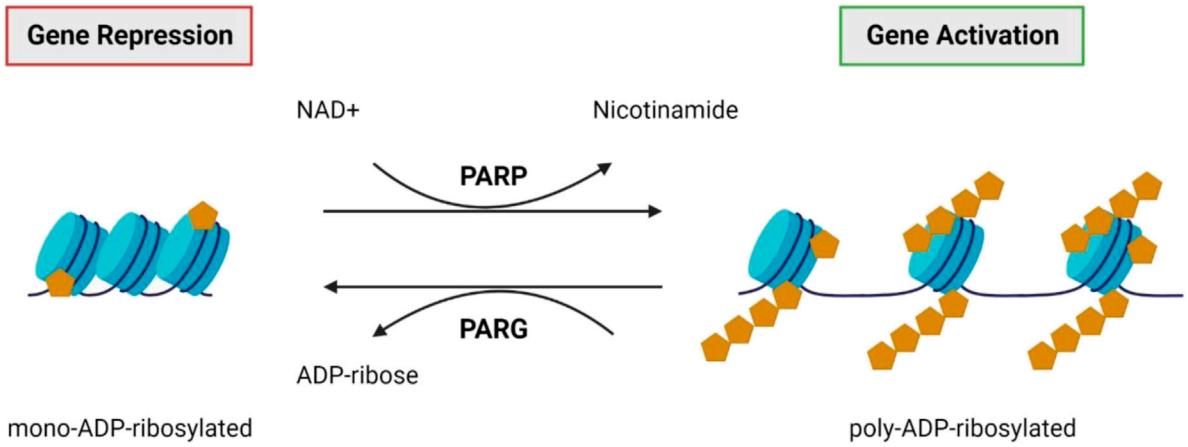

FIGURE 7
PARP and PARG. Poly (ADP-ribose) polymerases (PARPs) catalyse the attachment of poly-ADP-ribose units on the glutamic or aspartic acid residues of the target protein (Tong et al., 2001; Kraus and Lis, 2003; Quénet et al., 2009). Generally, this results in transcriptional activation via chromatin de-condensation and altered promoter and enhancer activity (Kraus and Lis, 2003; Quénet et al., 2009). This reaction is reversible by poly (ADP-ribose) glycohydrolase (PARG) activity (Quénet et al., 2009).

dominant RP with different mutations in the rhodopsin gene, P23H and S334ter. A significant activation of PARP was seen during cell death in these two models, which coincided with increased cellular oxidative stress, the activation of calpain, a protein linked to both apoptotic and necrotic cell death processes, and a reduction in its endogenous inhibitor calpastatin (Kaur et al., 2011). Another study looked at the impact of PARP in retinal degeneration using a *Parp1* knockout (*Parp1*$^{-/-}$) (Sahaboglu et al., 2010). The retina of the *Parp1*$^{-/-}$ mouse line was found to be morphologically similar to wildtype; however, there was a significant resistance to retinal degeneration when induced by blocking phosphodiesterase 6 (PDE6), an essential component of the phototransduction pathway. In contrast, application of the same PDE6 blocker caused rapid retinal degeneration in wildtype controls (Sahaboglu et al., 2010). The observed resistance to PDE6 induced retinal degeneration in *Parp1*$^{-/-}$ mutants suggests that PARP1 may be involved in photoreceptor degeneration via PARP-mediated cell death or a closely related mechanism (Sahaboglu et al., 2010). The role of PARP1 is largely opposed by its functional antagonist, poly-ADP-glycohydrolase (PARG), and another study by the same group investigated its effect in a *Parg110* knockout (*Parg110*$^{-/-}$) mouse. *Parg110*$^{-/-}$ mice were morphologically and functionally indistinguishable from wildtype mice, and when *Parg110*$^{-/-}$ mice were exposed to the PDE6 inhibitor there was a significant resistance to treatment, similar to that seen in *Parp1*$^{-/-}$ mice (Sahaboglu et al., 2014). The authors postulated that this resistance was due to low levels of PARP activity and reduced PAR accumulation, suggesting a positive regulation of PARP1 that must usually be present but is absent in the *Parg110*$^{-/-}$ retinae (Sahaboglu et al., 2014). Despite the initial assessment of PARG110 as a functional antagonist, this study revealed that there is, in fact, a positive feedback loop between PARP1 and PARG110, which is thought to be especially active in pathological conditions (Sahaboglu et al., 2014).

3.3.3 Is PARP overexpression or activation a consistent finding in IRDs?

More broadly, PARP overactivity was consistently elevated compared to wildtype controls in ten models of IRD, namely the P23H and S334ter rat models of autosomal dominant RP, *rd1*, *rd2*, *rd10*, *Cngb1*$^{-/-}$ and *Rho*$^{-/-}$ mice models of autosomal recessive RP, the *Rpe65*$^{-/-}$ model of Leber's congenital amaurosis and the *Pde6c*^{cpfl1} and *Cnga3*$^{-/-}$ models of achromatopsia (Arango-Gonzalez et al., 2014). This study also highlighted the consistent overactivity of other molecules involved in a non-apoptotic cell death pathway, including calpains, protein kinase G and HDAC. These observations suggest that similar mechanisms may modulate cell death in these ten models and may allow for generic neuroprotection using drugs that target these molecules across multiple models of IRD. Jiao et al. (2016) examined four additional models of RP, all with mutations in the *Pde6a* gene (three homozygous point mutations *Pde6a* R562W, D670G, V685M, and one compound heterozygous *Pde6a*$^{V685M/R562W}$). In each of the four models there appeared to be PARP overactivation and PAR accumulation which correlated with the progression of photoreceptor degeneration (Jiao et al., 2016). Interestingly, the models that possessed the most rapid photoreceptor degeneration (V685M, *Pde6a*$^{V685M/R562W}$) seemed to have lower levels of PARP activity. In contrast, in the slower degeneration models (R562W, D670G) there was a greater amount of PARP activity in dying cells. In the D670G mutant, the mildest form of all four models, almost 100% of PARP-positive cells were also TUNEL-positive (Jiao et al., 2016). This study also reported that pharmacological PARP inhibition using PJ34, was neuroprotective in all models to varying extents (Jiao et al., 2016). All models displayed a reduction in TUNEL-positive cells after treatment as well as an increase in the number of photoreceptor rows. There appeared to be an inverse

correlation between the strength of the genetic insult and the efficacy of PJ34, with the D670G model, which has the slowest degeneration, having the best treatment effects (Jiao et al., 2016). Furthermore, addition of PJ34 to retinal explant cultures preserved the number of photoreceptor rows in all models except for the V685M at 10 days, but this effect was no longer evident by 16 days, an effect that could be due to the short-term viability of retinal explants or, perhaps, loss of treatment efficacy (Jiao et al., 2016). Similar effects of PJ34 were noted in two other mouse models of RP. There was a decrease in levels of poly(ADP-ribosyl)ation and photoreceptor cell death in *rd1* retinal explants treated with PJ34 (Paquet-Durand et al., 2007), while *rd2* explants had a reduction in photoreceptor death, decreased poly(ADP ribosyl)ation, and improved rhodopsin localisation in the outer segments of rods (Sahaboglu et al., 2017).

Interestingly, a study in the *Nmnat1*$^{V9M/V9M}$ mouse model of IRD, which harbours a mutation in a gene responsible for NAD+ biosynthesis, showed that PARP activity was elevated during disease progression, with increased PAR expression in the photoreceptors (Greenwald et al., 2021). As PARP is a consumer of nuclear NAD+, this finding may suggest the photoreceptors in the *Nmnat1*$^{V9M/V9M}$ mouse might be dying via PARthanatos. This unique cell death pathway occurs due to the overactivation of PARP and overproduction of PAR rather than through classic apoptotic pathways (Fatokun et al., 2014; Greenwald et al., 2021). This hypothesis was further validated in a subsequent study by the same group where RNA sequencing of *Nmnat1*$^{V9M/V9M}$ retinae at 3 weeks of age showed a significant upregulation in the expression of *Parp1*, *Parp3*, *Tiparp* (*Parp7*), *Parp9*, *Parp12*, *Zchav1* (*Parp13*), *Parp14* and *Parp16* (Brown et al., 2022). By 4 weeks of age, PARP activity was significantly increased compared to wildtype controls (Brown et al., 2022). These increases in *Parp* expression appeared to coincide with reduced NAD+ activity, increased DNA damage, and increased immune reactivity in the retina (Brown et al., 2022). Furthermore, PARP upregulation has also been linked to endoplasmic reticulum (ER) stress-mediated cell death. In a model of achromatopsia caused by a mutation in the *ATF6* gene, which is best known for its role in transducing signals related to ER stress, patient fibroblasts harbouring the *ATF6*$^{Y567N/Y567N}$ mutation were more sensitive to ER stress and PARP overexpression (Chiang et al., 2017; Hillary and FitzGerald, 2018). Lastly, use of a monoclonal antibody that targets TNF-alpha in *rd10* RP mice resulted in a significant reduction in photoreceptor cell death, concurrently reducing PAR content, an indirect measurement of PARP activity (Martínez-Fernández de la Cámara et al., 2015).

3.3.4 The implication of PARP inhibition on photoreceptor cell death

Because dysregulated PARP activity seems to be a consistent feature during the death of photoreceptors in IRD, and the use of PJ34 to inhibit PARP appeared beneficial, multiple other PARP inhibitors have been tested to assess their effectiveness in preclinical models. These include inhibitors that are FDA-approved or in late stages of clinical trials, with the hope for easier drug repurposing in the future. R503, ABT-888 (in phase 3 clinical trials) and Olaparib (FDA-approved for use in ovarian cancer treatment) were all tested for their effectiveness in *rd1* mice, with R503 and ABT-888 showing relative toxicity at low drug concentrations (Sahaboglu et al., 2016). Contrastingly, the FDA-approved Olaparib, which targets PARP1 and PARP2 isoforms, did not show toxicity and exhibited photoreceptor protection after treatment, in both short-term (treatment starting at P7 and finishing at P11) and long-term experiments (P7-P17). Olaparib reduced the number of TUNEL-positive cells and decreased PARylation while preserving ONL thickness (Sahaboglu et al., 2016). There was also a reduction in cGMP levels, thought to be an essential component of cell death in this model (Sahaboglu et al., 2016). However, this neuroprotective effect was lost by P24 (Sahaboglu et al., 2016). In a separate study, another two PARP inhibitors, BMN-673 (FDA-approved) and 3-aminobenzamine were utilised in the *rd1* mouse, and both were able to reduce photoreceptor cell death by 25%–40%. The authors suggested this survival may be due to a relationship between PARP and the highly conserved kinase GSK and Wnt/catenin pathways, which are involved in various cellular processes such as differentiation, adult tissue homeostasis and apoptosis (Antolín and Mestres, 2014; Yang et al., 2016; Pai et al., 2017; Sahaboglu et al., 2020). Before treatment, there was a reduction in GSK-alpha immunoreactivity in *rd1* retinae in the ganglion cell and inner cell layers, and a small but not significant reduction in the ONL. When treated with the PARP inhibitors, these expression levels were reversed towards wildtype levels. Beta-catenin showed a significantly lower expression in the RPE, but no significant reduction in the ganglion cell layer and inner nuclear layer. These changes were partially neutralised by BMN-673 in the ganglion cell layer and the RPE, and by 3-aminobenzamide in the ganglion cell layer, RPE and the inner nuclear layer (Sahaboglu et al., 2020).

Given the data suggesting the influence of PARP in multiple IRDs, and the fact that PARP inhibition generally enhances photoreceptor survival (summary in Figure 8), the next steps in this field should include developing a firm understanding of the mechanisms behind this protection. Analysis of PARP inhibition in clinical trials involving IRD patients should be undertaken to determine if PARP inhibitors can benefit all patients or only a small subset dependent on genotype or mutation, and determine the safety of long-term treatment and its effect on disease progression.

3.4 Interactions between different post-translational modifications

Post-translational modifications such as DNA methylation, histone acetylation, histone methylation and poly(ADP-ribosyl)ation all have complex interactions and functional interplay. Several studies in IRD have highlighted these complex relationships, emphasising that epigenetic modifications do not take place in isolation (Nakao, 2001; Lee et al., 2006; Ummarino et al., 2021; Khalid et al., 2022; Miller et al., 2022). In 2010, Sancho-Pelluz and colleagues discovered that both HDAC and PARP were overactive in *rd1* mice (Sancho-Pelluz et al., 2010). Interestingly, they found that HDAC overactivity preceded PARP overactivity by approximately 2 days, with these findings later validated in a separate study that observed the same pattern of HDAC overactivity preceding PARP overactivity in ten different models of IRD (Sancho-Pelluz et al., 2010; Arango-Gonzalez et al., 2014). Additionally, it was found that PARP overactivity coincided with the peak of cell death, a determination based on positive TUNEL staining (Arango-

Gonzalez et al., 2014). Notably, they found that calpain and PARP overactivity coincided with TUNEL staining, indicating that they may be involved in the final stages of cell death, as TUNEL labels DNA nick-ends which are associated with final stages of cell death, while HDAC overactivity and cGMP accumulation appeared to be found earlier in the cell death process (Arango-Gonzalez et al., 2014). Dong et al. (2023) also showed that treating *rd1* explants with the PARP inhibitor Olaparib improved photoreceptor survival and reduced HDAC activity (Dong et al., 2023). In a similar line, overexpression of HDAC4 using electroporation significantly increased rod photoreceptor survival in *rd1* mice retinae (Guo et al., 2015). HDAC4 overexpression led to a 50% decrease in *Parp1* expression, along with other markers for cell death, cell cycle genes, and oxidative and endoplasmic reticulum stress, suggesting that *Parp1*, with other vital genes, may be involved in the protective effect seen with HDAC4 overexpression (Guo et al., 2015).

HDAC has also been shown to interact with other epigenetic modifications, such as histone methylation, where treatment with the pan-HDAC inhibitor TSA in the *Pde6c*^{cpfl1} mouse model of achromatopsia resulted in changes to histone methylation status. H3K27me3 levels which are severely reduced in *Pde6c*^{cpfl1} mice compared to wildtype, were partially restored to wildtype levels upon treatment, highlighting the effect that HDAC inhibition has on histone methylation (Miller et al., 2022). HDAC has also been shown to interact with DNA methylation via DMNT activity in *rd1* and *rd2* mice as well as in S334ter and P23H rat models of RP. Each model showed 5mC positive cells had very low or absent levels of acetylated lysine, suggesting a key interplay between HDAC and DNMT (Farinelli et al., 2014). Functional interplay between DNA methylation changes and poly(ADP-ribosyl)

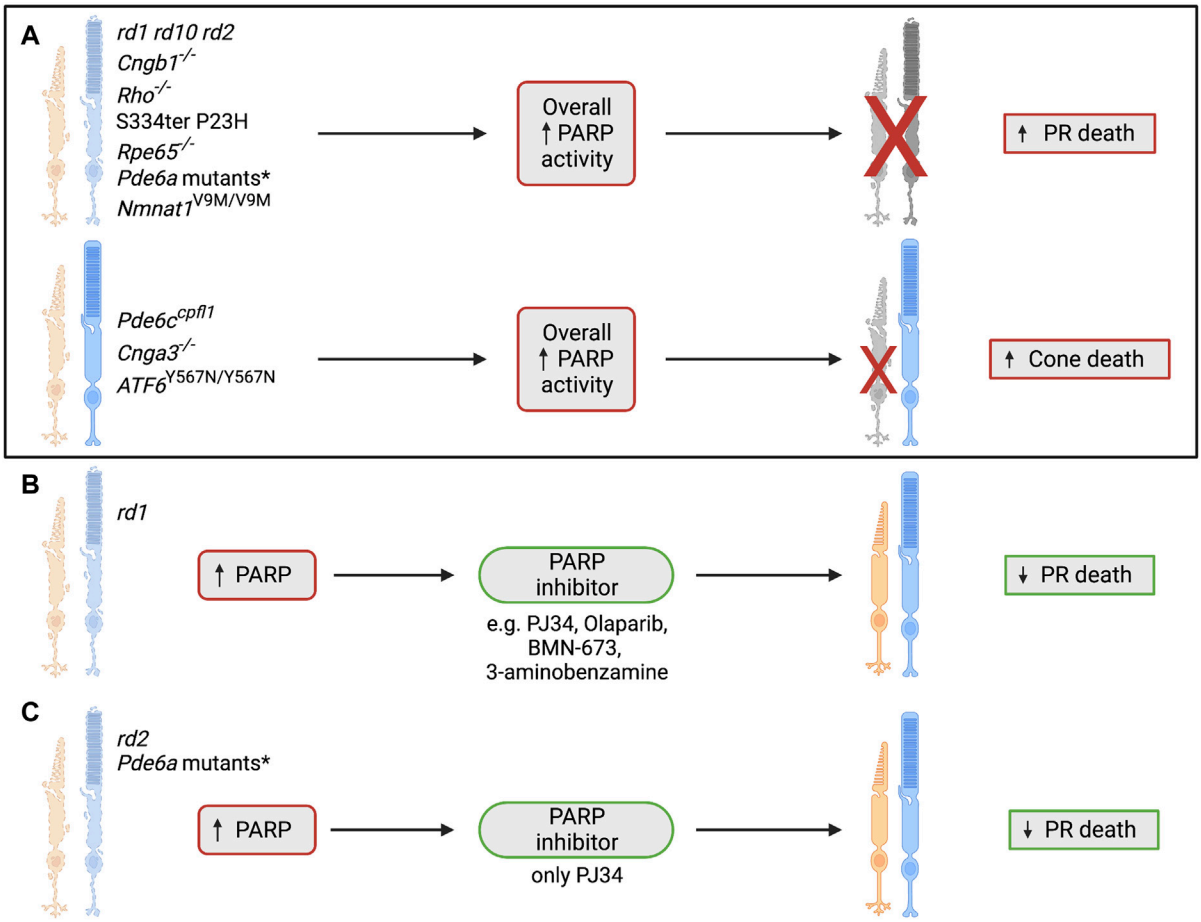

FIGURE 8
The role of poly(ADP-ribosyl)ation and PARP in IRDs. **(A)** PARP overactivity has previously been shown in many IRD models, including autosomal dominant RP, autosomal recessive RP, Leber's congenital amaurosis, cone/rod dystrophy and achromatopsia. This consistent overactivity of PARP has been shown to coincide with photoreceptor cell death, suggesting a link between these two processes (Paquet-Durand et al., 2007; Kaur et al., 2011; Arango-Gonzalez et al., 2014; Jiao et al., 2016; Chiang et al., 2017; Greenwald et al., 2021). *The *Pde6a* mutant models that have shown an increase in overall PARP activity are *Pde6a* R562W, *Pde6a* D670G, *Pde6a* V685M and *Pde6a*$^{V685M/R562W}$ (Jiao et al., 2016). **(B)** Testing of several PARP inhibitors has taken place in the *rd1* model and has indicated PARP inhibition as a strong candidate for neuroprotection of photoreceptors in IRD. Photoreceptor survival has been noted after administration of PJ34, Olaparib, BMN-673, and 3-aminobenzamine (Paquet-Durand et al., 2007; Sahaboglu et al., 2016; Sahaboglu et al., 2020). **(C)** Various IRD models have been used to test the PARP inhibitor PJ34, including the *rd1*, *rd2*, *Pde6a* R562W, *Pde6a* D670G, *Pde6a* V685M and *Pde6a*$^{V685M/R562W}$ models. PJ34 has shown neuroprotective benefits in all mentioned models and reduces photoreceptor death after administration (Paquet-Durand et al., 2007; Jiao et al., 2016; Sahaboglu et al., 2017). *The *Pde6a* mutant models that have shown a reduction in photoreceptor death after treatment with PJ34 are *Pde6a* R562W, *Pde6a* D670G, *Pde6a* V685M and *Pde6a*$^{V685M/R562W}$ (Jiao et al., 2016). PR = photoreceptor.

ation has been suggested; for instance, a study on *rd1* retinae revealed that many cells in the ONL that were positive for 5mC staining were also positive for PAR staining (Wahlin et al., 2013; Ummarino et al., 2021). Contrastingly, another study showed that PARP inhibition during the peak of degeneration in *rd1* retinae, did not cause any changes to 5mC and 5hmC levels, suggesting that DNA methylation may actually be unrelated or upstream to PARP activity (Sahaboglu et al., 2016).

The understanding of interactions between different epigenetic modifications in the context of IRD is still in relative infancy. In the future these types of studies may help us understand the neuroprotective effects of these drugs on a mechanistic level and may be used to leverage the use of multiple epigenetic modifying drugs for a synergistic and protective effect.

4 Conclusion

The potential role of epigenetic modifiers in IRD pathology has been gaining new insights in recent years. Roles for DNA methylation and histone modifications such as deacetylation, methylation, and poly(ADP-ribosyl)ation have been suggested, with modulation of each being a potential therapeutic target. The development of new cell-specific epigenetic techniques such as CUT&Tag, for example, will greatly assist in elucidating the role of histone modifications in IRD disease processes and its potential for therapeutic targeting. While understanding DNA methylation and histone methylation in IRD is still quite a new field, the influence of PARP and HDACs have been more extensively studied. PARP inhibition has been tested in multiple preclinical models and a better understanding of the mechanisms that underlie its neuroprotective action will only improve therapeutic options in the future. Both pan- and selective HDAC inhibition have shown promising potential in various preclinical models, although the HDAC inhibitor VPA remains the only drug that has so far proceeded to clinical trials. However, likely due to its different impact depending on the genetic basis of the IRD, its further use is currently discouraged due to inconsistent results in these clinical studies. A better understanding of how HDAC inhibitors affect people with different genotypes will facilitate future clinical translation of these types of drugs. There may also be sex differences in epigenetic regulation and drug metabolism that need to be considered (Gegenhuber and Tollkuhn, 2019; Li et al., 2019; Oliva et al., 2020; Saravanan et al., 2023). Clearly, interaction between each of these epigenetic regulators are very complex, with functional relationships via diverse molecules and intracellular pathways. In order to best understand these complex relationships, further omics studies are needed, ideally concurrently, which would allow for a better understanding of cell and mutation specific differences. Using multiple omics platforms in parallel would also allow for superior discernment of the changes underpinning the protective effects of epigenetic modulating drugs. This in-depth grasp of cellular mechanisms will be essential before successful translation of therapies to the clinic.

Author contributions

AM, AH, DT, and LC contributed to the conception of this review. AM wrote the first draft of the manuscript. RJ and AM created and edited the figures. All authors contributed to the article and approved the submitted version.

Acknowledgments

Figures in this manuscript were created using BioRender.com.

Conflict of interest

The authors declare that the research was conducted in the absence of any commercial or financial relationships that could be construed as a potential conflict of interest.

Publisher's note

Supplementary material

The Supplementary Material for this article can be found online at: https://www.frontiersin.org/articles/10.3389/fcell.2023.1224078/full#supplementary-material

References

Antolín, A. A., and Mestres, J. (2014). Linking off-target kinase pharmacology to the differential cellular effects observed among PARP inhibitors. *Oncotarget* 5 (10), 3023–3028. doi:10.18632/oncotarget.1814

Arango-Gonzalez, B., Trifunović, D., Sahaboglu, A., Kranz, K., Michalakis, S., Farinelli, P., et al. (2014). Identification of a common non-apoptotic cell death mechanism in hereditary retinal degeneration. *PLoS One* 9 (11), e112142. doi:10.1371/journal.pone.0112142

Balaiya, S., Abu-Amero, K. K., Kondkar, A. A., and Chalam, K. V. (2017). Sirtuins expression and their role in retinal diseases. *Oxidative Med. Cell. Longev.* 2017, 3187594. doi:10.1155/2017/3187594

Bannister, A. J., and Kouzarides, T. (2011). Regulation of chromatin by histone modifications. *Cell Res.* 21 (3), 381–395. doi:10.1038/cr.2011.22

Basavarajappa, B. S., and Subbanna, S. (2021). Histone methylation regulation in neurodegenerative disorders. *Int. J. Mol. Sci.* 22 (9), 4654. doi:10.3390/ijms22094654

Berger, W., Kloeckener-Gruissem, B., and Neidhardt, J. (2010). The molecular basis of human retinal and vitreoretinal diseases. *Prog. Retin Eye Res.* 29 (5), 335–375. doi:10.1016/j.preteyeres.2010.03.004

Bhalla, S., Joshi, D., Bhullar, S., Kasuga, D., Park, Y., and Kay, C. N. (2013). Long-term follow-up for efficacy and safety of treatment of retinitis pigmentosa with valproic acid. *Br. J. Ophthalmol.* 97 (7), 895–899. doi:10.1136/bjophthalmol-2013-303084

Bieliauskas, A. V., and Pflum, M. K. H. (2008). Isoform-selective histone deacetylase inhibitors. *Chem. Soc. Rev.* 37 (7), 1402–1413. doi:10.1039/b703830p

Birch, D. G., Bernstein, P. S., Iannacone, A., Pennesi, M. E., Lam, B. L., Heckenlively, J., et al. (2018). Effect of oral valproic acid vs placebo for vision loss in patients with autosomal dominant retinitis pigmentosa: A randomized phase 2 multicenter placebo-controlled clinical trial. *JAMA Ophthalmol.* 136 (8), 849–856. doi:10.1001/jamaophthalmol.2018.1171

Brown, E. E., Scandura, M. J., Mehrotra, S., Wang, Y., Du, J., and Pierce, E. A. (2022). Reduced nuclear NAD+ drives DNA damage and subsequent immune activation in the retina. *Hum. Mol. Genet.* 31 (9), 1370–1388. doi:10.1093/hmg/ddab324

Brunet, A. A., Harvey, A. R., and Carvalho, L. S. (2022). Primary and secondary cone cell death mechanisms in inherited retinal diseases and potential treatment options. *Int. J. Mol. Sci.* 23 (2), 726. doi:10.3390/ijms23020726

Center DSTUoTHS (2020). Center DSTUoTHS. RetNet 1996-2020. Available from: https://sph.uth.edu/retnet/.

Chandramowlishwaran, P., Vijay, A., Abraham, D., Li, G., Mwangi, S. M., and Srinivasan, S. (2020). Role of sirtuins in modulating neurodegeneration of the enteric nervous system and central nervous system. *Front. Neurosci.* 14, 614331. doi:10.3389/fnins.2020.614331

Chen, B., and Cepko, C. L. (2009). HDAC4 regulates neuronal survival in normal and diseased retinas. *Sci. (New York, NY)* 323 (5911), 256–259. doi:10.1126/science.1166226

Chiang, W. C., Chan, P., Wissinger, B., Vincent, A., Skorczyk-Werner, A., Krawczyński, M. R., et al. (2017). Achromatopsia mutations target sequential steps of ATF6 activation. *Proc. Natl. Acad. Sci. U. S. A.* 114 (2), 400–405. doi:10.1073/pnas.1606387114

Clemson, C. M. (2010). *Development of a multi-site phase II clinical trial of valproic acid for retinitis pigmentosa.*

Clemson, C. M., Tzekov, R., Krebs, M., Checchi, J. M., Bigelow, C., and Kaushal, S. (2011). Therapeutic potential of valproic acid for retinitis pigmentosa. *Br. J. Ophthalmol.* 95 (1), 89–93. doi:10.1136/bjo.2009.175356

Dong, Y., Yan, J., Yang, M., Xu, W., Hu, Z., Paquet-Durand, F., et al. (2023). Inherited retinal degeneration: Towards the development of a combination therapy targeting histone deacetylase, poly (ADP-Ribose) polymerase, and calpain. *Biomolecules* 13 (4), 581. doi:10.3390/biom13040581

Farinelli, P., Perera, A., Arango-Gonzalez, B., Trifunovic, D., Wagner, M., Carell, T., et al. (2014). DNA methylation and differential gene regulation in photoreceptor cell death. *Cell Death Dis.* 5 (12), e1558–e. doi:10.1038/cddis.2014.512

Fatokun, A. A., Dawson, V. L., and Dawson, T. M. (2014). Parthanatos: Mitochondrial-linked mechanisms and therapeutic opportunities. *Br. J. Pharmacol.* 171 (8), 2000–2016. doi:10.1111/bph.12416

Galvin, O., Chi, G., Brady, L., Hippert, C., Del Valle Rubido, M., Daly, A., et al. (2020). The impact of inherited retinal diseases in the republic of Ireland (ROI) and the United Kingdom (UK) from a cost-of-illness perspective. *Clin. Ophthalmol. Auckl. NZ)* 14, 707–719. doi:10.2147/OPTH.S241928

Gegenhuber, B., and Tollkuhn, J. (2019). Sex differences in the epigenome: A cause or consequence of sexual differentiation of the brain? *Genes (Basel)* 10 (6), 432. doi:10.3390/genes10060432

Greenwald, S. H., Brown, E. E., Scandura, M. J., Hennessey, E., Farmer, R., Du, J., et al. (2021). Mutant Nmnat1 leads to a retina-specific decrease of NAD+ accompanied by increased poly(ADP-ribose) in a mouse model of NMNAT1-associated retinal degeneration. *Hum. Mol. Genet.* 30 (8), 644–657. doi:10.1093/hmg/ddab070

Greer, E. L., and Shi, Y. (2012). Histone methylation: A dynamic mark in health, disease and inheritance. *Nat. Rev. Genet.* 13 (5), 343–357. doi:10.1038/nrg3173

Guo, X., Wang, S-B., Xu, H., Ribic, A., Mohns, E. J., Zhou, Y., et al. (2015). A short N-terminal domain of HDAC4 preserves photoreceptors and restores visual function in retinitis pigmentosa. *Nat. Commun.* 6, 8005. doi:10.1038/ncomms9005

Hillary, R. F., and FitzGerald, U. (2018). A lifetime of stress: ATF6 in development and homeostasis. *J. Biomed. Sci.* 25 (1), 48. doi:10.1186/s12929-018-0453-1

Iraha, S., Hirami, Y., Ota, S., Sunagawa, G. A., Mandai, M., Tanihara, H., et al. (2016). Efficacy of valproic acid for retinitis pigmentosa patients: A pilot study. *Clin. Ophthalmol.* 10, 1375–1384. doi:10.2147/OPTH.S109995

Jaliffa, C., Ameqrane, I., Dansault, A., Leemput, J., Vieira, V., Lacassagne, E., et al. (2009). Sirt1 involvement in rd10 mouse retinal degeneration. *Invest. Ophthalmol. Vis. Sci.* 50 (8), 3562–3572. doi:10.1167/iovs.08-2817

Jiao, K., Sahaboglu, A., Zrenner, E., Ueffing, M., Ekström, P. A. R., and Paquet-Durand, F. (2016). Efficacy of PARP inhibition in Pde6a mutant mouse models for retinitis pigmentosa depends on the quality and composition of individual human mutations. *Cell Death Discov.* 2 (1), 16040. doi:10.1038/cddiscovery.2016.40

Jin, B., Li, Y., and Robertson, K. D. (2011). DNA methylation: Superior or subordinate in the epigenetic hierarchy? *Genes Cancer* 2 (6), 607–617. doi:10.1177/1947601910393957

Kaur, J., Mencl, S., Sahaboglu, A., Farinelli, P., van Veen, T., Zrenner, E., et al. (2011). Calpain and PARP activation during photoreceptor cell death in P23H and S334ter rhodopsin mutant rats. *PLoS One* 6 (7), e22181. doi:10.1371/journal.pone.0022181

Kaushal, S., Noorwez, S. M., Tzekov, R., Huang, D., Li, Y., and Wen, R. (2010). The effect of valproic acid in mouse models of RP. *Investigative Ophthalmol. Vis. Sci.* 51 (13), 3735.

Keeler, C. E. (1924). The inheritance of a retinal abnormality in white mice. *Proc. Natl. Acad. Sci. U. S. A.* 10 (7), 329–333. doi:10.1073/pnas.10.7.329

Khalid, U., Simovic, M., Hammann, L. A., Iskar, M., Wong, J. K. L., Kumar, R., et al. (2022). A synergistic interaction between HDAC- and PARP inhibitors in childhood tumors with chromothripsis. *Int. J. Cancer* 151 (4), 590–606. doi:10.1002/ijc.34027

Kraus, W. L., and Lis, J. T. (2003). PARP goes transcription. *Cell* 113 (6), 677–683. doi:10.1016/s0092-8674(03)00433-1

Kumar, A., Midha, N., Gogia, V., Gupta, S., Sehra, S., and Chohan, A. (2014). Efficacy of oral valproic acid in patients with retinitis pigmentosa. *J. Ocular Pharmacol. Ther.* 30 (7), 580–586. doi:10.1089/jop.2013.0166

Langelier, M. F., Eisemann, T., Riccio, A. A., and Pascal, J. M. (2018). PARP family enzymes: Regulation and catalysis of the poly(ADP-ribose) posttranslational modification. *Curr. Opin. Struct. Biol.* 53, 187–198. doi:10.1016/j.sbi.2018.11.002

LaVail, M. M., and Sidman, R. L. (1974). C57BL/6J mice with inherited retinal degeneration. *Archives Ophthalmol.* 91 (5), 394–400. doi:10.1001/archopht.1974.03900060406015

Lee, M. G., Wynder, C., Bochar, D. A., Hakimi, M. A., Cooch, N., and Shiekhattar, R. (2006). Functional interplay between histone demethylase and deacetylase enzymes. *Mol. Cell Biol.* 26 (17), 6395–6402. doi:10.1128/MCB.00723-06

Leyk, J., Daly, C., Janssen-Bienhold, U., Kennedy, B. N., and Richter-Landsberg, C. (2017). HDAC6 inhibition by tubastatin A is protective against oxidative stress in a photoreceptor cell line and restores visual function in a zebrafish model of inherited blindness. *Cell Death Dis.* 8 (8), e3028–e. doi:10.1038/cddis.2017.415

Li, B., Gografe, S., Munchow, A., Lopez-Toledano, M., Pan, Z. H., and Shen, W. (2019). Sex-related differences in the progressive retinal degeneration of the rd10 mouse. *Exp. Eye Res.* 187, 107773. doi:10.1016/j.exer.2019.107773

Locke, W. J., Guanzon, D., Ma, C., Liew, Y. J., Duesing, K. R., Fung, K. Y. C., et al. (2019). DNA methylation cancer biomarkers: Translation to the clinic. *Front. Genet.* 10, 1150. doi:10.3389/fgene.2019.01150

Maguire, A. M., Bennett, J., Aleman, E. M., Leroy, B. P., and Aleman, T. S. (2021). Clinical perspective: Treating RPE65-associated retinal dystrophy. *Mol. Ther.* 29 (2), 442–463. doi:10.1016/j.ymthe.2020.11.029

Martínez-Fernández de la Cámara, C., Hernández-Pinto, A. M., Olivares-González, L., Cuevas-Martín, C., Sánchez-Aragó, M., Hervás, D., et al. (2015). Adalimumab reduces photoreceptor cell death in A mouse model of retinal degeneration. *Sci. Rep.* 5, 11764. doi:10.1038/srep11764

Miller, A. L., Fuller-Carter, P. I., Masarini, K., Samardzija, M., Carter, K. W., Rashwan, R., et al. (2022). Increased H3K27 trimethylation contributes to cone survival in a mouse model of cone dystrophy. *Cell Mol. Life Sci.* 79 (8), 409. doi:10.1007/s00018-022-04436-6

Mitton, K. P., Guzman, A. E., Deshpande, M., Byrd, D., DeLooff, C., Mkoyan, K., et al. (2014). Different effects of valproic acid on photoreceptor loss in Rd1 and Rd10 retinal degeneration mice. *Mol. Vis.* 20, 1527–1544.

Moore, L. D., Le, T., and Fan, G. (2013). DNA methylation and its basic function. *Neuropsychopharmacology* 38 (1), 23–38. doi:10.1038/npp.2012.112

Nakao, M. (2001). Epigenetics: Interaction of DNA methylation and chromatin. *Gene* 278 (1), 25–31. doi:10.1016/s0378-1119(01)00721-1

Oliva, M., Munoz-Aguirre, M., Kim-Hellmuth, S., Wucher, V., Gewirtz, A. D. H., Cotter, D. J., et al. (2020). The impact of sex on gene expression across human tissues. *Science* 369 (6509), eaba3066. doi:10.1126/science.aba3066

Pai, S. G., Carneiro, B. A., Mota, J. M., Costa, R., Leite, C. A., Barroso-Sousa, R., et al. (2017). Wnt/beta-catenin pathway: Modulating anticancer immune response. *J. Hematol. Oncol.* 10 (1), 101. doi:10.1186/s13045-017-0471-6

Paquet-Durand, F., Silva, J., Talukdar, T., Johnson, L. E., Azadi, S., van Veen, T., et al. (2007). Excessive activation of poly(ADP-ribose) polymerase contributes to inherited photoreceptor degeneration in the retinal degeneration 1 mouse. *J. Neurosci.* 27 (38), 10311–10319. doi:10.1523/JNEUROSCI.1514-07.2007

Park, S-Y., and Kim, J-S. (2020). A short guide to histone deacetylases including recent progress on class II enzymes. *Exp. Mol. Med.* 52 (2), 204–212. doi:10.1038/s12276-020-0382-4

Perron, N. R., Nasarre, C., Bandyopadhyay, M., Beeson, C. C., and Rohrer, B. (2021). SAHA is neuroprotective in *in vitro* and *in situ* models of retinitis pigmentosa. *Mol. Vis.* 27, 151–160.

Popova, E. Y., Imamura Kawasawa, Y., Zhang, S. S-M., and Barnstable, C. J. (2021). Inhibition of epigenetic modifiers LSD1 and HDAC1 blocks rod photoreceptor death in mouse models of retinitis pigmentosa. *J. Neurosci.* 41 (31), 6775–6792. doi:10.1523/JNEUROSCI.3102-20.2021

Portera-Cailliau, C., Sung, C. H., Nathans, J., and Adler, R. (1994). Apoptotic photoreceptor cell death in mouse models of retinitis pigmentosa. *Proc. Natl. Acad. Sci. U. S. A.* 91 (3), 974–978. doi:10.1073/pnas.91.3.974

Quénet, D., El Ramy, R., Schreiber, V., and Dantzer, F. (2009). The role of poly(ADP-ribosyl)ation in epigenetic events. *Int. J. Biochem. Cell Biol.* 41 (1), 60–65. doi:10.1016/j.biocel.2008.07.023

Rasmussen, K. D., and Helin, K. (2016). Role of TET enzymes in DNA methylation, development, and cancer. *Genes Dev.* 30 (7), 733–750. doi:10.1101/gad.276568.115

Rodriguez, F., Yushenova, I. A., DiCorpo, D., and Arkhipova, I. R. (2022). Bacterial N4-methylcytosine as an epigenetic mark in eukaryotic DNA. *Nat. Commun.* 13 (1), 1072. doi:10.1038/s41467-022-28471-w

Sahaboglu, A., Barth, M., Secer, E., Amo, E. M. D., Urtti, A., Arsenijevic, Y., et al. (2016). Olaparib significantly delays photoreceptor loss in a model for hereditary retinal degeneration. *Sci. Rep.* 6 (1), 39537. doi:10.1038/srep39537

Sahaboglu, A., Miranda, M., Canjuga, D., Avci-Adali, M., Savytska, N., Secer, E., et al. (2020). Drug repurposing studies of PARP inhibitors as a new therapy for inherited retinal degeneration. *Cell. Mol. Life Sci.* 77 (11), 2199–2216. doi:10.1007/s00018-019-03283-2

Sahaboglu, A., Sharif, A., Feng, L., Secer, E., Zrenner, E., and Paquet-Durand, F. (2017). Temporal progression of PARP activity in the Prph2 mutant rd2 mouse: Neuroprotective effects of the PARP inhibitor PJ34. *PLoS One* 12 (7), e0181374. doi:10.1371/journal.pone.0181374

Sahaboglu, A., Tanimoto, N., Bolz, S., Garrido, M. G., Ueffing, M., Seeliger, M. W., et al. (2014). Knockout of PARG110 confers resistance to cGMP-induced toxicity in mammalian photoreceptors. *Cell Death Dis.* 5 (5), e1234–e. doi:10.1038/cddis.2014.208

Sahaboglu, A., Tanimoto, N., Kaur, J., Sancho-Pelluz, J., Huber, G., Fahl, E., et al. (2010). PARP1 gene knock-out increases resistance to retinal degeneration without affecting retinal function. *PLOS ONE* 5 (11), e15495. doi:10.1371/journal.pone.0015495

Samardzija, M., Corna, A., Gomez-Sintes, R., Jarboui, M. A., Armento, A., Roger, J. E., et al. (2020). *HDAC inhibition ameliorates cone survival in retinitis pigmentosa mice*. Cell Death & Differentiation.

Samardzija, M., Masarini, K., Ueffing, M., and Trifunović, D. (Editors) (2019). "HDAC inhibition prevents primary cone degeneration even after the onset of degeneration," *Retinal degenerative diseases* (Cham: Springer International Publishing).

Sancho-Pelluz, J., Alavi, M. V., Sahaboglu, A., Kustermann, S., Farinelli, P., Azadi, S., et al. (2010). Excessive HDAC activation is critical for neurodegeneration in the rd1 mouse. *Cell Death Dis.* 1 (2), e24. doi:10.1038/cddis.2010.4

Sandberg, M. A., Rosner, B., Weigel-DiFranco, C., and Berson, E. L. (2011). Lack of scientific rationale for use of valproic acid for retinitis pigmentosa. *Br. J. Ophthalmol.* 95 (5), 744. doi:10.1136/bjo.2010.198176

Saravanan, M., Xu, R., Roby, O., Wang, Y., Zhu, S., Lu, A., et al. (2023). Tissue-specific sex difference in mouse eye and brain metabolome under fed and fasted states. *Investigative Ophthalmol. Vis. Sci.* 64 (3), 18. doi:10.1167/iovs.64.3.18

Shanmugam, P. M., Minija, C. K., Ramanjulu, R., Tekwani, P., and Saxena, M. (2012). Effect of short-term oral valproic acid on vision and visual field in retinitis pigmentosa. *Ophthalmol. Ther.* 1 (1), 6. doi:10.1007/s40123-012-0006-8

Sisk, R. A. (2012). Valproic acid treatment may be harmful in non-dominant forms of retinitis pigmentosa. *Br. J. Ophthalmol.* 96 (8), 1154–1155. doi:10.1136/bjophthalmol-2012-301950

Song, Y., Wu, F., and Wu, J. (2016). Targeting histone methylation for cancer therapy: Enzymes, inhibitors, biological activity and perspectives. *J. Hematol. Oncol.* 9 (1), 49. doi:10.1186/s13045-016-0279-9

Sundaramurthi, H., Roche, S. L., Grice, G. L., Moran, A., Dillion, E. T., Campiani, G., et al. (2020). Selective histone deacetylase 6 inhibitors restore cone photoreceptor vision or outer segment morphology in zebrafish and mouse models of retinal blindness. *Front. Cell Dev. Biol.* 8, 689. doi:10.3389/fcell.2020.00689

Tong, W-M., Cortes, U., and Wang, Z-Q. (2001). Poly(ADP-ribose) polymerase: A guardian angel protecting the genome and suppressing tumorigenesis. *Biochimica Biophysica Acta (BBA) - Rev. Cancer* 1552 (1), 27–37. doi:10.1016/s0304-419x(01)00035-x

Totan, Y., Güler, E., Yüce, A., and Dervişogulları, M. S. (2017). The adverse effects of valproic acid on visual functions in the treatment of retinitis pigmentosa. *Indian J. Ophthalmol.* 65 (10), 984–988. doi:10.4103/ijo.IJO_978_16

Trifunović, D., Arango-Gonzalez, B., Comitato, A., Barth, M., Del Amo, E. M., Kulkarni, M., et al. (2016). HDAC inhibition in the cpfl1 mouse protects degenerating cone photoreceptors *in vivo*. *Hum. Mol. Genet.* 25 (20), 4462–4472. doi:10.1093/hmg/ddw275

Trifunović, D., Petridou, E., Comitato, A., Marigo, V., Ueffing, M., and Paquet-Durand, F. (Editors) (2018). "Primary rod and cone degeneration is prevented by HDAC inhibition," *Retinal degenerative diseases* (Cham: Springer International Publishing).

Ummarino, S., Hausman, C., and Di Ruscio, A. (2021). The PARP way to epigenetic changes. *Genes (Basel).* 12 (3), 446. doi:10.3390/genes12030446

Vent-Schmidt, R. Y. J., Wen, R. H., Zong, Z., Chiu, C. N., Tam, B. M., May, C. G., et al. (2017). Opposing effects of valproic acid treatment mediated by histone deacetylase inhibitor activity in four transgenic *X. laevis* models of retinitis pigmentosa. *J. Neurosci.* 37 (4), 1039–1054. doi:10.1523/JNEUROSCI.1647-16.2016

Vishwakarma, S., Iyer, L. R., Muley, M., Singh, P. K., Shastry, A., Saxena, A., et al. (2013). Tubastatin, a selective histone deacetylase 6 inhibitor shows anti-inflammatory and anti-rheumatic effects. *Int. Immunopharmacol.* 16 (1), 72–78. doi:10.1016/j.intimp.2013.03.016

Wahlin, K. J., Enke, R. A., Fuller, J. A., Kalesnykas, G., Zack, D. J., and Merbs, S. L. (2013). Epigenetics and cell death: DNA hypermethylation in programmed retinal cell death. *PLOS ONE* 8 (11), e79140. doi:10.1371/journal.pone.0079140

Xiao, C. L., Zhu, S., He, M., Chen, D., Zhang, Q., Chen, Y., et al. (2018). N(6)-Methyladenine DNA modification in the human genome. *Mol. Cell* 71 (2), 306–318.e7. doi:10.1016/j.molcel.2018.06.015

Yang, E., Tacchelly-Benites, O., Wang, Z., Randall, M. P., Tian, A., Benchabane, H., et al. (2016). Wnt pathway activation by ADP-ribosylation. *Nat. Commun.* 7, 11430. doi:10.1038/ncomms11430

Zheng, S., Xiao, L., Liu, Y., Wang, Y., Cheng, L., Zhang, J., et al. (2018). DZNep inhibits H3K27me3 deposition and delays retinal degeneration in the rd1 mice. *Cell death Dis.* 9 (3), 310. doi:10.1038/s41419-018-0349-8

frontiers | Frontiers in Cell and Developmental Biology

TYPE Original Research
PUBLISHED 24 August 2023
DOI 10.3389/fcell.2023.1252547

OPEN ACCESS

EDITED BY
Glenn Prazere Lobo,
University of Minnesota Twin Cities, United States

REVIEWED BY
Tadao Maeda,
Kobe City Medical Center General Hospital, Japan
James A. Poulter,
University of Leeds, United Kingdom

*CORRESPONDENCE
Marion Jeanne,
jeanne.marion@gene.com

†These authors share first authorship

RECEIVED 03 July 2023
ACCEPTED 14 August 2023
PUBLISHED 24 August 2023

CITATION
Jones MK, Orozco LD, Qin H, Truong T, Caplazi P, Elstrott J, Modrusan Z, Chaney SY and Jeanne M (2023), Integration of human stem cell-derived *in vitro* systems and mouse preclinical models identifies complex pathophysiologic mechanisms in retinal dystrophy.
Front. Cell Dev. Biol. 11:1252547.
doi: 10.3389/fcell.2023.1252547

Integration of human stem cell-derived *in vitro* systems and mouse preclinical models identifies complex pathophysiologic mechanisms in retinal dystrophy

Melissa K. Jones[1,2†], Luz D. Orozco[3†], Han Qin[1], Tom Truong[4], Patrick Caplazi[5], Justin Elstrott[6], Zora Modrusan[7], Shawnta Y. Chaney[4] and Marion Jeanne[1*]

[1]Department of Neuroscience, Genentech Inc., South San Francisco, CA, United States, [2]Product Development Clinical Science Ophthalmology, Genentech Inc., South San Francisco, CA, United States, [3]Department of Bioinformatics, Genentech Inc., South San Francisco, CA, United States, [4]Department of Translational Immunology, Genentech Inc., South San Francisco, CA, United States, [5]Department of Research Pathology, Genentech Inc., South San Francisco, CA, United States, [6]Department of Translational Imaging, Genentech Inc., South San Francisco, CA, United States, [7]Department of Microchemistry, Proteomics, Lipidomics and Next-Generation Sequencing, Genentech Inc., South San Francisco, CA, United States

Rare *DRAM2* coding variants cause retinal dystrophy with early macular involvement via unknown mechanisms. We found that *DRAM2* is ubiquitously expressed in the human eye and expression changes were observed in eyes with more common maculopathy such as Age-related Macular Degeneration (AMD). To gain insights into pathogenicity of DRAM2-related retinopathy, we used a combination of *in vitro* and *in vivo* models. We found that *DRAM2* loss in human pluripotent stem cell (hPSC)-derived retinal organoids caused the presence of additional mesenchymal cells. Interestingly, *Dram2* loss in mice also caused increased proliferation of cells from the choroid *in vitro* and exacerbated choroidal neovascular lesions *in vivo*. Furthermore, we observed that *DRAM2* loss in human retinal pigment epithelial (RPE) cells resulted in increased susceptibility to stress-induced cell death *in vitro* and that *Dram2* loss in mice caused age-related photoreceptor degeneration. This highlights the complexity of DRAM2 function, as its loss in choroidal cells provided a proliferative advantage, whereas its loss in post-mitotic cells, such as photoreceptor and RPE cells, increased degeneration susceptibility. Different models such as human pluripotent stem cell-derived systems and mice can be leveraged to study and model human retinal dystrophies; however, cell type and species-specific expression must be taken into account when selecting relevant systems.

KEYWORDS

retinal dystrophy, human stem cells, retinal organoids, mouse models, single cell sequencing, *DRAM2*, disease modeling

1 Introduction

Inherited retinal dystrophy (IRD) is a broad category of phenotypically and genetically heterogeneous disorders that affects about 1 in 3,000 people and is characterized by progressive and irreversible vision loss (Sahel et al., 2015). Sub-classifications of IRDs include further categorization into cell- or region-specific loss, including rod or cone/rod dystrophies and macular dystrophies, with the underlying pathogenesis ultimately due to photoreceptor degeneration. Mutations in greater than 270 genes have been identified as causative factors leading to IRDs (Bohórquez et al., 2021), with mutations in over 80 genes for the most common form, retinitis pigmentosa (RP) (Bravo-Gil et al., 2017). Luxturna® (voretigene neparvovec-ryzl; Spark Therapeutics, Inc.) was the first FDA-approved gene therapy to treat patients with confirmed biallelic *RPE65* mutation-associated retinal dystrophy (Bennett et al., 2016; Maguire et al., 2019). This first approved pharmacologic treatment for IRDs caused by RPE65 mutations constituted a breakthrough therapy, and other therapies for a range of rare IRDs are now under clinical assessment (Prado et al., 2020).

The decreasing cost of emerging technologies, such as genome sequencing for personalized medicine, is changing the way patient care is approached, with treatment plans being increasingly tailored to each individual. Identification of pathologic mechanisms associated with genetic variations is therefore of foremost importance as it guides medical decisions and development of new therapeutic approaches. Recent technological advances in biomedical science, such as single cell sequencing, have allowed a deeper dive into tissue composition and disease pathophysiology (Tang et al., 2019). Even though in-depth molecular and cellular compositions of retinas from different species have been established (Shekhar et al., 2016; Rheaume et al., 2018; Liang et al., 2019; Peng et al., 2019; Yan et al., 2020a; 2020b; Lu et al., 2020; Orozco et al., 2020; Yamagata et al., 2021), constructing atlases of human disease such as IRDs remains challenging, as samples are rare, accessible only post-mortem, and usually not accompanied by a precise clinical diagnosis. Therefore, animal models are commonly used to model and study retinal diseases (Pennesi et al., 2012; Winkler et al., 2020). The development of *in vitro* human pluripotent stem cell (hPSC)-derived systems relevant to the eye, such as retinal organoids, has also provided researchers with new tools to study human-specific mechanisms, as they recapitulate retinal development and are comparable to human fetal retinal tissue (Cowan et al., 2020; Sridhar et al., 2020). Additionally, human induced pluripotent stem cell (iPSC)-derived retinal organoids generated from IRD patient cells have been used for *in vitro* modeling (Deng et al., 2018; Guo et al., 2019; Li et al., 2019; Lukovic et al., 2020; Kruczek et al., 2021). Of course, both animal models and human stem cell-derived *in vitro* systems have limitations, and as negative results are rarely published, it is hard to evaluate how successful they are at recapitulating aspects of particular IRDs.

DRAM2-associated retinopathy, also called cone-rod dystrophy 21 (CORD21), is a rare autosomal recessive IRD caused by coding variants in the *DNA-damage Regulated Autophagy Modulator 2* (*DRAM2*) gene (El-Asrag et al., 2015; Sergouniotis et al., 2015; Birtel et al., 2018; Abad-Morales et al., 2019; Kuniyoshi et al., 2020; Krašovec et al., 2022). *DRAM2*-retinopathy patients are usually asymptomatic in the first 2 decades of life, but then develop progressive central vision loss, associated with characteristic clinical features such as fine white/yellow dots, well-defined atrophic areas in the central retina, and bone-spicule pigmentation in the periphery. Following early maculopathy, visual acuity loss progresses and peripheral retinal degeneration is usually present in the later stages of the disease (El-Asrag et al., 2015; Krašovec et al., 2022).

DRAM2, also known as *Transmembrane protein 77* (*TMEM77*), encodes a 266-amino acid protein with six putative transmembrane domains localized in lysosomes (O'Prey et al., 2009; Park et al., 2009). DRAM2 was named after its homologue DRAM1, a key autophagy modulator and p53-cell death regulator (Crighton et al., 2007; O'Prey et al., 2009); however, DRAM2 cellular function remains unclear and controversial. DRAM2 has been involved in cell death (Park et al., 2009; Bai et al., 2016; Wudu et al., 2019), autophagy (Yoon et al., 2012) and more recently inflammation (Li et al., 2020; Liu et al., 2020). Of note, DRAM2 cellular function has often been studied in the context of oncogenicity and tumor cell treatment response, and not in the context of neurodegeneration or retinal dystrophy.

The purpose of our study was to use *DRAM2* loss as genetic perturbation and compare *in vitro* human and *in vivo* mouse models to determine if they could be leveraged to decipher pathophysiologic mechanisms of complex retinal dystrophy.

2 Materials and methods

2.1 Animal maintenance and ocular examination

All animal experiments were approved by the Genentech Institutional Animal Care and Use Committee (IACUC) and comply with the Institute for Lab Animals' guidelines for the humane care and use of laboratory animals. Animals were housed with *ad libitum* access to water and food and on a 14 h light/10 h dark cycle except for the animals subjected to the constant light exposure (CLE) model. Both males and females were used for experiments, with the exception of the animals used for single cell RNA sequencing and sodium iodate model, for which only males were used.

For ocular examination (fundus imaging, fluorescein angiography, optical coherence tomography (OCT) scanning and electroretinography (ERG) recording), mice were anesthetized by intraperitoneal injection of ketamine (70–80 mg/kg body weight) and xylazine (15 mg/kg body weight). Pupils were dilated with drops of Tropicamide Ophthalmic Solution USP 1% (Akorn). Drops of Systane lubricant eye drop (Alcon) were applied bilaterally to prevent corneal dehydration during the procedure. After ocular examination, anesthetized mice were placed on a pre-warmed warming plate at 37°C until they awakened.

Fundus images were obtained using the Spectralis HRA + OCT system (Heidelberg Engineering). To adjust for rodent optics, the system was modified according to the manufacturer's recommendations with a 55-degree wide-field lens placed in front of the camera.

Fluorescein angiography was performed with the Spectralis HRA + OCT system (Heidelberg Engineering). After anesthesia, mice were intraperitoneally injected with fluorescein AK-FLUOR (Akorn) at 5 µg/g body weight in physiological saline. Animals were orientated on a stage so that the optic nerve would be visible in the same location in each image and images acquired with a 488 nm light filter at 5- and 10-min post fluorescein injection.

Retinal thickness was measured by OCT scans using a Bioptigen Envisu R machine (Leica Microsystems, IL, United States). Total retina thickness was defined as the width from the nerve fiber layer to the RPE/choroid layer on the cross-sectional images. Retinal segmentation was automatically determined using an algorithm (Matlab software, MathWorks).

ERG recordings were performed with the Celeris electrophysiology system (Diagnosys). Mice were dark-adapted overnight before ERG recording, and all procedures were performed under low-level red light. Mouse body temperature was maintained on a 37°C homeothermic plate. A reference electrode was inserted subcutaneously through the forehead and a ground electrode was inserted subcutaneously at the base of the tail. Electrodes with a light-stimulator were placed on both eyes. Under scotopic conditions, eyes were stimulated with six flash-intensities at 0.001, 0.01, 0.05, 0.1, 2 and 4 cd s/m^2. After 5 min of light adaptation, eyes were then stimulated with photopic flash of 4 intensities at 2, 5, 50 and 250 cd.S/m^2. Recorded signals were bandpass-filtered at 0.15–1,000 Hz and sampled at 2 kHz. All of the recorded data points were analyzed using a custom Matlab software (MathWorks) with a-wave amplitude measured from the baseline to the trough of the a-wave while b-wave amplitude from the trough of the a-wave to the peak of the b-wave. Responses to three to five flashes of light stimulation were averaged.

2.2 Mouse ocular pre-clinical models

For the constant light exposure (CLE) degeneration model, animals were housed in transparent plastic boxes and exposed to 100,000 lux of white LED lighting (measured using an Extech HD450 light meter) for 24 h per day for 7 days. Each animal was administered with pupil dilator eye-drops twice daily (Atropine Sulphate 1% Akorn).

For the sodium iodate ($NaIO_3$) degeneration model, male mice were intravenously injected with 20 mg/kg body weight of $NaIO_3$ (Sigma-Aldrich) or saline control.

For the laser-induced choroidal neovascularization (CNV) injury model, animals received analgesic (buprenorphine, 0.05 mg/kg) intraperitoneally the day of the procedure. Mice were then anesthetized by intraperitoneal injection of ketamine (70–80 mg/kg body weight) and xylazine (15 mg/kg body weight). Pupils were dilated with drops of Tropicamide Ophthalmic Solution USP 1% (Akorn). Neovascularization was induced in each eye using an image-guided laser system (Micron III, Phoenix Research Laboratories) with a 532 nm wavelength (laser spot size of 100 µm, 320 mW power and 80 m duration). Three burns in eye at the 3, 6, and 12 o'clock positions around the optic nerve were made, and each burn was made 2–3 optic disk diameters (about 200–300 µm) from the optic nerve. Cases of hemorrhage induced by the laser were excluded from the analysis. After the procedure, a topical antibiotic (Neomycin and Polymyxin B Sulfates and Bacitracin Zinc Ophthalmic Ointment, Bausch & Lomb) was applied to both eyes and the mice were placed on a pre-warmed warming plate at 37°C until they awakened. CNV lesions were outlined and the surface area of each lesion was quantified using the Imaris software.

2.3 Histopathology, *in situ* hybridization and immunofluorescence

Postmortem human donor eyes were obtained from the Lions Eye Institute for Transplant and Research in Tampa, Florida. After 24-h fixation in 10% neutral-buffered formalin (NBF), both human and mouse eyes were transferred into 70% ethanol until paraffin embedding in an automated paraffin tissue processor. The formalin fixed paraffin embedded (FFPE) sections were subjected to deparaffinization before further processing. Hematoxylin-eosin (H&E) staining was performed according to standard protocol using an Automated Slide Stainer.

The *in situ* hybridization (ISH) RNAScope™ 2.5 HD-RED manual assay (Advanced Cell Diagnostics (ACD)) was performed on 4 µm-thick formalin-fixed paraffin-embedded sections of human or mouse eyes according to the ACD protocol. Probes against the ubiquitously expressed isomerase PPIB were used as positive control, and probes against bacterial DapB were used as negative control. ISH on mouse eye sections were performed using a 20 ZZ probe targeting 263-1479 of NM_001025582.2, and the ISH on human eye sections were performed using a 20 ZZ probe targeting 369-1475 of NM_001349881.1. All the probes were provided by ACD. After deparaffinization in xylene and endogenous peroxidase activity inhibition by H_2O_2 (10 min), sections were permeabilized and submitted to heat (15 min at 100°C) and protease IV treatment (20 min at 40°C). After probe hybridization for 2 h at 40°C, the signal was chemically amplified using the kit reagents and detected using the FastRED dye. The sections were then counterstained with Hematoxylin and mounted using VectaMount (Vector Labs, H-5000).

For immunofluorescent labeling, cells or retinal organoid sections were fixed in 4% paraformaldehyde and blocked/permeabilized with 10% normal donkey serum/0.1% Triton X-100/PBS. Cells or sections were incubated for 2 h with primary antibodies against: Zonula occludens-1 (ZO-1) (1:100; 61-7300, ThermoFisher), Melanocyte inducing transcription factor (MiTF) (1:200; ab12039, Abcam), Visual system homeobox (CHX10/VSX2) (1:200; SC-365519, Santa Cruz), Orthodenticle homeobox 2 (OTX2) (1:200; AB9566-I, Milipore), Rhodopsin (1:200; SC-57432, Santa Cruz), Arrestin 3 (ARR3) (1:200; AB15282, Millipore), Matrix Gla protein (MGP) (1:500; MA5-26799, Invitrogen), and Decorin (DCN) (1:100; AF143, R&D). Respective secondary antibodies were conjugated to either Alexa Fluor 488 or Alexa Fluor 594 (Invitrogen) and used at 1:500. Sections were mounted using Mowiol containing DAPI for nucleus staining.

2.4 Cell culture, treatments and functional assays

Human primary retinal pigment epithelial (hRPE) cells (Lonza #00194987) were maintained in Retinal Pigment Epithelial Cell Growth Medium (RtEGM; Lonza) per manufacturer protocols.

The pluripotent human embryonic stem cell (hPSC) line H1 was purchased from WiCell (WA01, (Thomson et al., 1998)) and experiments were performed prior to passage 40. hPSCs were maintained on growth factor reduced Matrigel (BD Biosciences) coated plates with mTeSR1 medium (Stemcell Technologies) according to WiCell protocols. Cells were passaged every 5–7 days at 80% confluence using Gentle Cell Dissociation Reagent (Stemcell Technologies). Colonies containing clearly visible differentiated cells were mechanically removed before passaging.

For isolation and culture of mouse RPE/choroid cells, mouse eyes were enucleated and the anterior chamber, the lens and the neural retina were removed. The RPE/choroid were then dissociated with papain solution (40 U papain in 10 mL DPBS) for 45 min at 37°C. Papain was neutralized in a trypsin inhibitor solution (0.15% ovomucoid in DPBS), and the tissue was triturated to dissociated cells. Following trituration, the cells were pelleted, resuspended, and cultured in RtEGM for experiments.

For cell confluency and cell survival assays (using the cell-impermeable DNA-binding dye DRAQ7), cells were imaged using the Incucyte S3 (Essen BioScience) and quantified using the Incucyte Cell-by-Cell Analysis Software Module. For the *in vitro* degeneration pre-clinical models, sodium iodate ($NaIO_3$) at 5 mM or *N*-retinylidene-*N*-retinylethanolamine (A2E) at 30 μM was added to the culture medium.

To conjugate fluorescence to the outer segments, bovine rod photoreceptor outer segments (POS; Invision BioResources) were labeled with FITC Isomer I (Sigma-Aldrich) per published protocol (Parinot et al., 2014). Briefly, FITC Isomer I was reconstituted in carbonate buffer (final concentration 2.5 mg/mL) and rotated for 1 h at room temperature (RT) in the dark. POS from 50 eyes (Lot #bROS-210820) were resuspended in DMEM, FITC was added, and rotated for 1.5 h at RT in the dark. FITC labeled POS (FITC-POS) were washed 4x with DMEM, centrifuged, and resuspended. The total number of particles were counted and diluted to 8 x 10^7 particles/mL for storage at −80°C until use. To perform the phagocytosis assay, FITC-POS (approximately 8×10^6 particles) were fed to the RPE cells for 6 h in the dark at 37°C (n = 4 transwells/replicate, n = 3 technical replicates). Following incubation, cells were washed 3x with RPE maintenance media (RPEMM) and either fixed in 4% PFA for 10 min at RT for ICC or prepared for flow cytometry analysis. To quantify the FITC-POS phagocytized, flow cytometry was performed (BD FACSymphony S6). Following washing with RPEMM, RPE cells were dissociated for 10 min in trypsin-EDTA, collected, filtered in a 35 μm cell strainer, and stored in cold FACS buffer (1X PBS, 0.5% BSA, 0.05% sodium azide).

2.5 Genetic CRISPR/Cas9 knockout and lentiviral knockdown

Dram2 knockout mice were generated by targeted mutation using CRISPR/Cas9 technology to delete exon 4. The resulting allele was named *Dram2*^{tm1Jean} in accordance with the guidelines from the International Committee on Standardized Genetic Nomenclature for Mice. To simplify our notations, the functionally null *Dram2*^{tm1Jean} allele is denoted knockout (ko) hereafter. Electroporation-based strategy of C57BL/6J zygotes with 25 ng μL^{-1} wild-type Cas9 mRNA (Life Technologies) and 13 ng μL^{-1} *in vitro*-transcribed two single-guide RNA into mouse zygotes was used (Modzelewski et al., 2018). Target sequences of sgRNA used to knockout exon4 were 5′- AGCATACTGTTAGCA AATCA (PAM: AGG, CFD algorithm score of 92) and 5′-TTATCT AAACCTAAGTTGCA (PAM:AGG, CFD algorithm score of 84). The 585 bp knockout region corresponds to GRCm38/mm10 chr3: 106,561,518- 106,562,102. Tail DNA from resulting offspring was analyzed by PCR and sequencing. Genotyping was carried out using the following primers: 5′-CTAAGACAATAACTGATGAATGGT, 5′-AGCGAGCAAGAGAACATAA, and 5′-ACACACAAGACA GGAACTT.

For generation of the *DRAM2* knockout (KO1 and KO2) hPSC lines, a guide RNA (gRNA) targeting *DRAM2* exon3 (5′-AAGGTA AAGCCGGGTCTATA) was designed and generated using GeneArt Precision gRNA Synthesis Kit (Invitrogen). hPSCs were trypsinized to single cells and electroporated with gRNA and rCas9 protein (ThermoFisher) using Human Amaxa P3 Primary Cell 96-well Nucleofector Kit on 4D-nucleofector X unit with program CB-150 according to the manufacturer's protocols (Lonza). After electroporation, cells were plated onto Matrigel coated cell culture plates with mTeSR1 PLUS medium in the presence of the 10 μM ROCK inhibitor Y-27632 (Selleckchem). After 10 days, single colonies were picked and expanded. To screen clones, genomic DNA was isolated using the Puregene Cell Kit (Qiagen) then PCR amplified with High-Fidelity 2X PCR Master Mix (NEB) using two primers flanking the target region (5′-ACTTCGTACGCA GTAAGC' and 5′-GGCTAAAGTAGGATGAGG). PCR products were cloned into a T-vector (Promega), and sequenced. Two different hPSC clones homozygous for *DRAM2* knockout (KO1 and KO2) were selected for experiments.

For gene knockdown, shRNAs targeting *DRAM2* in lentiviral vector pGIPZ-CMV-tGFP-IRES-puro were purchased from Dharmacon (RHS4430-200179097 and RHS4430-200259023). To produce lentiviruses, HEK 293T cells at 60%–70% confluency were transfected in 10 cm plates with 5 μg of the lentiviral vectors together with packaging plasmids 3.5 μg delta8.9 and 1.7 μg VSVG using Lipofectamine 2000 (ThermoFisher). After 72 h, viral supernatants were harvested, filtered, titered, and stored at −80°C. Cells were infected in the culture medium in presence of virus for 48 h. *DRAM2* knockdown was confirmed by qRT-PCR. RNA was isolated using the RNeasy Plus Mini RNA Isolation kit (QIAGEN) and reverse-transcribed using the High-Capacity cDNA Reverse Transcription kit (Applied BioSystems). The cDNA reaction was diluted 1:5 in TE (10 mM Tris-Cl/1 mM EDTA, pH 7.6) and used in SsoFast EvaGreen Supermix with Low ROX (BioRad). Reactions were run in triplicates on a ViiA 7 machine (Applied BioSystems) according to the manufacturer's instructions. Values were normalized to the housekeeping gene expression GAPDH and then to expression in uninfected cells. Data are from triplicate PCR reactions, and error bars represent standard deviation. Primers used were: *DRAM2* 5′-TCAGCAAGGCCTCAGTTTCC and 5′-GTAGCAATGCATAAAACT GCCG; *GAPDH* 5′-CTGCACCACCAACTGCTTAG' and 5′-TTCAGC TCAGGGATGACCTT.

2.6 hPSC directed differentiation into RPE cells and retinal organoids

Retinal pigment epithelial (RPE) cells were differentiated from hPSCs per published protocol with some modifications

(Maruotti et al., 2015). Briefly, hPSCs were seeded at high density (20,000 cells per cm^2) on growth factor-reduced Matrigel (BD Biosciences)-coated plates with mTeSR1 medium in 5% CO_2. Cells were maintained for 10 days until forming a monolayer. From days 11–25, cells were given differentiation media which included DMEM/F12, 15% knockout serum replacement (KOSR; Invitrogen), 2 mM glutamine, 0.1 mM NEAA (Invitrogen), and 10 mM nicotinamide. After day 25, cells were switched to maintenance media (RPEMM) containing DMEM, F12, and 2% B27 without vitamin A (Invitrogen). At day 35, RPE were passaged using Accumax (Sigma) incubated for 20 min at 37°C. Cells were centrifuged at 130 x g for 3 min, filtered through a 40-µm nylon mesh (BD Falcon) and counted. Cells were plated at a density of 300,000 cells per cm^2 onto growth factor-reduced Matrigel (BD Biosciences)-coated plates or transwells (Corning).

Retinal organoids were differentiated from hPSCs based on a previously described protocol with modifications (Idelson et al., 2009; Meyer et al., 2009; Zhong et al., 2014; Gong et al., 2015). Briefly, hPSCs were detached by Gentle Cell Dissociation Reagent (Stemcell Technologies), dissociated into small clumps and cultured in suspension with mTeSR1 medium and 10 µM Y-27632 (Selleckchem) to induce aggregate formation. Aggregates were gradually transitioned into neural-induction medium (NIM) containing DMEM/F12 (1:1), 1% N2 supplement (Gibco), 1x non-essential amino acids (NEAA; Gibco), 2 µg/mL heparin (Sigma), by replacing the medium with a 3:1 ratio of mTeSR1/NIM on day 1, 1:1 on day 2% and 100% NIM on day 3. On day 7, aggregates were seeded onto Matrigel (growth factor-reduced; BD Biosciences) coated dishes containing NIM at an approximate density of 20 aggregates per cm^2. Starting day 16, the media was switched to retinal differentiation medium (RDM) containing DMEM/F12 (3:1) supplemented with 2% B27 (minus vitamin A; Gibco), 1x NEAA and 1x penicillin and streptomycin and was changed daily. Around day 28, horseshoe-shaped neural retina domains were collected and cultured in RDM, where they gradually formed 3D eye organoids. Thereafter, the media was changed twice a week. To mature eye organoids, the medium was supplemented with 10% fetal bovine serum, 100 µM Taurine (Sigma) and 1x GlutaMAX starting from day 42. To promote photoreceptor maturation, the retinal organoids were supplemented with 1 µM all-trans retinoic acid (RA) from weeks 10–14. Subsequently, RA concentration was decreased to 0.5 µM, and B27 supplement was switched to N2 supplement. Retinal organoids were cultured for up to 12 months.

2.7 Single cell RNA sequencing and bioinformatic analysis

Mouse and retinal organoid single-cell suspensions were prepared by adapting previously described methods (Macosko et al., 2015). Briefly, mouse retinas, mouse RPE/choroid preparations, and hPSC-derived retinal organoids were digested in papain solution (40U papain in 10 mL DPBS) for 45 min at 37°C. Papain was then neutralized in a trypsin inhibitor solution (0.15% ovomucoid in DPBS) and the tissue was triturated to generate a single-cell suspension. Following trituration, the cells were pelleted, resuspended, and filtered through a 20 µm Nitex mesh filter to eliminate any clumped cells. The cells were then diluted in DPBS with 3% FBS to 200 to 1,000 cells/µL. The scRNAseq library was generated using Chromium Single Cell 3′ Reagent Kit v2 (10X Genomics) per manufacturer's instructions. Human donor eye single-nuclei suspensions were prepared from frozen sections and used for library preparation (Chromium single cell 3′ kit v2 or v3, 10X Genomics) and nucSequencing as described in (Orozco et al., 2020).

Single-nuclei RNAseq data were processed using cellranger from 10X. Since RNA derived from nuclei for the human single-nucleus RNAseq dataset was used, both exonic and intronic reads were considered for downstream analysis by including introns in the pre-processing step of the human reference genome sequence. For the single-cell RNAseq datasets, only exons were in the step to pre-processing the genomes. For alignment, the human reference genome GRCh38, and the mouse reference genome mm10 were used. The algorithm outputs a count matrix of cells by genes, which was used for down-stream analysis, and the clustering and dimensionality reduction analysis that is output by cellranger was not utilized.

Further downstream analysis was performed using Seurat. For normalization, UMIs using the "LogNormalize" method was utilized, and integration of the cells using CCA using experiment "Batch" as the batching variable was performed. For dimensionality reduction, we selected variable genes based on dispersion, then used these to compute principal components and UMAP dimensional reductions. Clusters of transcriptionally related cells corresponding to cell types or cell subtypes by using the graph-based clustering Louvain algorithm were generated and implemented in the Seurat function "FindClusters." Cluster markers, i.e., gene expression markers that were more highly expressed in each cluster relative to all other clusters, using the "FindAllMarkers" function were searched, based on the non-parametric Wilcoxon rank-sum test. Cluster marker genes were considered if they were expressed in at least 10% of the cells in the cluster, with a minimum difference of 30% in the fraction of cells expressing the marker between two clusters, and a minimum log2 fold change in expression of 0.25.

For pseudo-bulk differential expression analysis, pseudo-bulk datasets were derived from each dataset by aggregating the cells of each sample of the same cell type using "aggregateAcrossCells" in scran as described (McCarthy et al., 2017). For n donors and m cell types, it creates n*m total possible pseudo-bulks, which are aggregates of cells of a single cell type from a single donor. The resulting pseudo-bulk count matrix was then normalized to a normalized count statistic using "logNormCounts" in scran, and size factors were calculated using edgeR (Robinson et al., 2010). Differential expression was performed on this data-set to compare control *versus* DRAM2 KO samples, for each cell type, using the voom-limma method for bulk RNAseq as described in the following.

For bulk RNAseq differential expression analysis, sequencing data analysis was performed as previously described (Durinck et al., 2015). Briefly, sequencing reads were mapped to the reference human genome (GRCh38), using the GSNAP short read aligner (Wu and Nacu, 2010). Transcript models used for differential expression were based on GENCODE annotations. Expression counts per gene were quantified using HTSeqGenie (Pau and Reeder, 2022). Expression counts were normalized to a normalized count statistic using "logNormCounts" in scran, and

size factors were estimated using edgeR. Differential expression between bulk RNAseq samples using linear modeling with the voom/limma package (Law et al., 2014), and adjusted *p*-values for multiple testing using the Benjamini–Hochberg method were performed. Genes were considered differentially expressed if they had adjusted *p*-value < 0.05 and absolute fold change > 2.

In all heatmaps, color is the Z score of the expression level scaled by rows.

All datasets are available in the NCBI gene expression omnibus (GEO) database:

Already published datasets from Orozco et al. (2020): Bulk RNA seq of retinas and RPE/choroids (GSE135092) and Single-nucleus RNA seq of human retinas (GSE135133).

New datasets generated during this study are accessible in the reference series GSE220627 at https://www.ncbi.nlm.nih.gov/geo/query/acc.cgi?acc=GSE220627.

It includes three subseries.

- the hPSC-derived retinal organoids scRNA sequencing data (GSE220624)
- the mouse RPE/Choroid scRNA sequencing data (GSE220625).
- the mouse retina scRNA sequencing data (GSE220626).

2.8 Statistical analysis and software

Statistical analyses were performed using GraphPad Prism 9. Means+/-standard deviation are shown on all graphs. Exact values of numbers of samples used are described in Results or Figure Legends. All figures were created with BioRender (BioRender.com).

2.9 Gene and disease references

Cone-rod dystrophy 21 (CORD21): MIM# 616502; *DNA-damage Regulated Autophagy Modulator 2* (*DRAM2*) gene: MIM# 613360; DRAM1 gene: MIM# 610776; *CNGB3* gene: MIM# 605080; achromatopsia 3: MIM# 262300; *POC1B* gene: MIM# 614783; cone-rod dystrophy associated with *POC1B* mutations: MIM#615973; *CRB1* gene: MIM# 604210; retinal dystrophies associated with *CRB1* mutations: MIM# 613835, 172870, 600105; *BEST1* gene: MIM# 607854.

3 Results

3.1 DRAM2 is ubiquitously expressed in the human eye and expression changes are associated with macular degeneration

Rare biallelic *DRAM2* variants causing putative loss of DRAM2 function have been associated with retinal dystrophy (El-Asrag et al., 2015; Sergouniotis et al., 2015; Birtel et al., 2018; Kuniyoshi et al., 2020; Krašovec et al., 2022). Early in the third decade of life, patients become symptomatic, suffering from maculopathy and progressive central visual loss. To know if DRAM2 could also be involved in more common maculopathies, such as Age-related Macular Degeneration (AMD), we investigated whether *DRAM2* expression level in the eye was altered in AMD patients. Most AMD patients have early or intermediate AMD, characterized by build-up of drusen under the retina, and mild to no visual symptoms. However, they become at risk of severe vision loss as the disease progresses to advanced AMD, characterized by either degeneration of macular photoreceptors and their underlying retinal pigment epithelium (RPE) and/or growth of pathogenic blood vessels from the choroid into the retina. Using bulk RNA sequencing of macula and non-macula retinas and RPE/Choroids from human donor eyes (99 donors had no history of ocular disease and 23 donors were diagnosed with advanced AMD (Orozco et al., 2020)), we found that *DRAM2* expression was slightly lower in AMD retinas and RPE/Choroids compared to non-AMD controls ($p < 0.05$ and $p < 0.01$, respectively; Figure 1A). *DRAM2* has been described as expressed in photoreceptors and RPE cells in mice (El-Asrag et al., 2015), therefore, we checked if decreased *DRAM2* expression in AMD samples could simply reflect degeneration and loss of these particular cells during the disease process. *RCVRN*, a photoreceptor marker, showed decreased expression in AMD retinas compared to non-AMD retinas ($p < 0.0001$), confirming substantial photoreceptor loss (Figure 1B, left). However, *BEST1*, a RPE cell marker, had similar expression levels in AMD and non-AMD RPE/Choroid samples (Figure 1B, right), suggesting that RPE atrophy was minimal in these patient samples. When assessing association of DRAM2 expression to either RCVRN or BEST1 expression within each sample, we did not find significant correlation, suggesting that lower DRAM2 expression in AMD samples is not just due to photoreceptor or RPE cell loss (retina $R^2 = 0.28$, and RPE/Choroid $R^2 = 0.0001$).

To further investigate *DRAM2* expression at the cell type level, we leveraged single-nucleus RNA sequencing (scNucSeq) data from 4 donor eyes with no retinal disease diagnosis (Orozco et al., 2020). We found that *DRAM2* is ubiquitously expressed in the human eye, with expression detected notably in neurons (photoreceptors, interneurons and retinal ganglion cells (RGCs)), RPE cells, glia, mesenchymal and myeloid cells (Figures 1C, D left). This absence of cell type-specific *DRAM2* expression uncovered in the eye was also confirmed in other organs using single cell transcriptomics datasets from 13 tissues and blood, where *DRAM2* was ubiquitously expressed in all the different cell types identified (the Human Protein Atlas (Karlsson et al., 2021)) (Figure 1D, right).

Finally, we confirmed broad *DRAM2* expression in the human and mouse eyes by *in situ* hybridization (ISH) (Figure 1E and Supplementary Figure S1A). In non-AMD donor eyes, *DRAM2* mRNA was sparsely detected in the ganglion cell layer (GCL), the inner nuclear layer (INL), the outer nuclear layer (ONL), the retinal pigment epithelium (RPE) and the choriocapillaris (CC) (Figure 1E, top panels: representative image in the macula). In advanced dry AMD donor eyes, *DRAM2* mRNA was also sparsely detected in all the different retinal layers (Figure 1E, bottom panels, representative image in the macula). Of note, a relatively abundant signal was associated with a very few cells in the choriocapillaris, where the RPE was destroyed in the AMD lesions (Figure 1E, arrows in panel (7)). Unfortunately, no anti-DRAM2 antibody with a satisfactory specificity profile was identified to be able to confirm these finding at the protein level.

In conclusion, we found that *DRAM2* is ubiquitously expressed in the human eye and expression levels are low and comparable across the different retinal layers. No cell type-specific expression was observed in the eye or other tissues for which data were

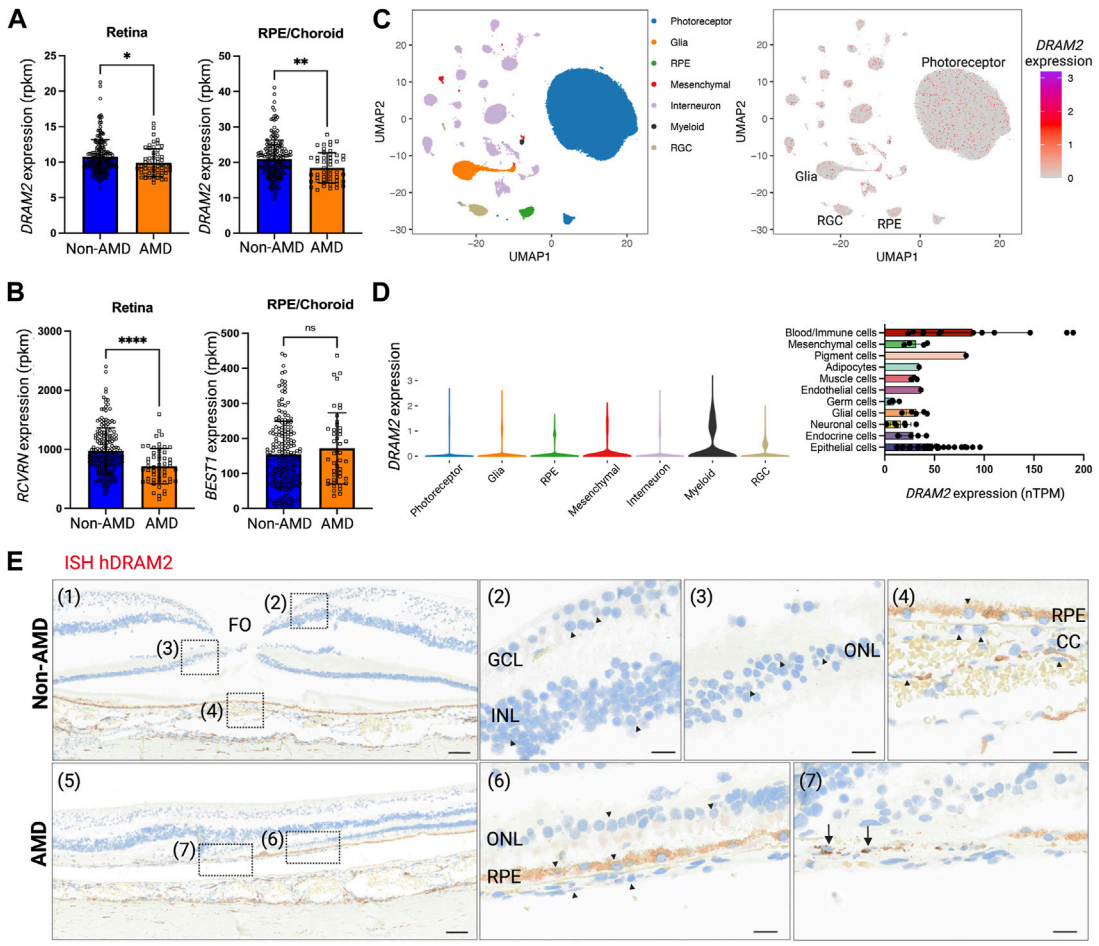

FIGURE 1
Human *DRAM2* is ubiquitously expressed in the eye. **(A)** *DRAM2* expression (rpkm) in human non-Age-related Macular Degeneration (AMD) or AMD retina and retinal pigment epithelium (RPE)/choroid samples (n = 49 to 198, Unpaired t-test, *$p < 0.05$, **$p < 0.01$). **(B)** Expression of key markers for photoreceptors (*RCVRN*) and RPE cells (*BEST1*) in human non-AMD or AMD retina and RPE/choroid samples (n = 49 to 198, unpaired t-test, ****$p <$ 0.0001, ns: not significant $p > 0.05$). **(C)** *DRAM2* expression in single nuclei RNA sequencing of human non-AMD eyes (n = 4); data from (Orozco et al., 2020). **(D)** *DRAM2* expression in different cell types (left panel, snRNA seq from non-AMD eyes (n = 4); data from (Orozco et al., 2020)) and other organs (right panel, scRNA seq data compiled from the Human Protein Atlas (Karlsson et al., 2021)). **(E)** *In situ* hybridization (ISH) of *DRAM2* mRNA in human non-AMD (top panels) and AMD (bottom panels) donor eyes. Representative images from n = 4 non-AMD eyes and 8 AMD eyes. Nuclear stain is in blue, natural pigment in the RPE is in brown and the ISH signal in red. (1) Area of fovea (FO). (2) *DRAM2* signal is sparsely disseminated in the ganglion cell layer (GCL) as well as inner nuclear layer (INL). (3) *DRAM2* signal is also sparsely disseminated in the outer nuclear layer (ONL), i.e., associated with photoreceptors nuclei. (4) Sparse *DRAM2* signal localizes to cells of the choriocapillaris (CC) and retinal pigment epithelium (RPE). (5) Lesion edge in an AMD donor eye. (6) Adjacent to the lesion, sparse *DRAM2* signal is disseminated in the stretch of contiguous RPE and the few residual photoreceptors in the ONL. (7) Within the lesion, a relatively abundant DRAM2 signal is associated with cells in the area of the destroyed RPE (black arrows). (FO, fovea; GCL, ganglion cell layer; INL, inner nuclear layer; ONL, outer nuclear layer; RPE, retinal pigment epithelium; CC, choriocapillaris). Scale bar: 100 µm on panels (1) and (5), and 20 µm on panels (2), (3), (4), (6) and (7).

available. We observed expression changes at the transcriptional level when investigating AMD eyes, with overall lower expression in diseased retinas and RPE/choroids.

3.2 DRAM2 loss in human pluripotent stem cell (hPSC)-retinal organoids results in the presence of extra cells with a mesenchymal gene signature

Since *DRAM2* is ubiquitously expressed in the human retina, we investigated the consequences of *DRAM2* loss in human retinal organoids, as they contain most retinal cell types (Cowan et al., 2020; Sridhar et al., 2020). First, we created two independent hPSC *DRAM2* biallelic knockout lines (KO1 and KO2) using CRISPR/Cas9 (Supplementary Figure S1E, F). Then, we generated retinal organoids by directed differentiation of hPSC wild-type (WT), *DRAM2* KO1 and KO2, as previously described (Figure 2A; [43–46]. Eye cups expressing early markers for the RPE (MITF) and neural retina (VSX2) were detected after 1 month of differentiation (Figure 2A). These eye cups were manually detached and cultured to form three-dimensional retinal organoids with photoreceptor progenitor cells (OTX2) at 2 months, and rod and cone photoreceptor cells (RHO positive and ARR3 positive cells, respectively) at 5 months (Figure 2A). *DRAM2* WT, KO1 and KO2 hPSC-retinal organoids showed

10.3389/fcell.2023.1252547

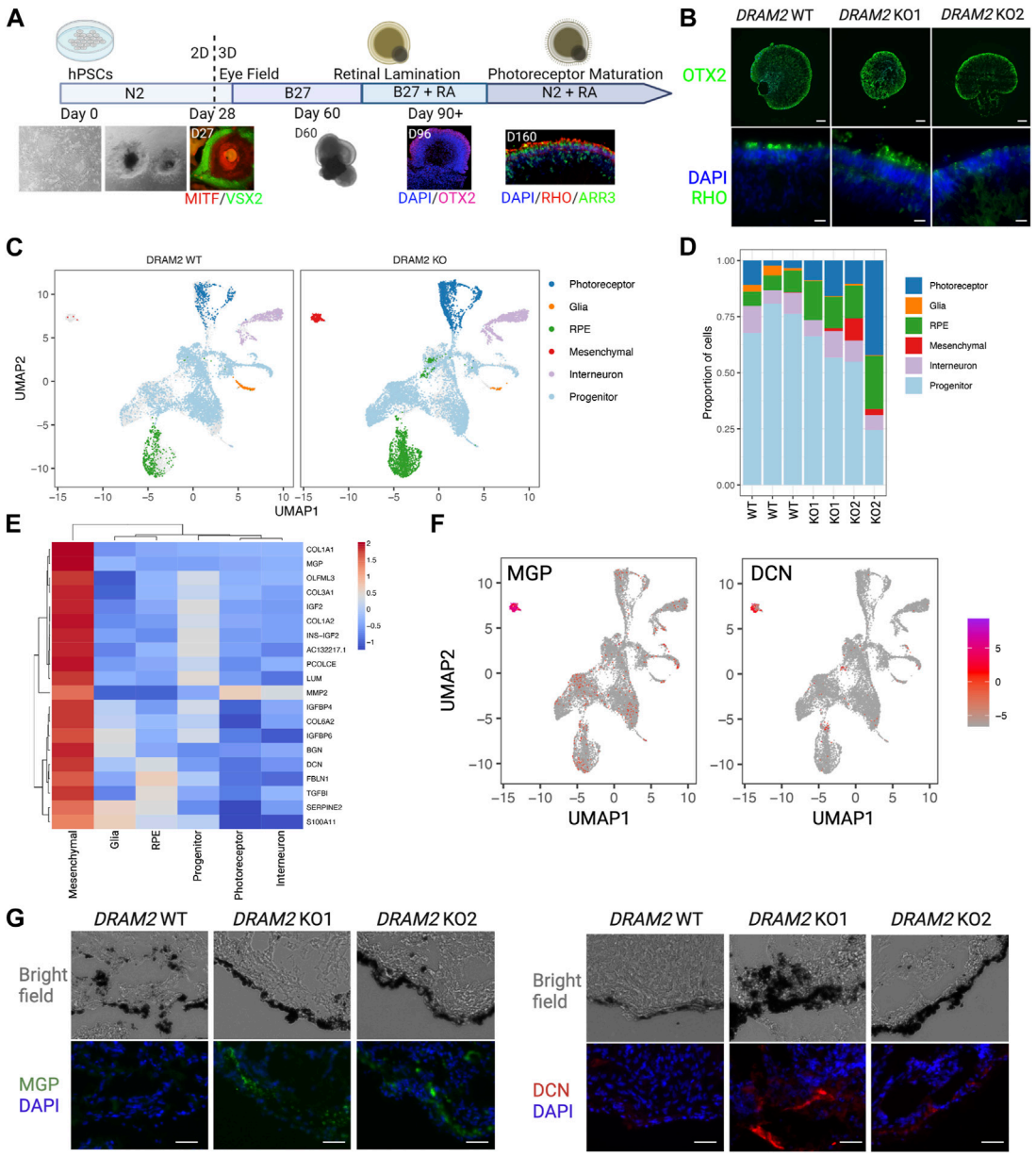

FIGURE 2
Absence of transcriptional changes in hPSC-retinal organoids knockout for *DRAM2* but presence of an extra cell cluster with mesenchymal signature **(A)** Overview of the differentiation protocol of human pluripotent stem cells (hPSC)-derived retinal organoids. MITF: RPE progenitor marker; VSX2, neuronal progenitor marker; OTX2, retinal progenitor marker; RHO, rod photoreceptor marker; ARR3, cone photoreceptor marker. **(B)** Representative immunofluorescent images of *DRAM2* WT, KO1, and KO2 hPSC-derived retinal organoids. Scale bars in upper panels: 100 µm. At day 160, retinal organoids express retinal progenitor (OTX2) and photoreceptor markers (RHO). Scale bars in bottom panels: 20 µm. **(C)** UMAP representation of single cell RNA sequencing (scRNAseq) of *DRAM2* WT and KO hPSC-derived retinal organoids identifying 6 clusters of different cell types. **(D)** Proportion of the different cell types from identified cell clusters from the scRNAseq of *DRAM2* WT and KO retinal organoids. **(E)** Heatmap showing expression of the mesenchymal markers by cell type (pseudobulk, genotypes pooled). **(F)** UMAP representation of *Matrix Gla Protein* (*MGP*) and *decorin* (*DCN*) expression in the scRNAseq of retinal organoids, showing predominant expression in the mesenchymal cluster. **(G)** Representative images of immunolabeling of MGP (left) and DCN (right) in *DRAM2* WT, KO1, and KO2 hPSC-derived retinal organoids. Scale bars: 25 µm.

some variability in shape and size that is inherent to organoid directed differentiation; however, no obvious consistent morphological differences were observed between the two genotypes. They all showed spontaneous retinal lamination with photoreceptors localized on the outer layer in contact with the culture media (Figure 2B). To further analyze the hPSC-retinal organoids, we matured them until 12 months of age and performed scRNA sequencing. Clustering the cells based on their gene expression identified five distinct cell populations in both the *DRAM2* WT and KO retinal organoids including: photoreceptors, glial cells, RPE cells, interneurons, and progenitor cells (Figure 2C). Cell composition was variable between the different retinal organoids and our limited number of replicates (n = 3 for *DRAM2* WT and n = 4 for *DRAM2* KO) does not allow us to

determine if any of the cell type proportion differences between WT and KO organoids are biologically relevant (Figure 2D). Differentially Expressed Genes (DEGs) analysis of the whole retinal organoids did not show any significant differences between *DRAM2 WT* and *KO* organoids, with the exception of *PRSS56* (FDR = 0.048) (Supplementary Figure S1B). This gene has been described as being expressed mainly first in retinal progenitors and then Muller Glia in the mouse retina (Paylakhi et al., 2018). Since these are cell types that are overall more present in *DRAM2 WT* organoids, the lower *PRSS56* expression in *DRAM2 KO* organoids is most likely reflecting the presence of a lower cell number expressing it (Supplementary Figure S1B). Indeed, when pseudobulk DEG analysis was done comparing *DRAM2 WT* and *KO* within each cell type, no genes were identified as significantly up or downregulated.

We were able to notice that an extra cluster was present in the *DRAM2* KO retinal organoids (average cell identified: 1 cell per WT organoid and 67 cells per KO organoid) (Figure 2D). We identified this extra *DRAM2* KO cluster as mesenchymal cells based on cluster marker genes (Figure 2E). We validated the existence of the extra cluster in *DRAM2* KO organoids using Matrix Gla Protein (*MGP*) and Decorin (*DCN*) as marker genes (Figure 2F). Using immunolabeling, we confirmed that they were both not detected in *DRAM2* WT organoids. Interestingly, we found that MGP and DCN were expressed by cells localized next to RPE cells in the *DRAM2* KO organoids, and not within the self-laminated neuroretina of the hPSC-organoids (Figure 2G).

In summary, we found that *DRAM2* loss in hPSC-retinal organoids does not affect cells at the transcriptional level, but induces the presence of additional mesenchymal cells, which localize near RPE cells.

3.3 DRAM2 loss exacerbates toxicity-induced human RPE cell death *in vitro*

Since we observed the strongest *DRAM2* mRNA signal in cells localized within the RPE layer in AMD lesions (Figure 1E) and identified extra mesenchymal cells next to RPE cells in *DRAM2* KO retinal organoids (Figure 2G), we investigated the consequences of *DRAM2* loss in human RPE cells. We used two different *in vitro* systems: 1) lentivirus-shRNAs to knockdown *DRAM2* expression in human primary RPE cells (hRPE) and 2) CRISPR/Cas9 to knockout *DRAM2* in human pluripotent stem cell-derived RPE cells (hPSC-RPE) (Figure 3A). RPE cells with *DRAM2* knockdown or knockout were fully differentiated before being challenged by either *N*-retinylidene-*N*-retinylethanolamine (A2E) or sodium iodate ($NaIO_3$). At the cellular level, A2E is a toxic visual cycle by-product found in lipofuscin deposits within RPE cells (Crouch et al., 2015; Parmar et al., 2018) $NaIO_3$ is known to induce oxidative stress, complement cascade activation, necroptosis and apoptosis (Balmer et al., 2015; Hanus et al., 2016; Berkowitz et al., 2017; Enzbrenner et al., 2021).

We first induced *DRAM2* knockdown in primary hRPE cells. High lentiviral infection efficiency was validated using GFP co-expression with the shRNAs, and two independent shRNAs targeting *DRAM2* were used with an approximately 10-fold knockdown efficiency determined by qRT-PCR (Figure 3B). The hRPE cells were then allowed to fully mature for at least 4 weeks before A2E or $NaIO_3$ treatment and cell survival analysis. *DRAM2* knockdown in hRPE exacerbated both A2E- and $NaIO_3$-induced cell death as compared to control RPE cells (Figure 3C). After A2E treatment, 50% of the hRPE cells expressing *DRAM2* shRNA1 or shRNA2 died after 114 and 102 h respectively, whereas the median survival for the hRPE cells expressing the control shRNA was 126 h. Similarly, after $NaIO_3$ treatment, 50% of the hRPE cells expressing *DRAM2* shRNA1 or shRNA2 died after 64 and 78 h respectively, whereas the median survival for the hRPE cells expressing the control shRNA was 118 h (Figure 3C).

We then replicated these findings in *DRAM2* knockout hPSC-RPE cells. *DRAM2* WT, KO1 and KO2 hPSC were differentiated into RPE cells and allowed to mature for at least 4 weeks (Figure 3D). No obvious phenotypic differences were observed between hPSC-RPE wild-type (WT) and KO1 or KO2 during the directed differentiation process, showing that DRAM2 does not play a critical role in RPE differentiation and survival. All hPSC-RPE cell lines formed a monolayer, became pigmented, and expressed the RPE marker ZO-1 (Figure 3D). Furthermore, mature hPSC-RPE cells were similarly functional as both *DRAM2* KO1 and KO2 cells were able to phagocytize photoreceptor outer segments (POS) as efficiently as the WT cells (Figure 3E). However, after A2E treatment, 50% of the hPSC-RPE KO1 and KO2 died after 42 and 50 h respectively, whereas the median survival for the hPSC-RPE WT was 72 h. Similarly, after $NaIO_3$ treatment, 50% of both the hPSC-RPE KO1 and KO2 died after 34 h, whereas the median survival for the hPSC-RPE WT was 86 h (Figure 3F).

In conclusion, *DRAM2* loss by either knockdown or knockout in human RPE cells resulted in decreased survival after challenges by A2E or $NaIO_3$ *in vitro*, showing that DRAM2 plays a role in resistance of human RPE cells to stress-induced cell death.

3.4 Dram2 loss causes mild age-related retinal dystrophy with absence of functional deficit in mice

To further study the effect of *Dram2* loss on retinal homeostasis, a constitutive CRISPR/Cas9 knockout (ko) C57BL/6J mouse strain was generated (Supplementary Figure S1C), and the disruption was confirmed by genomic DNA sequencing. The mouse ko region of Exon 4 corresponds to known patient biallelic mutations that cause retinal dystrophy (Supplementary Figure S1D; (El-Asrag et al., 2015)). *Dram2 wt/wt*, *wt/ko* and *ko/ko* mice were aged up to 24 months and no gross phenotypic differences were observed or detected by necropsy analysis. Ocular examination by fundus imaging, fluorescence angiography, and histological staining also did not reveal obvious phenotypic abnormalities in *Dram2 wt/ko* and *ko/ko* mice (Figure 4A). However, after 18 months, the total retinal thickness measured by live spectral-domain optical coherence tomography (SD-OCT) was slightly, but significantly decreased in *Dram2 ko/ko* mice as compared with their wild-type and heterozygous littermates (5 µm loss after 18 months, $p < 0.05$; Figure 4B). To determine the cell type contributing to loss in retinal thickness, a second cohort of *Dram2 wt/wt*, *wt/ko* and *ko/ko* mice was generated and aged. A small significant total retinal thickness loss in *Dram2 ko/ko* mice was replicated (reaching 7 µm loss after

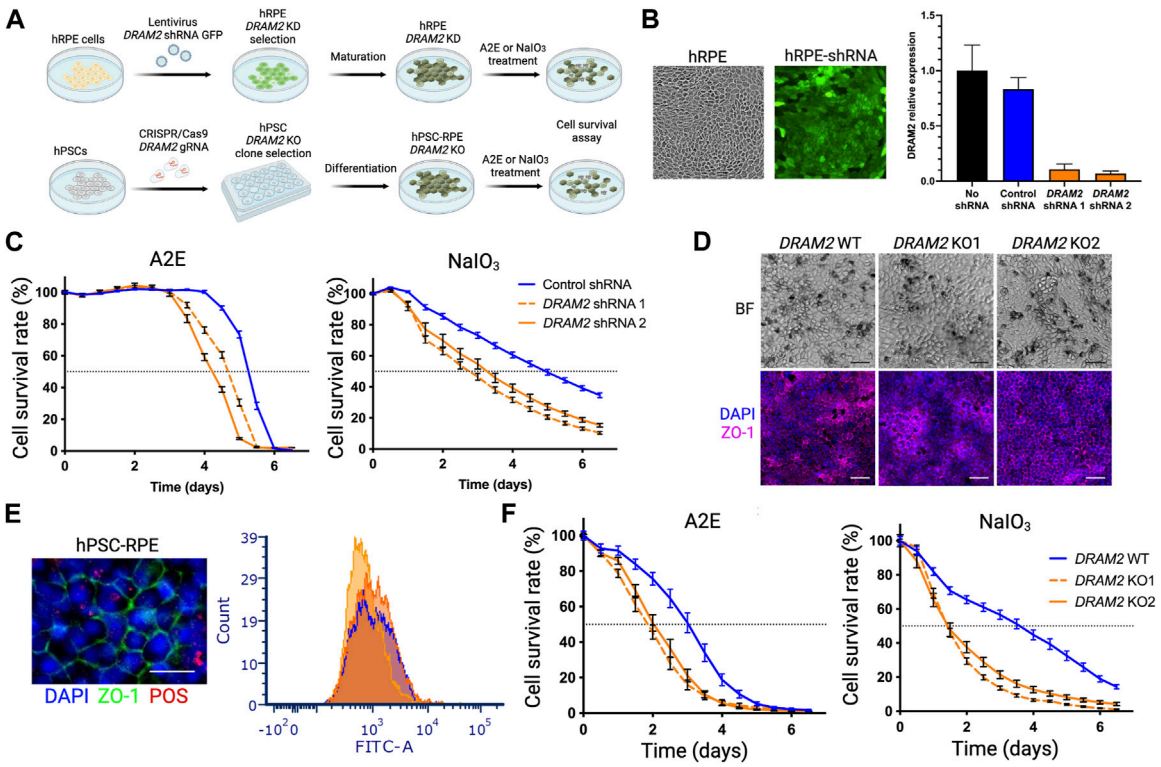

FIGURE 3
Dram2 loss exacerbates toxicity-induced human RPE cell death *in vitro* **(A)** Experimental design of loss of *DRAM2* experiments in human cells. hRPE, human primary retinal pigment epithelial (RPE) cells; KD, knockdown; A2E, N-retinylidene-N-retinylethanolamine; $NaOI_3$, Sodium Iodate; hPSC, human pluripotent stem cells; KO, Knockout. **(B)** Representative image of hRPE after infection with lentivirus expressing *DRAM2* shRNA and GFP (left) and knockdown efficiency of the two different *DRAM2* shRNAs assessed by quantitative RT-PCR (qPCR) analysis of *DRAM2* expression (right) **(C)** hRPE cell survival following treatment with A2E (30 μM; left) and $NaIO_3$ (5 mM; right). Dotted horizontal line marks the median survival (50% of the cells alive). **(D)** Differentiation of *DRAM2* WT and KO human pluripotent stem cells (hPSCs) into RPE (hPSC-RPE) showing pigmentation (top row, BF: Bright Field) and expression of RPE maker ZO-1 (bottom row). Scale bars: 50 μm. **(E)** Representative immunofluorescent image (left) of RPE marker ZO-1 (green) in hPSC-RPE *DRAM2* WT, KO1, and KO2 and phagocytosis of FITC-labeled Photoreceptor Outer Segments (POS; red). Scale bar: 20 μm. Phagocytosis capacity of the cells was assessed by quantification of cells with internalized FITC-POS by flow cytometry (*DRAM2* WT: blue line, *DRAM2* KO1 and 2: orange lines). **(F)** hPSC-RPE cell survival following treatment with A2E (30 μM; left) and $NaIO_3$ (5 mM; right). Dotted horizontal line marks the median survival.

24 months, $p < 0.05$; Figure 4C). The loss was found to be due to photoreceptor degeneration, while none of the other retinal layers (retinal nerve fiber layer (RNFL), retinal ganglion cell (RGC) layer, inner nuclear layer (INL), inner plexiform layer (IPL) or the choriocapillaris) showed thinning (Figure 4C and Supplementary Figure S3A). Since human *DRAM2* mutations cause cone-rod dystrophy, we investigated if cone photoreceptors were also affected in the mouse ko. Indeed, quantification of cone arrestin-3 (ARR3) positive cells at 4 months already identified significant loss in cone photoreceptor cells in *Dram2 ko/ko* mice ($p < 0.05$; Figures 4D, E). RPE cells were also quantified at the same age and no significant difference was detected in the number of ZO-1 positive cells from the center (closest to the optic nerve head), middle, and periphery (Figure 4E). This suggests that the age-related cone loss observed in *Dram2 ko/ko* mice is not secondary to RPE cell loss. To determine if photoreceptor loss caused visual deficit in *Dram2 ko/ko* mice, electroretinography (ERG) was performed on 21-month-old mice. No differences in rod (scotopic) or cone (photopic) responses were detected between *Dram2 wt/wt*, *wt/ko* and *ko/ko* mice (Figure 4F). These results show that loss of *Dram2* leads to age-related photoreceptor degeneration, but the severity of the retinal dystrophy is not sufficient to impact visual function in mice.

To investigate ongoing gene expression differences between *Dram2 wt/wt* and *ko/ko* mice, single-cell RNA sequencing (scRNAseq) was performed in 12-month-old retinas. Unsupervised cluster analysis identified five distinct cell populations in the retinas, including photoreceptors, glia, RPE cells, mesenchymal cells and interneurons (Figure 4G). The percentage of the different cell types was not significantly different between the two genotypes with the exception of the RPE cells (0.34% ± 0.005 in *Dram2 wt/wt* retinas and 0.19% ± 0.07 in *Dram2 ko/ko* retinas). However, presence of RPE cells in the cell preparation is an artifact of retina isolation and only a total of 10–25 RPE cells per retina were identified by scRNAseq. As expected, the vast majority of cells were photoreceptors (91.4% ± 4.4 in *Dram2 wt/wt* retinas and 93.7% ± 2.2 in *Dram2 ko/ko* retinas, Figure 4H). Significant Differentially Expressed Genes (DEGs) were identified only in interneurons (51 genes), mesenchymal cells (56 genes), and RPE cells (5 genes) (Supplementary Table S1). Strikingly, no significant DEGs were detected in photoreceptor cells from *Dram2 wt/wt* and *ko/ko* retinas (FDR <0.05).

10.3389/fcell.2023.1252547

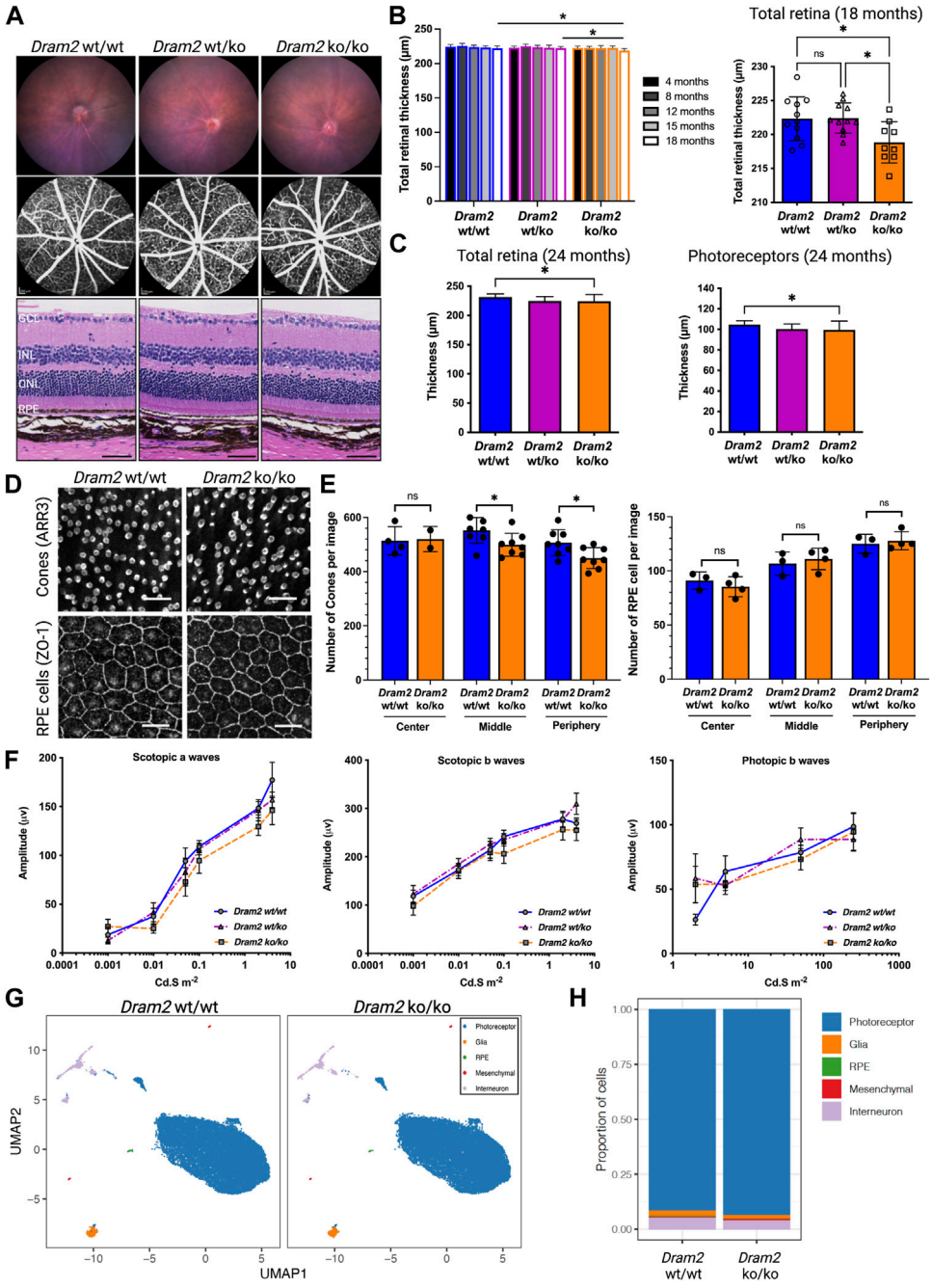

FIGURE 4
Dram2 loss causes very mild age-related photoreceptor degeneration with absence of functional deficit or transcriptional changes in mice. **(A)** Fundus imaging (top row) and fundus angiography (middle row) at 4-month of age. Histopathological (bottom row) analyses of *Dram2* wt/wt, wt/ko, and ko/ko mice at 24 months (Hematoxylin Eosin, 200 µm from the optic nerve head). GCL, ganglion cell layer; INL, inner nuclear layer; ONL, outer nuclear layer; RPE, retinal pigment epithelium. Scale bar, 50 µm. **(B)** Optical coherence tomography (OCT) analysis followed by automated segmentation of retinal thickness in *Dram2* wt/wt, wt/ko, and ko/ko. Time course of retinal thickness of all genotypes from 4 to 18-month of age (left; n = 8–14 mice per genotype; one-way ANOVA *$p < 0.05$) and between the genotypes at 18-month of age (right; n = 9–11 mice per genotype; one-way ANOVA *$p < 0.05$; ns, not significant). **(C)** Total retinal thickness at 24 months (left) and photoreceptor layer thickness (right) of *Dram2* wt/wt, wt/ko, and ko/ko mice (n = 16–27 mice per genotype, one-way ANOVA *$p < 0.05$). Automated 8-layer retinal segmentation was performed on this cohort of mice and only the photoreceptor layer (Outer nuclear layer (ONL) + inner segment + outer segment) showed significant difference between *Dram2* wt/wt and *Dram2* ko/ko mice (other layers shown in Supplementary Figure S3A). **(D)** Representative immunofluorescent image of cone photoreceptor cells (ARR3; top row) and RPE cells (ZO-1; bottom row) from peripheral retina. Scale bar, 25 µm. **(E)** Quantification of cone photoreceptor cells (left) and RPE cells (right) in *Dram2* wt/wt and *Dram2* ko/ko retinas (Mann-Whitney test, *$p < 0.05$, ns, not significant). **(F)** Electroretinography (ERG) analysis of *Dram2* wt/wt, wt/ko, and ko/ko mice at 21 months. (mean±SEM, n = 9–10 mice per genotype). **(G)** UMAP representations of single cell RNA sequencing (scRNAseq) analysis of *Dram2* wt/wt and ko/ko retinas **(H)** Proportion of cell types per genotype identified from the scRNAseq analysis.

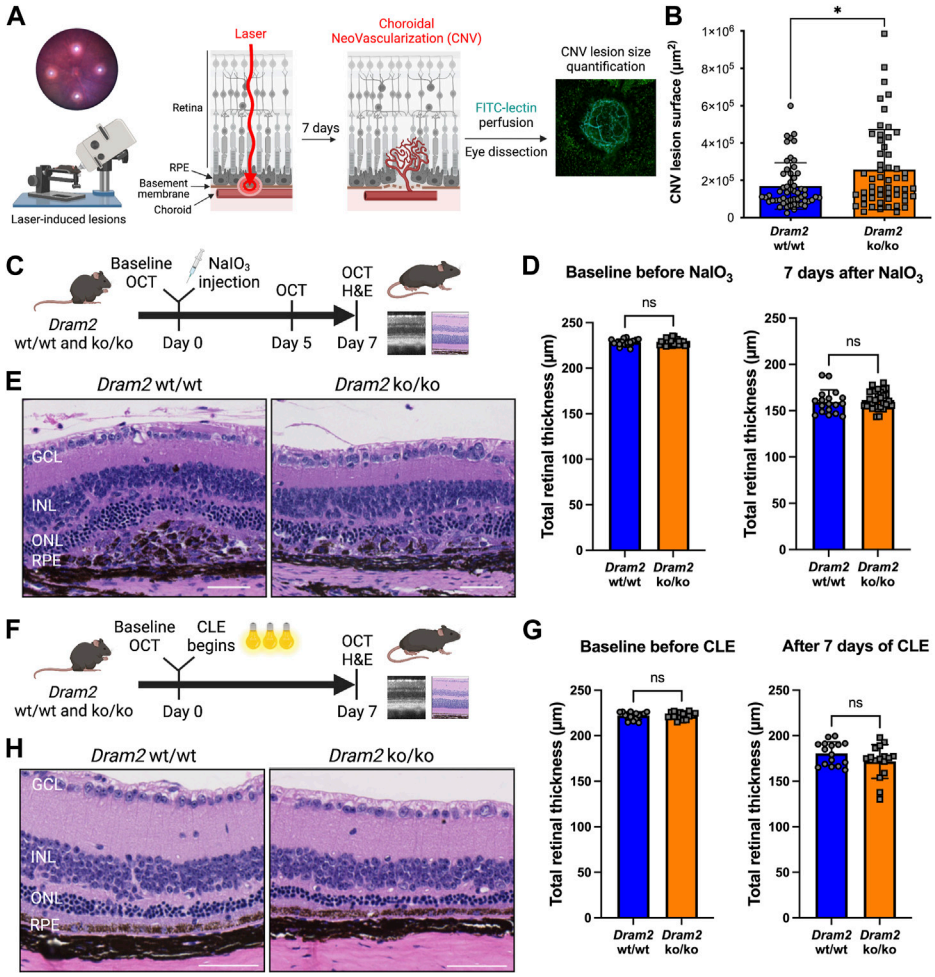

FIGURE 5
Dram2 loss exacerbates choroidal neovascularization lesions but does not exacerbate retinal dystrophy in mouse pre-clinical models involving photoreceptor or RPE injury **(A)** Experimental design of the laser-induced choroidal neovascularization (CNV) mouse pre-clinical model. **(B)** Quantification of CNV lesion surface size (in μm^2) 7 days after disruption of the basement membrane by the laser burn in *Dram2* wt/wt and ko/ko retinas (n = 55 lesions per genotype, unpaired t-test, *: $p < 0.05$). **(C)** Experimental design of the sodium iodate ($NaIO_3$) degeneration model (three independent cohorts, n = 9 to 15 mice per genotype at 5–18 weeks of age). OCT, optical coherence tomography; H&E, hematoxylin and eosin. **(D)** Retinal thickness in the NaIO3 experiment measured by OCT in *Dram2* wt/wt and ko/ko mice at baseline (left) and 7 days (right) after $NaIO_3$ treatment. Unpaired t-test; ns, not significant. **(E)** Histopathological analysis of *Dram2* wt/wt (left) and ko/ko (right) retinas after $NaIO_3$ treatment. **(F)** Experimental design of the constant light exposure (CLE) degeneration model (three independent cohorts, n = 8 mice per genotype at 33–40 weeks of age). **(G)** Retinal thickness in the CLE experiment measured by OCT in *Dram2* wt/wt and ko/ko mice at baseline (day 0, left) and after 7 days of exposure (right). Unpaired t-test; ns, not significant. **(H)** Histopathological analysis of *Dram2* wt/wt and ko/ko retinas after CLE (day 7). Scale bars = 50 µm. GCL, ganglion cell layer; INL, inner nuclear layer; ONL, outer nuclear layer; RPE, retinal pigment epithelium.

In conclusion, although no transcriptional changes were detected at 12 months, *Dram2* loss causes a mild age-related retinal degeneration starting at 18 months, which is restricted to photoreceptor cells and not severe enough to affect vision in mice even at 21 months.

3.5 Dram2 loss exacerbates choroidal neovascular lesions but not retinal degeneration caused by acute photoreceptor or RPE injury

Since *Dram2* loss causes a slow-progressing and mild retinal dystrophy in mice, we tested if the phenotype could be exacerbated by additional environmental stress. We selected three pre-clinical models commonly used to model AMD: 1) the laser-induced choroidal neovascularization (CNV) model (Lambert et al., 2013), 2) the sodium iodate model ($NaIO_3$), in which photoreceptor degeneration happens secondarily to RPE-specific toxicity-induced cell death (Balmer et al., 2015; Zhang et al., 2021) and 3) the constant light exposure model (CLE), in which phototoxicity directly causes photoreceptor death (Natoli et al., 2016), (Figure 5).

Because we identified an extra mesenchymal-like cluster in *DRAM2* KO organoids (Figure 2C) and because *DRAM2* silencing has been associated with increased tumor growth and resistance to apoptosis (Park et al., 2009; Bai et al., 2016; Wudu et al., 2019), we wanted to know if *DRAM2* loss could have consequences on cell survival, proliferation or/and migration of mesenchymal-like

cells. Since we identified *DRAM2* expression changes in the choriocapillaris in AMD eyes (Figure 1E), we used the laser-induced choroidal neovascularization (CNV) pre-clinical model to challenge cells around this area (Figure 5A). In this model, the Bruch's membrane between the choriocapillaris and the RPE is disrupted using a laser burn, and the resulting CNV lesions involve endothelial cells, pericytes, fibroblasts and mesenchymal cells, with blood vessels growing into the retina (Lambert et al., 2013). One week after the laser induction, the CNV lesion surface areas are quantified. Interestingly, a significant increase in the lesion size in *Dram2 ko/ko* mice was detected, with mean lesion size being 256,857 μm^2, compared to the *Dram2 wt/wt* mean lesion size of 169,340 μm^2 (Figure 5B, p-value = 0.0102).

To further investigate the role of Dram2 loss at the cellular level, we isolated choroidal and RPE cells from *Dram2 wt/wt* and *ko/ko* mice. Eyes were enucleated and after removal of the anterior chamber, the lens and the retina, the choroid containing RPE cells was dissected, dissociated and cultured for 7 days (Supplementary Figure S2A). The cells were collected and scRNAseq was performed. Clustering cells based on their gene expression identified 8 clusters of different cell types including: RPE cells, two distinct fibroblast clusters (fibroblast 1 and 2), fibroblast proliferating cells, fibroblast-like cells, endothelial cells, pericytes, and myeloid cells (Supplementary Figure S2B). There were no significant differences in cell type composition between *Dram2 wt/wt* and *ko/ko* RPE/Choroids (Supplementary Figure S2C) and most of the cells were fibroblastic cells expressing characteristic cell markers (Supplementary Figure S2D). The fibroblasts (1 and 2), fibroblasts proliferating, and fibroblast-like cells were sub-clustered further, but again, no differences were revealed between the *Dram2 wt/wt* and *ko/ko* samples (Supplementary Figure S2E). Interestingly, when we plated the cells, we observed that the RPE/Choroid cells from *Dram2 ko/ko* mice reached 20% confluency in a little over 3 days (78 h), whereas it took a little over 5 days (126 h) for the cells from *Dram2 wt/wt* mice to reach a similar level of confluency (Supplementary Figure S2F). This finding suggests that the CNV lesion exacerbation observed in *Dram2 ko/ko* mice is caused by a choroidal cell proliferative advantage.

We then tested if the exacerbation of $NaIO_3$-induced RPE cell death observed *in vitro* in absence of DRAM2 could be replicated *in vivo* (Figure 5C). Intravenous administration of $NaIO_3$ induces rapid and specific RPE cell death and as the RPE plays a critical role in the maintenance and survival of the overlying photoreceptors (Boulton and Dayhaw-Barker, 2001), the RPE loss is followed by photoreceptor degeneration. SD-OCT analysis five and 7 days after treatment with $NaIO_3$ revealed no significant differences in retinal thickness between *Dram2 wt/wt* and *ko/ko* mice (Supplementary Figure S3C and Figure 5D). Histological examination at day 7 confirmed thinning of the photoreceptor layer (ONL and segments) (Figure 5E), destruction of the RPE monolayer and ongoing wound healing in the subretinal space (Supplementary Figure S3B). Lesion scoring of the combined RPE and ONL damage showed similar severity in *Dram2 wt/wt* and *ko/ko* mouse retinas (Supplementary Figure S3D). These results indicate that loss of *Dram2* does not exacerbate photoreceptor loss following $NaIO_3$-induced RPE damage.

Finally, we tested if the age-related photoreceptor loss observed in the *Dram2 ko/ko* mice could be exacerbated by light toxicity (Figure 5F). Mice were subjected to constant light exposure (CLE) for 7 days. SD-OCT analysis showed that after a week of exposure to bright light, *Dram2 wt/wt* mice lost 66 ± 23 μm of retinal thickness and *ko/ko* mice lost 69 ± 20 μm, revealing no significant difference between the two genotypes (Figure 5G). Histological examination confirmed that the retinal degeneration affected photoreceptors, with significant thinning of the ONL and photoreceptor inner/outer segments (Figure 5H and Supplementary Figure S3E). Lesion scoring of the damaged areas showed similar severity of retinal dystrophy in *Dram2 wt/wt* and *ko/ko* mouse retinas (Supplementary Figure S3F). These results show that loss of *Dram2* does not exacerbate photoreceptor loss following acute light-induced damage.

Collectively, our results show that *Dram2* loss in mice does not exacerbate retinal dystrophy induced by acute photoreceptor- or RPE-injury, but it exacerbates proliferation of choroidal cells, resulting in more severe choroidal neovascular lesions.

3.6 Integration of data from different *in vitro* and *in vivo* systems reveals complexity of human disease pathophysiology

To gain further insights into relevance of hPSC-retinal organoids and mouse retinas to study and model human retinal dystrophies, we compared our scRNA seq datasets generated from *DRAM2* WT organoids and *Dram2 wt/wt* retinas to a previously published single nuclei sequencing of non-AMD human donor eyes (Orozco et al., 2020) (Figure 6A). Twelve-month old wild-type hPSC-retinal organoids had five main cell types, including photoreceptors, glia, RPE, interneurons, and progenitors (Figure 6B). Adult wild-type mouse retinas had three main cell types (photoreceptors, glia and interneurons) (Figure 6C) and adult human donor eyes had seven main classes of cells (photoreceptors, glia, RPE, mesenchymal, interneurons, myeloid, and retinal ganglion cells (RGC)) (Figure 6D). As described previously, very few mesenchymal cells were detected in wild-type retinal organoids, and few mesenchymal and RPE cells were captured in the mouse retina dataset. The main difference between the three datasets was that progenitors, which are absent in adult mouse and human retinas, constitute the majority of hPSC-retinal organoid cells; whereas photoreceptors are the main cell type detected in mouse and human retinas. Key marker genes for each cell type in the three datasets were identified (Figures 6E–G). Clustering the coinciding cell types between the three sample sets showed grouping of the same cell types together, and highly comparable expression of top cell type marker genes (Figure 6H). The fact that when using top marker genes, the different cell types clustered together across the three datasets is not surprising as they are very specialized cells with distinct characteristics and functions (e.g., light sensitivity for photoreceptors: OPN1MW, OPN1SW; recycling of visual cycle components by RPE cells: RBP1, RLBP1). What was less anticipated is that when we selected panels of genes involved in several biological processes common to all cell types, such as apoptosis, autophagy or lysosomal function, cell clustering once again grouped the different cell types together, independently of the

10.3389/fcell.2023.1252547

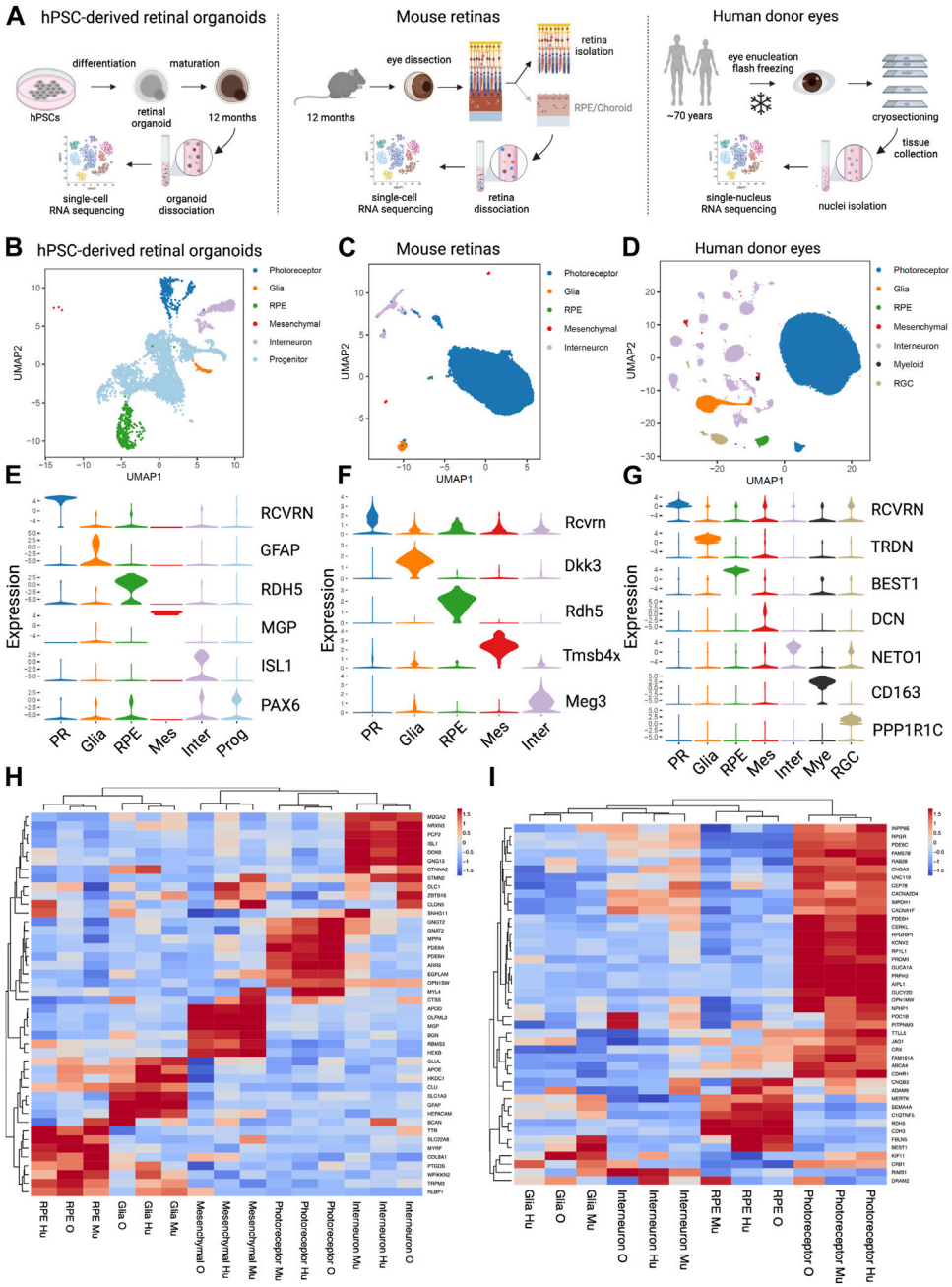

FIGURE 6
Comparative analysis of single cell analysis of human stem cell-derived retinal organoids, mouse retina and human retina **(A)** Diagrams of the experimental designs to generate single cell RNA sequencing (scRNA seq) data from human Pluripotent Stem Cells (hPSCs)-derived retinal organoids (left), scRNA seq data from mouse retinas (middle) and single nucleus RNA sequencing (snRNA seq) data from human eyes (right). **(B)** UMAP representation of the hPSC- retinal organoid scRNAseq analysis. **(C)** UMAP representation of the mouse retinal scRNAseq analysis. **(D)** UMAP representation of the human eyes snRNAseq analysis. **(E)** Violin plot of key marker genes expression for identified cell types in hPSC- retinal organoids. PR, photoreceptor; RPE, retinal pigment epithelium; Mes, mesenchymal; Inter, interneurons; Prog, progenitors. **(F)** Violin plot of key marker genes expression for identified cell types in mouse retinas. PR, photoreceptor; RPE, retinal pigment epithelium; Mes, mesenchymal; Inter, interneurons. **(G)** Violin plot of key marker genes expression for identified cell types in human eyes. PR, photoreceptor; RPE, retinal pigment epithelium; Mes, mesenchymal; Inter, interneurons; Mye, myeloid cells; RGC, retinal ganglion cells. **(H)** Heatmap of the unsupervised hierarchical cluster analysis of top marker genes per cell types identified in all three datasets. Mu, mouse retina scRNAseq; O, hPSC- retinal organoid scRNAseq; Hu, human snRNAseq. **(I)** Heatmap of the hierarchical cluster analysis of known cone-rod macular dystrophy genes expressed in the three datasets. Mu, mouse retina scRNAseq; O, hPSC-retinal organoid scRNAseq; Hu, human snRNAseq.

dataset origin (Supplementary Figures S4A–C). These findings confirmed that hPSC-retinal organoids and mouse retinas are overall relevant models for studying human retinal biology. There are still limitations to these models. For example, when we selected a panel of genes involved in phagocytosis, cell clustering grouped the RPE cells from the hPSC-retinal organoids with the Glia

cells from mouse and human retinas; while RPE cells from mouse and human retinas clustered together (Supplementary Figure S4D). This suggests that to study some human RPE biological processes such as phagocytosis, for example, using hPSC-derived RPE cells or mouse eyes will be more relevant than the RPE cells growing within the hPSC-retinal organoids.

Next, we clustered cell types using a panel of genes associated with retinal dystrophies. A compiled list of genes known to be involved in cone, cone-rod, and macular dystrophies was generated (Birtel et al., 2018; Gill et al., 2019). Clustering based on gene expression from the three sample sets showed the photoreceptors, interneurons, Glia and RPE cell types cluster by cell type and not by data source or species (Figure 6I). The vast majority of the retinal dystrophy genes (70% of them) have their strongest expression level in photoreceptor cells, and a smaller subset of genes (about 20%) is most highly expressed in RPE cells. Integration of the three datasets revealed that *DRAM2* has the highest expression in human interneurons, retinal organoid photoreceptors, and mouse RPE cells (Figure 6I). We used a combination of different systems and models to be able to uncover different aspects of DRAM2-retinopathy pathophysiology. Indeed, these particular system/cell types combination alone (i.e., photoreceptors in organoids or RPE in the mouse model) did not reveal any phenotype in absence of *DRAM2*.

In conclusion, different models such as hPSC-retinal organoids or mice can be leveraged to study and model human retinal dystrophies, however, cell type specific and species-specific expression of a gene of interest must be taken into account when picking the most relevant system. When a gene of interest is ubiquitously expressed or expressed in different cell types, such as *DRAM2*, then a combination of models is most likely to be useful to uncover the different pathophysiologic mechanisms underlying the disease.

4 Discussion

Before discussing our findings, we would like to acknowledge limitations of our study. First, transcript levels do not always directly correlate to protein expression, and our expression data are primarily based on mRNA expression levels. Unfortunately, we could not identify a commercially available anti-DRAM2 antibody with satisfactory selectivity validation in our hands to perform analysis at the protein level. Another limitation is that we used fetal human primary RPE cells and embryonic stem cell-derived RPE/retinal organoids to study a disease with an age-related component. Organoids accurately depict early retinal development (Sridhar et al., 2020); however, AMD occurs after decades of life and cannot be replicated *in vitro*. We aged hPSC-retinal organoids in culture for 12 months and our *Dram2 ko/ko* mice up to 24 months to recapitulate some aging features, but both models were kept in favorable and well-controlled conditions and do not mimic the environmental stress that patients experience over their lifetime. To study and potentially model *DRAM2*-retinopathy, we used knockdown or knockout in cells or mice, whereas patients carry point mutations in *DRAM2*. This choice was based on findings suggesting that patients with at least one loss-of-function variant present with earlier disease onset compared to patients carrying only missense or in-frame deletions (Sergouniotis et al., 2015). This was recently confirmed by a genotype-phenotype correlation analysis showing that non-null variants can result in milder disease (Krašovec et al., 2022). Finally, we used acute pre-clinical models. DRAM2-retinopathy is a slow progressive disease and chronic models would be more appropriate. Unfortunately, the lack of disease-relevant models is a common limitation in the age-related retinal degeneration field.

Despite some limitations, our study provides novel insight regarding different *in vitro* and *in vivo* models commonly used to study retinal dystrophies, including AMD. Since biallelic *DRAM2* variants cause retinal dystrophy with early macular involvement (El-Asrag et al., 2015; Sergouniotis et al., 2015; Birtel et al., 2018; Kuniyoshi et al., 2020; Krašovec et al., 2022), and we identify lower *DRAM2* expression in AMD patient eyes (Figure 1A), we decided to use *DRAM2* as a case study. By assessing the different phenotypes resulting from *DRAM2* loss in these various systems, our ultimate goal was to gain insights on *DRAM2*-retinopathy pathophysiology and understand the limitations of these different systems better. Interestingly, we found that *DRAM2* loss had different consequences depending on the species, the cell types analyzed and the model used. For example, while we did not see any phenotype exacerbation in the *DRAM2 ko/ko* mice after $NaIO_3$ treatment (Figures 5C–E), we found that *DRAM2* loss exacerbated cell death after $NaIO_3$ treatment in closely monitored human RPE cells *in vitro* (Figure 3). Similarly, the inherent variability of human PSC-derived retinal organoids did not allow us to identify differences in photoreceptor number between *DRAM2* WT and KO organoids even after a year of maturation (Figures 2B–D), however we were able to detect a mild spontaneous age-related photoreceptor dystrophy in *Dram2 ko/ko* mice (Figures 4B–E). Of note, the retinal organoid system, despite not being useful to study *DRAM2* loss consequences in photoreceptors, was critical in discovering its role in mesenchymal cell proliferation and ECM production (Figures 2C–G). This led us to test the choroidal neovascularization pre-clinical model and we observed exacerbation of the CNV lesions in absence of DRAM2 (Figure 5B). The fact that different systems did not always provide concordant results is not surprising. This is inherent to the differences in nature (*in vitro versus in vivo*), timeline (age-related *versus* acute), and readouts associated with each model. Our work highlights the importance of integration of data from different systems, of which pros and cons are taken into account, when studying complex human diseases.

As part of our study, we also performed a comparative single-cell transcriptomic analysis of the different systems. The results provide insights on which models to select when studying a particular gene or pathway. For example, *POC1B* is highly expressed in human and mouse photoreceptors but not highly expressed in hPSC-retinal organoid photoreceptors (Figure 6I). POC1B is critical for the photoreceptor connecting cilium and *POC1B* mutations cause cone-rod dystrophy (Beck et al., 2014). Lower *POC1B* expression in retinal organoid photoreceptors could reflect that their inner and outer segments are shorter and less fully developed compared to *in vivo* photoreceptors and they may not be the preferred system to study POC1B function. Another example is *CRB1*, which is expressed in photoreceptors from the three datasets. *CRB1*

mutations cause variable severe retinal dystrophies with photoreceptor degeneration. However, *CRB1* is expressed in mouse and human glial cells at a higher level than in photoreceptors (Figure 6I). This is interesting because *CRB1*-associated retinal dystrophies also involve inflammation and vascular leaks (Bujakowska et al., 2012). Therefore, mice may be a better model to study *CRB1* mutations over hPSC-retinal organoids, as the organoids would not integrate vascular and glial-dependent pathogenic features to the photoreceptor degeneration. Finally, comparison of the different datasets can help with tool development, such as selection of cell type specific promoters for creation of cell line reporters or conditional mouse models. It can also help understanding existing tools better. For example, BEST1, also known as *VMD2*, is a gene highly expressed in human RPE cells and is considered a RPE cell marker (Marquardt et al., 1998; Petrukhin et al., 1998) (Figure 6G). However, we found that in the mouse retina, BEST1 is actually highly expressed in glial cells (Figure 6I). This can explain why transgenes placed under the control of a VMD2 promoter in transgenic mice do not show the intended RPE specific expression and are also expressed in Muller glia (Le et al., 2008; Ueki et al., 2009).

Knowing in which cell type a gene is highly expressed is important when considering which system to select for its investigation. However, the fact that a gene at the transcriptional level is more expressed in a cell type does not necessarily mean that this cell type will be driving disease pathophysiology. For example, in the human dataset, *CNGB3* is most highly expressed in RPE cells and to a lower extent in photoreceptors. However, *CNGB3* mutations cause achromatopsia 3, which is characterized by loss of color vision and photoreceptor degeneration (Kohl et al., 2005; Wiszniewski et al., 2007). *CNGB3* encodes a channel subunit located in the plasma membrane and is essential for generation of light-evoked electrical responses in cones (Kohl et al., 2000; Sundin et al., 2000). Studying its function in RPE cells only, where is it most highly expressed in the human eye, would not have explained how its loss of function causes achromatopsia. It is therefore important to keep in mind that expression in different cell types may translate into different consequences in term of disease mechanism, independently of the relative level of expression in the different cell types. DRAM2 turned out to be a great example of this, as it is ubiquitously expressed in the eye.

Leveraging results obtained with the different systems, we were able to recapitulate the pathognomonic clinical features of *DRAM2*-retinopathy. In patients with loss of function *DRAM2* mutations, the first sign of disease is central vision loss in the third decade of life, with early macular involvement and photoreceptor loss (Krašovec et al., 2022). In primates, the center of the macula, called the fovea, is responsible for this central vision and contains 99% of the total cone photoreceptors (Perry and Cowey, 1985). Mouse do not have a macula and fovea, so we were not able to determine if this structure is also the first affected in *Dram2* knockout animals. However, we noticed that indeed early on (4-month-old), cone photoreceptors were lost in *Dram2 ko/ko* mice compared to *wt/wt* littermates (Figure 4E). Cones in mice represent only 3% of the photoreceptors, with the majority of photoreceptors being rods (Jeon et al., 1998). The fact that when we noticed cone loss, the outer retinal layer (i.e., photoreceptor layer) was not overall thinner suggests that at that time, rods were not yet affected in the mouse mutant. As we aged the mice (18-month-old), we observed outer retinal layer thinning, showing late onset of widespread rod degeneration (Figure 4C). As the mouse retina is thought to be similar to the primate peripheral retina (Jeon et al., 1998), this finding mimics the late onset of peripheral vision loss described by patients in their fifth decade. In addition to this early cone involvement followed by rod degeneration (i.e., cone-rod dystrophy), another aspect of DRAM2-retinopathy was identified in our mouse model. Indeed, many patients have bone-spicule pigmentation, which is characterized by migration of cells from the RPE to perivascular sites and accumulation of ECM components around the blood vessels (Li et al., 1995). Although we did not observe spontaneous RPE disturbance in *Dram2 ko/ko* mice, we observed exacerbation of neovascular lesions with ECM deposition around the blood vessels, when the RPE basement membrane was physically disrupted in the CNV model. We also observed an extra cell cluster in *DRAM2* KO retinal organoids, which was characterized by a mesenchymal gene signature with high expression of ECM genes (Figure 2E). Finally, we were able to observed a decreased hRPE cell-resistance to death induced by stressful *in vitro* conditions in absence or lower expression of *DRAM2* (Figure 3). This models the distinctive peripheral RPE disruption phenotype observed in patients with nonsense mutations or decreased *DRAM2* expression (Krašovec et al., 2022). Although the different cell specific effects we uncovered are consistent with DRAM2-retinopathy and AMD clinical presentation, the exact cellular mechanisms are still unclear. It would be interesting to link DRAM2's proposed role in autophagy to these phenotypes and understand why despite being expressed everywhere in the body, *DRAM2* mutations only affect the retina in patients. We have come a long way in term of identification of human genetics hits associated with disease, mapping their expression to individual cell types of interest and integration of these data to point towards putative pathogenic molecular mechanisms. We now have to keep developing retinal dystrophy models further, to be able to dissect these mechanisms in a disease-relevant manner and identify viable therapeutic approaches.

In conclusion, using different human pluripotent stem cell-derived *in vitro* systems and *in vivo* mouse pre-clinical models, we were able to uncover the complexity of DRAM2 function. We found that its loss in choroidal cells provided a proliferative advantage, whereas its loss in post-mitotic cells such as photoreceptor and RPE cells increased degeneration susceptibility. Our work highlights the importance of integration of data from different systems, of which pros and cons are taken into account, when studying complex human diseases. Indeed, we found that each system on its own provided only limited insights into DRAM2-disease mechanisms. However, integration of data from several systems allowed deeper understanding of the pathophysiology of retinal dystrophy associated with DRAM2 loss of function.

Data availability statement

The datasets presented in this study can be found in online repositories. The names of the repository/repositories and accession

number(s) can be found below: https://www.ncbi.nlm.nih.gov/geo/, GSE220627.

Ethics statement

The studies involving humans were approved by Lions Eye Institute for Transplant and Research ethics committee. The studies were conducted in accordance with the local legislation and institutional requirements. The human samples used in this study were acquired from Lions Eye Institute for Transplant and Research. Written informed consent for participation was not required from the participants or the participants' legal guardians/next of kin in accordance with the national legislation and institutional requirements. The animal study was approved by Genentech Institutional Animal Care and Use Committee (IACUC). The study was conducted in accordance with the local legislation and institutional requirements. No potentially identifiable images or data are presented in this study.

Author contributions

Conceptualization, MKJ, LO, HQ, and MJ; methodology, MKJ, LO, HQ, JE, and SC; software, LO and JE; validation, MKJ, LO, SC, and MJ; formal analysis, MKJ, LO and MJ; investigation, MJ, LO, HQ, TT, PC, and MJ; resources, ZM; data curation, LO; writing—original draft preparation, MKJ, and MJ; writing—review and editing, MKJ, LO, HQ, JE, ZM, SC, and MJ; visualization, MKJ, LO, and MJ; supervision, MJ; project administration, MJ. All authors contributed to the article and approved the submitted version.

Acknowledgments

The authors thank Sarah Gierke for assistance with image acquisition, the FACS Core for assistance with flow cytometry analysis, colleagues in the animal facility including Chris Dela Cruz for assistance with mouse breeding and genotyping, Nianfeng Ge, Sreedevi Chalasani, Janet Tao, Sarahjane Saturnion Nghiem and Linda Rangell for expert assistance with histology and *in-situ* hybridization, and Christine Clarke for assistance with uploading the datasets to a publicly accessible repository.

Conflict of interest

At the time of the study, all authors were full time employees of Genentech Inc. (a member of the Roche group) with stock and stock options in Roche.

Publisher's note

Supplementary material

The Supplementary Material for this article can be found online at: https://www.frontiersin.org/articles/10.3389/fcell.2023.1252547/full#supplementary-material

References

Abad-Morales, V., Burés-Jelstrup, A., Navarro, R., Ruiz-Nogales, S., Méndez-Vendrell, P., Corcóstegui, B., et al. (2019). Characterization of the cone-rod dystrophy retinal phenotype caused by novel homozygous DRAM2 mutations. *Exp. Eye Res.* 187, 107752. doi:10.1016/j.exer.2019.107752

Bai, S., Tian, B., Li, A., Yao, Q., Zhang, G., and Li, F. (2016). MicroRNA-125b promotes tumor growth and suppresses apoptosis by targeting DRAM2 in retinoblastoma. *Eye* 30, 1630–1638. doi:10.1038/eye.2016.189

Balmer, J., Zulliger, R., Roberti, S., and Enzmann, V. (2015). Retinal cell death caused by sodium iodate involves multiple caspase-dependent and caspase-independent cell-death pathways. *Int. J. Mol. Sci.* 16, 15086–15103. doi:10.3390/ijms160715086

Beck, B. B., Phillips, J. B., Bartram, M. P., Wegner, J., Thoenes, M., Pannes, A., et al. (2014). Mutation of POC1B in a severe syndromic retinal ciliopathy. *Hum. Mutat.* 35, 1153–1162. doi:10.1002/humu.22618

Bennett, J., Wellman, J., Marshall, K. A., McCague, S., Ashtari, M., DiStefano-Pappas, J., et al. (2016). Safety and durability of effect of contralateral-eye administration of AAV2 gene therapy in patients with childhood-onset blindness caused by RPE65 mutations: A follow-on phase 1 trial. *Lancet Lond Engl.* 388, 661–672. doi:10.1016/s0140-6736(16)30371-3

Berkowitz, B. A., Podolsky, R. H., Lenning, J., Khetarpal, N., Tran, C., Wu, J. Y., et al. (2017). Sodium iodate produces a strain-dependent retinal oxidative stress response measured *in vivo* using QUEST MRI. *Invest. Ophth Vis. Sci.* 58, 3286–3293. doi:10.1167/iovs.17-21850

Birtel, J., Eisenberger, T., Gliem, M., Müller, P. L., Herrmann, P., Betz, C., et al. (2018). Clinical and genetic characteristics of 251 consecutive patients with macular and cone/cone-rod dystrophy. *Sci. Rep-uk* 8, 4824. doi:10.1038/s41598-018-22096-0

Bohórquez, B. G., Aller, E., Muñoz, A. R., Jaijo, T., García, G. G., and Millán, J. M. (2021). Updating the genetic landscape of inherited retinal dystrophies. *Front. Cell Dev. Biol.* 9, 645600. doi:10.3389/fcell.2021.645600

Boulton, M., and Dayhaw-Barker, P. (2001). The role of the retinal pigment epithelium: topographical variation and ageing changes. *Eye Lond Engl.* 15, 384–389. doi:10.1038/eye.2001.141

Bravo-Gil, N., Pozo, M. G., Martín-Sánchez, M., Méndez-Vidal, C., Rúa, E. R., Borrego, S., et al. (2017). Unravelling the genetic basis of simplex Retinitis Pigmentosa cases. *Sci. Rep-uk* 7, 41937. doi:10.1038/srep41937

Bujakowska, K., Audo, I., Mohand-Saïd, S., Lancelot, M., Antonio, A., Germain, A., et al. (2012). CRB1 mutations in inherited retinal dystrophies. *Hum. Mutat.* 33, 306–315. doi:10.1002/humu.21653

Cowan, C. S., Renner, M., Gennaro, M. D., Gross-Scherf, B., Goldblum, D., Hou, Y., et al. (2020). Cell types of the human retina and its organoids at single-cell resolution. *Cell* 182, 1623–1640. doi:10.1016/j.cell.2020.08.013

Crighton, D., Wilkinson, S., and Ryan, K. M. (2007). DRAM links autophagy to p53 and programmed cell death. *Autophagy* 3, 72–74. doi:10.4161/auto.3438

Crouch, R. K., Koutalos, Y., Kono, M., Schey, K., and Ablonczy, Z. (2015). A2E and lipofuscin. *Prog. Mol. Biol. Transl.* 134, 449–463. doi:10.1016/bs.pmbts.2015.06.005

Deng, W.-L., Gao, M.-L., Lei, X.-L., Lv, J.-N., Zhao, H., He, K.-W., et al. (2018). Gene correction reverses ciliopathy and photoreceptor loss in iPSC-derived retinal organoids from retinitis pigmentosa patients. *Stem Cell Rep.* 10, 1267–1281. doi:10.1016/j.stemcr.2018.02.003

Durinck, S., Stawiski, E. W., Pavía-Jiménez, A., Modrusan, Z., Kapur, P., Jaiswal, B. S., et al. (2015). Spectrum of diverse genomic alterations define non–clear cell renal carcinoma subtypes. *Nat. Genet.* 47, 13–21. doi:10.1038/ng.3146

El-Asrag, M. E., Sergouniotis, P. I., McKibbin, M., Plagnol, V., Sheridan, E., Waseem, N., et al. (2015). Biallelic mutations in the autophagy regulator DRAM2 cause retinal dystrophy with early macular involvement. *Am. J. Hum. Genet.* 96, 948–954. doi:10.1016/j.ajhg.2015.04.006

Enzbrenner, A., Zulliger, R., Biber, J., Pousa, A. M. Q., Schäfer, N., Stucki, C., et al. (2021). Sodium iodate-induced degeneration results in local complement changes and inflammatory processes in murine retina. *Int. J. Mol. Sci.* 22, 9218. doi:10.3390/ijms22179218

Gill, J. S., Georgiou, M., Kalitzeos, A., Moore, A. T., and Michaelides, M. (2019). Progressive cone and cone-rod dystrophies: clinical features, molecular genetics and prospects for therapy. *Br. J. Ophthalmol.* 103, 711–720. doi:10.1136/bjophthalmol-2018-313278

Gong, J., Fields, M. A., Moreira, E. F., Bowrey, H. E., Gooz, M., Ablonczy, Z., et al. (2015). Differentiation of human protein-induced pluripotent stem cells toward a retinal pigment epithelial cell fate. *Plos One* 10, e0143272. doi:10.1371/journal.pone.0143272

Guo, Y., Wang, P., Ma, J. H., Cui, Z., Yu, Q., Liu, S., et al. (2019). Modeling retinitis pigmentosa: retinal organoids generated from the iPSCs of a patient with the USH2A mutation show early developmental abnormalities. *Front. Cell Neurosci.* 13, 361. doi:10.3389/fncel.2019.00361

Hanus, J., Anderson, C., Sarraf, D., Ma, J., and Wang, S. (2016). Retinal pigment epithelial cell necroptosis in response to sodium iodate. *Cell Death Discov.* 2, 16054. doi:10.1038/cddiscovery.2016.54

Idelson, M., Alper, R., Obolensky, A., Ben-Shushan, E., Hemo, I., Yachimovich-Cohen, N., et al. (2009). Directed differentiation of human embryonic stem cells into functional retinal pigment epithelium cells. *Cell Stem Cell* 5, 396–408. doi:10.1016/j.stem.2009.07.002

Jeon, C. J., Strettoi, E., and Masland, R. H. (1998). The major cell populations of the mouse retina. *J. Neurosci. Off. J. Soc. Neurosci.* 18, 8936–8946. doi:10.1523/JNEUROSCI.18-21-08936.1998

Karlsson, M., Zhang, C., Méar, L., Zhong, W., Digre, A., Katona, B., et al. (2021). A single-cell type transcriptomics map of human tissues. *Sci. Adv.* 7, eabh2169. doi:10.1126/sciadv.abh2169

Kohl, S., Baumann, B., Broghammer, M., Jägle, H., Sieving, P., Kellner, U., et al. (2000). Mutations in the CNGB3 gene encoding the β-subunit of the cone photoreceptor cGMP-gated channel are responsible for achromatopsia (ACHM3) linked to chromosome 8q21. *Hum. Mol. Genet.* 9, 2107–2116. doi:10.1093/hmg/9.14.2107

Kohl, S., Varsanyi, B., Antunes, G. A., Baumann, B., Hoyng, C. B., Jägle, H., et al. (2005). CNGB3 mutations account for 50% of all cases with autosomal recessive achromatopsia. *Eur. J. Hum. Genet. Ejhg* 13, 302–308. doi:10.1038/sj.ejhg.5201269

Krašovec, T., Volk, M., Habjan, M. Š., Hawlina, M., Valentinčič, N. V., and Fakin, A. (2022). The clinical spectrum and disease course of DRAM2 retinopathy. *Int. J. Mol. Sci.* 23, 7398. doi:10.3390/ijms23137398

Kruczek, K., Qu, Z., Gentry, J., Fadl, B. R., Gieser, L., Hiriyanna, S., et al. (2021). Gene therapy of dominant CRX-leber congenital amaurosis using patient stem cell-derived retinal organoids. *Stem Cell Rep.* 16, 252–263. doi:10.1016/j.stemcr.2020.12.018

Kuniyoshi, K., Hayashi, T., Kameya, S., Katagiri, S., Mizobuchi, K., Tachibana, T., et al. (2020). Clinical course and electron microscopic findings in lymphocytes of patients with DRAM2-associated retinopathy. *Int. J. Mol. Sci.* 21, 1331. doi:10.3390/ijms21041331

Lambert, V., Lecomte, J., Hansen, S., Blacher, S., Gonzalez, M.-L. A., Struman, I., et al. (2013). Laser-induced choroidal neovascularization model to study age-related macular degeneration in mice. *Nat. Protoc.* 8, 2197–2211. doi:10.1038/nprot.2013.135

Law, C. W., Chen, Y., Shi, W., and Smyth, G. K. (2014). voom: precision weights unlock linear model analysis tools for RNA-seq read counts. *Genome Biol.* 15, R29. doi:10.1186/gb-2014-15-2-r29

Le, Y.-Z., Zheng, W., Rao, P.-C., Zheng, L., Anderson, R. E., Esumi, N., et al. (2008). Inducible expression of cre recombinase in the retinal pigmented epithelium. *Investig. Opthalmology Vis. Sci.* 49, 1248–1253. doi:10.1167/iovs.07-1105

Li, G., Gao, G., Wang, P., Song, X., Xu, P., Xie, B., et al. (2019). Generation and characterization of induced pluripotent stem cells and retinal organoids from a leber's congenital amaurosis patient with novel RPE65 mutations. *Front. Mol. Neurosci.* 12, 212. doi:10.3389/fnmol.2019.00212

Li, H., Lu, C., Yao, W., Xu, L., Zhou, J., and Zheng, B. (2020). Dexmedetomidine inhibits inflammatory response and autophagy through the circLrp1b/miR-27a-3p/Dram2 pathway in a rat model of traumatic brain injury. *Aging* 12 (21), 21687–21705. doi:10.18632/aging.103975

Li, Z.-Y., Possin, D. E., and Milam, A. H. (1995). Histopathology of bone spicule pigmentation in retinitis pigmentosa. *Ophthalmology* 102 (5), 805–816. doi:10.1016/s0161-6420(95)30953-0

Liang, Q., Dharmat, R., Owen, L., Shakoor, A., Li, Y., Kim, S., et al. (2019). Single-nuclei RNA-seq on human retinal tissue provides improved transcriptome profiling. *Nat. Commun.* 10, 5743. doi:10.1038/s41467-019-12917-9

Liu, G., Wan, Q., Li, J., Hu, X., Gu, X., and Xu, S. (2020). Silencing miR-125b-5p attenuates inflammatory response and apoptosis inhibition in mycobacterium tuberculosis-infected human macrophages by targeting DNA damage-regulated autophagy modulator 2 (DRAM2). *Cell Cycle* 19, 3182–3194. doi:10.1080/15384101.2020.1838792

Lu, Y., Shiau, F., Yi, W., Lu, S., Wu, Q., Pearson, J. D., et al. (2020). Single-cell analysis of human retina identifies evolutionarily conserved and species-specific mechanisms controlling development. *Dev. Cell* 53, 473–491. doi:10.1016/j.devcel.2020.04.009

Lukovic, D., Castro, A. A., Kaya, K. D., Munezero, D., Gieser, L., Davó-Martínez, C., et al. (2020). Retinal organoids derived from hiPSCs of an AIPL1-LCA patient maintain cytoarchitecture despite reduced levels of mutant AIPL1. *Sci. Rep-uk* 10, 5426. doi:10.1038/s41598-020-62047-2

Macosko, E. Z., Basu, A., Satija, R., Nemesh, J., Shekhar, K., Goldman, M., et al. (2015). Highly parallel genome-wide expression profiling of individual cells using nanoliter droplets. *Cell* 161, 1202–1214. doi:10.1016/j.cell.2015.05.002

Maguire, A. M., Russell, S., Wellman, J. A., Chung, D. C., Yu, Z.-F., Tillman, A., et al. (2019). Efficacy, safety, and durability of voretigene neparvovec-rzyl in RPE65 mutation–associated inherited retinal dystrophy results of phase 1 and 3 trials. *Ophthalmology* 126, 1273–1285. doi:10.1016/j.ophtha.2019.06.017

Marquardt, A., Stöhr, H., Passmore, L. A., Krämer, F., Rivera, A., and Weber, B. H. F. (1998). Mutations in a novel gene, VMD2; encoding a protein of unknown properties cause juvenile-onset vitelliform macular dystrophy (Best's Disease). *Hum. Mol. Genet.* 7, 1517–1525. doi:10.1093/hmg/7.9.1517

Maruotti, J., Sripathi, S. R., Bharti, K., Fuller, J., Wahlin, K. J., Ranganathan, V., et al. (2015). Small-molecule–directed, efficient generation of retinal pigment epithelium from human pluripotent stem cells. *Proc. Natl. Acad. Sci.* 112, 10950–10955. doi:10.1073/pnas.1422818112

McCarthy, D. J., Campbell, K. R., Lun, A. T. L., and Wills, Q. F. (2017). Scater: pre-processing, quality control, normalization and visualization of single-cell RNA-seq data in R. *Bioinformatics* 33, 1179–1186. doi:10.1093/bioinformatics/btw777

Meyer, J. S., Shearer, R. L., Capowski, E. E., Wright, L. S., Wallace, K. A., McMillan, E. L., et al. (2009). Modeling early retinal development with human embryonic and induced pluripotent stem cells. *PNAS* 106, 16698–16703. doi:10.1073/pnas.0905245106

Modzelewski, A. J., Chen, S., Willis, B. J., Lloyd, K. C. K., Wood, J. A., and He, L. (2018). Efficient mouse genome engineering by CRISPR-EZ technology. *Nat. Protoc.* 13, 1253–1274. doi:10.1038/nprot.2018.012

Natoli, R., Jiao, H., Barnett, N. L., Fernando, N., Valter, K., Provis, J. M., et al. (2016). A model of progressive photo-oxidative degeneration and inflammation in the pigmented C57BL/6J mouse retina. *Exp. Eye Res.* 147, 114–127. doi:10.1016/j.exer.2016.04.015

O'Prey, J., Skommer, J., Wilkinson, S., and Ryan, K. M. (2009). Analysis of DRAM-related proteins reveals evolutionarily conserved and divergent roles in the control of autophagy. *Cell Cycle* 8, 2260–2265. doi:10.4161/cc.8.14.9050

Orozco, L. D., Chen, H.-H., Cox, C., Katschke, K. J., Arceo, R., Espiritu, C., et al. (2020). Integration of eQTL and a Single-Cell Atlas in the Human Eye Identifies Causal Genes for Age-Related Macular Degeneration. *Cell Rep.* 30, 1246–1259. doi:10.1016/j.celrep.2019.12.082

Parinot, C., Rieu, Q., Chatagnon, J., Finnemann, S. C., and Nandrot, E. F. (2014). Large-Scale Purification of Porcine or Bovine Photoreceptor Outer Segments for Phagocytosis Assays on Retinal Pigment Epithelial Cells. *J. Vis. Exp.* 12, 52100. doi:10.3791/52100

Park, S.-M., Kim, K., Lee, E.-J., Kim, B.-K., Lee, T. J., Seo, T., et al. (2009). Reduced expression of DRAM2/TMEM77 in tumor cells interferes with cell death. *Biochem. Bioph Res. Co.* 390, 1340–1344. doi:10.1016/j.bbrc.2009.10.149

Parmar, V. M., Parmar, T., Arai, E., Perusek, L., and Maeda, A. (2018). A2E-associated cell death and inflammation in retinal pigmented epithelial cells from human induced pluripotent stem cells. *Stem Cell Res.* 27, 95–104. doi:10.1016/j.scr.2018.01.014

Pau, G., and Reeder, J. (2022). *HTSeqGenie: A NGS analysis pipeline*. Available at: https://bioconductor.org/packages/release/bioc/html/HTSeqGenie.html.

Paylakhi, S., Labelle-Dumais, C., Tolman, N. G., Sellarole, M. A., Seymens, Y., Saunders, J., et al. (2018). Müller glia-derived PRSS56 is required to sustain ocular axial growth and prevent refractive error. *Plos Genet.* 14, e1007244. doi:10.1371/journal.pgen.1007244

Peng, Y.-R., Shekhar, K., Yan, W., Herrmann, D., Sappington, A., Bryman, G. S., et al. (2019). Molecular Classification and Comparative Taxonomics of Foveal and Peripheral Cells in Primate Retina. *Cell* 176, 1222–1237. doi:10.1016/j.cell.2019.01.004

Pennesi, M. E., Neuringer, M., and Courtney, R. J. (2012). Animal models of age related macular degeneration. *Mol. Asp. Med.* 33, 487–509. doi:10.1016/j.mam.2012.06.003

Perry, V. H., and Cowey, A. (1985). The ganglion cell and cone distributions in the monkey's retina: implications for central magnification factors. *Vis. Res.* 25, 1795–1810. doi:10.1016/0042-6989(85)90004-5

Petrukhin, K., Koisti, M. J., Bakall, B., Li, W., Xie, G., Marknell, T., et al. (1998). Identification of the gene responsible for Best macular dystrophy. *Nat. Genet.* 19, 241–247. doi:10.1038/915

Prado, D. A., Acosta-Acero, M., and Maldonado, R. S. (2020). Gene therapy beyond luxturna: a new horizon of the treatment for inherited retinal disease. *Curr. Opin. Ophthalmol.* 31, 147–154. doi:10.1097/icu.0000000000000660

Rheaume, B. A., Jereen, A., Bolisetty, M., Sajid, M. S., Yang, Y., Renna, K., et al. (2018). Single cell transcriptome profiling of retinal ganglion cells identifies cellular subtypes. *Nat. Commun.* 9, 2759. doi:10.1038/s41467-018-05134-3

Robinson, M. D., McCarthy, D. J., and Smyth, G. K. (2010). edgeR: a Bioconductor package for differential expression analysis of digital gene expression data. *Bioinformatics* 26, 139–140. doi:10.1093/bioinformatics/btp616

Sahel, J.-A., Marazova, K., and Audo, I. (2015). Clinical Characteristics and Current Therapies for Inherited Retinal Degenerations. *Csh Perspect. Med.* 5, a017111. doi:10.1101/cshperspect.a017111

Sergouniotis, P. I., McKibbin, M., Robson, A. G., Bolz, H. J., Baere, E., Düller, P. L. M., et al. (2015). Disease Expression in Autosomal Recessive Retinal Dystrophy Associated With Mutations in the DRAM2 Gene. *IOVS* 56, 8083–8090. doi:10.1167/iovs.15-17604

Shekhar, K., Lapan, S. W., Whitney, I. E., Tran, N. M., Macosko, E. Z., Kowalczyk, M., et al. (2016). Comprehensive Classification of Retinal Bipolar Neurons by Single-Cell Transcriptomics. *Cell* 166, 1308–1323. doi:10.1016/j.cell.2016.07.054

Sridhar, A., Hoshino, A., Finkbeiner, C. R., Chitsazan, A., Dai, L., Haugan, A. K., et al. (2020). Single-Cell Transcriptomic Comparison of Human Fetal Retina, hPSC-Derived Retinal Organoids, and Long-Term Retinal Cultures. *Cell Rep.* 30, 1644–1659. doi:10.1016/j.celrep.2020.01.007

Sundin, O. H., Yang, J.-M., Li, Y., Zhu, D., Hurd, J. N., Mitchell, T. N., et al. (2000). Genetic basis of total colourblindness among the Pingelapese islanders. *Nat. Genet.* 25, 289–293. doi:10.1038/77162

Tang, X., Huang, Y., Lei, J., Luo, H., and Zhu, X. (2019). The single-cell sequencing: new developments and medical applications. *Cell Biosci.* 9, 53. doi:10.1186/s13578-019-0314-y

Thomson, J. A., Itskovitz-Eldor, J., Shapiro, S. S., Waknitz, M. A., Swiergiel, J. J., Marshall, V. S., et al. (1998). Embryonic Stem Cell Lines Derived from Human Blastocysts. *Science* 282, 1145–1147. doi:10.1126/science.282.5391.1145

Ueki, Y., Ash, J. D., Zhu, M., Zheng, L., and Le, Y.-Z. (2009). Expression of Cre recombinase in retinal Müller cells. *Vis. Res.* 49, 615–621. doi:10.1016/j.visres.2009.01.012

Winkler, P. A., Occelli, L. M., and Petersen-Jones, S. M. (2020). Large Animal Models of Inherited Retinal Degenerations: A Review. *Cells* 9, 882. doi:10.3390/cells9040882

Wiszniewski, W., Lewis, R. A., and Lupski, J. R. (2007). Achromatopsia: the CNGB3 p.T383fsX mutation results from a founder effect and is responsible for the visual phenotype in the original report of uniparental disomy 14. *Hum. Genet.* 121, 433–439. doi:10.1007/s00439-006-0314-y

Wu, T. D., and Nacu, S. (2010). Fast and SNP-tolerant detection of complex variants and splicing in short reads. *Bioinformatics* 26, 873–881. doi:10.1093/bioinformatics/btq057

Wudu, M., Ren, H., Hui, L., Jiang, J., Zhang, S., Xu, Y., et al. (2019). DRAM2 acts as an oncogene in non-small cell lung cancer and suppresses the expression of p53. *J. Exp. Clin. Canc Res.* 38, 72. doi:10.1186/s13046-019-1068-4

Yamagata, M., Yan, W., and Sanes, J. R. (2021). A cell atlas of the chick retina based on single-cell transcriptomics. *Elife* 10, e63907. doi:10.7554/elife.63907

Yan, W., Laboulaye, M. A., Tran, N. M., Whitney, I. E., Benhar, I., and Sanes, J. R. (2020a). Mouse Retinal Cell Atlas: molecular Identification of over Sixty Amacrine Cell Types. *J. Neurosci.* 40, 5177–5195. doi:10.1523/jneurosci.0471-20.2020

Yan, W., Peng, Y.-R., Zyl, T., Regev, A., Shekhar, K., Juric, D., et al. (2020b). Cell Atlas of The Human Fovea and Peripheral Retina. *Sci. Rep-uk* 10, 9802. doi:10.1038/s41598-020-66092-9

Yoon, J.-H., Her, S., Kim, M., Jang, I.-S., and Park, J. (2012). The expression of damage-regulated autophagy modulator 2 (DRAM2) contributes to autophagy induction. *Mol. Biol. Rep.* 39, 1087–1093. doi:10.1007/s11033-011-0835-x

Zhang, N., Zhang, X., Girardot, P. E., Chrenek, M. A., Sellers, J. T., Li, Y., et al. (2021). Electrophysiologic and Morphologic Strain Differences in a Low-Dose NaIO3-Induced Retinal Pigment Epithelium Damage Model. *Transl. Vis. Sci. Technol.* 10, 10. doi:10.1167/tvst.10.8.10

Zhong, X., Gutierrez, C., Xue, T., Hampton, C., Vergara, M. N., Cao, L.-H., et al. (2014). Generation of three dimensional retinal tissue with functional photoreceptors from human iPSCs. *Nat. Commun.* 5, 4047. doi:10.1038/ncomms5047

frontiers | Frontiers in Genetics

TYPE Original Research
PUBLISHED 07 September 2023
DOI 10.3389/fgene.2023.1234032

OPEN ACCESS

EDITED BY
José M. Millan,
La Fe Health Research Institute, Spain

REVIEWED BY
Nicolas Sylvius,
University of Leicester, United Kingdom
John Chiang,
Molecular Vision Laboratory,
United States

*CORRESPONDENCE
Javier Ruiz-Ederra,
javier.ruize@ehu.eus
Susanne Roosing,
susanne.roosing@radboudumc.nl

RECEIVED 03 June 2023
ACCEPTED 15 August 2023
PUBLISHED 07 September 2023

CITATION
Rodríguez-Hidalgo M, de Bruijn SE, Corradi Z, Rodenburg K, Lara-López A, Valverde-Megías A, Ávila-Fernández A, Fernandez-Caballero L, Del Pozo-Valero M, Corominas J, Gilissen C, Irigoyen C, Cremers FPM, Ayuso C, Ruiz-Ederra J and Roosing S (2023), *ABCA4* c.6480-35A>G, a novel branchpoint variant associated with Stargardt disease.
Front. Genet. 14:1234032.
doi: 10.3389/fgene.2023.1234032

ABCA4 c.6480-35A>G, a novel branchpoint variant associated with Stargardt disease

María Rodríguez-Hidalgo[1,2], Suzanne E. de Bruijn[3], Zelia Corradi[3], Kim Rodenburg[3], Araceli Lara-López[4], Alicia Valverde-Megías[5], Almudena Ávila-Fernández[6,7], Lidia Fernandez-Caballero[6,7], Marta Del Pozo-Valero[6,7], Jordi Corominas[3,8], Christian Gilissen[3,8], Cristina Irigoyen[1,9], Frans P. M. Cremers[3], Carmen Ayuso[6,7], Javier Ruiz-Ederra[1,10]* and Susanne Roosing[3]*

[1]Department of Neuroscience, Biodonostia Health Research Institute, Donostia-San Sebastián, Spain, [2]Department of Genetic, Physical Anthropology and Animal Physiology, University of the Basque Country UPV/EHU, Leioa, Spain, [3]Department of Human Genetics, Radboud University Medical Center, Nijmegen, Netherlands, [4]Miramoon Pharma S.L., Donostia-San Sebastián, Spain, [5]Ophthalmology Service, San Carlos Clinical Hospital of Madrid, Madrid, Spain, [6]Department of Genetics, Health Research Institute-Fundación Jiménez Díaz University Hospital, Universidad Autónoma de Madrid (IIS-FJD, UAM), Madrid, Spain, [7]Center for Biomedical Network Research on Rare Diseases (CIBERER), Instituto de Salud Carlos III, Madrid, Spain, [8]Radboud Institute of Molecular Life Sciences, Radboud University Medical Center, Nijmegen, Netherlands, [9]Ophthalmology Service, Donostia Universy Hospital, Donostia-San Sebastián, Spain, [10]Department of Ophthalmology, University of the Basque Country (UPV/EHU), San Sebastián, Spain

Introduction: Inherited retinal dystrophies (IRDs) can be caused by variants in more than 280 genes. The ATP-binding cassette transporter type A4 (*ABCA4*) gene is one of these genes and has been linked to Stargardt disease type 1 (STGD1), fundus flavimaculatus, cone–rod dystrophy (CRD), and pan-retinal CRD. Approximately 25% of the reported *ABCA4* variants affect RNA splicing. In most cases, it is necessary to perform a functional assay to determine the effect of these variants.

Methods: Whole genome sequencing (WGS) was performed in one Spanish proband with Stargardt disease. The putative pathogenicity of c.6480-35A>G on splicing was investigated both *in silico* and *in vitro*. The *in silico* approach was based on the deep-learning tool SpliceAI. For the *in vitro* approach we used a midigene splice assay in HEK293T cells, based on a previously established wild-type midigene (BA29) containing *ABCA4* exons 46 to 48.

Results: Through the analysis of WGS data, we identified two candidate variants in *ABCA4* in one proband: a previously described deletion, c.699_768+342del (p.(Gln234Phefs*5)), and a novel branchpoint variant, c.6480-35A>G. Segregation analysis confirmed that the variants were in *trans*. For the branchpoint variant, SpliceAI predicted an acceptor gain with a high score (0.47) at position c.6480-47. A midigene splice assay in HEK293T cells revealed the inclusion of the last 47 nucleotides of intron 47 creating a premature stop codon and allowed to categorize the variant as moderately severe. Subsequent analysis revealed the presence of this variant as a second allele besides c.1958G>A p.(Arg653His) in an additional Spanish proband in a large cohort of IRD cases.

Conclusion: A splice-altering effect of the branchpoint variant, confirmed by the midigene splice assay, along with the identification of this variant in a second unrelated individual affected with STGD, provides sufficient evidence to classify the variant as likely pathogenic. In addition, this research highlights the importance

of studying non-coding regions and performing functional assays to provide a conclusive molecular diagnosis.

KEYWORDS

branchpoint variant, midigene splice assay, whole genome sequencing, *ABCA4*, Stargardt disease

1 Introduction

Inherited retinal dystrophies (IRDs) are a clinically complex and heterogenous group of visual impairment disorders that can result in progressive vision loss and eventual blindness. Today, there are more than 280 genes that have been associated with IRDs (https://web.sph.uth.edu/RetNet/home.htm).

ABCA4 is among the most commonly mutated genes associated with IRDs (Quazi and Molday, 2014; Perea-Romero et al., 2021). The gene encodes the ATP-binding cassette transporter type A4 (ABCA4), a retina-specific protein that is expressed in the outer segments of photoreceptors and functions to process the metabolites of vitamin A in the visual cycle (Sun et al., 1999; Tsybovsky et al., 2010; Molday, 2015). Dysfunction of ABCA4 leads to the accumulation of cytotoxic products (lipofuscin) in the photoreceptors and retinal pigment epithelium and can manifest in different phenotypes such as Stargardt disease type 1 (STGD1), fundus flavimaculatus, cone–rod dystrophy (CRD), and pan-retinal CRD (Allikmets et al., 1997; Cremers et al., 1998; Rozet et al., 1999; Maugeri et al., 2000; Cremers et al., 2020).

A genotype–phenotype correlation model was proposed to explain the wide range of phenotypes associated with biallelic pathogenic variants in *ABCA4*. This genotype–phenotype correlation model links the residual activity of the ABCA4 protein to the severity of retinal dystrophy (van Driel et al., 1998; Maugeri et al., 1999). The model categorizes variants as deleterious (no activity; null allele), severe, moderately severe, or mild (also mentioned as hypomorphic). Some mild variants, such as c.5603A>T (p.(Asn1868Ile)), when in *trans* with a severe variant, show incomplete penetrance (Runhart et al., 2018). Patients with two severe variants or null alleles present with pan-retinal CRD, while a severe variant combined with a moderately severe variant results in CRD. On the other hand, a combination of a severe and mild variant or two moderately severe variants gives rise to classic STGD1 (Cremers et al., 2020). A combination of a severe variant with a mild-incomplete penetrant variant most often results in late-onset STGD1.

More than 2,300 unique variants have been reported for *ABCA4* (http://www.lovd.nl/ABCA4) since being first reported in 1997 (Allikmets et al., 1997; Cornelis et al., 2017; Cornelis et al., 2022; Cornelis et al., 2023). A wide variety of causative genetic defects have been reported that include missense and nonsense variants, indels, canonical, non-canonical splice site defects, and deep-intronic variants. Approximately 25% of these variants affect RNA splicing by altering one or more of the key splicing elements (Khan et al., 2020; Corradi et al., 2022).

The splicing process is a complex phenomenon that involves a large number of proteins with various interactions between the *cis* and *trans* elements. The *cis* elements are the DNA sequences that define exons, introns, and other regulatory sequences necessary for proper splicing. The branchpoint sequence (BPS) is one of the key cis-acting elements, together with the canonical 5′ splice donor site (SDS) and the canonical 3′ splice acceptor site (SAS). The BPS is a short degenerate motif typically located upstream from the SAS and followed by a cytosine- and thymidine-rich sequence called the polypyrimidine tract. The BPS is recognized by proteins involved in the formation of the spliceosome complex and is thought to play a key role in positioning the spliceosome at the correct location for efficient splicing. Additionally, there are exonic and intronic regulators that act as enhancers or silencers (Anna and Monika, 2018; Tang et al., 2020).

In recent years, causative variants in *cis* elements, which include the BPS, have been described to disrupt pre-mRNA splicing, leading to dysfunctional proteins and retinal disease (Leman et al., 2020; Corradi et al., 2022; Fadaie et al., 2022; Reurink et al., 2023). *In silico* prediction tools can identify potential splicing variants and their putative effect, but lack accuracy for novel intronic variants outside of the splice site consensus sequence (Ohno et al., 2018; Rowlands et al., 2021). However, the introduction of SpliceAI provides an accurate prediction for deep-intronic variants (Riepe et al., 2021). According to the ACMG guidelines, however, these tools only serve as indicators of splicing aberrations and are not standalone evidence for determining pathogenicity (Richards et al., 2015). Experimental studies, such as the minigene splice assays, are crucial for determining the functional impact of variants that affect RNA splicing and increasing our knowledge of these variants. These studies enable accurate classification of the severity of variants and, together with the genotype–phenotype correlation model, provide conclusive clinical diagnoses, appropriate genetic counseling, and information about disease progression.

In this study, we describe the pathogenicity of a near-exon aberrant RNA (NEAR) splice variant, c.6480-35A>G in *ABCA4*, which alters the BPS upstream of exon 48 at its most critical position. We explore the effect of c.6480-35A>G using a midigene splice assay and show the relevance of assessing branchpoint motif regions in IRDs.

2 Materials and methods

2.1 Clinical evaluation

The participants were clinically examined by an experienced ophthalmologist. The clinical diagnoses were based on ophthalmological examinations, which included assessment of visual acuity, detailed fundoscopic examination, fundus photography, fundus autofluorescence (FAF), and optical coherence tomography (OCT), and electrophysiological evaluations, which included full-field flash electroretinography (ERG) and multifocal ERG, following the International Society for Clinical Electrophysiology of Vision standards (McCulloch et al., 2015).

All procedures performed in this study involving human participants received approval from the ethical standards of the

Ethics Committee for Drug Research in the Basque Country, Spain (CEIm-E), and the Ethics Committee of Fundación Jiménez Díaz University Hospital (CEIm-FJD) and were performed in accordance with the 2013 Declaration of Helsinki or comparable ethical standards. Prior to this study, informed consent was obtained from all participants or their legal representatives.

2.2 Whole genome sequencing

A proband was diagnosed with STGD1 at the Donostia University Hospital and without a previous genetic diagnosis. To identify the genetic defect for this individual, whole genome sequencing (WGS) was performed. DNA was provided by the Basque Biobank (www.biobancovasco.org) and was processed following standard operation procedures. WGS was performed by BGI on a BGISeq-500 using a 2 × 150 base pairs (bp) paired-end module, with a minimal median coverage per genome of 30-fold. The Burrows–Wheeler Aligner V.0.7814 (Li and Durbin, 2009) was used to map the WGS data to the human genome build GRCh38/hg38.

Single-nucleotide variants (SNVs) and small indels (<50 bp) were called using the Genome Analysis Toolkit HaplotypeCaller (McKenna et al., 2010). The SNVs and indels were annotated using an in-house developed pipeline based on Variant Effect Predictor (VEP V.104) and GENCODE V.34 basic gene annotations. Annotations included chromosomal location and position, reads, percent of variation, variant type (deletion, insertion, and substitution), gene component (e.g., intron, exon, splice site, 5′-UTR, 3′-UTR, and intragenic), protein effect (e.g., missense, synonymous, frameshift, and in-frame), various *in silico* prediction scores (e.g., CADD_PHRED, REVEL, and SpliceAI), Gene Ontology description, gene and disease OMIM description, gene regulation, expression data, and population frequency databases (gnomAD and in-house variant frequency whole exome sequencing/WGS data), among others.

Structural variants (SVs) were called using the Manta structural variant caller (Chen et al., 2016), based on read-pair signals (split reads and discordant read pairs) and read-depth signals (copy number changes), and the default parameters were used. The copy number variants (CNVs) were called using the Canvas Copy Number Variant Caller (Roller et al., 2016), based on read-depth evidence, and the default parameters were used. SVs and CNVs were annotated using an in-house developed pipeline based on ANNOVAR and GENCODE V.34 basic gene annotations. Annotations included chromosomal location and position, zygosity, type (e.g., deletion, duplication), gene overlap and component (e.g., intronic, exonic, intragenic), gene and disease OMIM description, gene boundary start and end, percentage overlap, and frequency of population frequency databases (1000 Genomes and in-house variant frequency SV data), among others.

2.3 Variant prioritization and selection

The WGS data were filtered and prioritized in two steps. First, an automatized in-house pipeline in RStudio V.4.1.3 (RStudio Team, 2020) was used, followed by a manual prioritization of the remaining variants. The SNVs and indels, from coding and non-coding regions, were filtered on the basis of a minor allele frequency of <1% in the gnomAD database v.2.1 (Karczewski et al., 2020) and an in-house variant frequency in the whole exome sequencing/WGS database from Radboudumc, which included 708 control samples. Nonsense, stop- or start-codon altering, frameshift, in-frame, missense, and (canonical) splice site variants were selected for detailed interrogation. Missense variants were prioritized based on score thresholds of different *in silico* prediction tools: CADD_PHRED (range: 1–99; predicted pathogenic ≥15) (Rentzsch et al., 2019) and REVEL (range: 0–1; predicted pathogenic ≥0.3) (Ioannidis et al., 2016). All coding and non-coding variants, were filtered on the splice predicting tool SpliceAI delta score (range: 0–1; predicted pathogenic ≥0.2) (Jaganathan et al., 2019) for gain or loss of a SDS or SAS. The Alamut™ Visual Plus 1.4 software was used as a visual aid to identify the position in which SpliceAI delta scores were predicted and characterize the genomic context of the variant, such as BPSs. Coding SVs and CNVs were filtered based on a minor allele frequency of <1% in the 1000 Genomes database (Zheng-Bradley et al., 2017). Inversion and duplication events were only considered when disrupting an IRD-associated gene (https://web.sph.uth.edu/RetNet/home.htm, accessed 1/11/2022), i.e., when at least one breakpoint was located within the respective gene. Compound heterozygous or homozygous candidate variants (recessive) or heterozygous candidate variants (dominant) that overlapped with IRD-associated genes were selected for validation and segregation analysis.

2.4 Midigene splice assay

The interrogation of a putative causal splice site variant, c.6480-35A>G in *ABCA4* (GenBank: NM_000350.2), was carried out using a midigene splice assay. A previously created wild-type midigene construct (BA29) was used that contained *ABCA4* exons 46–48 in the pDONR201 vector (Invitrogen) using Gateway cloning (Sangermano et al., 2018). The splice assay was performed in accordance with the previously described protocol (Sangermano et al., 2018; Corradi et al., 2022). In short, a construct harboring the c.6480-35A>G variant was generated through site-directed mutagenesis from the wild-type midigene construct followed by Gateway cloning. Subsequently, the wild-type and mutant constructs were transfected separately in HEK293T (Human Embryonic Kidney, ATCC# CRL-3216) cells. Transfection of the mutant construct was performed in duplicate using polyethylenimine (PEI) as a transfection reagent. After 48 h of incubation, RNA was collected using the NucleoSpin RNA kit (MACHEREY-NAGEL, Düren, Germany), and the transcripts were analyzed by reverse transcription polymerase chain reaction (RT-PCR) with primers located in exons 46 and 48, using the iScript cDNA Synthesis Kit (Bio-Rad, Hercules, CA, United States). RT-PCR was performed as follows: 2 min at 94°C, followed by 35 cycles of 30 s at 94°C, 30 s at 58°C, and 5 min at 72°C, with a final extension step of 2 min at 72°C. The RT-PCR product mixture was separated on a 2% agarose gel, and the product was verified by Sanger sequencing. Details on the primers used for mutagenesis, RT-PCR, and Sanger sequencing are presented in Supplementary Table S1. After agarose gel electrophoresis, a semi-quantification analysis of the ratios between different RNA products was carried out using the Fiji software (Schindelin et al., 2012) as previously described (Corradi et al., 2022).

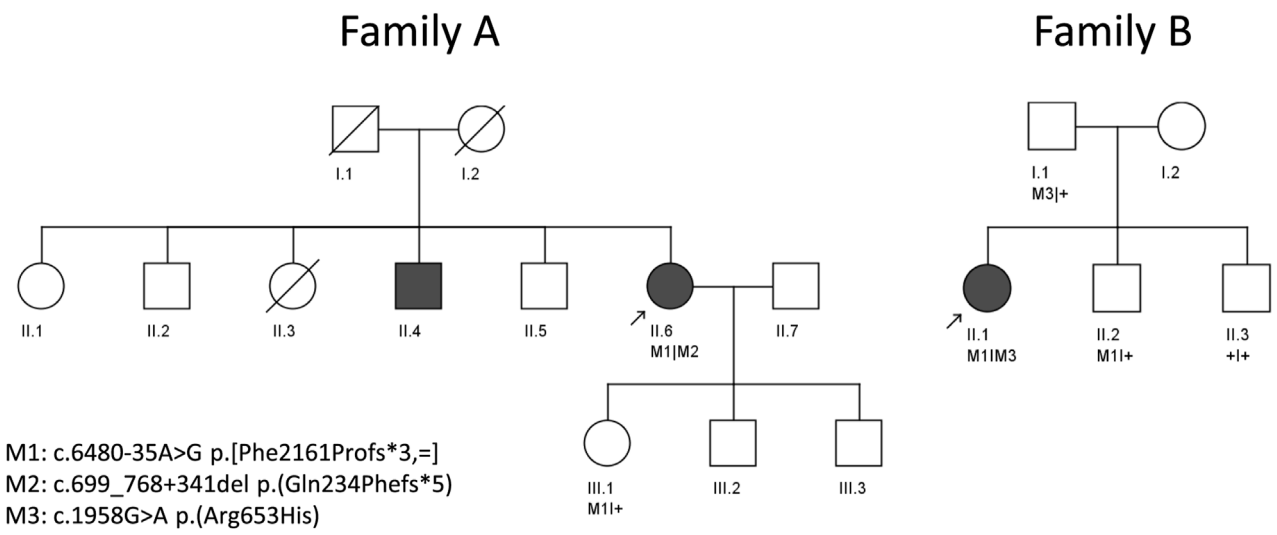

FIGURE 1
Pedigrees of two unrelated individuals analyzed in this study. Arrows indicate the proband in each family.

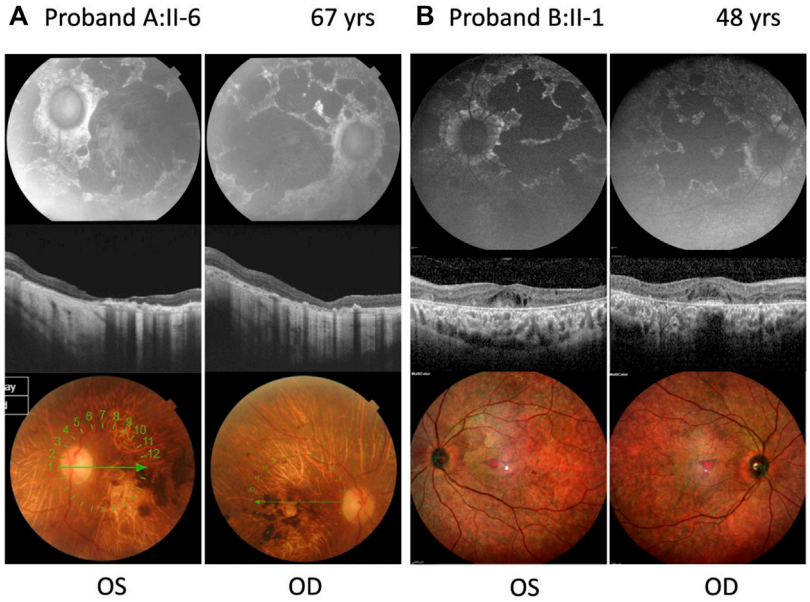

FIGURE 2
Ophthalmic features of compound heterozygous retinopathy cases carrying c.6480-35A>G. Fundus autofluorescence (upper panel), OCT (middle panel), and color fundus (lower panel) for left (OS) and right (OD) eyes. **(A)** Proband A:II-6 carrying c.699_768+341del p.(Gln234Phefs*5) as the second allele. **(B)** Proband B:II-1 carrying c.1958G>A p.(Arg653His) as the second allele. Years, yrs.

3 Results

3.1 Clinical findings

Pedigrees of the two studied families of Spanish origin with candidate variants in *ABCA4* are shown in Figure 1. Both probands presented with advanced STGD1 (Family A and B). An overview of the clinical characteristics is provided in Figure 2 and Table 1.

Proband A:II-6 (Figure 2A) had an onset of visual complaints at the age of 21 years and was diagnosed with STGD1, with a mean visual acuity of 1.8 logMAR at the age of 67 years. The FAF images showed patchy areas of hypo-autofluorescence in the posterior pole with peripapillary sparing. OCT revealed atrophy of the outer retina layers and a loss of photoreceptors in the foveal region. The fundus images showed macular, posterior pole, and mid-peripheral chorioretinal atrophy, without flecks and with bone spicules in

10.3389/fgene.2023.1234032

TABLE 1 Clinical characteristics of *ABCA4* retinopathy probands with c.6480-35A>G.

Patient ID (institution ID)	Sex	Age (yrs)	Initial symptom, age (yrs)	Initial clinical diagnosis	Age at last examination (yrs)	Visual acuity (logMAR)		Foveal photoreceptors	Fundus autofluorescence abnormalities	Electroretinogram
						OS	OD			
A:II-6 (RP145)	F	67	21	Stargardt disease	67	1.3	1.3	Loss of photoreceptors in foveal region	Patchy areas of hypo-autofluorescence in the posterior pole. Preservation of peripapillary regions	Severe cone and rod responses (57 years)
B:II-1 (MD-1378)	F	51	41	Stargardt disease	48	0	0	Loss of photoreceptors in perifoveal region	Area of RPE atrophy and hypo-autofluorescence	Severe alterations of rod responses and moderate–severe alterations in cones

F, female; OD, right eye; OS, left eye; RPE, retinal pigment epithelium; yrs, years.

the mid-periphery. ERG of the proband at the age of 53 years showed severely altered cone and rod responses (extinguished in the right eye). The abnormal cone and rod responses progression to a CRD diagnosis. Unfortunately, we had no access to any ophthalmologic data nor was the DNA of the affected brother available to confirm segregation.

Proband B:II-1 (Figure 2B) was diagnosed with STGD1 at the age of 41 years, through FAF, OCT, and fundus examination (Supplementary Figure S1). An ophthalmic examination at the age of 48 years revealed a normal visual acuity (0 logMAR), with severe constriction of the visual field, suggesting foveal sparing. Multicolor and FAF images showed diffuse retinal atrophy and hypo-autofluorescence involving the whole retinal posterior pole and mid-periphery. The OCT OD image showed the foveolar area with identifiable external retinal layers in less than the central 100 microns, and the OCT OS image showed severe disturbances in the foveal photoreceptors line and the presence of cystic spaces. ERG revealed moderate–severe alterations in cones and severe alterations of rod responses, suggesting advanced STGD1.

3.2 Identification of c.6480-35A>G in *ABCA4* by whole genome sequencing

To study potential candidate variants in IRD-associated genes, we performed WGS in proband A:II-6. This case remained genetically unexplained after previous genetic testing through a gene panel containing 316 IRD-associated genes (Ezquerra-Inchausti et al., 2018) and CGH arrays. In total, 5,055,143 SNVs/indels were detected through WGS. From 151,997 variants with a gnomAD AF ≤1% in the general population, 559 variants were considered potentially pathogenic, as they met our inclusion criteria as a nonsense, stop- or start-codon altering, frameshift variant, in-frame insertion or deletion, potentially pathogenic missense, and (canonical) splice site variants. From 559 variants, no homozygous variants were identified, and 16 heterozygous SNVs/indels were located in IRD-associated genes. Next, 10,536 SVs and 1,307 CNVs were called by Manta and Canvas, respectively, of which 689 SVs and 255 CNVs overlapped a coding region and had an AF ≤1% in the 1000 Genomes database. From 93 SV/CNVs spanning an IRD-associated gene, only one SV had at least one breakpoint within an IRD-associated gene. Collectively for the SNV and CNV/SV data, this yielded one single compound heterozygous situation in the *ABCA4* gene.

A novel intronic variant c.6480-35A>G (chr1(GRCh38): g.93998145T>C) was observed, which was absent from the control populations in gnomAD and located outside the SAS consensus sequence, which implies a potential impact on additional splicing elements like the BPS. Moreover, c.6480-35A>G alters the recognition score for the branchpoint algorithm, embedded in Alamut Visual Plus (range: 0–100) from 91.48 in the wild-type to zero in the mutant as a result of the removal of the branchpoint "A" nucleotide from the motif (Figure 3 upper panel). The c.6480-35A>G variant has little to no effect on splicing of the canonical SAS, as shown by the Splice score prediction algorithms. For the cryptic SAS at position c.6480-47, NNSPLICE predicts a 4.9% higher score than the wild-type situation, GeneSplicer predicts a 12.1% lower score, and no changes in the

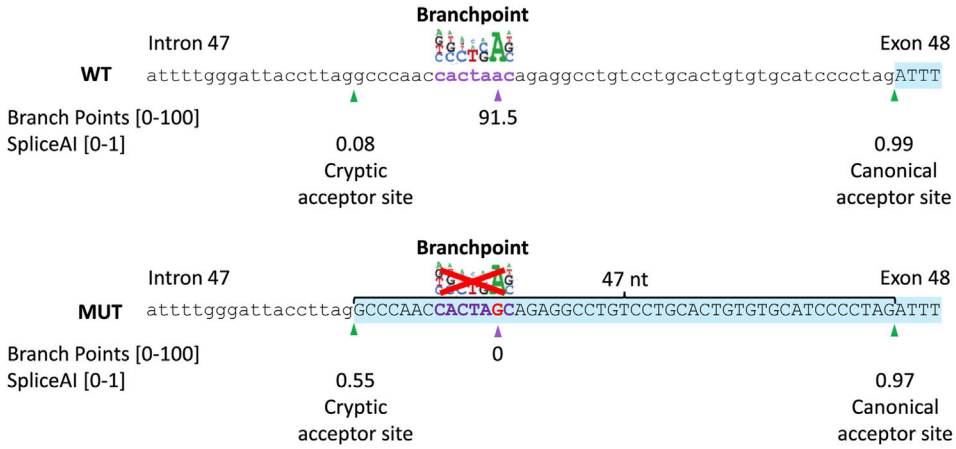

FIGURE 3
In silico prediction scores of the c.6480-35A>G variant. Schematic representation of the intron 47–exon 48 boundary sequence of *ABCA4*, branchpoint, and splice prediction in the wild-type (WT; upper panel) and c.6480-35A>G (MUT; lower panel) situation. The branchpoint algorithm predicts the abolishment of the branchpoint. SpliceAI predicts a 0.47 increase in the probability of activation of a cryptic acceptor site in intron 47 (47 nt upstream of the canonical acceptor site).

score values of MaxEntScan and SpliceSiteFinder-like. Nevertheless, the SpliceAI algorithm predicts a significant strengthening of the cryptic SAS in intron 47 (47 nt upstream of the canonical SAS) with delta scores of 0.47 and a loss of the canonical SAS of exon 48, with a delta score of 0.02 (Figure 3 lowel panel). The SV consisted of a deletion of 411 bp in *ABCA4* spanning 70 bp of exon 6 and 341 bp of intron 6, c.699_768+341del; p.(Gln234Phefs*5), as was previously identified in the Spanish population (Del Pozo-Valero et al., 2020).

The clinical/whole exome sequencing data from a Spanish cohort (the Fundación Jiménez Díaz cohort) of 52 probands with Stargardt disease and 26 probands with CRD, and one likely pathogenic or pathogenic variant in *ABCA4* were investigated for the presence of c.6480-35A>G. This analysis revealed a second case, proband B:II-1. This individual carried the c.1958G>A; p.(Arg653His) variant, a known likely pathogenic variant. Segregation analysis confirmed that in both families, the variants were compound heterozygous as available unaffected relatives carried one of these two variants in a heterozygous state. Additional analysis of the whole exome sequencing data of 1,935 genetically unexplained cases did not reveal probands carrying the variant of interest.

3.3 Midigene splice assay results

To assess pathogenicity of c.6480-35A>G, a midigene splice assay was performed (Figure 4). HEK293T cells were transfected either with a wild-type midigene construct spanning *ABCA4* exon 46–48 or a mutant construct carrying c.6480-35A>G within the same region.

After RNA isolation and RT-PCR analysis of the individual midigenes, a predicted 378 nt fragment was detected corresponding to the *ABCA4* wild-type mRNA, for the wild-type. In addition, a 285 nt fragment showing exon 47 skipping of *ABCA4* mRNA was observed, resulting in an in-frame deletion of 31 amino acid residues (p.(Ser2129_Lys2160delinsArg)). In the mutant midigenes, a 425 nt fragment (~67% of the PCR product) was observed in addition to the wild-type fragment (~30% of the PCR product) and a minimal contribution of the exon 47 skipping event. Sanger sequencing verified that the 425 nt fragment corresponded to the inclusion of the last 47 nt of intron 47 at the 5′ start of exon 48, likely due to the activation of a cryptic SAS at position c.6480-47, as predicted by SpliceAI. This inclusion results in a frameshift that includes a premature stop codon along with conventionally spliced mRNA (p.[Phe2161Profs*3,=]).

4 Discussion

In this study, we identified a novel pathogenic branchpoint variant, c.6480-35A>G, in *ABCA4* using WGS and a subsequent dedicated midigene splice assay. The variant abolishes the putative branchpoint of intron 47, leading to a 47 nt retention of intron 47 due to the activation of a cryptic SAS. The severity of a variant can be determined by the percentage of correct RNA remaining in the midigene splice assay in HEK293T cells (Sangermano et al., 2018; Cremers et al., 2020). The midigene splice assay revealed a moderately severe (range: 20%–40% normal RNA, FPMC, unpublished data) effect for c.6480-35A>G as 30.4% of the wild-type fragment remained alongside the mutant fragments after semi-quantification analysis. This knowledge is important for consideration of disease presentation and prognosis as the residual activity of the ABCA4 protein correlates with the severity of *ABCA4*-associated retinopathy.

The genotype–phenotype correlations in our study cohort also suggest the effect of variant c.6480-35A>G as moderately severe (likely pathogenic based on the ACMG classification). Different phenotypes were observed in the two probands carrying the variant c.6480-35A>G. In particular, A:II-6, who carries the variant in *trans* with c.699_768+341del; p.(Gln234Phefs*5), showed a more severe phenotype associated with STGD1 and additional degeneration of the cone and/or rod photoreceptor cells over time, leading to a

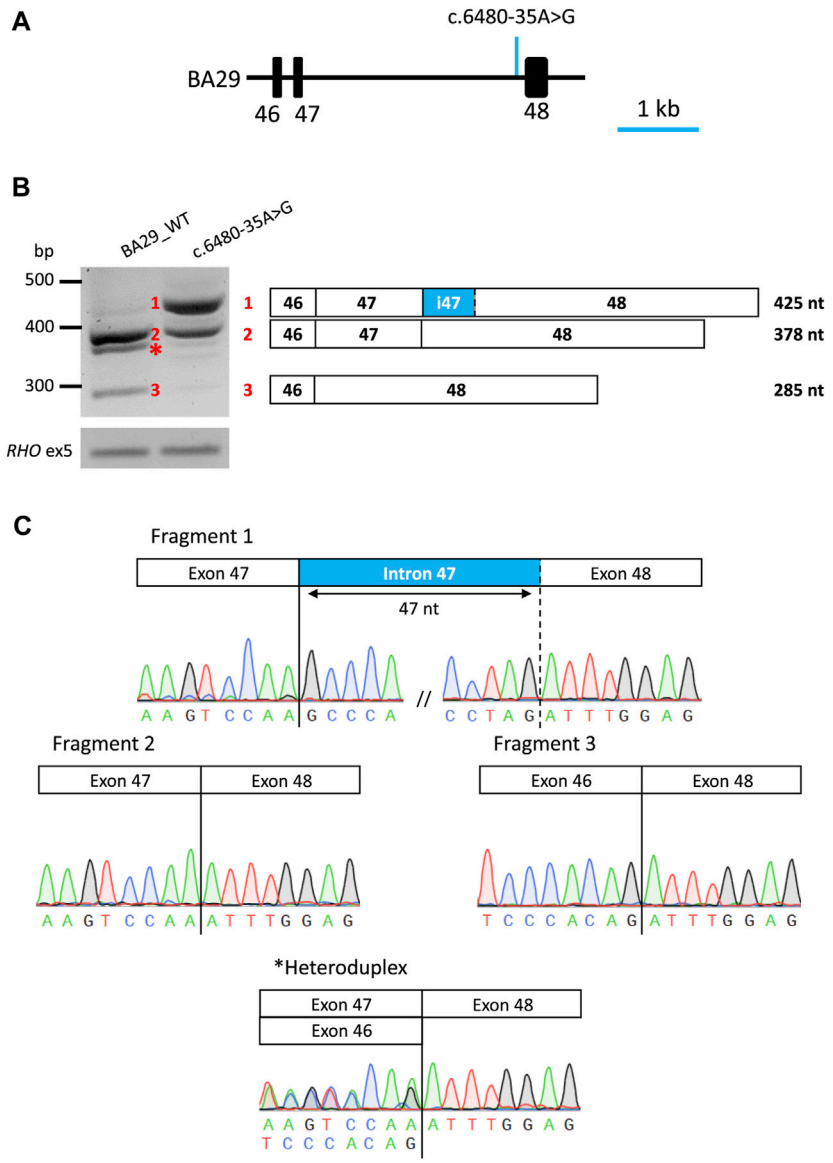

FIGURE 4
Overview of midigene assay results of variant c.6480-35A>G in HEK293T cells. **(A)** Schematic representation of wt midigene (BA29_WT) where the position of the variant is indicated by an arrow. **(B)** Gel image of RT-PCR products of wild-type and mutant constructs. The rhodopsin exon 5 (*RHO* ex5) RT-PCR was used as a control for transfection efficiency. Schematic representation of the three RT-PCR products identified in the gel. Wt midigene reveals the expected 378 nt wt fragment (Fragment 2) and the exon 47 skipping fragment (Fragment 3). Mutant midigene reveals a partial intron 47 inclusion of 45 nt 5′ (Fragment 1) and 30.4% of the remaining wt fragment (Fragment 2). Fiji software was used for a semi-quantification of the fragments in the mutant construct. **(C)** Sanger sequence analysis of the RT-PCR fragments. The chromatograms show the breakpoints in all fragments. * Heteroduplex fragment.

phenotype that more closely resembles CRD. The variant c.699_768+341del is a null variant, is classified as severe and was previously associated with both STGD1 and CRD (Del Pozo-Valero et al., 2020). According to our data, individuals with STGD1 who have one severe variant in combination with one moderately severe variant may progress to CRD. Therefore, additional ophthalmologic assessments, which include ERG, should be taken into account. B:II-1, who carries c.6480-35A>G in *trans* with c.1958G>A; p.(Arg653His), showed a milder phenotype associated to late-onset STGD1. The variant c.1958G>A has been previously associated with STGD1 (Jiang et al., 2016; Sung et al., 2019; Garces et al., 2020; Ma et al., 2021). Moreover, it has been previously classified to have a mild/moderate effect by Garces et al. (2020) and a severe effect by Cornelis et al. (2022). The phenotypic assessment of the proband B:II-1 suggests a moderately severe effect of c.1958G>A.

Only recently, the first BPS variants associated with IRDs have been identified in *BBS1* (Fadaie et al., 2022) and *ABCA4* (Corradi et al., 2022), while the recognition of the BPS is crucial for the formation of the lariat structure prior to intron excision from pre-

mRNA. Identification of pathogenic BPS variants may be hampered by the challenges of recognition of the BPS sites due to its localization and the conserved motif of BPSs. While the majority of BPSs have been identified in a window of 18–44 nt upstream of the SAS, BPSs located up to 400 nt away from the SAS have also been found (Gooding et al., 2006). The limited number of experimentally validated wild-type and mutated BPSs has posed challenges in developing effective tools to predict the impact of variants upstream of SASs. Alamut Visual Plus prediction tools such as NNSPLICE indicated an increase of 4.9% for the cryptic SAS at position c.6480-47, while GeneSplicer indicated a reduction of 12.1% at position c.6480-47. However, the branchpoint prediction incorporated in Alamut Visual Plus showed a predictive score for the wild-type (91.5), which is completely abolished in the mutant. Moreover, SpliceAI accurately predicted partial intron retention as confirmed by our *in vitro* splice assay, which highlights that SpliceAI proves to be effective in predicting the impact of BPS variants on splicing.

To assess the effect of the variant, *in vitro* splice assays using HEK293T cells have been previously shown to accurately recapitulate splice defects affecting consensus splice site sequences at the exon–intron junctions, as well as most variants that generate new splice sites or enhance cryptic splice sites in introns, leading to pseudo-exon inclusion, exon elongation, or intron retention (Sangermano et al., 2018; Bauwens et al., 2019; Valero et al., 2019; Westin et al., 2021; Viering et al., 2022). The midigene assay in this study effectively demonstrated that the c.6480-35A>G variant resulted in an altered splicing pattern. However, we also observed exon 47 skipping in wild-type mRNA. It remains to be determined whether this is a natural exon skipping event or an artifact due to the lack of retina-specific factors in HEK293T cells and the artificial nature of the midigene system. Therefore, the analysis of retina mRNA, photoreceptor precursor cells, or retinal organoids generated from induced pluripotent stem cells derived from patient offer a more relevant context for observing the variant's effects (Vig et al., 2020; Mullin et al., 2021).

To date, there are no FDA-approved therapies for *ABCA4*-associated retinopathy, but several experimental treatments are being studied. Antisense oligonucleotide (AON)–based therapeutic strategies have shown effectiveness in modulating splicing and obtaining correct transcripts in *ABCA4* in several studies (Albert et al., 2018; Garanto et al., 2019; Sangermano et al., 2019; Tomkiewicz et al., 2021; Kaltak et al., 2023). Nevertheless, the use of AONs to treat the effects of c.6480-35A>G could potentially result in its binding to the region upstream of the canonical SAS that may disrupt regulatory motifs and the binding of auxiliary splice proteins. Additionally, recent studies have shown the efficiency of the CRISPR/Cas9 system in correcting variants in the *ABCA4* gene without off-target genomic alterations (De Angeli et al., 2022; Siles et al., 2023). These are promising areas of research that could potentially lead to effective treatments for *ABCA4*-associated retinopathy, but more research is required to determine their safety and effectiveness in clinical trials.

In conclusion, we have identified a novel variant in *ABCA4*, c.6480-35A>G, which disrupts a predicted branchpoint, leading to inclusion of 47 nt in the mRNA resulting in protein truncation. This variant was observed in two unrelated individuals of Spanish descent. We determined that c.6480-35A>G can be classified as moderately severe. In combination with a deletion with a severe effect, it underlies STGD1 progressing to CRD in proband A:II-6. In proband B:II-1, this variant, in *trans* with a moderately severe missense variant, led to late-onset STGD1. Furthermore, this study emphasizes the significance of investigating non-coding regions and conducting functional assays to establish a better molecular diagnosis.

Data availability statement

The variant data presented in this study have been submitted to the "Global Variome shared LOVD" and it can be accessed using the url: https://databases.lovd.nl/shared/references/DOI:10.3389/fgene.2023.1234032.

Ethics statement

The studies involving humans were approved by the Ethics Committee for Drug Research in the Basque Country, Spain (CEIm-E) and the Ethics Committee of Fundación Jiménez Díaz University Hospital (CEIm-FJD). The studies were conducted in accordance with the local legislation and institutional requirements. The participants provided their written informed consent to participate in this study.

Author contributions

MR-H performed laboratory experiments, data analyses, and sequencing analyses. ZC, KR, and AL-L provided laboratory support. AA-F, LF-C, and CA collected clinical cases and performed sequencing analysis. CI and AA-F collected clinical cases and performed clinical examinations of patients. CG and JC provided infrastructure and bioinformatic expert input. FPMC, JR-E, SR, and SEdB provided strategic support, expert input, and supervision for the project. MR-H, SEdB, and SR contributed significantly to design of the study. MR-H, SEdB, JR-E, and SR wrote the manuscript. All authors contributed to the article and approved the submitted version.

Funding

The study was funded by the National Institute of Health Carlos III and co-funded by the European Union, project no. PI20/01186 (to CI) project no. PI22/00321 (to CA). This work was also supported by the Education Department of the Basque Government, grant no. PRE_2019_1_0325 (to MR-H), the Education Department of the Basque Government, grant no. 325 EP_2022_1_0060 (to MR-H), EMBO Scientific Exchange Grant, grant no 9507 (to MR-H), and University Chair UAM-IIS-FJD of Genomics Medicine (to CA). This work was also supported by the Basque Retinitis Pigmentosa Foundation (to JR-E). The work of SEdB was funded by the European Union's

Horizon 2020 Research and Innovation Programme under the EJP RD COFUND-EJP N° 825575 (to FPMC and SR). The work of KR was supported by grant awards from Fighting Blindness Ireland (FB18CRE) (to FPMC and SR). The work of KR and SR was funded by the Foundation Fighting Blindness (FFB)–career development award (CD-GE-0621-0809-RAD) (to SR).

Acknowledgments

The authors thank Galuh D. N. Astuti and P. Minguez for bioinformatic assistance and Stéphanie S. Cornelis for expert opinion in variant classification.

Conflict of interest

Author AL-L was employed by Miramoon Pharma S.L.

The remaining authors declare that the research was conducted in the absence of any commercial or financial relationships that could be construed as a potential conflict of interest.

Publisher's note

Supplementary material

The Supplementary Material for this article can be found online at: https://www.frontiersin.org/articles/10.3389/fgene.2023.1234032/full#supplementary-material

SUPPLEMENTARY FIGURE S1
Ophthalmic features of proband B:II-1 at two ages. Fundus autofluorescence (upper panel), OCT (middle panel), and color fundus (lower panel) for left (OS) and right (OD) eyes. **(A)** Proband B:II-1 at 41 years. **(B)** Proband B:II-1 at 48 years.

SUPPLEMENTARY TABLE S1
Oligonucleotides employed in this study.

References

Albert, S., Garanto, A., Sangermano, R., Khan, M., Bax, N. M., Hoyng, C. B., et al. (2018). Identification and rescue of splice defects caused by two neighboring deep-intronic ABCA4 mutations underlying Stargardt disease. *Am. J. Hum. Genet.* 102 (4), 517–527. doi:10.1016/j.ajhg.2018.02.008

Allikmets, R., Singh, N., Sun, H., Shroyer, N. F., Hutchinson, A., Chidambaram, A., et al. (1997). A photoreceptor cell-specific ATP-binding transporter gene (ABCR) is mutated in recessive Stargardt macular dystrophy. *Nat. Genet.* 15 (3), 236–246. doi:10.1038/ng0397-236

Anna, A., and Monika, G. (2018). Splicing mutations in human genetic disorders: examples, detection, and confirmation. *J. Appl. Genet.* 59, 253–268. doi:10.1007/s13353-018-0444-7

Bauwens, M., Garanto, A., Sangermano, R., Naessens, S., Weisschuh, N., De Zaeytijd, J., et al. (2019). ABCA4-associated disease as a model for missing heritability in autosomal recessive disorders: novel noncoding splice, cis-regulatory, structural, and recurrent hypomorphic variants. *Genet. Med.* 21 (8), 1761–1771. doi:10.1038/s41436-018-0420-y

Chen, X., Schulz-Trieglaff, O., Shaw, R., Barnes, B., Schlesinger, F., Källberg, M., et al. (2016). Manta: rapid detection of structural variants and indels for germline and cancer sequencing applications. *Bioinformatics* 32 (8), 1220–1222. doi:10.1093/bioinformatics/btv710

Cornelis, S. S., Runhart, E. H., Bauwens, M., Corradi, Z., De Baere, E., Roosing, S., et al. (2022). Personalized genetic counseling for Stargardt disease: offspring risk estimates based on variant severity. *Am. J. Hum. Genet.* 109 (3), 498–507. doi:10.1016/j.ajhg.2022.01.008

Cornelis, S. S., Bauwens, M., Haer-Wigman, L., De Bruyne, M., Pantrangi, M., De Baere, E., et al. (2023). *Compendium of clinical variant classification for 2,247 unique ABCA4 variants to improve genetic medicine access for Stargardt Disease*.

Cornelis, S. S., Bax, N. M., Zernant, J., Allikmets, R., Fritsche, L. G., den Dunnen, J. T., et al. (2017). *In silico* functional meta-analysis of 5,962 ABCA4 variants in 3,928 retinal dystrophy cases. *Hum. Mutat.* 38 (4), 400–408. doi:10.1002/humu.23165

Corradi, Z., Salameh, M., Khan, M., Héon, E., Mishra, K., Hitti-Malin, R. J., et al. (2022). ABCA4 c 859-25a> G, a frequent Palestinian founder mutation affecting the intron 7 branchpoint, is associated with early-onset Stargardt disease. *Investigative Ophthalmol. Vis. Sci.* 63 (4), 20. doi:10.1167/iovs.63.4.20

Cremers, F. P., Lee, W., Collin, R. W., and Allikmets, R. (2020). Clinical spectrum, genetic complexity and therapeutic approaches for retinal disease caused by ABCA4 mutations. *Prog. Retin. eye Res.* 79, 100861. doi:10.1016/j.preteyeres.2020.100861

Cremers, F. P., van de Pol, D. J., van Driel, M., den Hollander, A. I., van Haren, F. J., Knoers, N. V., et al. (1998). Autosomal recessive retinitis pigmentosa and cone-rod dystrophy caused by splice site mutations in the Stargardt's disease gene ABCR. *Hum. Mol. Genet.* 7 (3), 355–362. doi:10.1093/hmg/7.3.355

De Angeli, P., Reuter, P., Hauser, S., Schöls, L., Stingl, K., Wissinger, B., et al. (2022). Effective splicing restoration of a deep-intronic ABCA4 variant in cone photoreceptor precursor cells by CRISPR/SpCas9 approaches. *Mol. Therapy-Nucleic Acids* 29, 511–524. doi:10.1016/j.omtn.2022.07.023

Del Pozo-Valero, M., Riveiro-Alvarez, R., Blanco-Kelly, F., Aguirre-Lamban, J., Martin-Merida, I., Iancu, I.-F., et al. (2020). Genotype–phenotype correlations in a Spanish cohort of 506 families with biallelic ABCA4 pathogenic variants. *Am. J. Ophthalmol.* 219, 195–204. doi:10.1016/j.ajo.2020.06.027

Ezquerra-Inchausti, M., Anasagasti, A., Barandika, O., Garay-Aramburu, G., Galdós, M., López de Munain, A., et al. (2018). A new approach based on targeted pooled DNA sequencing identifies novel mutations in patients with Inherited Retinal Dystrophies. *Sci. Rep.* 8 (1), 15457–15512. doi:10.1038/s41598-018-33810-3

Fadaie, Z., Whelan, L., Dockery, A., Li, C. H., van den Born, L. I., Hoyng, C. B., et al. (2022). BBS1 branchpoint variant is associated with non-syndromic retinitis pigmentosa. *J. Med. Genet.* 59 (5), 438–444. doi:10.1136/jmedgenet-2020-107626

Garanto, A., Duijkers, L., Tomkiewicz, T. Z., and Collin, R. W. (2019). Antisense oligonucleotide screening to optimize the rescue of the splicing defect caused by the recurrent deep-intronic ABCA4 variant c 4539+ 2001G> A in Stargardt disease. *Genes* 10 (6), 452. doi:10.3390/genes10060452

Garces, F. A., Scortecci, J. F., and Molday, R. S. (2020). Functional characterization of ABCA4 missense variants linked to Stargardt macular degeneration. *Int. J. Mol. Sci.* 22 (1), 185. doi:10.3390/ijms22010185

Gooding, C., Clark, F., Wollerton, M. C., Grellscheid, S.-N., Groom, H., and Smith, C. W. (2006). A class of human exons with predicted distant branch points revealed by analysis of AG dinucleotide exclusion zones. *Genome Biol.* 7, 1–19. doi:10.1186/gb-2006-7-1-r1

Ioannidis, N. M., Rothstein, J. H., Pejaver, V., Middha, S., McDonnell, S. K., Baheti, S., et al. (2016). Revel: an ensemble method for predicting the pathogenicity of rare missense variants. *Am. J. Hum. Genet.* 99 (4), 877–885. doi:10.1016/j.ajhg.2016.08.016

Jaganathan, K., Panagiotopoulou, S. K., McRae, J. F., Darbandi, S. F., Knowles, D., Li, Y. I., et al. (2019). Predicting splicing from primary sequence with deep learning. *Cell* 176 (3), 535–548. doi:10.1016/j.cell.2018.12.015

Jiang, F., Pan, Z., Xu, K., Tian, L., Xie, Y., Zhang, X., et al. (2016). Screening of ABCA4 gene in a Chinese cohort with Stargardt disease or cone-rod dystrophy with a report on 85 novel mutations. *Investigative Ophthalmol. Vis. Sci.* 57 (1), 145–152. doi:10.1167/iovs.15-18190

Kaltak, M., de Bruijn, P., Piccolo, D., Lee, S.-E., Dulla, K., Hoogenboezem, T., et al. (2023). Antisense oligonucleotide therapy corrects splicing in the common Stargardt disease type 1-causing variant ABCA4 c 5461-10T> C. *Mol. Therapy-Nucleic Acids* 18 (31), 674–688. doi:10.1016/j.omtn.2023.02.020

Karczewski, K. J., Francioli, L. C., Tiao, G., Cummings, B. B., Alföldi, J., Wang, Q., et al. (2020). The mutational constraint spectrum quantified from variation in 141,456 humans. *Nature* 581 (7809), 434–443. doi:10.1038/s41586-020-2308-7

Khan, M., Cornelis, S. S., Pozo-Valero, M. D., Whelan, L., Runhart, E. H., Mishra, K., et al. (2020). Resolving the dark matter of ABCA4 for 1054 Stargardt disease probands through integrated genomics and transcriptomics. *Genet. Med.* 22 (7), 1235–1246. doi:10.1038/s41436-020-0787-4

Leman, R., Tubeuf, H., Raad, S., Tournier, I., Derambure, C., Lanos, R., et al. (2020). Assessment of branch point prediction tools to predict physiological branch points and their alteration by variants. *BMC genomics* 21, 86–12. doi:10.1186/s12864-020-6484-5

Li, H., and Durbin, R. (2009). Fast and accurate short read alignment with Burrows–Wheeler transform. *bioinformatics* 25 (14), 1754–1760. doi:10.1093/bioinformatics/btp324

Ma, D. J., Lee, H.-S., Kim, K., Choi, S., Jang, I., Cho, S.-H., et al. (2021). Whole-exome sequencing in 168 Korean patients with inherited retinal degeneration. *BMC Med. Genomics* 14 (1), 74–12. doi:10.1186/s12920-021-00874-6

Maugeri, A., Klevering, B. J., Rohrschneider, K., Blankenagel, A., Brunner, H. G., Deutman, A. F., et al. (2000). Mutations in the ABCA4 (ABCR) gene are the major cause of autosomal recessive cone-rod dystrophy. *Am. J. Hum. Genet.* 67 (4), 960–966. doi:10.1086/303079

Maugeri, A., van Driel, M. A., van de Pol, D. J., Klevering, B. J., van Haren, F. J., Tijmes, N., et al. (1999). The 2588G→ C mutation in the ABCR gene is a mild frequent founder mutation in the Western European population and allows the classification of ABCR mutations in patients with Stargardt disease. *Am. J. Hum. Genet.* 64 (4), 1024–1035. doi:10.1086/302323

McCulloch, D. L., Marmor, M. F., Brigell, M. G., Hamilton, R., Holder, G. E., Tzekov, R., et al. (2015). ISCEV Standard for full-field clinical electroretinography (2015 update). *Doc. Ophthalmol.* 130 (1), 1–12. doi:10.1007/s10633-014-9473-7

McKenna, A., Hanna, M., Banks, E., Sivachenko, A., Cibulskis, K., Kernytsky, A., et al. (2010). The genome analysis Toolkit: A MapReduce framework for analyzing next-generation DNA sequencing data. *Genome Res.* 20 (9), 1297–1303. doi:10.1101/gr.107524.110

Molday, R. S. (2015). Insights into the molecular properties of ABCA4 and its role in the visual cycle and Stargardt disease. *Prog. Mol. Biol. Transl. Sci.* 134, 415–431. doi:10.1016/bs.pmbts.2015.06.008

Mullin, N. K., Voigt, A. P., Cooke, J. A., Bohrer, L. R., Burnight, E. R., Stone, E. M., et al. (2021). Patient derived stem cells for discovery and validation of novel pathogenic variants in inherited retinal disease. *Prog. Retin. eye Res.* 83, 100918. doi:10.1016/j.preteyeres.2020.100918

Ohno, K., Takeda, J. i., and Masuda, A. (2018). Rules and tools to predict the splicing effects of exonic and intronic mutations. *Wiley Interdiscip. Rev. RNA* 9 (1), e1451. doi:10.1002/wrna.1451

Perea-Romero, I., Gordo, G., Iancu, I. F., Del Pozo-Valero, M., Almoguera, B., Blanco-Kelly, F., et al. (2021). Genetic landscape of 6089 inherited retinal dystrophies affected cases in Spain and their therapeutic and extended epidemiological implications. *Sci. Rep.* 11 (1), 1526. doi:10.1038/s41598-021-81093-y

Quazi, F., and Molday, R. S. (2014). ATP-binding cassette transporter ABCA4 and chemical isomerization protect photoreceptor cells from the toxic accumulation of excess 11-cis-retinal. *Proc. Natl. Acad. Sci.* 111 (13), 5024–5029. doi:10.1073/pnas.1400780111

Rentzsch, P., Witten, D., Cooper, G. M., Shendure, J., and Kircher, M. (2019). Cadd: predicting the deleteriousness of variants throughout the human genome. *Nucleic acids Res.* 47 (D1), D886–D894. doi:10.1093/nar/gky1016

Reurink, J., Weisschuh, N., Garanto, A., Dockery, A., van den Born, L. I., Fajardy, I., et al. (2023). Whole genome sequencing for USH2A-associated disease reveals several pathogenic deep-intronic variants that are amenable to splice correction. *Hum. Genet. Genomics Adv.* 4, 100181. doi:10.1016/j.xhgg.2023.100181

Richards, S., Aziz, N., Bale, S., Bick, D., Das, S., Gastier-Foster, J., et al. (2015). Standards and guidelines for the interpretation of sequence variants: A joint consensus recommendation of the American college of medical genetics and genomics and the association for molecular pathology. *Genet. Med.* 17 (5), 405–424. doi:10.1038/gim.2015.30

Riepe, T. V., Khan, M., Roosing, S., Cremers, F. P., and 't Hoen, P. A. (2021). Benchmarking deep learning splice prediction tools using functional splice assays. *Hum. Mutat.* 42 (7), 799–810. doi:10.1002/humu.24212

Roller, E., Ivakhno, S., Lee, S., Royce, T., and Tanner, S. (2016). Canvas: versatile and scalable detection of copy number variants. *Bioinformatics* 32 (15), 2375–2377. doi:10.1093/bioinformatics/btw163

Rowlands, C., Thomas, H. B., Lord, J., Wai, H. A., Arno, G., Beaman, G., et al. (2021). Comparison of *in silico* strategies to prioritize rare genomic variants impacting RNA splicing for the diagnosis of genomic disorders. *Sci. Rep.* 11 (1), 20607. doi:10.1038/s41598-021-99747-2

Rozet, J.-M., Gerber, S., Ghazi, I., Perrault, I., Ducroq, D., Souied, E., et al. (1999). Mutations of the retinal specific ATP binding transporter gene (ABCR) in a single family segregating both autosomal recessive retinitis pigmentosa RP19 and Stargardt disease: evidence of clinical heterogeneity at this locus. *J. Med. Genet.* 36 (6), 447–451.

RStudio Team (2020). *RStudio: Integrated development for R*. Boston Massachusetts: RStudio.

Runhart, E. H., Sangermano, R., Cornelis, S. S., Verheij, J. B., Plomp, A. S., Boon, C. J., et al. (2018). The common ABCA4 variant p. Asn1868Ile shows nonpenetrance and variable expression of Stargardt disease when present in trans with severe variants. *Investigative Ophthalmol. Vis. Sci.* 59 (8), 3220–3231. doi:10.1167/iovs.18-23881

Sangermano, R., Garanto, A., Khan, M., Runhart, E. H., Bauwens, M., Bax, N. M., et al. (2019). Deep-intronic ABCA4 variants explain missing heritability in Stargardt disease and allow correction of splice defects by antisense oligonucleotides. *Genet. Med.* 21 (8), 1751–1760. doi:10.1038/s41436-018-0414-9

Sangermano, R., Khan, M., Cornelis, S. S., Richelle, V., Albert, S., Garanto, A., et al. (2018). ABCA4 midigenes reveal the full splice spectrum of all reported noncanonical splice site variants in Stargardt disease. *Genome Res.* 28 (1), 100–110. doi:10.1101/gr.226621.117

Schindelin, J., Arganda-Carreras, I., Frise, E., Kaynig, V., Longair, M., Pietzsch, T., et al. (2012). Fiji: an open-source platform for biological-image analysis. *Nat. methods* 9 (7), 676–682. doi:10.1038/nmeth.2019

Siles, L., Ruiz-Nogales, S., Navinés-Ferrer, A., Méndez-Vendrell, P., and Pomares, E. (2023). Efficient correction of ABCA4 variants by CRISPR/Cas9 in hiPSCs derived from Stargardt disease patients. *Mol. Therapy-Nucleic Acids* 32, 64–79. doi:10.1016/j.omtn.2023.02.032

Sun, H., Molday, R. S., and Nathans, J. (1999). Retinal stimulates ATP hydrolysis by purified and reconstituted ABCR, the photoreceptor-specific ATP-binding cassette transporter responsible for Stargardt disease. *J. Biol. Chem.* 274 (12), 8269–8281. doi:10.1074/jbc.274.12.8269

Sung, Y., Choi, S. W., Shim, S. H., and Song, W. K. (2019). Clinical and genetic characteristics analysis of Korean patients with Stargardt disease using targeted exome sequencing. *Ophthalmologica* 241 (1), 38–48. doi:10.1159/000490073

Tang, S. J., Shen, H., An, O., Hong, H., Li, J., Song, Y., et al. (2020). Cis-and trans-regulations of pre-mRNA splicing by RNA editing enzymes influence cancer development. *Nat. Commun.* 11 (1), 799. doi:10.1038/s41467-020-14621-5

Tomkiewicz, T. Z., Suárez-Herrera, N., Cremers, F. P., Collin, R. W., and Garanto, A. (2021). Antisense oligonucleotide-based rescue of aberrant splicing defects caused by 15 pathogenic variants in ABCA4. *Int. J. Mol. Sci.* 22 (9), 4621. doi:10.3390/ijms22094621

Tsybovsky, Y., Molday, R. S., and Palczewski, K. (2010). The ATP-binding cassette transporter ABCA4: structural and functional properties and role in retinal disease. *Inflamm. Retin. Dis. complement Biol. pathology* 703, 105–125. doi:10.1007/978-1-4419-5635-4_8

Valero, R., de Castro-Miró, M., Jiménez-Ochoa, S., Rodríguez-Ezcurra, J. J., Marfany, G., and Gonzàlez-Duarte, R. (2019). Aberrant splicing events associated to CDH23 noncanonical splice site mutations in a proband with atypical Usher syndrome 1. *Genes* 10 (10), 732. doi:10.3390/genes10100732

van Driel, M. A., Maugeri, A., Klevering, B. J., Hoyng, C. B., and Cremers, F. P. (1998). ABCR unites what ophthalmologists divide (s). *Ophthalmic Genet.* 19 (3), 117–122. doi:10.1076/opge.19.3.117.2187

Viering, D., Hureaux, M., Neveling, K., Latta, F., Kwint, M., Blanchard, A., et al. (2022). Long read sequencing identifies novel pathogenic intronic variants in gitelman syndrome. *J. Am. Soc. Nephrol.* 34 (2), 333–345. doi:10.1681/ASN.2022050627

Vig, A., Poulter, J. A., Ottaviani, D., Tavares, E., Toropova, K., Tracewska, A. M., et al. (2020). DYNC2H1 hypomorphic or retina-predominant variants cause nonsyndromic retinal degeneration. *Genet. Med.* 22 (12), 2041–2051. doi:10.1038/s41436-020-0915-1

Westin, I. M., Jonsson, F., Österman, L., Holmberg, M., Burstedt, M., and Golovleva, I. (2021). EYS mutations and implementation of minigene assay for variant classification in EYS-associated retinitis pigmentosa in northern Sweden. *Sci. Rep.* 11 (1), 7696–7712. doi:10.1038/s41598-021-87224-9

Zheng-Bradley, X., Streeter, I., Fairley, S., Richardson, D., Clarke, L., Flicek, P., et al. (2017). Alignment of 1000 Genomes Project reads to reference assembly GRCh38. *Gigascience* 6 (7), 1–8. doi:10.1093/gigascience/gix038

Frontiers in
Cell and Developmental Biology

Explores the fundamental biological processes of life, covering intracellular and extracellular dynamics.

The world's most cited developmental biology journal, advancing our understanding of the fundamental processes of life. It explores a wide spectrum of cell and developmental biology, covering intracellular and extracellular dynamics.

Discover the latest Research Topics

See more →

Frontiers

Avenue du Tribunal-Fédéral 34
1005 Lausanne, Switzerland
frontiersin.org

Contact us

+41 (0)21 510 17 00
frontiersin.org/about/contact